



HAL
open science

The cingulo-habenular pathway in the emotional consequences of chronic pain in the rodent : behavioural, functional and molecular characterisation

Sarah H. Journée

► **To cite this version:**

Sarah H. Journée. The cingulo-habenular pathway in the emotional consequences of chronic pain in the rodent : behavioural, functional and molecular characterisation. Neuroscience. Université de Strasbourg, 2023. English. NNT : 2023STRAJ021 . tel-04957247

HAL Id: tel-04957247

<https://theses.hal.science/tel-04957247v1>

Submitted on 19 Feb 2025

HAL is a multi-disciplinary open access archive for the deposit and dissemination of scientific research documents, whether they are published or not. The documents may come from teaching and research institutions in France or abroad, or from public or private research centers.

L'archive ouverte pluridisciplinaire **HAL**, est destinée au dépôt et à la diffusion de documents scientifiques de niveau recherche, publiés ou non, émanant des établissements d'enseignement et de recherche français ou étrangers, des laboratoires publics ou privés.

ÉCOLE DOCTORALE DES SCIENCES DE LA VIE ET DE LA SANTÉ
CNRS UPR3212 – Institut des Neurosciences Cellulaires et Intégratives

THÈSE présentée par :

Sarah JOURNÉE

soutenue le : 28 juin 2023

pour obtenir le grade de : **Docteur de l'université de Strasbourg**

Discipline/ Spécialité : Neurosciences

**La voie cingulo-habénulaire dans les
conséquences émotionnelles de la douleur
chronique chez le rongeur : caractérisation
comportementale, fonctionnelle et
moléculaire**

**The cingulo-habenular pathway in the emotional
consequences of chronic pain in the rodent:
behavioural, functional and molecular characterisation**

THÈSE dirigée par :

Mme YALCIN Ipek

DR, INCI, Université de Strasbourg, France

RAPPORTEURS :

Mme BELZUNG Catherine

Pr, Inserm U1253, Université de Tours, France

M. MORON CONCEPCION Jose

Pr, Washington University School of Medicine in St. Louis, USA

AUTRES MEMBRES DU JURY :

M. MENDOZA Jorge

DR, INCI, Université de Strasbourg, France

To my grandpa

À mon papi

« La seule trace qui vaille est celle qu'on se crée,
à la pointe extrême de ce qu'on peut. »

A. Damasio,
La Horde du Contrevent

Content

Content	- 1 -
Acknowledgements/Remerciements	- 3 -
Liste des publications	- 7 -
Liste des communications orales et affichées	- 8 -
Résumé de thèse en français	- 9 -
Abbreviations	- 15 -
General Introduction	- 17 -
<i>Pain & Nociception</i>	- 17 -
Chronic pain	- 19 -
Neuropathic pain	- 19 -
The study of pain in rodents	- 23 -
Rodent models of neuropathic pain – The cuff model	- 25 -
<i>Chronic pain and its emotional component and consequences</i>	- 28 -
Aversion	- 28 -
General Anxiety Disorder	- 31 -
Major Depressive Disorder	- 33 -
Animal models of chronic pain-induced emotional disorders.....	- 34 -
Structures implicated in the comorbidity of chronic pain and emotional disorders	- 36 -
Highlight - Chronic pain and mood disorders comorbidity: Deciphering underlying brain circuits.	- 38 -
<i>The anterior cingulate cortex (ACC)</i>	- 42 -
Overview	- 42 -
Review - Janus Effect of the Anterior Cingulate Cortex: Pain and Emotion	- 42 -
The ACC to lateral habenula pathway	- 65 -
<i>The lateral habenula (LHb)</i>	- 66 -
Neuroanatomy, cytoarchitecture and neuronal properties of LHb.....	- 67 -
Connectivity	- 68 -
Functions.....	- 69 -
Role in emotional disorders	- 71 -
Role in chronic pain.....	- 72 -
Role in the emotional consequences of chronic pain.....	- 74 -
Research objectives	- 77 -
Material and Methods	- 79 -
<i>Animals</i>	- 79 -
<i>Surgical procedures</i>	- 79 -
<i>Chronic variable stress model (CVS)</i>	- 81 -
<i>Optogenetic stimulation procedures</i>	- 82 -
<i>Fiberphotometry</i>	- 83 -
<i>Behavioral assessment</i>	- 83 -

<i>Emotionality z-scores</i>	- 88 -
<i>Ex vivo electrophysiological recordings</i>	- 88 -
<i>Plasmid and AAV generation</i>	- 89 -
<i>Immunohistochemistry</i>	- 91 -
<i>Viral Translating Ribosome Affinity Purification (vTRAP) & RNA extraction</i>	- 91 -
<i>qRT-PCR</i>	- 92 -
<i>RNA-sequencing</i>	- 93 -
<i>RNA-sequencing analysis</i>	- 94 -
<i>Statistical analysis</i>	- 95 -
Results	- 101 -
<i>General overview</i>	- 101 -
<i>Article: The cingulo-habenular pathway plays a key role in aversive processing and participates in chronic pain- but not stress-induced anxiodepressive like consequences</i>	- 101 -
Abstract	- 102 -
Introduction	- 103 -
Material and Methods	- 105 -
Results	- 109 -
Discussion	- 129 -
General Discussion	- 141 -
<i>Overview & interpretation</i>	- 141 -
The calcium fluctuation of ACC→LHb neurons	- 141 -
The behavioural characterisation of the ACC-LHb pathway	- 142 -
The transcriptional signature of ACC→LHb neurons in chronic pain.....	- 144 -
Concluding remarks	- 146 -
<i>Limitations of the study</i>	- 147 -
The optogenetic model	- 147 -
The cuff model	- 150 -
The vTRAP	- 152 -
The fiber photometry.....	- 153 -
<i>Perspectives & open questions</i>	- 154 -
What is the primary role of the ACC-LHb pathway?.....	- 155 -
To whom does the ACC speak?.....	- 155 -
Concluding remarks	- 156 -
Bibliography	- 157 -
Appendix	- 192 -

Acknowledgements/Remerciements

First off, I would like to thank my jury members Pr Dr Catherine Belzung, Pr Dr Jose Moron-Concepcion and Dr Jorge Mendoza for making time in their busy schedule to review and evaluate my thesis work. I am looking forward to discussing it in person with you.

For this long list of acknowledgments, I will of course start with Ipek, the first pillar of this thesis work. To start with, I want to thank you for believing in me and trusting me even before the start of this thesis. Knowing that you believed enough in my abilities to entrust me with a PhD project after only 2 months of internship during my master 1 and mostly after I told you that I wanted to do my master 2 internship in another country really pushed me forward and allowed me to trust myself a little bit more. Our talk after the results of my master 2 defence that left me really down still resonates, when you told me “Sometimes the questions you get don’t let you shine, but it doesn’t mean that you are bad at something.”. This sentence attributes you at least half of my achievement during the doctoral school contest, as it kept me going forward when I wanted to give up. Thank you for being this inspiration and teaching me (and others I hope), that being a successful woman in science is possible, but most of all, being a kind, considerate, but nonetheless scientifically and humanly powerful woman in science is possible. I hope the future in research sees more Ipeks.

Thank you for putting up with me during these almost 4 years, I know that I can be pretty stubborn and pessimistic at times. I was delighted to proofread your emails, but also to be your special guide in the good food quest in Strasbourg (which is probably one of my biggest accomplishments during these 4 years, in close second with the completion of this work). Finally, thank you for believing in me when I did not.

PS: Remember to take some time off!

Jorge, there is of course a second thanks to you. My neuroscience life started with you when you were my tutor in PRT, but also through our discussions which convinced me to pursue with these PhD studies. Having you on my CST was a strength, both scientifically but also personally, during these 4 long year and I am thrilled to cross the finish line of this doctorate with you in my jury.

Un grand merci également au personnel administratif, ingénieur, technicien, et j’en passe, sans qui les thèses et la recherche seraient en bien mauvaise posture.

Merci dans un désordre alphabétique à Antoine, Betty, Bruno, Charles, Dom, Julie, Guillaume, Mélanie, Olivier, Pierre H, Sebahat, Sophie, Stéphane.

Pour la suite, j’aimerais célébrer mon (notre?) bureau, qui a été le théâtre de bien des rires, des choses étranges, des blagues vaseuses (et carambar surtout) et des tests topitos.

Léa -salamèche- À mon arrivée en master 1 c’est toi qui m’as formée, ce que tu as fait à nouveau quand je suis retombée dans l’équipe 2 ans plus tard pour commencer ma thèse. Tu

as été sans contexte le deuxième pilier de cette thèse et ton départ a fait vaciller beaucoup d'acquis que j'avais dans le laboratoire. Une amie a aussi disparu de ma proximité, plus personne pour râler de concert, aller boire des bières à 15h l'été, gossiper, fomenter des plans démoniaques, énerver Quentin (j'ai fait ce que j'ai pu) ou encore juste me rassurer sur mes résultats de thèse. Merci de m'avoir accompagnée dans mes premiers pas et dans les suivants aussi. Je suis persuadée que tu seras excellente dans la suite de ta carrière, que tu continues en science ou ailles ouvrir un refuge pour chiens, chevaux et chinchillas au fin fond de la Chine. Marion -bulbizarre- Ma secrétaire favorite (je rigole, mais juste un peu), je te transmets le flambeau des questions qui m'a été transmis par Léa. Merci d'avoir corrigé mes emails pour les rendre plus agréables. Merci pour une de mes plus récentes addiction, Haikyuu, qui m'a permis de bien procrastiner pendant l'écriture de ma thèse. Merci aussi pour toutes ces discussions, ces rires, ces tentatives d'aller au sport, ce support mental que tu m'as apporté au jour le jour.

Quentin -carapuce- Proclamé meilleur ingénieur et personne, ta gentillesse n'a d'égal que ton ego, peu importe ce que tu veux laisser penser aux autres. Merci d'avoir été le meilleur voisin de bureau qu'on puisse espérer, te voir écouter des groupes étranges en compilant tes résultats de von Frey refaisait mes journées. J'ai peu d'espoir de te voir rentrer un jour du Canada, mais je suis sûre que tu y feras bien des adeptes.

Maxime -carapuce (il semblerait qu'il te soit difficile de ne pas copier)- De tout fraîchement arrivé, tu es devenu mon frenemy numero uno. Merci pour les post-its, les expressions improbables, les kilos de sucre que je t'ai volé, les gossips, et merci de m'avoir écouté me plaindre et de m'avoir soutenue dans ces dernières (souvent à raison, et peut-être quelques fois à tort). Tu as repris le flambeau du bureau avec brio, et j'espère que tu le transmettra où tu iras.

Une pensée à Baptiste, qui apparemment m'aurait transmis tous ses tics et ses humeurs en me transmettant son bureau à son départ. Ils ne savaient juste pas encore que nous étions juste des jumeaux de caractères.

Grobin, meilleur fan de Nicolas Cage, meilleur partenaire de chirurgies, meilleur partenaire de comportement, meilleur partenaire de fou rire, (meilleur) ingénieur, troisième et dernier pilier de cette thèse (oui, elle était clairement bancal, j'aurai dû m'en douter). Je ne saurai te remercier assez de tout ce que tu as fait pour moi durant les trois ans que nous avons partagés. Tu es un peu l'ange gardien de cette thèse, je pense que sans toi j'aurai déjà tout arrêté une bonne centaine de fois. On rencontre rarement des personnes plus extraordinaires que N. Cage, tu en fais partie. Merci pour ces situations gênantes et d'avoir embrassé la vie malaisante que je mène. Et bien que nous ayons commencé en tant que collègues, je finis cette thèse avec le bonheur de t'appeler ami. C'est partie pour la best life.

Mes mentors ensuite (vous le saviez !), Clémentine, Victor and Elliott. Je commencerai dans l'ordre alphabétique pour qu'il n'y ait pas de jalousies

Clémentine, d'une personne qu'on m'avait présentée comme une légende vivante, tu es devenue une amie. Merci pour ta présence, ton écoute, ta bizarrerie qui m'a fait me sentir moins seule. Garde cette pêche et, je l'espère, transmets là à beaucoup d'étudiants, ils en auront bien besoin. J'ai hâte de te retrouver teinte en gris quand je t'aurai également volé ton idée. Elliott, merci de me rappeler que « Ga ! » est une réponse tout à fait appropriée à toutes les questions de la vie.

Victor, on t'avait présenté comme une personne terrifiante, et j'angoissais de te voir arriver au laboratoire pour au final découvrir une personne géniale. Peu de regrets, à part peut-être de ne pas avoir fait plus de chirurgies à tes côtés, ce qui aurait été une occasion de plus de discuter. Tu m'as fait reprendre (un peu, ce qui est déjà beaucoup) espoir en la recherche et a su me remotiver dans la pente descendante qu'a été cette fin de thèse. Merci pour nos discussions, qu'elles soient scientifiques, féministes ou autre, merci de montrer qu'une remise en question dans la recherche actuelle est possible et, je le pense, bénéfique pour le futur.

Noémie, les bottes de Quentin étaient bien grandes, mais tu les as remplies avec brio. Merci d'avoir été là pour m'accompagner pour mon shot de bubble tea et d'avoir été une source non tarissable de compliments sur ma personne qui m'ont bien aidé ces derniers mois.

Enora, notre temps au laboratoire ensembles aura été bref, mais du peu que j'en ai vu, je suis persuadée que tu sauras tenir la maison debout. Ne t'oublie pas dans la recherche, prends des vacances, elles te permettront de mieux repartir, et reste cette personne géniale, passionnée et bienveillante que tu es.

Finally, a big thank you to all the other students, more or less recent, from the team, who probably saw me more than once walking with firm and fast steps in the corridors, and with whom I've shared countless discussions, meals, beers, and sometimes science. Thank you to Ilona, Marilou, Alba, Beyza, Heba, Jérémy, Vandana, Susana, Mithil, Hanus, Margot², Benjamin, Pierre-Alexis and Nicolas Cage.

Un grand merci aux copains de thèse, la team des J : Jamille, Jarion, Jangel, Jéo. Jamille et Jarion, merci de votre présence au jour le jour dans l'équipe, mais aussi au yoga, par la pensée pendant le tricot, pendant les pauses partagées, les repas, les rires, les discussions mouvementées. Jarion, merci d'avoir été plus d'une fois une partenaire rebelle. Théo et Angel, merci de votre joie de vivre qui se propage sans limites, j'ai hâte de boire cette bière de post thèse avec vous.

L'instant fourre-tout est arrivé, sponsored par Doctoneuro, garant d'une bonne part de ma santé mentale durant ce doctorat et tisseur de liens depuis des années. Beaucoup sont devenus des amis, en partie grâce à cette asso qui fait un travail incroyable grâce à vous/nous. Merci à Baptiste (best président, vice-président, secrétaire et CARE, hâte de voir la suite !), Robin (j'attends le déguisement de lapin à ma thèse), Valod (je reviendrai empiler des trucs

sur ton bureau, n'ait crainte), Karim (continue de me faire rire pitié), Valentin (belle surchemise), Louise, Lucien, Federica, Charlotte, Henrico, Matthieu, Noëmi, Clémence, Guillaume, Colette, Théo, ...

Bien sûr il y a les amis d'autres sphères, ceux qui garantissent que le doctorat reste au laboratoire. Merci à Mathieu, Gauthier et Big Boss. Merci à Amira pour les cinémas, les repas et les photos/vidéos de chat. Merci Célia d'être présente dès que le besoin s'en ressent et d'être toujours partante pour un thé ou une discussion sur l'avenir, et de toujours poser la question qui fâche : « Comment ça va ? ». Merci à ma Camie, qui a connu mon année questionnement en architecture puis a été là à chaque fois par-delà les frontières qui nous séparent toujours. Merci à toi Paul de me remplir de joie et faire envoler tous mes soucis à chaque fois qu'on se voit. Merci à mes gow de licence Trine, Goti et Dylan, même si les réunions sont rares, c'est toujours un plaisir de voir la diversité de parcours possibles après une L1 de bio, et surtout toujours un bonheur de voir que malgré les années la connexion reste présente. Merci à Adrien, mon doctorant corse finlandais, téléchargeur de papiers personnalisés. J'espère encore emporter la victoire et finir ce doctorat avant toi. Merci à Morgane qui n'a de cesse de m'informer sur ma mauvaise utilisation des virus et qui est responsable de mon addiction aux Spritz. Merci à la team collègue/lycée, Mathilde ma Docteure lyonnaise préférée et ma Madeleine parisienne (qui l'eut cru), qui me soutiennent et me fascinent de leur brillance. Merci à Maiko et Mathilde, mes strasbourgeoises préférées, dont les discussions de plantes, tricot, chat, dessin, vie autour d'un thé, de sucreries et d'onigiri m'ont énormément aidée pendant cette thèse à comprendre le plus important. Thanks to Emelie and Jiadi, I can't wait to see you again. Same for you Bonnie, I miss you dearly. Finalement à mes amisœurs, mes sœurs de cœur, Inès et Valentine, je ne saurais souligner en quoi votre soutien durant cette thèse a été salvateur. Je m'arrêterai à ceci, vous savez déjà à quel point je vous aime et vous êtes essentielles. Thanks for putting up with my bad temper.

Merci finalement à ma famille : papa, maman, Juliette, Marion, mamie, Catherine, Philippe, Luc, Gabriel, Alexis, Héloïse, Edouard, Paty. J'ai la chance d'avoir une famille comme vous, présente et aimante. Merci à mes parents de m'avoir soutenue et de continuer à me soutenir dans mon parcours, même s'ils ne comprennent pas forcément toute l'ampleur de ce que je fais. Merci à mes sestras pour leur présence au jour le jour et leur amour inconditionnel. Un merci félin à Hera et Loki, qui eux ne comprennent clairement pas ce que je fais, mais qui m'ont apporté un soutien émotionnel non négligeable durant cette thèse.

Enfin, pour finir, je ferai court pour ne pas finir dans le cheesy que tu détestes tant, mais merci Monsieur. Merci d'être là au jour le jour, de me calmer, m'apaiser, me radicaliser, m'écouter, me faire rire, m'apprendre à m'accepter. J'ai hâte que ta thèse soit finie pour qu'on puisse faire pousser plein de trucs, se rebeller et cuisiner des plats délicieux. Merci d'amour.

À mon papi et son double doctorat, tu me manques et j'aurai aimé que tu sois là.

Liste des publications

Articles publiés :

Becker LJ*, **JOURNÉE SH***, Lutz PE, Yalcin I (2020) Comorbidity of chronic pain and anxiodepressive disorders: Deciphering underlying brain circuits. *Neurosci Biobehav Rev*, 115, 131-133. (*equal contribution)

Megat S, Hugel S, **JOURNÉE SH**, Bohren Y, Lacaud A, Lelièvre V, Doridot S, Villa P, Bourguignon JJ, Salvat E, Schlichter R, Freund-Mercier MJ, Yalcin I, Barrot M (2022) Antiallodynic action of phosphodiesterase inhibitors in a mouse model of peripheral nerve injury. *Neuropharmacol*, 205, 108909.

Becker LJ, Fillinger C, Waegaert R, **JOURNÉE SH**, Hener P, Ayazgök B, Humo M, Karatas M, Thouaye M, Gaikwad M, Degiorgis L, Santin M, Mondino M, Barrot M, El Chérif I, Turecki G, Belzeaux R, Veinante P, Harsan LA, Hugel S, Lutz PE, Yalcin I. (2023) The basolateral amygdala-anterior cingulate pathway contributes to depression and its comorbidity with chronic pain. *Nat. Commun.*

Koskinen M-K, Laine MA, Abdollahzadeh A, Gigliotta A, Mazzini G, **JOURNÉE SH**, Alenius V, Trontti K, Tohka J, Hyytiä P, Sierra A, Hovatta I. (2023) Nodes of Ranvier remodeling in chronic psychosocial stress and anxiety. *Neuropsychopharmacol*

Articles en révision :

JOURNÉE SH*, Mathis VP*, Fillinger C, Veinante P, Yalcin I. Janus Effect of the Anterior Cingulate Cortex: Pain and Emotion. *Neurosci Biobehav* (*equal contribution)

Articles en préparation :

JOURNÉE SH*, Mathis VP*, Waegaert R, Gaikwad M, Thouaye M, Hugel S, Leboulleux Q, Willem N, Becker L, Ozkan S, Lutz PE, Yalcin I. The cingulo-habenular pathway plays a key role in aversive processing and participates in chronic pain- but not stress-induced anxiodepressive like consequences. (*equal contribution)

Liste des communications orales et affichées

FENS 2022, Paris, France.

Understanding the emotional consequences of chronic pain: Insight from ACC-LHb pathway.

JOURNÉE SH, Waegaert R, Leboulleux Q, Barrot M, Mathis VP, Yalcin I. (poster)

Lake Como School of Neuroscience 2022, Côme, Italie.

Role of the ACC-LHb pathway in the emotional consequences of chronic pain.

JOURNÉE SH, Waegaert R, Barrot M, Mathis VP, Yalcin I (communication orale)

Euridol Day 2021, Strasbourg, France.

Role of the ACC-LHb pathway in the emotional consequences of chronic pain.

JOURNÉE SH, Waegaert R, Barrot M, Mathis VP, Yalcin I (communication orale)

RIKEN CBS école d'été 2021," Reconstructing emotion, from molecules and circuits to concepts.", Japon.

Role of the ACC-LHb pathway in the emotional consequences of chronic pain.

JOURNÉE SH, Waegaert R, Becker LJ, Mathis VP, Barrot M, Yalcin I (poster)

Congrès NeuroFrance 2020, Strasbourg, France.

Role of the ACC-LHb pathway in the emotional consequences of chronic pain.

JOURNÉE SH, Waegaert R, Becker LJ, Mathis VP, Barrot M, Yalcin I (poster)

Résumé de thèse en français

Introduction

La douleur chronique, définie comme une douleur persistante ou récurrente de plus de trois mois, affecte 30% de la population française. Cette expérience sensorielle désagréable détériore significativement la vie des patients et peut devenir invalidante. Il est en effet fréquent que les patients douloureux chroniques développent des troubles de l'humeur ou anxieux, tel qu'un trouble dépressif majeur ou un trouble anxieux généralisé. Cette comorbidité touche entre 30% et 80% des patients atteints de douleur chronique suivant le type de douleur considéré, faisant de cette dernière l'un des facteurs de risque pour le développement de troubles émotionnels. De plus, ces troubles semblent aggraver la sensation de douleur chez les patients souffrant de douleurs chroniques. Cette forte comorbidité complique grandement le diagnostic ainsi que le choix de stratégies thérapeutiques.

Au cours des deux dernières décennies, de nombreux modèles rongeurs ont été développés afin de modéliser et étudier la comorbidité entre douleur chronique et troubles émotionnels. Si ces modèles ont permis de mieux décrire les mécanismes neurobiologiques impliqués dans ce phénomène clinique grave, les circuits neuronaux sous-tendant le développement et le maintien des troubles émotionnels induits par la douleur chronique restent encore majoritairement inconnus. Au sein de notre équipe, nous utilisons un modèle de douleur neuropathique, qui est une douleur causée par une lésion ou maladie du système nerveux somatosensoriel. Ce dernier consiste en l'implantation d'un manchon en polyéthylène autour de la branche principale du nerf sciatique. Ce modèle, dit du « cuff », induit non seulement une hypersensibilité mécanique après la chirurgie, mais provoque également des symptômes de types anxiodépressifs. Ces symptômes somatosensoriels et émotionnels suivent une chronologie précise et similaire à celle retrouvée chez des patients douloureux, à savoir dans un premier temps le développement de l'hypersensibilité mécanique, suivi par l'apparition de symptôme anxieux, puis de symptômes dépressifs, lesquels subsistent après la disparition de la composante somatosensorielle.

De nombreuses études, réalisées ces dernières années chez l'Homme ou dans des modèles animaux, ont mis en lumière des structures cérébrales impliquées dans la douleur chronique, les troubles émotionnels, mais également leur comorbidité. Parmi ces structures, le cortex cingulaire antérieur (CCA) joue un rôle crucial dans la physiopathologie de la douleur

chronique et des troubles anxiodépressifs. C'est en effet l'un des principaux modulateurs du système régulant les émotions. Par exemple, chez des patients atteints de douleurs chroniques associées à des troubles dépressifs, une stimulation magnétique transcrânienne ou une ablation chirurgicale du CCA ont amélioré les symptômes résultant des deux pathologies. Au niveau fondamental, notre équipe a d'ores et déjà confirmé le rôle primordial joué par le CCA dans le contrôle émotionnel : 1) chez des souris naïves, l'activation optogénétique des cellules pyramidales glutamatergiques du CCA est suffisante pour déclencher des comportements de type anxiodépressifs ; 2) dans notre modèle murin du cuff, une lésion ou une inactivation optogénétique du CCA contrecarrent les symptômes anxiodépressifs sans affecter l'allodynie mécanique. Ces résultats ont ainsi mis en évidence le rôle majeur du CCA dans les conséquences émotionnelles de la douleur chronique. Cependant, ces comorbidités ne dépendent pas d'une seule structure cérébrale, mais sont des pathologies dites de réseau. En effet, l'altération du CCA provoquée par la douleur chronique peut ensuite se « propager » aux structures qu'il contacte. Afin de mieux comprendre et décrire ce phénomène, grâce à des techniques de traçage et d'imagerie cérébrale chez le rongeur, notre équipe a commencé à étudier le connectome du CCA et a ainsi mis en évidence des efférences du CCA potentiellement impliquées dans le développement des conséquences émotionnelles de la douleur chronique. Notamment, une connexion entre le CCA et l'habénula latérale (HbL) semble pouvoir jouer un rôle important dans la comorbidité entre douleur chronique et troubles émotionnels. Notamment, il a été démontré que l'HbL est impliquée dans des processus aversifs et qu'une altération de son activité participe au développement de symptômes dépressifs, y compris induits par une douleur chronique.

Ma thèse s'est donc déroulée dans ce cadre conceptuel, visant à caractériser la voie cingulo-habénulaire dans les conséquences émotionnelles de la douleur chronique chez la souris. Dans un premier temps nous avons évalué si la voie cortico-habénulaire (CCA-HbL) participait au développement de la comorbidité entre douleur chronique et troubles émotionnels. Dans un second temps, nous avons cherché à savoir si les altérations moléculaires observées au sein de cette voie pouvaient être impliquées dans les changements neuro-adaptatifs et comportementaux observés.

Pour répondre à ces questions, nous avons combiné des outils optogénétiques, d'imagerie calcique (par la technique de « fiber photometry ») et de biologie moléculaire et avons défini 3 grands objectifs :

- 1) étudier l'impact de la manipulation de la voie CCA-HbL sur les comportements émotionnels et nociceptifs ;
- 2) caractériser l'activité des neurones du CCA projetant vers l'HbL ;
- 3) identifier des modifications transcriptomiques des neurones du CCA projetant vers l'HbL.

Étude de l'impact de la manipulation optogénétique de la voie CCA-HbL sur les comportements émotionnels et nociceptifs

La première étape de ce travail de thèse a été de caractériser comportementalement le rôle de la voie CCA-HbL dans les réponses nociceptives et émotionnelles. Pour cela, nous avons utilisé une approche optogénétique consistant en l'expression d'opsines (des protéines photo-activables), par l'intermédiaire de vecteurs viraux, permettant soit l'activation (channelrhodopsine – ChR2) soit l'inhibition (archéorhodopsine – Arch) lors d'une stimulation lumineuse. Lors de nos expériences nous avons opté pour une stratégie virale rétrograde permettant la manipulation optogénétique des neurones du CCA-projetant à l'HbL. Nous avons ensuite évalué l'effet de la manipulation de la voie CCA-HbL sur la douleur, l'anxiété et la dépression grâce à une batterie de tests comportementaux incluant des tests d'allodynie mécanique (filaments de von Frey), d'aspect aversif d'une douleur persistante (évitement en temps réel, conditionnement de préférence de place) et des tests d'anxiété et de dépression (test du clair-obscur, test d'hyponéophagie, test de nage forcée), chez des souris libres de leurs mouvements. L'inhibition neuronale a eu lieu chez des souris neuropathiques et contrôles avec une stimulation unique (continue, 5 min). Nous avons ainsi montré que l'inhibition de la voie CCA-HbL suffisait à prévenir les comportements de type dépressifs, mais pas douloureux, provoqués par une douleur chronique. Afin de mieux comprendre le rôle de cette voie dans les troubles émotionnels, nous avons également utilisé un modèle murin de stress chronique léger. De façon surprenante, la même manipulation de la voie CCA-HbL n'a pas impacté les conséquences émotionnelles provoquées par le stress chronique, suggérant ainsi que la voie CCA-HbL est spécifique aux troubles anxiodépressifs induits par une douleur chronique.

Nous nous sommes ensuite demandé si l'activation de cette voie chez des animaux naïfs, ne présentant pas de douleur, était suffisante pour induire des comportements de type anxiodépressifs. Une stimulation unique n'a provoqué aucune réponse comportementale. Cependant, il est connu que l'apparition de troubles de type anxiodépressifs suite à une

douleur chronique est progressive. Une activation unique n'étant potentiellement pas suffisante, nous avons alors choisi de tester l'effet de stimulations répétées, soit une stimulation de 30 minutes par jour durant quatre jours consécutifs. Les tests comportementaux ont été réalisés à la suite de ce protocole et sans stimulation. Cette activation chronique de la voie CCA-HbL a déclenché quant à elle des comportements de type anxieux et dépressifs chez des animaux naïfs. Ces résultats viennent confirmer l'implication de la voie CCA-HbL dans les processus émotionnels et suggèrent qu'une plasticité est mise en place par notre protocole de stimulation chronique qui provoquerait en conséquence des comportements de type anxiodépressifs. Ceci reste cohérent avec nos résultats dans le modèle neuropathique, dans lequel les comportements de type anxiodépressifs mettent plusieurs semaines à se mettre en place, à l'instar de l'hyperactivité du CCA, ce qui suppose également une plasticité du CCA.

Caractérisation de l'activité des neurones du CCA projetant vers l'HbL

La seconde étape de ce projet de thèse a été de caractériser l'activité globale des neurones du CCA projetant vers l'HbL dans notre modèle neuropathique en regard de l'activité totale des neurones du CCA. Pour ce faire, nous avons utilisé une approche d'imagerie calcique *in vivo* consistant en l'expression de biosenseurs calciques par l'intermédiaire de vecteurs viraux. Cette technique, appelée « fiber photometry », permet de mesurer les fluctuations de calcium, considérées comme un reflet de l'activité neuronale, via une fibre optique implantée à demeure et des biosenseurs calciques qui émettent de la fluorescence lorsqu'ils sont au contact d'ion calcium. Afin de cibler la totalité des neurones du CCA et également les neurones du CCA projetant vers l'HbL, nous avons utilisé une stratégie virale double, avec d'une part l'injection d'un virus rétrograde dans l'HbL, et d'autre part l'injection d'un virus local dans l'ACC. Les virus permettent chacun l'expression de biosenseurs calciques différents (GCaMP6m et jRGECO1a) avec chacun une longueur d'onde d'excitation et une fluorescence spécifique, afin de pouvoir enregistrer les deux signaux chez les mêmes animaux. Les animaux neuropathiques et contrôles ont été enregistrés lors des tests comportementaux décrits précédemment (filament de Von Frey, test du clair-obscur, test d'hyponéophagie). L'analyse des fluctuations de calcium au sein de l'ensemble des neurones du CCA mais aussi, plus spécifiquement, des neurones CCA projetant à l'HbL nous permettra d'évaluer si cette dernière population joue un rôle particulier dans les comportements susmentionnés. De plus,

la comparaison des fluctuations calciques entre animaux neuropathiques et contrôles nous permettra de mieux comprendre les mécanismes cellulaires sous-tendant le développement des troubles émotionnels provoqués par la douleur au sein de la voie CCA-HbL. Toutes ces expériences sont en cours et devraient se terminer courant mars 2023.

Caractérisation moléculaire des neurones du CCA projetant vers l'HbL

À la suite de notre caractérisation comportementale, nous avons cherché à étudier l'impact de la comorbidité entre douleur chronique et troubles anxiodépressifs sur l'expression des gènes dans les neurones du CCA projetant à l'HbL. Pour caractériser la signature moléculaire des neurones du CCA projetant vers l'ACC, nous avons utilisé la technique de « viral Translating Ribosome Affinity Purification » (vTRAP). Cette technique repose sur le marquage génétique de la protéine ribosomale Rpl10a et l'immunopurification des ribosomes d'un type cellulaire spécifique de façon à ne récupérer que les ARN messagers en transcription. Ici, un vecteur viral exprimant des protéines Rpl10a marquée avec la protéine mCherry a été injecté dans l'HbL et transporté de manière rétrograde pour immunoprécipiter uniquement les ribosomes des neurones du CCA projetant vers l'HbL. Ces ribosomes ont été traités pour l'extraction d'ARN et les ARN en transcription ont ensuite été analysés grâce à du séquençage ARN à haut débit. La comparaison des ARN de souris neuropathiques et contrôles nous permettent d'identifier les altérations transcriptomiques conséquentes à une douleur chronique associée à des troubles émotionnels (en cours). Nous allons pour ce faire effectuer différentes analyses. La première méthode est celle du Gene Set Enrichment Analysis (GSEA) qui permet d'identifier des classes de gènes et des réseaux ontologiques représentés différemment entre nos deux conditions (contrôles et neuropathiques). Ensuite, nous utiliserons une approche de biologie des systèmes, c'est-à-dire une analyse des réseaux de co-expression de gènes qui permet de comparer la signature de l'expression génique de deux échantillons. Cette seconde approche nous permettra d'évaluer quels sont les gènes conservés ou non entre le transcriptome complet du CCA et le transcriptome caractéristique des neurones du CCA projetant à l'HbL, afin d'identifier des gènes spécifiquement dérégulés dans la voie CCA-HbL chez nos animaux neuropathiques, qui devraient être confirmés par PCR d'ici la soutenance de thèse (en cours). Ces résultats nous permettraient par la suite de sélectionner un gène cible et de le manipuler dans notre modèle du cuff afin d'établir un lien causal entre les modifications moléculaires observées et les troubles émotionnels induits par une douleur chronique.

Conclusion

Ce travail de thèse a permis de mettre en évidence le rôle important joué par la voie CCA-HbL dans les comportements émotionnels, notamment à la suite d'une douleur chronique. En effet, de manière intéressante l'inhibition de la voie CCA-HbL n'a un effet sur les comportements émotionnels que dans notre modèle de douleur neuropathique, mais pas dans un modèle de stress chronique. De plus, bien que l'HbL soit impliquée dans les processus nociceptifs, il semblerait que l'inhibition des neurones projetant vers cette dernière n'ait aucun impact sur la réponse nociceptive. Il est probable que les neurones de la voie CCA-HbL soient soumis à une plasticité, étant donné qu'une stimulation unique de ces derniers ne suffit pas à évoquer des comportements de type anxiodépressif, à l'inverse d'un protocole chronique. L'étude de l'activité des neurones du CCA projetant vers l'HbL nous permettra de caractériser fonctionnellement de façon plus poussée la voie CCA-HbL. Enfin, les données transcriptionnelles obtenues nous permettront d'apporter un lien de causalité entre la dérégulation de gènes cibles et les conséquences émotionnelles de la douleur chronique.

Ce projet de thèse aura été l'occasion de caractériser pour la première fois la contribution de la voie CCA-HbL dans les conséquences émotionnelles de la douleur chronique, et ce de façon comportementale, fonctionnelle et transcriptionnelle, plaçant ainsi cette voie dans la circuiterie de la comorbidité entre douleur chronique et troubles émotionnels. Les résultats de ce projet de thèse feront l'objet d'un article scientifique. Ce dernier est en cours d'écriture et nous espérons pouvoir le soumettre d'ici la fin de cette thèse.

Abbreviations

ACC: anterior cingulate cortex	LH: lateral hypothalamus
ACC_{→LHb} neurons: LHb projecting ACC neurons	LHb: lateral habenula
ArchT: archeorhodopsin	LHbL: lateral part of the lateral habenula
BDNF: brain derived neurotrophic factor	LHbM: medial part of the lateral habenula
BLA: basolateral amygdala	LPO: lateral preoptic area
CaMKII: calcium/calmodulin-dependent protein kinase II	LTP: long term potentiation
CCI: chronic constriction injury	MDD: major depressive disorder
CeA: central amygdala	MeCP2: Methyl-CpG binding protein 2
CFA: complete Freund's adjuvant	MHb: medial habenula
ChR2: channelrhodopsin	MRI: magnetic resonance imaging
CMS: chronic mild stress	NAC: nucleus accumbens
CPA: conditioned place aversion	NP: neuropathic pain
CPID: chronic pain induced depression	NSF: novelty suppressed feeding test
CPP: conditioned place preference	OFT: open-field test
CRS: chronic restraint stress	PAG: periaqueductal gray
CUS: chronic unpredictable stress	PEAP: place escape-avoidance paradigm
CVS: chronic variable stress	PFC: prefrontal cortex
DBS: deep brain stimulation	PF_{Glu}: posterior thalamic nucleus glutamatergic neurons
DEGs: differentially expressed genes	PO_{Glu}: parafascicular thalamic nucleus glutamatergic neurons
DRN: dorsal raphe nucleus	PP2A: protein phosphatase 2A
DSM-V: Diagnostic and Statistical Manual of Mental Disorders, Fifth Edition	RRHO2: rank rank hypergeometric overlap
EPM: elevated plus maze	RTA: real-time aversion
EPN: entopeduncular nucleus	SC: spinal cord
EOM: elevated zero maze	SN: substantia nigra
fMRI: functional magnetic resonance imaging	SNI: spinal nerve injury
FST: forced swim test	SNRIs: selective serotonergic and noradrenergic reuptake inhibitors
GAD: generalised anxiety disorder	SSRIs: selective serotonergic reuptake inhibitors
Glu: glutamatergic	TCAs: tricyclic antidepressants
Hb: habenula	TP: time point
HIV: human immunodeficiency virus	TST: tail suspension test
IASP: International Association for the Study of Pain	tVTA: tail of the ventral tegmental area
IC: insular cortex	UST: urine sniffing test
ICD: International Classification of Diseases	vF: von Frey
IP: immunoprecipitated transcriptome	VTA: ventral tegmental area
LC: locus coeruleus	vTRAP: viral translating ribosome affinity purification
LD: light dark test	WHO: World Health Organization

General Introduction

Pain

“An unpleasant sensory and emotional experience associated with, or resembling that associated with, actual or potential tissue damage.”

Notes

- Pain is always a personal experience that is influenced to varying degrees by biological, psychological, and social factors.
- Pain and nociception are different phenomena. Pain cannot be inferred solely from activity in sensory neurons.
- Through their life experiences, individuals learn the concept of pain.
- A person’s report of an experience as pain should be respected.*
- Although pain usually serves an adaptive role, it may have adverse effects on function and social and psychological well-being.
- Verbal description is only one of several behaviors to express pain; inability to communicate does not negate the possibility that a human or a nonhuman animal experiences pain.

Etymology

Middle English, from Anglo-French *peine* (pain, suffering), from Latin *poena* (penalty, punishment), in turn from Greek *poinë* (payment, penalty, recompense).

*The Declaration of Montréal, a document developed during the First International Pain Summit on September 3, 2010, states that “Access to pain management is a fundamental human right.”

Figure 1. IASP revised definition of pain (Raja *et al.*, 2020)

Pain & Nociception

Pain is defined in the Oxford Dictionary as *“the feelings that you have in your body when you have been hurt or when you are sick”*. This definition is well known by the general public and raises two interesting points: the concept of feelings, something that you feel through the mind or through the senses and the fact that pain arises in abnormal situations. However, this definition does not account for the valence of these feelings, which is central in pain. On the other hand, in clinical settings, the International Association for the Study of Pain (IASP) used to define pain as an *“unpleasant sensory and emotional experience associated with actual or potential tissue damage, or described in terms of such damage”* (Bonica, 1979). Pain is thus distinct from nociception, defined as the neural process of encoding noxious stimuli (IASP), which solely relies on peripheral nociceptors-mediated detection of potentially damaging stimuli; whereas pain is a conscious concept. Nociception can thus occur without pain sensation and vice versa. Interestingly, compared to the more general dictionary definition, in the IASP definition the somatosensory discriminative and emotional components of pain are clearly separated. After 40 years of *status quo*, this definition was recently revised to take into consideration nuances and complexity of pain. Indeed, pain is now defined as *“an unpleasant sensory and emotional experience associated with, or resembling that associated with, actual or potential tissue damage”* (Raja et al., 2020). This definition is now accompanied by key notes to provide a better context (Figure 1) and be more inclusive. It was brought by a multinational task force and relies partly on reviews and essays to reconsider the definition of pain. Within the proposed revisions, Cohen *et al.* (2018) offered the following: *“Pain is a mutually recognizable somatic experience that reflects a person’s apprehension of threat to their bodily or existential integrity”*. Although this definition does not account for several important points of the current definition of pain, in particular the different components of pain, it highlights the primal survival value of acute pain, which is supposed to be a red flag for an underlying condition (i.e., actual or potential tissue damage) and usually disappears with it.

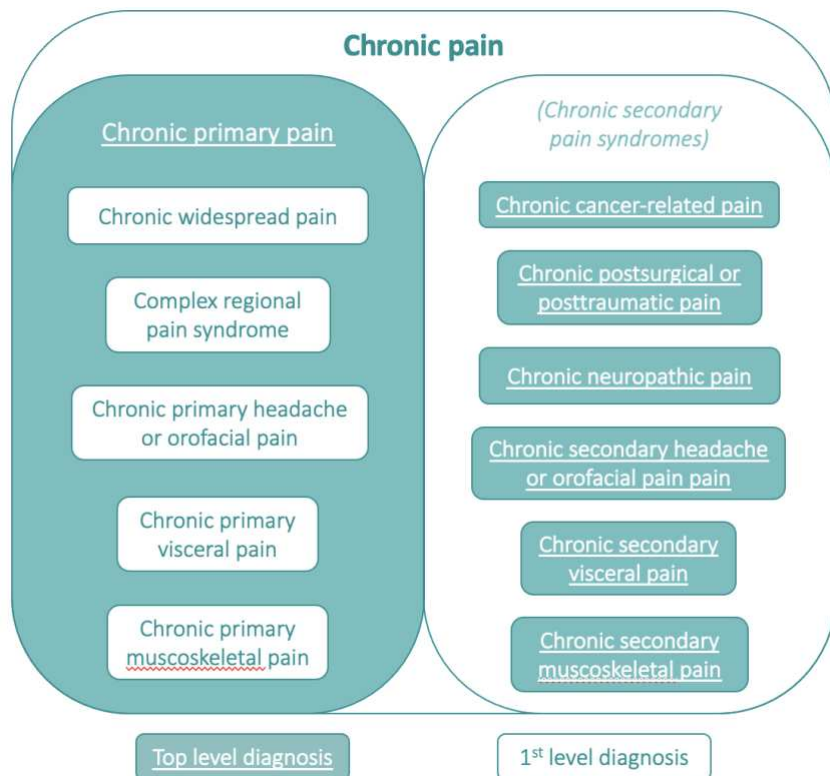


Figure 2. ICD-11 classification of chronic pain. Adapted from Treede et al. (2019)

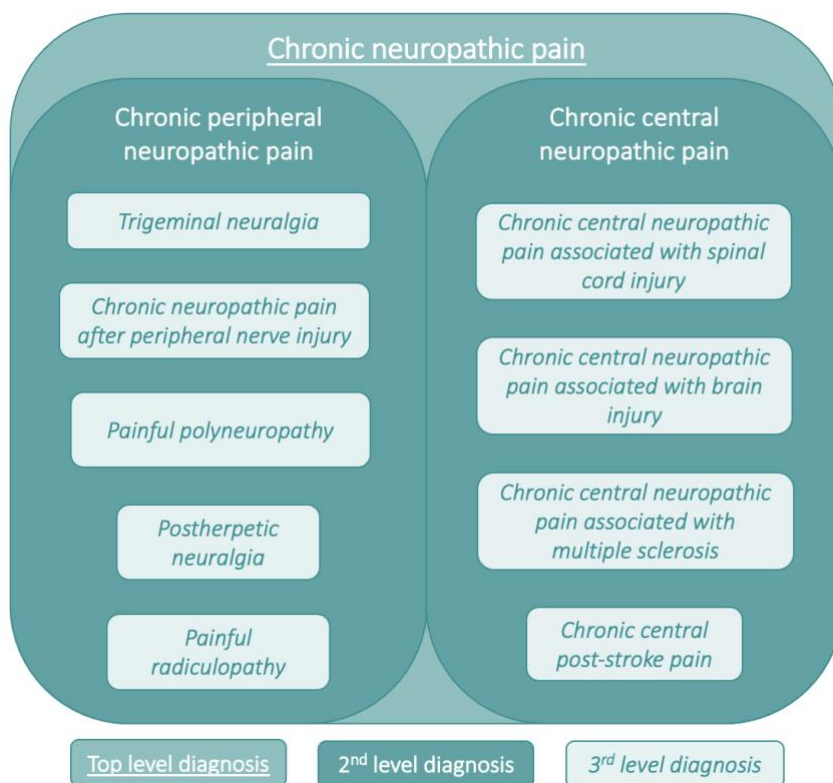


Figure 3. ICD-11 classification of chronic neuropathic pain. Adapted from Scholz et al. (2019)

Chronic pain

While acute pain is usually considered as a symptom of another condition (e.g., sickness or injury) and has an evolutionary significance in terms of survival because it serves to avoid and/or limit potential threats to one's own integrity, chronic pain does not seem to have any survival value. Chronic pain may arise because the condition that caused it cannot be treated correctly, but also when the treatments were successful. To describe chronic pain, a solely temporal criterion was chosen, and it is nowadays defined as a pain that lasts or recurs for more than 3 months. The World Health Organization (WHO) International Classification of Diseases (ICD) classifies pain conditions into chronic primary and chronic secondary pain syndromes based on IASP systematic classification (Treede et al., 2019, 2015). Chronic primary pain is considered as a disease in itself and encompasses numerous pain syndromes, (e.g., chronic widespread pain, complex regional pain syndrome, etc.). On the other hand, chronic secondary pains are conceived as symptoms to other medical conditions and include cancer-related, postsurgical/posttraumatic, neuropathic, secondary headache/orofacial, secondary visceral and secondary musculoskeletal pain (Figure 2) (Treede et al., 2019). When the pain becomes chronic, it usually is either a core or leading complaint from patients, which makes it a debilitating condition. The weight on the patients' health and quality of life can be overwhelming, which in turns becomes a massive socio-economic burden to society (Phillips and Harper, 2011), especially when considering that about an estimated 20% of the world population is affected by it (Global Burden of Disease Study 2013 Collaborators, 2015).

Neuropathic pain

Although ICD classification is mainly based on the variety in aetiologies and severities of pain conditions and the need for treatment strategies specificity (Treede et al., 2019), these different pain conditions are usually divided into two types of pain based on their aetiology: nociceptive pain and neuropathic pain (Cohen and Mao, 2014; Kosek et al., 2016; Treede et al., 2008). Nociceptive pain is characterised by actual or potential non-neural tissular damage and due to activation of nociceptors (e.g., inflammatory pain), while neuropathic pain occurs after a lesion or a disease affecting

Neuropathic pain

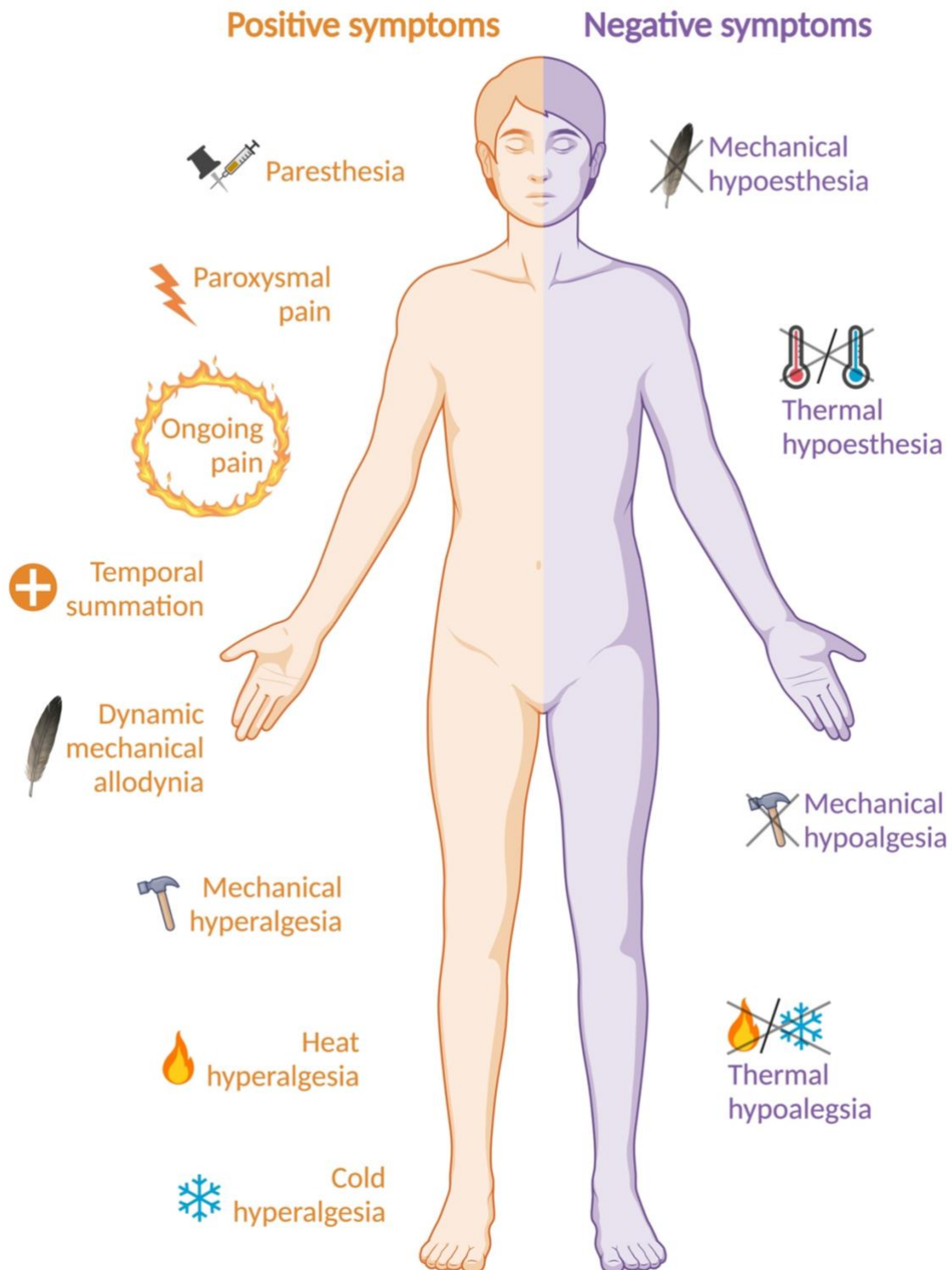


Figure 4. Symptoms of chronic neuropathic pain. Positive symptoms refer to a gain of somatosensory function and negative symptoms to a loss of somatosensory function.

the somatosensory nervous system. This classification into nociceptive and neuropathic pain has been criticised, largely because it overlooks dysfunctions to the nervous system without confirmed activation of nociceptors, which are present in pain groups such as fibromyalgia patients (Kosek et al., 2016).

Chronic neuropathic pain is estimated to affect 7-10% of the world population, contributing greatly to the global burden of disease (van Hecke et al., 2014). It can be divided in two main categories, peripheral and central (Gierthmühlen and Baron, 2016; Scholz et al., 2019), which are further classified into different subtypes based on the cause of the neuropathy (Figure 3; ICD-11). Another division could be done based solely on the cause of the neuropathic pain, i.e., whether it arises from a lesion of the nervous system (e.g., spinal cord -SC- or brain injury) or due to a disease (e.g., diabetes, multiple sclerosis, herpes, etc.) (Scholz et al., 2019). In chronic neuropathic pain, a diverse range of somatosensory symptoms can be described, classified in negative symptoms, i.e., loss of somatosensory function, and positive symptoms, i.e., gain of somatosensory function (Figure 4) (Gierthmühlen and Baron, 2016). Negative symptoms are always evoked by a stimulus, while positive symptoms can be either spontaneous or evoked. Negative symptoms encompass mechanical and thermal hypæsthesia, which correspond to reduced perception/sensation to mechanical or cold/warm stimuli respectively; and mechanical and thermal hypoalgesia correspond to reduced sensation to painful mechanical stimuli/blunt pressure or to painful thermal stimuli respectively. Positive spontaneous symptoms include paresthesia, i.e., nonpainful ongoing sensation described as “pins and needles”, paroxysmal pain, i.e., electric shock-like attacks, and ongoing pain, which is often reported as “burning pain”. Finally, positive evoked symptoms can be divided in three main categories: temporal summation, dynamic mechanical allodynia and mechanical/cold/heat hyperalgesia. Temporal summation refers to sharp superficial pain of increasing intensity that is evoked by repeated painful static mechanical stimuli. Allodynia, defined by IASP as “*pain due to a stimulus that does not normally provoke pain*”, corresponds to a painful response to an ordinarily non-nociceptive stimulus. On the other hand, hyperalgesia refers to “*increased pain to a stimulus that normally provokes pain*” (IASP), meaning a suprathreshold stimulus elicits the same painful response than would usually a lower threshold stimulus do (Figure 5). Despite this symptomatic diversity, some symptoms

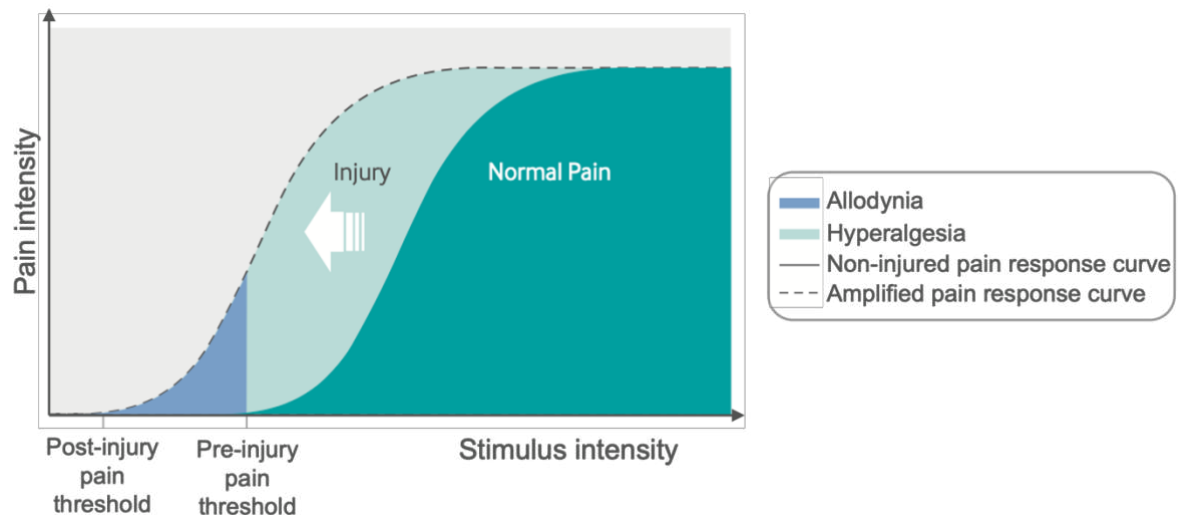


Figure 5. Schematic diagram illustrating allodynia and hyperalgesia after injury compared to normal pain. *Adapted from Cohen and Mao (2014)*

Diagnostic criteria for chronic neuropathic pain

Pain must persist or recur for ≥ 3 months and fulfil at least criteria A and D below. Criteria B and C increase the level of diagnostic certainty.

A. The pain is characterised by both of the following:

- A.1. History of relevant neurological lesion or disease
- A.2. Pain distribution neuroanatomically plausible

B. Pain is associated with sensory signs in the same neuroanatomically plausible distribution

C. Diagnostic test confirming a lesion or disease of the somatosensory nervous system explaining the pain

D. Not better accounted for by another diagnosis of chronic pain

Comments

Negative or positive sensory signs consistent with the distribution of the pain may be sufficient to indicate the presence of a lesion or disease of the peripheral somatosensory nervous system. The clinical examination may be supplemented by laboratory tests, e.g., quantitative sensory testing.

Figure 6. Diagnostic criteria used for chronic neuropathic pain (IASP)

are prominent in neuropathic pain patients. For instance, around 15-20% of patients present allodynia and hyperalgesia (Jensen and Finnerup, 2014). Mechanical allodynia and hyperalgesia are present in three types based on the nature of the stimulus: dynamic (e.g., brush), punctate (e.g., filament, pinprick) and static (pressure); while thermal allodynia and hyperalgesia are usually divided between cold and heat (Jensen and Finnerup, 2014).

These somatosensory symptoms are accompanied by a range of sleep and psychosocial comorbidities, which complicates the understanding of the pathophysiology of this disease and the treatments strategies. In addition to the 3 months threshold for chronic pain, criteria used for diagnosis of chronic neuropathic pain are as follows: the pain is characterized by a history of neurological lesion or disease; the pain distribution is neuroanatomically plausible with the cause and is not better accounted for by another diagnosis of chronic pain. Additional criteria can increase the certainty of diagnosis (Figure 6; IASP).

Current pharmacological treatments for chronic neuropathic pain comprise first-, second- and third-line treatments and focus on the treatment of symptoms. First-line treatments encompass anticonvulsants -gabapentin or pregabalin-, and classical antidepressant, such as tricyclic antidepressants (TCAs) -nortriptyline or desipramine- and selective serotonin noradrenaline reuptake inhibitors -duloxetine or venlafaxine. Second line and third line treatments include lidocaine, capsaicin, tramadol or tapentadol, and strong opioids and botulinum toxin type A respectively (Attal et al., 2010; Colloca et al., 2017; Dworkin et al., 2007; Finnerup et al., 2021, 2015). Non-pharmacological treatments such as neuromuscular or neuronal stimulations can also be found in clinical settings, but either as auxiliary therapies or in the case of ineffective drug treatment.

The study of pain in rodents

One of the important things to consider when looking at chronic pain in animals is the definition of chronicity. While in patients the usual timepoint used to classify pain as chronic is three months, it is not possible to just apply the same timepoint to animal models, mainly because of the biological disparities between humans and rodents. Nowadays, most chronic pain rodent models rely on what we could call persistent pain.

In the case of chronic inflammatory pain models, such persistence is usually attained with a unique long lasting (>3 weeks) injection of an inflammatory agent (e.g., Complete Freund's Adjuvant - CFA). On the other hand, for chronic neuropathic pain, specifically in injury models, it is considered that the pain is persistent, thus chronic, because the injury itself is not healed (Kremer et al., 2021).

One must also be careful when considering pain in animal models. Indeed, as stated earlier, the sensation (nociception) and its interpretation (pain) are two different components that, although closely related, are still distinct. The assessment of pain in patients relies mainly on verbal evaluations, which is not possible in animals. Therefore, all the tests used to evaluate "pain" in rodents are indeed nociceptive tests that do not rely on the interpretation of a stimulus (Kremer et al., 2021). All nociceptive tests are thus based on reflexes, but their interpretation in the literature is often confusing. Indeed, a lot of articles often refer to increased sensitivity measured by reflexes' means as allodynia, although the definition of allodynia involves a painful component that is not quantifiable in rodents. However, nociceptive tests used in rodent studies cover both thermal and mechanical components, with even a differentiation between dynamic (e.g., brush test) and punctate (e.g., von Frey filaments) mechanical sensitivity (Kremer et al., 2021), which still makes them a good output compared to pain observed in humans. Changes in one of the components should therefore be mentioned as thermal or mechanical hypersensitivity rather than thermal or mechanical allodynia as to not mislead the reader.

To characterise the presence of thermal/mechanical hypersensitivity in pain models, several nociceptive tests have been developed in rodents and are based either on thermal or mechanical stimuli (Figure 7) (Barrot, 2012; Kremer et al., 2021).

Tests relying on withdrawal reflexes include the tail flick test (D'amour and Smith, 1941), based on the withdrawal reflex of the tail to a heat beam or a hot bath, while hot/cold plate tests (Bennett and Xie, 1988; Hunskaar et al., 1985; Woolfe and Macdonald, 1944) and Hargreaves test (Hargreaves et al., 1988), based on thermal (hot, cold or laser) stimulation of the paw. Some thermal nociceptive tests rely on the observation and quantification of nociceptive behaviours, such as the acetone test (Yoon et al., 1994), which application produces a cold stimulus. Finally, the most common mechanical nociceptive test is the von Frey test, for which calibrated von Frey

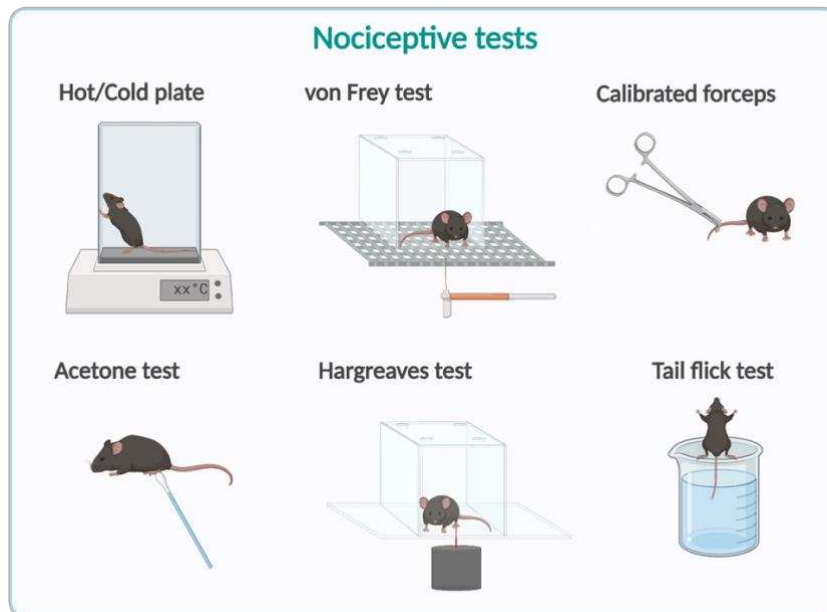


Figure 7. Schematic representation of tests used for the evaluation of nociceptive behaviours.

filaments of increasing pressure are applied to the hindpaw of the animal (Chaplan et al., 1994). This test relies on the pressure threshold needed to elicit a nociceptive response.

Rodent models of neuropathic pain – The cuff model

During the last decades, several rodent models have been developed to understand better the physiopathology of chronic neuropathic pain and to improve treatment strategies (Colleoni and Sacerdote, 2010; Jaggi et al., 2011; Kumar et al., 2018).

It is noteworthy that the vast majority of rodent animal models of neuropathic pain are traumatic, even though most prevalent chronic neuropathic pain is induced by diabetes (Kremer et al., 2021; van Hecke et al., 2014). Diabetes- (e.g., streptozotocin-induced or genetic models), drug- (e.g., chemotherapy or anti-HIV agents), virus-induced (e.g., HIV or post-herpetic) and bone cancer pain-induced neuropathic pain models are however also currently used in preclinical settings to understand the mechanisms underlying different aetiologies of neuropathic pain (Jaggi et al., 2011). On the other hand, traumatic injury models are usually based on injuries of spinal nerves (peripheral neuropathic pain), and for a few on injuries of the spinal cord (central neuropathic pain) (Figure 8) (Kremer et al., 2021). They often rely on the

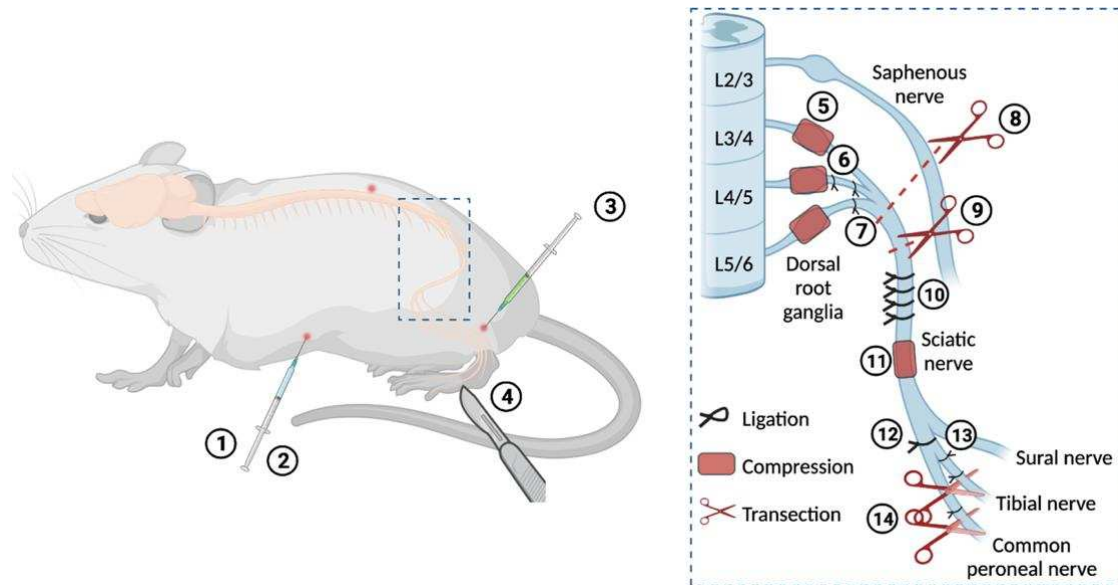


Figure 8. Experimental models of neuropathic pain (NP). (1) Chemotherapy induced NP; (2) chemically induced diabetic NP; (3) bone-cancer pain by injection of cancer cells in the bone marrow; (4) postsurgical pain by incision of tissues and muscle; (5) chronic constriction of multiple dorsal root ganglia; (6) L5 spinal nerve ligation; (7) sciatic nerve ligation; (8) complete axotomy; (9) partial axotomy; (10) chronic constriction injury; (11) sciatic nerve cuffing (cuff); (12) partial sciatic nerve ligation; (13) tibial nerve transection; (14) spared nerve injury. The nerve roots' insertion may vary according to strains, hence the double numbering on lumbar sections. For diabetes induced NP models, genetic or hypercaloric diet induced can also be used.

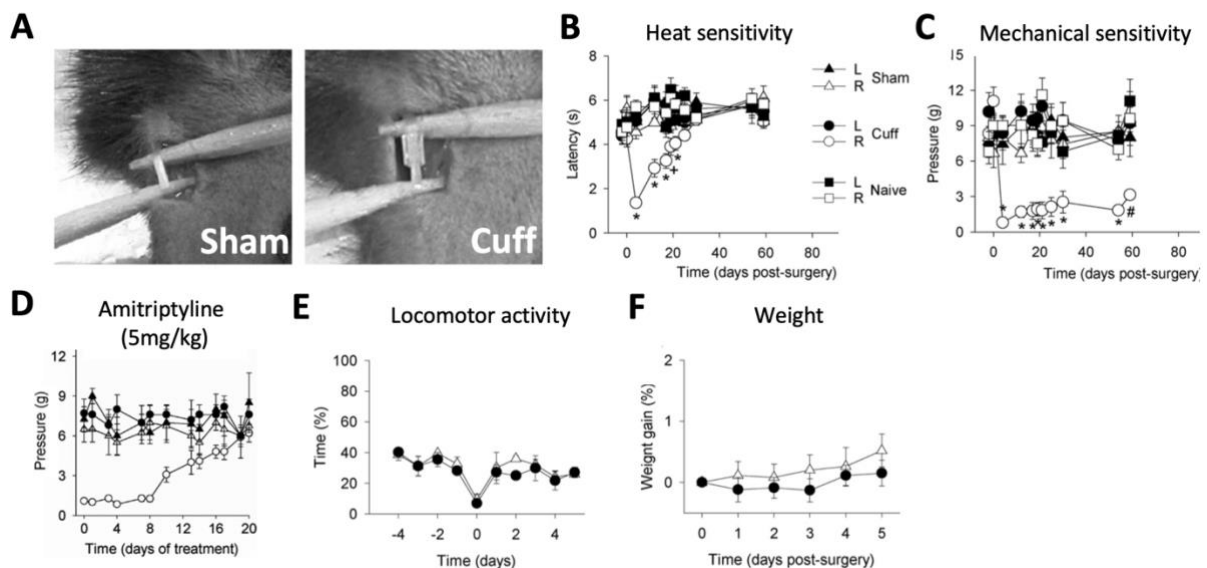


Figure 9. Cuff implantation on the sciatic nerve (A) induces a heat hypersensitivity in the ipsilateral paw during the first 3 weeks post-surgery (B) while the mechanical hypersensitivity is sustained for at least 12 weeks post-surgery (C). Treatment with the tricyclic antidepressant amitriptyline alleviates the mechanical hypersensitivity (D). Both weight and locomotor activity are not affected by the cuff. Adapted from Benbouzid et al. (2008a, 2008b)

transection, ligation, constriction or cuffing of the sciatic nerve (e.g., complete sciatic nerve transection, partial sciatic nerve ligation, chronic constriction injury or cuffing-induced sciatic nerve injury models respectively). The most frequently used sciatic nerve model, the chronic constriction injury model (CCI), originates in the 90s. Bennett and Xie (1988) designed a model of peripheral mononeuropathy in rats that would elicit symptoms as seen in humans, which most of the current models at the time failed to do. The CCI model is produced by loose constrictive ligatures around the common sciatic nerve, which elicited “hyperalgesia” (i.e., increased sensitivity), “allodynia” (i.e., hypersensitivity) and possibly spontaneous pain. However, in this model, there is a great variation in the neuronal fibre spectrum altered, with different populations and percentages of fibres affected by the ligation. The cuffing-induced sciatic nerve injury, also known as the cuff model, was first developed in rat in 1996 (Mosconi and Kruger, 1996) as a mean to fill this reproducibility gap. Implantation of a fixed-diameter polyethylene tube allows standardising and reducing the variability between studies. I will now focus more specifically on this model as it is the one used in this thesis work. Cuffing of the sciatic nerve does produce nociceptive behaviours in rats resembling that of peripheral nerve injury patients, but also reproducible decrease of axon numbers, degeneration and inflammatory reaction (Mosconi and Kruger, 1996). This model was later adapted to C57BL/6J mice in our team (Benbouzid et al., 2008b). We showed that the cuffing of the right sciatic nerve induces thermal hypersensitivity during the first three weeks after surgery and mechanical hypersensitivity for at least 12 weeks after induction (Figure 9) (Yalcin et al., 2014). Interestingly, this model does not induce any locomotor or weight changes, nor hindlimb auto mutilation or autophagy (Benbouzid et al., 2008b) which can be found in various models of peripheral neuropathic pain (Zeltser et al., 2000). In addition, it was shown that treatments generally used for neuropathic pain such as the anticonvulsant gabapentin or carbamazepine, chronic TCAs nortriptyline, amitriptyline or desipramine, the SNRI duloxetine, the opioid drug morphine or ketamine suppressed the cuff-induced mechanical hypersensitivity (Benbouzid et al., 2008b, 2008a; Salvat et al., 2018). Altogether, it seems that the cuff model is a standardised, reproducible and pertinent model for the study of neuropathic pain and its treatments.

Chronic pain and its emotional component and consequences

The definition of pain highlights not only the somatosensory discriminative component of pain, but also the emotional experience, hence component, of pain. In addition to the sensory symptoms and the unpleasantness of pain, when pain becomes chronic it is frequently comorbid with emotional dysregulations, which aggravates the patients' quality of life, complicates the treatment strategies and often worsen the pain sensation (Kirsh, 2010). Amongst psychiatric disorders comorbid to chronic pain, anxiety and depression are the most prevalent (Attal et al., 2010; Means-Christensen et al., 2008). Indeed, while the development of anxiety and depression in the general population is close to 20-30% (Santomauro et al., 2021), this prevalence reaches 30 to 80% when looking at chronic pain patients depending on the type of pain considered (Bair et al., 2003; de Heer et al., 2014; Demyttenaere et al., 2007; Gureje et al., 2008; Von Korff et al., 2005; Williams, 2003). On the other hand, around half of patients diagnosed with major depressive disorder (MDD) report pain problems (Meints and Edwards, 2018; Williams, 2003). This comorbidity is thus even more important to address because the link between chronic pain and emotional disorders is bidirectional, with each acting as a risk factor for the other (Bandelow, 2015; Fishbain et al., 1997).

Aversion

The aversiveness of pain, especially in chronic pain patients, is an important factor to consider, because it might lead to strategies to avoid pain. The desire to avoid pain can thus be considered a good indicator of the emotional component of pain (Price, 2000). Aversion refers to a strong feeling of not liking something or someone. Because of its unpleasantness, pain is, in itself, aversive. Even though aversion *per se* is not a disorder, it is closely linked to anxiety and depression, and probably precipitates the development of these disorders. Indeed, neural circuits associated with aversion present maladaptive changes in anxiety and depression (Chen, 2022). As stated earlier, pain is not fully assessable in rodents, however, the aversiveness of pain on the other hand is an output that is measurable and is an indirect factor for the assessment of pain. Some paradigms have been developed in the last 20 years to assess aversion in the context of pain (Figure 10) (Kremer et al., 2021). The place escape-avoidance

paradigm (PEAP) relies on the selection of the animal between a safe environment (i.e., dark area) associated with mechanical stimuli or an unsafe environment (i.e., lit area) without mechanical stimuli (LaBuda and Fuchs, 2000). To assess the aversiveness of thermal stimuli Moqrich *et al.* (2005), designed a thermotaxis assay, giving the choice to the animal between two surfaces with different temperatures. In addition, ongoing pain indirect measure can be achieved with place preference/aversion (CPP, CPA) paradigms relying on the injection of pain-relieving drug (Barthas *et al.*, 2015), or in the inflammatory agents respectively (e.g., formalin) (Johansen *et al.*, 2001). One compartment is coupled with the injection of the pain-relieving drug or the inflammatory agent, while the other is coupled with a saline injection during the conditioning. On the day of the test, the time spent in each compartment is monitored to assess the potential aversiveness or preference of the injected solution.

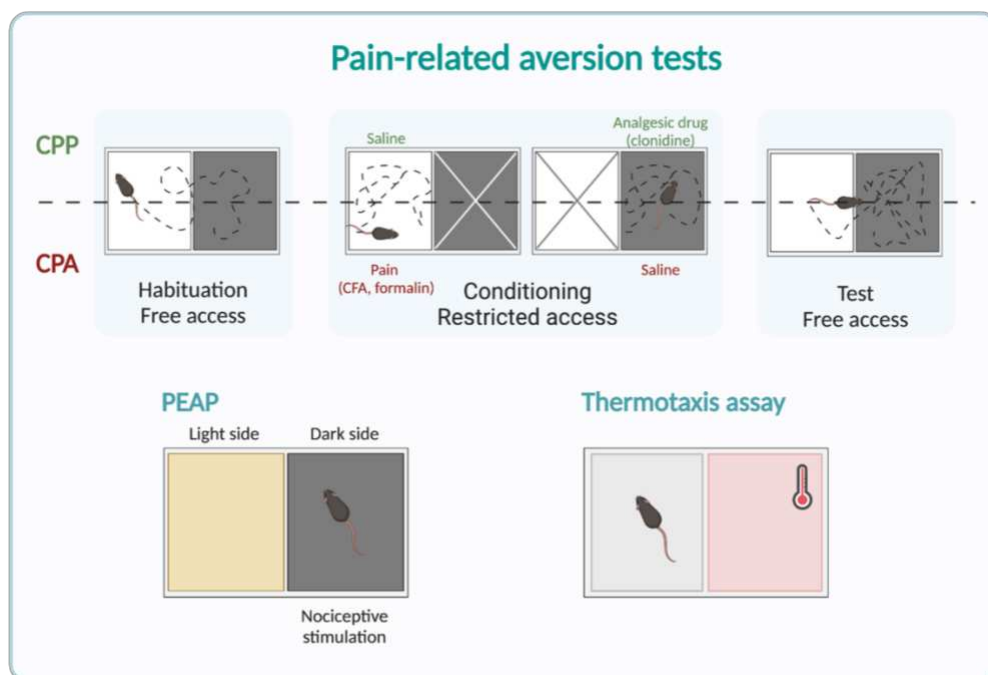


Figure 10. Schematic representation of tests used for the evaluation of aversive behaviours. CPA, conditioned place aversion; CPP, conditioned place preference; PEAP, place escape avoidance paradigm.



Figure 11. ICD-11 classification of anxiety or fear related disorders.

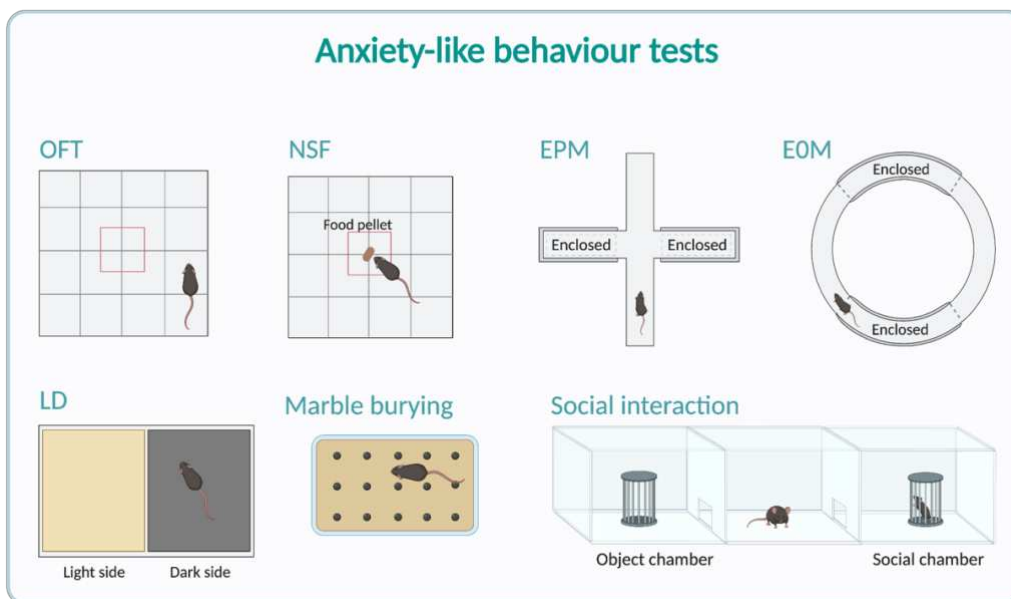


Figure 12. Schematic representation of tests used for the evaluation of anxiety-like behaviours. EPM, elevated plus maze; EOM, elevated zero maze; LD, light-dark test; NSF, novelty suppressed feeding test; OFT, open-field test.

General Anxiety Disorder

Chronic pain is frequently associated with anxiety, which is a feeling of unease, such as worry or fear, towards everyday situations or specific items. The Diagnostic and Statistical Manual of Mental Disorders, Fifth Edition (DSM-V) classifies anxiety disorders based mainly on their aetiology and specifies 11 different types of anxiety disorders (Figure 11).

For the scope of this thesis, I will provide a particular focus on generalised anxiety disorder (GAD). GAD is characterised by excessive anxiety and worry for most days for at least 6 months. The anxiety/worry is not focused on a single trigger and is not explained by another mental disorder, and associates with at least 3 symptoms of the following: restlessness, fatigue, difficulty concentrating, irritability, muscle tension and sleep disturbances. Finally, the anxiety, worry and/or physical symptoms are causing significant distress or impairment in the patients' life (DSM-V).

Treatments for GAD will depend greatly on the severity of the disorder, reflected by the severity of the symptoms. All GAD patients require psychotherapy, mostly cognitive behavioural therapy that can be associated with pharmacological treatment. First-line treatments for GAD are selective serotonin reuptake inhibitors (SSRIs) - sertraline, escitalopram or paroxetine- followed by SNRIs -duloxetine or venlafaxine-, and the anticonvulsant pregabalin. Benzodiazepines -diazepam- are usually used for short-term treatment during severe periods of anxiety when all the aforementioned treatments are unresponsive (Bandelow et al., 2017). Anxiety-like behaviours are well characterised in rodent models and several tests are routinely used. These tests present a good predictive validity as they respond to anxiolytic drugs. They rely on the innate behaviour of rodents, which tend to avoid open and lit areas for the profit of closed dark ones, offering more security. Therefore, tests currently used in lab settings are the open-field test, elevated mazes, light-dark box (Crawley and Goodwin, 1980). In addition, tests based on avoidance behaviours, such as social interaction or marble burying, are also used as they are considered to represent a good output of anxiety-like behaviours (Figure 12) (Kremer et al., 2021).

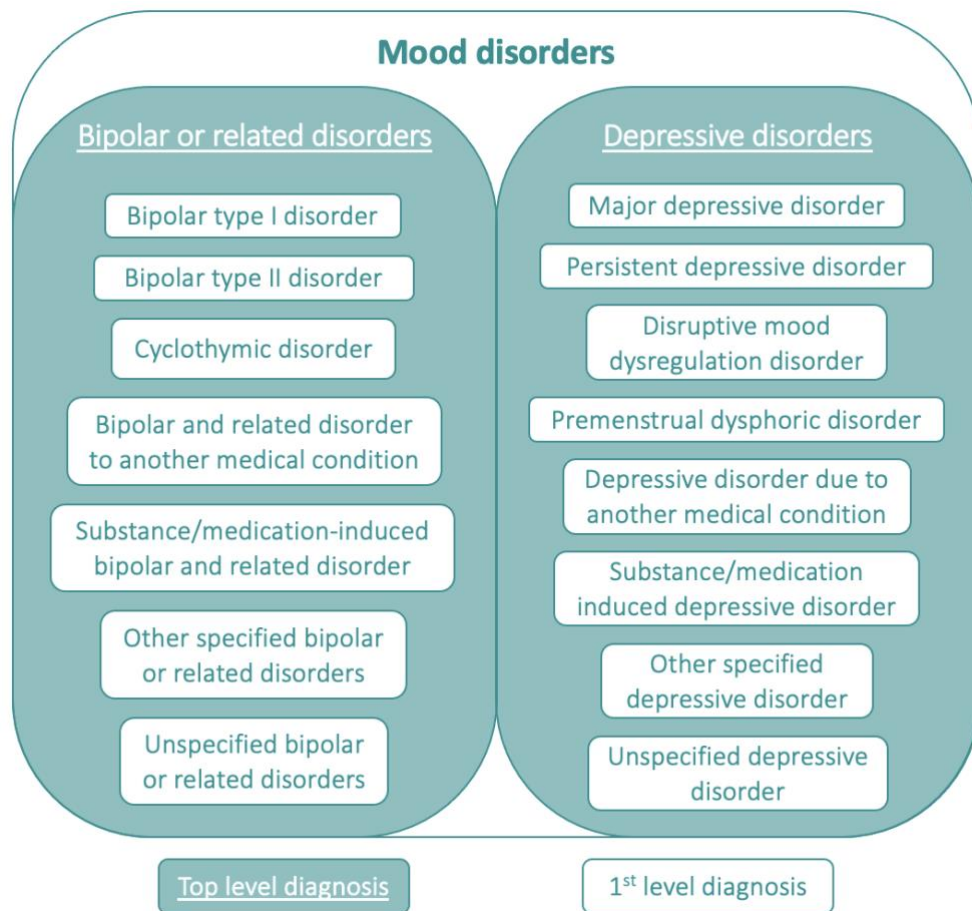


Figure 13. ICD-11 classification of mood disorders.

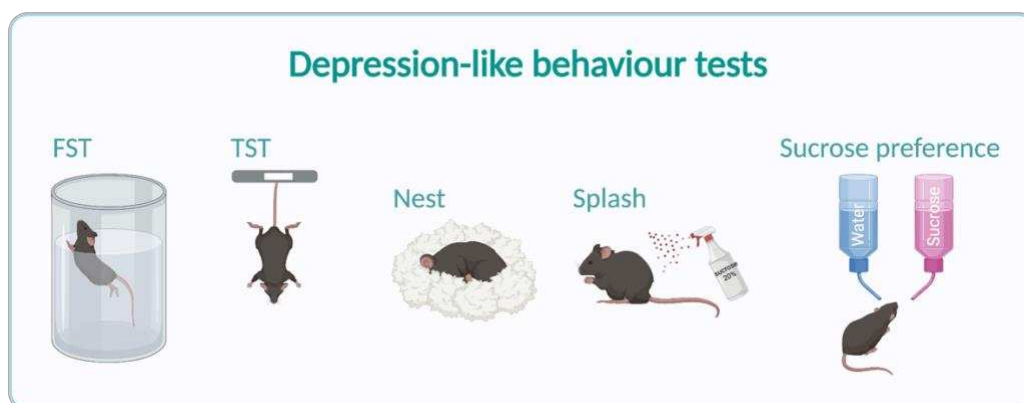


Figure 14. Schematic representation of tests used for the evaluation of depressive-like behaviours. FST, forced swim test; TST, tail suspension test.

Major Depressive Disorder

Like anxiety disorders, depression is often associated with chronic pain and falls within the mood disorders. There are various mood disorders that are classified by the DSM-V depending on their duration, timing and supposed aetiology. Their first division is between bipolar or related disorders and depressive disorders, the first containing 7 types of bipolar disorders and the latter 7 types of depressive disorders (Figure 13) (Spijker and Claes, 2014).

I will in this thesis focus solely on major depressive disorder (MDD), which is characterised by the presence of two core symptoms: depressed mood or loss of interest or pleasure (anhedonia). These primary symptoms are accompanied by additional symptoms: insomnia, feelings of guilt, decreased energy levels, decreased concentration, decreased appetite, psychomotor activity changes, and recurrent suicidal ideation/attempts or acts of self-harm. Out of all the primary and secondary symptoms, at least 5 should be present for almost every day for 2 weeks or more (DSM-V).

Like for GAD, treatments for MDD will vary depending on the severity of the disorder, ranging from mild, some impact on the patients' daily life, to severe, the patients find it impossible to get through daily life. The severities are further detailed and assessable by a scale provided in DSM-V. For all severities, therapies such as cognitive behavioural therapies are always recommended. For moderate and severe depression, pharmacological treatments in the form of antidepressants are prescribed. They comprise classical antidepressants such as SSRIs -paroxetine, fluoxetine or citalopram-, SNRIs -venlafaxine or duloxetine- and TCAs -imipramine or amitriptyline-, and other antidepressants such as the serotonin modulator and stimulator vortioxetine or the noradrenergic and specific serotonergic antidepressant mirtazapine (Kupfer et al., 2012).

Depressive-like behaviours can be observed in rodents, and they rely mainly on three features: well-being of the animal, anhedonia and despair. For the well-being, tests commonly used are the splash test for the grooming behaviour and the nest test. For the anhedonic component, the sucrose preference test is the most widely used. Finally, tests relying on despair-like behaviour, such as the tail suspension test (TST) (Steru et al., 1985) or the forced swim test (FST) (Porsolt et al., 1977), are the most widely used

and described in the literature (Figure 14; Kremer *et al.*, 2021). However, their predictive validity has been widely criticised due to their answer not only to antidepressant drugs, but also to psychostimulants (Porsolt *et al.*, 1978). In addition, these two tests rely widely on stress-coping behaviours, which are impaired in depression, but also in other conditions such as autism (Commons *et al.*, 2017). Therefore, as for anxiety-like behaviours, one must be careful to select a battery of tests to correctly assess the behavioural output of animals as not to misinterpret the results.

Animal models of chronic pain-induced emotional disorders

Due to the various aetiology of anxiety and depression, several animal models were established. These models have been developed based on the causes of the disease: early life stress (e.g., maternal separation), social stress (e.g., social defeat), environmental factors (e.g., unpredictable chronic mild stress, restraint stress, predator stress) or biological causes (e.g., genetic models, corticosterone drinking, inflammation-induced depression by lipopolysaccharide injection) (Planchez *et al.*, 2019). However, these models, although valid and important to understand the pathophysiology of these diseases, are only displaying either anxiety, depression or the comorbidity of both. Stress is indeed the first cause of anxiety and depression, but it is also well known that they can co-occur with a range of other conditions, including chronic pain.

While chronic pain, anxiety and depression have been widely studied individually, only in the last 20 years the comorbidity between these disorders has been more closely examined. Interestingly, no matter the chronic pain type considered, aversion and/or anxiodepressive-like behaviours can usually be measured consequentially to pain (Kremer *et al.*, 2021). However, while most studies reported anxiodepressive-like behaviours following chronic pain, some studies could not reveal anxiodepressive-like behaviours concurrent to chronic pain. Such a phenomenon could be explained by the fact that for the development of anxiety- and depressive-like symptoms concurrent to chronic pain, time is a critical factor (Humo *et al.*, 2020; Yalcin and Barrot, 2014). Indeed, in some of the studies reporting no emotional consequences (Hasnie *et al.*, 2007; Pitzer *et al.*, 2019; Urban *et al.*, 2011), anxiodepressive-like behaviour tests were performed in the first weeks following the pain induction, during which no

anxiodepressive-like consequences can be found in some models, while they are present at later time points (Alba-Delgado et al., 2013; Yalcin et al., 2011). However, when anxiodepressive-like consequences are observed, they almost always follow the same timeline, with first the appearance of anxiety-like behaviours, then later depressive-like behaviours, with some exceptions (Humo et al., 2020).

Tests	Time (weeks)						
	2-3	4-5	6-7	8-9	10-14	15-17	
Hargreaves	+	0	0	0	0	0	Heat hypersensitivity
von Frey	+	+	+	+	+/11	0	Mechanical hypersensitivity
CPP		+	+	+	+	+	Aversion
LD	0/+	+	+	+	+	0	Anxiety-like
NSF	0	0/+	+	+	+	+	Anxiety-like
Splash	0	0	+	+	+	+/0	Depression-like
FST	0	0	0	+	+	+	Depression-like

Figure 15. Summary of the tests used, and the results obtained for the cuff model in male mice. 0, no phenotype; +, phenotype present. CPP, conditioned place preference; FST, forced swim test; LD, light-dark test; NSF, novelty suppressed feeding test. *Adapted from Yalcin et al. (2011)*

In our cuff model, the development of the emotional consequences of pain follows a strict timeline in male mice, which is different in females (Figure 15) (Yalcin et al., 2011). Accordingly, the mechanical hypersensitivity is present from the first week after the surgery and sustained until at least post-operative week 11 (Sellmeijer et al., 2018), while anxiety-like behaviours start appearing from post-operative week 4-5 onward, and depressive-like behaviours are only notable from post-operative week 6, alongside with the aversiveness of ongoing pain, as displayed in a CPP with clonidine (Yalcin et al., 2011). Interestingly, when the animals spontaneously recover from the mechanical hypersensitivity, they also recover from anxiety-, but not aversion nor depressive-like behaviours, which are sustained until post-operative week 18 (Sellmeijer et al., 2018). After week 18, the mice do not display any mechanical hypersensitivity, nor ongoing pain and anxiodepressive-like behaviours. Therefore, it is possible to define 4 time points (TP) following the surgery: TP1, when only the mechanical hypersensitivity is present; TP2, when both mechanical hypersensitivity, aversiveness and

anxiodepressive like consequences are present; TP3, which corresponds to the disappearance of both mechanical hypersensitivity and anxiety-like behaviours; and TP4, for which all behaviours are back to control levels (Figure 15) (Sellmeijer et al., 2018). The sustained emotional consequences of chronic neuropathic pain support the idea that emotional dysfunction can persist even after the recovery from evoked nociceptive responses, pointing out the possibility of long-term plasticity in the brain underlying these behaviours.

Structures implicated in the comorbidity of chronic pain and emotional disorders

Thanks to progress in imaging techniques, the so-called pain matrix has been highlighted, which includes several brain regions or networks that are intimately interconnected (Figure 16). Their coordinated activity elicits sensory, emotional and cognitive processes, which gives rise to the response known as pain. Regions that are consistently activated throughout studies include the primary and secondary cortices (S1 & S2), the anterior cingulate cortex (ACC), the insular cortex (IC), the prefrontal cortex (PFC), the thalamus, basal ganglia, periaqueductal gray (PAG) and cerebellum (Mercer Lindsay et al., 2021; Schweinhardt and Bushnell, 2010). In addition, some regions are responding less consistently to noxious stimuli: the basal ganglia, parabrachial complex, posterior cingulate, amygdala, hypothalamus, and supplementary motor area (Mercer Lindsay et al., 2021). While most of the studies have been performed in healthy volunteers with acute pain stimulus, some groups have started to explore pain processing in chronic pain patients. Magnetic resonance imaging (MRI) has thus allowed to confirm the implication of brain structures of the “pain matrix” in chronic pain states, with alterations in the PFC, thalamus, IC, ACC, and white matter tracts (Apkarian et al., 2004; Foerster et al., 2012; Ichesco et al., 2014; Lieberman et al., 2014). In addition, studies comparing healthy volunteers with chronic pain patients have highlighted specific structural alterations depending on the component of pain examined (Brown et al., 2011; Lee et al., 2021, 2021; Liang et al., 2013; Wager et al., 2013). These results all confirm that pain is based on several interconnected brain structures, which are all respectively responsible for one or more modalities of the pain experience (Mercer Lindsay et al., 2021).

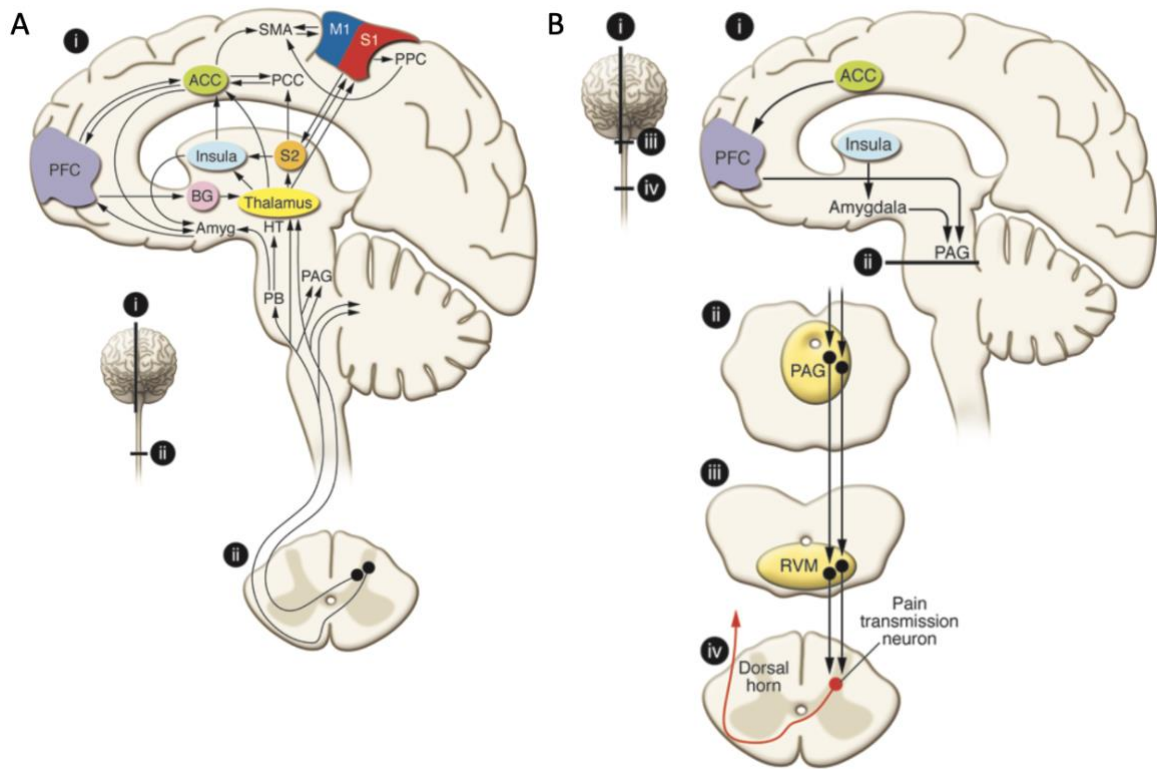


Figure 16. Pain pathways in the human brain. (A) Schematic representation of ascending pain pathways and brain regions involved in pain processing. (B) Descending pain modulatory pathways that might be involved in psychological modulation of pain. ACC; anterior cingulate cortex; Amyg, amygdala; BG, basal ganglia; HT, hypothalamus; M1, primary motor cortex; PB, parabrachial nuclei; PAG, periaqueductal gray; PCC, posterior cingulate cortex; PFC, prefrontal cortex; PPC, posterior parietal cortex; VM, rostral ventral medulla; SMA, supplemental motor area; S1, primary somatosensory cortex. *Adapted from Schweinhardt and Bushnell (2010)*

Beside changes observed in humans, Hubbard *et al.* (2015), by using functional MRI in a neuropathic pain model in rats, also showed changes in the somatosensory and cingulate cortices of painful animals. In addition, thanks to the use of animal models of chronic pain-induced emotional disorders, the contribution of brain structures to this comorbidity have started to be addressed. Optogenetic and chemogenetic studies have also allowed deciphering the brain structures implicated in anxiety (Chen *et al.*, 2022; Zhuo, 2016) and depression (Sheng *et al.*, 2017). Interestingly structures of the corticolimbic pathway, which is well-known for its implication in anxiety and depression, were shown to be implicated in the anxiodepressive consequences of pain in various chronic pain models (Bravo *et al.*, 2020; Thompson and Neugebauer, 2019). These include the PFC (Lee *et al.*, 2015), ACC (Barthas *et al.*, 2015; Sellmeijer *et al.*,

2018; Zhang et al., 2017), amygdala (Seno et al., 2018), hippocampus (Ma et al., 2019; Tajerian et al., 2014), locus coeruleus (LC) (Llorca-Torralba et al., 2022, 2019, 2018) and lateral habenula (LHb) (Li et al., 2017).

Highlight - Chronic pain and mood disorders comorbidity: Deciphering underlying brain circuits.

The following section is a recently published highlight in response to the Bravo *et al.* (2020) review. It focuses on brain circuits implicated in the comorbidity between anxiodepressive disorders and chronic pain in rodent models, as opposed to single brain structures. In addition, it presents new tools used in preclinical settings to dissect circuits with high temporal and spatial specificity. This highlight emphasises on the importance of considering and studying circuitries as a whole.



Contents lists available at ScienceDirect

Neuroscience and Biobehavioral Reviews

journal homepage: www.elsevier.com/locate/neubiorev

Comorbidity of chronic pain and anxiodepressive disorders: Deciphering underlying brain circuits

Léa J. Becker^{a,1}, Sarah H. Journée^{a,1}, Pierre-Eric Lutz (MD PhD)^{a,b}, Ipek Yalcin (PharmD PhD)^{a,c,*}^a Centre National de la Recherche Scientifique, Université de Strasbourg, Fédération de Médecine Translationnelle de Strasbourg, Institut des Neurosciences Cellulaires et Intégratives UPR3212, 67000 Strasbourg, France^b Douglas Mental Health University Institute, McGill University, Montréal, Canada^c Department of Psychiatry and Neuroscience, Université Laval, Québec, Canada

ARTICLE INFO

Keywords:

Chronic pain
Anxiety
Depression
Brain circuits
Comorbidity
Optogenetic
Chemogenetic

Chronic pain and anxiodepressive disorders are well-known for being intimately related and for influencing each other, but the mechanisms underlying this clinically significant comorbidity remain largely unknown. In this issue, Bravo et al. (2020) address this challenging topic by focusing on brain structures implicated in their bidirectional relationship. By reviewing lesion, pharmacologic, optogenetic or chemogenetic studies, they nicely recapitulate the role of individual brain structures (such as the prefrontal cortex - PFC, the amygdala, the nucleus accumbens - NAc, the locus coeruleus - LC, and the hippocampus) in the anxiodepressive disorders-pain dyad.

Even though studies focusing on individual brain regions improve our understanding of pathophysiology, it is also essential to reach circuitry level of understanding. Indeed, most central nervous system disorders are linked to alterations in brain circuits rather than to changes occurring in single structures. While this issue was difficult to explore until recently, the rapid development of optogenetic and chemogenetic tools now allows the targeting of anatomically defined neuronal pathways (Fig. 1A). Regarding chronic pain-induced emotional dysregulation (CPED), a few preclinical studies have started to unravel critical brain circuits (Fig. 1B), which link together some of the brain regions highlighted by Bravo et al.

Lee and collaborators (2015) first showed that optogenetic activation of PFC neurons terminals within the NAc blocks both nociceptive

and negative affective behaviors in neuropathic animals (Fig. 1A). To further identify the neurochemical identity of this pathway, they combined optogenetic and pharmacological manipulations, and infused an AMPA receptor antagonist into the NAc, which blocked the effects of the optogenetic modulation.

The amygdala is another major hub for CPED. Llorca-Torralba and colleagues (2019) demonstrated that chemogenetic silencing of LC noradrenergic neurons projecting to the basolateral amygdala (Fig. 1A) relieved pain-induced anxiety-like behaviors in neuropathic rats, without affecting mechanical hypersensitivity.

To decipher potentially divergent contributions from subpopulations of neurons located in the same brain structure but sending projections to distinct target sites, Hirschberg and colleagues highlighted another approach (2017). The authors used retrograde viruses injected in the PFC or spinal cord (SC) to target ascending and descending projections from noradrenergic neurons of the LC, respectively (Fig. 1A). They showed that chemogenetic activation of the LC-SC pathway had an anti-nociceptive effect, while the activation of LC-PFC projections enhanced aversive and anxiety-like behaviors. This study along with that of Llorca-Torralba et al. (2019) point out that refining the analysis of specific neuronal subpopulations based on their efferences can reveal distinct and even functionally opposite effects in the modulation of the sensory and affective components of pain.

* Corresponding author at: Institut des Neurosciences Cellulaires et Intégratives UPR3212, 8 allée du général Rouvillois, 67000 Strasbourg, France.

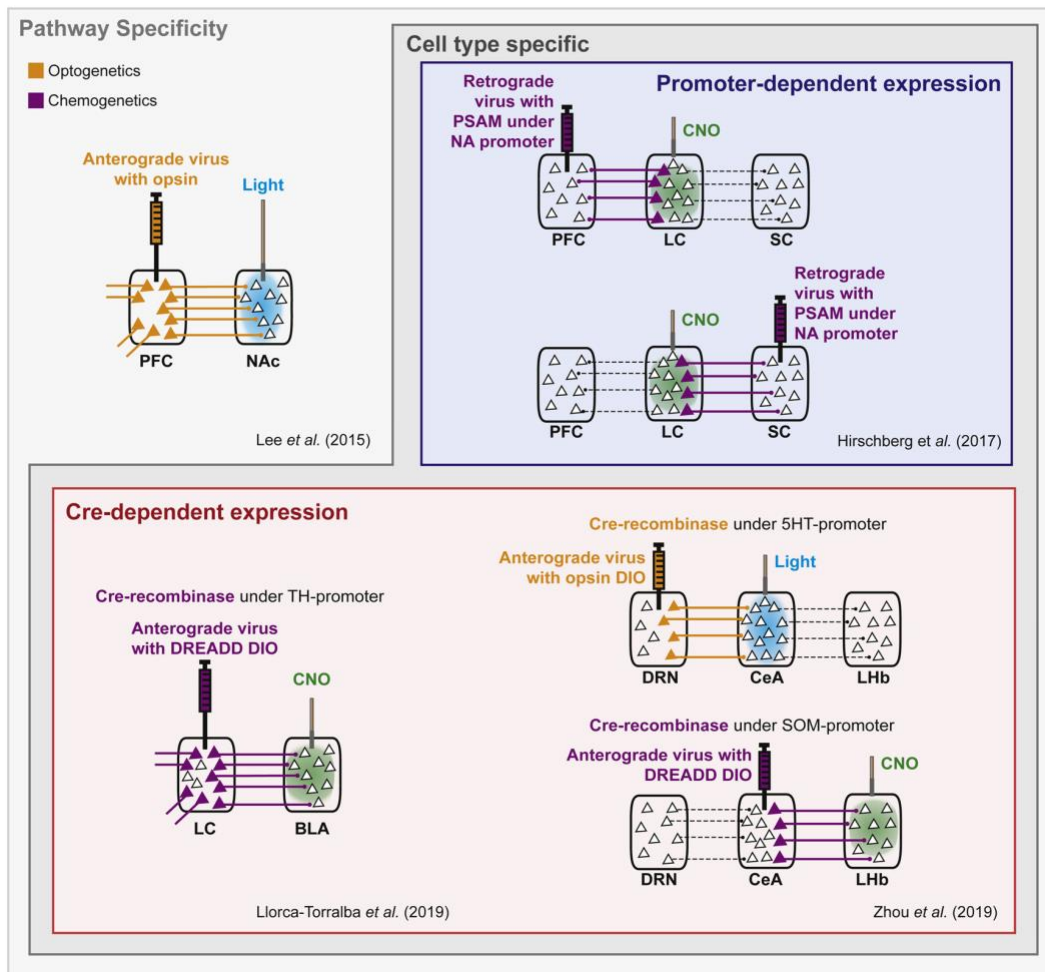
E-mail addresses: lea.becker@inci-cnrs.unistra.fr (L.J. Becker), s.journee@inci-cnrs.unistra.fr (S.H. Journée), pelutz@inci-cnrs.unistra.fr (P.-E. Lutz), iyalcin@inci-cnrs.unistra.fr (I. Yalcin).¹ equal contribution.<https://doi.org/10.1016/j.neubiorev.2020.05.013>

Received 23 April 2020; Accepted 26 May 2020

Available online 30 May 2020

0149-7634/ © 2020 Elsevier Ltd. All rights reserved.

A



B

In chronic pain models:

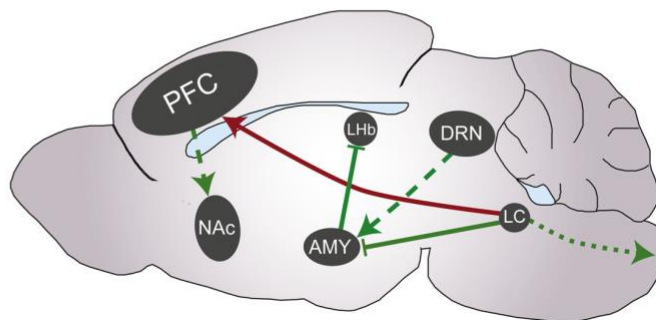
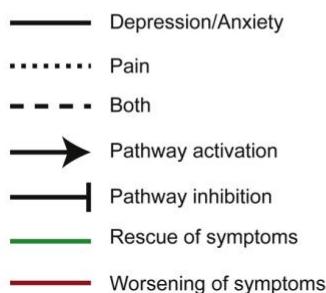


Fig. 1. Tools and approaches used to dissect neuronal circuitry underlying chronic pain-induced emotional dysregulation. **A.** Optogenetic and chemogenetic techniques used to dissect brain circuits. *Upper left panel:* mPFC-NAc specificity reached by injection of anterogradely transported opsin in the PFC and by an optic fiber implantation in the NAc (Lee et al., 2015). *Upper right panel:* Cell-type specificity by promoter-dependent expression: injection in the PFC or SC of a retrograde virus expressing DREADD under the synthetic promoter PRS targeting noradrenergic (NA) neurons. Cell bodies of NA neurons expressing DREADD and projecting either the PFC or SC are stimulated by CNO injection in the LC through a cannula (Hirschberg et al., 2017). *Lower panel:* Cell-type specificity by Cre-dependent expression. *Left:* Injection of an anterogradely transported DREADD in the LC. DREADD will be expressed in neurons expressing the Cre recombinase under the TH promoter. Axon terminals expressing DREADD in the BLA are stimulated by CNO injection through a cannula (Llorca-Torralba et al., 2019). *Right:* Injection of an anterogradely transported opsin or DREADD in the DRN or the CeA. The opsins/DREADD will only be expressed in neurons expressing Cre-recombinase under the Pet-1 (5 H T neurons, injected in the DRN) or SOM (injected in the CeA) promoters. Axon terminals expressing opsin/DREADD in the CeA or the LHb are stimulated by light/CNO injection through an optic fiber/cannula (Zhou et al., 2019). **B.** The figure depicts neuronal circuits underlying the comorbidity between pain and depression/anxiety, as dissected using optogenetics/DREADD in the following publications (see main text for details): mPFC-NAc pathway, see Lee et al., 2015; LC-mPFC and LC-spinal cord pathways, see Hirschberg et al., 2017; LC-AMY pathway, see Llorca-Torralba et al., 2019; DRN-AMY-LHb pathways, see Zhou et al., 2019. Abbreviations: 5-HT: serotonin; AMY: amygdala; BLA: basolateral amygdala; CeA: central nucleus of the amygdala; CNO: clozapine-N-oxide; DREADD: designer receptor exclusively activated by designer drugs; DRN: dorsal raphe nucleus; LC: locus coeruleus; LHb: lateral habenula; PFC: prefrontal cortex; PSAM: pharmaco-selective actuator module; NA: noradrenaline; NAc: nucleus accumbens; SC: spinal cord; SOM: somatostatin; TH: tyrosine hydroxylase.

While the different studies discussed so far assessed pathways involving two brain structures, circuits underlying pain perception and emotional regulation are likely to be more complex. Recently, Zhou and collaborators (2019) dissected an ascending pathway involved in pain-induced depressive-like behavior that is composed of the dorsal raphe nucleus (DRN), the central nucleus of the amygdala (CeA), and the lateral habenula (LHb), using both chemo- and optogenetics. Their results demonstrated that inhibition of serotonergic DRN neurons terminals in the CeA (Fig. 1A) resulted in depressive-like behavior in naive mice, while activation of this pathway in neuropathic animals produced antidepressant-like and antinociceptive effects. DRN serotonergic neurons preferentially target somatostatin neurons in the CeA, which in turn project to the LHb. Surprisingly, electrophysiological recordings showed that activation of CeA somatostatin fibers elicited excitatory responses in the LHb. Indeed, even though most somatostatin neurons are GABAergic, a small population of them is in fact excitatory. Silencing those fibers in the LHb (Fig. 1A) rescued chronic pain-induced depressive-like behavior, while activation of this pathway in naive animals conversely induced depressive-like behavior. Finally, by combining optogenetics with neuronal tracing and electrophysiology, they assessed the whole DRN-CeA-LHb circuit and showed that CPED in their model stems from the loss of serotonergic inhibition of LHb-projecting neurons of the CeA.

Taken altogether, these results deepen our understanding of the interconnected pathways that differentially modulate affective and sensory components of pain. Nevertheless, more research will be needed to better understand the big picture of CPED. While existing studies have proven the strength of opto- and chemogenetics in combination with pharmacological or electrophysiological approaches, future studies should consider additional levels of analysis. Within this line, cell-type, pathway-specific, or single-cell RNA-sequencing all have the potential to reveal underlying molecular mechanisms. On the other hand, techniques such as fiber photometry or calcium imaging, which are now more and more used *in vivo* and even in freely-moving rodents,

give more precise information at cellular and cell-specific levels. Finally, the use of functional magnetic resonance imaging (fMRI) or diffusion tensor imaging could give a more global insight in brain pathway alterations in CPED. Such non-invasive approaches allow for longitudinal studies and offer promising perspectives when considering that temporality is crucial when it comes to chronic pain and its affective consequences.

We believe that the leap forward in novel techniques and their combination with more classical approaches will lead to a better understanding of the circuits underlying the anxiodepressive disorders-pain dyad.

Acknowledgments

This work was supported by the Fondation de France (N° Engt: 00081244), the Fondation pour la Recherche Médicale (“Équipe FRM”, EQU201903007809; and ARF20160936006, PEL), the Fondation Deniker (“Bourses 2016”, PEL) and the French National Research Agency through the Programme d’Investissement d’Avenir (under the contract “ANR-17-EURE-0022”).

References

- Bravo, L., Llorca-Torralba, M., Suárez-Pereira, I., Berrocoso, E., 2020. Pain in neuropsychiatry: insight from animal models. *Neurosci. Biobehav. R.*
- Hirschberg, S., Li, Y., Randall, A., Kremer, E.J., Pickering, A.E., 2017. Functional dichotomy in spinal-vs prefrontal-projecting locus coeruleus modules splits descending noradrenergic analgesia from ascending aversion and anxiety in rats. *Elife* 6, e29808.
- Lee, M., Manders, T.R., Eberle, S.E., Su, C., D’amour, J., Yang, R., Lin, H.Y., Deisseroth, K., Froemke, R.C., Wang, J., 2015. Activation of corticostriatal circuitry relieves chronic neuropathic pain. *J. Neurosci.* 35 (13), 5247–5259.
- Llorca-Torralba, M., Suárez-Pereira, I., Bravo, L., Camarena-Delgado, C., Garcia-Partida, J.A., Mico, J.A., Berrocoso, E., 2019. Chemogenetic silencing of the locus coeruleus-basolateral amygdala pathway abolishes pain-induced anxiety and enhanced aversive learning in rats. *Biol. Psychiat.* 85 (12), 1021–1035.
- Zhou, W., Jin, Y., Meng, Q., Zhu, X., Bai, T., Tian, Y., et al., 2019. A neural circuit for comorbid depressive symptoms in chronic pain. *Nat. Neurosci.* 22 (10), 1649–1658.

The anterior cingulate cortex (ACC)

Overview

The following section focusing on the role on the ACC in the emotional consequences of chronic pain has been submitted as a review in Neuroscience & Biobehavioural Reviews. It consists of an outline of preclinical evidence from molecular, neuroimaging, behavioural, pharmacological and biochemical studies published during the last 20 years that address the role of the ACC in pain related aversion and anxiodepressive consequences of chronic pain. Finally, we discussed the next steps needed for strengthening our understanding of the role of the ACC in the chronic pain and emotional disorder dyad.

Review - Janus Effect of the Anterior Cingulate Cortex: Pain and Emotion

Janus Effect of the Anterior Cingulate Cortex: Pain and Emotion

Authors and affiliations: Sarah H. Journée^{a,1}, Victor P. Mathis^{a,1}, Fillinger C^a, Veinante P^a, Ipek Yalcin^{a,b*}

^a: Centre National de la Recherche Scientifique, Université de Strasbourg, Institut des Neurosciences Cellulaires et Intégratives, Strasbourg, France

^b: Department of Psychiatry and Neuroscience, Université Laval, Québec QC G1V 0A6, Canada

¹: equal contribution

* Corresponding author:

Dr. Ipek Yalcin, INCI CNRS, 8 allée du Général Rouvillois, 67000 Strasbourg, France. *E-mail address:* yalcin@inci-cnrs.unistra.fr

Highlights:

- ACC plays a critical role in emotional and pain processing.
- ACC is essential for the emotional component as well as anxio-depressive consequences of chronic pain.
- Imbalance of glutamatergic and GABAergic transmission in the ACC is one of the key mechanisms for the aversive- and anxiodepressive-consequences of chronic pain.
- Recent technological advances and development of several rodent model of chronic pain strengthen our mechanistic understanding underlying the complex role of the ACC in emotion and pain dyad.

Abstract

Over the past 20 years, clinical and preclinical studies point to the anterior cingulate cortex (ACC) as a site of interest for several neurological and psychiatric conditions. Indeed, the ACC plays a critical role in emotion, autonomic regulation, pain processing, attention, memory and decision making. Increasing number of studies demonstrated the involvement of the ACC in the emotional component of pain and its comorbidity with emotional disorders such as anxiety and depression. Thanks to the development of animal models combined with state-of-the-art technologies, we now have a better mechanistic understanding of the ACC functions. Hence, the primary aim of this review is to compile the most recent preclinical studies on the ACC's role in the emotional component and consequences of chronic pain. We thus described the electrophysiological, molecular and anatomical alterations in the ACC induced by pain and considered how these alterations might affect ACC circuits. Finally, we discussed the next steps that are needed to strengthen our understanding of the implication of the ACC in emotional and pain processing.

Key words: Anterior cingulate cortex, ACC, pain, chronic pain, aversion, anxiety, depression, circuits, rodent models.

Abbreviation list

ACC: anterior cingulate cortex
ALB: anxiety-like behaviors
AMPA: α -amino-3-hydroxy-5-methyl-4-isoxazolepropionic acid
BDNF: brain derived neurotrophic factor
BLA: basolateral nucleus of the amygdala
CaMKII α : calmodulin-kinase II α
CB: cannabidiol
CPA: conditioned place aversion
CPEB1: cytoplasmic polyadenylation element binding protein 1
CPP: conditioned place preference
DLB: depressive-like behaviors
E/I: excitatory/inhibitory
EPM: elevated plus maze
FST: forced swim test
GABA: γ -aminobutyric acid
GAD: generalized anxiety disorder
Glu: glutamatergic
HCN: hyperpolarization-activated cyclic nucleotide-gated
IDO: indoleamine 2,3-dioxygenase
Ins: insular cortex
LC: locus coeruleus
LD: light-dark box test
mGluR5: metabotropic glutamate receptor 5
MAPK: mitogen-activated protein kinase
MKP-1: MAPK phosphatase 1
MCC: middle cingulate cortex
MD: mediodorsal thalamus
MDD: major depressive disorder
N: nucleus
NAc: nucleus accumbens
NMDA: N-methyl D-aspartate
OFT: open field test
p: phosphorylated
PAG: periaqueductal gray
PCC: posterior cingulate cortex
PEAP: place escape/avoidance paradigm
PFC: prefrontal cortex
PKC γ : gamma isoform of the protein kinase C
PRA: pain-related aversion
PV: parvalbumin
PVN: paraventricular nucleus
R: receptor
rACC: rostral anterior cingulate cortex
RS: retrosplenial cortex
r-tDCS: repetitive transcranial direct current stimulation
SI: social interaction
SNARE: soluble N-ethylmaleimide-sensitive factor attachment protein receptors
SOM: somatostatin
S1: primary somatosensory cortex
S2: secondary somatosensory cortex
TST: tail suspension test
VTA: ventral tegmental area
5HT: serotonin

1. Introduction

Major depressive disorder (MDD) and generalized anxiety disorder (GAD) are some of the leading causes of disability worldwide (World Health Organization, 2009), contributing to the global burden of diseases (Santomauro et al., 2021; Whiteford et al., 2013). Although chronic stress is considered as the major risk factor for MDD and GAD, other pathologies can also trigger or worsen MDD/GAD. These comorbidities are in part responsible for treatment failures and decrease the patients' quality of life. Aside from the well-known comorbidity between depression and anxiety themselves, chronic pain is an important determinant for MDD/GAD (Means-Christensen et al., 2008). Depending on the pain condition, between 30-80% of chronic pain patients develop MDD or GAD in their lifespan (Bair et al., 2003; de Heer et al., 2014; Demyttenaere et al., 2007; Gureje et al., 2008; Von Korff et al., 2005; Williams, 2003). On the other hand, 50-60% of patients diagnosed with MDD report chronic pain (Meints and Edwards, 2018; Williams, 2003). However, despite numerous clinical studies reporting this comorbidity (Bair et al., 2003; de Heer et al., 2014; Demyttenaere et al., 2007; Gureje et al., 2008; Von Korff et al., 2005; Williams, 2003) the underlying cerebral mechanisms still remain unclear.

In the last two decades, the development of preclinical settings and rodent models of chronic pain have greatly improved our understanding of the neurobiological mechanisms implicated in this important clinical issue (Bravo et al., 2020; Kremer et al., 2021). One hypothesis for the comorbidity between chronic pain and emotional disorders is based on a shared neuroanatomical substrate hypothesis, suggesting that **i)** specific brain regions processing pain are also involved in emotional processing, and **ii)** alterations induced by chronic pain in these regions may alter emotional processing, eventually resulting in psychiatric disorders. Indeed, in different pain conditions, recent human and rodent imaging studies reported morphological and functional alterations in the pain matrix, including the primary (S1) and secondary somatosensory (S2), insular (Ins) and anterior cingulate cortices (ACC) (Apkarian et al., 2005), and in the mesolimbic and corticolimbic pathways, well-known for their implication in emotional processing (Serafini et al., 2020). Among these brain structures, the ACC is at the interface between sensory, cognitive and emotional processes (Vogt, 2005), acting as a hub for both pain and emotional processing (Shackman et al., 2011). Among other evidence, clinical studies reported a positive effect of transcranial magnetic stimulation of the ACC (Best and Pavel, 2017) and bilateral anterior cingulotomy (Deng et al., 2019) on pain and depressive symptoms in chronic pain patients also suffering from MDD. These findings pointed out for a strong and dual role of the ACC in pain and its emotional comorbidities. Since the correlates of human ACC can be found in both primates and rodents (van Heukelum et al., 2020), this brain structure became a region of interest in preclinical studies.

As the role of the ACC in the somatosensory component of pain have already been exhaustively documented (Bliss et al., 2016; Descalzi et al., 2009), this review will outline preclinical studies published between 2004 and 2022 focusing only on its role in the emotional component of chronic pain. In that purpose, the publications were chosen using a combination of three keywords [(pain) and (aversion or anxiety or depression) and (anterior cingulate cortex or cingulate or ACC or prefrontal

Box 1. Chronic pain models cited in this review.

Neuropathic pain	Inflammatory pain	Visceral pain
<i>Bone cancer pain (BCP)</i> : injection of cultured cancer cells into the tibial bone marrow	<i>Chronic facial inflammatory (CFI)</i> : injection of CFA in the vibrissae pad	<i>Acetic acid</i> : intraperitoneal acetic acid injection
<i>Chemotherapy induced</i> : administration of chemotherapeutics	<i>Complete Freund adjuvant (CFA)</i> : hindpaw injection of CFA	<i>Chronic pancreatitis</i> : intraductal administration of trinitrobenzene sulfonic acid
<i>Chronic constriction injury (CCI)</i> : ligation of the sciatic nerve	<i>Formalin</i> : hindpaw injection of formalin	<i>Colitis (DSS)</i> : dextran sulfate sodium in the water
<i>CCI-ION</i> : CCI of the infraorbital nerve	<i>Monoarthritis</i> : injection of CFA in the tibiotarsal joint	<i>Colorectal distension (CRD)</i> : application of pressure inside the colon and rectum with saline
<i>Common peroneal nerve ligation (CPNL)</i> : ligation of the common peroneal nerve		<i>Irritable bowel syndrome (IBS)</i> : zymosan injection
<i>Complete axotomy</i> : removal of a small part of the sciatic and saphenous nerves		
<i>Cuff</i> : compressing the main branch of the sciatic nerve by a polyethylene tube		
<i>Chronic constriction of multiple dorsal root ganglia (CCD)</i> : compression of the DRG of three lumbar nerves		
<i>Partial axotomy</i> : removal of a small part of the sciatic nerve		
<i>Partial sciatic nerve ligation (PSNL)</i> : ligation of half of the sciatic nerve		
<i>Spinal nerve injury (SNI)</i> : ligation of two branches of the sciatic nerve		
<i>Spinal nerve ligation (SNL)</i> : ligation of the spinal nerve of one or more spinal ganglia		
<i>Tibial nerve transection (TNT)</i> : transection of the tibial nerve		
<i>Postsurgical</i> : incision of the skin, deep tissues and muscle of the hindpaw		

NB: this list is non-exhaustive.

cortex or PFC) (Fig. 1). It is noteworthy to mention that the ACC neuroanatomical description differs in the literature (Fillinger et al., 2017a, 2017b; van Heukelum et al., 2020), which might explain some contradictory findings concerning its role in physiological and pathological conditions. Here, based on the Paxinos and Franklin atlas (Paxinos and Franklin, 2012), we selected the scientific papers focusing only on the area **24a**, **24b** and **32**, for which the majority of the scientific papers were found. Most of these studies interested in neuropathic and inflammatory pain (see Kremer et al., 2021 for detail), with few articles focusing on visceral or cancer pain (BOX 1 for preclinical models cited in this review).



Figure 1. Search and analysis strategies.

PubMed was used to search for original studies using a combination of the following terms: [Pain] AND [Aversion OR Anxiety OR Depression] AND [ACC OR Cingulate OR Anterior Cingulate Cortex OR PFC OR Prefrontal Cortex]. Clinical data, reviews and irrelevant publications were excluded. Numbers in light colors (yellow, green and blue) correspond to the total amount of articles for each specific key word combination. Numbers in white correspond to the papers used in this review. Overlapping papers among different topics are indicated in the intersections. *Abbreviations: ACC, anterior cingulate cortex; PFC, prefrontal cortex.*

In this review, after a brief description and comparison of the neuroanatomy of the ACC across species, we will highlight the significant role of this cerebral hub at the interface between pain and its emotional components. Finally, we will discuss the next steps needed for strengthening our understanding of the role of the ACC in the emotional component and consequences of pain.

2. Neuroanatomy of the ACC

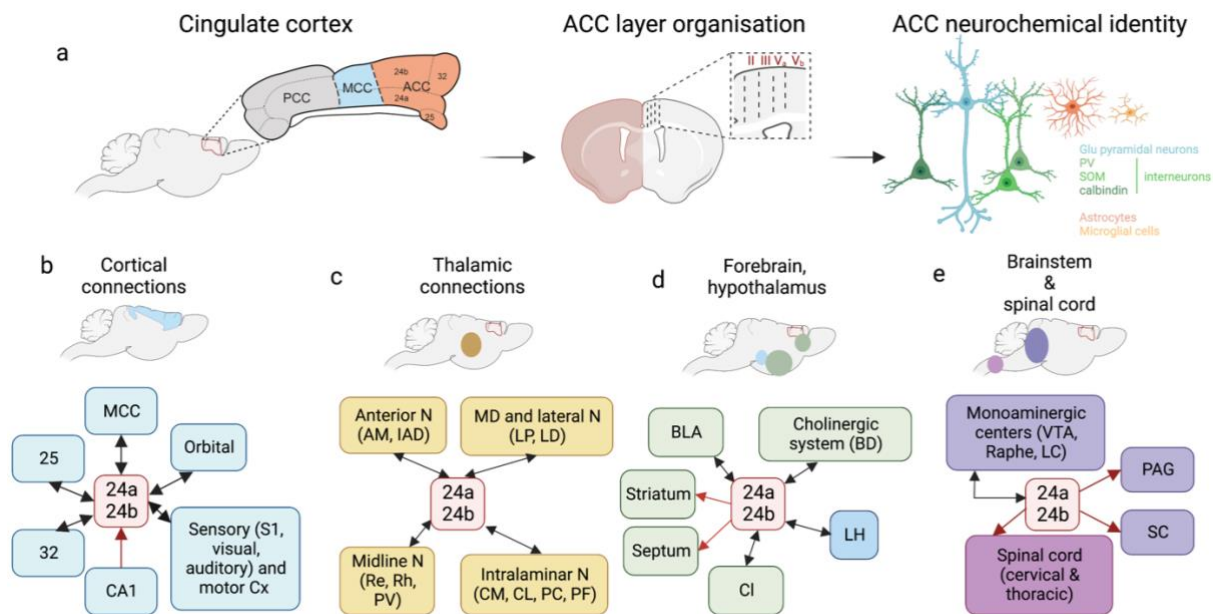
In humans and non-human primates, the cingulate cortex belongs to the medial wall of the cerebral cortex (Palomero-Gallagher et al., 2009; van Heukelum et al., 2020; Vogt et al., 1996). Along the anteroposterior axis, four subregions including the anterior (ACC), the middle (MCC) and posterior (PCC) cingulate cortex as well as the retrosplenial cortices (RS) compose this gyrus [Fig.2a, (Vogt, 2005)]. Comparative studies based on the cytoarchitecture and the homology with the primate cingulate cortex, described only the ACC, MCC and RS in rodents (Vogt and Paxinos, 2014). The ACC is an agranular cortex lacking a true layer IV, composed in rodents by the area 24, further divided into 24a (ventral) and 24b (dorsal), and the areas 25, 32 and 33 – the latter being absent in mice (Fig.2a). These areas contain both pyramidal neurons and interneurons distinctly distributed in terms of density and connectome over different layers and subdivisions (Gabbott et al., 1997). There are far more glutamatergic (Glu) neurons (around 80%) than GABAergic neurons in all ACC layers, apart from layer I, the latter including heterogeneous subpopulations based on calcium binding proteins [parvalbumin (PV), calbindin or calretinin] and peptides, such as somatostatin (SOM) (Gabbott et al., 1997).

Concerning its neuroanatomical connections, the ACC presents a wide connectome, similar across species, with only few differences in term of density of connections (for details see Fillinger et al., 2017a, 2017b; van Heukelum et al., 2020). Briefly, connections of the areas 24a/24b can be divided in four sub-networks, 1) cortical, 2) thalamic, which are the denser connections of the ACC and mostly reciprocal, 3) forebrain and hypothalamus and 4) brainstem centers, which receive stronger and wider ACC inputs than providing afferent (**Fig.2b-d**).

At the cortical level, beside strong interconnections, areas 24a and 24b are reciprocally connected with frontal regions, mostly with the rest of the ACC and the orbital cortex, as well as the sensory and temporal cortices. As an exception, the hippocampal region sends moderate projections to the ACC but does not receive any afferents from it. In regards to the thalamo-cortico-thalamic connections, four main groups of nuclei can be highlighted as cingulate privileged interlocutors: the anterior nuclei - mostly the anteromedial nucleus, the mediodorsal nucleus, the midline nuclei - primarily the reuniens and rhomboid nuclei, and finally the intralaminar nuclei with the centromedial, central lateral, paracentral and parafascicular thalamic nuclei (Fillinger et al., 2017a, 2017b).

In the forebrain, the basolateral nucleus of the amygdala (BLA) and the claustrum are densely and reciprocally connected to the ACC, along with a lesser contribution of the lateral and anterior hypothalamus. Additionally, the lateral septum, as well as the dorsal, and to a lesser extent the ventral, striatum receive a dense ACC input. In the brainstem, monoaminergic centers [ventral tegmental area (VTA), substantia nigra, dorsal and median raphe and the locus coeruleus (LC)] are bidirectionnally connected with the ACC (Fillinger et al., 2017a, 2017b). In addition, the ACC sends unidirectional projections to the superior colliculus and the pretectal nuclei, as well as to the periaqueductal gray (PAG), more specifically to the dorsolateral column from 24a and the lateral/ventrolateral columns from

24b, in mice. Finally, ACC neurons have been found to project to the cervical and thoracic spinal cord in rodents (T. Chen et al., 2018).



NB: not exhaustive.

Figure 2. Neuroanatomical and neurochemical description of the ACC.

(a) Graphical representation of the mouse cingulate cortex, composed by the posterior (PCC; grey), middle (MCC; blue) and anterior cingulate cortex (ACC; orange). Specifically, the ACC is an agranular cortical region comprising the Brodmann areas 24a and 24b, 25 and 32, lacking a true layer IV (middle panel) and composed by multiple different cell types (right panel). Concerning its neurochemical identity, beside the vast majority of glutamatergic neurons (80%), it contains PV, SOM and calbindin GABAergic neurons and non-neuronal cells, such as microglia and astrocytes. (b-e) The areas 24a and 24b of the ACC have a wide connectome that can be divided into 4 sub-categories. The ACC cortical connections (b; light blue) are mostly reciprocal (double arrows), such as its connections with the thalamus (c; gold) and the forebrain (d; light green) and the hypothalamus (d; blue). The ACC has also reciprocal connections with the monoaminergic centers and sends projections to the PAG, SC (violet) and the spinal cord (purple), mostly to the cervical and thoracic levels (e). *Abbreviations: ACC, anterior cingulate cortex; AM, anteromedial nucleus; DBB, diagonal band of Broca; BLA, basolateral nucleus of the amygdala; CA1, hippocampal subfield 1; CM, central medial N; CL, centrolateral N; Cl, claustrum; Cx, cortex; Glu, glutamatergic; IAD, interanterodorsal N; LH, lateral hypothalamus; LC, locus coeruleus; LD, laterodorsal N; LP, lateroposterior N; MCC, midcingulate cortex; MD, mediodorsal N; N, nucleus; PAG, periaqueductal gray; PC, paracentral N; PCC, posterior cingulate cortex; PV, parvalbumin; Re, N reuniens; Rh, rhomboid N; SC, superior colliculus; SOM, somatostatin; VTA, ventral tegmental area.*

3. Role of the ACC in pain-related aversion

The affective dimension of pain refers primarily to the feeling of unpleasantness and secondary to the long-term impact of suffering from pain. Such aspects of pain participate in shaping subsequent pain-related behaviors and reflect aversive and motivational aspects of pain. Hence, pain-related aversion (PRA) leads to behavioral avoidance or extinction of behaviors associated with noxious stimuli.

Numerous clinical studies have demonstrated the critical role of the ACC in the affective dimension of pain in human (see: Brotis et al., 2009). In regard to preclinical studies, several paradigms were developed as a mean to evaluate PRA in rodents [Fig.3, (Kremer et al., 2021)]. The place

escape/avoidance paradigm (PEAP) - measuring the escape behavior of animals from an evoked painful stimulus, place conditioning paradigms - relying on the association of a context with either painful stimuli in conditioned place aversion (CPA) or pain-relief via an analgesic drug in conditioned place preference (CPP), are the most frequently used tests to evaluate the aversive component of pain. Lesioning studies were part of the milestones to question the involvement of the ACC in PRA. It was reported that ACC lesion (using electrolytic or excitotoxic procedures) in rats, blocks the avoidance to a context paired with acute inflammatory pain (Gao et al., 2004; Shi et al., 2020; Yi et al., 2011). This lesion also prevent the aversiveness of ongoing pain in both neuropathic (Barthas et al., 2015; Juarez-Salinas et al., 2019; LaGraize et al., 2004; Li et al., 2022; Qu et al., 2011) and inflammatory pain models (Johansen et al., 2001). Interestingly, none of these studies reported an effect on mechanical hypersensitivity. In contrary, lesion of the posterior insular cortex blocks the maintenance of mechanical hypersensitivity (Gao et al., 2004; Shi et al., 2020) without affecting the aversive component of neuropathic pain (Barthas et al., 2015). Accordingly, the ACC seems to be essential for the aversive component of pain. The next section will thus outline cellular and molecular alterations in the ACC as well as its circuits implicated in PRA.

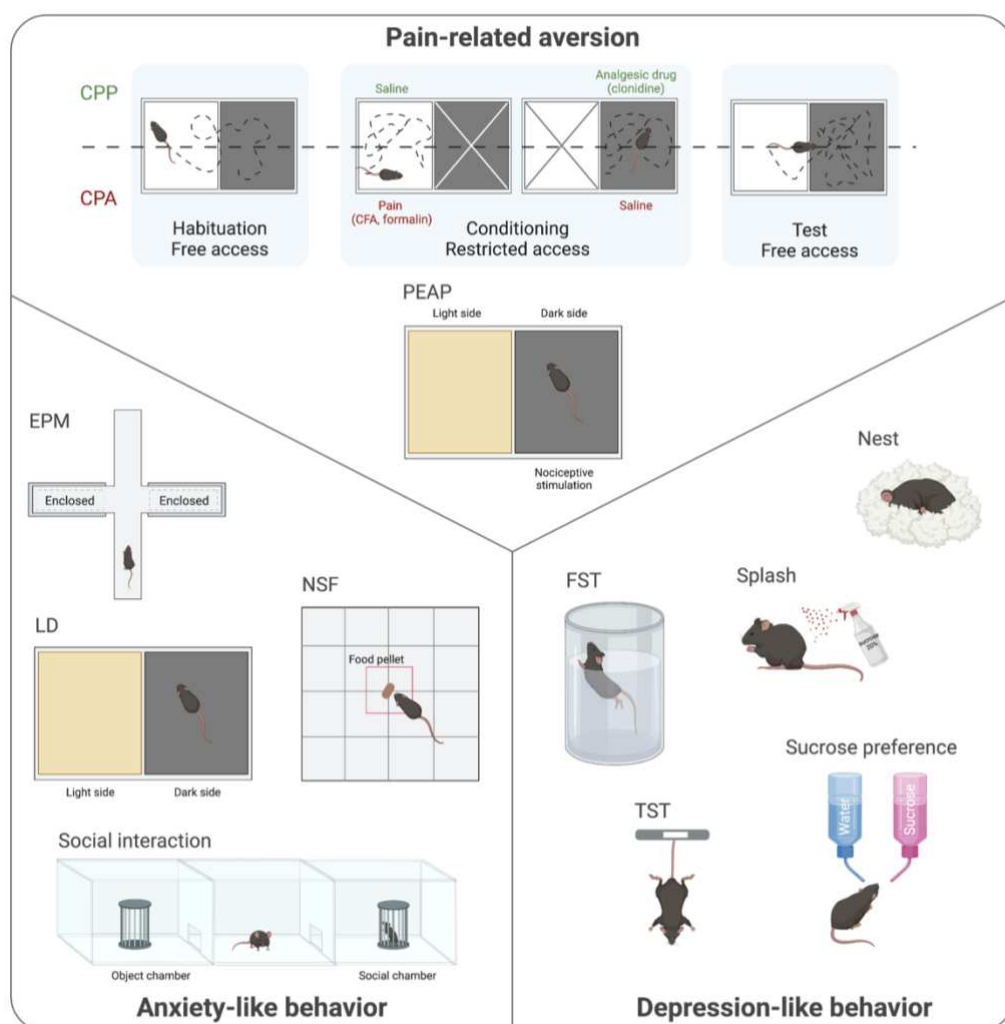


Figure 3. Classical tests used to evaluate pain-related aversion, anxiety- and depressive-like behaviors in rodents.

Numerous behavioral tests were developed to test pain-related aversion (upper panel), anxiety- (lower left panel) and depressive-like (lower right panel) behaviors in rodents. Most of the pain-related aversion tests are based on the preference that animals experiencing pain develop toward an analgesic drug paired with a specific area (CPP) or the avoidance of pain-associated environments (CPA and PEAP). Tests assessing anxiety-like behavior rely on the natural conflict between innate behaviors (exploration, feeding, and socialization) and innate fear (open lit areas, foreign objects, unfamiliar individual). Paradigms evaluating depressive-like behavior in rodent assess either self-centered behaviors, such as nest building or grooming behaviors or despair-like behaviors as in the tail suspension or forced swim tests. In regard to anhedonia, the most used test so far is the sucrose preference test that measures the preference for a sweet solution (1 to 5% sucrose solution) compared to water. *Abbreviations: CFA, complete Freund adjuvant; CPA, conditioned place aversion; CPP, conditioned place preference; EPM, elevated plus maze; FST, forced swim test; LD, light-dark test; NSF, novelty-suppressed feeding test; PEAP, place escape-avoidance paradigm; TST, tail suspension test.*

3.1. Electrophysiological changes and functional alterations

Recent technological advances have accelerated the study of the functional alterations of the ACC in PRA. In different pain models and pain-related paradigms, in rodents, *in vivo* single unit recordings in anesthetized animals (Cao et al., 2012; Sellmeijer et al., 2018), extracellular recordings in freely moving rats (Zhang et al., 2017), and *in vitro* whole cell patch clamp recordings (Lançon et al., 2021; Sellmeijer et al., 2018; Zhang et al., 2021) have shown an increased firing activity of ACC neurons associated with PRA. This shift towards ACC hyperactivity might be due to an imbalance between excitatory and inhibitory (E/I) neurons within the ACC. Recent *in vivo* studies, aiming at modulating ACC activity, suggest a primary role of the pyramidal cells in this imbalance (Bliss et al., 2016; Zhu et al., 2022). Indeed, cell-type specific opto- or chemogenetic inhibition of ACC Glu neurons alleviates the aversiveness of ongoing pain without affecting mechanical allodynia in inflammatory and neuropathic pain models (Sellmeijer et al., 2018; Zhang et al., 2017, 2021). On the contrary, optogenetic activation of ACC pyramidal neurons in naive animals induces aversion (Tan et al., 2017; Zhang et al., 2017) similar to that of pain models. Interestingly, Gan and colleagues (Gan et al., 2021) reported that repetitive transcranial direct current stimulation (r-tDCS) of the prefrontal cortex not only blocks aversion, but also mechanical and thermal nociceptive behaviors in a neuropathic pain mice model. This latest effect could be explained by the fact that the application of r-tDCS is not restricted to the ACC and might affect other prefrontal areas. In a similar manner, high frequency electrical stimulation of the ACC also rescues PRA, while low frequency stimulation increases it (Liu et al., 2021). In a pharmacological perspective, a single dose of ketamine induces a prolonged suppression of the hyperactivity of the ACC pyramidal neurons that is associated with a reduction of the aversive response to noxious stimuli in rodent pain models. Strikingly, this anti-aversive effect persists long after the cessation of the anti-nociceptive effects of ketamine (Zhou et al., 2018). These results support the hypothesis postulating that ACC excitatory neurons' hyperactivity might be at the origin of the pain aversiveness.

On the other hand, it was also reported that ACC hyperactivity could be due to a loss of GABAergic inhibitory control. Indeed, the local administration of the GABA-A receptor agonist, muscimol, into the

rostral ACC (rACC) reduces PRA after nerve injury (LaGraize and Fuchs, 2007; Tang et al., 2005). Using chemotherapy-induced neuropathic pain model, Juarez-Salinas and colleagues (Juarez-Salinas et al., 2019) showed that the transplantation of inhibitory interneuron progenitor cells into the ACC was sufficient to restore a GABA-A mediated inhibitory control of host pyramidal cells and to block PRA in the CPP paradigm. These findings demonstrate the complexity of the functional alterations induced by chronic pain in the ACC. Hence, further experiments are required to decipher what mechanism comes first: an increase in excitatory cells activity followed by a dysregulation of the E/I balance or an alteration of local inhibitory circuits triggering the ACC hyperactivity.

To further dissect what cell types are implicated in PRA, Zhang and colleagues (Zhang et al., 2021) focused on ACC neurons expressing the gamma isoform of the protein kinase C (PKC γ). They showed that chemogenetic activation these ACC PKC γ neurons induces mechanical hypersensitivity and aversion in naive animals, while in neuropathic pain condition these neurons are hyperexcitable and their inhibition blocks mechanical allodynia and aversiveness of ongoing pain.

While the aforementioned studies were mainly performed in male rodents, it is important to take into consideration sex differences in pain research (Bartley and Fillingim, 2013; Mogil, 2020), even though it might be more difficult to study the affective consequences of pain in females (Cardenas et al., 2020). A pioneer study from Jarrin and colleagues (Jarrin et al., 2020) compared the role of ACC Glu neurons in PRA in male and female rats in an inflammatory pain model and showed that the optogenetic activation of calmodulin-kinase II α (CaMKII α)-expressing Glu neurons decreases formalin-induced nociceptive behaviors during conditioning without affecting formalin-induced CPP in males while this activation increases nociceptive behavior in females. However, the optogenetic inhibition of ACC Glu neurons reduces PRA in both males and females without affecting the nociceptive behaviors. Further studies will be necessary to fully understand potential sex differences regarding the functional role of the ACC and its cell types implicated in PRA.

3.2. ACC circuits

Besides the ACC microcircuits alterations, the whole ACC network is affected by chronic pain conditions and some of the aforementioned mechanisms likely spread to ACC outputs and impact ACC macrocircuits that participate in PRA. The recent advances in the development of viral approaches enabled the study of specific ACC circuits in the affective component of pain. For instance, inhibition of the mediodorsal (MD) thalamic nucleus projections to the ACC creates CPP in animals with nerve injury, while its activation exacerbates PRA with strikingly no effect in naive animals (Meda et al., 2019). In the same study, the authors also showed that optogenetically inhibiting BLA inputs to ACC elicited PRA (Meda et al., 2019). On the contrary, it was shown that chemogenetic activation of LC neurons projecting to the ACC exacerbates spontaneous pain and produces aversion, in the a neuropathic pain model (Hirschberg et al., 2017). As for the MD-ACC manipulation described above, the LC-ACC manipulation did not affect pain related behaviors in naive mice. In regard to cortico-cortical

connections, Singh and colleagues demonstrated that the optogenetic activation of the primary somatosensory cortex S1 increased the proportion of ACC neurons that respond to noxious stimuli, suggesting that S1 inputs reinforce nociceptive response in the ACC (Singh et al., 2020). They further observed an enhanced S1-ACC connectivity in chronic pain state and showed that the optogenetic inhibition of this pathway effectively relieved the aversive component of chronic pain.

Concerning the ACC output neurons, Gao and colleagues (Gao et al., 2020), using a chemogenetic approach, showed that inhibition of CaMKII ACC neurons projecting to both the nucleus accumbens (NAc) and VTA induced a place preference for the compartment associated with the inhibition in neuropathic rats, while activation of these pathways induced aversive behavior in naive animals suggesting an important role of this circuit in PRA.

3.3. Molecular and cellular changes

An increasing number of studies brought new knowledge about molecular mechanisms underlying ACC hyperactivity and PRA. Several groups reported an increase in brain derived neurotrophic factor (BDNF), its receptor TrkB, phosphorylated ERK (pERK), phosphorylated mTOR (p-mTOR) and mitogen-activated protein kinase (MAPK) in the ACC in different pain models (Cao et al., 2014, 2009; Galan-Arriero et al., 2014; Han et al., 2014; Li et al., 2022; Lu et al., 2016; Thibault et al., 2014; Wang et al., 2017; Zhang et al., 2016, 2018). Strikingly, blockade of one of these targets seems to rescue PRA (Thibault et al., 2014). Indeed, blocking the receptor TrkB in the ACC rescues PRA in cancer pain (Li et al., 2022) while the BDNF injection into the ACC is sufficient to induce aversion in naive animals (Thibault et al., 2014; Zhang et al., 2016). Interestingly, by blocking p-mTOR in the rACC after formalin injection, Zhang and colleagues (Zhang et al., 2018) did not only rescue PRA, but also prevented NMDA (N-methyl D-aspartate) receptor 2B upregulation in the rACC, known to be overexpressed in the ACC in pain conditions (Li et al., 2009), suggesting a complex interaction between all these factors. Accordingly, blocking/silencing ACC NMDA subunits, with an antagonist or small interfering RNA, in inflammatory, neuropathic and cancer pain rescues PRA, but not mechanical hypersensitivity nor acute pain (Feng et al., 2016; Guo et al., 2015; Lei et al., 2004; Li et al., 2009; Zhou et al., 2018). Similarly, blocking D-serine, an endogenous ligand for NMDA receptors, either by enzymatic degradation or an antagonist of the glycine site of NMDA receptors, also attenuates CPA produced by inflammatory pain (Ren et al., 2006), strengthening the role of Glu signaling in PRA. Galan-Arriero and colleagues (Galan-Arriero et al., 2014) also showed an increase in ACC metabotropic Glu receptor 5 (mGluR5) expression in neuropathic rats. Accordingly, preventing this increase by p38a MAPK inhibition or by blocking Glu receptor (R) with kynurenic acid in the ACC is sufficient to prevent aversion induced by inflammation, while their stimulation in naive animals produces CPA (Galan-Arriero et al., 2014; Johansen and Fields, 2004). Kang and colleagues also showed that inhibiting ACC Glu positive cells in their inflammatory model induces CPP but also alleviates mechanical hypersensitivity in mice (Kang et al., 2017). Collectively, these results confirm the crucial role played by the glutamatergic system in PRA and seem

to indicate that chronic pain-induced molecular alterations facilitate the glutamatergic transmission in the ACC in various pain models.

However, we cannot only consider ACC Glu signaling since several pharmacological studies highlight the crucial role of the ACC GABAergic transmission. Indeed, local ACC or rACC infusion of muscimol attenuates PRA but not spontaneous pain after formalin or mechanical hypersensitivity (LaGraize and Fuchs, 2007; Wang et al., 2005). Altogether, these electrophysiological and molecular findings confirm the shift toward ACC hyperactivity in chronic pain condition and reinforce the hypothesis that an imbalance of glutamatergic and GABAergic transmissions is a key mechanism governing PRA. However, further studies are required to decipher whether these alterations are the cause or consequences of the comorbidity between chronic pain and emotional disorders.

Alongside with Glu and GABAergic systems, several neuromodulators have been implicated in PRA. In neuropathic rats, bilateral administration of morphine into the rACC is sufficient to produce CPP (Gomtsian et al., 2018; LaGraize et al., 2006; Navratilova et al., 2015) while the microinjection of the opioid antagonist, naloxone, into the ACC prevented morphine-induced CPP (Navratilova et al., 2015), suggesting a key role of the opioid system. More specifically, the administration of the delta opioid receptor agonist into rACC prevents inflammatory pain-induced CPA (Ma et al., 2022), while kappa opioid receptor antagonist blocks the electroacupuncture rescue of CFA-induced CPA (Zhang et al., 2011).

The role of monoamine signaling such as serotonin (5HT) and dopamine has also been described in PRA. Santello and colleagues (Santello et al., 2017) demonstrated that injection of a selective 5HT_{7R} antagonist into the ACC reduces both mechanical hypersensitivity and PRA by enhancing the function of hyperpolarization-activated cyclic nucleotide-gated (HCN) channels that are downregulated in ACC layer V neurons. In addition, it was shown that dopamine D_{1R} agonists rescue the decreased activity of HCN channel in neuropathic mice, which in turn inhibits ACC hyperactivity (Lançon et al., 2021). Interestingly, chronic systemic L-DOPA or carbidopa treatments rescue not only ACC HCN channel function but also mechanical and cold hypersensitivity as well as PRA. Hence, besides the ACC E/I imbalance, several modulatory systems appear to be implicated in PRA, which might be additional targets for new treatment strategies.

These vast alterations in diverse neurotransmission systems can be related to overexpression of ACC SIP30, one of many SNAREs (soluble N-ethylmaleimide-sensitive factor attachment protein receptors) which are essential for the regulation of neurotransmitter-containing synaptic vesicles exocytosis. Indeed, expression of SIP30 is modified by pain conditions and its local silencing reduces aversion without affecting mechanical hypersensitivity (Han et al., 2014). However, the exact nature of the neurotransmitters affected by SIP30 silencing is yet to be studied.

Finally, some studies also point to neuroinflammation as well as non-neuronal cells as key factors for PRA. Indeed, an increase in astrocytic markers, such as GFAP/S100B, and inflammatory cytokines including IL-1B/TNF- α , have been observed in the ACC in inflammatory rat models (Chen et al., 2012;

Lu et al., 2011). In addition, local injection of an astroglia-specific toxin can prevent PRA (Chen et al., 2012). Moreover, Wang and colleagues (Wang et al., 2020) showed increased ACC immune system activity indicators such as Kynurenine/Tryptophan ratio and IDO (indoleamine 2,3-dioxygenase) enzyme for tryptophan catabolism to kynurenine in a neuropathic pain model. The inhibition of the latter was shown to reverse PRA as well as cold and mechanical hypersensitivity.

Overall, these recent findings (**Table 1**) demonstrate the complexity of the role of the ACC in PRA implicating multiple mechanisms and highlight the necessity to decipher the underlying mechanisms not only at the microcircuitry level but also at the macrocircuitry one.

4. Role of the ACC in the anxiodepressive-like consequences of chronic pain

In the past two decades, several paradigms addressing the anxiodepressive-like consequences of chronic pain were developed in rodents [(for detail see Kremer et al., 2021); (Fig. 3)]. In general, the evaluation of anxiety-like behaviors (ALB) in rodents relies on the conflict between innate behaviors (exploration, feeding, and socialization) and innate fear (open lit areas, foreign objects or unfamiliar individual). Hence, the most used tests are the elevated plus maze (EPM), open-field (OFT), light-dark box (LD), social interaction (SI) or burrowing tests. Regarding depressive-like behaviors (DLB), the currently available paradigms mostly assess despair-like [forced swim (FST) or tail suspension tests (TST)], anhedonia-like symptoms (sucrose preference test) or animals' well-being (splash, nest tests), and only partially model the depressive symptoms observed in human.

Using these tests, lesion studies showed that ACC ablation prevents both ALB (Zeng et al., 2018) and DLB (Barthas et al., 2015) in models of remifentanyl induced hyperalgesia and neuropathic pain. It was also shown that optogenetic inhibition of ACC pyramidal neurons is sufficient to rescue neuropathic pain-induced anxiodepressive-like behaviors in mice (Sellmeijer et al., 2018). Furthermore, a longitudinal imaging study in rats demonstrated a correlation between decreased ACC volume and anxiety-like consequences of neuropathic pain (Seminowicz et al., 2009). Similar to PRA, these results demonstrate the crucial role of the ACC in the emotional consequences of pain. The next sections will focus on the cellular and molecular alterations in the ACC as well as in its networks in the anxiodepressive-consequences of chronic pain.

4.1. Electrophysiological changes and functional alterations

As reported in PRA, the ACC E/I balance is shifted toward hyperactivity as increased firing activity and excitability of ACC neurons that accompanies anxiodepressive-like behaviors were reported in the context of cutaneous mechanical stimulation (Matsumoto et al., 2020), neuropathic pain (Sellmeijer et al., 2018; Zhao et al., 2020), inflammatory pain (Ducret et al., 2022; Zhou et al., 2022) and visceral pain (Brenner et al., 2021; Ren et al., 2022; Zhang et al., 2014). Likewise, ACC activity alterations were observed after chronic stress, which also leads to increased pain sensitivity (Liu et al., 2019). Interestingly, Sellmeijer and colleagues (Sellmeijer et al., 2018) studied ACC spontaneous neuronal

activity along the time-dependent evolution of neuropathic pain symptoms and showed that chronic pain-induced ACC hyperactivity was only observed when animals displayed depressive-like consequences. They also described an enhancement of excitatory synaptic transmission in the ACC coinciding with DLB in neuropathic pain. Furthermore, inhibiting ACC pyramidal neurons using optogenetic approach was sufficient to block these behavioral alterations (Sellmeijer et al., 2018). Again, the shift in ACC E/I activity balance is likely not only due to Glu signaling alterations. Both the activity of PV and SOM interneurons in the ACC are decreased in chronic inflammatory model, and chemogenetic activation of PV interneurons alleviates mechanical hypersensitivity and ALB (Shao et al., 2021a, 2021b). Concurrently, this manipulation reduces pain induced ACC c-Fos levels and hyperexcitability of Glu neurons (Shao et al., 2021a, 2021b). On the contrary, chemogenetic inhibition of ACC GABAergic interneurons in naive animals induces ALB by enhancing ACC Glu neurons excitability and reducing inhibitory synaptic transmission (Shao et al., 2021b). It was also shown that chemogenetic inhibition of Glu neurons or activation of GABA neurons relieved both mechanical hypersensitivity and DLB in inflammatory and neuropathic mouse models (Zhu et al., 2021), while optogenetic inhibition of ACC Glu neurons rescued hyperalgesia and ALB induced by chronic pancreatitis (Ren et al., 2022). These results suggest again a key role for ACC inhibitory neurons and a complex alteration of the ACC E/I balance in pain condition that could trigger anxiodepressive behaviors.

4.2. ACC circuits

Aforementioned ACC alterations might be the consequence of alterations that occur in upstream circuits and most likely propagate to downstream circuits. Although the literature remains minor yet, Zhu and colleagues (Zhu et al., 2022) showed that chemogenetic activation of rACC Glu neurons projecting to the ventrolateral PAG provokes mechanical hypersensitivity and ALB, while the inhibition of this pathway prevents such symptoms in a neuropathic pain model. Similarly, the chemogenetic activation of the ACC-thalamus pathway in naive rats induces ALB while chemogenetic inhibition of this pathway rescues ALB in a CFA rat model (Shen et al., 2021). Recent studies also highlighted the crucial role of the reciprocal thalamo-cortical circuits in DLB triggered by chronic pain (Zhu et al., 2021). Indeed, in mice, Zhu and colleagues showed the specific role of the Glu projection from the parafascicular thalamic nucleus onto both GABAergic and Glu ACC neurons in depressive-like states, while the projection from the posterior thalamic nucleus to the ACC specifically mediates mechanical hypersensitivity (Zhu et al., 2021). The ACC connections from the paraventricular nucleus (PVN) of the hypothalamus also play a role in the comorbidity between neuropathic pain and anxiety, as the optogenetic activation of the PVN-ACC pathway reduces both mechanical hypersensitivity and ALB (Li et al., 2021a). In addition, chemogenetic inhibition of the pathway from the LC, the principal brain region secreting noradrenaline, to the ACC reversed DLB in a rat neuropathic pain model (Llorca-Torralba et al., 2022). Finally, Becker and colleagues (Becker et al., 2022) showed that the BLA-ACC pathway is implicated in the depressive-

like but not anxiety-like consequences of neuropathic pain as its optogenetic inhibition rescues depressive-like behavior in neuropathic pain, and its chronic activation in naive mice mimics depressive-like behaviors.

Hence, as for PRA, ACC sub-circuits are likely implicated in the development of the anxiodepressive consequences of chronic pain. Nevertheless, further studies are required to precisely map and link these circuits with the behavioral outputs.

4.3. Molecular and cellular changes

As for PRA, several groups reported robust changes in the intracellular MAPK/ERK pathway in the anxiodepressive-like consequences of chronic pain (Barthas et al., 2017; Humo et al., 2020; Xiao et al., 2021). For instance, in a genome-wide study, ACC MAPK signaling pathway was the most significantly altered at both early and late phase of neuropathic pain (Barthas et al., 2017). In another transcriptomic study, Su and colleagues (Su et al., 2021) showed that most of the differentially expressed-genes in the ACC in neuropathic pain were related to anxiety and depression rather than pain itself, confirming the crucial role of the ACC in emotion, and that MAPK signaling was one of the most dysregulated pathway. In accordance, the expression of MAPK phosphatase 1 (MKP-1), a negative regulator of this pathway, dephosphorylating downstream proteins such as pERK and phosphorylated CREB (pCREB), was robustly increased in neuropathic pain (Barthas et al., 2017; Humo et al., 2020; Wen et al., 2022). In addition, blocking MKP-1 with an antagonist or knocking it down rescued or prevented anxiodepressive-like behaviors induced by chronic pain (Barthas et al., 2017; Humo et al., 2020), highlighting the importance of the MAPK pathway as well as its regulators in pain-induced molecular changes in the ACC and the emotional consequences of pain. Strikingly, it was also shown that classical and fast-acting antidepressant drugs such as fluoxetine and ketamine can normalize ACC MKP-1 levels. Besides MKP-1, increased level of ACC pERK levels (Dai et al., 2011; Luo et al., 2015; Pereira-Silva et al., 2020; Shao et al., 2015; Zhong et al., 2012), decreased levels of pCREB and BDNF (Bravo et al., 2012; Cong et al., 2021; Imbe and Kimura, 2017; Ishikawa et al., 2014, 2015; Pan et al., 2018; Yasuda et al., 2014) were reported in animals showing ALB and DLB following chronic pain induction. More specifically, in both visceral and incisional pain, the expression of the ACC pERK increases biphasically (Dai et al., 2011; Zhong et al., 2012). During the first phase, both allodynia and ALB are rescued by pERK inhibition, while in the second phase this inhibition only affects ALB (Dai et al., 2011; Zhong et al., 2012). Interestingly, stimulating BDNF synthesis, via 4-methylcatechol intracerebroventricular injection, increases ACC BDNF levels, decreases ACC pERK levels and prevents thermal hypersensitivity and DLB in neuropathic pain (Ishikawa et al., 2014). Similarly, ACC knock-down of CREB or the systemic injection of the CREB inhibitor rescues mechanical and heat hypersensitivity, ALB, as well as CREB, pCREB and BDNF levels in a neuropathic rat model (Wen et al., 2022). It was shown that different treatment strategies used for pain and mood disorders, such as imipramine (Ishikawa et al., 2014), neurotrophin (Ishikawa et al., 2015) or ketamine (Pan et al., 2018), also recruit the

MAPK/ERK pathway by altering pERK, pCREB and BDNF levels in the ACC. Interestingly, the inhaled anesthetic sevoflurane also influences ACC pERK levels in rats and has a positive effect on the nociceptive and anxiety components of inflammatory pain (Luo et al., 2015). On the contrary, intravenous anesthetics such as propofol and pentobarbital sodium do not produce the same effect and only block the nociceptive response (Luo et al., 2015). Besides pharmacological agents, paramedical approaches such as manual acupuncture and electroacupuncture were shown to alleviate mechanical hypersensitivity and anxiodepressive-like behaviors (Cong et al., 2021; Shao et al., 2021a, 2015; Shen et al., 2021; Zhu et al., 2022), as well as pERK overexpression (Shao et al., 2015) or BDNF/CREB downregulation (Cong et al., 2021).

In addition to pERK, pCREB and BDNF, Glu signaling and its receptors also play a critical role in the pain/anxiodepressive dyad (Du et al., 2017; Guo et al., 2018; Sun et al., 2016; Wang et al., 2019; Zeng et al., 2018). Indeed, the expression of ACC AMPA (α -amino-3-hydroxy-5-methyl-4-isoxazolepropionic acid receptor) and NMDA receptors were increased in inflammatory (Du et al., 2017; Sun et al., 2016; Wang et al., 2020), visceral (Ren et al., 2022; Wang et al., 2019) and remifentanil-induced pain (Zeng et al., 2018). In addition, it seems that AMPA-R/NMDA-R ratio plays an important role as it was reduced in the rACC of an inflammatory-pain model (Ducret et al., 2022). Accordingly, pharmacological studies further supported the implication of AMPA-R and NMDA-R in the comorbidity of chronic pain and emotional disorders. For instance, blockade of both ACC AMPA-R and NMDA-R, using CNQX or AP-5, reversed mechanical hyperalgesia in a chronic pancreatitis model (Ren et al., 2022). Moreover, the ACC injection of an antagonist of AMPA-R subunit pGluR1 prevented ALB and remifentanil-induced hyperalgesia and also decreased ACC c-Fos overexpression (Zeng et al., 2018). Along with GluR1, several groups also reported dysregulation of other related proteins such as increased levels of protein kinases PKCzeta and PKMzeta (Du et al., 2017) or CPEB1 (Cytoplasmic Polyadenylation Element Binding Protein 1) in the ACC (Wang et al., 2019). Interestingly, blocking PKCzeta or knocking down CPEB1 alleviated pain, ALB and increased GluR1 levels. On the other hand, it was reported that mGluR5 expression was decreased in a model of inflammatory pain (Guo et al., 2018) and positive allosteric modulation of mGluR5 alleviated both CFA-induced ALB and allodynia. These findings suggest a differential role for AMPAR, NMDAR and mGluR5. Besides these intracellular mechanisms, extracellular alterations might trigger or facilitate intracellular changes. Li and colleagues (Li et al., 2021b) indeed showed, in neuropathic pain, a downregulation of LAMB1, one key component of the extracellular matrix with a dual role in tissues architecture and cell signaling, that accompanies anxiodepressive-like behaviors. These results suggest a yet understudied role of the extracellular matrix in chronic pain and its emotional consequences. Indeed, such extracellular pain-induced modifications might lead to strong alterations in neurotransmission. Interestingly, in a transcriptomic study, downregulation of neurotransmitter release and extracellular matrix genes were observed 2 weeks post neuropathic pain induction in the ACC of female, but not male mice (Dai et al.,

2022). This supports the need for more studies including both sexes as there are sex-specific differences already in control animals as well as in neuropathic animals.

Besides neurons, glial cells are also implicated in the anxiodepressive-consequences of chronic pain. Indeed, inflammatory (Sun et al., 2016) and neuropathic pain (Wang et al., 2020) induce microgliosis, astrogliosis and increase proinflammatory cytokines expression such as TNF- α and IL6 levels in the ACC. Imaging studies further support the alterations in glial cells. Using manganese-enhanced magnetic resonance imaging, McIlwrath and colleagues showed increased T1 and T2 signals and bilateral astrogliosis within the ACC (McIlwrath et al., 2020). The implication of glial cells and cytokines in the anxiodepressive-like consequences of chronic pain was also supported by Wang and colleagues (Wang et al., 2020) showing that chronic IDO1 inhibitors not only alleviates mechanical and thermal hypersensitivity, but also prevents the ALB by blocking cytokines and microglial activation. A sex-dependent mechanism could also be at play here, as Michailidis and colleagues (Michailidis et al., 2021) reported a sexual dimorphism in DLB and microglial markers. In this study, male mice displayed DLB earlier than female mice in a neuropathic mouse model and the authors observed an increased number of microglial cells in the contralateral ACC of female but not male neuropathic mice.

Similar to PRA, opioid signaling is implicated in pain-induced ALB as an increase of astrocytes in the ACC due to the dysfunction of delta opioid system in neuropathic animals displaying ALB was reported (Narita et al., 2006). Similarly, 5HT signaling plays an important role since ACC injection of the selective 5HT reuptake inhibitor paroxetine, commonly used as an antidepressant drug, rescued anxiodepressive consequences, but not mechanical hypersensitivity, in animals with neuropathic pain (Matsuzawa-Yanagida et al., 2008). In addition, Zhou and colleagues (Zhou et al., 2022) described lower 5HT levels in the ACC in inflammatory pain-model and that knock-down of 5HT1A-R in the ACC of naive animals mimicked ALB, while 5HT7-R knockdown induced mechanical hypersensitivity, which points to a dual and differential role for 5HT signaling in chronic-pain induced emotional disorders. Likewise, chronic cannabidiol (CB) treatment, was shown to rescue mechanical, heat and cold hypersensitivity as well as ALB, with an increase of CB1-R numbers in the ACC post-treatment (Silva-Cardoso et al., 2021). Finally, oxytocin also seems to play a role in the emotional consequences of neuropathic pain as an acute administration of oxytocin in the ACC attenuated mechanical hypersensitivity and ALB. Interestingly, this effect was shown to act through a reduction in the ratio of E/I transmission in the ACC, with a greater enhancement of inhibitory transmission due to the reduction of evoked excitatory postsynaptic currents amplitude concurrently with the depolarization and increased firing rate of interneurons (Li et al., 2021a).

In conclusion, these studies focusing on the role of the ACC in anxiety- (**Table 2**) and depressive-like (**Table 3**) consequences of chronic pain demonstrate the complexity of the underlying mechanisms. Interestingly, multiple mechanisms deciphered have commonalities with the aversive component of pain (**Fig.4**).

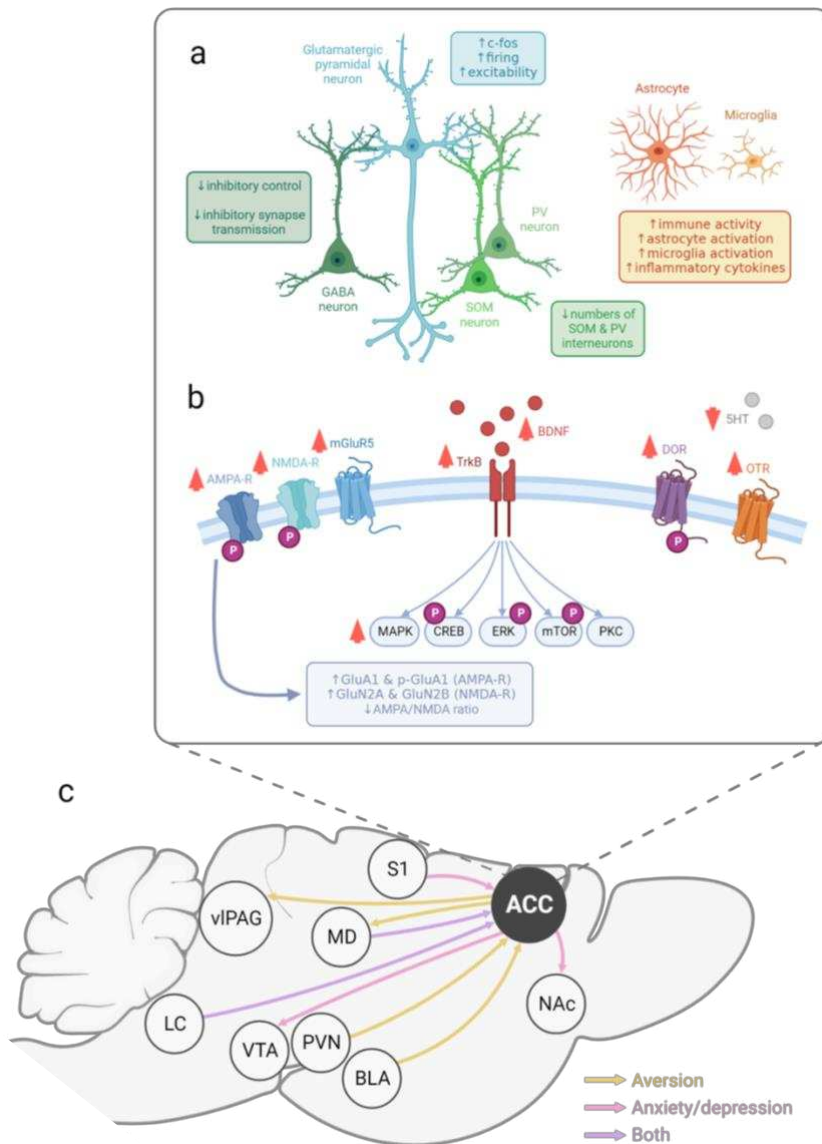


Figure 4. Illustration of the chronic pain-induced molecular and cellular alterations observed in the ACC and its network.

(a) Chronic pain triggers an E/I imbalance shifting the ACC activity toward hyperactivity. Several studies reported increased c-Fos expression, enhanced activity and excitability in ACC pyramidal cells. On the contrary, a loss of inhibitory control has also been observed in chronic pain models, with a decrease in transmission at inhibitory synapses. Morphological alterations were also reported, notably a diminution of the number of SOM and PV neurons, in chronic pain conditions. (b) These functional alterations are concomitant with pain-induced molecular modifications including glutamatergic receptor sub-units (AMPA, NMDA, mGluR5) overexpression, MAP/ERK, mTOR and PKC signaling pathway overactivation as well as alterations in opioid, oxytocinergic and serotonergic systems. (c) All these alterations likely affect the whole ACC connectome. Different studies already highlighted the implication of specific ACC pathways in the chronic pain-induced emotional disorders, such as aversion (yellow), anxiety and depression (pink) or both (violet). *Abbreviations: ACC, anterior cingulate cortex; AMPA, α -amino-3-hydroxy-5-methyl-4-isoxazolepropionic acid; BDNF, brain derived neurotrophic factor; BLA, basolateral nucleus of the amygdala; CREB, c-AMP response element-binding protein; DOR, delta opioid receptor; ERK, extracellular signal-regulated kinases; LC, locus coeruleus; NAc, nucleus accumbens; LP, lateroposterior nucleus; MAPK, mitogen-activated protein kinase; MD, mediodorsal thalamus; mGluR5, metabotropic glutamate receptor 5; mTOR, mechanistic target of rapamycin; NMDA, N-methyl D-aspartate; OTR, oxytocin receptor; PKC, protein kinase C; PV, parvalbumin; PVN, paraventricular nucleus; SOM, somatostatin; S1, primary somatosensory cortex; viPAG, ventrolateral periaqueductal gray; VTA, ventral tegmental area; 5-HT: serotonin.*

5. Conclusion and future directions

Even though the studies that we discussed in this present review strongly support the idea that the ACC is a critical hub, and it is hyperactive when animals experience pain-related aversion or anxiodepressive-like behaviours, further research is needed to fully understand how local ACC alterations occur and what cell types are implicated. Indeed, most of the studies described the role of excitatory cells but the exact implication of inhibitory neurons in the ACC E/I imbalance must be further studied. Indeed, compensatory mechanisms, that could explain such shift in specific cell type activity, cannot be excluded. Moreover, our knowledge concerning the role of the ACC extracellular matrix or non-neuronal cells, such as astrocytes and microglia, is still limited (Kuzumaki et al., 2007; Narita et al., 2006; Panigada and Gosselin, 2011) and should be further explored.

Beside the local mechanisms, the pain-induced shift of the ACC E/I balance toward a hyperactive state likely affects the whole ACC connectome, which likely participates in the development and maintenance of pain-induced emotional disorders. Hence, it appears essential to understand how ACC alterations affect its whole network. Thanks to recent technological advancements in brain imaging and brain activity manipulation, we start to decipher the role of ACC inputs and outputs in the emotional consequences of chronic pain (Gao et al., 2020; Hirschberg et al., 2017; Li et al., 2021a; Llorca-Torralba et al., 2022; Meda et al., 2019; Shen et al., 2021; Singh et al., 2020; Zhu et al., 2022; Zhu et al., 2021). Multi-site fiber photometry (Sych et al., 2019), as well as functional magnetic resonance imaging (McIlwrath et al., 2020; Van der Linden et al., 2007), will now allow the study of large scale brain circuits and will likely bring valuable insight about ACC networks. In addition, these techniques provide necessary tools for longitudinal studies, from the initiation of pain until the development of pain-induced emotional disorders, for description of subtle and time-dependent brain dynamic changes, as well as new potential targets for the development of personalized treatments against emotional disorders in patients suffering from chronic pain.

Acknowledgement: This work was supported by the Centre National de la Recherche Scientifique (contract UPR3212), the University of Strasbourg, the Fondation pour la Recherche Médicale (“Equipe FRM, EQU201903007809 (IY), ARF202110013920 (VM)), a NARSAD Young Investigator Grant from the Brain & Behavior Research Foundation (24736; IY), the French National Research Agency (ANR) through the Programme d'Investissement d'Avenir EURIDOL graduate school of pain ANR-17-EURE-0022 (SJ), ANR-18-CE37-0004 (IY), ANR-18-CE19-0006-03 (IY) and IdEx Attractivité Université de Strasbourg (IY). Figures are created with BioRender.com.

Table 1. Pain related aversion

Species	Pain type	Models	Tests	Observation in the ACC in pain related aversion	Reference
Rats	NP, Inf	CCI, formalin	F-CPA	↑ pERK, PKA & pCREB	Cao et al., 2009
Rats	Visceral	CRD	CPA	↑ neuronal firing in response to colorectal distension	Cao et al., 2012
Rats	Inf	Formalin	F-CPA	↑ p38/MAPK & MKK3/6 activation in GABAergic neurons and microglia	Cao et al., 2014
Rats	Inf	CFA	PEAP	↑ GFAP levels	Chen et al., 2012
Rats	NP	SCI	PEAP	↑ mGluR5 & OX42 levels	Galan-Arriero et al., 2014
Mice	NP	SNI	CPP, PEAP	↑ activity	Gan et al., 2021
Rats	NP	CCI	CPP	neurons projecting to the NAc/VTA are hyperexcitable	Gao et al., 2020
Rats	NP	CCI	CPA	↑ ERK, PKA & CREB activation and SIP30 levels	Han et al., 2014
Mice, Rats	NP, Inf	SNI, postsurgical	CPP	↑ ACC pyramidal neurons excitability	Lançon et al., 2021
Rats	Inf	Formalin	F-CPA	↑ cFos+ cells in layers II-VI	Lei et al., 2004
Rats	Inf	Formalin	F-CPA	↑ NR2AR/NR2BR & cFos, ↑ amplitude of NMDA currents	Li et al., 2009
Rats	NP	BCP	CPA, PEAP	↑ BDNF levels	Li et al., 2022
Rats	Inf	Formalin	F-CPA	↑ GFAP/S100B (astrocyte), IL1b/TNFα (inf. cytokines) mRNA & protein	Lu et al., 2011
Rats	Inf	Formalin	F-CPA	↑ p-mTOR & p-p70S6K levels	Lu et al., 2016
Rats	Inf	CFA	CPA	↑ discharge frequencies in the CFA-compartment of CPA	Ma et al., 2022
Mice	NP	CCI	PEAP	↓ HCN channels in apical dendrites of layer V neurons	Santello et al., 2017
Mice	NP	Cuff	CPP	↑ firing, enhancement of excitatory synapse transmission	Sellmeijer et al., 2018
Rats	Inf	CFA	passive avoidance	↑ BDNF, pERK & BDNF+ cells	Thibault et al., 2014
Rats	NP	SNI	CPA	↑ BDNF, TrkB & pERK levels	Wang et al., 2017
Mice, Rats	Inf, NP	Formalin, SNL	CPP	↑ Kyn/Trp ratio, IDO1, GFAP, IL66, pNMDA2BR, pCDK5, pMAP2 & pTau levels and spine density	Wang et al., 2020
Rats	Inf	Formalin	F-CPA	↑ estrogen levels	Xiao et al., 2013
Rats	NP	SNI	CPP	↑ BDNF, TrkB & NR2B levels	Zhang et al., 2016
Rats	Inf	CFA	CPA	↑ firing rate post acute stimulus	Zhang et al., 2017
Rats	Inf	Formalin	CPA	↑ BDNF, p-mTOR, p-p70S6K & NR2B levels	Zhang et al., 2018
Mice	NP	CCI	CPP	↑ excitability, cfos and excitability of PKCγ neurons	Zhang et al., 2021
Rats	Inf/NP	CFA, SNI	CPA	layer V/VI hyperactivity	Zhou et al., 2018
Mice	NP	Cuff	CPP	ACC lesion blocks pain relief (CPP)	Barthas et al., 2015
Rats	NP	BCP	CPA	NR2BR antagonist injection in the rACC rescues PRA	Feng et al., 2016
Rats	Inf	Formalin	F-CPA	ACC lesion reduces the magnitude of PRA	Gao et al., 2004
Rats	NP	SNL	CPP	Morphine injection in the rACC rescues PRA	Gomtsian et al., 2018
Rats	NP	SNL	CPA	Silencing of NR2BR in the rACC rescues PRA	Guo et al., 2015
Rats	NP	TNT	CPP	LC-ACC chemogenetic activation induces PRA	Hirschberg et al., 2017
Rats	Inf	Formalin	F-CPA	Optogenetic inhibition of ACC Glu+ neurons reduces PRA	Jarrin et al., 2020
Rats	Inf	Formalin	F-CPA	Blockade of Glu-R in the rACC prevents PRA	Johansen & Fields, 2004
Rats	Inf	Formalin	F-CPA	rACC lesion rescues F-CPA	Johansen et al., 2001
Mice	NP	SNI, Chemotherapy	CPP	rACC lesion rescues F-CPA	Juarez-Salinas et al., 2019
Mice	Inf	CFA	CPP	Glu+ cells inhibition creates CPP, PV+ cells activation alleviates mechanical hypersensitivity	Kang et al., 2017
Rats	NP	SNL	PEAP	GABAA & GABAB agonist injection in the rACC attenuate PEAP	LaGraize and Fuchs, 2007
Rats	NP	SNL	PEAP	ACC lesion prevents PRA	LaGraize et al., 2004
Rats	NP	SNL	PEAP	Morphine injection in the ACC rescues PRA	LaGraize et al., 2006
Rats	Acute pain	Acute pain	CPA	ACC high frequency stimulation rescues PRA, while low frequency increases PRA	Liu et al., 2021
Mice	NP	SNI, chemotherapy	CPP	Optogenetic inhibition of MD-ACC pathway induces CPP, BLA-ACC activation elicits CPP	Meda et al., 2019
Rats	NP	Postsurgical, SNL	CPP	Injection of morphine in the rACC produces CPP	Navratilova et al., 2015
Rats	NP	Partial/complete axotomy, SNL	CPP	rACC lesion blocks pain relief (CPP)	Qu et al., 2011
Rats	Inf	Formalin	F-CPA	rACC degradation of d-serine & blockade of NMDA receptor attenuates F-CPA	Ren et al., 2006
Rats	Inf	CFA	CFA-CPA	ACC lesion improves PRA	Shi et al., 2020
Rats	Inf, NP	CFA, SNI	CPA, CPP	S1-ACC inhibition induces CPP	Singh et al., 2020
Mice	NP, Inf	SNI, CFA	CPA	ACC optogenetic stimulation leads to CPA	Tan et al., 2017
Mice, Rats	Acute pain	Acute pain	CPP	GABAA receptor agonist in the ACC reduces unpleasant pain memories	Tang et al., 2005
Rats	Inf	Formalin	F-CPA	GABAA blockade rescues PRA	Wang et al., 2005
Rats	Inf	Formalin	F-CPA	ACC lesion rescues PRA	Yi et al., 2011
Rats	Inf	CFA	CPA	rACC KOR antagonist injection blocks electroacupuncture rescue of CPA	Zhang et al., 2011

Abbreviations: ACC, anterior cingulate cortex; BCP, bone cancer pain; BLA, basolateral nucleus of the amygdala; CCI, chronic constriction injury; CDK5, cyclin-dependant kinase 5; CFA, complete Freund adjuvant; CPA, conditioned place aversion; CPP, conditioned place preference; CRD, colorectal distension; CREB, cAMP response element-binding protein; ERK, extracellular signal-regulated kinase; GABA, γ -aminobutyric acid; GFAP, glial fibrillary acidic protein; Glu, glutamate; HCN, hyperpolarization-activated cyclic nucleotide-gated; IDO1, indoleamine 2,3-dioxygenase 1; IL, interleukin; Inf, inflammatory; F-CPA, formalin-induced CPA; KOR, kappa opioid receptor; Kyn, kynurenine; LC, locus coeruleus; MAPK, mitogen-activated protein kinase; MAP2, microtubule-associated protein 2; MD, mediodorsal thalamus; mGluR5, metabotropic Glu receptor 5; mTOR, mammalian target of rapamycin; NAc, nucleus accumbens; NMDA, N-methyl D-aspartate; NP, neuropathic; NR2A, NMDA subunit NR2A; NR2B, NMDA subunit NR2B; p, phosphorylated; PEAP, place escape/avoidance paradigm; PK, protein kinase; PRA, pain-related aversion; PV, parvalbumin; R, receptor; rACC, rostral ACC; SIP30, SNAP25 interacting protein of 30; SNI, spinal nerve injury; SNL, spinal nerve ligation; S1, somatosensory cortex 1; TNF α , tumor necrosis factor alpha; TNT, tibial nerve transection; TrkB, tropomyosin receptor kinase B; Trp, tryptophan; VTA, ventral tegmental area

Table 2. Anxiety-like consequences of chronic pain

Species	Pain type	Models	Tests	Observation in the ACC in pain-induced anxiety	Reference
Mice	NP	Cuff	NSF	↑ MKP1, pCREB, cFos and active epigenetic regulations on mcp1 gene	Barthas et al., 2017
Mice	Visceral	Colitis	OFT	↑ cfos levels	Brenner et al., 2021
Rats	NP, Inf	Postsurgical	EPM, OFT	↑ pERK1/2 levels biphasically in time	Dai et al., 2011
Rats	Inf	CFA	OFT, EZM	↑ PKCzeta, PKMzeta and GluR1 levels	Du et al., 2017
Rats	Inf	CFI	EPM, LD	↑ fos in layers II-III/IV, ↓ AMPA/NMDA ratio	Ducret et al., 2022
Mice	Inf	CFA	OFT	↓ number and function of mGluR5	Guo et al., 2018
Mice	Inf, NP	SNI, CFA	EPM, OFT	↑ ECM genes expression, ↓ LAMB1 gene expression	Li et al., 2021b
Mice	NP	CPNL	EPM, OFT	↑ oxytocin receptor expression	Li et al., 2021a
Rats	Inf	Formalin	OFT	↑ pERK levels	Luo et al., 2015
Rats	Acute pain	vF	EPM, OFT	↑ firing in response to cutaneous mechanical stimulation	Mastumoto et al., 2020
Rats	NP	CCI-ION	EPM, LD	↑ T1 and T2 signal (edema and astrogliosis resp.)	McIlwrath et al., 2020
Mice	NP	SNL	EPM, LD	↑ pDOR immunoreactivity, ↓ DOR function	Narita et al., 2006
Rats	Visceral	chronic pancreatitis	EPM, OFT	↑ fos+ cells in layers II/III & V/VI, vGluT1, membrane GluR1 & pGluR1 (AMPA), membrane NR2B & pNR2B (NMDAR)	Ren et al., 2022
Mice	NP	Cuff	LD, NSF	↑ firing rates, enhancement of excitatory synapse transmission	Sellmeijer et al., 2018
Rats	NP	SNI	EPM, OFT	↓ volume, correlated to mechanical hypersensitivity	Seminowicz et al., 2009
Rats	NP	SNL	EZM	↑ pERK1/2+ cells and pERK levels in layers II-VI	Shao et al., 2015
Rats	Inf	CFA	OFT, EZM, NSF	↓ PV and SOM interneurons	Shao et al., 2021a
Rats	Inf	CFA	OFT, EZM, NSF, marble	↑ fos levels and excitability of pyramidal cells, ↓ PV+ cells in layer V and ↓ inhibitory synaptic transmission	Shao et al., 2021b
Mice	Inf	CFA	EPM, OFT	↑ astrocytes & microglia activation and GluN2A/GluN2B, GluA1, CaMKII-α, pP38 & pJNK MAPK & TNFα/IL6 levels	Sun et al., 2016
Mice	Visceral	IBS	EPM, OFT	↑ GluA1, pGluA1, synaptophysin, PSD95 & CPEB1 levels	Wang et al., 2019
Rats	Inf, NP	Formalin, SNL	OFT	↑ Kyn/Trp ratio, IDO1, GFAP, IL66, pNMDA2BR, pCDK5, pMAP2 & pTau levels and spine density	Wang et al., 2020
Rats	NP	SNI	EPM, OFT, NSF	↑ fos, PSD95, neuroligin2, CREB, pCREB, CaMKIIα levels	Wen et al., 2022
Rats	OIH	Remifentanyl	EPM, OFT	↑ pGluR1 and cfos levels, ↓ Arc levels	Zeng et al., 2018
Mice	Visceral	IBS	EPM, OFT, LD	↑ fos expression in layers II-III	Zhang et al., 2014
Rats	NP	CCD	EPM, OFT	↑ pyramidal neurons excitability, ↓ function of BKCa channels	Zhao et al., 2020
Mice	Visceral	Acetic acid	EPM, OFT	↑ pERK1/2+ cells	Zhong et al., 2012
Mice	Inf	CFA	EPM, OFT	↑ fos, ↓ 5HT levels	Zhou et al., 2022

Table 2. (continued)

Species	Pain type	Models	Tests	Observation in the ACC in pain-induced anxiety after manipulation	Reference
Mice	NP	Cuff	NSF, marble	ACC lesion prevents ALB	Barthas et al., 2015
Rats	NP	TNT	OFT	LC-ACC chemogenetic activation induces ALB	Hirschberg et al., 2017
Mice, Rats	NP	SNL	EPM, LD	Paroxetine (SSRI) injection into the ACC rescues ALB	Matsuzawa-Yanagida et al., 2008
Rats	Inf	CFA	OFT	Chemogenetic inhibition of rACC-thalamus rescues ALB	Shen et al., 2021
Rats	NP	CCI	OFT	Subchronic CBD treatment increases CB1 & TRPV1 receptors in the ACC	Silva-Cardoso et al., 2021
Mice	NP	SNI	EPM, OFT	Chemogenetic inhibition of rACC(Glu)-vIPAG pathway rescues mechanical hypersensitivity & ALB	Zhu et al., 2022

Abbreviations: ACC, anterior cingulate cortex; ALB, anxiety-like behavior; AMPA, α-amino-3-hydroxy-5-methyl-4-isoxazolepropionic acid; BKCa, large-conductance voltage- and Ca²⁺-activated potassium channel; CaMKIIα, calcium calmodulin-dependent protein kinase II alpha; CBD, cannabidiol; CB1, cannabinoid receptor type 1; CCD, chronic constriction of multiple dorsal root ganglia; CCI, chronic constriction injury; CCI-ION, CCI of the infraorbital nerve; CDK5, cyclin-dependent kinase 5; CFA, complete Freund adjuvant; CFI, chronic facial inflammatory; CPEB1, Cytoplasmic Polyadenylation Element Binding Protein 1; CPNL, common peroneal nerve ligation; CREB, cAMP response element-binding protein; CRS, chronic restraint stress; DOR, delta opioid receptor; ECM, extracellular matrix; EPM, elevated plus maze; ERK, extracellular kinase-regulated kinase; EZM, elevated zero maze; GFAP, glial fibrillary acidic protein; Glu, glutamate; IBS, irritable bowel syndrome; IDO, indoleamine 2,3-dioxygenase 1; IL, interleukin; Inf, inflammatory; Kyn, kynurenine; LAMB1, laminin subunit beta 1; LC, locus coeruleus; LD, light-dark; LPS, lipopolysaccharide; MAPK, mitogen-activated protein kinase, mGluR5; metabotropic Glu receptor 5; MKP1, MAPK phosphatase 1; NMDA, N-methyl D-aspartate; NR2B, NMDA subunit NR2B; NSF, novelty suppressed feeding; NP, neuropathic; OIH, opioid-induced hyperalgesia; OFT, open field test; p, phosphorylated; PK, protein kinase; PSD95, postsynaptic density protein 95; PV, parvalbumin; R, receptor; rACC, rostral ACC; SNI, spinal nerve injury; SNL, spinal nerve ligation; SOM, somatostatin; SSRI, selective serotonin reuptake inhibitor; TNFα, tumor necrosis factor alpha; TNT, tibial nerve transection; Trp, tryptophan; TRPV1, transient receptor potential vanilloide 1; UCMS, unpredictable chronic mild stress; vF, von Frey; vGluT1, vesicular Glu transporter 1; vIPAG, ventrolateral periaqueductal gray; 5HT, serotonin

Table 3. Depressive-like consequences of chronic pain

Species	Pain type	Models	Tests	Observation in the ACC in pain-induced depression	Reference
Mice	NP	Cuff	splash, FST	↑ MKP1, pCREB, cFos and active epigenetic regulations on mcp1 gene	Barthas et al., 2017
Rats	NP	CCI	FST, anhedonia	↑ pERK, ↓ neuronal density	Bravo et al., 2012
Mice	NP	CCI	FST, TST	↓ 5HT, BDNF & CREB levels	Cong et al., 2021
Mice ♀	NP	SNI	splash, FST, TST	Transcriptomic differences stronger in females with neurotransmitter release & ECM impacted	Dai et al., 2022
Mice	NP	Cuff	splash, FST, NSF	↑ MKP1 levels, ↓ pERK levels	Humo et al., 2020
Rats	Inf	FST + CFA	FST	↑ pCREB+ and Egr1+ cells	Imbe & Kimura, 2017
Rats	NP	CCI	FST	↑ pERK1/2+ cells, ↓ BDNF levels	Ishikawa et al., 2014
Rats	NP	CCI	FST	↑ pERK1/2+ cells, ↓ pCREB & BDNF levels	Ishikawa et al., 2015
Mice	Inf, NP	SNI, CFA	TST, SPT	↑ ECM genes expression, ↓LAMB1 gene expression	Li et al., 2021b
Rats	Depression-induced pain	Chronic FST	FST	↑ activity of neurons	Liu et al., 2019
Rats	NP	CCI	FST	LC-rACC projection is activated after pain	Llorca-Torralba et al., 2022
Mice	NP	SNI	FST, TST, SPT	↑ microglia in females	Michailidis et al., 2021
Rats	NP	SNI	FST, SPT	↓ neuroligin1 & BDNF levels	Pan et al., 2018
Rats	Inf	Monoarthritis	FST	↑ pERK levels	Pereira-Silva et al., 2020
Rats	Visceral	Chronic pancreatitis	FST	↑ fos+ cells in layers II/III & V/VI, vGluT1, membrane GluR1 & pGluR1, membrane NR2B & pNR2B	Ren et al., 2022
Mice	NP	Cuff	splash, FST, NSF	↑ firing rates, enhancement of excitatory synapse transmission	Sellmeijer et al., 2018
Rats	NP	SNI	FST, NSF	↑ fos, PSD95, neuroligin2, CREB, pCREB, CaMKIIa levels	Wen et al., 2022
Mice	NP	Cuff	/	MAPK pathway is altered at 2w & 8w post surgery	Xiao et al., 2021
Rats	NP	CCI	FST	↑ pERK1/2+ cells, ↓ pCREB+ cells & BDNF levels	Yasuda et al., 2014
Mice	Inf, NP	CFA, SNI	FST, TST, SI	↑ spike number & cFos in Glu+ neurons, ↓excitability of GABA+ neurons	Zhu et al., 2021

Species	Pain type	Models	Tests	Observation in the ACC in pain-induced depression after manipulation	Reference
Mice	NP	Cuff	splash, FST	ACC lesion or optogenetic inhibition of CaMKII+ cells prevent DLB	Barthas et al., 2015 Sellmeijer et al., 2018

Abbreviations: ACC, anterior cingulate cortex; BDNF, brain-derived neurotrophic factor; CaMKIIa, calcium calmodulin-dependent protein kinase II alpha; CCI, chronic constriction injury; CFA, complete Freund adjuvant; CREB, cAMP response element-binding protein; DLB, depression-like behavior; ECM, extracellular matrix; Egr1, early growth factor 1; ERK, extracellular signal-regulated kinase; FST, forced swim test; GABA, γ -aminobutyric acid; Glu, glutamate; Inf, inflammatory; LAMB1, laminin subunit beta 1; LC, locus coeruleus; LPS, lipopolysaccharide; MAPK, MAPK, mitogen-activated protein kinase; MKP1, MAPK phosphatase 1; NMDA, N-methyl D-aspartate; NR2B, NMDA subunit NR2B; NP, neuropathic; NSF, novelty-suppressed feeding; p, phosphatase; PSD95, postsynaptic density protein 95; R, receptor; rACC, rostral ACC; SI, social interaction; SNI, spinal nerve injury; SPT, sucrose preference test; TST, tail suspension test; vGluT1, vesicular Glu transporter 1; 5HT, serotonin; ♀, study realized in both males and females, if not specified, only males were used

The ACC to lateral habenula pathway

Even nowadays, most of the studies focus on a single brain area in the chronic pain and emotional disorders dyad. However, changes occurring in hub structures such as the ACC are likely coming from afferent brain structures and propagating to efferent structures. It is thus important to consider the ACC's circuitry in order to decipher the contribution of its afferents in the comorbidity between chronic pain and emotional disorders, but also how it affects downstream targets, which could worsen the development and maintenance of the comorbidity. Previous results from our team have already highlighted the critical role of basolateral amygdala (BLA) projections to the ACC in the depressive-consequences of chronic pain (Becker et al., 2023). Indeed, inhibition of the BLA-ACC pathway in our cuff model rescued depressive-like behaviours, but not anxiety-like and nociceptive behaviours. It is now important to study how information arriving to the ACC are conveyed to other brain areas. Our team's work on the ACC connectome (Figure 17A) (Fillinger et al., 2017a, 2017b) Fillinger *et al.*, 2016; 2017) showed a connection between the ACC and the lateral habenula (LHb). Additionally, our resting state functional MRI (fMRI) in collaboration with ICube (UMR7357) demonstrated decreased functional connectivity alterations between the ACC and the habenula in neuropathic animals (Figure 17B; unpublished data). Altogether these results pinpoint the possible implication of the ACC-LHb pathway in the emotional consequences of chronic neuropathic pain.

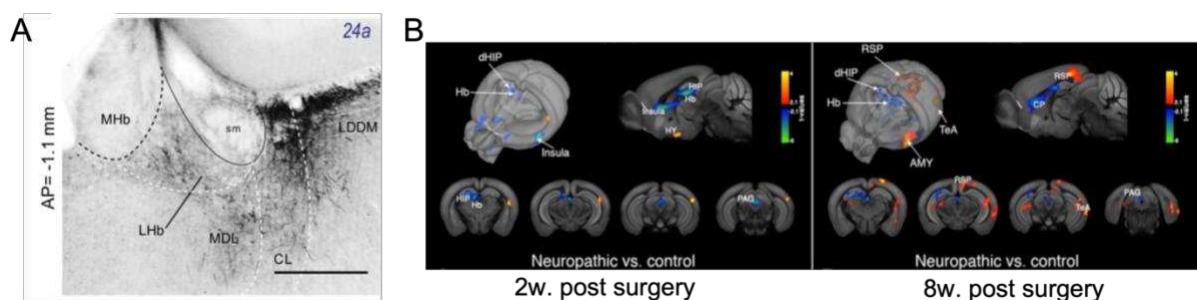


Figure 17. (A) Injections of an anterograde tracer in area 24a of the ACC moderately labels the LHb. (B) fMRI Inter-group statistical differences of ACC functional connectivity highlights a decreased functional connectivity between the ACC and the Hb. ACC, anterior cingulate cortex; AMY, amygdala; CL, centrolateral thalamic nucleus; CP, caudate putamen; dHip, dorsal hippocampus; Hb; habenula; HIP, hippocampus; HY, hypothalamus; LDDM, dorsomedial part of the laterodorsal thalamic nucleus; LHb, lateral habenula; MDL, lateral part of the mediodorsal thalamic nucleus; MHb, medial habenula; PAG, periaqueductal gray; RSP, retrosplenial cortex; sm, stria medullaris; TeA, temporal association cortex. Adapted from Fillinger *et al.* (2017b)

The lateral habenula (LHb)

The habenula (Hb) is a paired epithalamic structure conserved throughout evolution and located on the dorsomedial surface of the caudal thalamus (Stephenson-Jones et al., 2012). In mammals (and amniotes more widely), it is symmetrical and consists in two major nuclear complexes: the smaller medial habenula (MHb), comprising dense small neurons, and the larger LHb, which consists of larger neurons more loosely packed (Figure 18A) (Aizawa et al., 2012; Zahm and Root, 2017). Since the focus of my thesis work was the LHb, I will highlight its neuroanatomical organisation, function, and especially its role in pain and emotional disorders in the following subsections.

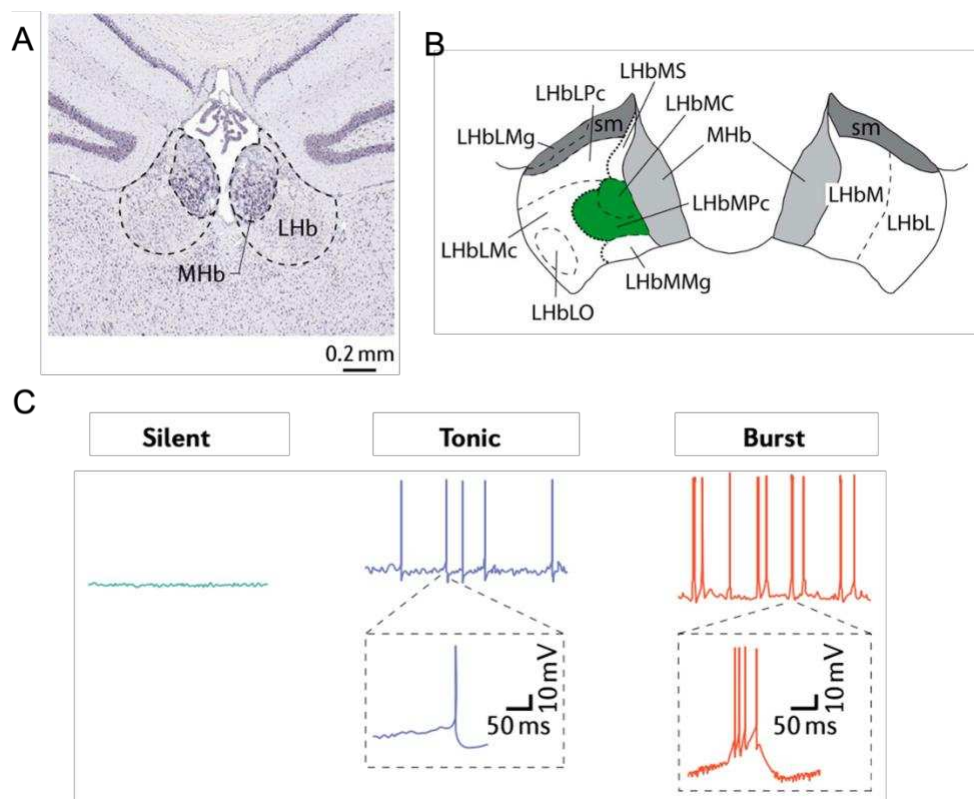


Figure 18. (A) Lateral habenula (LHb) and medial habenula (MHb) anatomical localisation. (B) A first subdivision of the LHb can be done between its medial (LHbM) and lateral parts (LHbL). Further division segregates the magnocellular subnucleus of the lateral division of the LHb (LHbLMc), the marginal subnucleus of the lateral division of the LHb (LHbLMg), the oval subnucleus of the lateral division of the LHb (LHbLO), the parvocellular subnucleus of the lateral division of the LHb (LHbLPC), the central subnucleus of the medial division of the LHb (LHbMC), the marginal subnucleus of the medial division of the LHb (LHbMMg), the parvocellular subnucleus of the medial division of the LHb (LHbMPc) and the superior subnucleus of the medial division of the LHb (LHbMS). (C) LHb neurons exhibit different activity patterns depicted here, with silent, tonic or bursting neurons, regardless of their localisation. *Adapted from Zahm and Root (2017) and Hu et al. (2020).*

Neuroanatomy, cytoarchitecture and neuronal properties of LHb

In humans, 5 LHb subregions have been identified based on Nissl staining (Díaz et al., 2011), whereas in rodents, thanks to tracing, immunohistology and electrophysiological studies, up to 10 LHb subregions have been described (Figure 18B) (Aizawa et al., 2012; Wagner et al., 2014; Weiss and Veh, 2011), which can be divided between the lateral (LHbL) and medial part of the LHB (LHbM).

The LHb is composed of mainly 4 categories of projection neurons: spherical, fusiform, polymorphic and vertical; and of neurogliaform cells which are supposedly interneurons (Weiss and Veh, 2011). These different projection neurons are found throughout the whole LHb, thus are not specific of one particular subregion. Electrophysiological recordings of these different types of neurons allowed the characterisation of different discharge profiles, which are not linked to the neuron's morphology (Kowski et al., 2009; Weiss and Veh, 2011). They include silent neurons, neurons with regular tonic repetitive firing of single action potentials, neurons with irregular tonic repetitive firing of single action potentials or neurons with rhythmic burst firing of trains of single action potential (Figure 18C). Interestingly, Sakhi and collaborators (2014a, 2014b) have described in mice a daily profile of firing activity based on circadian rhythms.

This heterogeneity is also found when focusing on the neurochemical profile of LHb neurons, which present a huge variety of neuronal markers (Aizawa et al., 2012; Wagner et al., 2014). Firstly, most of LHb neurons are glutamatergic, evidenced by the presence of the vesicular glutamate transporter 2, with a small proportion of GABAergic neurons, which can sparsely be found in the oval part of the LHbL (Aizawa et al., 2012; Brinschwitz et al., 2010). However, a recent single-cell transcriptional profiling study in mice could not find any evidence of GABAergic neurons in the LHb. Indeed, they only observed expression of the GABA synthetic enzyme *Gad2* and the GABA transporter *Slc6a1* throughout the LHb, but not of *Slc32a1* or *Slc18a2*, which are needed for vesicular loading of GABA (Wallace et al., 2020). This could be explained by the relatively small number of GABAergic cells in the LHb. In addition, an important concentration of tyrosine hydroxylase, the enzyme responsible for the synthesis of dopamine and norepinephrine was observed in the rats LHb, but not in the mice (Wagner et al., 2014). In subregions of the LHb, acetylcholine degradation enzyme and

vesicular transporter can also be observed (Aizawa et al., 2012; Wagner et al., 2016). Finally, neuropeptides, such as vasopressin, substance P, somatostatin or melatonin, can also be observed in the LHb (Salaberry and Mendoza, 2015; Zahm and Root, 2017). Concerning receptors expressed in LHb neurons, glutamatergic AMPA, NMDA and metabotropic receptors (mGluR1, 3 and 5) have been identified (Li et al., 2011; Maroteaux and Mameli, 2012; Meye et al., 2013; Valentinova and Mameli, 2016; Wagner et al., 2016). GABAergic receptors GABA_A and GABA_B are also found in the LHb (Meye et al., 2013). In addition, an heterogeneous expression of monoaminergic receptors throughout the LHb have been observed, such as the dopamine type 2 receptor, the serotonin type 2c receptor (Aizawa et al., 2012).

Altogether, these results indicate a great variety in LHb neurons, strongly suggesting its role as an integrative structure.

Connectivity

The central anatomical localisation of the LHb makes it a potential relay hub. Indeed, most of its afferents are forebrain structures, while its efferents are in the midbrain and brainstem (Figure 19).

The first studies of the LHb connectome were performed in rats by Herkenham and Nauta (1979, 1977). They mainly described the main afferent of the LHb: the entopeduncular nucleus (EPN; the rodent homolog of the internal segment of the globus pallidus), one of the principal outputs of the basal ganglia. Other major LHb afferents include the lateral hypothalamus (LH) or the lateral preoptic area (LPO) (Herkenham and Nauta, 1977). Otherwise, the LHb also receives weaker afferents from the ventral pallidum, the nucleus accumbens, the olfactory bulb, the retina, the suprachiasmatic nucleus, the septum, the diagonal band of Broca, the bed nucleus of the stria terminalis, the lamina I of the dorsal horn of the spinal cord, the nucleus incertus, the periaqueductal gray, the MHb, the insular cortex and the PFC (Herkenham and Nauta, 1977; Kim and Chang, 2005; Kim and Lee, 2012; Zahm and Root, 2017). PFC projections arise from its three divisions, the infralimbic, prelimbic and cingulate cortices and are terminating specifically in subregions of the LHb (Kim and Lee, 2012). Some connections are reciprocal, such as the afferents from the raphe nuclei or the ventral tegmental area (VTA) (Herkenham and Nauta, 1979; Zahm and Root, 2017). At

the functional level, these projections arise from different structures processing either sensory, emotional, limbic signals or internal state information.

Concerning efferents of the Lhb, the principal targets of the Lhb are monoaminergic centres: the serotonergic median and dorsal raphe nuclei, and the dopaminergic substantia nigra (SN) and VTA (Herkenham and Nauta, 1979). The Lhb also interestingly targets the inhibitory region of the two dopaminergic centres, the tail of the VTA (tVTA). Other efferents include the nucleus incertus, the mamillary and supramamillary nuclei, several thalamic nuclei, the ventral pallidum and or periaqueductal gray (Herkenham and Nauta, 1979).

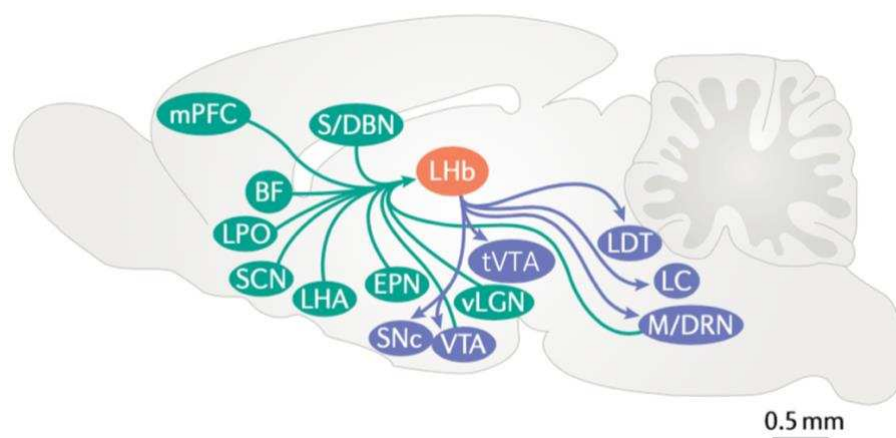


Figure 19. Schematic representation of the afferents (green) and efferents (blue) of the lateral habenula (Lhb, orange). BF, basal forebrain; EPN, entopeduncular nucleus; LC, locus coeruleus; LDT, laterodorsal tegmental nucleus; LHA, lateral hypothalamic area; LPO, lateral preoptic area; M/DRN, medial/dorsal raphe nucleus; mPFC, medial prefrontal cortex; SCN, suprachiasmatic nucleus; S/DBN, septum and diagonal band of Broca; SNc, substantia nigra pars compacta; tVTA, tail of the ventral tegmental area; vLGN, ventral lateral geniculate nucleus; VTA, ventral tegmental area.

Adapted from Hu et al. (2020).

Functions

The connectivity of the Lhb places it as a perfect candidate for an integrative role between forebrain limbic and midbrain/brainstem regions, thus modulating different functions through its control on monoaminergic structures. Indeed, through direct and indirect connection onto the VTA, the SN and the raphe, and indirectly towards the tVTA (Brinschwitz et al., 2010; Zahm and Root, 2017) it induces a tonic inhibition on dopamine and serotonin release (Matsumoto and Hikosaka, 2007). Therefore, the Lhb

can fine-tune the liberation of monoamines in the brain based on the information it receives on sensory, emotional and internal state changes.

The LHb regulates many physiological functions, including reward and aversion, pain, sleep and circadian rhythms, cognition, navigation and maternal behaviours and motor functions (Hu et al., 2020).

Concerning reward and aversion, it is well described that the LHb is activated by aversive stimuli and omission of rewards, while its activity decreases in a rewarding condition (Matsumoto and Hikosaka, 2007), especially in non-human primates. This is in line with its position upstream to the dopaminergic reward centres: when a reward happens, LHb's activity decreases, which in turns disinhibits the dopaminergic cells. Inversely, LHb's activity increases and the dopaminergic neurons' activity decreases in the response to a punishment or an omission of reward. Since the LHb does not only react to aversive stimuli (e.g., a punishment), but also to an omission of reward when it was expected, it is believed that the LHb is in fact involved in the re-evaluation of the current situation, i.e., value change, and therefore is important for the following actions that need to be taken (Hikosaka, 2010). In addition, through its connection towards serotonergic centres, the LHb is thought to play a role in value state, i.e., the value of a stimulus, encoded by serotonergic neurons. They indeed exhibit a change in their tonic activity after the value of the reward is updated. Control on both value state (serotonergic neurons) and value change (dopaminergic neurons) places the LHb as a perfect hub to control reward-based decision making (Hu et al., 2020). On the aversive side, the LHb is also well-known to encode aversive states. Indeed, in rodents several negative emotional stimuli or stressors (e.g., inescapable foot/tail shocks, physical restraint, maternal deprivation, social defeat stress, etc.) elicit a neural activation in LHb cells, as reflected by increased *Fos* expression, calcium activity and spontaneous firing recorded in electrophysiological recordings (*in vivo* & *ex vivo*) (Benabid and Jeaugey, 1989; Carr et al., 1998; Chastrette et al., 1991; Wirtshafter et al., 1994). Interestingly, an aversive state can be produced by stimulating excitatory afferents to the LHb, or efferents from the LHb towards the tVTA or the VTA, confirming the important role of the LHb in the modulation of aversion (Hu et al., 2020). Because of its role in both reward and aversion, and its afferents from structures processing

sensory inputs, the LHb is essential for behavioural flexibility, which allows an animal to adapt its behaviour based on internal states and external cues.

Role in emotional disorders

Due to its role as an “anti-reward” centre, the LHb is thought to be implicated in multiple psychiatric disorders in which the reward system is malfunctioning.

The most well-known psychiatric condition in which there is a malfunction of the LHb is depression. Indeed, clinical studies have reported (i) an increased activity of the LHb in depressive patients (Morris, 1999), (ii) rapid and sustained relief from depression after deep brain stimulation (DBS) of the lateral habenula in a therapy-refractory patient (Sartorius et al., 2010; Sartorius and Henn, 2007). Its activation in depression is consistent with the monoamine hypothesis of depression, which postulates that depletion in monoamines drives the disease, as it regulates monoaminergic brain centres, thus monoamine release. Preclinical studies showed that the LHb is hyperactive in three different rat models of depression, including stress-, drug injection- and chronic amphetamine-induced depression models (Caldecott-Hazard et al., 1988). This hyperactivity is thought to be driven by an increase in the percentage of bursting neurons, which are not numerous under normal physiological conditions, but doubles in several rodent models of depression (Han et al., 2015; Seo et al., 2018; Yang et al., 2018). Cui and collaborators (2018) have highlighted that this bursting activity is potentially due in parts to astrocytes and glial potassium channel Kir4.1. Indeed, Kir4.1 is upregulated in depressive-like rats. Kir4.1 overexpression in LHb astrocytes of naïve mice drives depressive-like behaviours and the increased burst firing associated with it. The implication of burst firing neurons in depression was further explored by Yang and colleagues (2018), showing that an optogenetic activation driving LHb burst firing in naïve mice produced depressive-like behaviours. Several other studies manipulating the LHb in rodents to activate or inhibit it resulted in depressive-like behaviours in naïve animals or antidepressant effects in depression models respectively (Cui et al., 2018; Lecca et al., 2016; Li et al., 2013). Deep brain stimulation was also performed in a rat model of depression and rescues depressive-like symptoms in the same way as in humans (Meng et al., 2011). Considering that the LHb receives multiple sensory inputs, and that depression is a disease based on

circuitry changes, the implication of afferents to the LHb have been recently explored. The VTA-LHb (Root et al., 2018) and EPN-LHb (Shabel et al., 2014) pathways for example were shown to have an increased probability of synaptic release in depressive-like animals, while LH-LHb synaptic potentiation occurs in stress-induced depression (Zheng et al., 2022). In addition, the EPN-LHb pathway, which co-releases GABA and glutamate onto LHb synapses, exhibits an imbalance of co-released transmitters, favoring glutamate release, thus probably over activating LHb neurons (Shabel et al., 2014).

At the level of the LHb itself, postsynaptic mechanisms have been highlighted, with increased activity of calcium/calmodulin-dependent protein kinase II subunit-beta (CaMKIIbeta) (Li et al., 2013) and of protein phosphatase 2A (PP2A) (Lecca et al., 2016). On one hand, CaMKIIbeta is regulating AMPARs trafficking. Thus, an increase in its activity or its upregulation leads to increased AMPARs found at the synapse, resulting in enhanced synaptic efficacy (Li et al., 2013). On the other hand, PP2A regulates GABA_B receptor signaling and an increase in its activity reduces GABA_B receptor inhibitory currents, which results in increased neuronal activity (Lecca et al., 2016). Both these mechanisms have been described in depressive-like animals, and their induction in naïve animals creates depressive-like phenotypes (Lecca et al., 2016; Li et al., 2013).

In summary, all these studies seem to emphasize the crucial role of the LHb in depression, with several mechanisms tightly interacting and creating a hyperactivity of the LHb, which drives depressive phenotypes.

Role in chronic pain

While the LHb's role in reward and aversion, and thus emotional disorders is well described and almost common sense when knowing its physiological role in reward-based decision making and behavioural flexibility, there is also a potential role for the LHb in the processing of pain. It is indeed well located within the pain transmission system as it receives direct inputs from the spinal cord or indirect through the LH or the NAc, and is also contacted by cortical areas processing pain, such as the insular cortex. In addition, it sends efferents to pain modulatory regions, i.e., the PAG and dorsal raphe nucleus (DRN).

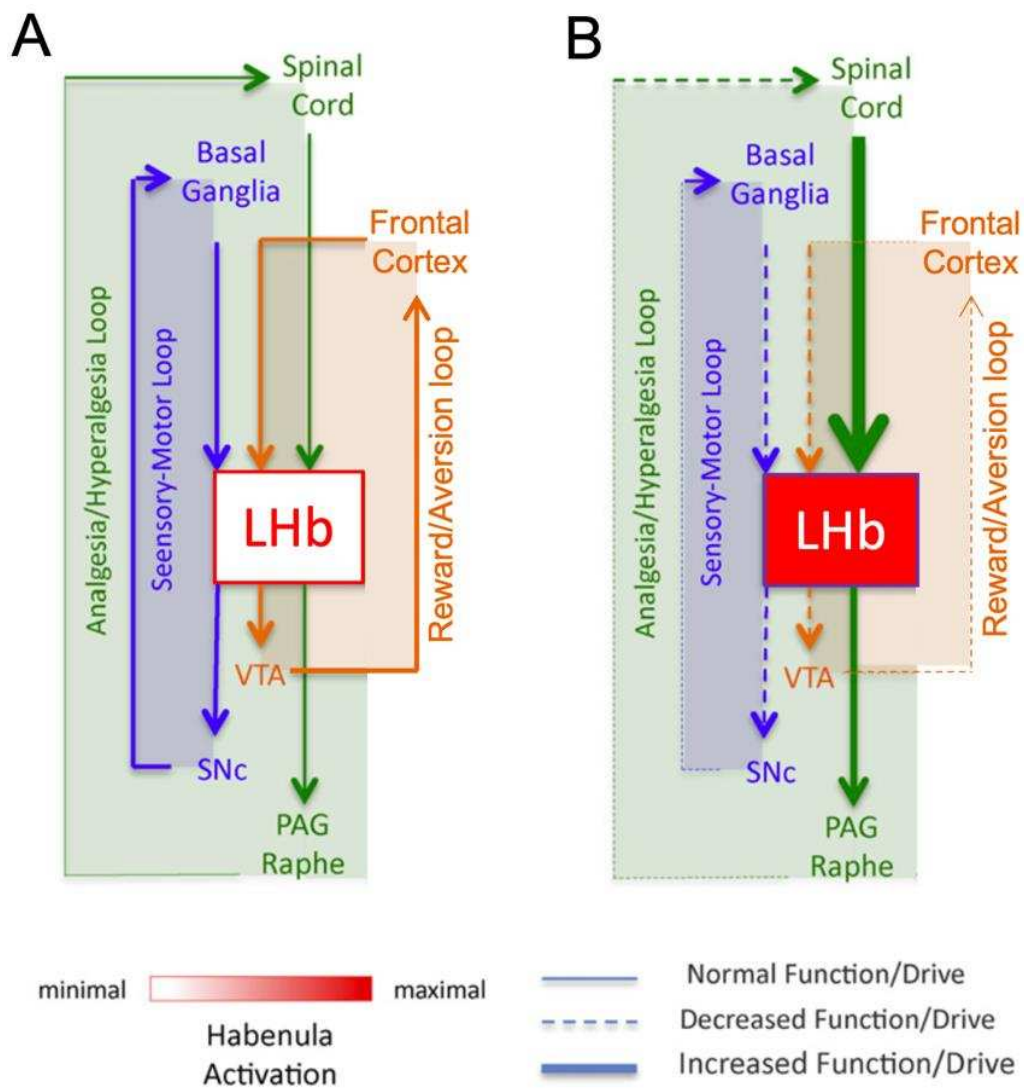


Figure 20. Schematic model of lateral habenula (LHb) circuit divided between functional loops under normal physiological conditions (A) and in the context of chronic pain (B). In chronic pain, there is an imbalance between all the functional loops, which reinforces the activation of the LHb. PAG, periaqueductal gray; SNc, substantia nigra pars compacta; VTA, ventral tegmental area. *Adapted from Shelton et al. (2012).*

Interestingly, in anaesthetised rats, electrophysiological recordings have highlighted an excitatory response of LHb neurons after peripheral noxious stimuli (Benabid and Jeaugey, 1989; Gao et al., 1996). In addition, infusion of morphine in the Hb produces analgesia. These results in acute pain pinpoint the LHb as a potential actor in chronic pain (Shelton et al., 2012). A few studies focusing on rodents' chronic pain models have shown the LHb implication in this important clinical issue.

Paulson and collaborators have also shown the implication of the Hb in a neuroimaging study, with increased Hb activity in rats after spinal cord damage (Paulson et al., 2005) or diabetes-induced neuropathic pain (Paulson et al., 2007). In humans, this result was confirmed by a few fMRI studies (Roiser et al., 2009; Ullsperger and von Cramon, 2003). However, these results take the Hb as a whole as the current fMRI resolution is not sufficient to distinguish its subregions.

A possible model for the LHb implication in chronic pain was proposed by Shelton and collaborators (2012). As stated earlier, the LHb is connected to several brain regions, placing it as hub between sensory, emotional and internal state processing regions. The LHb circuitry can therefore be divided into several distinct, but interconnected loops based on its afferents and efferents (Figure 20A): pain processing (i.e., afference from SC and afferences to PAG & DRN), reward/aversion (i.e., afferences from PFC and efferences to dopaminergic & serotonergic centres, especially VTA) and sensory motor (afference from basal ganglia and efference to SN). In chronic pain conditions, these functional circuits' weight is differentially distributed, causing an imbalance between the loops, therefore probably reinforcing pain (Figure 20B).

Role in the emotional consequences of chronic pain

As mentioned earlier, the role of the LHb in depression has been widely studied, but mostly in stress-, environment-induced or genetic rodent models. Because the LHb is thought to be a key actor in chronic pain, a few groups have started to look more closely at the LHb and its role in the emotional consequences of chronic pain.

Li and collaborators (2016) have shown that LHb neurons discharge at a higher frequency in a model of depression, and that almost 75% of these high-frequency neurons were activated by a formalin injection, i.e., by a noxious stimulus. c-Fos expression was interestingly increase in depressive rats, in control rats with formalin

injection, but even more in depressive rats that received a formalin injection, which was reversed by the TCA clomipramine treatment. This could mean that both conditions (i.e., depression and noxious stimuli) are potentiating each other and therefore LHB neuronal response. This fits well with the behavioural output that was observed, in which the depressive-like rats were exhibiting stronger responses to noxious stimuli compared to controls. The same group next examined the LHB in the context of chronic pain-induced mood disorders (Li et al., 2017). In a rat model of chronic constriction injury inducing a depressive-like phenotype, they demonstrated that the LHB has an increased activity, concurrent with increased CaMKIIbeta expression. Interestingly, DRN activity was decreased, supporting that depression induced by chronic pain could be driven by LHB-DRN pathway hyperactivity. On the other hand, lesion of the LHB was able to improve both mechanical hypersensitivity and depressive-like behaviours (Li et al., 2017), similarly to what they observed when lesioning the LHB in their rat model of depression with increased hypersensitivity (Li et al., 2016).

Another group, working this time with a mice model of trigeminal neuralgia in which orofacial mechanical hypersensitivity is associated with anxiety-like behaviours, also studied the role of the LHB in this comorbidity (Cui et al., 2020; W.-W. Zhang et al., 2023; Zhuang et al., 2022). They showed that their model induced an increased excitability of LHB neurons, which correlated with behavioural outputs. Gene expression analysis revealed that *Tacr3*, a gene previously involved in other diseases, was downregulated in their model. When overexpressing this gene in the LHB of their trigeminal neuralgia model, they showed that this alleviated anxiety-like behaviour, mechanical hypersensitivity and LHB hyperactivity, in the same way as bilateral chemogenetic inhibition of glutamatergic (Glu+) neurons (Cui et al., 2020). More recently, the same group showed that bilateral chemogenetic activation of LHB Glu+ neurons in naïve mice induced orofacial mechanical hypersensitivity and anxiety-like behaviours, same as in their model (Zhuang et al., 2022). They revealed an increased phosphorylation of NMDA receptors and CaMKII in LHB neurons, and that bilateral inhibition of NMDA and CaMKII alleviated to some extent both nociceptive and anxiety-like behaviours. On the opposite, bilateral chemogenetic activation of CaMKII+ neurons triggered mechanical hypersensitivity and anxiety-like behaviours in naïve

animals, supporting their role in the comorbidity. Finally, in their newest study, they investigated the role of tachykinin receptor 3, which is encoded by the *Tacr3* gene, in the LHb in chronic pain-induced anxiety (W.-W. Zhang et al., 2023). Pharmacological activation or inhibition of NK3R reduced the hyperexcitability of LHb neurons or induced hyperactivity, respectively. Activation of this receptor by its ligand neurokinin B, which is released by the PAG into the LHb, rescued chronic-pain induced anxiety-like symptoms (W.-W. Zhang et al., 2023). These results point to the PAG-LHb pathway as a good candidate for future therapeutical approaches.

In terms of circuits involving the LHb and implicated in the emotional consequences of chronic pain, Zhou and collaborators (2019) realised an elegant study, in which they highlighted the role of central amygdala somatostatin neurons contacting LHb Glu+ neurons in the spinal nerve injury (SNI) model in mice. Optogenetic activation of this pathway in naïve animals induced depressive-like behaviours, whereas its optogenetic inhibition alleviated chronic pain-induced depressive-like behaviours.

It is particularly interesting to note that, even though the LHb seems implicated in both chronic pain and its emotional consequences, manipulating different afferent pathways can produce different outcomes. However, it is unknown whether the cells in the LHb that are activated by different pathways are the same or not, or if there are different LHb subpopulations, with some dealing with the emotional component of pain only, and some involved for both the somatosensory and emotional components of pain. Further studies are therefore needed to properly pinpoint the contribution of different afferents and the integrative role of the LHb in this comorbidity.

Research objectives

Even though the comorbidity of chronic pain and emotional disorder has a high incidence in the population worldwide (Global Burden of Disease Study, 2013), it is currently poorly described. To understand the underlying mechanisms of this comorbidity, it is crucial to consider **where** and **how** changes occur in the brain.

Our team has already extensively studied the role of the ACC in the emotional consequences of pain using a preclinical model of sciatic nerve constriction -the cuff model-, consisting in the sciatic nerve compression and resulting in both persistent mechanical hypersensitivity and emotional consequences in a time-dependent manner (Barthas et al., 2017, 2015; Yalcin et al., 2011). Our previous rodent studies support the implication of the ACC in mood control: (i) in naive mice, optogenetic activation of glutamatergic pyramidal neurons is sufficient to trigger anxiodepressive-like behaviours (Barthas et al., 2015) and (ii) in our chronic neuropathic pain model, a lesion (Barthas et al., 2015) or an optogenetic inactivation (Sellmeijer et al., 2018) of the ACC prevents or reverses depressive-like symptoms without affecting physical pain (mechanical allodynia) (Barthas et al., 2015; Sellmeijer et al., 2018). In addition, using resting state fMRI in rodents, in collaboration with ICube (UMR7357), our team demonstrated an overall brain network reorganization during chronic pain (unpublished data). These results especially highlight modifications of the cortico-habenulo-tegmental pathway, showing that functional connectivity between the ACC and the habenula is altered after peripheral nerve injury.

With the help of optogenetic, calcium imaging (with the fiber photometry technique) and molecular biology tools, we aimed at describing and understanding the role of the ACC-LHb pathway in the emotional consequences of chronic neuropathic pain.

This thesis was built around three objectives:

1. To characterise the activity of ACC neurons projecting to the LHb.
2. To study the impact of optogenetic manipulations of the ACC-LHb pathway on emotional and nociceptive behaviours.
3. To identify transcriptomic modifications of ACC neurons projecting to the LHb.

The combination of these three aims provided a behavioural, functional and molecular characterisation of the ACC-LHb pathway in the comorbidity of chronic neuropathic pain

and emotional disorders. In particular, the third objective yields specific molecular targets which can be manipulated in our cuff model to understand the causal link between the dysregulation of target genes and the emotional consequences of chronic pain.

My thesis work will allow to understand the place of the ACC-LHb pathway in the chronic pain/emotional disorder dyad circuitry, adding to what was already established in our team with the involvement of the basolateral amygdala to ACC pathway in the depressive-like consequences of chronic neuropathic pain (Becker et al., 2023).

Materials & Methods

Material and Methods

The following section is composed of the Extended Material and Methods of the scientific article that can be found in the Results section.

Animals

Male adult C57BL/6J mice (RRID: IMSR JAX: 000664, Charles River, l'Arbresle, France) were used. Mice were 8 weeks old at the beginning of experimental procedures, group-housed with a maximum of 5 animals per cage and kept under a reversed 12h light/dark cycle (lights on: 8pm and off: 8am). Animals had *ad libitum* access to food and water throughout the experiments. After the optogenetic fiber implantation, animals were single housed to avoid possible damage to the implant. We conducted all the behavioral tests during the dark phase, under red light. Our animal facility (Chronobiotron) is registered for animal experimentation (Agreement B6748225), and protocols were approved by the local ethical committee of the University of Strasbourg (CREMEAS, APAFIS17390-2018103014097465v8) and performed according to animal care and use guidelines of the European Community Council Directive (EU 2010/63).

Surgical procedures

Surgical procedures were performed under zoletil/xylazine anesthesia (Zoletil 50 43mg/kg, Paxman 7mg/kg, ip; Centravet). For stereotaxic surgery, a local anesthetic was delivered subcutaneously at the incision site (Lurocaïne 4mg/kg, Bupivacaïne 4mg/kg, sc; Centravet) and an anti-inflammatory drug was injected at the end of the surgery (Meloxicam 5mg/kg, sc; Centravet). Right after the surgeries, mice were visually inspected for any sign of discomfort and their body weight recorded each day until their weight and condition stabilized, after which their weight was recorded weekly.

Neuropathic pain model: Cuff surgery

Before surgery, mice were assigned to experimental groups based on their baselines to not have any discrepancies in mechanical nociceptive threshold between groups. Chronic neuropathic pain was induced by placing a 2mm PE-20 polyethylene tube (Cuff, Ø 0.38 mm inward diameter / 1.09 mm outward diameter, Harvard Apparatus, Les Ulis, France) around the main branch of the right sciatic nerve. After the induction of anesthesia, the

right leg was shaved, a skin incision (~0.5 cm, parallel to the femur and approximately 1.5 mm anterior to the femur) was made and the sciatic nerve was exposed. Then, the 2 mm PE-20 cuff was placed around the sciatic nerve and pressed to close it around the nerve. The skin was then sutured, and the animal placed back in a new clean cage. The Sham group underwent the same procedure without the cuff implantation (Yalcin et al., 2014).

Virus injection

After general anesthesia, mice were placed in a stereotaxic frame (Kopf Instruments). 0.25µl of AAVrg-CaMKIIa-ChR2(H134R)-mCherry (Addgene #26975-AAVrg, Deisseroth), AAVrg-CaMKIIa-ArchT-GFP(PV2527) (Addgene #99039-AAVrg, Boyden) or AAVrg-CaMKIIa-m.Cherry-RPL10a-WPRE-SV40 (IGBMC) were injected bilaterally into the LHb using a glass pipette (0.0625µl/30sec, coordinates for the LHb, anteroposterior (AP): -1.7mm from bregma, lateral (L): +/-0.4mm, dorsoventral (DV): -2.7mm from the brain surface). For fiberphotometry, the same method was used to unilaterally inject 0.25 µl of AAVrg-Syn.NES-jRGECO1a.WPRE.SV40 (Addgene # 100854-AAVrg) into the LHb and 0.5 µl of AAV5-Syn-GCaMP6m-WPRE-SV40 (Addgene # 100841-AAV5) into the ACC (coordinates: AP: +0.7mm, L: +/-0.2mm, from the bregma, DV: -1.5mm from the brain). After injection, the glass pipette was let in place for 8-10min before removal and the skin was sutured. Following surgery, animals were left undisturbed for at least two weeks before cannula implantation.

Optic fiber and optogenetic cannula implantation

Two weeks after virus injection, optic fiber or optogenetic cannula (1.7mm long and 220µm in diameter) was implanted unilaterally into the ACC (AP: +0.7mm L: +/- 0.2mm DV: -1.5mm; for optogenetic stimulation: MFC 220/250-0.66_1.7mm_RM3_FLT; for fiber photometry: MFC_400/430-0.66_1.7mm_MF1.25_FLT; Doric Lenses). Cannulas were implanted half in the left hemisphere and half in the right hemisphere in a randomized manner for each experimental group. All animals underwent the implantation, whether they were in the stimulated or non-stimulated group.

For the chronic variable stress (CVS) and fiber photometry, both virus injection and optic fiber implantation were done simultaneously.

Intracardiac perfusion

To verify the virus injection localization at the end of the experiment, animals were anesthetized with Euthasol (182mg/kg) or Ketamine/Xylazine (Ketamine 1000 160mg/kg, Paxman 20mg/kg ip; Centravet) and perfused with 30mL of 0.1M phosphate buffer (PB, pH 7.4) followed by 100mL of 4% paraformaldehyde solution (PFA) in 0.1M PB. Brains were extracted, post fixed overnight and kept in 0.1M PB saline (PBS) at 4°C until cutting. Coronal sections (40µm) were obtained using a vibratome (VT 1000S, Leica, Deerfield, IL) and serially collected in PBS (1X) and sodium azide (0,04M) solution. Sections were then serially mounted with Vectashield medium (Vector laboratories) and localization of the fluorescence was checked using an epifluorescence microscope (Nikon 80i, FITC filter). Only animals well-injected bilaterally in the LHb (injection site restricted to the LHb with no transfection in the thalamus) and with correct virus expression in the ACC (marked cell bodies in the ACC with no expression in the rest of the cortex) were kept for further analyses (see Extended Table 1 for excluded animals).

Extended Table 1 – Animals selection based on injection sites.

	Acute activation	Chronic activation	Inhibition in CPID	Inhibition in CVS
Selected animals	18 stim	17 stim	41 stim	23 stim
Discarded animals	19 stim	18 stim	40 stim	11 stim

Chronic variable stress model (CVS)

CVS consists of three different stressors that were repeated and alternated over a period of 21d. CVS group were submitted to stressors as follows: 100 random mild foot shocks at 0.45 mA for 1h (10 mice/chamber), a tail suspension stress for 1 h, and a restraint stress in which mice are placed inside 50 mL Falcon tubes for 1 h. The three stressors were then repeated for the next 21 d in the same order. Control mice remained unstressed and kept group housed, while stressed animals were housed individually. The CVS paradigm started 3 to 7 days after virus injection and cannula implantation. Directly after the last stressor, both control and CVS groups were each further divided into two subgroups (non-stimulated and stimulated animals) and subjected to a battery of behavioral tests.

Optogenetic stimulation procedures

After 3 to 7 days of recovery, we either activated or inhibited the ACC-LHb pathway. ACC-LHb pathway was activated by a blue light emitting diode (LED) with a peak wavelength of 463nm (LEDFRJ-B FC, Doric Lenses) or inhibited with a green light emitting laser with a peak wavelength of 520nm (Miniature Fiber Coupled Laser Diode Module, Doric Lenses). From the light source, the light travelled through the fiber optic patch cable (MFP 240/250/900-0.63 0.75m FC CM3, Doric Lenses) to the implant cannula. For non-stimulated animals the light remained switched off.

Activation paradigm:

Blue light was delivered by pulses generated through a universal serial bus connected transistor-transistor logic pulse generator (OPTG 4, Doric Lenses) connected to a LED driver (LEDRV 2CH v.2, Doric Lenses). Transistor-transistor logic pulses were generated by an open-source software developed by Doric Lenses (USBTTL V1.9). Stimulated animals received repetitive stimulation sequences of 10s consisting of 8s at 10Hz with 40ms pulses and 2s without stimulation. Light intensity at the fiber optic patch cable was measured using a photodetector (UNO, Gentec, Quebec, Canada) and set at 8mW.

For the acute activation paradigm of the ACC-LHB pathway, the 10s sequence was repeated during 30min prior (Light-Dark test or Forced Swim Test) or during behavioral testing (Real-Time Aversion and Novelty Suppressed Feeding test).

For the chronic stimulation paradigm, the 30min sequence took place each day for 4 consecutive days and the animals were subjected to behavioral tests in the following week without stimulation during the tests.

Both activation paradigms were performed in naïve animals in two groups: stimulated and non-stimulated animals.

Inhibition paradigm:

Green light was delivered in a continuous manner during 5min prior (Light-Dark test and Forced Swim Test) or during behavioral testing (Locomotor activity test, Real-Time Aversion, Conditioned Place Preference, Novelty Suppressed Feeding test and von Frey test). The onset and end of stimulation were manually directed. Light intensity at the fiber optic patch cable was as stated before and set at 12mW. The inhibition and behavioral tests were performed 8 weeks after the cuff surgery in CPID animals and the day after the last stressor in CVS animals.

Fiberphotometry

Before any recording, mice were habituated to the procedure (to the handling procedure and then to freely move with the patch cord) for at least 3 days. Mice were connected with the fiber photometry patch cord and then rest for ~1 min before starting any behavioural test. Each recording was synchronized with the ANY-maze (Aniphy®) video tracking system, using TTLs signals. The fiber photometry setup used two light-emitting LEDs: 410-420 nm LED sinusoidally modulated at 333.786 Hz and a 460-490 nm LED sinusoidally modulated at 208.616 Hz (Doric®) merged in a iFMC6-G2 MiniCube (Doric®) that combines the two wavelengths excitation light streams and separate them from the emission light. On-line real-time demodulation of the fluorescence due to the 410-420nm and the 460-490 nm excitations was performed by Doric Neuroscience studio software (V6; Doric®). The MiniCube was connected to a fiberoptic rotary joint (Doric®) connected to the cannula. Calcium signals were collected at a sampling frequency of 12 kHz. We equalized the 410-420 and 460-490 nm signals to record an equivalent signal/noise ratio. Custom-generated MATLAB® scripts were then used to down-sample and normalize the fluorescence signal. The fluorescence from the control channel (F_{405} , isobestic point) was filtered using a polyfit regression giving a fitted control (F_{405c}). $\Delta F/F$ was calculated as $(F_{465} - F_{405c})/F_{405}$. The deviation of each sample from the averaged signal of a given period was calculated with a Z-score [$z=(x-\mu)/\sigma$]. This score indicates how many standard deviations (σ) an observation (x) is above or below the mean of the full recording session (μ). Bins of appropriate time periods (in seconds) were calculated for each peri-event and then compared around the time-locked events.

Behavioral assessment

All the behavioral tests were performed during the dark phase, under red light. Animals never submitted to same tests twice. The forced swim test (FST) was always performed as a final test. Body weights were measured weekly. Experimenters were always blind to the pain conditions and to the optogenetic stimulation for the chronic activation paradigm. All behavioral apparatus were cleaned with 70% ethanol between each animal. For the chronic optogenetic activation paradigm, all the tests were performed from the day following the four consecutive days of stimulation, without stimulation. For the

fiberphotometry experiments, the recordings were done during the behavioral tests. A summary of the tests performed for each animal cohort is provided in [Extended Data Table 2](#).

Extended Table 2 – Summary of tests performed by each cohort.

	Locomotor activity	vF	RTA	CPP	LD	NSF	FST	Splash	UST	Restraint	Shocks
Whole ACC fiber photometry											
Dual ACC & ACC-LHb fiber photometry											
Acute activation											
Chronic activation											
Inhibition in CPID											
Inhibition in CVS											
vTRAP in CPID											

[Locomotor activity](#)

Spontaneous locomotor activity was monitored for each experimental group. Mice were tested in an open field apparatus (unknown environment, 40x40x30cm plexiglas). The mice were placed in a corner and permitted to freely explore the apparatus.

The total distance travelled, time spent inactive (resting time), time spent along the edges of the apparatus and time spent in the center of the apparatus were automatically recorded by the ANY-maze software (Aniphy) over 5min. For optogenetic inhibition, the tests were performed during the light stimulation.

[Nociceptive behavior](#)

The mechanical threshold was assessed before surgery (baseline) and on a weekly basis after surgery with the von Frey filaments test. During each session, the animals were individually habituated (5 min) in transparent, bottomless plastic boxes placed on a mesh

platform. For the testing, filaments of different pressure (0.4–8.0 g; Bioseb, Chaville, France) were applied to the ventral surface of each hindpaw in an ascending fashion. A positive response for a given pressure corresponds to withdrawal or licking of the stimulated hindpaw for 3 out of 5 applications. The mechanical sensitivity threshold was defined as a response to 2 consecutive filaments.

For the optogenetic inhibition, the mice were first wired, habituated in von Frey boxes (5min) and tested for mechanical sensitivity without light stimulation following the aforementioned protocol. Then, after 5min, the light was turned on and the mice were tested a second time for mechanical sensitivity. For the fiberphotometry experiment, the mice were first wired, habituated in von Frey boxes (5min) and tested for mechanical sensitivity.

Real-time aversion (RTA)

The apparatus consists of 2 connected Plexiglas chambers (size 20cmx20cmx30cm) distinguished by the wall patterns. On the first day (pre-test), animals were free to explore the apparatus 10min and the time spent in each chamber was measured to control for the lack of spontaneous preference for one compartment. Animals spending more than 75% or less than 25% of the total time in one chamber were excluded from the study. The second day (test), animals were plugged to the light source, placed between the 2 chambers, and let free to explore for 10min. The light was turned on when the mouse entered its head and forepaws in the stimulation-paired chamber and turned off when it left the compartment. The total time spent in the stimulation-paired chamber was measured.

Conditioned place preference (CPP)

Mice were individually placed in the conditioned place preference apparatus, with 2 chambers and 1 corridor distinguished by the wall and floor patterns (Imetronic, Pessac, France; 32x20x15cm). Photocells beam breaks were recorded using Polyplace software (Imetronic, Pessac, France). On the first day (habituation), animals were free to explore the apparatus 5min and the time spent in each chamber was measured to control for the lack of spontaneous preference for one compartment. On the second and third days (conditioning), the mice were plugged to the light source. First, the animals were maintained during 5min in one chamber, without optogenetic inhibition. Then, 4h later

they were placed during 5min in the other chamber, with optogenetic inhibition (continuous). On the 4th day (test), the time spent in each chamber was recorded during 5min.

Light-dark test (LD)

The apparatus consists of light and dark boxes (19x19x15cm each). The lit compartment was brightly illuminated (>1000 lux). Mice were placed in the dark compartment (<5 lux) in the beginning of the test, and the time spent in the lit compartment was recorded during 5min. For acute activation and inhibition, the test was performed immediately after the light stimulation. The time spent in each compartment and the latency to enter the light side were automatically recorded.

For fiberphotometry, the test was performed during the recording in an automated light/dark box (Imetronic, Pessac, France). The apparatus contained two interconnected compartments (each 19x19x15cm). A gutter made on top of the apparatus (7mm) allowed the optical patch cord to follow the animal during the test and to stimulate and record the animal. One of the compartments was illuminated during the test session (1500 lux, 'light' side) and the other non-illuminated (<5 lux, 'dark' side). The entrance in each compartment was automatically detected by infra-red beams and corresponding TTLs signals were sent to the fiber photometry console (Poly software, Imetronics®). Percentages of time spent in each side were then calculated $[(\text{time in light side}/\text{total time}) * 100]$.

Novelty suppressed feeding test (NSF)

The apparatus consists of an open field (40x40x30cm) with the floor covered with 1cm of sawdust. Twenty-four hours prior to the test, food was removed from the home cage. At the time of testing, a single pellet of food was placed on a paper in the center of the box. The animal was then placed in a corner of the box and the latency to eat the pellet was recorded within a 5min period. The test was stopped as soon as the animal ate the pellet. For acute activation and inhibition, the optogenetic stimulation was conducted during the test.

For fiber photometry recordings, TTLs signals were sent to the fiber photometry console (ANY-maze, Aniphy®) when mice touched and ate the food. For fiber recording purposes,

animals were left undisturbed after eating the pellet and recorded for 5 min and multiple eating episodes were recorded for each mice.

Forced swim test (FST)

FST was conducted by gently lowering the mouse into a glass cylinder (height 26.5cm, diameter 18.5cm) containing 17.5cm of water (24,5°+/-1°C) during 6 min. The mouse was considered immobile when it floated in the water and made only small movements to keep its head above water. For acute activation and inhibition, the test was performed immediately after the light stimulation.

Splash test

The test animal was placed in a new cage and a 20% sucrose solution (Erstein, France) was sprayed on the dorsal coat of the mouse. Grooming duration was then measured during 5min.

For fiber photometry recordings, the grooming behavior was recorded (ANY-maze, Aniphy®). An experienced experimenter triggered a TTL signal, sent to the fiber photometry console, for the initiation and termination of each grooming episode.

Urine sniffing test (UST)

Reward seeking/anhedonia-like behaviours were assessed with the urine sniffing test (UST), adapted from Malkesman *et al.*, (2010). Animals were placed in a new familiar cage with the floor covered with sawdust. Two cotton tips were placed in two holes made in the Plexiglas cage (extended 1cm, 5cm above the sawdust in the cage) allowing the animals to freely explore each tip and the patch cords to follow this exploration. Before each test the cotton tips were impregnated with 20uL of male or female urine (same mouse line and age-matched animals). Two identical zones [representing 9% of the full apparatus (682cm²)] were virtually delimited around the cotton tips, considered as “male” and “female” zone accordingly. The animals were always placed in the center of the cage and permitted to freely explore the apparatus for 5min. For each zone and in the full apparatus, the time spent, average speed, latency to enter the zone, and the immobility time were automatically recorded (ANY-maze, Aniphy®). We also recorded the latency to sniff each cotton tip, the total cotton tip investigation time, and the longest cotton tip investigation. TTLs signals corresponding to each cotton tip investigation were manually triggered and sent to the fiber photometry console (ANY-maze, Aniphy®)

Restraint stress

An acute restraint stress was performed to assess the Ca²⁺ response to a stressful event. After a 1-min baseline period, mice were restrained by an experimenter and familiar experimenter for 5 s after which they were released, and an additional 1-min was recorded.

Unpredictable electrical shocks

Ca²⁺ response to foot shocks was assessed in a chamber with electrified grid floors. After a 1-min baseline period with no scheduled events, mice were exposed to one unpredictable electrical foot shock for 1 s (0.6 mA) and left for an additional minute in the chamber.

Emotionality z-scores

Emotionality z-scores were computed as previously described by (Guilloux et al., 2011). First, individual z-score values were calculated for each mouse in each test using the following formula: $z = (X - \mu) / \sigma$ where X represents the individual data for the observed parameter while μ and σ represent the mean and standard deviation of the control group. The directionality of scores was adjusted so that increased score values reflect increased dimensionality (anxiety- or depressive-like behaviors). For instance, decreased time spend in the light box in LD test was converted into positive standard deviation changes compared to group means indicating increased anxiety-like behaviors. Conversely, increased immobility time in the FST was not converted since it is a direct indicator of increased depressive-like behaviors. Finally, z values obtained for each test were averaged to obtain a single emotionality score:

$$\text{Emotionality z-score} = Z_{\text{test1}} + Z_{\text{test2}} + \dots + Z_{\text{testn}} / \text{Number of tests.}$$

Ex vivo electrophysiological recordings

We performed whole-cell patch clamp recordings of ACC pyramidal neurons. We recorded from mCherry- or GFP-expressing neurons of mice bilaterally injected with an retrograde AAV in the LHb driving the expression of either the channelrhodopsin 2 (ChR2) or the archeorhodopsin T (ArchT) under the control of the CaMKIIa promoter (with AAVrg-CaMKIIa-ChR2(H134R)-mCherry and AAVrg-CaMKIIa-ArchT-GFP(PV2527), respectively).

For these experiments, mice were anaesthetized with urethane (1.9g/kg) and killed by decapitation, their brain was removed and immediately immersed in cold (0°C-4°C) sucrose-based ACSF containing the following (in mM): 2 kynurenic acid, 248 sucrose, 11 glucose, 26 NaHCO₃, 2 KCl, 1.25 KH₂PO₄, 2 CaCl₂, and 1.3 MgSO₄ (bubbled with 95% O₂ and 5% CO₂). Transverse slices (300 μm thick) were cut with a vibratome (VT1000S, Leica). Slices were maintained at room temperature in a chamber filled with ACSF containing the following (in mM): 126 NaCl, 26 NaHCO₃, 2.5 KCl, 1.25 NaH₂PO₄, 2 CaCl₂, 2 MgCl₂, and 10 glucose (bubbled with 95% O₂ and 5% CO₂; pH 7.3; 310mOsm measured). Slices were transferred to a recording chamber and continuously superfused with ACSF saturated with 95% O₂ and 5% CO₂. ACC neurons expressing mCherry or GFP were recorded in the whole-cell patch-clamp configuration. Recording electrodes (3.5-4.5MΩ) were pulled from borosilicate glass capillaries (1.2mm inner diameter, 1.69mm outer diameter, Warner Instruments, Harvard Apparatus) using a P1000 electrode puller (Sutter Instruments). Recording electrodes were filled with, in mM: 140 KCl, 2 MgCl₂, 10 HEPES, 2 MgATP; pH 7.3. The pH of intrapipette solutions was adjusted to 7.3 with KOH, and osmolarity to 310mOsm with sucrose. The ACC was illuminated with the same system used for the *in vivo* experiments (see above) triggered with WinWCP 5.7.2, the optic fiber being localized in the recording chamber at 3 mm from the recorded neuron. The current injected was adapted for the neuron to have a membrane potential of about -60mV. Recordings were acquired with WinWCP 5.7.2 (courtesy of Dr. J. Dempster, University of Strathclyde, Glasgow, United Kingdom). All recordings were performed at 34°C.

Plasmid and AAV generation

Plasmid construction

For translating ribosome affinity purification, pAAV-CaMKII-mCherry-RPL10a-WPRE-SV40 plasmid was constructed. mCherry-RPL10a from plasmid pAAV-hSyn-Flex-mCherry-RPL10a (IGBMC) was cloned by in-fusion cloning into the plasmid pAAV-CaMKII-ArchT-GFP(PV2527) (Addgene #99039). The vector pAAV-CaMKII-ArchT-GFP-WPRE-SV40(PV2527) was linearized by digestion with the enzymes BamHI and HindIII and deposited on 1% agarose gel. It was extracted and purified using the gel extraction kit QIAquick. mCherry-RPL10a fragment of the pAAV-hSyn-Flex-mCherry-RPL10a was

amplified by PCR using CloneAmp HiFi Polymerase and the following primers: for-AGGTTGATTATCGATAAGCTTCTAATACAGACGCTGGGGCT and rev-TCTGGGGGCAGCGGGGATCCCTAGCCACCATGGTGAGCAAG. The primers were designed according to the in-fusion cloning method, in order to generate PCR products with a sequence homology of 15bp with the vector extremities. PCR products were deposited on 1% agarose gel and extracted and purified as the vector. Both the vector and the insert were quantified on gel and using Nanodrop. The in-fusion cloning was performed with 150ng of purified insert, 50ng of purified linearized vector and 5X In-Fusion HD Enzyme Premix in a total volume of 10µL for 15min at 50°C. An aliquot of 2.5µL of this reaction media was used to transform 50µL of “stellar” competent cells by thermic shock. After incubation at 37°C with 500µL of SOC medium, the bacterial pellet was spread on LB agar ampicillin-100 plates and placed at 37°C overnight. 4 colonies were selected to realize minipreps. The extracted DNA was digested by BamHI and HindIII cloning enzymes and deposited on 1% agarose gel. A 2023bp corresponding to the size of the insert was highlighted in the 4 minipreps, which were further sequenced with the Sanger method and analyzed to confirm the presence of the insert. A maxipreparation was realized from miniprep 2 and provided to the Molecular Biology and Virus platform of IGBMC for further AAV preparation.

[AAV preparation and purification](#)

AAV generation was performed by the Molecular Biology and Virus platform at IGBMC (Strasbourg, France).

Recombinant adeno-associated virus AAV serotype 2-retro were generated by a triple transfection of HEK293T-derived cell line using Polyethylenimine (PEI) transfection reagent and the 3 following plasmids: pAAV-CamKII-mCherry-RPL10a-WPRE-SV40pA, pAAV2-retro helper (Addgene #81070) encoding the AAV serotype 2-retro capsid and pHelper (Agilent) encoding the adenovirus helper functions. 48hours after transfection, AAV2-retro vectors were harvested from cell lysate treated with Benzonase (Merck) at 120U/mL. They were further purified by gradient ultracentrifugation with Iodixanol (Optiprep™ density gradient medium) followed by dialysis and concentration against Dulbecco’s Phosphate Buffered Saline (DPBS) using centrifugal filters (Amicon Ultra-15 Centrifugal Filter Devices 100K, Millipore). Viral titers were quantified by Real-Time PCR

using the LightCycler480 SYBR Green I Master (Roche) and primers targeting mCherry sequence (for: CAGAGGCTGAAGCTGAAGGA, rev: GCTTCTTGGCCTTGTAGGTG). Titers are expressed as genome copy per milliliter (GC/mL).

Immunohistochemistry

For the vTRAP study, animals were perfused (see Intracardiac perfusion) 3 weeks after the AAVrg-CaMKIIa-mCherry-RPL10a-WPRE-SV40 virus injection. 40µm sections with the ACC were washed in PBS (3x10min) and pre-incubated in PBS containing Triton X-100 (0.3%) and donkey serum (5%) for 2h. Sections were then incubated overnight at +4°C in PBS containing Triton X-100 (0.3%) and one of the following primary antibodies: rabbit anti-NeuN (1:200, Abcam, 104225), rabbit anti-GFAP (1:200, United States Biological, G2032-27) or rabbit anti-Olig2 (1:200, Merck-Millipore, AB9610). Sections were then washed in PBS (3x10min), incubated with donkey anti-rabbit A488 secondary antibody (1:400, Jackson ImmunoResearch, 711-165-152) in PBS containing Triton X-100 (0.3%) for 2h and washed in PBS (3x10min). Sections were finally serially mounted with DAPI.

Viral Translating Ribosome Affinity Purification (vTRAP) & RNA extraction

Bilateral ACC dissection was performed 3 weeks after virus injection. The ACC was freshly and quickly manually dissected from animals killed by cervical dislocation. Translated mRNA purification was made following Heiman *et al.* (2014) protocol for TRAP and tissues were immediately put in a pre-chilled tissue-lysis buffer (20mM HEPES KOH [pH 7.3], 150mM KCl, 12mM MgCl₂, 1M DTT, 100µg/mL cycloheximide, protease inhibitors, and RNase inhibitors) and homogenized using a homogenizer (Fisher Scientific). To remove large cells debris, the homogenates were centrifuged (2000 x g, 4°C) for 10min and NP-40 (1%) and DHPC (30mM) were added to the supernatant. After incubating the samples 5min on ice, the lysate was centrifuged (20000 x g) to remove non solubilized material and the supernatant was collected. At the same time, mCherry antibodies coupled to magnetic beads were resuspended and washed three times in low-salt buffer (HEPES KOH [7.3pH], 150mM KCl, 12mM MgCl₂, 0.5mM DTT, 100µg/mL cycloheximide). 250µL of the total tissue lysate was collected to separate the total RNA of the ACC (input) tissue from the immunoprecipitated (IP) transcriptome of ACC-LHb cells. Then, 200µL of freshly

prepared magnetic beads were added to each sample and were incubated overnight at 4°C with end-over-end agitation. After 14-16h of incubation, the beads were collected on a pre-chilled magnetic rack and the liquid was collected to separate the unbound fraction's RNA (unbound) from the IP. The beads were then washed four times with high salt buffer (HEPES KOH [7.3pH], 350mM KCl, 12mM MgCl₂, 1% NP-40, 0.5mM DTT, 100µg/mL cycloheximide). After the last wash, the high salt buffer was removed and beads were resuspended in nanoprep lysis buffer (20mM HEPES KOH [pH 7.3], 150mM KCl, 12mM MgCl₂, 1M DTT, 100µg/mL cycloheximide, protease inhibitors, RNase inhibitors and β-mercaptoethanol). RNA transcripts were separated from the beads after thorough vortexing followed by 10min incubation at room temperature. RNA extraction was performed on input, unbound and IP fractions for each sample by adding an equal volume of 80% sulfolane and following the protocol from the Absolutely Nanoprep kit (Agilent), including the extra DNase treatment. The extracted RNAs were stored at -80°C until qRT-PCR and sequencing.

The vTRAP was performed in two different cohorts. The first cohort was composed of naïve animals to validate the vTRAP virus and technique, in which RNA sequencing was performed in both IP and input fractions of 3 animals. The second experiment was performed in sham and cuff animals in our CPID model, in which RNA sequencing was done only in the IP fraction of 8 sham and 8 cuff animals.

qRT-PCR

qRT-PCR was performed to validate the vTRAP procedure and to preselect the best enriched samples for RNA-sequencing. For this purpose, RNA extracted after vTRAP was used to generate cDNA using Mastercycler 534X (Eppendorf) as followed. 10 µL of RNA/sample were added to a mix of 10 µL water, 2 µL dNTPs (10mM), 4 µL of a mix of Oligo(dT) (10mM) and RHX (20mM) and annealed for 5min at 65°C in the Mastercycler. The samples were then left to chill on ice for 3min. Then, 8µL of First Strand Buffer (5X), 4µL of DTT (0.1M) and 2µL of M-MLV Reverse Transcriptase (400U/sample) were added to each sample. The samples were then placed back in the PCR machine with the following steps: reverse transcription step at 37°C for 75min followed by inactivation step at 95°C for 15min and lag step at 4°C.

RT-qPCR was performed on a 384-wells QuantStudio5 Real-Time PCR system (Applied Biosystem) using SYBR Green, with initialization step at 95°C for 20s followed by amplification step for 40 cycles of 1s 95°C denaturation, 20s 60°C annealing and 1s 95°C extension. Experiments were performed with triplicate sample deposits on the amplification plate. Relative abundance of each RNA target gene transcript was normalized to the endogenous control gene *Gapdh* RNA. Data were analyzed according to the standard curve method. Primers are available in [Extended Table 3](#).

Extended Table 3 – Primers for qRT-PCR

Gene name	Rev/Fw	Sequence
<i>Gapdh</i>	Rev	TGGGATGGAAATTGTGAGGGAG
	Fw	TGGCCTCCAAGGAGTAAGAAAC
<i>Mcherry</i>	Rev	CTTGGAGCCGTACATGAACTGAGG
	Fw	GAACGGCCACGAGTTCGAGA
<i>Camk2</i>	Rev	AAGAAAACAGTGCAGACAGGAGATC
	Fw	TGGGTTTGGCTCTTGTATGGA
<i>Gad65</i>	Rev	GTGCGCAAAGTGGAGGTACAA
	Fw	CATTGATAAGTGTGGAGCTAGCA
<i>Gad67</i>	Rev	TCGGCTCTGTCACAGGAGTA
	Fw	CCTCTCCGGATCTCTCCCTT
<i>Gfap</i>	Rev	CTCCTCTGTCTTTGCATGTTACTG
	Fw	ACAGCGGCCCTGAGAGAGAT

RNA-sequencing

RNA-sequencing was performed by the Genomeast platform at IGBMC (Strasbourg, France), using Clontech SMART-Seq v4 Ultra Low Input RNA Kit for Sequencing User Manual (PN 091817) and the Illumina Nextera XT DNA Library Prep Kit Reference Guide (PN 15031942). Full length cDNA were generated from 1ng of total RNA using SMART-SeqX v4 UltraX Low Input RNA Kit for Sequencing (Takara Bio Europe, Saint Germain en Laye, France) according to manufacturer’s instructions with 12 cycles of PCR for cDNA amplification by Seq-Amp polymerase. Six hundreds pg of pre-amplified cDNA were then used as input for Tn5 transposon tagmentation by the Nextera XT DNA Library Preparation Kit (96 samples) (Illumina, San Diego, USA) followed by 12 cycles of library amplification. Following purification with SPRIselect beads (Beckman-Coulter, Villepinte, France), the

size and concentration of libraries were assessed by capillary electrophoresis. Libraries were sequenced on an Illumina NextSeq 2000 sequencer as single read 50 base reads. Image analysis and base calling were performed using RTA version 2.7.7 and BCL Convert version 3.8.4.

RNA-sequencing analysis

Reads were preprocessed to remove adapter, polyA and low-quality sequences (Phred quality score below 20). After this preprocessing, reads shorter than 40 bases were discarded for further analysis. These preprocessing steps were performed using cutadapt version 1.10. Reads were mapped to rRNA sequences using bowtie version 2.2.8 and reads mapping to rRNA sequences were removed for further analysis. Reads were mapped onto the mm10 assembly of the *Mus musculus* genome, using STAR version 2.5.3a. Gene expression quantification was performed from uniquely aligned reads using htseq-count version 0.6.1p1, with annotations from Ensembl version 102 and “union” mode. Only non-ambiguously assigned reads to a gene have been retained for further analyses. Read counts were then normalized across samples with the median-of-ratios method proposed by Anders and Huber⁹¹, to make these counts comparable between samples. Principal Component Analysis was computed on regularized logarithm transformed data calculated with the method proposed by Love and collaborators⁹². Differential expression analysis was performed using R and the Bioconductor package DESeq2 version 1.16.1.

For the first cohort, the fold-changes were calculated for IP vs input (a positive fold-change corresponding to an increased gene expression in the IP compared to the input), while for the second cohort the fold-changes were computed for cuff vs sham (a positive fold-change corresponding to an increased gene expression in cuff animals compared to sham animals, in ACC neurons projecting to the LHb).

Gene ontology

Enrichment for functional terms in differentially expressed genes (DEGs) was performed using WEBGSTALL for kegg pathway, biological process and molecular function. Analysis was restricted to the genes differentially expressed at nominal p-value < 0.05.

Gene Set Enrichment Analysis (GSEA)

All genes were ranked independently based on the fold changes obtained from their respective differential expression analysis. GSEA was performed as previously described using the GSEA Preranked tool and gene sets related to PFC cell types (Zhong et al., 2018).

Rank-rank hypergeometric overlap (RRHO) analysis

In order to compare IP vs input (naïve) and IP vs IP (cuff vs sham) RNA-Sequencing data, we used the Rank-rank hypergeometric overlap (RRHO2) procedure, as described by Cahill *et al.* (2018), using the R package available at: <https://github.com/Caleb-Huo/RRHO2>. Genes in each data set were ranked based on the following metric: $-\log_{10}(\text{p-value}) \times \text{sign}(\log_2 \text{ Fold Change})$. Then, the RRHO2 function was applied to the 2 gene lists at default parameters (with stepsize equal to the square root of the list length). Significance of hypergeometric overlaps between IP vs input (naïve) and IP vs IP (cuff vs sham) gene expression changes are reported as \log_{10} raw p-values.

Statistical analysis

Statistical analyses were performed in GraphPad Prism v9.0.2 software. Data are expressed as mean \pm SEM, with statistical significance set as * $p < 0.05$, ** $p < 0.01$, *** $p < 0.001$.

Data were first tested for normality using the Shapiro-Wilk normality test. If data passed the normality test, student's t-test (unpaired, two-tailed), One-Way Repeated Measures ANOVA, and Two-way ANOVA followed by Sidak, Bonferroni or Newman-Keuls post hoc tests were used when appropriate. If data failed the normality test, Mann-Whitney non-parametric analysis (two-tailed) was used. All statistical analyses are summarized in Extended Data Table 4 and 5.

Extended Table 4 – Statistical analysis for the main figures.

Figure	Experiment	Assessment	Treatment	Test	Group (n)	Analysis	Statistics
1D	Whole ACC fiberphotometry	Mechanical (paw withdrawal) threshold	Cuff surgery	vF	Sham (14) Cuff (15)	Time x Surgery Mixed Effect Model with Geisser-Greenhouse correction of sphericity	Time: p<0.0001 ; **** Surgery: p<0.0001 ; **** Time x Surgery: p<0.0001 ; ****
1E	Whole ACC fiberphotometry	Emotionality	Cuff surgery	Emotionality score (Splash + NSF + LD)	Sham (14) Cuff (15)	Unpaired t-test (two tailed)	F(14,13)=1.894 p=0.0161 ; *
1F''	Whole ACC fiberphotometry	ACC Ca2+ dynamics in CPID	Cuff surgery	Splash	Sham (14) Cuff (15)	Paired t-tests	Sham start grooming: t=4.078, df=14 Cuff start grooming: t=2.863, df=14 Sham stop grooming: t=3.514, df=14 Cuff stop grooming: t=4.723, df=14
1G'	Whole ACC fiberphotometry	ACC Ca2+ dynamics in CPID	Cuff surgery	NSF eat	Sham (14) Cuff (15)	Time x Surgery 2-way ANOVA repeated measures	Time: p<0.0001 ; **** Surgery: p=0.0235 ; * Time x Surgery: p=0.9628 ; ns
1G''	Whole ACC fiberphotometry	ACC Ca2+ dynamics in CPID	Cuff surgery	NSF touch + eat	Sham (14) Cuff (15)	Time x Surgery 2-way ANOVA repeated measures	Time: p<0.0001 ; **** Surgery: p=0.0250 ; * Time x Surgery: p=0.4118 ; ns
1H'	Whole ACC fiberphotometry	ACC Ca2+ dynamics in CPID	Cuff surgery	LD entry in light	Sham (14) Cuff (15)	Time x Surgery 2-way ANOVA repeated measures	Time: p<0.0001 ; **** Surgery: p=0.0347 ; * Time x Surgery: p=0.1486 ; ns
1I'	Whole ACC fiberphotometry	ACC Ca2+ dynamics in CPID	Cuff surgery	UST female scent	Sham (14) Cuff (15)	Time x Surgery 2-way ANOVA repeated measures	Time: p<0.0001 ; **** Surgery: p=0.0877 ; ns Time x Surgery: p=0.0011 ; **
2D	Dual ACC & ACC-LHb fiberphotometry	Mechanical (paw withdrawal) threshold	Cuff surgery	vF	Sham (8) Cuff (6)	Time x Surgery 2-way ANOVA repeated measures	Time: p<0.0001 ; **** Surgery: p=0.0002 ; *** Time x Surgery: p=0.0163 ; *
2E	Dual ACC & ACC-LHb fiberphotometry	Emotionality	Cuff surgery	Emotionality score (Splash + NSF + LD)	Sham (8) Cuff (6)	Unpaired t-test (two tailed)	F(5,7)=1.920 p=0.3532 ; ns
2F'	Dual ACC & ACC-LHb fiberphotometry	ACC-LHb Ca2+ dynamics in CPID	Cuff surgery	Splash grooming initiation	Sham (8) Cuff (6)	Time x Surgery 2-way ANOVA repeated measures	Time: p=0.6843 ; ns Surgery: p=0.8966 ; ns Time x Surgery: p=0.2163 ; ns
2F''	Dual ACC & ACC-LHb fiberphotometry	ACC-LHb Ca2+ dynamics in CPID	Cuff surgery	Splash grooming termination	Sham (8) Cuff (6)	Time x Surgery 2-way ANOVA repeated measures	Time: p=0.8561 ; ns Surgery: p=0.9980 ; ns Time x Surgery: p=0.9198 ; ns
2G'	Dual ACC & ACC-LHb fiberphotometry	ACC-LHb Ca2+ dynamics in CPID	Cuff surgery	NSF eat	Sham (8) Cuff (6)	Time x Surgery 2-way ANOVA repeated measures	Time: p=0.0588 ; ns Surgery: p=0.4756 ; ns Time x Surgery: p=0.9154 ; ns
2H	Dual ACC & ACC-LHb fiberphotometry	ACC-LHb Ca2+ dynamics in CPID	Cuff surgery	UST female scent	Sham (8) Cuff (6)	Time x Surgery 2-way ANOVA repeated measures	Time: p=0.6068 ; ns Surgery: p=0.6969 ; ns Time x Surgery: p=0.2316 ; ns
2I'	Dual ACC & ACC-LHb fiberphotometry	ACC-LHb Ca2+ dynamics in CPID	Cuff surgery	LD entry in light	Sham (8) Cuff (6)	Time x Surgery 2-way ANOVA repeated measures	Time: p=0.1915 ; ns Surgery: p=0.9189 ; ns Time x Surgery: p=0.3143 ; ns
2J'	Dual ACC & ACC-LHb fiberphotometry	ACC-LHb Ca2+ dynamics in CPID	Cuff surgery	Restraint stress	Sham (8) Cuff (6)	1-way ANOVA	F=0.03390 p=0.0005, ***

Extended Table 4 – Statistical analysis for the main figures, extended.

2K'	Dual ACC & ACC-LHb fiberphotometry	ACC-LHb Ca2+ dynamics in CPID	Cuff surgery	Unpredictable electrical shock	Sham (8) Cuff (6)	Paired t-test (two tailed)	t=2.510, df=13 p=0.0261, *
3E	Acute ACC-LHb optogenetic activation	Aversion	Acute ACC-LHb optogenetic activation	RTA pre test	No stim (19) Stim (8)	Unpaired t-test (two tailed)	F(7,8)=1.196 p=0.7035 ; ns
3F	Acute ACC-LHb optogenetic activation	Aversion	Acute ACC-LHb optogenetic activation	RTA delta	No stim (19) Stim (8)	Unpaired t-test (two tailed)	F(7,18)=1.251 p=0.0514 ; ns
3G	Acute ACC-LHb optogenetic activation	Anxiety-like behavior	Acute ACC-LHb optogenetic activation	LD	No stim (21) Stim (15)	Unpaired t-test (two tailed)	F(14,20)=1.268 p=0.7858 ; ns
3H	Acute ACC-LHb optogenetic activation	Anxiodepressive-like behavior	Acute ACC-LHb optogenetic activation	NSF	No stim (19) Stim (15)	Unpaired t-test (two tailed)	F(14,18)=2.499 p=0.2566 ; ns
3I	Acute ACC-LHb optogenetic activation	Depressive-like behavior	Acute ACC-LHb optogenetic activation	FST	No stim (21) Stim (15)	Unpaired t-test (two tailed)	F(20,14)=1.492 p=0.7550 ; ns
3J	Acute ACC-LHb optogenetic activation	Emotionality	Acute ACC-LHb optogenetic activation	Emotionality score (LD + NSF + FST)	No stim (21) Stim (15)	Unpaired t-test (two tailed)	F(14,20)=1.219 p=0.4378 ; ns
4C	Chronic ACC-LHb optogenetic activation	Anxiety-like behavior	Chronic ACC-LHb optogenetic activation	LD	No stim (23) Stim (16)	Mann-Whitney test (two tailed)	U=104.5 p=0.0224 ; *
4D	Chronic ACC-LHb optogenetic activation	Anxiodepressive-like behavior	Chronic ACC-LHb optogenetic activation	NSF	No stim (13) Stim (13)	Unpaired t-test (two tailed)	F(12,12)=1.696 p=0.0467 ; *
4E	Chronic ACC-LHb optogenetic activation	Depressive-like behavior	Chronic ACC-LHb optogenetic activation	FST	No stim (23) Stim (16)	Unpaired t-test (two tailed)	F(22,15)=1.502 p=0.0595 ; ns
4F	Chronic ACC-LHb optogenetic activation	Emotionality	Chronic ACC-LHb optogenetic activation	Emotionality score (LD + NSF + FST)	No stim (23) Stim (16)	Unpaired t-test (two tailed)	F(15,22)=1.220 p=0.0004 ; ***
4G	Chronic ACC-LHb optogenetic activation	Aversion	Chronic ACC-LHb optogenetic activation	RTA pre test	No stim (12) Stim (10)	Mann-Whitney test (two tailed)	U=57.50 p=0.8850 ; ns
4H	Chronic ACC-LHb optogenetic activation	Aversion	Chronic ACC-LHb optogenetic activation	RTA delta	No stim (12) Stim (10)	Unpaired t-test (two tailed)	F(9,11)=1.082 p=0.8406 ; ns
4I	Chronic ACC-LHb optogenetic activation	Depressive-like behavior	Chronic ACC-LHb optogenetic activation	FST + 2 weeks	No stim (12) Stim (10)	Unpaired t-test (two tailed)	F(9,11)=1.133 p=0.7054 ; ns
4J	Chronic ACC-LHb optogenetic activation	Locomotor activity in unknown environment	Chronic ACC-LHb optogenetic activation	Locomotor activity	No stim (12) Stim (10)	Unpaired t-test (two tailed)	F(9,11)=2.983 p=0.1465 ; ns
5E	ACC-LHb optogenetic inhibition in CPID	Mechanical (paw withdrawal) threshold	Cuff surgery x ACC-LHb inhibition	vF	Sham () Cuff ()	Time x Surgery Mixed Effect Model with Geisser-Greenhouse correction of sphericity	Time: p<0.0001 ; **** Surgery: p<0.0001 ; **** Time x Surgery: p<0.0001 ; ****
5F	ACC-LHb optogenetic inhibition in CPID	Mechanical (paw withdrawal) threshold with stimulation	Cuff surgery x ACC-LHb inhibition	vF + stimulation	Sham no stim () Cuff no stim () Sham stim () Cuff stim ()	Optogenetic inhibition x Surgery x Time 3-way ANOVA repeated measures	Stimulation: F(1,75)=0.01144 p=0.9144 ; ns Surgery: F(1,75)=21.45 p<0.0001 ; **** Time: F(1,75)=1.958 p=0.1659 ; ns Stimulation x Surgery: F(1,75)=0.0001 p=0.9849 ; ns Time x Surgery: F(1,75)=2.134 p=0.1501 ; ns Time x Stimulation: F(1,75)=0.147 p=0.7054 ; ns Time x Stimulation x Surgery: F(1,75)=0.0001 p=0.9849 ; ns
5G	ACC-LHb optogenetic inhibition in CPID	Anxiety-like behavior	Cuff surgery x ACC-LHb inhibition	LD	Sham no stim (20) Cuff no stim (22) Sham stim (17) Cuff stim (13)	Optogenetic inhibition x Surgery 2-way ANOVA	Stimulation: F(1,67)=0.6711 p=0.4151 ; ns Surgery: F(1,67)=7.826 p=0.0067 ; ** Stimulation x Surgery: F(1,67)=0.0001 p=0.9849 ; ns
5H	ACC-LHb optogenetic inhibition in CPID	Anxiodepressive-like behavior	Cuff surgery x ACC-LHb inhibition	NSF	Sham no stim (20) Cuff no stim (22) Sham stim (14) Cuff stim (12)	Optogenetic inhibition x Surgery 2-way ANOVA	Stimulation: F(1,64)=1.665 p=0.2031 ; ns Surgery: F(1,64)=0.3990 p=0.5298 ; ns Stimulation x Surgery: F(1,64)=6.4 p=0.0174 ; **

Extended Table 4 – Statistical analysis for the main figures, extended bis.

5I	ACC-LHb optogenetic inhibition in CPID	Depressive-like behavior	Cuff surgery x ACC-LHb inhibition	FST	Sham no stim (20) Cuff no stim (20) Sham stim (15) Cuff stim (12)	Optogenetic inhibition x Surgery 2-way ANOVA	Stimulation: $F(1,67)=1.732$ $p=0.19$; Surgery: $F(1,67)=3.259$ $p=0.0757$; Stimulation x Surgery: $F(1,67)=4.2$
5J	ACC-LHb optogenetic inhibition in CPID	Emotionality	Cuff surgery x ACC-LHb inhibition	Emotionality score (LD + NSF + FST)	Sham no stim (20) Cuff no stim (22) Sham stim (17) Cuff stim (13)	Optogenetic inhibition x Surgery 2-way ANOVA	Stimulation: $F(1,68)=3.303$ $p=0.07$; Surgery: $F(1,68)=6.647$ $p=0.0121$; Stimulation x Surgery: $F(1,68)=5.3$
5K	ACC-LHb optogenetic inhibition in CPID	Aversion	Cuff surgery x ACC-LHb inhibition	RTA pre test	Sham no stim (8) Cuff no stim (9) Sham stim (9) Cuff stim (9)	Optogenetic inhibition x Surgery 2-way ANOVA	Stimulation: $F(1,31)=0.1266$ $p=0.73$; Surgery: $F(1,31)=0.05083$ $p=0.823$; Stimulation x Surgery: $F(1,31)=4.5$
5L	ACC-LHb optogenetic inhibition in CPID	Aversion	Cuff surgery x ACC-LHb inhibition	RTA delta	Sham no stim (8) Cuff no stim (9) Sham stim (9) Cuff stim (9)	Optogenetic inhibition x Surgery 2-way ANOVA	Stimulation: $F(1,31)=0.3515$ $p=0.56$; Surgery: $F(1,31)=0.1032$ $p=0.7501$; Stimulation x Surgery: $F(1,31)=3.5$
5M	ACC-LHb optogenetic inhibition in CPID	Place preference	Cuff surgery x ACC-LHb inhibition	CPP pre test	Sham no stim (6) Cuff no stim (6) Sham stim (5) Cuff stim (6)	Optogenetic inhibition x Surgery 2-way ANOVA	Stimulation: $F(1,19)=0.0005964$ $p=0.96$; Surgery: $F(1,19)=0.2041$ $p=0.6565$; Stimulation x Surgery: $F(1,19)=0.0$
5N	ACC-LHb optogenetic inhibition in CPID	Place preference	Cuff surgery x ACC-LHb inhibition	CPP delta	Sham no stim (6) Cuff no stim (6) Sham stim (5) Cuff stim (6)	Optogenetic inhibition x Surgery 2-way ANOVA	Stimulation: $F(1,19)=0.3443$ $p=0.56$; Surgery: $F(1,19)=0.008750$ $p=0.92$; Stimulation x Surgery: $F(1,19)=0.2$
5O	ACC-LHb optogenetic inhibition in CPID	Locomotor activity in unknown environment	Cuff surgery x ACC-LHb inhibition	Locomotor activity	Sham no stim (12) Cuff no stim (14) Sham stim (10) Cuff stim (9)	Optogenetic inhibition x Surgery 2-way ANOVA	Stimulation: $F(1,33)=0.01263$ $p=0.91$; Surgery: $F(1,33)=0.7519$ $p=0.3921$; Stimulation x Surgery: $F(1,33)=0.2$
6C	ACC-LHb optogenetic inhibition in CVS	Anxiety-like behavior	Chronic variable stress x ACC-LHb inhibition	LD	Ctrl no stim (17) Stress no stim (22) Control stim (11) Stress stim (9)	Optogenetic inhibition x Stress 2-way ANOVA	Stimulation: $F(1,55)=0.4740$ $p=0.49$; Stress: $F(1,55)=1.020$ $p=0.3170$; Stimulation x Stress: $F(1,55)=0.05$
6D	ACC-LHb optogenetic inhibition in CVS	Anxiodepressive-like behavior	Chronic variable stress x ACC-LHb inhibition	NSF	Ctrl no stim (17) Stress no stim (22) Control stim (11) Stress stim (10)	Optogenetic inhibition x Stress 2-way ANOVA	Stimulation: $F(1,56)=0.9477$ $p=0.33$; Stress: $F(1,56)=3.836$ $p=0.0552$; Stimulation x Stress: $F(1,56)=0.42$
6E	ACC-LHb optogenetic inhibition in CVS	Depressive-like behavior	Chronic variable stress x ACC-LHb inhibition	FST	Ctrl no stim (17) Stress no stim (22) Control stim (11) Stress stim (9)	Optogenetic inhibition x Stress 2-way ANOVA	Stimulation: $F(1,55)=1.009$ $p=0.32$; Stress: $F(1,55)=7.157$ $p=0.0098$; Interaction: $F(1,55)=0.8530$ $p=0.36$
6F	ACC-LHb optogenetic inhibition in CVS	Emotionality	Chronic variable stress x ACC-LHb inhibition	Emotionality score (LD + NSF + FST)	Ctrl no stim (17) Stress no stim (22) Control stim (11) Stress stim (10)	Optogenetic inhibition x Stress 2-way ANOVA	Stimulation: $F(1,58)=1.099$ $p=0.30$; Stress: $F(1,58)=7.670$ $p=0.0075$; Interaction: $F(1,58)=0.9973$ $p=0.32$
8C	vTRAP in CPID	Mechanical (paw withdrawal) threshold	Cuff surgery x vTRAP	vF	Sham (8) Cuff (8)	Time x Surgery 2-way ANOVA repeated measures	Time: $p=0.0052$; ** Surgery: $p<0.0001$; **** Time x Surgery: $p<0.0001$; ****
8D	vTRAP in CPID	Emotionality	Cuff surgery x vTRAP	Emotionality score (Splash + NSF)	Sham (8) Cuff (8)	Unpaired t-test (two tailed)	$F(7,7)=2.148$ $p=0039$; **

Extended Table 5 – Statistical analysis for the supplementary figures.

Figure	Experiment	Assessment	Treatment	Test	Group (n)	Analysis	Statistics
S1A	Whole ACC fiberphotometry	Depressive-like behavior	Cuff surgery	Splash	Sham (14) Cuff (15)	Mann-Whitney test (two tailed)	U=91 p=0.553
S1B	Whole ACC fiberphotometry	Anxiodepressive-like behavior	Cuff surgery	NSF	Sham (14) Cuff (15)	Unpaired t-test (two tailed)	F(13,14) p=0.447
S1C	Whole ACC fiberphotometry	Anxiety-like behavior	Cuff surgery	LD	Sham (14) Cuff (15)	Unpaired t-test (two tailed)	F(13,14) p=0.008
S1D	Whole ACC fiberphotometry	Depressive-like behavior	Cuff surgery	UST	Sham (7) Cuff (6)	Unpaired t-test (two tailed)	F(6,5)= p=0.514
S1E	Whole ACC fiberphotometry	ACC Ca ²⁺ dynamics in CPID	Cuff surgery	Splash grooming initiation	Sham (14) Cuff (15)	Time x Surgery 2-way ANOVA repeated measures	Time: p Surgery Time x
S1F	Whole ACC fiberphotometry	ACC Ca ²⁺ dynamics in CPID	Cuff surgery	Splash grooming termination	Sham (14) Cuff (15)	Time x Surgery 2-way ANOVA repeated measures	Time: p Surgery Time x
S1H	Whole ACC fiberphotometry	ACC Ca ²⁺ dynamics in CPID	Cuff surgery	NSF touch only	Sham (14) Cuff (15)	Time x Surgery 2-way ANOVA repeated measures	Time: p Surgery Time x
S1J	Whole ACC fiberphotometry	ACC Ca ²⁺ dynamics in CPID	Cuff surgery	LD entry in dark	Sham (14) Cuff (15)	Time x Surgery 2-way ANOVA repeated measures	Time: p Surgery Time x
S1L	Whole ACC fiberphotometry	ACC Ca ²⁺ dynamics in CPID	Cuff surgery	UST male scent	Sham (14) Cuff (15)	Time x Surgery 2-way ANOVA repeated measures	Time: p Surgery Time x
S2A	Dual ACC & ACC-LHb fiberphotometry	Depressive-like behavior	Cuff surgery	Splash	Sham (8) Cuff (6)	Unpaired t-test (two tailed)	U=21 p=0.754
S2B	Dual ACC & ACC-LHb fiberphotometry	Anxiodepressive-like behavior	Cuff surgery	NSF	Sham (8) Cuff (6)	Unpaired t-test (two tailed)	F(5,7)= p=0.755
S2C	Dual ACC & ACC-LHb fiberphotometry	Depressive-like behavior	Cuff surgery	UST	Sham (8) Cuff (6)	Mann-Whitney test (two tailed)	U=15 p=0.445
S2D	Dual ACC & ACC-LHb fiberphotometry	Anxiety-like behavior	Cuff surgery	LD	Sham (8) Cuff (6)	Unpaired t-test (two tailed)	F(5,7)= p=0.779

Extended Table 5 – Statistical analysis for the supplementary figures, extended.

S2H	Dual ACC & ACC-LHb fiberphotometry	ACC-LHb Ca2+ dynamics in CPID	Cuff surgery	UST male scent	Sham (8) Cuff (6)	Time x Surgery 2-way ANOVA repeated measures	Time: p Surgery Time x
S2J	Dual ACC & ACC-LHb fiberphotometry	ACC-LHb Ca2+ dynamics in CPID	Cuff surgery	LD entry in dark	Sham (8) Cuff (6)	Time x Surgery 2-way ANOVA repeated measures	Time: p Surgery Time x
S2K	Dual ACC & ACC-LHb fiberphotometry	ACC-LHb Ca2+ dynamics in CPID	Cuff surgery	Restraint stress	Sham (8) Cuff (6)	Time x Surgery 2-way ANOVA repeated measures	Time: p Surgery Time x
S2L	Dual ACC & ACC-LHb fiberphotometry	ACC Ca2+ dynamics in CPID	Cuff surgery	Restraint stress	Sham (8) Cuff (6)	1-way ANOVA	F=0.00 p=0.00
S2M	Dual ACC & ACC-LHb fiberphotometry	ACC-LHb Ca2+ dynamics in CPID	Cuff surgery	Unpredictable electrical shock	Sham (8) Cuff (6)	Time x Surgery 2-way ANOVA repeated measures	Time: p Surgery Time x
S2N	Dual ACC & ACC-LHb fiberphotometry	ACC Ca2+ dynamics in CPID	Cuff surgery	Unpredictable electrical shock	Sham (8) Cuff (6)	Paired t-test (two tailed)	t=5.374 p=0.00
S3A	Acute ACC-LHb optogenetic activation	Electrophysiological properties of Chr2	Acute ACC-LHb optogenetic activation	Voltage clamp	n=3	One way ANOVA	F=2.874 p=0.21
S3B	Acute ACC-LHb optogenetic activation	Electrophysiological properties of Chr2	Acute ACC-LHb optogenetic activation	Current clamps	n=4	One way ANOVA	F=20.9 p=0.00
S3C	Acute ACC-LHb optogenetic activation	Electrophysiological properties of ArchT	Acute ACC-LHb optogenetic activation	Voltage clamp	n=4	Paired t-test (two tailed)	t=0.267 p=0.80
S3D	Acute ACC-LHb optogenetic activation	Electrophysiological properties of ArchT	Acute ACC-LHb optogenetic activation	Current clamps	n=4	One way ANOVA	F=14.8 p=0.03
S4A	Chronic ACC-LHb optogenetic activation	Anxiodepressive-like behavior	Chronic ACC-LHb optogenetic activation	NSF	No stim (8) Stim (8)	Unpaired t-test (two tailed)	F(7,7)= p=0.61
S4B	Chronic ACC-LHb optogenetic activation	Depressive-like behavior	Chronic ACC-LHb optogenetic activation	Splash	No stim (8) Stim (8)	Unpaired t-test (two tailed)	F(7,7)= p=0.00
S4E	Chronic ACC-LHb optogenetic activation	FC linear regression	Chronic ACC-LHb optogenetic activation	Correlation	n=31389	Spearman's correlation	r=0.733
S4F	Chronic ACC-LHb optogenetic activation	p-value linear regression	Chronic ACC-LHb optogenetic activation	Correlation	n=31212	Spearman's correlation	r=0.622

Results

General overview

The following section is composed of original data obtained over the course of my doctoral studies in the form a scientific article, as a first version that will be submitted shortly. It is co-authored by Dr Victor Mathis and myself. He carried out the fiberphotometry experiments in the whole ACC, which represent the first part of the article, and we worked together on the fiberphotometry experiments aiming at characterising the ACC neurons projecting to the LHb. I conducted the remaining part of the article, comprising the optogenetic characterisation of the ACC-LHb pathway in naïve, chronic pain and chronic stress animals, as well as the molecular characterisation of LHb-projecting ACC neurons.

Article: The cingulo-habenular pathway plays a key role in aversive processing and participates in chronic pain- but not stress-induced anxiodepressive like consequences.

Authors and affiliations: Sarah H. Journée^{a#}, Victor P. Mathis^{a#}, Robin Waegaert^a, Mithil Gaikwad^{a,b}, Maxime Thouaye^a, Sylvain Hugel^a, Quentin Leboulleux^a, Noémie Willem^a, Léa Becker^{a,c}, Sebahat Ozkan^a, Pierre-Eric Lutz^{a,d}, Ipek Yalcin^{a,b*}.

^a: Centre National de la Recherche Scientifique, Université de Strasbourg, Institut des Neurosciences Cellulaires et Intégratives, Strasbourg, France

^b: Department of Psychiatry and Neuroscience, Université Laval, Québec QC G1V 0A6, Canada

^c: Department of Anesthesiology, Center for Clinical Pharmacology, Washington University in St. Louis, St. Louis, MO, USA

^d: Douglas Mental Health University Institute, Montreal, QC, Canada

#: These authors contributed equally to this work

*: corresponding author

Address correspondence to Ipek Yalcin Ph.D., Institut des Neurosciences Cellulaires et Intégratives, UPR3212 CNRS, 5 rue Blaise Pascal, Strasbourg cedex 67084, France; E-mail: yalcin@inci-cnrs.unistra.fr.

Abstract

The anterior cingulate cortex (ACC) has a major role in behavioral adaptation notably by integrating information related to aversion and emotions. Preclinical and clinical studies showed that the comorbidity of chronic pain and mood disorders is associated with functional and structural alterations in the ACC. However, how these changes propagate to downstream structures of the ACC is yet to be studied. The lateral habenula (LHb) seems to be an interesting target based on its well-known roles in mood regulation, and strong anatomo-functional connection with the ACC. Here, we thus aimed at deciphering the role of ACC neurons projecting to LHb in chronic pain and its comorbidity with depression. Using calcium imaging recordings in freely moving mice, we first compared the Ca²⁺ dynamics of all ACC neurons with ACC neurons projecting to the LHb only (ACC→LHb). We observed that ACC→LHb neurons present a unique Ca²⁺ signature in response to aversive events. Then, using optogenetic approach, we evaluated the functional role of ACC→LHb neurons. We observed that their chronic, but not acute, activation induces long lasting anxiodepressive-like behaviors while the inhibition of this specific neuronal populations is sufficient to prevent the anxiodepressive-like consequences induced by chronic pain, but not chronic stress. Finally, combining vTRAP and RNAseq approaches, we showed that chronic pain induces epigenetic adaptations and alters RNA processing in ACC neurons projecting to LHb. Overall, these results confirm the important role of the cingulo-habenular pathway in chronic pain-induced emotional disorders.

Abbreviations

ACC: anterior cingulate cortex

BLA: basolateral amygdala

CaMKIIa: calcium/calmodulin kinase 2a

CPP: conditioned place preference

Ctrl: control

CVS: chronic variable stress

FST: forced swim test

LD: light dark

LHb: lateral habenula

MeCP2: methyl-CPG-binding protein 2

NSF: novelty suppressed feeding test

RTA: real time aversion

UST: urine sniffing test

vF: von Frey

vTRAP: viral translating ribosome affinity purification

Introduction

The anterior cingulate cortex (ACC) is a higher-order brain region integrating a multitude of information related to potential negative/positive outcomes and emotions. Accordingly, it participates in risk assessment and action selection (Johansen and Fields, 2004; Kolling et al., 2016a, 2016b; Monosov et al., 2020; Procyk et al., 2000; Quilodran et al., 2008; Rigney et al., 2018; Rolls, 2019; Rushworth et al., 2011; Shackman et al., 2011). It has notably been described that the ACC mediates action selection depending on the level of uncertainty and volatility of a given situation (Monosov et al., 2020), confirming its key role in behavioral adaptation (Brockett et al., 2020; Quilodran et al., 2008). fMRI studies have highlighted the implication of the ACC in anxiety and mood disorders (Chen et al., 2018; Shin et al., 2001) and more recently, the advancement in deep brain stimulation brought additional insights about the ACC functions. For instance, a recent study demonstrates a robust anxiolytic response to cingulum bundle stimulation in patients treated for epilepsy (Bijanki et al., 2019). Additionally, one of the most promising use of ACC deep brain stimulation (DBS) protocols concerns the treatment of patient affected by treatment-resistant depression (Holtzheimer et al., 2017; Riva-Posse et al., 2018). These findings suggest that, beside its primary role in behavioral coordination and action selection, the ACC is a key brain region in mood regulation (Etkin et al., 2011; Rolls, 2019; Stevens et al., 2011). In that regard, it has been shown that risk factors associated with emotional disorders, such as chronic pain, alter the ACC neuronal activity (Barthas et al., 2015; Shin et al., 2001; Stevens et al., 2011). For instance, in a mouse model of neuropathic pain, the ACC becomes hyperactive (Barthas et al., 2015) concomitant with the emergence of pain-induced anxiodepressive consequences (Sellmeijer et al., 2018). Hence, the ACC appears not only as a potential promising target in the treatment of mood disorders (Figeo et al., 2022; Holtzheimer et al., 2017; Mayberg et al., 2005) but also in the comorbidity between chronic pain and anxiodepressive symptoms (Humo et al., 2019). However, how these alterations in the ACC propagate within the ACC network is yet to be studied. It is then of critical importance to understand how specific ACC pathways participate in behavioral adaptations, emotion or pain processing and development of mood disorders.

Among the ACC wide connectome (Fillinger et al., 2017a, 2017b), numerous brain areas are known to be implicated in the development of mood disorders. Notably, ACC-related neurocircuits have been specifically described in the control of the social transfer of pain and analgesia or stressful events (Smith et al., 2021), or the vulnerability to chronic pain (Becker

et al., 2023; Lee et al., 2022; Zhu et al., 2021). However, since most of the ACC brain connections are reciprocal, it is difficult to evaluate whether alterations come from the ACC or from the other brain structure. Recent studies showed that alterations in the cingulo-amygdala circuit control emotional processing and participate in mood disorders. Indeed, the activation of ACC neurons projecting to amygdala is sufficient to inhibit innate fear responses (Jhang et al., 2018) while the activation of the basolateral amygdala (BLA) neurons projecting to ACC can drive the ACC hyperactivity and trigger anxiodepressive-like phenotypes in mice (Becker et al., 2023). Surprisingly, very little is known about the role of the unidirectional connection from the ACC to the lateral habenula (LHb) (Kim and Lee, 2012; Mathis et al., 2017, 2021). Indeed, this latest has been extensively described in aversion, anxiety and stress processing (Baker et al., 2022; Cerniauskas et al., 2019; Lecca et al., 2017; Mathis et al., 2018, 2015; Proulx et al., 2014; Shabel et al., 2012; Trusel et al., 2019) as well as in action evaluation and selection based on the potential outcomes (Hikosaka, 2010; Stephenson-Jones et al., 2016; Stopper and Floresco, 2014). Moreover, its implication in depression is well established in both preclinical models (Cui et al., 2018; Lecca et al., 2016, 2014; Li et al., 2013) and in Human (Sartorius et al., 2010; Sartorius and Henn, 2007). Indeed, deep brain stimulation of the LHb was notably found to rescue depressive symptoms (Sartorius et al., 2010; Sartorius and Henn, 2007). The overlap between ACC and LHb functions, combined with their common implication in depression, suggests that the LHb could be an important relay for the ACC, as already observed for other prefrontal cortical areas (Benekareddy et al., 2018; Mathis et al., 2017). Hence, the study of the ACC-LHb pathway might bring new knowledge to better apprehend whether and how ACC alterations propagate to other brain regions implicated in emotion regulation and action selection eventually contributing to emotional disorders.

In this study, we evaluated whether the chronic-pain induced alterations occurring in the ACC (Barthas et al., 2015; Sellmeijer et al., 2018) affect the ACC-LHb pathway. Using calcium imaging recordings in freely moving mice, we first performed a thorough evaluation of the Ca^{2+} dynamic alterations induced by chronic pain in the ACC. After, this first characterization, using multi-colors fiber photometry recordings we observed that the LHb projecting ACC neurons ($ACC \rightarrow LHb$) present a unique Ca^{2+} signature in response to aversive events, compared to the whole ACC neuronal population. Then, using an optogenetic approach, we further evaluated the functional role of $ACC \rightarrow LHb$ neurons. Notably, we observed that their chronic,

but not acute, activation induces long lasting anxiodepressive-like behaviors, while inhibition of the ACC→LHb pathway is sufficient to prevent the anxiodepressive-like consequences induced by chronic pain, but not chronic stress. Finally, using vTRAP and RNAseq approaches, we characterized the molecular identity of the ACC→LHb neurons and found that chronic pain specifically alters genes implicated in epigenetic adaptations and RNA processing in these neurons. Our results suggest that ACC→LHb pathway is strongly implicated in emotional processing especially in the anxiodepressive-like consequences of neuropathic pain. Molecular alterations identified in this particular cell types will help us to better understand the physiological and pathological role of the ACC output neurons in emotion and related disorders.

Material and Methods

See Supplement for Extended Materials and Methods

Animals

All experiments were conducted in adult male C57BL/6J mice (Charles River, L'Arbresle, France) in a reversed 12h light/dark cycle. Protocols were approved by the local ethical committee of the University of Strasbourg (CREMEAS) and performed according to guidelines of the European Community Council Directive (EU 2010/63).

Surgical procedures

Surgical procedures were performed under zoletil/xylazine anesthesia (Zoletil 50 43mg/kg, Paxman 7mg/kg, ip; Centravet).

Chronic neuropathic pain was induced by placing a polyethylene cuff around the common branch of the right sciatic nerve of the animal (Yalcin et al., 2014). The control group (sham) underwent the same procedure without cuff implantation.

Based on the Mouse Brain Atlas (Franklin and Paxinos, 2013), the following coordinates were used for viral transfection and optical fiber implantation: the ACC (AP: +0.7mm, L: +/-0.3mm, DV: -1.4mm) and LHb (AP: -1.7mm, L: +/-0.4mm, DV: -2.7mm). 0.25µl of AAVrg-CaMKIIa-ChR2(H134R)-mCherry (Addgene), AAVrg-CaMKIIa-ArchT-GFP(PV2527) (Addgene) or AAVrg-CaMKIIa-m.Cherry-RPL10a-WPRE-SV40 (IGBMC) were injected bilaterally into the LHb. For

fiberphotometry, the same method was used to unilaterally inject 0.25 μ l of AAVrg-Syn.NES-jRGECO1a.WPRE.SV40 (Addgene) into the LHb and 0.5 μ l of AAV5-Syn-GCaMP6m-WPRE-SV40 (Addgene) into the ACC. At the end of the experiments, animals underwent intracardiac perfusion to check the site of injection ([see Extended Table 1 for exclusion criteria](#)).

Chronic Variable Stress model (CVS)

During 21 days, stressed mice were subjected each day for 1h to one stressor, with a succession of three different stressors: 100 electrical footshocks, tail suspension and restraint stress (falcon tube). Control mice remained unstressed and kept group housed, while stressed mice were housed individually.

Optogenetic stimulation procedures

After 3 to 7 days of cannula implantation, the ACC-LHb pathway was either activated or inhibited using optogenetic approach. For non-stimulated animals the light remained switched off.

[Activation paradigm](#): Stimulated animals received repetitive blue light (463nm)_stimulation sequences of 10s consisting of 8s at 10Hz with 40ms pulses and 2s without stimulation. For the acute activation paradigm of the ACC-LHB pathway, the 10s sequence was repeated during 30min prior (LD, FST) or during behavioral testing (RTA, NSF). For the chronic stimulation paradigm, the 30min sequence took place each day for 4 consecutive days and the animals were subjected to behavioral tests in the following week without stimulation during the tests. Both activation paradigms were performed in naïve animals.

[Inhibition paradigm](#): Green light (520nm) was delivered in a continuous manner during 5min prior (LD, FST) or during behavioral testing (locomotor activity, RTA, CPP, NSF and vF). The inhibition and behavioral tests were performed 8 weeks after the cuff surgery and the day after the last stressor in CVS animals.

Fiberphotometry

Fiber photometry data were collected with a Doric system at a sampling frequency of 12kHz. The 405- and 465-nm signals were equalized to record an equivalent signal/noise ratio. Data have been analyzed with custom MATLAB scripts. The dynamic of fluorescence was calculated

as: $\Delta F/F = (F_{465} - F_{405f})/F_{405c}$. The deviation of each sample from the averaged signal of a given period was calculated with a z-score.

Behavioral assessment

All the behavioral tests were performed during the dark phase, under red light. A summary of the tests performed by each animal cohort is provided in [Extended Data Table 2](#).

The mechanical threshold of hindpaw withdrawal was determined weekly using von Frey filaments (vF; Bioseb, Chaville, France) before and after peripheral nerve injury. Aversion and preference due to the optogenetic stimulation were measured with real-time aversion (RTA) and conditioned place preference (CPP) respectively. For anxiodepressive-like behaviors, the light-dark (LD), novelty suppressed feeding (NSF), forced swim (FST), splash and urine sniffing (UST) tests were conducted. To record responses to stressful events, a 5s restraint stress and unpredictable foot shocks were performed. Locomotor activity was measured in the home cage and in an open field.

Emotionality z-score

Emotionality z-scores were computed as previously described by (Guilloux et al., 2011). First, individual z-score values were calculated for each mouse in each test using the following formula: $z = (X - \mu)/\sigma$ where X represents the individual data for the observed parameter while μ and σ represent the mean and standard deviation of the control group. Finally, z values obtained for each test were averaged to obtain a single emotionality score:

Emotionality z-score = $Z_{test1} + Z_{test2} + \dots + Z_{testn} / \text{Number of tests}$.

Ex vivo electrophysiology

Patch-clamp recordings of the ACC pyramidal neurons were performed using acute slices prepared from 8- to 12-week-old mice, the ACC being illuminated with the same system used for the in vivo experiments.

Immunohistochemistry

For the vTRAP study, to verify in which neuronal type the virus is expressed, the animals were perfused 3 weeks after virus injection and NeuN, Olig2 or GFAP immunostaining were performed.

Plasmid and AAV generation

For translating ribosome affinity purification, pAAV-CaMKII-mCherry-RPL10a-WPRE-SV40 plasmid was constructed by in-fusion cloning. AAV generation was performed by the Molecular Biology and Virus platform at IGBMC (Strasbourg, France) to generate the AAVrg-CaMKIIa-mCherry-RPL10a-WPRE-SV40 virus.

Viral Translating Ribosome Affinity Purification (vTRAP) & RNA extraction

Bilateral ACC dissection was performed 3 weeks after virus injection. The ACC was freshly and quickly manually dissected from animals killed by cervical dislocation. Translated mRNA purification was made following Heiman *et al.* (2014) protocol for TRAP and directly followed by RNA extraction with the Absolutely Nanoprep kit (Agilent). The extracted RNAs were stored at -80°C until qRT-PCR and sequencing.

The vTRAP was performed in two different cohorts. The first cohort was composed of naïve animals, in which RNA sequencing was performed in both IP and input fractions of 3 animals. The second experiment was performed in sham and cuff animals in our cuff model, in which RNA sequencing was done only in the IP fraction of 8 sham and 8 cuff animals.

qRT-PCR

qRT-qPCR was performed on a 384-wells QuantStudio5 Real-Time PCR system (Applied Biosystem) using Sybr Green. Relative abundance of each RNA target gene transcript was normalized to the endogenous control gene *Gapdh* RNA. Primers can be found in [Extended Data Table 3](#).

RNA sequencing

RNA-sequencing was performed by the Genomeast platform at IGBMC (Strasbourg, France), using Clontech SMART-Seq v4 Ultra Low Input RNA Kit for Sequencing User Manual (PN 091817) and the Illumina Nextera XT DNA Library Prep Kit Reference Guide (PN 15031942). Libraries were sequenced on an Illumina NextSeq 2000 sequencer.

RNA sequencing analysis

Reads were processed by the Genomeast platform at IGBMC (Strasbourg, France). Gene expression quantification was performed from uniquely aligned reads using htseq-

count90version 0.6.1p1, with annotations from Ensembl version 102. Differential expression analysis was performed using R and the Bioconductor package DESeq2.

For the first cohort, the fold-changes were calculated for IP vs input, while for the second cohort the fold-changes were computed for cuff vs sham. From these data, gene ontology, Gene Set Enrichment Analysis (GSEA) and Rank-Rank Hypergeometric Overlap (RRHO) analyses were performed on both data sets.

Statistical analysis

Statistical analyses were performed in GraphPad Prism v9.0.2 software. Data are expressed as mean±SEM, with statistical significance set as * $p < 0.05$, ** $p < 0.01$, *** $p < 0.001$.

Data were first tested for normality using the Shapiro-Wilk normality test. If data passed the normality test, student's t-test (unpaired, two-tailed), One-Way Repeated Measures ANOVA, and Two-way ANOVA followed by Bonferroni or Newman-Keuls post hoc tests were used when appropriate. If data failed the normality test, Mann-Whitney non-parametric analysis (two-tailed) was used. All statistical analyses are summarized in [Extended Data Table 4](#).

Results

The Anterior Cingulate Cortex Ca^{2+} is slightly affected by chronic pain.

First, using calcium imaging techniques, we evaluated whether chronic neuropathic pain alters the ACC Ca^{2+} fluctuations during behavioral emotional tests. Here, mice underwent a sciatic nerve compression ("Cuff" model) that induces long-term mechanical hypersensitivity associated with the development of anxiodepressive-like behaviors (Fig.1 and S1) and were injected with an AAV expressing the calcium biosensor GcAMP6m and implanted with an optic fiber in the ACC (Fig. 1A-C). As expected, peripheral nerve injury induced an ipsilateral mechanical hypersensitivity in cuff animals that lasted for 8 weeks (Fig.1D; Mixed Effect Model, time as repeated measure: Time, Surgery & Time x Surgery: $p < 0.0001$; 2-8 PO weeks: $cuff_{ipsi} < sham_{ipsi}$, $cuff_{ipsi} < sham_{contra}$, $cuff_{ipsi} < cuff_{contra}$, $p < 0.01$). As already described (Barthas et al., 2015; Sellmeijer et al., 2018; Yalcin et al., 2011), eight weeks after the cuff surgery, neuropathic animals start to display anxiodepressive disorders (Fig. S1A-D). Nonetheless, as for other animal models of psychiatric condition (Krishnan et al., 2007; Nasca et al., 2019), within the population not all the individuals display the full spectrum of anxiodepressive-like

symptoms, and accordingly our data showed a remarkable variability between tests and within groups. In this study, we sought to evaluate the impact of chronic pain onto ACC's Ca²⁺ activity, and so decided to keep all the animals and calculated an emotionality score (Guilloux et al., 2011). Overall, cuff animals displayed a higher emotionality score compared to sham mice (Fig.1E; t-test: $p=0.0161$), suggesting a shift towards emotional disorders in our cohorts, confirming the comorbidity between chronic pain and emotional disorders.

We further evaluated the impact of chronic neuropathic pain on the ACC Ca²⁺ dynamic during the anxiodepressive tests. In that purpose, we recorded and compared the ACC Ca²⁺ signals between Sham and Cuff mice performing each aforementioned test. It has been described that chronic pain, and especially sciatic nerve compression, induces a shift towards ACC hyperactivity (Sellmeijer et al., 2018). Hence, we anticipated important differences in ACC signals between the two groups. However, only subtle changes were observable. Strikingly, no differences were observed for the Ca²⁺ dynamics during the initiation and termination of each grooming episode between neuropathic and control animals for the splash test (Fig.1F-F'' and Fig.S1E-F). Overall, for both groups, we observed a strong reduction of the ACC Ca²⁺ signal as soon as the animals started grooming (t-test: sham, $p=0.0015$; cuff, $p=0.0125$) and a return to the initial signal immediately after the cessation of the grooming behavior (Fig.1F''; (t-test: sham, $p=0.0043$; cuff, $p=0.0003$). The analysis of the 1-sec bins +/-3 sec around the event confirmed this observation (Fig. S1E-F). The 2way-ANOVA corresponding to the grooming initiation (time as repeated measure, $F_{(1,26)}=22.51$, $p<0.0001$) revealed a strong difference between the 3 sec before and after the initiation for both groups. The post-hoc analysis revealed that the 3 sec before the grooming were not different from each other, whereas all the 3 sec after the initiation were different from the 3 sec before (Fig.1.F''). A similar but reversed pattern was observed for the termination (time as repeated measure, $F_{(1,26)}=33.40$, $p<0.0001$). Hence, this suggests that the ACC activity is decreased while mice engage in self-grooming and is increased when they stop this behavior. However, no effect of neuropathic pain was observed. On the contrary, in the NSF test, we observed an effect of the cuff surgery for the ACC signal when mice touched and ate the food pellet (Fig.1G-G'' and Fig.S1H-I). When mice ate the food, the 2-way ANOVA showed time and surgery effects (Fig.1G'; 2-way ANOVA, time as repeated measure: Time: $F_{(3,72)}=64.75$, $p<0.0001$; Surgery: $F_{(1,24)}=5.854$, $p=0.0235$; Time x Surgery $F_{(3,72)}=0.0945$, $p=0.9628$).

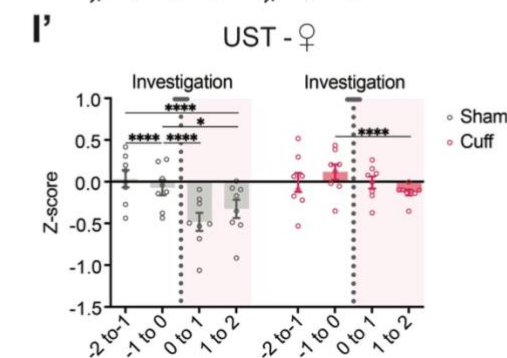
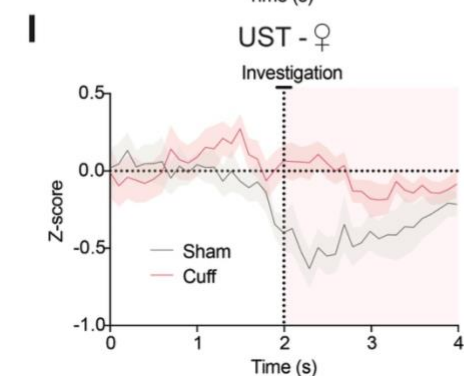
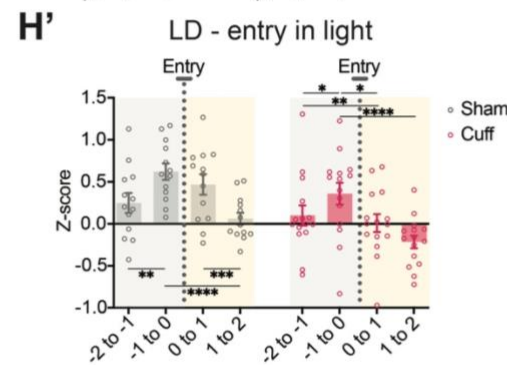
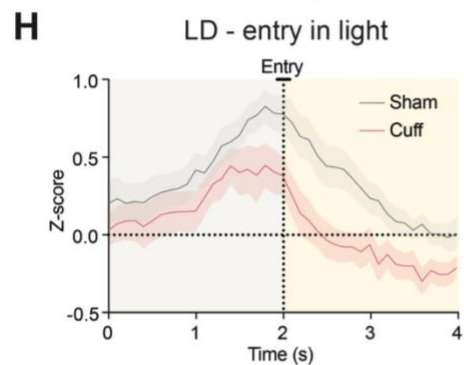
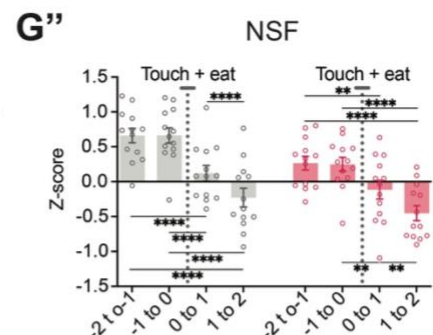
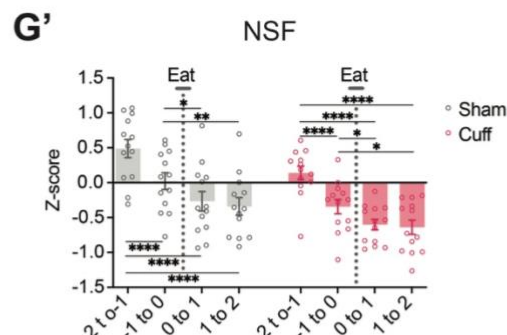
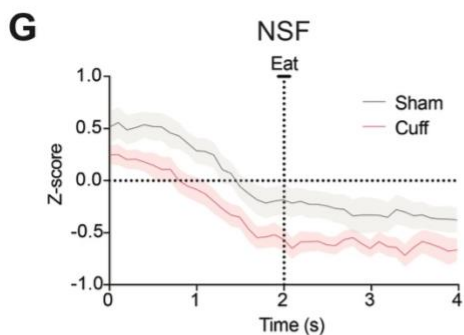
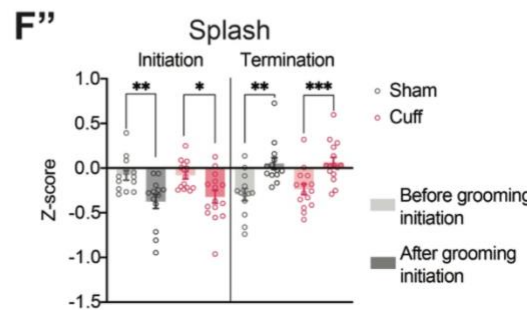
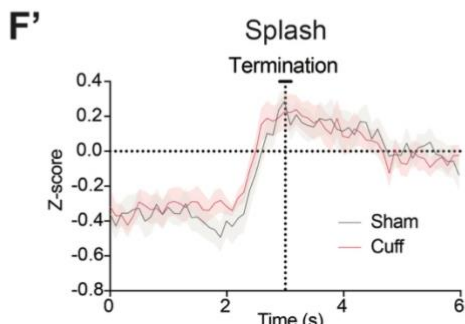
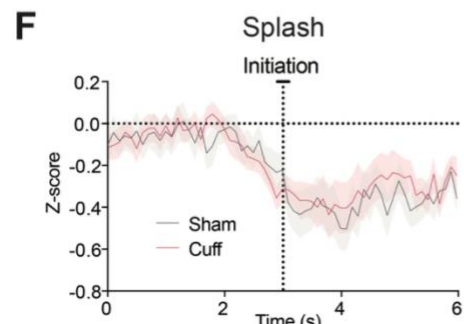
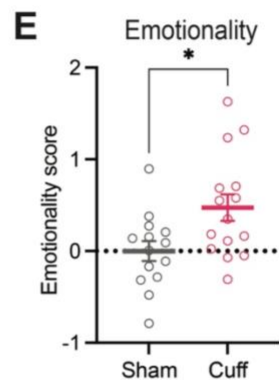
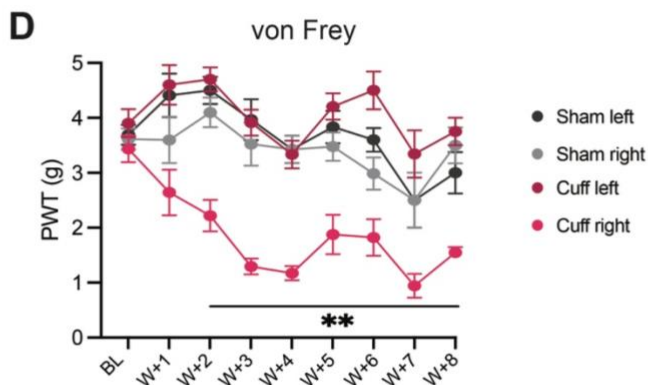
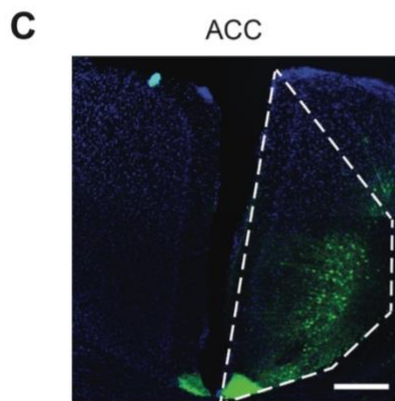
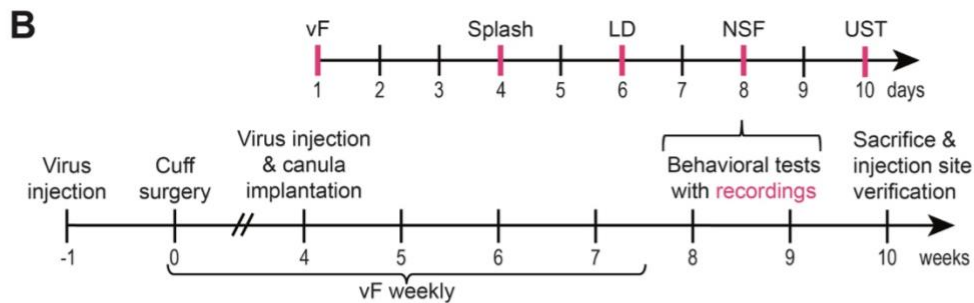
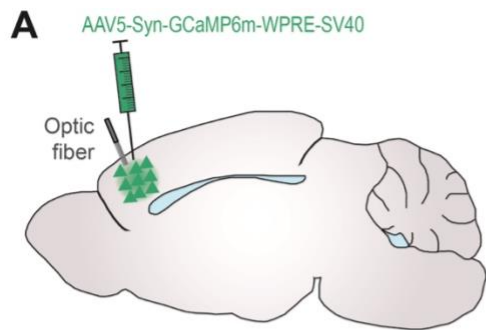


Figure 1. The effect of chronic pain on the ACC Ca²⁺ dynamic.

(A) Representation of the virus injections and fiber photometry cannula implantation strategy. **(B)** Timeframe of the experimental design (cuff surgery, virus injection, cannula implantation and behavioral tests with recordings). **(C)** Representative picture of the virus expression in the ACC; scale bar = 250µm. **(D)** Cuff animals present a decreased mechanical threshold in the ipsilateral paw compared to the contralateral paw and sham animals, 2 weeks after the surgery and onward. **(E)** Cuff animals exhibit an increased emotionality score, reflecting the development of anxiodepressive-like consequences. **(F-F'')** ACC Ca²⁺ dynamic during splash test. Representative Z-score trace during grooming initiation (**F'**) and grooming termination (**F''**) in the splash test. **(F'-F'')** Averaged 2-sec bin Z-score before and after grooming initiation and termination, for both groups. **(G-G'')** ACC Ca²⁺ dynamic during NSF test. **(G)** Representative Z-score trace of a recording when the animal eats the food pellet in the NSF. **(G')** Averaged 1-sec bin Z-score before and after the eating episode. **(G'')** Averaged 1-sec bin Z-score before and after touching the food pellet. We selected only the “touch events” that were followed by the food consumption. **(H-H')** ACC Ca²⁺ dynamic during LD test. Representative Z-score trace of a recording when the animal enters the light box (**H**). **(H')** Averaged 1-sec bin Z-score related to the entrance in the light compartment (from dark to light side). **(I-I')** ACC Ca²⁺ dynamic during UST for the female scent. Representative Z-score trace of a recording when the animal sniffs the female scent (**I**). **(I')** Averaged 1-sec bin Z-score before and after the female scent investigation. n=14-15 animals/group. Data are expressed as mean ± SEM. *p<.05, **<.01, ***p<.001, ****<.0001. ACC, anterior cingulate cortex; BL, baseline; LD, light-dark test; NSF, novelty suppressed feeding test; UST, urine sniffing test; vF, von Frey; w, week.

For the touch, we only observed a difference when mice touched and ate the food pellet (Fig.1G''; 2-way ANOVA, time as repeated measure: Time: $F_{(3,72)}=57.13$, $p<0.0001$; Surgery: $F_{(1,24)}=5.720$, $p=0.0250$; Time x Surgery $F_{(3,72)}=0.9697$, $p=0.4118$), but not when they touched without eating (Fig.S1H-I; 2-way ANOVA, time as repeated measure: Time: $F_{(3,69)}=4.157$, $p=0.0091$; Surgery: $F_{(1,23)}=2.064$, $p=0.1643$; Time x Surgery $F_{(3,69)}=0.4242$, $p=0.7362$). This confirms the key role played by the ACC in action selection. Indeed, these findings suggest that the ACC Ca²⁺ reduction is required to promote food intake. It also reveals that the ACC reactivity to the task is not affected by the pain condition.

For the LD test (Fig.1H-H' and Fig.S1J-K), only the ACC Ca²⁺ signal related to the entrance in the light side was different between groups (Fig.1H'; 2-way ANOVA, time as repeated measure: Time: $F_{(3,78)}=24.14$, $p<0.0001$; Surgery: $F_{(1,26)}=4.965$, $p=0.0347$; Time x Surgery $F_{(3,78)}=1.830$, $p=0.1486$). For the entrance in the dark side, the 2-way analysis revealed a time effect as well as a Surgery X time interaction (Fig.S1J-K; 2-way ANOVA, time as repeated measure: Time: $F_{(3,42)}=20.22$, $p<0.0001$; Surgery: $F_{(1,14)}=0.1746$, $p=0.6824$; Time x Surgery $F_{(3,42)}=3.194$, $p=0.0331$). Again, this suggests that the pain condition is not affecting the ACC Ca²⁺ dynamics.

Finally, we wanted to test despair-like behaviors using the classical forced swim test (FST) (Porsolt et al., 1977). Unfortunately, with our first batch of mice we observed the difficulty for tethered animals to perform the test. Hence, with our second cohort of mice, we choose to adapt the urine sniffing test (UST) (Malkesman et al., 2010; Morel et al., 2022), used to assess anhedonia, to evaluate ACC Ca²⁺ signal when male mice were exposed with a pleasant scent, female urine from same strain and age-matched animals (Fig.1I-I'). We chose to use male urine as a control. Although a Ca²⁺ fluctuation was observed when mice investigated both scent, no differences were observed between sham and cuff mice when sniffing the male scent (Fig.S1L-M; 2-way ANOVA, time as repeated measure: Time: $F_{(3,42)}=2.865$, $p=0.0479$; Surgery: $F_{(1,14)}=0.0002$, $p=0.9882$; Time x Surgery $F_{(3,42)}=1.859$, $p=0.1513$). The analysis showed that the dynamic of ACC Ca²⁺ signal of cuff mice is strongly reduced compared to sham mice in response to female scent (Fig.1I'; 2-way ANOVA, time as repeated measure: Time: $F_{(3,42)}=12.42$, $p<0.0001$; Surgery: $F_{(1,14)}=3.370$, $p=0.0877$; Time x Surgery $F_{(3,42)}=6.441$, $p=0.0011$), suggesting that the ACC of neuropathic animals is not reactive anymore to pleasant scent.

Altogether, these results suggest that, even though chronic pain induces important long-lasting alteration within the ACC that are correlated with the expression of anxiodepressive disorders²⁰, the ACC activity dynamic changes significantly with tests assessing motivation or anhedonia, but no innate behavior that are expressed by both groups.

ACC neurons projecting to the lateral habenula (ACC_{→LHb}) display a unique pattern of activity in response to aversive events in a pilot study.

Nevertheless, given the crucial role of the ACC in the development of emotional disorders especially in the context of chronic pain (Barthas et al., 2015; Becker et al., 2023; Sellmeijer et al., 2018), the subtle Ca²⁺ alterations observed within the ACC appeared surprising and suggest that chronic pain might affect only a very specific subset of ACC neurons. Among others, the ACC neurons projecting to the LHb are of particular interest. Indeed, the two areas share common functions, notably in relation with emotional processing and action selection, and are implicated in depression. Even though very little is known about the ACC-LHb pathway role, it was recently described that its pharmacological alteration is sufficient to alter behavioral selection in rats (Mathis et al., 2017), while its chemogenetic inhibition prevents stress integration (Mathis et al., 2021). Hence, we further sought to evaluate if the pain-

induced alteration occurring within the ACC affects specifically ACC neurons projecting to the LHb (ACC→LHb), and if so whether it could propagate to the LHb. In that purpose we used a dual-color fiber photometry. A retrograde AAV allowing the expression of the red-shifted calcium biosensor jRGECO and a local AAV-GcAMP6m were injected in the LHb and the ACC respectively (Fig.2A-C). This viral strategy allowed the simultaneous recording of Ca²⁺ fluctuations of the whole ACC neuronal population and ACC→LHb neurons in cuff animals with anxiodepressive-like behaviors (Fig.2D-E and Fig.S2A-D).

The most striking finding was that ACC→LHb neurons do not have a similar Ca²⁺ signature compared to the whole ACC. Indeed, these neurons do not present a specific Ca²⁺ fluctuation when mice start or stop grooming in the splash test. The analysis of 1sec bins revealed no time effect for both groups (Fig.2F-F'' and Fig.S2E; initiation of grooming: 2-way ANOVA time as repeated measure, Time: $F_{(1.347,16.36)}=0.2668$, $p=0.6843$; termination of grooming: time as repeated measure, Time: $F_{(1.464,17.57)}=0.09057$, $p=0.8561$) nor when they eat the food in the NSF test (Fig.2G-G'; 2-way ANOVA time as repeated measure, Time: $F_{(1.585,17.44)}=3.579$, $p=0.0588$). Similarly, these neurons did not present any dynamic in response to female scent in the UST (Fig.2H; 2-way ANOVA time as repeated measure, Time: $F_{(1.681, 18.49)}=0.4574$, $p=0.6068$), nor male scent (Fig.S2F-H), or to the entry of the light box (Fig.2I-I'; 2-way ANOVA time as repeated measure, Time: $F_{(1.733, 19.06)}=1.821$, $p=0.1915$) or dark box in the LD test (Fig.S2I-J).

Overall, these findings suggest that contrary to the whole ACC neuronal population, ACC→LHb neurons are not implicated in the tested behavioral paradigms.

Nonetheless, given the prominent role played by both the prefrontal cortex and the LHb in stress processing, we further sought to evaluate the Ca²⁺ response to stressful events. Accordingly, we evaluated the Ca²⁺ dynamics triggered in response to an acute 5-sec restraint stress protocol and an unpredictable electrical foot shock. Interestingly, we observed two different patterns. First, in response to the restraint stress, the analysis of 5-sec bins around and during the stress revealed a strong reduction of the Ca²⁺ signal (Fig.2J-J'; 1-way ANOVA time as repeated measure, $F_{(1.312, 17.06)}=15.58$, $p=0.0005$). The postdoc analysis revealed that the 5-sec of restraint stress as well the 5-sec following the restraint stress were similar ($p=0.1614$) but both different from the 5-sec before the restraint stress (bin 1 vs 2: $p=0.039$ and bin 1 vs 3: $p<0.0001$).

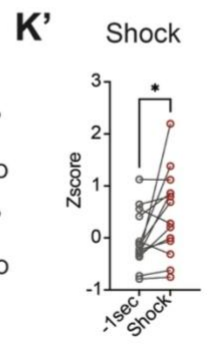
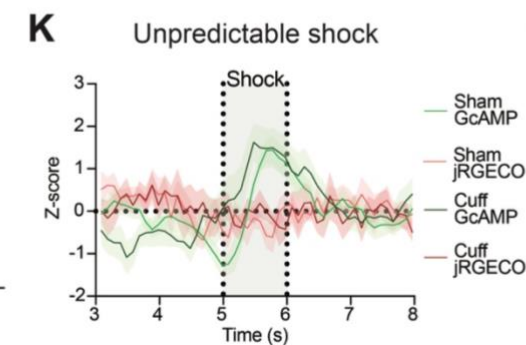
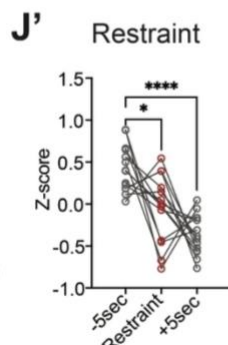
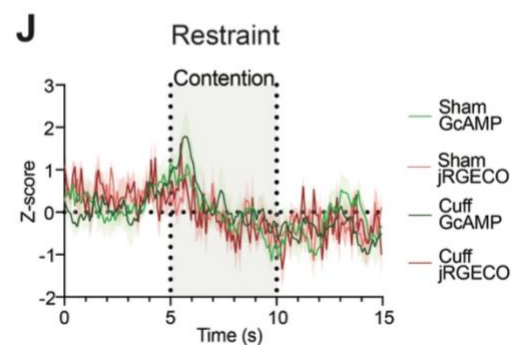
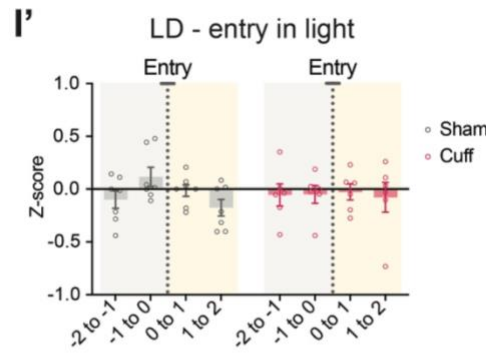
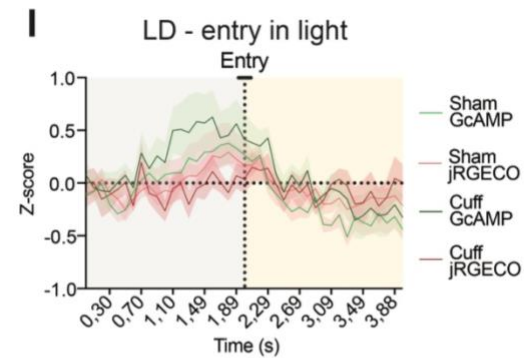
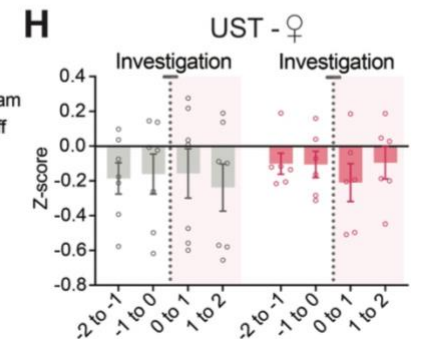
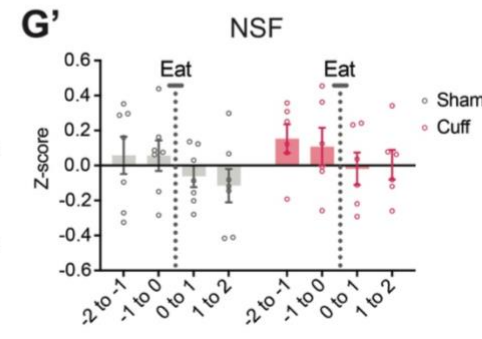
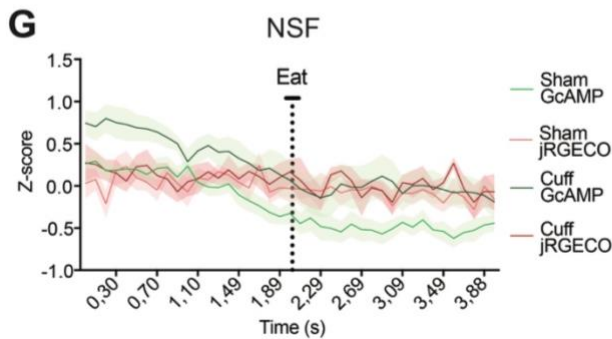
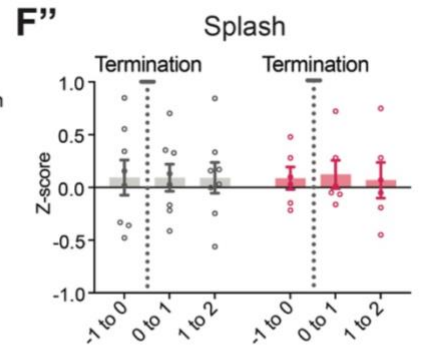
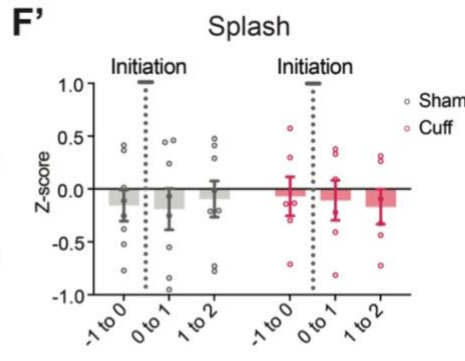
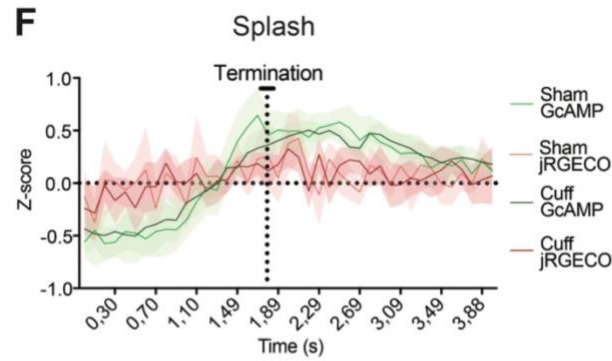
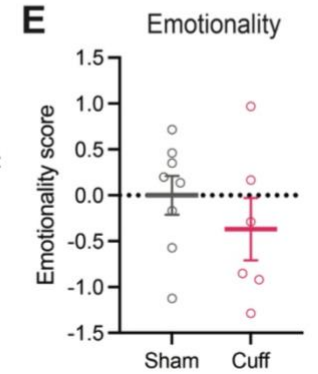
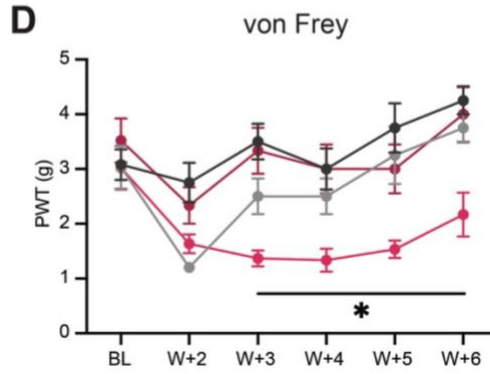
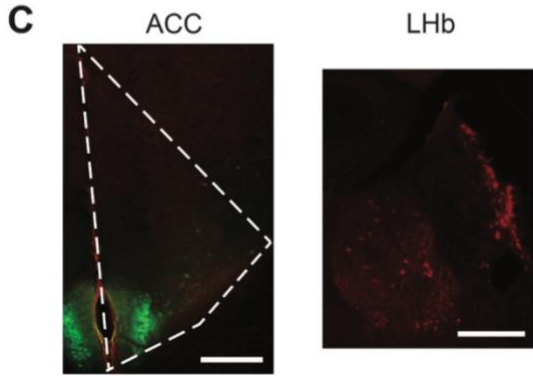
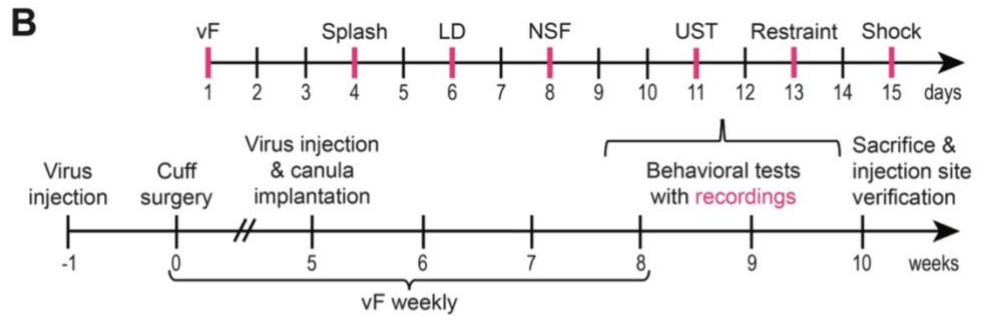
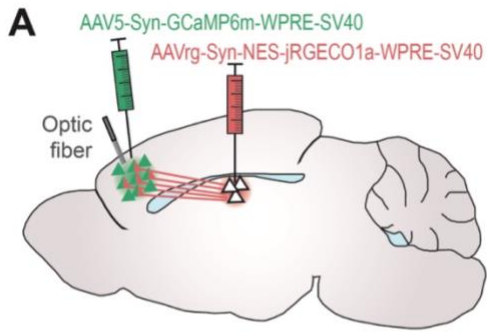


Figure 2. The effect of chronic pain on Ca²⁺ dynamic of ACC neurons projecting to LHb.

(A) Representation of the double virus injections and fiber photometry cannula implantation strategy. **(B)** Timeframe of the experimental design (cuff surgery, virus injection, cannula implantation and behavioral tests with recordings). **(C)** Representative picture of the expression of two viruses in the ACC and of the injection site in the LHb; scale bar = 250µm. **(D)** Cuff animals present a decreased mechanical threshold in the ipsilateral paw compared to the contralateral paw and sham animals, 2 weeks after the surgery and onward. **(E)** Cuff animals do not exhibit a difference in emotionality score. **(F-F'')** ACC and ACC→LHb Ca²⁺ dynamic during splash test. Representative Z-score trace of a recording during grooming termination **(F)**. **(F')** Averaged 1-sec bin Z-score before and after the grooming initiation for the jRGECO (ACC→LHb neurons), for both groups. **(F'')** Averaged 1-sec bin Z-score before and after the grooming termination. **(G-G')** ACC and ACC→LHb Ca²⁺ dynamic during NSF test. **(G)** Representative Z-score trace of a recording when the animal eats the food pellet in the NSF test. **(G')** Averaged 1-sec bin Z-score before and after the animals consumed the food pellet for the jRGECO (ACC→LHb neurons), for both groups. **(H)** ACC Ca²⁺ dynamic during UST for the female scent represented as averaged 1-sec bin Z-score before and after female scent investigation for the jRGECO (ACC→LHb neurons), for both groups. **(I-I')** ACC and ACC→LHb Ca²⁺ dynamic during LD test for the entry in the light box. **(I)** Representative Z-score trace of a recording when the animal enters the light box. **(I')** Averaged 1-sec bin Z-score related to the entrance in the light compartment (from dark to light side) for the jRGECO (ACC→LHb neurons), for both groups. **(J-J')** ACC and ACC→LHb Ca²⁺ dynamic during restraint stress. **(J)** Representative Z-score trace of a recording when the animal is put in 5 sec restraint stress. **(J')** Averaged 5-sec bin Z-score before, during and after the 5-sec restraint stress for the jRGECO (ACC→LHb neurons), both groups pooled. **(K-K')** ACC and ACC→LHb Ca²⁺ dynamic during unpredictable foot shock. **(K)** Representative Z-score trace of a recording when the animal is subjected to a 1sec unpredictable shock. **(K')** Averaged 1-sec bin Z-score before and during 1-sec electrical foot shock for the jRGECO (ACC→LHb neurons), both groups pooled. n=6-8 animals/group. Data are expressed as mean ± SEM. *p<.05, ****p<.0001. ACC, anterior cingulate cortex; BL, baseline; FST, forced swim test; LD, light-dark test; LHb, lateral habenula; NSF, novelty suppressed feeding test; UST, urine sniffing test; vF, von Frey.

Such a pattern is similar to what we observed for the whole ACC neuronal population (Fig.S2K), but opposite to what we and others (Huang et al., 2019) observed in the LHb. On the contrary, we observed a drastic increase in Ca²⁺ signals in response to a single unpredictable electrical foot shock (Fig.2K-K'; comparison between 1sec before the shock and the 1-sec shock: t-test: $t_{(13)}=2.510$, $p=0.0261$). A similar pattern was observed in the whole ACC neuronal population and the LHb (Fig.S2L), as already described in other studies for the LHb (Lecca et al., 2017; Trusel et al., 2019) or cortico-habenular neurons (Mathis et al., 2021). These results show for the first time that ACC→LHb neurons are not directly implicated in the aforementioned behavioral tasks but specifically signal aversive information that likely trigger an emotional response. Interestingly, their response is a mix of the ACC and LHb individual responses.

During the restraint stress the ACC→LHb neurons presented a dynamic similar to the one observed in the whole ACC neuronal population but opposite to what we observed in the LHb neurons (i.e., a reduction of the Ca²⁺ signal), while in response to the electrical foot shock the response was similar in the ACC, LHb and ACC→LHb neurons. This suggests that this specific neuronal population participates in the integration of stressful stimuli and the coordination of the ACC and LHb activities to likely modulate emotional behaviors. Hence, an alteration of these neurons might participate in emotional disorders. However, these data should be interpreted carefully as these are preliminary data performed on a small number of animals and that this experiment will need to be repeated.

The chronic, but not acute, optogenetic stimulation of ACC→LHb neurons induces anxiodepressive behaviors.

To further evaluate the involvement of the ACC-LHb pathway in emotional processing, we activated glutamatergic ACC neurons projecting to the LHb by injecting a retrograde AAV expressing ChR2-mCherry in the LHb and implanting an optic fiber in the ACC of naïve animals (Fig. 3A-C). Patch-clamp recordings confirmed that pulsed blue light stimulation (wavelength: 475nm, pulse duration: 40ms; frequency: 10Hz) evoked strong and stable inward currents in voltage clamp and action potentials in current clamp in mCherry-expressing ACC neurons (Fig. 3D). Evoked currents by the stimulation are stable in amplitude for the whole stimulation train whatever the stimulation frequency (Fig. S3A) and the proportion of pulses resulting in an action potential depends on the stimulation frequency (Fig. S3B). Using the same paradigm, we showed that a single stimulation session was not sufficient to trigger any alteration in spontaneous locomotor activity, real-time place avoidance or behaviors related to anxiety or depression. Indeed, no differences in aversive- and anxiodepressive-like behaviors were observed between stimulated and non-stimulated groups through the time spent in the stimulated box in the RTA (Fig. 1E; t-test: $p=0.0514$), the time spent in the lit compartment of the LD test (Fig. 3F; t-test: $p=0.7858$), the latency to eat in the NSF (Fig. 3G; t-test: $p=0.2566$) and the duration of immobility time in the FST (Fig. 3H; t-test: $p=0.7550$). As a more general measure of emotionality (Guilloux *et al.*, 2011), we also calculated emotionality scores for each animal across all 3 tests (LD, NSF, FST). Results confirmed that single stimulation of the ACC-LHb pathway does not induce any emotional deficits (Fig. 3I; t-test: $p=0.4378$).

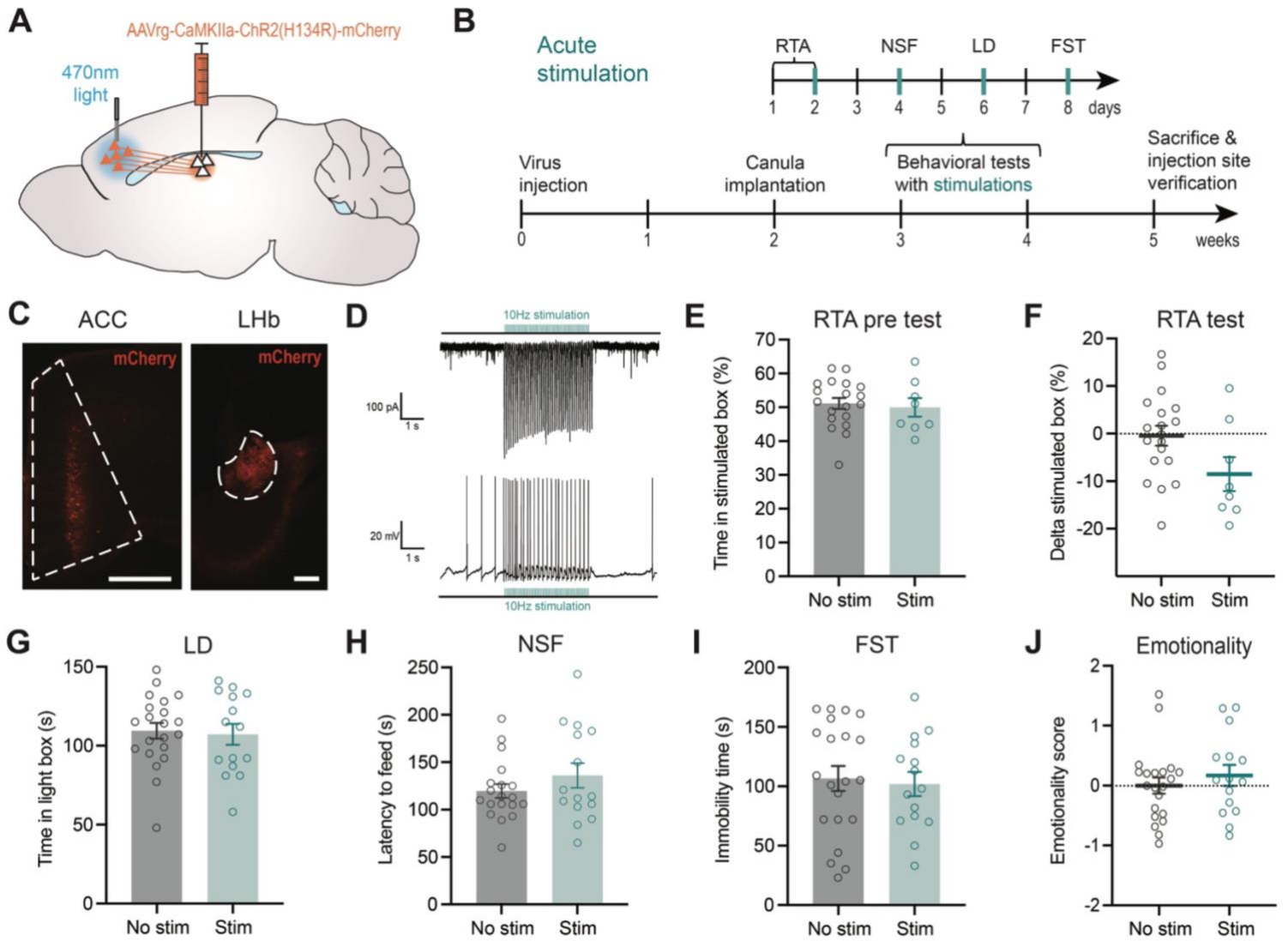


Figure 3. Acute optogenetic activation of ACC \rightarrow LHB neurons in naïve animals does not induce aversion and anxiodepressive-like behaviors.

(A) Representation of the virus injection and optogenetic cannula implantation strategy. **(B)** Timeframe of virus injection, cannula implantation and behavioral tests. **(C)** Representative picture of the injection site in the LHB and of the virus expression in the ACC; scale bar = 250 μ m. **(D)** Representative traces of the inward currents recorded in voltage clamp (upper panel) and of the action potentials recorded in current clamp (lower panel) induced by a 10 Hz optogenetic stimulation of an ACC neuron. Stimulated animals do not show any difference in the time spent in the stimulated box before **(E)** and during the stimulation **(F)** compared to controls in the RTA ($n=7-19$ animals/group). They also do not exhibit any difference in time spent in the light box of the LD ($n=15-21$ animals/group) **(G)**, in the latency to feed in the NSF ($n=15-19$ animals/group) **(H)** and in the immobility time in the FST ($n=15-21$ animals/group) **(I)**. Confirmed by the emotionality score combining LD, NSF and FST do not elicit difference between non-stimulated and stimulated animals ($n=15-21$ animals/group) **(J)**. Data are expressed as mean \pm SEM. ACC, anterior cingulate cortex; FST, forced swim test; LD, light-dark test; LHB, lateral habenula; NSF, novelty suppressed feeding test; No stim, non-stimulated; RTA, real time aversion; Stim, stimulated.

Considering that emotional deficits are chronic phenomena, an acute activation of the ACC-LHb pathway might not be enough to significantly recruit the ACC-LHb pathway. We therefore tested the effects of repeated stimulations over 4 consecutive days (Fig. 4A-B). Our results showed that chronic stimulation of the ACC-LHb pathway induced anxiodepressive-like behaviors since stimulated animals displayed decreased time spent in the lit box of the LD (Fig. 4C; Mann-Whitney: $p=0.0224$), increased latency to eat in the NSF (Fig. 4D; t-test: $p=0.0467$) and a tendency to increase immobility time in the FST (Fig. 4E; t-test: $p=0.0595$). This was confirmed when computing the emotionality score, with an increased emotional score, reflecting increased emotional disorders, in stimulated animals (Fig. 4F; t-test: $p=0.0004$). However, the aversive component was still not affected by this chronic activation (Fig. 4G; t-test: $p=0.8406$). Interestingly, the effect of chronic activation on behavioral outcomes disappears 2 weeks after the last stimulation in the FST test pointing out the reversible nature of the optogenetic paradigm (Fig. 4H; t-test: $p=0.7054$).

Since most of the behavioral tests used can be interfered by any locomotor activity deficits, spontaneous activity of stimulated and non-stimulated animals was measured in an open field. Our results demonstrated no differences between groups in distance travelled (Fig. 4I; open field: t-test: $p=0.5935$).

The acute inhibition of ACC \rightarrow LHb neurons is sufficient to counteract chronic neuropathic pain-induced but not stress-induced emotional consequences.

Since a chronic activation of the ACC-LHb pathway induces anxiodepressive-like behaviors and that ACC \rightarrow LHb neurons participate in emotional processing, we wondered whether inhibiting this pathway could rescue the anxiodepressive-like behaviors induced by either chronic pain or stress. To address this, we inhibited glutamatergic ACC neurons projecting to the LHb by injecting a retrograde AAV expressing ArchT-GFP in the LHb and implanting an optic fiber in the ACC (Fig. 5A-B). We first confirmed ArchT-GFP function by *ex vivo* electrophysiological recordings, which confirmed that our continuous optogenetic stimulation consistently evoked outward currents in GFP+ ACC neurons and inhibited their action potentials (Fig. 5C). The evoked current is stable in amplitude for the whole continuous stimulation (Fig. S3C). The action potential frequency is strongly inhibited at the beginning of the stimulation and then re-increases slowly until the end of it (Fig. S3D). To assess behavioral effects of inhibiting the BLA-ACC pathway in chronic pain or chronic stress model, the same viral vector was injected.

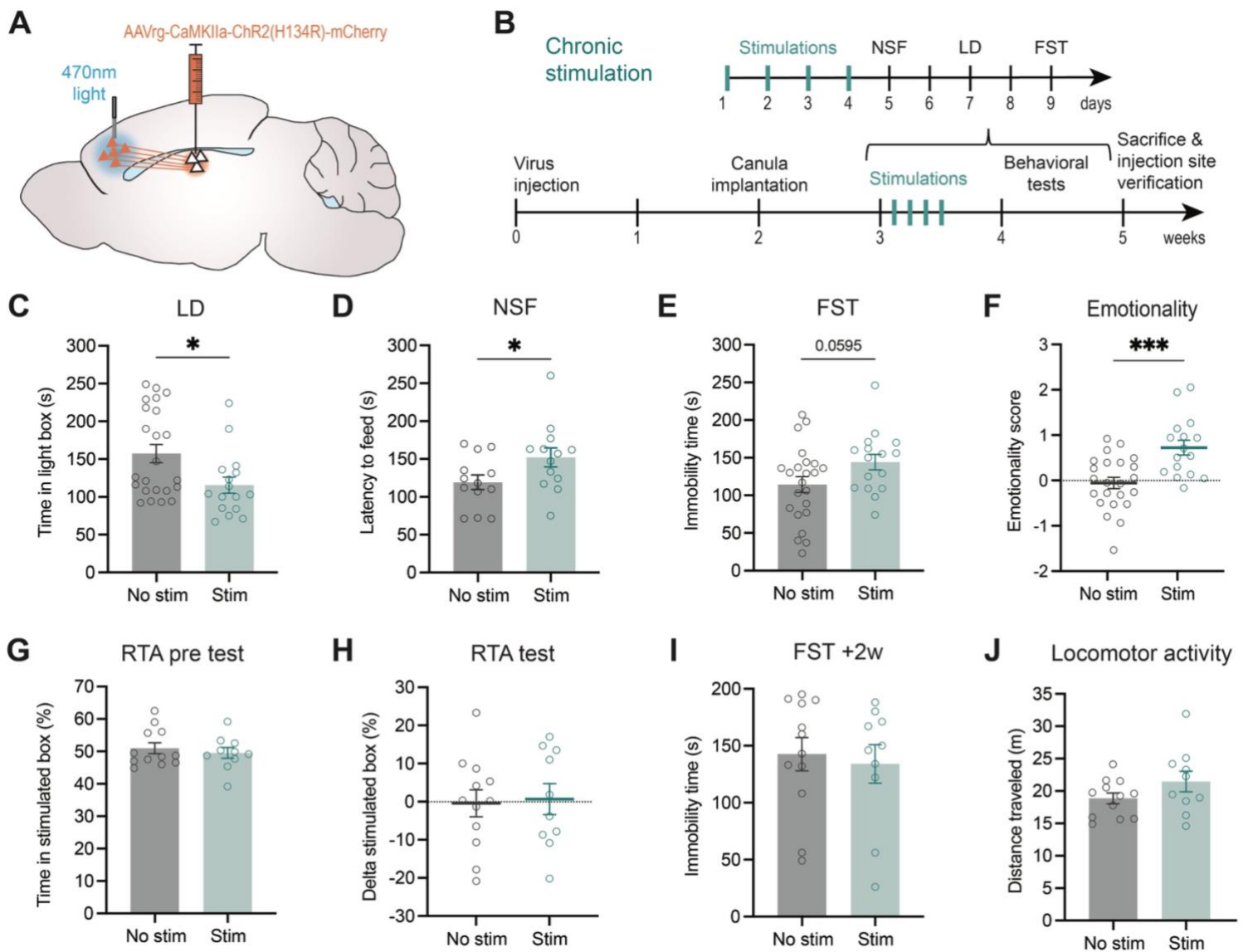


Figure 4. The chronic optogenetic stimulation of ACC_→LHB neurons induces anxiodepressive-like behaviors in naïve animals.

(A) Representation of the virus injection and optogenetic cannula implantation strategy. **(B)** Timeframe of virus injection, cannula implantation, chronic activation and behavioral tests. Stimulated animals present a decreased time spent in the light box of the LD (n=16-23 animals/group) **(C)**, an increased latency to feed in the NSF (n=13-13 animals/group) **(D)** and a tendency to increased immobility in the FST (n=16-23 animals/group) **(E)**, which is reflected by an increased emotionality score compared to non-stimulated mice (n=16-23 animals/group) **(F)**. However, chronic activation of this pathway does not produce any aversion to the stimulation as seen in the RTA with no difference before **(G)** or during the stimulation **(H)** (n=10-12 animals/group). 2 weeks post stimulation, the stimulated mice do not present any difference in immobility time compared to controls in the FST (n=10-12 animals/group) **(I)**. This chronic stimulation does not have any effect on the locomotor activity of the animals **(J)** as the distance traveled is the same for non-stimulated and stimulated mice in an open field (n=10-12 animals/group). Data are expressed as mean ± SEM. *p<.05, ***p<.001. ACC, anterior cingulate cortex; FST, forced swim test; HC, home cage; LD, light-dark test; LHB, lateral habenula; NSF, novelty suppressed feeding test; No stim, non-stimulated; RTA, real time aversion; Stim, stimulated; w, week.

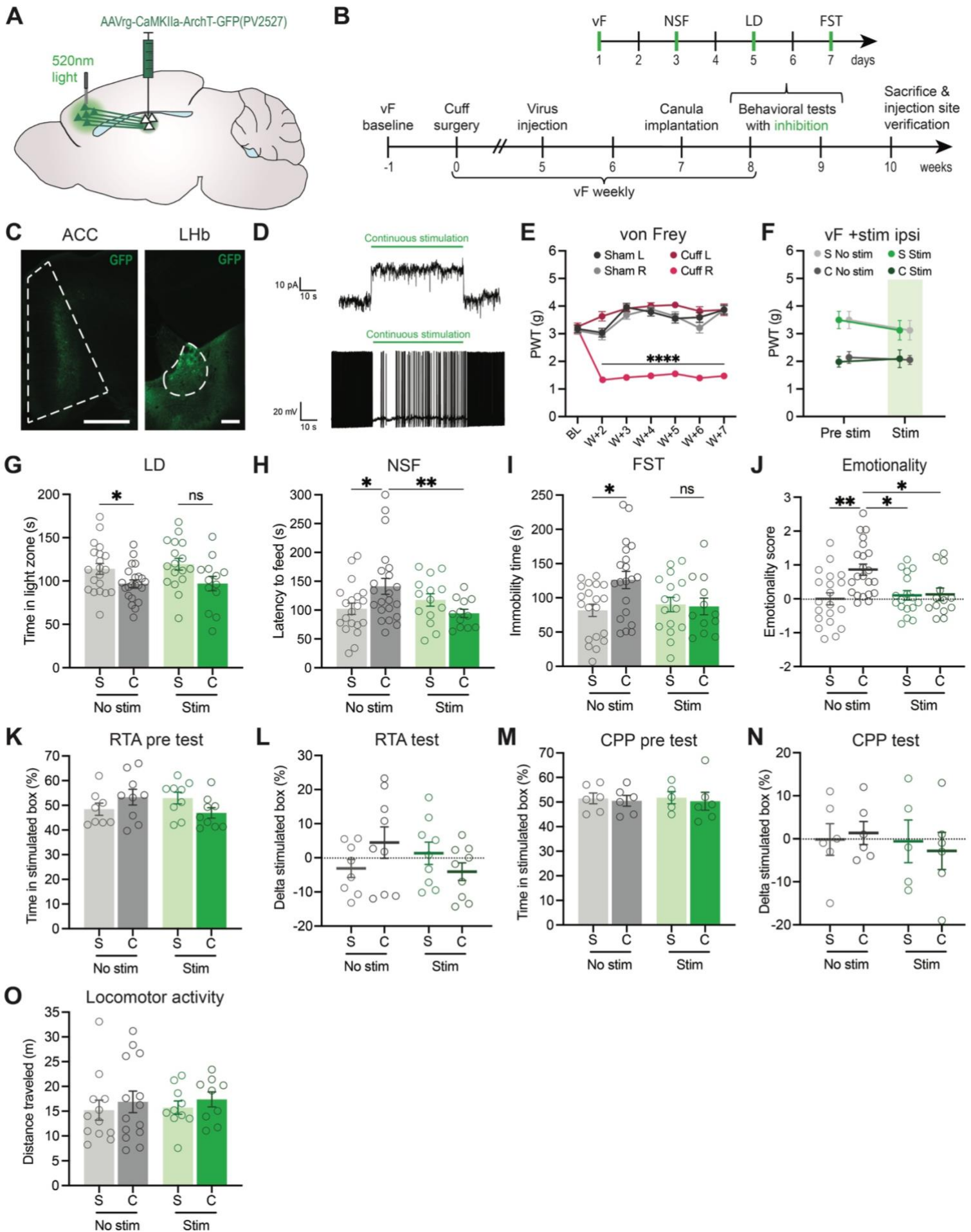


Figure 5. The inhibition of ACC→LHb neurons is sufficient to counteract chronic neuropathic pain-induced anxiodepressive-like behavior.

(A) Representation of the virus injection and optogenetic cannula implantation strategy. **(B)** Timeframe of cuff surgery, virus injection, cannula implantation and behavioral tests with inhibition. **(C)** Representative picture of the injection site in the LHb and of the virus expression in the ACC; scale bar = 250µm. **(D)** Representative trace of the hyperpolarization recorded in voltage clamp (upper panel) and of the decrease in action potentials frequency recorded in current clamp (lower panel) induced by a 10 Hz optogenetic stimulation of an ACC neuron. **(E)** Cuff animals present a decreased mechanical threshold in the ipsilateral paw compared to the contralateral paw and sham animals 2 weeks after the surgery and onward (n=35-38 animals/group). ACC-LHb inhibition do not affect the mechanical threshold in cuff animals (n=13-24 animals/group) **(F)**. Cuff animals exhibit decreased time spent in the light box of LD (n=13-22 animals/group) **(G)**, increased latency to feed in the NSF (n=12-22 animals/group) **(H)** and increased immobility time in the FST (n=12-20 animals/group) **(I)**, which is reflected by an increased emotionality score (n=13-22 animals/group) **(J)**. Acute inhibition does not elicit any difference in the LD **(G)**, however, it rescues depressive-like behaviors in the NSF **(H)** and in the FST **(I)**, as reflected in the emotionality score **(J)**. This inhibition does not produce any aversion, as seen in the RTA before **(K)** and during the stimulation **(L)** (n=8-9 animals/group). It did not elicit any preference either, as seen in the CPP between the habituation **(M)** and the stimulation **(N)** (n=5-6 animals/group). It also does not induce any differences in locomotor activity in an open field (n=7-14 animals/group) **(O)**. Data are expressed as mean ± SEM. *p<.05, **p<.01, ****p<.0001. ACC, anterior cingulate cortex; BL, baseline; C, cuff; CPP, conditioned place preference; FST, forced swim test; L, left; LD, light-dark test; LHb, lateral habenula; NSF, novelty suppressed feeding test; No stim, non-stimulated; R, right; RTA, real time aversion; S, sham; Stim, stimulated; vF, von Frey; w, week.

In our neuropathic pain model, as expected, we observed decreased mechanical sensitivity thresholds in the ipsilateral paw of cuff animals following the surgery (Fig. 5D; Mixed Effect Model, time as repeated measure: Time, Surgery & Time x Surgery: $p<0.0001$; 2-7 PO weeks: $cuff_{ipsi} < sham_{ipsi}$, $cuff_{ipsi} < sham_{contra}$, $cuff_{ipsi} < cuff_{contra}$, $p<0.0001$). We also observed anxiodepressive-like behaviors following chronic pain in cuff non stimulated animals with a decreased time spent in the lit box of the LD (Fig. 5F; 2-way ANOVA: Surgery: $F_{1,67}=7.826$ $p=0.0067$; Sham vs Cuff - No stim: $p=0.0337$), an increased latency to eat in the NSF (Fig. 5G; 2-way ANOVA: Interaction: $F_{1,64}=6.479$ $p=0.0133$; Sham No stim vs Cuff No stim: $p=0.0124$) and an increased immobility time in the FST (Fig. 5H; 2-way ANOVA: Interaction: $F_{1,67}=4.211$ $p=0.0443$; Sham No stim vs Cuff No stim: $p=0.0036$); all reflected by an increased emotionality score (Fig. 5I; 2-way ANOVA: Surgery: $F_{1,68}=6.647$ $p=0.0121$, Interaction: $F_{1,68}=5.740$ $p=0.0193$; Sham No stim vs Cuff No stim: $p=0.0002$). The inhibition of the ACC-LHb pathway did not have any effect on the mechanical hypersensitivity (Fig. 5E; 3-way ANOVA, time as repeated

measure: Interaction: $F_{1,35}=0.2849$ $p=0.5969$, ns). However, it prevented anxiodepressive-like behavior as displayed in the LD (Fig. 5F; 2-way ANOVA: Surgery: $F_{1,67}=7.826$ $p=0.0067$; Sham vs Cuff-Stim: $p=0.0702$; ns), in the NSF (Fig. 5G; 2-way ANOVA: Interaction: $F_{1,64}=6.479$ $p=0.0133$; Cuff No stim vs Cuff Stim: $p=0.0095$) and the FST (Fig. 5H; 2-way ANOVA: Interaction: $F_{1,67}=4.211$ $p=0.0443$; Cuff No stim vs Cuff Stim: $p=0.0255$), as confirmed by the emotionality score (Fig. 5I; 2-way ANOVA: Interaction: $F_{1,68}=5.740$ $p=0.0193$; Cuff No stim vs Cuff Stim: $p=0.0002$). This inhibition did not create any aversion as seen in the RTA (Fig. 5J, 2-way ANOVA: Interaction: $F_{1,31}=3.593$ $p=0.0674$, ns), nor did it prevent spontaneous pain in the CPP (Fig. 5K; 2-way ANOVA: Interaction: $F_{1,19}=0.2268$ $p=0.6394$, ns). We also verified that this inhibition did not have any impact on the locomotor activity (Fig. 5L; 2-way ANOVA: open-field - Interaction: $F_{1,41}=1.954$ $p=0.1697$, ns).

To study whether ACC-LHb pathway is specifically implicated in chronic pain induced depression or if its implication can be generalized to other cause of depression, we used the same optogenetic paradigm in the chronic variable stress model (Fig. 6A-B). Animals submitted to CVS for 3 weeks did not display anxiety-like behavior in the LD (Fig. 6C; 2-way ANOVA: Stress: $F_{1,55}=1.020$ $p=0.3170$, ns), although there was a trend in the NSF (Fig. 6D; 2-way ANOVA: Stress: $F_{1,56}=3.836$ $p=0.0552$). However, they exhibited depressive-like behavior as observed in the FST (Fig. 6E; 2-way ANOVA: Stress: $F_{1,55}=7.157$ $p=0.0098$; POST HOC: Ctrl No stim vs CVS No stim: $p=0.0064$). This was reflected by the emotionality score with an increased emotionality between stressed and non-stressed animals (Fig. 6F; 2-way ANOVA: Stress: $F_{1,55}=7.670$ $p=0.0075$; Ctrl No stim vs CVS No stim: $p=0.0061$).

Contrary to the cuff model, inhibition of the ACC-LHb pathway did not seem to prevent any depressive-like consequences as stimulated stressed animals presented a similar latency to eat and immobility time as controls. Likewise, the emotionality score did not seem to differ between non stimulated and stimulated stressed animals. However, the control stimulated animals had a tendency towards an increased emotionality compared to non-stimulated controls, which might explain why there is no significant difference between stimulated controls and stressed animals in the FST (Fig. 6E; 2-way ANOVA: Stress: $F_{1,55}=7.157$ $p=0.0098$; Ctrl Stim vs CVS Stim: $p=0.4895$) and in the emotionality score (Fig. 6F; 2-way ANOVA: Stress: $F_{1,55}=7.670$ $p=0.0075$; Ctrl Stim vs CVS Stim: $p=0.4656$). These results suggest that the ACC-LHb pathway is an important part of the circuit involved in chronic pain-induced anxiodepressive disorders, but not stress-induced depression.

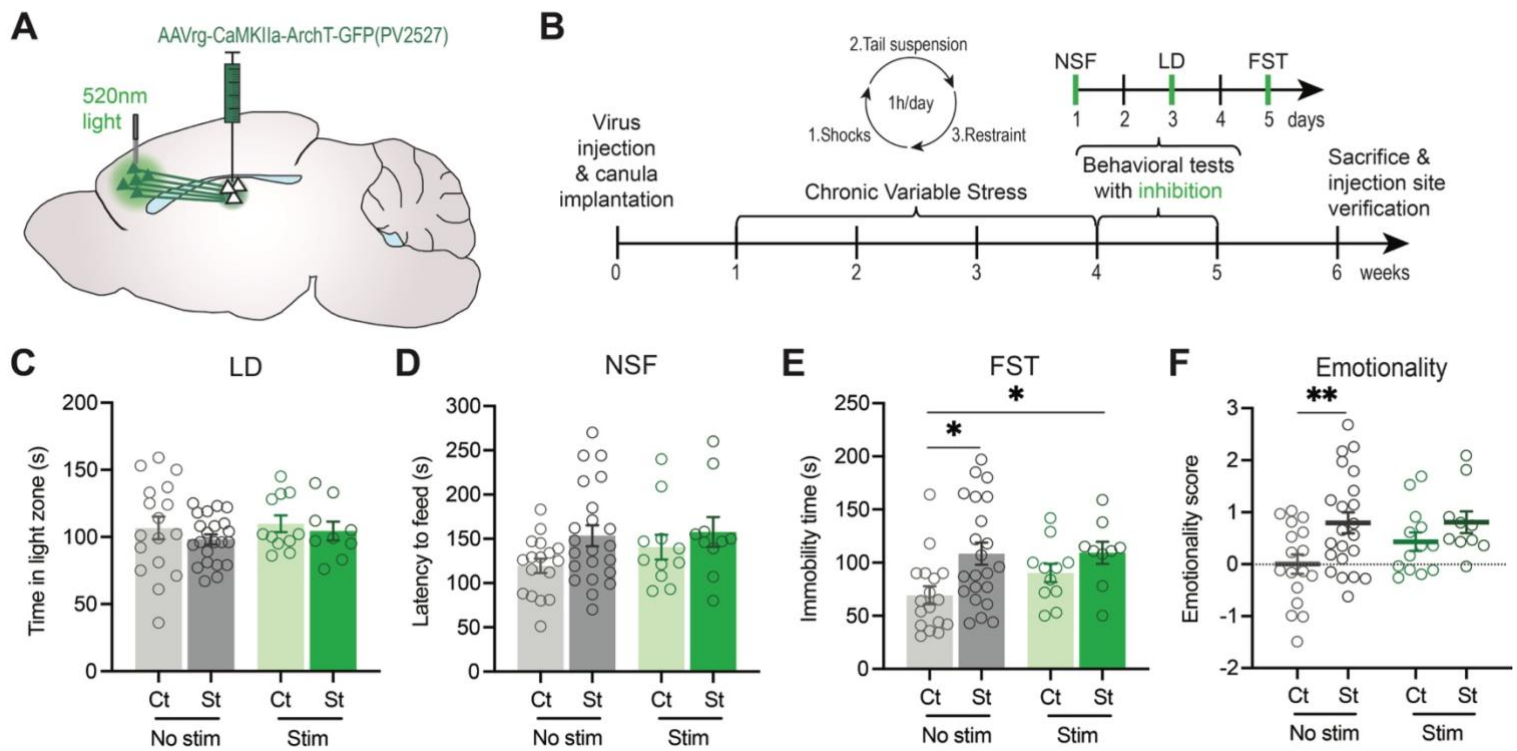


Figure 6. The optogenetic inhibition of ACC \rightarrow LHb neurons is not sufficient to counteract stress-induced emotional consequences.

(A) Representation of the virus injection and optogenetic cannula implantation strategy. **(B)** Timeframe of virus injection, cannula implantation, chronic variable stress and behavioral tests. Stressed animals do not present any anxiety-like behavior as seen with the time in the light box of the LD (n=9-22 animals/group) **(C)**. However, they do exhibit increased latency to feed in the NSF (n=10-22 animals/group) **(D)** and increased immobility time in the FST (n=9-22 animals/group) **(E)** that are not rescued by the ACC-LHb inhibition as seen in the emotionality score (n=10-22 animals/group) **(F)**. Data are expressed as mean \pm SEM. *p<.05, **p<.01. ACC, anterior cingulate cortex; Ct, control; CVS, chronic variable stress; FST, forced swim test; LD, light-dark test; LHb, lateral habenula; NSF, novelty suppressed feeding test; No stim, non-stimulated; St, stressed; Stim, stimulated.

Lateral habenula projecting ACC neurons display a unique molecular signature that is affected by chronic neuropathic pain.

To study the molecular signature of ACC neurons projecting to the LHb (ACC \rightarrow LHb), we generated a retrograde AAV containing a plasmid encoding the ribosomal protein RPL10a fused to the reporter protein mCherry, under the CaMKIIa promoter (AAVrg-CaMKIIa-mCherry-RPL10A-WPRE-SV40). After injection in the LHb, this allowed us to perform viral translating ribosome affinity purification (vTRAP), as described by Heiman *et al.* (2014), in order to collect only mRNA under transcription from ACC \rightarrow LHb. We first performed vTRAP in naïve animals to verify the viral approach used and to characterize ACC \rightarrow LHb neurons transcriptional signature (Fig. 7A-C).

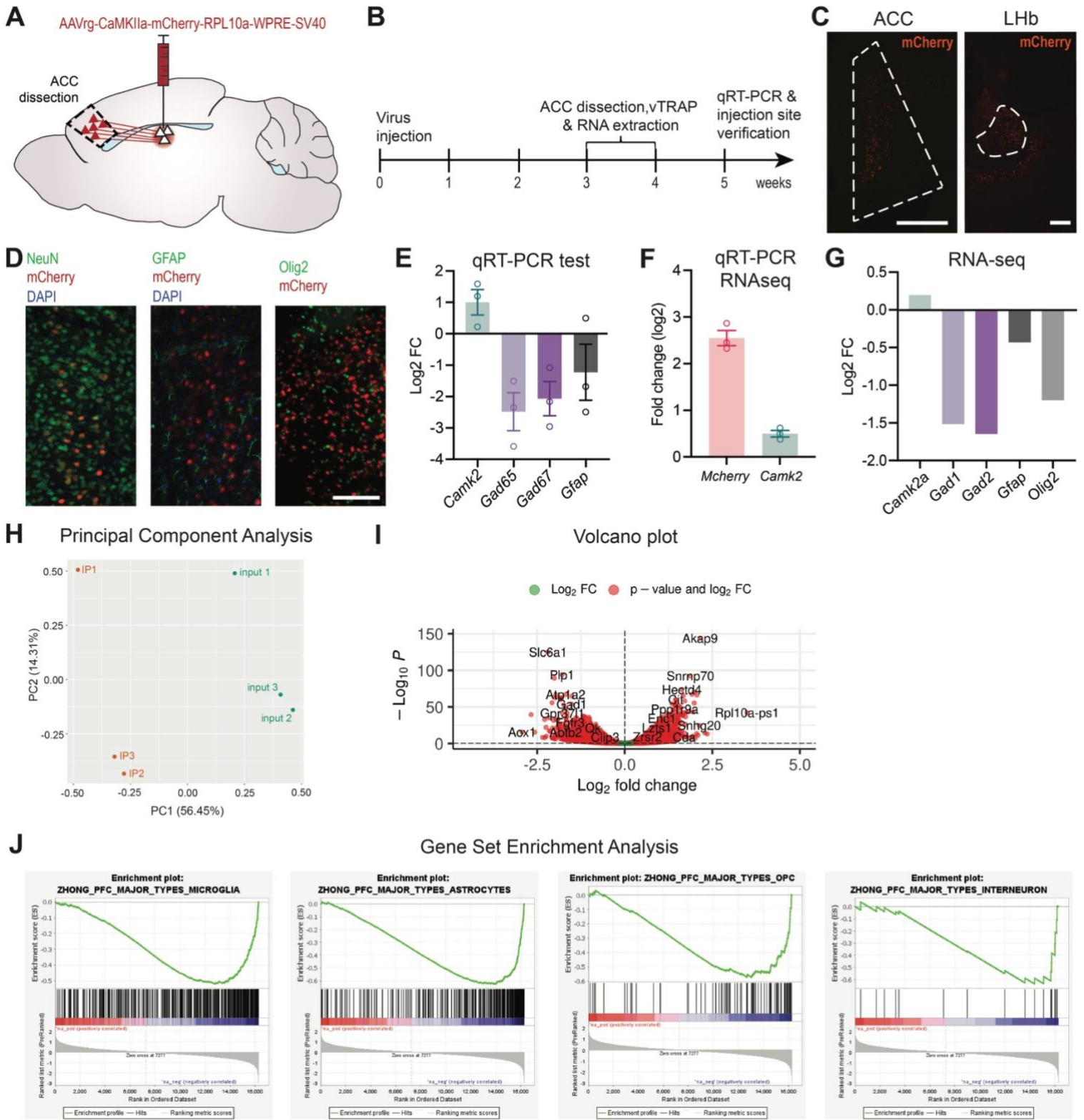


Figure 7. vTRAP of LHB-projecting ACC neurons in naïve animals.

(A) Representation of the virus injection and ACC dissection strategy. **(B)** Timeframe of virus injection, ACC dissection, vTRAP and RNA extraction. **(C)** Representative picture of the injection site in the LHB; scale bar = 250µm. **(D)** Representative fluorescence images showing cells positive for mCherry and NeuN (left panel), GFAP (middle panel) or Olig2 (right panel); scale bar = 100µm. **(E)** RT-qPCR analysis confirmed the enrichment in the immunoprecipitated (IP) portion in *Camk2*, with a depletion in *Gad65*, *Gad67* and *Gfap* (n=3 animals). **(F)** The samples selected for RNA sequencing presented a good enrichment in *Mcherry* and *Camk2*, which was further confirmed by the RNA sequencing results, with also depletion in *Gad1*, *Gad2*, *Gfap* and *Olig2* (n=3 animals) **(G)**. **(H)** Using Principal Component Analysis, robust differences were observed across groups (IP and input samples) at the genome-wide level. **(I)** 3310 transcripts were upregulated and 3943 transcripts were downregulated in the IP fraction compared to the input fraction. **(J)** GSEA analysis revealed depletion in genes associated with PFC microglia, astrocytes, oligodendrocytes precursor cells and interneurons. Data are expressed as mean ± SEM. ACC, anterior cingulate cortex; FC, fold change; IP, immunoprecipitated fraction; LHB, lateral habenula; PFC, prefrontal cortex.

The mCherry reporter was only present in cells expressing NeuN protein, thus neurons, but not in cells expressing the GFAP or Olig2 proteins (Fig. 7D; astrocytes or oligodendrocytes, respectively). These results were confirmed by qRT-PCR (Fig. 7E), with an enrichment in *Camk2* (glutamatergic marker) and a depletion in *Gad65*, *Gad67* (GABA markers) and *Gfap* (astrocytic marker) RNA in the immunoprecipitated section (IP) compared to the whole tissue (input). Before sending the three samples for RNA sequencing, we systematically checked that the IP was enriched in *Mcherry* and *Camk2* (Fig. 7F). Our RNAseq data confirmed the vTRAP of glutamatergic cells only, with an enrichment in *Camk2a* and a depletion in *Gad1*, *Gad2*, *Gfap* and *Olig2* (Fig. 7G). IP and input sections were well separated as expected in principal component analysis (PCA; Fig. 7H). In the IP fraction, 3310 transcripts were upregulated and 3943 transcripts were downregulated compared to the input fraction (Fig. 7I). We then used Gene Set Enrichment Analysis (GSEA, Fig. 7J) to interrogate gene sets related to prefrontal cortex cell types (Zhong et al., 2018). It confirmed that astrocytic (Fig. 7J, upper left panel), microglial (Fig. 7J, upper right panel), oligodendroglial (Fig. 7J, bottom left panel) and interneuronal (Fig. 7J, bottom right panel) genes are all downregulated in the IP fraction.

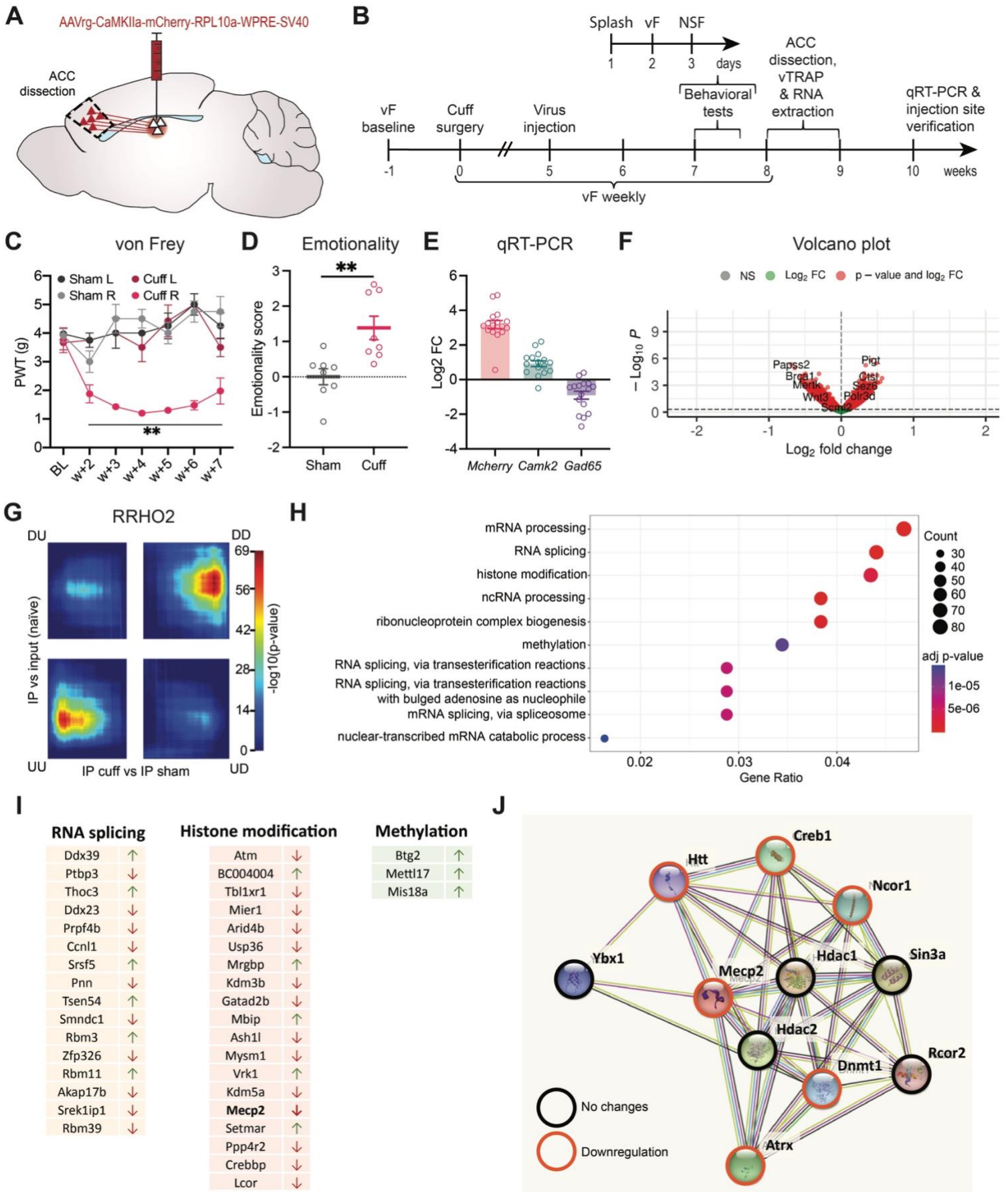


Figure 8. Lateral habenula projecting ACC neurons display a unique molecular signature that is affected by chronic neuropathic pain.

(A) Representation of the virus injection and ACC dissection strategy. **(B)** Timeframe of cuff surgery, virus injection, behavioral tests, ACC dissection, vTRAP and RNA extraction. **(C)** Cuff animals present a decreased mechanical threshold in the ipsilateral paw compared to the contralateral paw and sham animals, 2 weeks after the surgery and onward (n=8 animals/group). They also present a higher emotionality score, reflecting anxiodepressive-like behavior (NSF+splash) **(D)**. **(E)** RT-qPCR analysis confirmed the enrichment in the immunoprecipitated (IP) portion in *Mcherry* and *Camk2*, with a depletion in *Gad65* (n=8 animals/group). **(F)** 591 transcripts were upregulated and 828 were downregulated in cuff compared to sham animals. **(G)** RRHO2 identified shared transcriptomic changes in the ACC across naïve IP vs naïve input study and IP cuff vs IP sham study. Levels of significance for the rank overlap between the two studies are color-coded. **(H)** Gene ontology analysis on the overlapped genes of the two bottom panels (upregulated in IP vs input) revealed enrichments in GO terms related to RNA processing and epigenetic adaptations. **(I)** Genes significantly dysregulated in cuff animals from the GO terms of the RRHO2 analysis. *Mecp2* gene is of particular interest and genes its STRING network showed mainly downregulation in neuropathic animals displaying anxiodepressive-like behavior **(J)**. Data are expressed as mean \pm SEM. **p<.01. ACC, anterior cingulate cortex; BL, baseline; D, down; L, left; NSF, novelty suppressed feeding test, R, right; RRHO2, rank-rank hypergeometric analysis; U, up; vF, von Frey; w, week.

We then performed vTRAP in our cuff model at 8 weeks post-surgery and analyzed the obtained RNA by RNAseq using Illumina NextSeq 2000 RNAsequencer (Fig. 8A-B). Animals with peripheral nerve injury displayed decreased mechanical thresholds in the ipsilateral paw (Fig. 8C) and increased emotionality score (Fig. 8D) computed with NSF and Splash tests (Supplementary Fig. 4A-B). qRT-PCR confirmed that the samples sent for RNA sequencing did present an enrichment in *Mcherry* and *Camk2* and a depletion in *Gad65* (Fig. 8E). Two samples had a lower quality, but GSEA comparing the overlap between the IP effect (IP vs input, obtained from the naïve animal batch) and the cuff effect (IP cuff vs IP sham), with and without outliers (WITH_OL and WO_OL, respectively), showed a similar overlap and directionality (Supplementary Fig. 4C-D), with a good correlation for FC values (Supplementary Fig. 4E) and p-values (Supplementary Fig. 4F). Therefore, we continued the analyses with the outliers. In cuff IP, 591 transcripts were upregulated and 828 transcripts were downregulated compared to sham IP (Fig. 8F). A systematic threshold-free comparison, Rank Rank Hypergeometric Overlap (RRHO2), revealed large patterns of transcriptional dysregulation in similar directions in our IP effect and our cuff effect (Fig. 8G). Gene ontology (GO) analysis on overlapped genes in the two bottom panels (Supplementary Fig. 4G), for which genes were enriched in the IP

fraction, revealed enrichments in GO terms (Fig. 8H) related to RNA processing (mRNA processing, RNA splicing, ncRNA processing, ribonucleoprotein complex biogenesis) and epigenetic adaptations (histone modification or methylation). Interestingly, genes related to histone modifications or methylation have already been associated with depression or anxiety, such as *Ash11*, *Mysm1* or *Mecp2* (Fig. 8I). Lateral habenula projecting ACC neurons display a unique molecular signature that is affected by chronic neuropathic pain.

Discussion

The ACC has been described as a key player in emotional processing and psychiatric disorders such as anxiety and depression, more specifically in the context of chronic pain (Barthas et al., 2015; Etkin et al., 2011; Sellmeijer et al., 2018). In this study we showed that ACC neuronal dynamics seems to be blunted in cuff animals during female urine sniffing, hinting for its role in anhedonic behavior. On the other hand, while ACC neurons projecting to the LHb are not implicated in behavioral outputs observed in classical tests for anxiety- and depressive-like behaviors, they seem to react specifically to aversive events. By assessing this pathway's function, we showed that its chronic activation was able to induce anxiodepressive-like behaviors, while its inhibition in a chronic pain mice model was able to rescue consequent emotional disorders. This specific role in chronic pain-induced anxiodepressive-like behaviors could be due to the dysregulation of RNA processing and epigenetic adaptations in ACC \rightarrow LHb neurons that we uncovered with an RNAseq analysis.

Studying ACC neuronal dynamics during several classically used tests assessing anxiety- and depressive-like behaviors revealed specific Ca²⁺ fluctuations time-locked with grooming episodes, entries into light and dark zones, exploration and consumption of food (after food deprivation) as well as when mice investigated social scents. Overall, these tests showed ACC activity fluctuations when mice started or terminated a given behavior. This role in action initiation has already been observed in animal models and Humans (Brockett et al., 2020; Rolls, 2019; Srinivasan et al., 2013). Notably, it has been shown that ACC neurons fire on STOP trials in a Go-noGo task (Bryden et al., 2019). On the contrary, ACC lesion induces deficits in suppressing a motor action, likely through a default activation of the dorsomedial striatum (Brockett et al., 2020). Furthermore, using head restraint mice, Kim and colleagues (2021) showed that the pharmacological inhibition of the ACC altered the selection of actions. In the present study, most of the events require freely moving animals to engage in an action, which

should theoretically require a decrease in ACC activity. Accordingly, when mice initiate grooming in splash test, investigate social scents (both male and female) in the UST and eat the food pellet in NSF test, we observed strong and sustained reduction of the Ca^{2+} signal. Interestingly, in the NSF test, a clear dissociation is detected when mice touched the food and ate (Touch→eat) the pellet or not (Touch→do not eat). When mice touched the food and subsequently ate it, we can consider that after the “evaluation” of the food they took the decision to eat it. For this specific behavioral sequence, we observed a strong reduction in the ACC Ca^{2+} right after touching the food. This likely reflects the switch allowing the promotion of the action (i.e., eating). In the contrary, in the Touch→do not eat sequence the ACC signal does not fluctuate, suggesting that the ACC reduction of activity required to promote the food consumption is absent and so prevents the behavioral outcome. As for the splash test or the UST, the reduction seems to occur right after the initiation of the behavior, which likely suggests an integration of the information rather than the anticipation and the promotion of the given behavior. Surprisingly, this framework seems to not be adapted when mice explore a threatening context (LD test). In our conditions, we observed a similar increase in ACC Ca^{2+} signal right before the transition from one compartment to the other, regardless of the directionality. First, this suggests that the ACC is not tracking the aversive valence of the compartment the animals is entering. Then, contrary to the other behaviors, the ACC activity is increased before the animals engage in the transition from one compartment to the other. An important number of studies already described the presence of multiple sub-types of neurons in the ACC, able to encode reward-related information, detect error in prediction or participate in motor selection (Johansen and Fields, 2004; Kolling et al., 2016a, 2016b; Monosov et al., 2020; Procyk et al., 2000; Quilodran et al., 2008; Rigney et al., 2018; Shackman et al., 2011). However, in the present, using fiber photometry, we could not dissociate different cell populations and so must consider the local ACC activity. We thus consider that such an increase of ACC Ca^{2+} signal right before the transition, regardless of the directionality, might signal a critical change in the task context (i.e., change in the light condition) and is related to the evaluation of the ongoing action. An important aspect of this calcium dynamic to consider is its quick decrease once the animal has transitioned to one compartment, compared to the second before entering. This confirms our previous findings and reinforces the hypothesis that ACC Ca^{2+} activity must be reduced to promote the exploration. Hence, in the LD box, we can hypothesize that the increase right before the transition reflects the

evaluation of the ongoing action while the following inhibition of the ACC activity reflects the promotion of action. It is noteworthy to mention that most of the ACC Ca²⁺ dynamic observed were not different in sham and cuff animals. However, ACC Ca²⁺ dynamic related to the female scent sniffing was blunted, but not the one for the male scent. This latest result suggests that the information, here socially relevant, are not conveyed the same way in neuropathic mice and are likely not integrated within the ACC. Male mice have a preference toward female olfactory stimuli (Dhungel et al., 2019), suggesting that pleasant socially relevant stimulations are not integrated by the ACC of cuff mice. Such a shift in information processing might participate in the development of anhedonia-like behaviors. Altogether, these first results confirm the crucial role played by the ACC in the promotion of actions and the signaling of social information in freely moving mice tested in classical behavioral paradigms.

However, the information it sends to other brain regions might be altered, resulting in the development of anxiodepressive-like symptoms. It also suggests that among the multiple projections from the ACC, the LHb appears as an important candidate, notably because of its role as the anti-reward system. It is indeed important for the processing of aversive information and is also implicated in depressive-like behaviors and anxiety (Baker et al., 2022; Cui et al., 2018; Lecca et al., 2017, 2016; Lecourtier et al., 2023; Li et al., 2013; Mathis et al., 2015; Murphy et al., 1996; Sartorius et al., 2010; Sartorius and Henn, 2007). We thus recorded the Ca²⁺ dynamics of ACC→LHb neurons. Interestingly, these neurons do not participate as does the whole ACC neuronal population during the anxiodepressive behavioral paradigms tested in this study, but they are particularly responsive to aversive/stressful events. It is therefore likely that they are integrating aversive/stressful information, transmitting it to the LHb and therefore coordinating the ACC and LHb responses in the presence of such stimuli.

Since this ACC subpopulation possesses this unique stress relevant functional signature, we hypothesized that they might play an important role in emotional regulation and that their manipulation must affect emotional behaviors. Surprisingly, even though these neurons respond to acute stress stimuli such as restraint stress or an unpredictable foot shock, only their chronic optogenetic activation induced anxiodepressive-like behaviors. These results suggest that a long-term plasticity of the pathway is likely implicated and needed for the occurrence of these behaviors. This resembles greatly pain- and stress-induced symptoms which require a certain chronicity to be observed. However, inhibiting this pathway in animals submitted to chronic stress did not induce any changes in depressive-like behaviours

suggesting that this specific population is not implicated in emotional deficits induced by chronic stress. On the other hand, the inhibition of the ACC-LHb pathway was able to rescue anxiodepressive-like symptoms induced by neuropathic pain, highlighting its importance in chronic pain-induced emotional consequences. Of note, this inhibition had no effect on the mechanical hypersensitivity of the animals, confirming the essential role of the ACC in the emotional consequences of pain (Barthas et al., 2015). Since it has been reported that lesion of the LHb in the context of chronic pain was sufficient to reverse the mechanical hypersensitivity and the anxiodepressive-like behaviors (Li et al., 2017), we suggest that the role of the LHb in the somatosensorial component of chronic pain could therefore be due to other brain regions projecting to the LHb such as the insular cortex (Kim and Lee, 2012). With these results in mind, it seems that pain is affecting the ACC, probably from information it receives from other brain structures, such as the locus coeruleus (Hirschberg et al., 2017) or the BLA (Becker et al., 2023; Meda et al., 2019) and that the chronification of pain likely affects its network, notably the LHb. Altogether, it seems that ACC neurons projecting to the LHb is playing critical role in chronic pain but not stress induced depression.

Such a unique trait makes this pathway a crucial player in chronic pain-induced emotional disorders. In that regard, we further evaluated, at the molecular level, the chronic pain-induced alterations within the ACC-LHb neurons. We used vTRAP approach (Heiman et al., 2014), allowing us to study modifications in the transcriptome of ACC \rightarrow LHb neurons. Based on bioinformatic analyses, we found that transcriptomic changes occurring in animals with neuropathic pain were mostly related to RNA processing and epigenetic adaptations. There seems to be in particular a downregulation in the expression of *Ash11*, *Mysm1* or *Mecp2* genes in ACC \rightarrow LHb neurons in neuropathic pain condition, which have all been previously implicated in anxiety or depression. *Ash11*, a gene encoding the histone methyltransferase Ash11, was shown to be differentially expressed after chronic restraint stress in the dentate gyrus (Datson et al., 2013). *Mysm1* dysregulation has been widely observed in patients with major depression and mice with depressive-like behaviors. It encodes the deubiquitinase Mysm1, and its knockdown or pharmacological inhibition in astrocytes in mice alleviated depressive-like behaviors induced by chronic restraint stress (Zhang et al., 2023). Finally, *Mecp2* encodes the transcriptional regulator methyl-CPG-binding protein 2 (MeCP2), which binds to methylated genomic DNA. Alterations in its expression have been notably highlighted in the context of pain and depression (Hou et al., 2015; Jang et al., 2021; Murgatroyd et al., 2009;

Sánchez-Lafuente et al., 2022; Sun et al., 2021; Tao et al., 2020; Wang et al., 2011). Loss of MeCP2 was shown to cause more repression than activation of downstream genes in the hippocampus (Chahrour et al., 2008). Interestingly, genes associated to *Mecp2* in STRING network were mostly downregulated as well in our dataset. Its role as a transcriptional regulator puts *Mecp2* in a central position to affect a multitude of downstream genes, which could lead to the development of anxiodepressive-like behaviors. The following step is to verify these genes' expression in qRT-PCR in another set of animals submitted to neuropathic pain. Trying to reverse the anxiodepressive-like phenotype induced by chronic pain by overexpressing these genes in the cuff model could confirm their importance in ACC→LHb neurons in the emotional consequences of chronic pain. Such a modulation has already been successfully applied in our team with the inhibition of *Mkp1* in the cuff model (Humo et al., 2020) or of *Sema4a* in depression-induced by chronic activation of the BLA-ACC pathway (Becker et al., 2023).

In conclusion, the ACC neurons projecting to the LHb are implicated in emotional processing and more particularly chronic pain induced emotional dysfunction. The unique functional and molecular signature of this pathway in the context of chronic pain-induced emotional disorders makes it an interesting target for future therapeutical strategies.

Acknowledgments and Disclosure

This work was supported by the Centre National de la Recherche Scientifique (contract UPR3212), the University of Strasbourg, the Fondation pour la Recherche Médicale (FRM équipe EQU201903007809), the interdisciplinary Thematic Institute NeuroStra (ITI 2021-2028 program of the University of Strasbourg, CNRS and Inserm) through the IdEx Unistra (ANR-10-IDEX-0002) under the framework of the French Program *Investments for the Future* (ANR-10-IDEX-0002) and the French National Research Agency (ANR) through the French Program *Investments for the Future* EURIDOL Graduate School of Pain (University of Strasbourg; ANR-17-EURE-0022).

We would like to thank the UMS3415 Chronobiotron for animal care, Pascale Koebel and Paola Rossolillo from IGBMC for virus preparations, Christelle Thibault-Carpentier and Damien Plassard from IGBMC for the sequencing and bioinformatic collaboration. Sequencing was performed by the GenomEast platform, a member of the 'France Génomique' consortium (ANR-10-INBS-0009).

The authors report no biomedical financial interests or potential conflicts of interest.

Authors contribution

Behavioral experiments: *SHJ, RW, VPM, QL, NW, LB*; Molecular experiments: *SHJ*; Electrophysiological recordings: *SH*; Immunohistochemistry: *RW, MT*; Neuroanatomy: *SHJ, RW, MT*; Plasmid preparation: *SO*; Experimental design: *SHJ, PEL, IY*; Data analyses: *SHJ, MG, MT, PEL, IY*; Fundings: *IY*; Manuscript preparation: *SHJ, VPM, IY*.

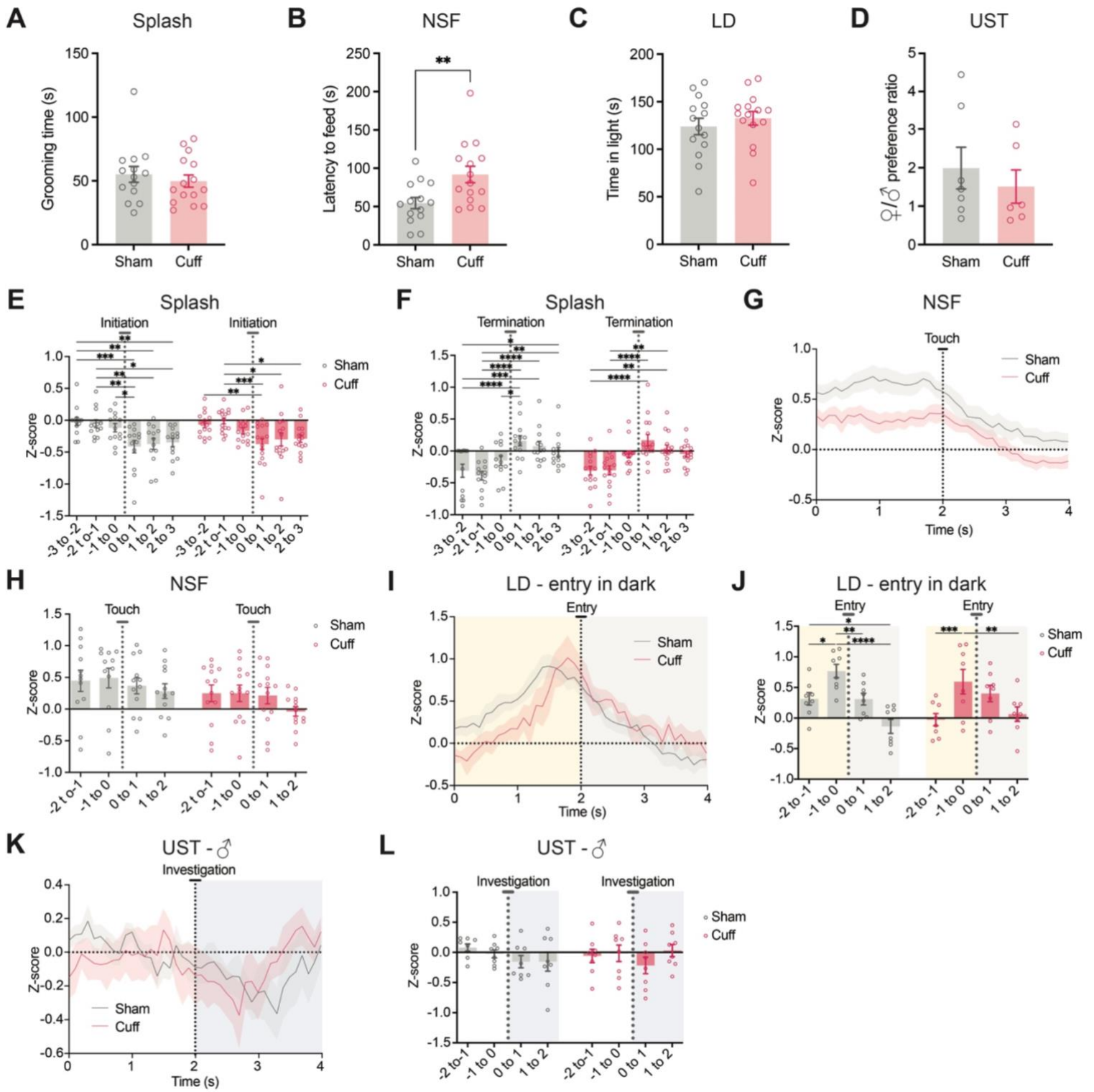


Figure S1. The effect of chronic pain on the ACC Ca²⁺ dynamic.

(A) Splash test grooming time is not different between sham and cuff animals. **(B)** NSF latency to feed is increased in cuff animals. **(C)** LD test time in light box is not different between sham and cuff animals. **(D)** UST preference ratio shows a tendency to decrease for cuff animals. **(E-F)** ACC Ca²⁺ dynamic during splash test. Averaged 1-sec bin Z-score before and after grooming initiation **(E)** and termination **(F)**, for both groups. **(G-H)** ACC Ca²⁺ dynamic recordings during NSF test. **(G)** Representative trace of a recording when the animal touches the food pellet in the NSF test. **(H)** Averaged 1-sec bin Z-score before and after the touching episode, for both groups. **(I-J)** ACC Ca²⁺ dynamic during LD test for the entry in the dark box. **(I)** Representative Z-score trace when the animal enters the dark box. **(J)** Averaged 1-sec bin Z-score related to the entrance to the dark compartment (from light to dark side). **(K-L)** ACC Ca²⁺ dynamic during UST for the male scent. **(K)** Representative Z-score trace of a recording when the animal sniffs the female scent. **(L)** Averaged 1-sec bin Z-score before and after the male scent investigation. n=14-15 animals/group. Data are expressed as mean \pm SEM. *p<.05, **<.01, ***p<.001, ****<.0001. LD, light-dark test; NSF, novelty suppressed feeding test; UST, urine sniffing test.

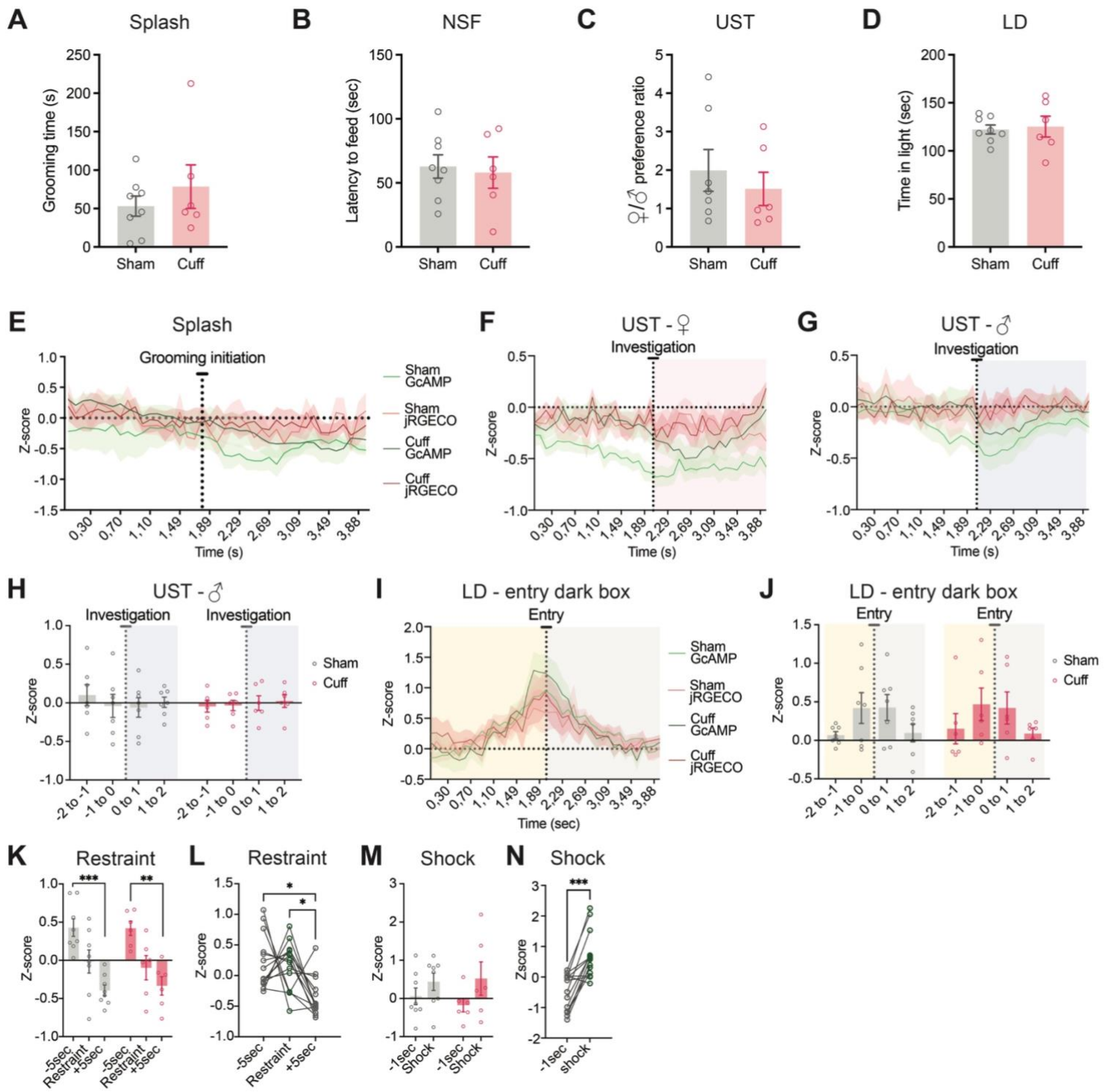


Figure S2. The effect of chronic pain on Ca²⁺ dynamic of ACC neurons projecting to LHb.

(A) Splash test grooming time is not different between sham and cuff animals. **(B)** NSF latency to feed is not different between sham and cuff animals. **(C)** UST preference ratio shows a tendency to decrease for cuff animals. **(D)** LD test time in light box is not different between sham and cuff animals. **(E)** ACC and ACC_{→LHb} Ca²⁺ dynamic during splash test, representative trace of a recording when the animal initiates grooming. **(F-H)** ACC and ACC_{→LHb} Ca²⁺ dynamic during UST. **(F)** Representative Z-score trace of a recording when the animal sniffs the female scent. **(G)** Representative Z-score trace of a recording when the animal sniffs the male scent. **(H)** Averaged 1-sec bin Z-score before and after the male scent investigation. **(I-J)** ACC and ACC_{→LHb} Ca²⁺ dynamic during LD test for the entry in the dark box. **(I)** Representative Z-score trace of a recording when the animal enters the dark box. **(J)** Averaged 1-sec bin Z-score related to the entrance to the light compartment (from dark to light side). **(K-L)** ACC and ACC_{→LHb} Ca²⁺ dynamic during restraint stress. **(K)** Averaged 5-sec bin Z-score before, during and after the 5-sec restraint stress for the jRGECO (ACC_{→LHb} neurons), for both groups. **(L)** Averaged 5-sec bin Z-score before, during and after the 5-sec restraint stress for the GcAMP (ACC neurons). **(M-N)** ACC and ACC_{→LHb} Ca²⁺ dynamic unpredictable foot shock. **(M)** Averaged 1-sec bin Z-score before and during 1-sec electrical foot shock for the jRGECO (ACC_{→LHb} neurons), for both groups. **(N)** Averaged 1-sec bin Z-score before and during 1-sec electrical foot shock for the GcAMP (ACC neurons). n=6-8 animals/group. Data are expressed as mean ± SEM. *p<.05, **<.01, ***p<.001. LD, light-dark test; NSF, novelty suppressed feeding test; UST, urine sniffing test.

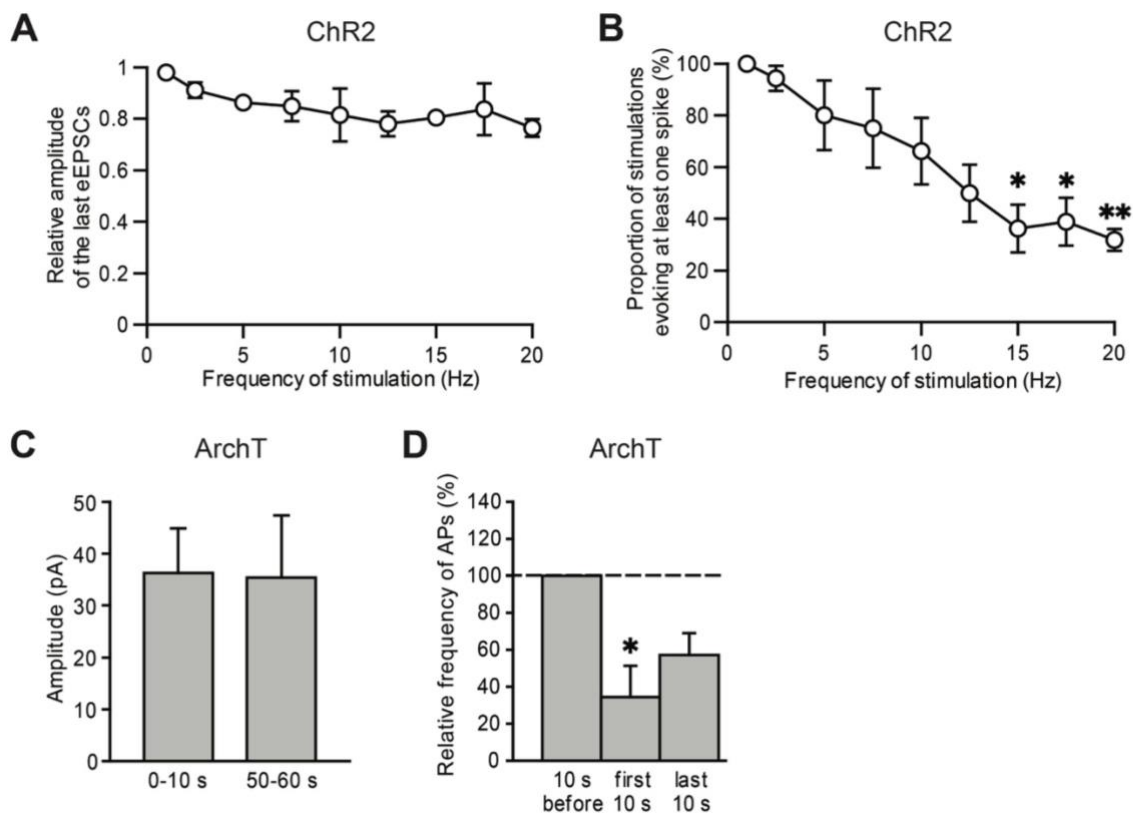


Figure S3. Electrophysiological recordings of neurons expressing the channelrhodopsin or the archeorhodopsin.

(A) Amplitude of the last eEPSCs of the stimulation depending on the stimulation frequency of the channelrhodopsin (ChR2) and relative to the amplitude of the eEPSC evoked by a 1Hz stimulation. **(B)** Proportion of stimulations evoking at least one spike depending on the stimulation frequency of the ChR2. **(C)** Amplitude of the current recorded during the first 10s and the last 10s of a 1-minute continuous inhibition via the archeorhodopsin (ArchT). **(D)** Frequency of action potentials during the first and last 10s of the continuous inhibition via the ArchT relative to the 10s before the inhibition. Data are expressed as mean \pm SEM. * $p < .05$, ** $p < .01$. ArchT, archeorhodopsin; ChR2, channelrhodopsin.

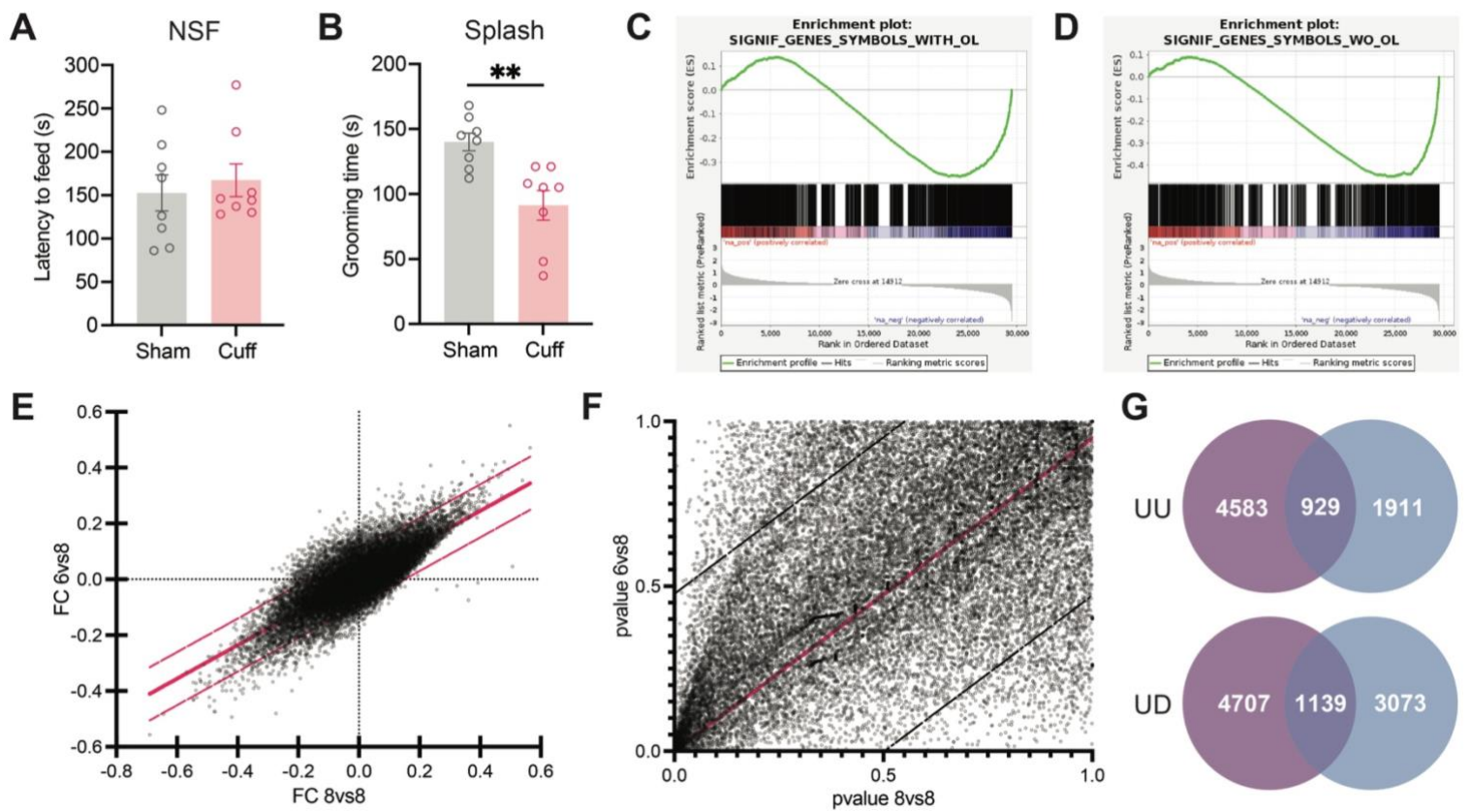


Figure S4. Lateral habenula projecting ACC neurons display a unique molecular signature that is affected by chronic neuropathic pain.

(A) NSF latency to feed is not different between sham and cuff animals. **(B)** Grooming time in the splash test is decreased in cuff animals. **(C-D)** GSEA reveals that there is a similar overlap with (WITH_OL) and without the technical outliers (WITHOUT_OL) with the IP portion of the vTRAP in naïve animals. **(E-F)** There is also a good correlation in fold change values **(E)** and p-values **(F)**. **(G)** RRHO2 reveals a good overlap between genes upregulated in the IP vs input (in naïve animals) and in cuff vs sham (IP only) in the upper panel (UU: 929 genes). There is also a good overlap between genes upregulated in the IP vs input (in naïve animals) and downregulated in cuff vs sham (IP only) in the bottom panel (UD: 929 genes). Data are expressed as mean \pm SEM. **<math>< .01</math>. FC, fold change; NSF, novelty suppressed feeding test; UD, up/down; UU, up/up.

General Discussion

Overview & interpretation

While the ACC has been widely studied in our team in the pain-emotional disorders dyad, the contribution of its networks to the development of anxiety and depression needs to be further studied. Our team started to tackle this topic, notably with the study of the BLA-ACC pathway and its role in the depressive consequences of chronic neuropathic and more widely depression in both mice and humans (Becker et al., 2023). However, the dysregulations present at the level of the ACC, in chronic neuropathic pain when anxiodepressive-like symptoms are present, probably do not stop there and are likely to propagate to downstream structures. We thus hypothesised that the projection from the ACC to the LHb, an epithalamic structure implicated in aversive processing, anxiety and depression, could play a role in the development and maintenance of the emotional consequences of chronic pain.

The calcium fluctuation of ACC \rightarrow LHb neurons

Our first aim was to understand the dynamics of neuronal activity in the ACC subpopulation that projects to the LHb in freely moving animals with a fiber photometry approach. Interestingly, the calcium dynamics of ACC \rightarrow LHb neurons were different to those of the whole ACC, and only responsive to aversive stimuli, but not to specific behavioural outputs recorded in anxiodepressive-like tests. In the characterisation of ACC calcium fluctuation, it is interesting that the response of ACC neurons in sham and cuff animals is almost similar for most of the behaviours analysed. This result, which could be surprising at first, is in accordance with the fact that the mice are already engaged in a specific behaviour when we look at the calcium fluctuation. It would therefore be interesting to see whether there are differences before the behaviour is performed, when the animal decides to engage or not in the behaviour, as observed in the NSF when mice only touch the food or when it touches and eats the food. However, such an analysis could require the development of more specific behavioural paradigms, which allow to know when the animal decides to perform a behaviour. While we saw no calcium fluctuations in anxiodepressive-like tests in ACC \rightarrow LHb neurons, it is likely that these neurons are not involved in the

execution of these specific behaviours but could be important in the processes leading to them. Indeed, as they exhibit a specific activity in response to stressful events such as a restraint or an unpredictable electric foot shock, they could be important for the processing and evaluation of aversive information that happen before the behaviour is engaged. Furthermore, while ACC \rightarrow LHb neurons are glutamatergic, the whole ACC recordings encompass all neuronal populations, including GABAergic neurons. Finally, recent papers have shown that some brain structures can present a functional dichotomy depending on their projections. For example, Hirschberg and colleagues (2017) highlighted that the LC-ACC and LC-SC pathways present a functional dichotomy, as their activation induces aversion/anxiety-like behaviours and antinociception respectively. It is thus conceivable that ACC \rightarrow LHb neurons are only implicated in aversive processing and that other ACC projections would be implicated in the behavioural outputs observed in anxiodepressive tests.

The behavioural characterisation of the ACC-LHb pathway

Secondly, we aimed at characterising the role of the ACC-LHb pathway in emotional processing using an optogenetic approach. We first activated this pathway in naïve animals. Interestingly, while the acute activation of this pathway did not result in any behavioural changes, the chronic optogenetic activation elicited anxiodepressive-like behaviours. This result is in line with previous work from our team in which only a chronic activation of the ACC was able to induce anxiodepressive-like behaviours (Barthas et al., 2015, 2017). This suggests that plasticity is at play and that it requires a chronic activation of the neurons. It is well known that long term potentiation (LTP) is one of these plastic mechanisms that can happen in the ACC (Bliss et al., 2016; Chen et al., 2021). Two types of LTP can occur in cortical excitatory synapses, presynaptic LTP (kainate-dependent) and postsynaptic LTP (NMDA-dependent) (Bliss et al., 2016). In the ACC, both LTP seem to play an important role in pain-induced hyperactivity, but also emotional consequences (Bliss et al., 2016; Koga et al., 2015; Li et al., 2021). As LTP can occur after repeated activity of neurons (Sandkühler, 2007), we suggest that only a chronic activation of ACC \rightarrow LHb neurons results in LTP, leading to anxiodepressive-like behaviours development.

Interestingly, the plastic mechanisms that could underlie the development of anxiodepressive-like behaviours in our chronic optogenetic paradigm resembled those that could occur in chronic pain-induced emotional disorders. Therefore, we inhibited the ACC-LHb pathway in our cuff model. A single inhibition led to alleviation of anxiodepressive-like symptoms, with no effect on the mechanical hypersensitivity of neuropathic pain. This result is not surprising as most of the papers studying the emotional consequences of pain have not reported any changes in the somatosensorial component of pain when manipulating the ACC (see the review in the ACC part of the Introduction).

In addition, it is well-known that the LHb is widely implicated in stress response, and therefore in stress-induced depression. Hence, we inhibited the ACC-LHb pathway in a chronic variable stress model in which animals are submitted to different environmental stress. We showed that inhibiting the ACC-LHb pathway do not alter the anxiodepressive-like behaviours observed in animals submitted to CVS suggesting that the ACC-LHb pathway, although driving anxiodepressive-like behaviours when chronically activated, is essential to chronic neuropathic pain-induced, but not stress-induced, emotional disorders. Knowing that the LHb is widely implicated in stress processing (Benabid and Jeaugey, 1989; Carr et al., 1998; Chastrette et al., 1991; Wirtshafter et al., 1994), the fact that blocking the ACC-LHb pathway is not sufficient to rescue stress-induced depression is surprising. However, several teams have been investigating the role of the ACC in the pain-emotional disorder dyad and have also found different underlying mechanisms when comparing it with models of stress-induced depression. For example, Li *et al.* (2021a) have compared an inflammatory model (chronic CFA), with a neuropathic model (SNI) and two stress-induced models: chronic corticosterone injection and chronic restraint stress. While all these models induced depressive-like behaviours, only did the chronic pain models exhibit a downregulation of the extracellular matrix protein laminin β 1 in the ACC. Similarly, in the thalamus, Zhu and colleagues (2021) have compared CFA, SNI, chronic restraint stress (CRS) and chronic unpredictable stress (CUS) models' impact. They have notably highlighted that posterior thalamic nucleus glutamatergic (PO_{Glu}) neurons have an increased excitability in CFA and SNI, but not CRS and CUS animals. On the opposite, parafascicular thalamic nucleus glutamatergic (PF_{Glu}) neurons have a decreased

excitability in CRS and CUS, but not CFA and SNI animals. These distinct subpopulations of neurons within the thalamus that underlie two different models of depressive-like behaviours are particularly interesting as it seems that there is a discrimination in several brain regions between stress- and pain-induced emotional consequences. In addition, these two populations were shown to project to different cortical areas: PO_{Glu} neurons to the primary somatosensory cortex and PF_{Glu} neurons to the ACC. Therefore, it is possible that the ACC-LHb pathway is only implicated in pain-induced anxiodepressive consequences, and it would thus be interesting to compare these results with other models of pain-induced emotional disorders such as an inflammatory model.

In addition, our preliminary fiber photometry results highlight that ACC_{→LHb} neurons seem to be responding to aversive stimuli only. As in chronic stress, all the stressors received during the CVS are aversive, it is possible that the ACC-LHb pathway has been over activated. Plastic changes occurring in the LHb could thus lead this specific connection to be ineffective, such as compensation mechanisms. On the opposite, in the context of chronic pain, this pathway is probably not as activated as in chronic variable stress, but could be more prone to be activated, because of the changes induced by chronic pain. This would be in line with results from Bravo and colleagues (2012), who observed that chronic mild stress (CMS) heightened the aversion to nociceptive stimuli in CCI animals, compared to animals subjected to only CMS, CCI or none. Their findings suggest that pain and stress could exacerbate each other's behavioural output. In our cuff model, it is thus possible that chronic pain is facilitating the communication between the ACC and the LHb to signal aversive events, leading to the development of the anxiodepressive-like comorbidity. By inhibiting the ACC-LHb pathway in chronic pain animals, it could block the facilitated communication, therefore blocking the emotional consequences of chronic pain.

The transcriptional signature of ACC_{→LHb} neurons in chronic pain

Because of the specificity of this pathway to chronic pain and its unique functional signature within the ACC in fiber photometry, we sought to understand whether these neurons presented a specific transcriptional alteration in our cuff model. From our

experiment, we ended with an IP (the immunoprecipitated RNA linked to ribosomes) and an input (the whole ACC RNA content) fraction for all the samples.

Our result showed that upregulated and downregulated genes in the cuff model compared to sham (IP cuff vs IP sham) correlated greatly to those in the IP of naïve animals (IP naïve vs input naïve), which confirmed that the vTRAP approach worked in our cuff and sham animals. When looking only at downregulated and upregulated genes in cuff animals that overlapped with genes upregulated in the IP of naïve animals, the gene ontology revealed terms widely associated with RNA processing and epigenetics.

Epigenetics processes have already been widely implicated in pain (Descalzi et al., 2009; Finnerup et al., 2021), depression (Penner-Goeke and Binder, 2019) and anxiety (Bartlett et al., 2017). More specifically, within the genes implicated in the gene ontology terms, *Mecp2* is an interesting target. Methyl-CpG binding protein 2 (MeCP2) is a transcriptional regulator that binds to methylated genomic DNA to regulate several physiological functions (Boyes and Bird, 1991; Guy et al., 2011; Lewis et al., 1992; Nan et al., 1997). It notably acts as a transcriptional repressor by binding to methylated CpG dinucleotides and recruiting corepressors and chromatin remodelling proteins (Jones et al., 1998). While it was extensively studied in neurodevelopmental disorders such as Rett syndrome, in which loss of MeCP2 function was shown to be associated with anxiety symptoms, alterations in its expression have more recently been highlighted in the context of pain or depression (Hou et al., 2015; Jang et al., 2021; Murgatroyd et al., 2009; Sánchez-Lafuente et al., 2022; Sun et al., 2021; Tao et al., 2020; Wang et al., 2011). Interestingly, gain of MeCP2 causes more activation than repression, while its loss causes more repression in the hippocampus (Chahrour et al., 2008). It would therefore not be surprising if most of downstream targets of MeCP2 were to be repressed in our context. Even though the results are not significantly different, we looked at the main direction for genes in the MeCP2 STRING network of association and found that most of them were downregulated in our data in cuff animals. Chahrour and colleagues' study also highlighted the upregulation of *Bdnf* in animals with gain of MeCP2 function and inversely downregulation in animals with loss of MeCP2 function. Increases in MeCP2 expression have been widely correlated with increased brain derived neurotrophic factor (BDNF) expression (Chang et al., 2006;

Klein et al., 2007). It would be interesting to check BDNF gene and protein expression in ACC \rightarrow LHb neurons as we did not see it in our RNAseq data. In addition, as we observe a decrease of *Mecp2* gene expression, it is also possible that the protein is not yet impacted. This could also be a compensatory mechanism to counteract chronic pain induced changes, it would therefore be interesting to study *Mecp2* expression at earlier time points also. Finally, the aforementioned studies have been performed in gain or loss of MeCP2 animal models, while in our case, the dysregulation of *Mecp2* is probably not as strong as any of their manipulations, as *Mecp2* is just downregulated and not completely suppressed.

In addition, studies in neuropathic animals were mostly performed in the spinal cord or in brain regions involved in the somatosensorial component of pain (Sun et al., 2021; Tao et al., 2020; Wang et al., 2011). This could explain the discrepancies between their upregulation of MeCP2 and the downregulation of *Mecp2* we observed in ACC \rightarrow LHb neurons, as the ACC is more involved in the emotional consequences of pain. Loss of MeCP2 function was also shown to be damaging to dendritic morphology, synaptic plasticity and neurotransmission (Na et al., 2013). However, before going further, it seems important to confirm *Mecp2* dysregulation in our model via qRT-PCR, and also to check MeCP2 protein levels. A deeper network analysis of *Mecp2* also seems essential to assess the potential changes its downregulation could generate.

In addition, this study remains descriptive, thus trying to target *Mecp2* in ACC \rightarrow LHb neurons by increasing its expression by viral means in our cuff model or silencing it with siRNA or shRNA in naïve animals would provide a causal link between its dysregulation and the observed phenotype. This strategy have already been successfully applied to *Mkp1* in the cuff model (Humo et al., 2020) and to *Sema4a* in BLA-ACC chronic activation-induced depression model (Becker et al., 2023).

Concluding remarks

This study is, to my knowledge, the first to study the role of the ACC-LHb pathway in the context of chronic pain-induced emotional disorders. It brings new knowledge about the functional connectivity, the behaviour and the transcriptional profile of a particular subset of ACC neurons projecting to the LHb (ACC \rightarrow LHb). It highlights the specificity of the ACC-LHb pathway in chronic pain-, but not stress-, induced emotional disorders, which goes in

the same direction as several published articles highlighting the dichotomy of several brain regions' projections. In addition, the epigenetic mechanisms that seem at play in this particular pathway in chronic pain animals are of great interest as they are influencing a wide variety of targets and thus biological functions.

The unique functional and molecular signature of this pathway in the context of chronic pain-induced emotional disorders makes it critical for understanding the pathophysiology of pain, anxiety and depression. This study provides some new keys and highlights the importance of studying circuitries to understand the pain-emotional disorder dyad.

Limitations of the study

In the following section, I will discuss several technical points and their possible limitations in my thesis work.

The optogenetic model

The optogenetic model, used in this study, might have an impact on the interpretation of some behavioural outcomes.

First, we systematically isolated animals in individual cages from the surgery onward until the end of the behavioural experiments. This social isolation was necessary at the beginning of the experiments, as we had no means to implant cannulas with the certainty that they would hold in place for as long as needed. However, social isolation is a known and reported factor for anxiety and depression in humans (Yanguas et al., 2018). While most of the studies using social isolation models focus on early social isolation, specifically in juvenile and adolescent rodents (Toth and Neumann, 2013), several studies in the last decades have started to address social isolation in adult rodents. Interestingly, social isolation in adolescent and adult mice was shown to have differential effects on behaviour, with more pronounced behavioural changes in adolescent mice (Lander et al., 2017). Nevertheless, several behavioural deficits have been observed in socially isolated adult mice, including higher locomotor activity in an open field and decreased home-cage activity, increased aggression, anxiety- and depressive-like behaviours, decreased cognitive and memory abilities (Clemenza et al., 2021; Funabashi et al., 2022; Ieraci et al., 2016; Lander et al., 2017). In addition, cellular

and molecular mechanisms that are keys in the pathophysiology of anxiety and depression can be found in socially isolated mice, such as dysregulation of corticosterone, BDNF, c-fos and GABA_A in the hippocampus or the prefrontal cortex (Berry et al., 2012; Chaibi et al., 2021; Ieraci et al., 2016). Typical social isolation models in adult mice often last for 6 weeks, while our social isolation lasted for 2-3 weeks at most. However, Liang's group have shown that 4 weeks social isolation was sufficient to induce anxiety-like behaviours, cognitive and memory impairments, as well as impairments in GABAergic transmission, decreased ATP levels, modulation of BDNF-TrkB signaling pathway and their downstream phosphorylation of MAPK pathway, changes in microglia and astrocytes density, size and morphology in the hippocampus (Al Omran et al., 2022a, 2022b; Silva et al., 2020; Watanabe et al., 2022a, 2022b, 2022c). In that regard, even 2-3 weeks social isolation could already be profoundly deleterious for the animals and could make them more prone to develop emotional disorders. However, in our study all the mice underwent social isolation, which can decrease the social isolation bias as all mice were treated equally in that regard. Fortunately, for the CVS protocol and the fiber photometry experiments, we developed a new implantation protocol that ensures that the cannulas can remain in place, without the need for social isolation. However, I have noted several discrepancies with the optogenetics experiments when analysing behavioural data from the vTRAP experiments or from our longitudinal genomic study in which I participated and that can be found in the appendix. Indeed, in these experiments, mice that underwent cuff surgery were group housed as there was no need to isolate them because of the absence of cannulas. In these settings, tests such as the NSF, which was key in my optogenetic study was not highlighting any more differences between sham and cuff animals when animals were group housed. However, other studies from our team have been performed in group housed animals in the cuff model, so it seems that it is rather an issue with the experimental settings used in my thesis rather than an actual issue with the cuff model (Humo et al., 2020; Sellmeijer et al., 2018). Knowing the changes that can occur in the brain after a few weeks of social isolation, it would not be surprising that social isolation is either priming ACC_→LHb neurons prior to their chronic activation, or multiplying the effects of neuropathic pain, thus worsening symptoms associated with anxiety or depression. Although the cuff model is still

working in group housed animals, it would be of great interest to test whether our chronic activation protocol in naïve group-housed animals would be sufficient or if priming by social isolation is key to the development of anxiodepressive-like behaviours that we observed.

The second technical point concerns the timing of the optogenetic stimulation. Indeed, some of our behavioural tests were not adapted to perform the stimulation during the test, because of material issues, such as for the LD test, or because of the incompatibility of the connection of the mice to an optogenetic cable during the test, like the FST. Since we did not see any differences in any tests in experimental paradigm with acute activation and tests were performed without the optogenetic stimulation in the chronic activation, we suggest that testing during or just after the activation does not interfere with the data. Concerning the optogenetic inhibition, although we tested our parameters in electrophysiological recordings, the continuous inhibition in freely moving animals lasted 5 minutes, hence 5 times the stimulation used in the electrophysiological protocols. However, while there is a decrease of around 50% of action potential firing during the inhibition, which is almost entirely sustained during the whole inhibition (Fig. S3D), it seems that *ex vivo*, the action potential firing comes back to basal levels right after the 60s of inhibition. This, in a way, is positive, because it seems that there is no rebound of activity from the inhibited neurons. However, we do not know what happens after 5mn of inhibition and if the neurons behave in the same way right after this specific inhibition. One important thing to take into consideration is that *ex vivo* is probably different from what happens in our freely moving animals. As circuits are intact *in vivo* compared to *ex vivo*, other mechanisms could lead to a sustained inhibition of the ACC-LHb pathway, which would be enough to alter subsequent behaviour. Another important concern for the electrophysiological recording is that it was only performed in naïve animals, and not in our neuropathic pain model. It is known from previous work in our team that the ACC is hyperactive at later time points of neuropathy, which are associated with anxiodepressive-like behaviours. Thus, we think that our inhibition acts differently in neurons that are hyperactive because of the neuropathy, which is supported by the inhibition of the ACC-LHb pathway in sham animals, which behaved the same way as sham non stimulated animals. This hints that our inhibition only has an effect when the neurons

are hyperactive or that they are silent in sham animals, and that inhibition right before or during the test does not change anything. To bypass this technical limitation, one possibility would be to do our inhibition using chemogenetic tools, which would allow us to have an inhibition of the ACC-LHb pathway during the tests. Otherwise, even though we did not see so far significant alterations in any Ca^{2+} fluctuations in LHb projecting ACC neurons during the behavioural tests in our fiber photometry experiment, it would be interesting to inhibit and record the neurons at the same time to have an idea of the overall activity of LHb projecting ACC neurons before, during and following the inhibition. This could provide us with a clearer picture of whether our inhibition is still effective following the 5mn inhibition.

The cuff model

Our neuropathic pain model, which consists of implanting a cuff on the main branch of the right sciatic nerve, has been well characterised and presents several advantages: it is highly reproducible, does not induce motor deficits or autophagy, and induces a sustained mechanical hypersensitivity, that associates with anxiodepressive-like behaviours at later timepoints (Yalcin et al., 2011). However, the cuffing of only the right sciatic nerve should be taken into consideration. For example, a study in rats reported a differential effect of left and right neuropathy induced by spared-nerve injury (Leite-Almeida et al., 2012). The left neuropathy was associated with anxiety-like behaviours without cognitive deficits, while the right neuropathy associated with cognitive deficits, without anxiety-like behaviours. Even though in our cuff model, it seems that the right neuropathy is indeed sufficient for the development of anxiodepressive-like behaviour, it would be of interest to also assess whether cuffing the left sciatic nerve would have the same effect, as it was already observed in other groups (internal communication from collaborators). This would be particularly important considering that the optogenetic cannula implantation is done randomly in either hemisphere. In humans, the ACC and PFC were shown to be lateralised in the context of emotional processing (Esteves et al., 2020, 2021). For example, Watanabe and colleagues (2015) have shown an asymmetry in the endogenous opioid system in the human ACC, which could be implicated in the lateralisation of emotion and pain processing. In addition, a study in mice have shown a lateralisation of the right ACC in

the context of observational fear, which is closely linked with negative emotions (Kim et al., 2012). In our cuff model, electrophysiological recordings did not show any lateralisation in term of hyperactivity, even though the cuff surgery is always performed on the right sciatic nerve (Sellmeijer et al., 2018). However, cuffing on the left sciatic nerve could bring new knowledge about the lateralisation of neuropathic pain, which would be extremely valuable for translational research in chronic pain.

In addition, one of the drawbacks of this study is the fact that we only performed experiments in male so far. The study of chronic pain and emotional disorders in female is however clinically relevant, as female patients make up to 70% of the chronic pain population (Berkley, 1997), while female patients are twice more likely to develop anxiety or depression compared to male patients (Gater et al., 1998; Kessler et al., 1995, 1994; Weissman et al., 1996, 1994). Although sex differences are widely studied in clinical settings, this is still not the case for preclinical research. Indeed, a review by Mogil (2012) have highlighted that in the journal PAIN, almost 4 papers out of 5 tested male animals only, while 5% papers tested both sexes without analysing possible sex differences. However, a few studies have been focusing on the study of chronic pain in male and female rodents and have reported different results, notably on the presentation of nociceptive symptoms, such as increased and longer hypersensitivity (Nicotra et al., 2014; Rahn et al., 2014; Sorge and Totsch, 2017; Vacca et al., 2014). In addition, responses to analgesic drugs such as opioids were shown to be different between males and females, mainly because of difference in kappa- and mu-opioid receptor mechanism of action (Bai et al., 2015; Mogil et al., 1993). Finally cellular and molecular differences have been highlighted, with for example higher levels of interleukin-1b, tumor necrosis factor-alpha and brain-derived neurotrophic factor in male CFA mice (Kuzawińska et al., 2014), or with a downregulation of genes associated with neurotransmitter release or extracellular matrix in the ACC of female SNI mice (Dai et al., 2022).

When I started my PhD thesis, the cuff model had only been characterised in male mice, which explains why we only performed the study in male animals. However, recent unpublished study from our group aiming at characterising the cuff model in female mice have showed that depressive but not anxiety-like behaviours can also be observed in female mice with a similar time course as reported in male mice. Such

differences in emotional behaviour concurrent to chronic pain could be explained by difference in the mechanisms underlying the development of this comorbidity between males and females. Therefore, an evaluation of our optogenetic activation and inhibition in female animals could allow us to have a better understanding of the mechanisms underlying chronic pain and its emotional consequences, while encompassing the entirety of the population suffering from this comorbidity. Such an experiment is already planned to first verify whether our chronic activation is sufficient to induce emotional consequences in female mice.

The vTRAP

The vTRAP approach constitutes a strong tool to interrogate the transcriptome of a specific brain cell population (Heiman et al., 2014). However, as this method relies on the purification with a fluorescent protein, it is thus dependant on the virus injection and expression. Although we selected the samples sent for RNAseq based on multiple factors, including the site of injection, the behaviour of the animals and the qRT-PCR results, the enrichment in mCherry was very variable between samples, which could be explained by the injection that was not perfectly performed or due to the improper viral transfection and expression. Even though this represents a technical limitation for the vTRAP method, the other alternative could have been to perform fluorescent-activated cell sorting (FACS) (Lanier, 2014), which allows to sort cells based upon the fluorescent characteristics of each cell, which would encounter the same limitations. Therefore, we selected the vTRAP method as it allows us to assess the translating RNA and not the full RNA content of the targeted neurons, which gives more precise information on the state of the neurons at a specific time point.

Finally, the RNAseq in our cuff model was only made on the IP fraction, which only allowed us to compare sham and cuff animals in this fraction, but not in light of the input fraction as we have already done this for another study. The analysis thus solely focused on comparing the IP vs input in naïve animals and the IP cuff vs IP sham. Even though we hypothesised that, using the RRHO2 tool, genes enriched in the IP vs input experiment and overlapping with genes from the cuff IP vs sham IP experiment would for sure be specific of our neurons of interest, there is still a possibility that the cuff surgery induces changes that are hidden by such an analysis. We also have no way to

make sure that the processes we observe and that the dysregulated genes are specific of only our IP population in cuff animals and not present in the whole ACC, as we only had the IP, but not the input of our sham and cuff animals. To tackle that question, it would be possible to perform an RRHO2 with our cuff IP vs sham IP and cuff input vs sham input from other RNAseq datasets of our laboratory that have been previously generated. This could confirm the specificity of the observed changes in our neuronal population only.

The fiber photometry

Fiber photometry is one of the new tools to monitor cellular events *in vivo* through fluorescent biosensors (Cui et al., 2014). The most well-known are calcium sensors, to monitor neuronal activity, but a plethora of other sensors have been developed to sense other specific neurotransmitters. It is however important to keep in mind that the recorded signals will be dependent on the number of neurons expressing the sensor and the level of expression in each neuron. It is therefore not possible to compare the raw signal between animals, and thus to know whether the ACC is hyperactive in cuff animals. However, the strength of the fiber photometry approach is to understand neuronal dynamics in response to specific behavioural outputs, such as the initiation of a grooming episode in the splash test or the entry into a zone in the LD test. The biggest issue I had with the fiber photometry experiment was that the mice were very stressed on a basal level, and they do not seem to have developed anxiodepressive-like behaviours. This absence of symptoms could be due to two things: the animals did not develop emotional consequences after chronic pain, i.e., an issue with our model, or the fiber photometry cable somehow impaired behaviour. To tackle that question, it would be interesting to perform a test before the fiber photometry recordings, such as the splash test to verify that mice indeed do develop anxiodepressive consequences following cuff surgery. This is to keep in mind for following batches of mice that will be needed to complete this experiment. It is thus complicated to conclude on the results we have got so far with the fiberphotometry, or at least to compare between sham and cuff animals. However, as we did not observe any calcium fluctuations in the anxiodepressive tests, we chose to still present all the results we got so far separating sham and cuff, as they still had a different surgery. For

the restraint and the unpredictable electrical foot shock, we chose to combine all the animals, as we saw no differences between sham and cuff animals. An additional batch with good behaviour is still needed to confirm whether there is an absence of differences between sham and cuff or if it was mainly due to the absence of emotional consequences. Indeed, it would not be surprising for the processing of aversive information to be different in cuff animals, which could explain the behavioural outcomes.

In addition, from the preliminary checks we have performed on the virus expression in the ACC, it seems that, while the GcAMP6 is well expressed in ACC neurons, jRGECO expression in ACC→LHb neurons is very poor. Indeed, not a lot of cells were infected with this approach compared to the amount we had for the optogenetic or vTRAP experiments. As the connection between the ACC and the LHb is mainly ipsilateral and that we implant the fiber only on one side of the ACC, we decided to only inject the virus unilaterally. However, there are also some contralateral connections from the ACC to the LHb, which could explain why we had such a poor expression efficiency. In addition, it is not impossible that our two viruses were competing in ACC→LHb neurons, which could be an additional explanation. Therefore, for the following experiments, it seems important to limit ourselves to only ACC→LHb neurons, with a bilateral injection in the LHb, to maximise our chances of having a sufficient fiberphotometry signal to confirm the results we have so far.

Perspectives & open questions

The present work has brought plenty of new knowledge about the ACC-LHb pathway, but it represents only a glimpse into this pathway.

Firstly, while the ACC-LHb pathway seems to be implicated in anxiodepressive-like behaviours, especially in the context of chronic pain, this study did not decipher the role of the ACC-LHb pathway under non pathological condition.

Secondly, it only focused on ACC neurons, leaving the LHb mainly out of the equation, apart from being the receiver of the information conveyed by the ACC.

This leaves two open questions that would benefit from additional studies to properly be able to understand the importance and the role of the ACC-LHb pathway.

What is the primary role of the ACC-LHb pathway?

The study of brain structures and networks are particularly important in the context of diseases and have led to the development of therapeutical approaches currently used in the clinic. However, understanding how the brain works under normal conditions seems essential to decipher how alterations could potentially affect physiology. While brain structures have been widely studied and are well known for their functions, such as action selection for the ACC or the LHb as an anti-reward centre, a lot of work is still needed to understand pathways and circuitries. This is especially the case in our study. We have started to tackle the question of the primary role of the ACC-LHb pathway with our fiber photometry experiment, but more work would be beneficial.

Indeed, while it seems that the ACC-LHb pathway is not implicated in the behavioural outputs recorded in our anxiodepressive tests, it is involved in the signalling of aversive events. Aversion and reward being two faces of the same coin, especially when it comes to the LHb, it would be particularly interesting to try to record ACC→LHb neurons in a rewarding task, or in a test combining reward and aversion such as the sucrose water quinine test (Yuan *et al.*, 2019).

This knowledge would allow for a more precise interpretation of optogenetic results and could bring new information to understand why the inhibition of this pathway seems only effective in the context of chronic pain-induced emotional behaviours.

To whom does the ACC speak?

The second important point to progress in understanding the ACC circuitry would be to understand where in the LHb the ACC projects and which neurons it contacts.

Indeed, the LHb comprises multiple subregions that are targeted by different prefrontal cortex areas in rat (Kim and Lee, 2012) and could therefore specifically project to different brain regions.

In addition, while the LHb is mainly composed of glutamatergic cells, it also contains GABAergic interneurons. Such targeting of specific cell subtypes was demonstrated by Zhou and colleagues (2019), who looked at central amygdala (CeA) somatostatin neurons projecting to the LHb in the context of chronic pain-induced depression. They

showed that these CeA neurons preferentially contacted glutamatergic LHb neurons, and that this connection was involved in pain-induced depressive-like behaviours. Knowing the targets of ACC neurons in the LHb would allow for a better understanding on how information sent from the ACC are processed and how they are transmitted to LHb downstream structures and participating in the physiopathology of chronic pain-induced emotional consequences.

Concluding remarks

Altogether, this project shed light on the role of the ACC-LHb pathway in the emotional consequences of chronic pain in mice. With the completion of the fiber photometry experiment in ACC \rightarrow LHb neurons, we will be able to assess the importance of this pathway in aversive signalling. In addition, our RNAseq results provide an overview of impairments in epigenetic mechanisms. Assessing the causal role between these impairments and emotional consequences of chronic pain could be a first step to uncover potential preclinical targets to open future therapeutic leads.

Bibliography

A

- Aizawa, H., Kobayashi, M., Tanaka, S., Fukai, T., Okamoto, H., 2012. Molecular characterization of the subnuclei in rat habenula. *J. Comp. Neurol.* 520, 4051–4066. <https://doi.org/10.1002/cne.23167>
- Al Omran, A.J., Shao, A.S., Watanabe, S., Zhang, Z., Zhang, J., Xue, C., Watanabe, J., Davies, D.L., Shao, X.M., Liang, J., 2022a. Social isolation induces neuroinflammation and microglia overactivation, while dihydromyricetin prevents and improves them. *J Neuroinflammation* 19, 2. <https://doi.org/10.1186/s12974-021-02368-9>
- Al Omran, A.J., Watanabe, S., Hong, E.C., Skinner, S.G., Zhang, M., Zhang, J., Shao, X.M., Liang, J., 2022b. Dihydromyricetin ameliorates social isolation-induced anxiety by modulating mitochondrial function, antioxidant enzymes, and BDNF. *Neurobiology of Stress* 21, 100499. <https://doi.org/10.1016/j.ynstr.2022.100499>
- Alba-Delgado, C., Llorca-Torralla, M., Horrillo, I., Ortega, J.E., Mico, J.A., Sánchez-Blázquez, P., Meana, J.J., Berrocoso, E., 2013. Chronic Pain Leads to Concomitant Noradrenergic Impairment and Mood Disorders. *Biological Psychiatry* 73, 54–62. <https://doi.org/10.1016/j.biopsych.2012.06.033>
- Apkarian, A.V., Bushnell, M.C., Treede, R.-D., Zubieta, J.-K., 2005. Human brain mechanisms of pain perception and regulation in health and disease. *European Journal of Pain* 9, 463–463. <https://doi.org/10.1016/j.ejpain.2004.11.001>
- Apkarian, A.V., Sosa, Y., Sonty, S., Levy, R.M., Harden, R.N., Parrish, T.B., Gitelman, D.R., 2004. Chronic Back Pain Is Associated with Decreased Prefrontal and Thalamic Gray Matter Density. *J. Neurosci.* 24, 10410–10415. <https://doi.org/10.1523/JNEUROSCI.2541-04.2004>
- Attal, N., Cruccu, G., Baron, R., Haanpää, M., Hansson, P., Jensen, T.S., Nurmikko, T., 2010. EFNS guidelines on the pharmacological treatment of neuropathic pain: 2010 revision. *European Journal of Neurology* 17, 1113. <https://doi.org/10.1111/j.1468-1331.2010.02999.x>

B

- Bai, X., Zhang, X., Li, Y., Lu, L., Li, B., He, X., 2015. Sex Differences in Peripheral Mu-Opioid Receptor Mediated Analgesia in Rat Orofacial Persistent Pain Model. *PLoS ONE* 10, e0122924. <https://doi.org/10.1371/journal.pone.0122924>
- Bair, M.J., Robinson, R.L., Katon, W., Kroenke, K., 2003. Depression and Pain Comorbidity: A Literature Review. *Arch Intern Med* 163, 2433. <https://doi.org/10.1001/archinte.163.20.2433>
- Baker, P.M., Mathis, V., Lecourtier, L., Simmons, S.C., Nugent, F.S., Hill, S., Mizumori, S.J.Y., 2022. Lateral Habenula Beyond Avoidance: Roles in Stress, Memory, and Decision-Making With Implications for Psychiatric Disorders. *Frontiers in Systems Neuroscience* 16.

- Bandelow, B., 2015. Generalized Anxiety Disorder and Pain, in: Finn, D.P., Leonard, B.E. (Eds.), *Modern Trends in Psychiatry*. S. Karger AG, pp. 153–165.
<https://doi.org/10.1159/000435939>
- Bandelow, B., Michaelis, S., Wedekind, D., 2017. Treatment of anxiety disorders. *Dialogues in Clinical Neuroscience* 19.
- Barrot, M., 2012. Tests and models of nociception and pain in rodents. *Neuroscience* 211, 39–50. <https://doi.org/10.1016/j.neuroscience.2011.12.041>
- Barthas, F., Humo, M., Gilsbach, R., Waltisperger, E., Karatas, M., Leman, S., Hein, L., Belzung, C., Boutillier, A.-L., Barrot, M., Yalcin, I., 2017. Cingulate Overexpression of Mitogen-Activated Protein Kinase Phosphatase-1 as a Key Factor for Depression. *Biological Psychiatry* 82, 370–379. <https://doi.org/10.1016/j.biopsych.2017.01.019>
- Barthas, F., Sellmeijer, J., Hugel, S., Waltisperger, E., Barrot, M., Yalcin, I., 2015. The Anterior Cingulate Cortex Is a Critical Hub for Pain-Induced Depression. *Biological Psychiatry* 77, 236–245. <https://doi.org/10.1016/j.biopsych.2014.08.004>
- Bartlett, A.A., Singh, R., Hunter, R.G., 2017. Anxiety and Epigenetics. *Adv Exp Med Biol* 978, 145–166. https://doi.org/10.1007/978-3-319-53889-1_8
- Bartley, E.J., Fillingim, R.B., 2013. Sex differences in pain: a brief review of clinical and experimental findings. *British Journal of Anaesthesia* 111, 52–58.
<https://doi.org/10.1093/bja/aet127>
- Becker, L.J., Fillinger, C., Waegaert, R., Hener, P., Ayazgok, B., Humo, M., Journée, S.H., Karatas, M., Degiorgis, L., Santin, M. des N., Mondino, M., Barrot, M., Ibrahim, E.C., Turecki, G., Belzeaux, R., Veinante, P., Harsan, L.A., Hugel, S., Lutz, P.-E., Yalcin, I., 2022. The basolateral amygdala-anterior cingulate pathway contributes to depression and its comorbidity with chronic pain. <https://doi.org/10.1101/2022.08.09.503276>
- Becker, L.J., Fillinger, C., Waegaert, R., Journée, S.H., Hener, P., Ayazgok, B., Humo, M., Karatas, M., Thouaye, M., Gaikwad, M., Degiorgis, L., Santin, M.D.N., Mondino, M., Barrot, M., Ibrahim, E.C., Turecki, G., Belzeaux, R., Veinante, P., Harsan, L.A., Hugel, S., Lutz, P.-E., Yalcin, I., 2023. The basolateral amygdala-anterior cingulate pathway contributes to depression-like behaviors and comorbidity with chronic pain behaviors in male mice. *Nat Commun* 14, 2198. <https://doi.org/10.1038/s41467-023-37878-y>
- Benabid, A.L., Jeaugey, L., 1989. Cells of the rat lateral habenula respond to high-threshold somatosensory inputs. *Neurosci Lett* 96, 289–294. [https://doi.org/10.1016/0304-3940\(89\)90393-5](https://doi.org/10.1016/0304-3940(89)90393-5)
- Benbouzid, M., Choucair-Jaafar, N., Yalcin, I., Waltisperger, E., Muller, A., Freund-Mercier, M.J., Barrot, M., 2008a. Chronic, but not acute, tricyclic antidepressant treatment alleviates neuropathic allodynia after sciatic nerve cuffing in mice. *European Journal of Pain* 12, 1008–1017. <https://doi.org/10.1016/j.ejpain.2008.01.010>
- Benbouzid, M., Pallage, V., Rajalu, M., Waltisperger, E., Doridot, S., Poisbeau, P., Freund-Mercier, M.J., Barrot, M., 2008b. Sciatic nerve cuffing in mice: A model of sustained neuropathic pain. *European Journal of Pain* 12, 591–599.
<https://doi.org/10.1016/j.ejpain.2007.10.002>

- Benekareddy, M., Stachniak, T.J., Bruns, A., Knoflach, F., Kienlin, M. von, Künnecke, B., Ghosh, A., 2018. Identification of a Corticohabenular Circuit Regulating Socially Directed Behavior. *Biological Psychiatry* 83, 607–617.
<https://doi.org/10.1016/j.biopsych.2017.10.032>
- Bennett, G.J., Xie, Y.-K., 1988. A peripheral mononeuropathy in rat that produces disorders of pain sensation like those seen in man. *Pain* 33, 87–107. [https://doi.org/10.1016/0304-3959\(88\)90209-6](https://doi.org/10.1016/0304-3959(88)90209-6)
- Berkley, K.J., 1997. Sex differences in pain. *Behav Brain Sci* 20, 371–380; discussion 435-513.
<https://doi.org/10.1017/s0140525x97221485>
- Berry, A., Bellisario, V., Capoccia, S., Tirassa, P., Calza, A., Alleva, E., Cirulli, F., 2012. Social deprivation stress is a triggering factor for the emergence of anxiety- and depression-like behaviours and leads to reduced brain BDNF levels in C57BL/6J mice. *Psychoneuroendocrinology* 37, 762–772.
<https://doi.org/10.1016/j.psyneuen.2011.09.007>
- Best, S., Pavel, D.G., 2017. Combined transcranial magnetic stimulation and ketamine for treatment of refractory mood disorder, anxiety, and pain: A case report 8, 4.
- Bijanki, K.R., Manns, J.R., Inman, C.S., Choi, K.S., Harati, S., Pedersen, N.P., Drane, D.L., Waters, A.C., Fasano, R.E., Mayberg, H.S., Willie, J.T., 2019. Cingulum stimulation enhances positive affect and anxiolysis to facilitate awake craniotomy. *J Clin Invest* 129, 1152–1166. <https://doi.org/10.1172/JCI120110>
- Bliss, T.V.P., Collingridge, G.L., Kaang, B.-K., Zhuo, M., 2016. Synaptic plasticity in the anterior cingulate cortex in acute and chronic pain. *Nat Rev Neurosci* 17, 485–496.
<https://doi.org/10.1038/nrn.2016.68>
- Bonica, J., 1979. Editorial The need of a taxonomy. *PAIN* 6, 247.
[https://doi.org/10.1016/0304-3959\(79\)90046-0](https://doi.org/10.1016/0304-3959(79)90046-0)
- Boyes, J., Bird, A., 1991. DNA methylation inhibits transcription indirectly via a methyl-CpG binding protein. *Cell* 64, 1123–1134. [https://doi.org/10.1016/0092-8674\(91\)90267-3](https://doi.org/10.1016/0092-8674(91)90267-3)
- Bravo, L., Llorca-Torralba, M., Suárez-Pereira, I., Berrocoso, E., 2020. Pain in neuropsychiatry: Insights from animal models. *Neuroscience & Biobehavioral Reviews* 115, 96–115.
<https://doi.org/10.1016/j.neubiorev.2020.04.029>
- Bravo, L., Mico, J.A., Rey-Brea, R., Pérez-Nievas, B., Leza, J.C., Berrocoso, E., 2012. Depressive-like States Heighten the Aversion to Painful Stimuli in a Rat Model of Comorbid Chronic Pain and Depression. *Anesthesiology* 117, 613–625.
<https://doi.org/10.1097/ALN.0b013e3182657b3e>
- Brenner, L., Zerlin, L., Tan, L.L., 2021. Functional disruption of cortical cingulate activity attenuates visceral hypersensitivity and anxiety induced by acute experimental colitis. *Sci Rep* 11, 2103. <https://doi.org/10.1038/s41598-021-81256-x>
- Brinschwitz, K., Dittgen, A., Madai, V.I., Lommel, R., Geisler, S., Veh, R.W., 2010. Glutamatergic axons from the lateral habenula mainly terminate on GABAergic neurons of the ventral midbrain. *Neuroscience* 168, 463–476.
<https://doi.org/10.1016/j.neuroscience.2010.03.050>

- Brockett, A.T., Tennyson, S.S., deBettencourt, C.A., Gaye, F., Roesch, M.R., 2020. Anterior cingulate cortex is necessary for adaptation of action plans. *Proc Natl Acad Sci U S A* 117, 6196–6204. <https://doi.org/10.1073/pnas.1919303117>
- Brotis, A.G., Kapsalaki, E.Z., Paterakis, K., Smith, J.R., Fountas, K.N., 2009. Historic Evolution of Open Cingulectomy and Stereotactic Cingulotomy in the Management of Medically Intractable Psychiatric Disorders, Pain and Drug Addiction. *SFN* 87, 271–291. <https://doi.org/10.1159/000226669>
- Brown, J.E., Chatterjee, N., Younger, J., Mackey, S., 2011. Towards a Physiology-Based Measure of Pain: Patterns of Human Brain Activity Distinguish Painful from Non-Painful Thermal Stimulation. *PLoS ONE* 6, e24124. <https://doi.org/10.1371/journal.pone.0024124>
- Bryden, D.W., Brockett, A.T., Blume, E., Heatley, K., Zhao, A., Roesch, M.R., 2019. Single Neurons in Anterior Cingulate Cortex Signal the Need to Change Action During Performance of a Stop-change Task that Induces Response Competition. *Cerebral Cortex* 29, 1020–1031. <https://doi.org/10.1093/cercor/bhy008>

C

- Caldecott-Hazard, S., Mazziotta, J., Phelps, M., 1988. Cerebral correlates of depressed behavior in rats, visualized using 14C- 2-deoxyglucose autoradiography. *J. Neurosci.* 8, 1951–1961. <https://doi.org/10.1523/JNEUROSCI.08-06-01951.1988>
- Cao, B., Zhang, X., Yan, N., Chen, S., Li, Y., 2012. Cholecystokinin enhances visceral pain-related affective memory via vagal afferent pathway in rats. *Mol Brain* 5, 19. <https://doi.org/10.1186/1756-6606-5-19>
- Cao, H., Gao, Y.-J., Ren, W.-H., Li, T.-T., Duan, K.-Z., Cui, Y.-H., Cao, X.-H., Zhao, Z.-Q., Ji, R.-R., Zhang, Y.-Q., 2009. Activation of Extracellular Signal-Regulated Kinase in the Anterior Cingulate Cortex Contributes to the Induction and Expression of Affective Pain. *Journal of Neuroscience* 29, 3307–3321. <https://doi.org/10.1523/JNEUROSCI.4300-08.2009>
- Cao, H., Zang, K.-K., Han, M., Zhao, Z.-Q., Wu, G.-C., Zhang, Y.-Q., 2014. Inhibition of p38 mitogen-activated protein kinase activation in the rostral anterior cingulate cortex attenuates pain-related negative emotion in rats. *Brain Research Bulletin* 107, 79–88. <https://doi.org/10.1016/j.brainresbull.2014.06.005>
- Cardenas, A., Caniglia, J., Keljalic, D., Dimitrov, E., 2020. Sex differences in the development of anxiodepressive-like behavior of mice subjected to sciatic nerve cuffing. *Pain* 161, 1861–1871. <https://doi.org/10.1097/j.pain.0000000000001875>
- Carr, K.D., Park, T.H., Zhang, Y., Stone, E.A., 1998. Neuroanatomical patterns of Fos-like immunoreactivity induced by naltrexone in food-restricted and ad libitum fed rats. *Brain Res* 779, 26–32. [https://doi.org/10.1016/s0006-8993\(97\)01074-3](https://doi.org/10.1016/s0006-8993(97)01074-3)
- Cerniauskas, I., Winterer, J., de Jong, J.W., Lukacsovich, D., Yang, H., Khan, F., Peck, J.R., Obayashi, S.K., Lilascharoen, V., Lim, B.K., Földy, C., Lammel, S., 2019. Chronic Stress Induces Activity, Synaptic, and Transcriptional Remodeling of the Lateral Habenula Associated with Deficits in Motivated Behaviors. *Neuron* 104, 899-915.e8. <https://doi.org/10.1016/j.neuron.2019.09.005>

- Chahrour, M., Jung, S.Y., Shaw, C., Zhou, X., Wong, S.T.C., Qin, J., Zoghbi, H.Y., 2008. MeCP2, a Key Contributor to Neurological Disease, Activates and Represses Transcription. *Science* 320, 1224–1229. <https://doi.org/10.1126/science.1153252>
- Chaibi, I., Bennis, M., Ba-M'Hamed, S., 2021. GABA-A receptor signaling in the anterior cingulate cortex modulates aggression and anxiety-related behaviors in socially isolated mice. *Brain Research* 1762, 147440. <https://doi.org/10.1016/j.brainres.2021.147440>
- Chang, Q., Khare, G., Dani, V., Nelson, S., Jaenisch, R., 2006. The Disease Progression of Mecp2 Mutant Mice Is Affected by the Level of BDNF Expression. *Neuron* 49, 341–348. <https://doi.org/10.1016/j.neuron.2005.12.027>
- Chaplan, S.R., Bach, F.W., Pogrel, J.W., Chung, J.M., Yaksh, T.L., 1994. Quantitative assessment of tactile allodynia in the rat paw. *J Neurosci Methods* 53, 55–63. [https://doi.org/10.1016/0165-0270\(94\)90144-9](https://doi.org/10.1016/0165-0270(94)90144-9)
- Chastrette, N., Pfaff, D.W., Gibbs, R.B., 1991. Effects of daytime and nighttime stress on Fos-like immunoreactivity in the paraventricular nucleus of the hypothalamus, the habenula, and the posterior paraventricular nucleus of the thalamus. *Brain Res* 563, 339–344. [https://doi.org/10.1016/0006-8993\(91\)91559-j](https://doi.org/10.1016/0006-8993(91)91559-j)
- Chen, F.-L., Dong, Y.-L., Zhang, Z.-J., Cao, D.-L., Xu, J., Hui, J., Zhu, L., Gao, Y.-J., 2012. Activation of astrocytes in the anterior cingulate cortex contributes to the affective component of pain in an inflammatory pain model. *Brain Research Bulletin* 87, 60–66. <https://doi.org/10.1016/j.brainresbull.2011.09.022>
- Chen, L., Wang, Y., Niu, C., Zhong, S., Hu, H., Chen, P., Zhang, S., Chen, G., Deng, F., Lai, S., Wang, J., Huang, L., Huang, R., 2018. Common and distinct abnormal frontal-limbic system structural and functional patterns in patients with major depression and bipolar disorder. *NeuroImage: Clinical* 20, 42–50. <https://doi.org/10.1016/j.nicl.2018.07.002>
- Chen, Q.-Y., Li, X.-H., Zhuo, M., 2021. NMDA receptors and synaptic plasticity in the anterior cingulate cortex. *Neuropharmacology* 197, 108749. <https://doi.org/10.1016/j.neuropharm.2021.108749>
- Chen, T., Taniguchi, W., Chen, Q.-Y., Tozaki-Saitoh, H., Song, Q., Liu, R.-H., Koga, K., Matsuda, T., Kaito-Sugimura, Y., Wang, J., Li, Z.-H., Lu, Y.-C., Inoue, K., Tsuda, M., Li, Y.-Q., Nakatsuka, T., Zhuo, M., 2018. Top-down descending facilitation of spinal sensory excitatory transmission from the anterior cingulate cortex. *Nat Commun* 9, 1886. <https://doi.org/10.1038/s41467-018-04309-2>
- Chen, T., Wang, J., Wang, Y.-Q., Chu, Y.-X., 2022. Current Understanding of the Neural Circuitry in the Comorbidity of Chronic Pain and Anxiety. *Neural Plasticity* 2022, 1–13. <https://doi.org/10.1155/2022/4217593>
- Chen, W., 2022. Neural circuits provide insights into reward and aversion. *Front. Neural Circuits* 16, 1002485. <https://doi.org/10.3389/fncir.2022.1002485>
- Clemenza, K., Weiss, S.H., Cheslack, K., Kandel, D.B., Kandel, E.R., Levine, A.A., 2021. Social isolation is closely linked to a marked reduction in physical activity in male mice. *J. Neurosci. Res.* 99, 1099–1107. <https://doi.org/10.1002/jnr.24777>

- Cohen, M., Quintner, J., van Rysewyk, S., 2018. Reconsidering the International Association for the Study of Pain definition of pain. *PR9* 3, e634.
<https://doi.org/10.1097/PR9.0000000000000634>
- Cohen, S.P., Mao, J., 2014. Neuropathic pain: mechanisms and their clinical implications. *BMJ* 348, f7656–f7656. <https://doi.org/10.1136/bmj.f7656>
- Colleoni, M., Sacerdote, P., 2010. Murine models of human neuropathic pain. *Biochimica et Biophysica Acta (BBA) - Molecular Basis of Disease* 1802, 924–933.
<https://doi.org/10.1016/j.bbadis.2009.10.012>
- Colloca, L., Ludman, T., Bouhassira, D., Baron, R., Dickenson, A.H., Yarnitsky, D., Freeman, R., Truini, A., Attal, N., Finnerup, N.B., Eccleston, C., Kalso, E., Bennett, D.L., Dworkin, R.H., Raja, S.N., 2017. Neuropathic pain. *Nat Rev Dis Primers* 3, 17002.
<https://doi.org/10.1038/nrdp.2017.2>
- Commons, K.G., Cholani, A.B., Babb, J.A., Ehlinger, D.G., 2017. The Rodent Forced Swim Test Measures Stress-Coping Strategy, Not Depression-like Behavior. *ACS Chem. Neurosci.* 8, 955–960. <https://doi.org/10.1021/acscchemneuro.7b00042>
- Cong, W., Peng, Y., Meng, B., Jia, X., Jin, Z., 2021. The effect of electroacupuncture on regulating pain and depression-like behaviors induced by chronic neuropathic pain. *Ann Palliat Med* 10, 104–113. <https://doi.org/10.21037/apm-20-1900>
- Crawley, J., Goodwin, F.K., 1980. Preliminary report of a simple animal behavior model for the anxiolytic effects of benzodiazepines. *Pharmacology Biochemistry and Behavior* 13, 167–170. [https://doi.org/10.1016/0091-3057\(80\)90067-2](https://doi.org/10.1016/0091-3057(80)90067-2)
- Cui, G., Jun, S.B., Jin, X., Luo, G., Pham, M.D., Lovinger, D.M., Vogel, S.S., Costa, R.M., 2014. Deep brain optical measurements of cell type-specific neural activity in behaving mice. *Nat Protoc* 9, 1213–1228. <https://doi.org/10.1038/nprot.2014.080>
- Cui, W.-Q., Zhang, W.-W., Chen, T., Li, Q., Xu, F., Mao-Ying, Q.-L., Mi, W.-L., Wang, Y.-Q., Chu, Y.-X., 2020. Tacr3 in the lateral habenula differentially regulates orofacial allodynia and anxiety-like behaviors in a mouse model of trigeminal neuralgia. *acta neuropathol commun* 8, 44. <https://doi.org/10.1186/s40478-020-00922-9>
- Cui, Y., Yang, Y., Ni, Z., Dong, Y., Cai, G., Foncelle, A., Ma, S., Sang, K., Tang, S., Li, Y., Shen, Y., Berry, H., Wu, S., Hu, H., 2018. Astroglial Kir4.1 in the lateral habenula drives neuronal bursts in depression. *Nature* 554, 323–327. <https://doi.org/10.1038/nature25752>

D

- Dai, R.-P., Li, C.-Q., Zhang, J.-W., Li, F., Shi, X.-D., Zhang, J.-Y., Zhou, X.-F., 2011. Biphasic Activation of Extracellular Signal-regulated Kinase in Anterior Cingulate Cortex Distinctly Regulates the Development of Pain-related Anxiety and Mechanical Hypersensitivity in Rats after Incision. *Anesthesiology* 115, 604–613.
<https://doi.org/10.1097/ALN.0b013e3182242045>

- Dai, W., Huang, S., Luo, Y., Cheng, X., Xia, P., Yang, M., Zhao, P., Zhang, Y., Lin, W.-J., Ye, X., 2022. Sex-Specific Transcriptomic Signatures in Brain Regions Critical for Neuropathic Pain-Induced Depression. *Front. Mol. Neurosci.* 15, 886916. <https://doi.org/10.3389/fnmol.2022.886916>
- D'amour, F.E., Smith, D.L., 1941. A Method for Determining Loss of Pain Sensation. *J Pharmacol Exp Ther* 72, 74–79.
- Datson, N.A., Van Den Oever, J.M.E., Korobko, O.B., Magarinos, A.M., De Kloet, E.R., McEwen, B.S., 2013. Previous History of Chronic Stress Changes the Transcriptional Response to Glucocorticoid Challenge in the Dentate Gyrus Region of the Male Rat Hippocampus. *Endocrinology* 154, 3261–3272. <https://doi.org/10.1210/en.2012-2233>
- de Heer, E.W., Gerrits, M.M.J.G., Beekman, A.T.F., Dekker, J., van Marwijk, H.W.J., de Waal, M.W.M., Spinhoven, P., Penninx, B.W.J.H., van der Feltz-Cornelis, C.M., 2014. The Association of Depression and Anxiety with Pain: A Study from NESDA. *PLoS ONE* 9, e106907. <https://doi.org/10.1371/journal.pone.0106907>
- Demyttenaere, K., Bruffaerts, R., Lee, S., Posada-Villa, J., Kovess, V., Angermeyer, M.C., Levinson, D., de Girolamo, G., Nakane, H., Mneimneh, Z., Lara, C., de Graaf, R., Scott, K.M., Gureje, O., Stein, D.J., Haro, J.M., Bromet, E.J., Kessler, R.C., Alonso, J., Von Korff, M., 2007. Mental disorders among persons with chronic back or neck pain: Results from the world mental health surveys. *Pain* 129, 332–342. <https://doi.org/10.1016/j.pain.2007.01.022>
- Deng, Z., Pan, Y., Li, D., Zhang, C., Jin, H., Wang, T., Zhan, S., Sun, B., 2019. Effect of Bilateral Anterior Cingulotomy on Chronic Neuropathic Pain with Severe Depression. *World Neurosurgery* 121, 196–200. <https://doi.org/10.1016/j.wneu.2018.10.008>
- Descalzi, G., Kim, S., Zhuo, M., 2009. Presynaptic and Postsynaptic Cortical Mechanisms of Chronic Pain. *Mol Neurobiol* 40, 253–259. <https://doi.org/10.1007/s12035-009-8085-9>
- Dhungel, S., Rai, D., Terada, M., Orikasa, C., Nishimori, K., Sakuma, Y., Kondo, Y., 2019. Oxytocin is indispensable for conspecific-odor preference and controls the initiation of female, but not male, sexual behavior in mice. *Neuroscience Research* 148, 34–41. <https://doi.org/10.1016/j.neures.2018.11.008>
- Díaz, E., Bravo, D., Rojas, X., Concha, M.L., 2011. Morphologic and immunohistochemical organization of the human habenular complex. *J Comp Neurol* 519, 3727–3747. <https://doi.org/10.1002/cne.22687>
- Du, J., Fang, Junfan, Wen, C., Shao, X., Liang, Y., Fang, Jianqiao, 2017. The Effect of Electroacupuncture on PKMzeta in the ACC in Regulating Anxiety-Like Behaviors in Rats Experiencing Chronic Inflammatory Pain. *Neural Plasticity* 2017, 1–13. <https://doi.org/10.1155/2017/3728752>
- Ducret, E., Jacquot, F., Descheemaeker, A., Dallel, R., Artola, A., 2022. Chronic facial inflammatory pain-induced anxiety is associated with bilateral deactivation of the rostral anterior cingulate cortex. *Brain Research Bulletin* 184, 88–98. <https://doi.org/10.1016/j.brainresbull.2022.03.012>

Dworkin, R.H., O'Connor, A.B., Backonja, M., Farrar, J.T., Finnerup, N.B., Jensen, T.S., Kalso, E.A., Loeser, J.D., Miaskowski, C., Nurmikko, T.J., Portenoy, R.K., Rice, A.S.C., Stacey, B.R., Treede, R.-D., Turk, D.C., Wallace, M.S., 2007. Pharmacologic management of neuropathic pain: Evidence-based recommendations. *Pain* 132, 237–251.
<https://doi.org/10.1016/j.pain.2007.08.033>

E

Esteves, M., Ganz, E., Sousa, N., Leite-Almeida, H., 2021. Asymmetrical Brain Plasticity: Physiology and Pathology. *Neuroscience* 454, 3–14.
<https://doi.org/10.1016/j.neuroscience.2020.01.022>

Esteves, M., Lopes, S.S., Almeida, A., Sousa, N., Leite-Almeida, H., 2020. Unmasking the relevance of hemispheric asymmetries—Break on through (to the other side). *Progress in Neurobiology* 192, 101823. <https://doi.org/10.1016/j.pneurobio.2020.101823>

Etkin, A., Egner, T., Kalisch, R., 2011. Emotional processing in anterior cingulate and medial prefrontal cortex. *Trends in Cognitive Sciences* 15, 85–93.
<https://doi.org/10.1016/j.tics.2010.11.004>

F

Feng, H., Chen, Z., Wang, G., Zhao, X., Liu, Z., 2016. Effect of the ifenprodil administered into rostral anterior cingulate cortex on pain-related aversion in rats with bone cancer pain. *BMC Anesthesiol* 16, 117. <https://doi.org/10.1186/s12871-016-0283-1>

Figeo, M., Riva-Posse, P., Choi, K.S., Bederson, L., Mayberg, H.S., Kopell, B.H., 2022. Deep Brain Stimulation for Depression. *Neurotherapeutics* 19, 1229–1245.
<https://doi.org/10.1007/s13311-022-01270-3>

Fillinger, C., Yalcin, I., Barrot, M., Veinante, P., 2017a. Afferents to anterior cingulate areas 24a and 24b and midcingulate areas 24a' and 24b' in the mouse. *Brain Struct Funct* 222, 1509–1532. <https://doi.org/10.1007/s00429-016-1290-1>

Fillinger, C., Yalcin, I., Barrot, M., Veinante, P., 2017b. Efferents of anterior cingulate areas 24a and 24b and midcingulate areas 24a' and 24b' in the mouse. *Brain Struct Funct*.
<https://doi.org/10.1007/s00429-017-1585-x>

Finnerup, N.B., Attal, N., Haroutounian, S., McNicol, E., Baron, R., Dworkin, R.H., Gilron, I., Haanpää, M., Hansson, P., Jensen, T.S., Kamerman, P.R., Lund, K., Moore, A., Raja, S.N., Rice, A.S.C., Rowbotham, M., Sena, E., Siddall, P., Smith, B.H., Wallace, M., 2015. Pharmacotherapy for neuropathic pain in adults: a systematic review and meta-analysis. *The Lancet Neurology* 14, 162–173. [https://doi.org/10.1016/S1474-4422\(14\)70251-0](https://doi.org/10.1016/S1474-4422(14)70251-0)

Finnerup, N.B., Kuner, R., Jensen, T.S., 2021. Neuropathic Pain: From Mechanisms to Treatment. *Physiological Reviews* 101, 259–301.
<https://doi.org/10.1152/physrev.00045.2019>

Fishbain, D.A., Cutler, R., Rosomoff, H.L., Rosomoff, R.S., 1997. Chronic pain-associated depression: antecedent or consequence of chronic pain? A review. *Clin J Pain* 13, 116–137. <https://doi.org/10.1097/00002508-199706000-00006>

- Foerster, B.R., Petrou, M., Edden, R.A.E., Sundgren, P.C., Schmidt-Wilcke, T., Lowe, S.E., Harte, S.E., Clauw, D.J., Harris, R.E., 2012. Reduced insular γ -aminobutyric acid in fibromyalgia. *Arthritis & Rheumatism* 64, 579–583. <https://doi.org/10.1002/art.33339>
- Franklin, K., Paxinos, G., 2013. Paxinos and Franklin's the Mouse Brain in Stereotaxic Coordinates - 5th Edition.
- Funabashi, D., Wakiyama, Y., Muto, N., Kita, I., Nishijima, T., 2022. Social isolation is a direct determinant of decreased home-cage activity in mice: A within-subjects study using a body-implantable actimeter. *Experimental Physiology* 107, 133–146. <https://doi.org/10.1113/EP090132>

G

- Gabbott, P.L.A., Dickie, B.G.M., Vaid, R.R., Headlam, A.J.N., Bacon, S.J., 1997. Local-circuit neurones in the medial prefrontal cortex (areas 25, 32 and 24b) in the rat: Morphology and quantitative distribution. *Journal of Comparative Neurology* 377, 465–499. [https://doi.org/10.1002/\(SICI\)1096-9861\(19970127\)377:4<465::AID-CNE1>3.0.CO;2-0](https://doi.org/10.1002/(SICI)1096-9861(19970127)377:4<465::AID-CNE1>3.0.CO;2-0)
- Galan-Arriero, I., Avila-Martin, G., Ferrer-Donato, A., Gomez-Soriano, J., Bravo-Esteban, E., Taylor, J., 2014. Oral administration of the p38 α MAPK inhibitor, UR13870, inhibits affective pain behavior after spinal cord injury. *Pain* 155, 2188–2198. <https://doi.org/10.1016/j.pain.2014.08.030>
- Gan, Z., Li, H., Naser, P.V., Han, Y., Tan, L.L., Oswald, M.J., Kuner, R., 2021. Repetitive non-invasive prefrontal stimulation reverses neuropathic pain via neural remodelling in mice. *Progress in Neurobiology* 201, 102009. <https://doi.org/10.1016/j.pneurobio.2021.102009>
- Gao, D.M., Hoffman, D., Benabid, A.L., 1996. Simultaneous recording of spontaneous activities and nociceptive responses from neurons in the pars compacta of substantia nigra and in the lateral habenula. *Eur J Neurosci* 8, 1474–1478. <https://doi.org/10.1111/j.1460-9568.1996.tb01609.x>
- Gao, S.-H., Shen, L.-L., Wen, H.-Z., Zhao, Y.-D., Chen, P.-H., Ruan, H.-Z., 2020. The projections from the anterior cingulate cortex to the nucleus accumbens and ventral tegmental area contribute to neuropathic pain-evoked aversion in rats. *Neurobiology of Disease* 140, 104862. <https://doi.org/10.1016/j.nbd.2020.104862>
- Gao, Y.-J., Ren, W.-H., Zhang, Y.-Q., Zhao, Z.-Q., 2004. Contributions of the anterior cingulate cortex and amygdala to pain- and fear-conditioned place avoidance in rats. *Pain* 110, 343–353. <https://doi.org/10.1016/j.pain.2004.04.030>
- Gater, R., Tansella, M., Korten, A., Tiemens, B.G., Mavreas, V.G., Olatawura, M.O., 1998. Sex Differences in the Prevalence and Detection of Depressive and Anxiety Disorders in General Health Care Settings: Report From the World Health Organization Collaborative Study on Psychological Problems in General Health Care. *Archives of General Psychiatry* 55, 405–413. <https://doi.org/10.1001/archpsyc.55.5.405>
- Gierthmühlen, J., Baron, R., 2016. Neuropathic Pain. *Semin Neurol* 36, 462–468. <https://doi.org/10.1055/s-0036-1584950>

- Global Burden of Disease Study 2013 Collaborators, 2015. Global, regional, and national incidence, prevalence, and years lived with disability for 301 acute and chronic diseases and injuries in 188 countries, 1990-2013: a systematic analysis for the Global Burden of Disease Study 2013. *Lancet* 386, 743–800. [https://doi.org/10.1016/S0140-6736\(15\)60692-4](https://doi.org/10.1016/S0140-6736(15)60692-4)
- Gomtsian, L., Bannister, K., Eyde, N., Robles, D., Dickenson, A.H., Porreca, F., Navratilova, E., 2018. Morphine effects within the rodent anterior cingulate cortex and rostral ventromedial medulla reveal separable modulation of affective and sensory qualities of acute or chronic pain. *Pain* 159, 2512–2521. <https://doi.org/10.1097/j.pain.0000000000001355>
- Guilloux, J.-P., Seney, M., Edgar, N., Sibille, E., 2011. Integrated behavioral z-scoring increases the sensitivity and reliability of behavioral phenotyping in mice: Relevance to emotionality and sex. *Journal of Neuroscience Methods* 197, 21–31. <https://doi.org/10.1016/j.jneumeth.2011.01.019>
- Guo, B., Wang, J., Yao, H., Ren, K., Chen, J., Yang, J., Cai, G., Liu, H., Fan, Y., Wang, W., Wu, S., 2018. Chronic Inflammatory Pain Impairs mGluR5-Mediated Depolarization-Induced Suppression of Excitation in the Anterior Cingulate Cortex. *Cerebral Cortex* 28, 2118–2130. <https://doi.org/10.1093/cercor/bhx117>
- Guo, S.-G., Lv, X.-H., Guan, S.-H., Li, H.-L., Qiao, Y., Feng, H., Cong, L., 2015. Silencing the NR2B gene in rat ACC neurons by lentivirus-delivered shRNA alleviates pain-related aversion 10.
- Gureje, O., Von Korff, M., Kola, L., Demyttenaere, K., He, Y., Posada-Villa, J., Lepine, J.P., Angermeyer, M.C., Levinson, D., de Girolamo, G., Iwata, N., Karam, A., Borges, G.L.G., de Graaf, R., Browne, M.O., Stein, D.J., Haro, J.M., Bromet, E.J., Kessler, R.C., Alonso, J., 2008. The relation between multiple pains and mental disorders: Results from the World Mental Health Surveys. *Pain* 135, 82–91. <https://doi.org/10.1016/j.pain.2007.05.005>
- Guy, J., Cheval, H., Selfridge, J., Bird, A., 2011. The Role of MeCP2 in the Brain. *Annu. Rev. Cell Dev. Biol.* 27, 631–652. <https://doi.org/10.1146/annurev-cellbio-092910-154121>

H

- Han, L.-N., Zhang, L., Li, L.-B., Sun, Y.-N., Wang, Y., Chen, L., Guo, Y., Zhang, Y.-M., Zhang, Q.-J., Liu, J., 2015. Activation of serotonin(2C) receptors in the lateral habenular nucleus increases the expression of depression-related behaviors in the hemiparkinsonian rat. *Neuropharmacology* 93, 68–79. <https://doi.org/10.1016/j.neuropharm.2015.01.024>
- Han, M., Xiao, X., Yang, Y., Huang, R.-Y., Cao, H., Zhao, Z.-Q., Zhang, Y.-Q., 2014. SIP30 Is Required for Neuropathic Pain-Evoked Aversion in Rats. *Journal of Neuroscience* 34, 346–355. <https://doi.org/10.1523/JNEUROSCI.3160-13.2014>
- Hargreaves, K., Dubner, R., Brown, F., Flores, C., Joris, J., 1988. A new and sensitive method for measuring thermal nociception in cutaneous hyperalgesia. *Pain* 32, 77–88. [https://doi.org/10.1016/0304-3959\(88\)90026-7](https://doi.org/10.1016/0304-3959(88)90026-7)

- Hasnie, F.S., Wallace, V.C.J., Hefner, K., Holmes, A., Rice, A.S.C., 2007. Mechanical and cold hypersensitivity in nerve-injured C57BL/6J mice is not associated with fear-avoidance- and depression-related behaviour. *British Journal of Anaesthesia* 98, 816–822. <https://doi.org/10.1093/bja/aem087>
- Heiman, M., Kulicke, R., Fenster, R.J., Greengard, P., Heintz, N., 2014. Cell type-specific mRNA purification by translating ribosome affinity purification (TRAP). *Nat Protoc* 9, 1282–1291. <https://doi.org/10.1038/nprot.2014.085>
- Herkenham, M., Nauta, W.J., 1979. Efferent connections of the habenular nuclei in the rat. *J Comp Neurol* 187, 19–47. <https://doi.org/10.1002/cne.901870103>
- Herkenham, M., Nauta, W.J., 1977. Afferent connections of the habenular nuclei in the rat. A horseradish peroxidase study, with a note on the fiber-of-passage problem. *J Comp Neurol* 173, 123–146. <https://doi.org/10.1002/cne.901730107>
- Hikosaka, O., 2010. The habenula: from stress evasion to value-based decision-making. *Nat Rev Neurosci* 11, 503–513. <https://doi.org/10.1038/nrn2866>
- Hirschberg, S., Li, Y., Randall, A., Kremer, E.J., Pickering, A.E., 2017. Functional dichotomy in spinal- vs prefrontal-projecting locus coeruleus modules splits descending noradrenergic analgesia from ascending aversion and anxiety in rats. *eLife* 6, e29808. <https://doi.org/10.7554/eLife.29808>
- Holtzheimer, P.E., Husain, M.M., Lisanby, S.H., Taylor, S.F., Whitworth, L.A., McClintock, S., Slavin, K.V., Berman, J., McKhann, G.M., Patil, P.G., Rittberg, B.R., Abosch, A., Pandurangi, A.K., Holloway, K.L., Lam, R.W., Honey, C.R., Neimat, J.S., Henderson, J.M., DeBattista, C., Rothschild, A.J., Pilitsis, J.G., Espinoza, R.T., Petrides, G., Mogilner, A.Y., Matthews, K., Peichel, D., Gross, R.E., Hamani, C., Lozano, A.M., Mayberg, H.S., 2017. Subcallosal cingulate deep brain stimulation for treatment-resistant depression: a multisite, randomised, sham-controlled trial. *Lancet Psychiatry* 4, 839–849. [https://doi.org/10.1016/S2215-0366\(17\)30371-1](https://doi.org/10.1016/S2215-0366(17)30371-1)
- Hou, Y.-Y., Cai, Y.-Q., Pan, Z.Z., 2015. Persistent Pain Maintains Morphine-Seeking Behavior after Morphine Withdrawal through Reduced MeCP2 Repression of Glua1 in Rat Central Amygdala. *J. Neurosci.* 35, 3689–3700. <https://doi.org/10.1523/JNEUROSCI.3453-14.2015>
- Hu, H., Cui, Y., Yang, Y., 2020. Circuits and functions of the lateral habenula in health and in disease. *Nat Rev Neurosci* 21, 277–295. <https://doi.org/10.1038/s41583-020-0292-4>
- Huang, L., Xi, Y., Peng, Y., Yang, Y., Huang, X., Fu, Y., Tao, Q., Xiao, J., Yuan, T., An, K., Zhao, H., Pu, M., Xu, F., Xue, T., Luo, M., So, K.-F., Ren, C., 2019. A Visual Circuit Related to Habenula Underlies the Antidepressive Effects of Light Therapy. *Neuron* 102, 128-142.e8. <https://doi.org/10.1016/j.neuron.2019.01.037>
- Hubbard, C.S., Khan, S.A., Xu, S., Cha, M., Masri, R., Seminowicz, D.A., 2015. Behavioral, metabolic and functional brain changes in a rat model of chronic neuropathic pain: A longitudinal MRI study. *NeuroImage* 107, 333–344. <https://doi.org/10.1016/j.neuroimage.2014.12.024>

Humo, M., Ayazgök, B., Becker, L.J., Waltisperger, E., Rantamäki, T., Yalcin, I., 2020. Ketamine induces rapid and sustained antidepressant-like effects in chronic pain induced depression: Role of MAPK signaling pathway. *Progress in Neuro-Psychopharmacology and Biological Psychiatry* 100, 109898. <https://doi.org/10.1016/j.pnpbp.2020.109898>

Humo, M., Lu, H., Yalcin, I., 2019. The molecular neurobiology of chronic pain-induced depression. *Cell Tissue Res* 377, 21–43. <https://doi.org/10.1007/s00441-019-03003-z>

Hunnskaar, S., Fasmer, O.B., Hole, K., 1985. Formalin test in mice, a useful technique for evaluating mild analgesics. *Journal of Neuroscience Methods* 14, 69–76. [https://doi.org/10.1016/0165-0270\(85\)90116-5](https://doi.org/10.1016/0165-0270(85)90116-5)

I

Ichesco, E., Schmidt-Wilcke, T., Bhavsar, R., Clauw, D.J., Peltier, S.J., Kim, J., Napadow, V., Hampson, J.P., Kairys, A.E., Williams, D.A., Harris, R.E., 2014. Altered Resting State Connectivity of the Insular Cortex in Individuals With Fibromyalgia. *The Journal of Pain* 15, 815-826.e1. <https://doi.org/10.1016/j.jpain.2014.04.007>

Ieraci, A., Mallei, A., Popoli, M., 2016. Social Isolation Stress Induces Anxious-Depressive-Like Behavior and Alterations of Neuroplasticity-Related Genes in Adult Male Mice. *Neural Plasticity* 2016, 1–13. <https://doi.org/10.1155/2016/6212983>

Imbe, H., Kimura, A., 2017. Attenuation of pCREB and Egr1 expression in the insular and anterior cingulate cortices associated with enhancement of CFA-evoked mechanical hypersensitivity after repeated forced swim stress. *Brain Research Bulletin* 134, 253–261. <https://doi.org/10.1016/j.brainresbull.2017.08.013>

Ishikawa, K., Yasuda, S., Fukuhara, K., Iwanaga, Y., Ida, Y., Ishikawa, J., Yamagata, H., Ono, M., Kakeda, T., Ishikawa, T., 2014. 4-Methylcatechol prevents derangements of brain-derived neurotrophic factor and TrkB-related signaling in anterior cingulate cortex in chronic pain with depression-like behavior. *NeuroReport* 25, 226–232. <https://doi.org/10.1097/WNR.0000000000000072>

Ishikawa, T., Yasuda, S., Minoda, S., Ibuki, T., Fukuhara, K., Iwanaga, Y., Ariyoshi, T., Sasaki, H., 2015. Neurotrophin® Ameliorates Chronic Pain via Induction of Brain-Derived Neurotrophic Factor. *Cell Mol Neurobiol* 35, 231–241. <https://doi.org/10.1007/s10571-014-0118-x>

J

Jaggi, A.S., Jain, V., Singh, N., 2011. Animal models of neuropathic pain: Animal models of neuropathic pain. *Fundamental & Clinical Pharmacology* 25, 1–28. <https://doi.org/10.1111/j.1472-8206.2009.00801.x>

Jang, J.-H., Song, E.-M., Do, Y.-H., Ahn, S., Oh, J.-Y., Hwang, T.-Y., Ryu, Y., Jeon, S., Song, M.-Y., Park, H.-J., 2021. Acupuncture alleviates chronic pain and comorbid conditions in a mouse model of neuropathic pain: the involvement of DNA methylation in the prefrontal cortex. *Pain* 162, 514–530. <https://doi.org/10.1097/j.pain.0000000000002031>

- Jarrin, S., Pandit, A., Roche, M., Finn, D.P., 2020. Differential Role of Anterior Cingulate Cortical Glutamatergic Neurons in Pain-Related Aversion Learning and Nociceptive Behaviors in Male and Female Rats. *Front. Behav. Neurosci.* 14, 139. <https://doi.org/10.3389/fnbeh.2020.00139>
- Jensen, T.S., Finnerup, N.B., 2014. Allodynia and hyperalgesia in neuropathic pain: clinical manifestations and mechanisms. *The Lancet Neurology* 13, 924–935. [https://doi.org/10.1016/S1474-4422\(14\)70102-4](https://doi.org/10.1016/S1474-4422(14)70102-4)
- Jhang, J., Lee, H., Kang, M.S., Lee, H.-S., Park, H., Han, J.-H., 2018. Anterior cingulate cortex and its input to the basolateral amygdala control innate fear response. *Nat Commun* 9, 2744. <https://doi.org/10.1038/s41467-018-05090-y>
- Johansen, J.P., Fields, H.L., 2004. Glutamatergic activation of anterior cingulate cortex produces an aversive teaching signal. *Nat Neurosci* 7, 398–403. <https://doi.org/10.1038/nn1207>
- Johansen, J.P., Fields, H.L., Manning, B.H., 2001. The affective component of pain in rodents: direct evidence for a contribution of the anterior cingulate cortex. *Proc Natl Acad Sci U S A* 98, 8077–8082. <https://doi.org/10.1073/pnas.141218998>
- Jones, P.L., Veenstra, G.J.C., Wade, P.A., Vermaak, D., Kass, S.U., Landsberger, N., Strouboulis, J., Wolffe, A.P., 1998. Methylated DNA and MeCP2 recruit histone deacetylase to repress transcription. *Nat Genet* 19, 187–191. <https://doi.org/10.1038/561>
- Juarez-Salinas, D.L., Braz, J.M., Etlin, A., Gee, S., Sohal, V., Basbaum, A.I., 2019. GABAergic cell transplants in the anterior cingulate cortex reduce neuropathic pain aversiveness. *Brain* 142, 2655–2669. <https://doi.org/10.1093/brain/awz203>

K

- Kang, S.J., Kim, S., Lee, J., Kwak, C., Lee, K., Zhuo, M., Kaang, B.-K., 2017. Inhibition of anterior cingulate cortex excitatory neuronal activity induces conditioned place preference in a mouse model of chronic inflammatory pain. *Korean J Physiol Pharmacol* 21, 487. <https://doi.org/10.4196/kjpp.2017.21.5.487>
- Kessler, R.C., McGonagle, K.A., Zhao, S., Nelson, C.B., Hughes, M., Eshleman, S., Wittchen, H.-U., Kendler, K.S., 1994. Lifetime and 12-Month Prevalence of DSM-III-R Psychiatric Disorders in the United States: Results From the National Comorbidity Survey. *Archives of General Psychiatry* 51, 8–19. <https://doi.org/10.1001/archpsyc.1994.03950010008002>
- Kessler, R.C., Sonnega, A., Bromet, E., Hughes, M., Nelson, C.B., 1995. Posttraumatic Stress Disorder in the National Comorbidity Survey. *Archives of General Psychiatry* 52, 1048–1060. <https://doi.org/10.1001/archpsyc.1995.03950240066012>
- Kim, J.-H., Ma, D.-H., Jung, E., Choi, I., Lee, S.-H., 2021. Gated feedforward inhibition in the frontal cortex releases goal-directed action. *Nat Neurosci* 24, 1452–1464. <https://doi.org/10.1038/s41593-021-00910-9>
- Kim, S., Mátyás, F., Lee, S., Acsády, L., Shin, H.-S., 2012. Lateralization of observational fear learning at the cortical but not thalamic level in mice. *Proc. Natl. Acad. Sci. U.S.A.* 109, 15497–15501. <https://doi.org/10.1073/pnas.1213903109>

- Kim, U., Chang, S.-Y., 2005. Dendritic morphology, local circuitry, and intrinsic electrophysiology of neurons in the rat medial and lateral habenular nuclei of the epithalamus. *J Comp Neurol* 483, 236–250. <https://doi.org/10.1002/cne.20410>
- Kim, U., Lee, T., 2012. Topography of descending projections from anterior insular and medial prefrontal regions to the lateral habenula of the epithalamus in the rat. *Eur J Neurosci* 35, 1253–1269. <https://doi.org/10.1111/j.1460-9568.2012.08030.x>
- Kirsh, K.L., 2010. Differentiating and Managing Common Psychiatric Comorbidities Seen in Chronic Pain Patients. *Journal of Pain & Palliative Care Pharmacotherapy* 24, 39–47. <https://doi.org/10.3109/15360280903583123>
- Klein, M.E., Liroy, D.T., Ma, L., Impey, S., Mandel, G., Goodman, R.H., 2007. Homeostatic regulation of MeCP2 expression by a CREB-induced microRNA. *Nat Neurosci* 10, 1513–1514. <https://doi.org/10.1038/nn2010>
- Koga, K., Descalzi, G., Chen, T., Ko, H.-G., Lu, J., Li, S., Son, J., Kim, T., Kwak, C., Haganir, R.L., Zhao, M., Kaang, B.-K., Collingridge, G.L., Zhuo, M., 2015. Coexistence of Two Forms of LTP in ACC Provides a Synaptic Mechanism for the Interactions between Anxiety and Chronic Pain. *Neuron* 85, 377–389. <https://doi.org/10.1016/j.neuron.2014.12.021>
- Kolling, N., Wittmann, M.K., Behrens, T.E.J., Boorman, E.D., Mars, R.B., Rushworth, M.F.S., 2016. Value, search, persistence and model updating in anterior cingulate cortex. *Nat Neurosci* 19, 1280–1285. <https://doi.org/10.1038/nn.4382>
- Kolling, Wittmann, M., Behrens, T., Boorman, E., Mars, R., Rushworth, M., 2016. Anterior cingulate cortex and the value of the environment, search, persistence, and model updating. *Nat Neurosci* 19, 1280–5. <https://doi.org/10.1038/nn.4382>
- Kosek, E., Cohen, M., Baron, R., Gebhart, G.F., Mico, J.-A., Rice, A.S.C., Rief, W., Sluka, A.K., 2016. Do we need a third mechanistic descriptor for chronic pain states? *Pain* 157, 1382–1386. <https://doi.org/10.1097/j.pain.0000000000000507>
- Kowski, A.B., Veh, R.W., Weiss, T., 2009. Dopaminergic activation excites rat lateral habenular neurons in vivo. *Neuroscience* 161, 1154–1165. <https://doi.org/10.1016/j.neuroscience.2009.04.026>
- Kremer, M., Becker, L.J., Barrot, M., Yalcin, I., 2021. How to study anxiety and depression in rodent models of chronic pain? *Eur J Neurosci* 53, 236–270. <https://doi.org/10.1111/ejn.14686>
- Krishnan, V., Han, M.-H., Graham, D.L., Berton, O., Renthal, W., Russo, S.J., LaPlant, Q., Graham, A., Lutter, M., Lagace, D.C., Ghose, S., Reister, R., Tannous, P., Green, T.A., Neve, R.L., Chakravarty, S., Kumar, A., Eisch, A.J., Self, D.W., Lee, F.S., Tamminga, C.A., Cooper, D.C., Gershenfeld, H.K., Nestler, E.J., 2007. Molecular Adaptations Underlying Susceptibility and Resistance to Social Defeat in Brain Reward Regions. *Cell* 131, 391–404. <https://doi.org/10.1016/j.cell.2007.09.018>
- Kumar, A., Kaur, H., Singh, A., 2018. Neuropathic Pain models caused by damage to central or peripheral nervous system. *Pharmacological Reports* 70, 206–216. <https://doi.org/10.1016/j.pharep.2017.09.009>

- Kupfer, D.J., Frank, E., Phillips, M.L., 2012. Major depressive disorder: new clinical, neurobiological, and treatment perspectives. *The Lancet* 379, 1045–1055. [https://doi.org/10.1016/S0140-6736\(11\)60602-8](https://doi.org/10.1016/S0140-6736(11)60602-8)
- Kuzawińska, O., Lis, K., Cudna, A., Bałkowiec-Iskra, E., 2014. Gender differences in the neurochemical response of trigeminal ganglion neurons to peripheral inflammation in mice. *Acta Neurobiol Exp (Wars)* 74, 227–232.
- Kuzumaki, N., Narita, Minoru, Narita, Michiko, Hareyama, N., Niikura, K., Nagumo, Y., Nozaki, H., Amano, T., Suzuki, T., 2007. Chronic pain-induced astrocyte activation in the cingulate cortex with no change in neural or glial differentiation from neural stem cells in mice. *Neuroscience Letters* 415, 22–27. <https://doi.org/10.1016/j.neulet.2006.12.057>

L

- LaBuda, C.J., Fuchs, P.N., 2000. A Behavioral Test Paradigm to Measure the Aversive Quality of Inflammatory and Neuropathic Pain in Rats. *Experimental Neurology* 163, 490–494. <https://doi.org/10.1006/exnr.2000.7395>
- LaGraize, S.C., Borzan, J., Peng, Y.B., Fuchs, P.N., 2006. Selective regulation of pain affect following activation of the opioid anterior cingulate cortex system. *Experimental Neurology* 197, 22–30. <https://doi.org/10.1016/j.expneurol.2005.05.008>
- LaGraize, S.C., Fuchs, P.N., 2007. GABAA but not GABAB receptors in the rostral anterior cingulate cortex selectively modulate pain-induced escape/avoidance behavior. *Experimental Neurology* 204, 182–194. <https://doi.org/10.1016/j.expneurol.2006.10.007>
- LaGraize, S.C., Labuda, C.J., Rutledge, M.A., Jackson, R.L., Fuchs, P.N., 2004. Differential effect of anterior cingulate cortex lesion on mechanical hypersensitivity and escape/avoidance behavior in an animal model of neuropathic pain. *Experimental Neurology* 188, 139–148. <https://doi.org/10.1016/j.expneurol.2004.04.003>
- Lançon, K., Qu, C., Navratilova, E., Porreca, F., Séguéla, P., 2021. Decreased dopaminergic inhibition of pyramidal neurons in anterior cingulate cortex maintains chronic neuropathic pain. *Cell Reports* 37, 109933. <https://doi.org/10.1016/j.celrep.2021.109933>
- Lander, S.S., Linder-Shacham, D., Gaisler-Salomon, I., 2017. Differential effects of social isolation in adolescent and adult mice on behavior and cortical gene expression. *Behavioural Brain Research* 316, 245–254. <https://doi.org/10.1016/j.bbr.2016.09.005>
- Lanier, L.L., 2014. Just the FACS. *The Journal of Immunology* 193, 2043–2044. <https://doi.org/10.4049/jimmunol.1401725>
- Lecca, S., Meye, F.J., Mameli, M., 2014. The lateral habenula in addiction and depression: an anatomical, synaptic and behavioral overview. *European Journal of Neuroscience* 39, 1170–1178. <https://doi.org/10.1111/ejn.12480>
- Lecca, S., Meye, F.J., Trusel, M., Tchenio, A., Harris, J., Schwarz, M.K., Burdakov, D., Georges, F., Mameli, M., 2017. Aversive stimuli drive hypothalamus-to-habenula excitation to promote escape behavior. *eLife* 6, e30697. <https://doi.org/10.7554/eLife.30697>

- Lecca, S., Pelosi, A., Tchenio, A., Moutkine, I., Lujan, R., Hervé, D., Mameli, M., 2016. Rescue of GABAB and GIRK function in the lateral habenula by protein phosphatase 2A inhibition ameliorates depression-like phenotypes in mice. *Nat Med* 22, 254–261. <https://doi.org/10.1038/nm.4037>
- Lecourtier, L., Durieux, L., Mathis, V., 2023. Alteration of Lateral Habenula Function Prevents the Proper Exploration of a Novel Environment. *Neuroscience* 514, 56–66. <https://doi.org/10.1016/j.neuroscience.2023.01.010>
- Lee, J.-J., Kim, H.J., Čeko, M., Park, B., Lee, S.A., Park, H., Roy, M., Kim, S.-G., Wager, T.D., Woo, C.-W., 2021. A neuroimaging biomarker for sustained experimental and clinical pain. *Nat Med* 27, 174–182. <https://doi.org/10.1038/s41591-020-1142-7>
- Lee, J.-Y., You, T., Lee, C.-H., Im, G.H., Seo, H., Woo, C.-W., Kim, S.-G., 2022. Role of anterior cingulate cortex inputs to periaqueductal gray for pain avoidance. *Curr Biol* 32, 2834–2847.e5. <https://doi.org/10.1016/j.cub.2022.04.090>
- Lee, M., Manders, T.R., Eberle, S.E., Su, C., D’amour, J., Yang, R., Lin, H.Y., Deisseroth, K., Froemke, R.C., Wang, J., 2015. Activation of Corticostriatal Circuitry Relieves Chronic Neuropathic Pain. *J. Neurosci.* 35, 5247–5259. <https://doi.org/10.1523/JNEUROSCI.3494-14.2015>
- Lei, L., Sun, S., Gao, Y., Zhao, Z., Zhang, Y., 2004. NMDA receptors in the anterior cingulate cortex mediate pain-related aversion. *Experimental Neurology* 189, 413–421. <https://doi.org/10.1016/j.expneurol.2004.06.012>
- Leite-Almeida, H., Cerqueira, J.J., Wei, H., Ribeiro-Costa, N., Anjos-Martins, H., Sousa, N., Pertovaara, A., Almeida, A., 2012. Differential effects of left/right neuropathy on rats’ anxiety and cognitive behavior. *Pain* 153, 2218–2225. <https://doi.org/10.1016/j.pain.2012.07.007>
- Lewis, J.D., Meehan, R.R., Henzel, W.J., Maurer-Fogy, I., Jeppesen, P., Klein, F., Bird, A., 1992. Purification, sequence, and cellular localization of a novel chromosomal protein that binds to Methylated DNA. *Cell* 69, 905–914. [https://doi.org/10.1016/0092-8674\(92\)90610-O](https://doi.org/10.1016/0092-8674(92)90610-O)
- Li, B., Piriz, J., Mirrione, M., Chung, C., Proulx, C.D., Schulz, D., Henn, F., Malinow, R., 2011. Synaptic potentiation onto habenula neurons in the learned helplessness model of depression. *Nature* 470, 535–539. <https://doi.org/10.1038/nature09742>
- Li, J., Li, Y., Zhang, B., Shen, X., Zhao, H., 2016. Why depression and pain often coexist and mutually reinforce: Role of the lateral habenula. *Experimental Neurology* 284, 106–113. <https://doi.org/10.1016/j.expneurol.2016.08.010>
- Li, J., Wang, X., Wang, H., Wang, R., Guo, Y., Xu, L., Zhang, G., Wu, J., Wang, G., 2022. The BDNF-TrkB signaling pathway in the rostral anterior cingulate cortex is involved in the development of pain aversion in rats with bone cancer via NR2B and ERK-CREB signaling. *Brain Research Bulletin* 185, 18–27. <https://doi.org/10.1016/j.brainresbull.2022.04.001>
- Li, K., Zhou, T., Liao, L., Yang, Z., Wong, C., Henn, F., Malinow, R., Yates, J.R., Hu, H., 2013. β CaMKII in lateral habenula mediates core symptoms of depression. *Science* 341, 1016–1020. <https://doi.org/10.1126/science.1240729>

- Li, T.-T., Ren, W.-H., Xiao, X., Nan, J., Cheng, L.-Z., Zhang, X.-H., Zhao, Z.-Q., Zhang, Y.-Q., 2009. NMDA NR2A and NR2B receptors in the rostral anterior cingulate cortex contribute to pain-related aversion in male rats. *Pain* 146, 183–193.
<https://doi.org/10.1016/j.pain.2009.07.027>
- Li, X.-H., Matsuura, T., Xue, M., Chen, Q.-Y., Liu, R.-H., Lu, J.-S., Shi, W., Fan, K., Zhou, Z., Miao, Z., Yang, J., Wei, S., Wei, F., Chen, T., Zhuo, M., 2021. Oxytocin in the anterior cingulate cortex attenuates neuropathic pain and emotional anxiety by inhibiting presynaptic long-term potentiation. *Cell Reports* 36, 109411.
<https://doi.org/10.1016/j.celrep.2021.109411>
- Li, Yanhui, Wang, Y., Xuan, C., Li, Yang, Piao, L., Li, J., Zhao, H., 2017. Role of the Lateral Habenula in Pain-Associated Depression. *Front. Behav. Neurosci.* 11.
<https://doi.org/10.3389/fnbeh.2017.00031>
- Li, Z.-Z., Han, W.-J., Sun, Z.-C., Chen, Y., Sun, J.-Y., Cai, G.-H., Liu, W.-N., Wang, T.-Z., Xie, Y.-D., Mao, H.-H., Wang, F., Ma, S.-B., Wang, F.-D., Xie, R.-G., Wu, S.-X., Luo, C., 2021. Extracellular matrix protein laminin β 1 regulates pain sensitivity and anxiodepression-like behaviors in mice. *Journal of Clinical Investigation* 131, e146323.
<https://doi.org/10.1172/JCI146323>
- Liang, M., Mouraux, A., Hu, L., Iannetti, G.D., 2013. Primary sensory cortices contain distinguishable spatial patterns of activity for each sense. *Nat Commun* 4, 1979.
<https://doi.org/10.1038/ncomms2979>
- Lieberman, G., Shpaner, M., Watts, R., Andrews, T., Filippi, C.G., Davis, M., Naylor, M.R., 2014. White Matter Involvement in Chronic Musculoskeletal Pain. *The Journal of Pain* 15, 1110–1119. <https://doi.org/10.1016/j.jpain.2014.08.002>
- Liu, L.-Y., Zhang, R.-L., Chen, L., Zhao, H.-Y., Cai, J., Wang, J.-K., Guo, D.-Q., Cui, Y.-J., Xing, G.-G., 2019. Chronic stress increases pain sensitivity via activation of the rACC–BLA pathway in rats. *Experimental Neurology* 313, 109–123.
<https://doi.org/10.1016/j.expneurol.2018.12.009>
- Liu, Y., Xu, H., Sun, G., Vemulapalli, B., Jee, H.J., Zhang, Q., Wang, J., 2021. Frequency Dependent Electrical Stimulation of PFC and ACC for Acute Pain Treatment in Rats. *Front. Pain Res.* 2, 728045. <https://doi.org/10.3389/fpain.2021.728045>
- Llorca-Torralba, M., Camarena-Delgado, C., Suárez-Pereira, I., Bravo, L., Mariscal, P., Garcia-Partida, J.A., López-Martín, C., Wei, H., Pertovaara, A., Mico, J.A., Berrocoso, E., 2022. Pain and depression comorbidity causes asymmetric plasticity in the locus coeruleus neurons. *Brain* 145, 154–167. <https://doi.org/10.1093/brain/awab239>
- Llorca-Torralba, M., Mico, J.A., Berrocoso, E., 2018. Behavioral effects of combined morphine and MK-801 administration to the locus coeruleus of a rat neuropathic pain model. *Progress in Neuro-Psychopharmacology and Biological Psychiatry* 84, 257–266.
<https://doi.org/10.1016/j.pnpbp.2018.03.007>

- Llorca-Torralba, M., Suárez-Pereira, I., Bravo, L., Camarena-Delgado, C., Garcia-Partida, J.A., Mico, J.A., Berrocoso, E., 2019. Chemogenetic Silencing of the Locus Coeruleus–Basolateral Amygdala Pathway Abolishes Pain-Induced Anxiety and Enhanced Aversive Learning in Rats. *Biological Psychiatry* 85, 1021–1035. <https://doi.org/10.1016/j.biopsych.2019.02.018>
- Lu, B., Jiang, J., Sun, J., Xiao, C., Meng, B., Zheng, J., Li, X., Wang, R., Wu, G., Chen, J., 2016. Inhibition of mammalian target of rapamycin activation in the rostral anterior cingulate cortex attenuates pain-related aversion in rats. *Behavioural Brain Research* 310, 51–58. <https://doi.org/10.1016/j.bbr.2016.05.011>
- Lu, Y., Zhu, L., Gao, Y.-J., 2011. Pain-related aversion induces astrocytic reaction and proinflammatory cytokine expression in the anterior cingulate cortex in rats. *Brain Research Bulletin* 84, 178–182. <https://doi.org/10.1016/j.brainresbull.2010.12.007>
- Luo, C., Zhang, Y.-L., Luo, W., Zhou, F.H., Li, C.-Q., Xu, J.-M., Dai, R.-P., 2015. Differential effects of general anesthetics on anxiety-like behavior in formalin-induced pain: involvement of ERK activation in the anterior cingulate cortex. *Psychopharmacology* 232, 4433–4444. <https://doi.org/10.1007/s00213-015-4071-2>

M

- Ma, L., Yue, L., Zhang, Y., Wang, Y., Han, B., Cui, S., Liu, F.-Y., Wan, Y., Yi, M., 2019. Spontaneous Pain Disrupts Ventral Hippocampal CA1-Infralimbic Cortex Connectivity and Modulates Pain Progression in Rats with Peripheral Inflammation. *Cell Reports* 29, 1579–1593.e6. <https://doi.org/10.1016/j.celrep.2019.10.002>
- Ma, Y., Qin, G.-H., Guo, X., Hao, N., Shi, Y., Li, H.-F., Zhao, X., Li, J.-G., Zhang, C., Zhang, Y., 2022. Activation of δ -opioid Receptors in Anterior Cingulate Cortex Alleviates Affective Pain in Rats. *Neuroscience* 494, 152–166. <https://doi.org/10.1016/j.neuroscience.2022.05.008>
- Malkesman, O., Scattoni, M.L., Paredes, D., Tragon, T., Pearson, B., Shaltiel, G., Chen, G., Crawley, J.N., Manji, H.K., 2010. The Female Urine Sniffing Test: A Novel Approach for Assessing Reward-Seeking Behavior in Rodents. *Biological Psychiatry* 67, 864–871. <https://doi.org/10.1016/j.biopsych.2009.10.018>
- Maroteaux, M., Mameli, M., 2012. Cocaine evokes projection-specific synaptic plasticity of lateral habenula neurons. *J Neurosci* 32, 12641–12646. <https://doi.org/10.1523/JNEUROSCI.2405-12.2012>
- Mathis, V., Barbelivien, A., Majchrzak, M., Mathis, C., Cassel, J.-C., Lecourtier, L., 2017. The Lateral Habenula as a Relay of Cortical Information to Process Working Memory. *Cereb Cortex* 27, 5485–5495. <https://doi.org/10.1093/cercor/bhw316>
- Mathis, V., Cosquer, B., Avallone, M., Cassel, J.-C., Lecourtier, L., 2015. Excitatory Transmission to the Lateral Habenula Is Critical for Encoding and Retrieval of Spatial Memory. *Neuropsychopharmacol* 40, 2843–2851. <https://doi.org/10.1038/npp.2015.140>

- Mathis, V., Cosquer, B., Barbelivien, A., Herbeaux, K., Bothorel, B., Sage-Ciocca, D., Poirel, V.-J., Mathis, C., Lecourtier, L., 2018. The lateral habenula interacts with the hypothalamo-pituitary adrenal axis response upon stressful cognitive demand in rats. *Behavioural Brain Research* 341, 63–70. <https://doi.org/10.1016/j.bbr.2017.12.016>
- Mathis, V.P., Williams, M., Fillinger, C., Kenny, P.J., 2021. Networks of habenula-projecting cortical neurons regulate cocaine seeking. *Sci Adv* 7, eabj2225. <https://doi.org/10.1126/sciadv.abj2225>
- Matsumoto, M., Hikosaka, O., 2007. Lateral habenula as a source of negative reward signals in dopamine neurons. *Nature* 447, 1111–1115. <https://doi.org/10.1038/nature05860>
- Matsumoto, Y., Fujino, Y., Furue, H., 2020. Anti-nociceptive and anxiolytic effects of systemic flupirtine and its direct inhibitory actions on in vivo neuronal mechanical sensory responses in the adult rat anterior cingulate cortex. *Biochemical and Biophysical Research Communications* 531, 528–534. <https://doi.org/10.1016/j.bbrc.2020.07.129>
- Matsuzawa-Yanagida, K., Narita, M., Nakajima, M., Kuzumaki, N., Niikura, K., Nozaki, H., Takagi, T., Tamai, E., Hareyama, N., Terada, M., Yamazaki, M., Suzuki, T., 2008. Usefulness of Antidepressants for Improving the Neuropathic Pain-Like State and Pain-Induced Anxiety through Actions at Different Brain Sites. *Neuropsychopharmacol* 33, 1952–1965. <https://doi.org/10.1038/sj.npp.1301590>
- Mayberg, H.S., Lozano, A.M., Voon, V., McNeely, H.E., Seminowicz, D., Hamani, C., Schwalb, J.M., Kennedy, S.H., 2005. Deep brain stimulation for treatment-resistant depression. *Neuron* 45, 651–660. <https://doi.org/10.1016/j.neuron.2005.02.014>
- McIlwrath, S.L., Montera, M.A., Gott, K.M., Yang, Y., Wilson, C.M., Selwyn, R., Westlund, K.N., 2020. Manganese-enhanced MRI reveals changes within brain anxiety and aversion circuitry in rats with chronic neuropathic pain- and anxiety-like behaviors. *NeuroImage* 223, 117343. <https://doi.org/10.1016/j.neuroimage.2020.117343>
- Means-Christensen, A.J., Roy-Byrne, P.P., Sherbourne, C.D., Craske, M.G., Stein, M.B., 2008. Relationships among pain, anxiety, and depression in primary care. *Depress. Anxiety* 25, 593–600. <https://doi.org/10.1002/da.20342>
- Meda, K.S., Patel, T., Braz, J.M., Malik, R., Turner, M.L., Seifika, H., Basbaum, A.I., Sohal, V.S., 2019. Microcircuit Mechanisms through which Mediodorsal Thalamic Input to Anterior Cingulate Cortex Exacerbates Pain-Related Aversion. *Neuron* 102, 944-959.e3. <https://doi.org/10.1016/j.neuron.2019.03.042>
- Meints, S.M., Edwards, R.R., 2018. Evaluating psychosocial contributions to chronic pain outcomes. *Progress in Neuro-Psychopharmacology and Biological Psychiatry* 87, 168–182. <https://doi.org/10.1016/j.pnpbp.2018.01.017>
- Meng, H., Wang, Y., Huang, M., Lin, W., Wang, S., Zhang, B., 2011. Chronic deep brain stimulation of the lateral habenula nucleus in a rat model of depression. *Brain Res* 1422, 32–38. <https://doi.org/10.1016/j.brainres.2011.08.041>
- Mercer Lindsay, N., Chen, C., Gilam, G., Mackey, S., Scherrer, G., 2021. Brain circuits for pain and its treatment. *Sci. Transl. Med.* 13, eabj7360. <https://doi.org/10.1126/scitranslmed.abj7360>

- Meye, F.J., Lecca, S., Valentinova, K., Mameli, M., 2013. Synaptic and cellular profile of neurons in the lateral habenula. *Front Hum Neurosci* 7, 860.
<https://doi.org/10.3389/fnhum.2013.00860>
- Michailidis, V., Lidhar, N.K., Cho, C., Martin, L.J., 2021. Characterizing Sex Differences in Depressive-Like Behavior and Glial Brain Cell Changes Following Peripheral Nerve Injury in Mice. *Front. Behav. Neurosci.* 15, 758251. <https://doi.org/10.3389/fnbeh.2021.758251>
- Mogil, J.S., 2020. Qualitative sex differences in pain processing: emerging evidence of a biased literature. *Nat Rev Neurosci* 21, 353–365. <https://doi.org/10.1038/s41583-020-0310-6>
- Mogil, J.S., 2012. Sex differences in pain and pain inhibition: multiple explanations of a controversial phenomenon. *Nat Rev Neurosci* 13, 859–866.
<https://doi.org/10.1038/nrn3360>
- Mogil, J.S., Sternberg, W.F., Kest, B., Marek, P., Liebeskind, J.C., 1993. Sex differences in the antagonism of swim stress-induced analgesia: effects of gonadectomy and estrogen replacement. *Pain* 53, 17–25. [https://doi.org/10.1016/0304-3959\(93\)90050-Y](https://doi.org/10.1016/0304-3959(93)90050-Y)
- Monosov, I.E., Haber, S.N., Leuthardt, E.C., Jezzi, A., 2020. Anterior Cingulate Cortex and the Control of Dynamic Behavior in Primates. *Curr Biol* 30, R1442–R1454.
<https://doi.org/10.1016/j.cub.2020.10.009>
- Moqrich, A., Hwang, S.W., Earley, T.J., Petrus, M.J., Murray, A.N., Spencer, K.S.R., Andahazy, M., Story, G.M., Patapoutian, A., 2005. Impaired Thermosensation in Mice Lacking TRPV3, a Heat and Camphor Sensor in the Skin. *Science* 307, 1468–1472.
<https://doi.org/10.1126/science.1108609>
- Morel, C., Montgomery, S.E., Li, L., Durand-de Cuttoli, R., Teichman, E.M., Juarez, B., Tzavaras, N., Ku, S.M., Flanigan, M.E., Cai, M., Walsh, J.J., Russo, S.J., Nestler, E.J., Calipari, E.S., Friedman, A.K., Han, M.-H., 2022. Midbrain projection to the basolateral amygdala encodes anxiety-like but not depression-like behaviors. *Nat Commun* 13, 1532.
<https://doi.org/10.1038/s41467-022-29155-1>
- Morris, R.G., 1999. D.O. Hebb: The Organization of Behavior, Wiley: New York; 1949. *Brain Res Bull* 50, 437. [https://doi.org/10.1016/s0361-9230\(99\)00182-3](https://doi.org/10.1016/s0361-9230(99)00182-3)
- Mosconi, T., Kruger, L., 1996. Fixed-diameter polyethylene cuffs applied to the rat sciatic nerve induce a painful neuropathy: ultrastructural morphometric analysis of axonal alterations. *Pain* 64, 37–57. [https://doi.org/10.1016/0304-3959\(95\)00077-1](https://doi.org/10.1016/0304-3959(95)00077-1)
- Murgatroyd, C., Patchev, A.V., Wu, Y., Micale, V., Bockmühl, Y., Fischer, D., Holsboer, F., Wotjak, C.T., Almeida, O.F.X., Spengler, D., 2009. Dynamic DNA methylation programs persistent adverse effects of early-life stress. *Nat Neurosci* 12, 1559–1566.
<https://doi.org/10.1038/nn.2436>
- Murphy, C.A., DiCamillo, A.M., Haun, F., Murray, M., 1996. Lesion of the habenular efferent pathway produces anxiety and locomotor hyperactivity in rats: a comparison of the effects of neonatal and adult lesions. *Behavioural Brain Research* 81, 43–52.
[https://doi.org/10.1016/S0166-4328\(96\)00041-1](https://doi.org/10.1016/S0166-4328(96)00041-1)

N

- Na, E.S., Nelson, E.D., Kavalali, E.T., Monteggia, L.M., 2013. The Impact of MeCP2 Loss- or Gain-of-Function on Synaptic Plasticity. *Neuropsychopharmacol* 38, 212–219. <https://doi.org/10.1038/npp.2012.116>
- Nan, X., Campoy, F.J., Bird, A., 1997. MeCP2 Is a Transcriptional Repressor with Abundant Binding Sites in Genomic Chromatin. *Cell* 88, 471–481. [https://doi.org/10.1016/S0092-8674\(00\)81887-5](https://doi.org/10.1016/S0092-8674(00)81887-5)
- Narita, Minoru, Kuzumaki, N., Narita, Michiko, Kaneko, C., Hareyama, N., Miyatake, M., Shindo, K., Miyoshi, K., Nakajima, M., Nagumo, Y., Sato, F., Wachi, H., Seyama, Y., Suzuki, T., 2006. Chronic pain-induced emotional dysfunction is associated with astrogliosis due to cortical delta-opioid receptor dysfunction. *J Neurochem* 97, 1369–1378. <https://doi.org/10.1111/j.1471-4159.2006.03824.x>
- Nasca, C., Menard, C., Hodes, G., Bigio, B., Pena, C., Lorsch, Z., Zelli, D., Ferris, A., Kana, V., Purushothaman, I., Dobbin, J., Nassim, M., DeAngelis, P., Merad, M., Rasgon, N., Meaney, M., Nestler, E.J., McEwen, B.S., Russo, S.J., 2019. Multidimensional Predictors of Susceptibility and Resilience to Social Defeat Stress. *Biological Psychiatry* 86, 483–491. <https://doi.org/10.1016/j.biopsych.2019.06.030>
- Navratilova, E., Xie, J.Y., Meske, D., Qu, C., Morimura, K., Okun, A., Arakawa, N., Ossipov, M., Fields, H.L., Porreca, F., 2015. Endogenous Opioid Activity in the Anterior Cingulate Cortex Is Required for Relief of Pain. *Journal of Neuroscience* 35, 7264–7271. <https://doi.org/10.1523/JNEUROSCI.3862-14.2015>
- Nicotra, L., Tuke, J., Grace, P.M., Rolan, P.E., Hutchinson, M.R., 2014. Sex differences in mechanical allodynia: how can it be preclinically quantified and analyzed? *Front. Behav. Neurosci.* 8. <https://doi.org/10.3389/fnbeh.2014.00040>

P

- Palomero-Gallagher, N., Vogt, B.A., Schleicher, A., Mayberg, H.S., Zilles, K., 2009. Receptor architecture of human cingulate cortex: Evaluation of the four-region neurobiological model. *Hum. Brain Mapp.* 30, 2336–2355. <https://doi.org/10.1002/hbm.20667>
- Pan, W., Zhang, G.-F., Li, H.-H., Ji, M.-H., Zhou, Z.-Q., Li, K.-Y., Yang, J.-J., 2018. Ketamine differentially restores diverse alterations of neuroligins in brain regions in a rat model of neuropathic pain-induced depression. *NeuroReport* 29, 863–869. <https://doi.org/10.1097/WNR.0000000000001045>
- Panigada, T., Gosselin, R.-D., 2011. Behavioural alteration in chronic pain: Are brain glia involved? *Medical Hypotheses* 77, 584–588. <https://doi.org/10.1016/j.mehy.2011.06.036>
- Paulson, P.E., Gorman, A.L., Yeziarski, R.P., Casey, K.L., Morrow, T.J., 2005. Differences in forebrain activation in two strains of rat at rest and after spinal cord injury. *Exp Neurol* 196, 413–421. <https://doi.org/10.1016/j.expneurol.2005.08.015>

- Paulson, P.E., Wiley, J.W., Morrow, T.J., 2007. Concurrent activation of the somatosensory forebrain and deactivation of periaqueductal gray associated with diabetes-induced neuropathic pain. *Exp Neurol* 208, 305–313.
<https://doi.org/10.1016/j.expneurol.2007.09.001>
- Paxinos and Franklin's the Mouse Brain in Stereotaxic Coordinates - 5th Edition [WWW Document], n.d. URL <https://www.elsevier.com/books/paxinos-and-franklins-the-mouse-brain-in-stereotaxic-coordinates/paxinos/978-0-12-816157-9> (accessed 11.16.22).
- Penner-Goeke, S., Binder, E.B., 2019. Epigenetics and depression. *Dialogues in Clinical Neuroscience* 21, 397–405. <https://doi.org/10.31887/DCNS.2019.21.4/ebinder>
- Pereira-Silva, R., Costa-Pereira, J.T., Alonso, R., Serrão, P., Martins, I., Neto, F.L., 2020. Attenuation of the Diffuse Noxious Inhibitory Controls in Chronic Joint Inflammatory Pain Is Accompanied by Anxiodepressive-Like Behaviors and Impairment of the Descending Noradrenergic Modulation. *IJMS* 21, 2973. <https://doi.org/10.3390/ijms21082973>
- Phillips, C.J., Harper, C., 2011. The economics associated with persistent pain. *Current Opinion in Supportive & Palliative Care* 5, 127–130.
<https://doi.org/10.1097/SPC.0b013e3283458fa9>
- Pitzer, C., La Porta, C., Treede, R.-D., Tappe-Theodor, A., 2019. Inflammatory and neuropathic pain conditions do not primarily evoke anxiety-like behaviours in C57BL/6 mice. *European Journal of Pain* 23, 285–306. <https://doi.org/10.1002/ejp.1303>
- Planchez, B., Surget, A., Belzung, C., 2019. Animal models of major depression: drawbacks and challenges. *J Neural Transm* 126, 1383–1408. <https://doi.org/10.1007/s00702-019-02084-y>
- Porsolt, R.D., Anton, G., Blavet, N., Jalfre, M., 1978. Behavioural despair in rats: A new model sensitive to antidepressant treatments. *European Journal of Pharmacology* 47, 379–391.
[https://doi.org/10.1016/0014-2999\(78\)90118-8](https://doi.org/10.1016/0014-2999(78)90118-8)
- Porsolt, R.D., Le Pichon, M., Jalfre, M., 1977. Depression: a new animal model sensitive to antidepressant treatments. *Nature* 266, 730–732. <https://doi.org/10.1038/266730a0>
- Price, D.D., 2000. Psychological and neural mechanisms of the affective dimension of pain. *Science* 288, 1769–1772. <https://doi.org/10.1126/science.288.5472.1769>
- Procyk, E., Tanaka, Y.L., Joseph, J.P., 2000. Anterior cingulate activity during routine and non-routine sequential behaviors in macaques. *Nat Neurosci* 3, 502–508.
<https://doi.org/10.1038/74880>
- Proulx, C.D., Hikosaka, O., Malinow, R., 2014. Reward processing by the lateral habenula in normal and depressive behaviors. *Nat Neurosci* 17, 1146–1152.
<https://doi.org/10.1038/nn.3779>

Q

- Qu, C., King, T., Okun, A., Lai, J., Fields, H.L., Porreca, F., 2011. Lesion of the rostral anterior cingulate cortex eliminates the aversiveness of spontaneous neuropathic pain following partial or complete axotomy. *Pain* 152, 1641–1648.
<https://doi.org/10.1016/j.pain.2011.03.002>

Quilodran, R., Rothé, M., Procyk, E., 2008. Behavioral shifts and action valuation in the anterior cingulate cortex. *Neuron* 57, 314–325.
<https://doi.org/10.1016/j.neuron.2007.11.031>

R

Rahn, E.J., Iannitti, T., Donahue, R.R., Taylor, B.K., 2014. Sex differences in a mouse model of multiple sclerosis: neuropathic pain behavior in females but not males and protection from neurological deficits during proestrus. *Biol Sex Differ* 5, 4.
<https://doi.org/10.1186/2042-6410-5-4>

Raja, S.N., Carr, D.B., Cohen, M., Finnerup, N.B., Flor, H., Gibson, S., Keefe, F.J., Mogil, J.S., Ringkamp, M., Sluka, K.A., Song, X.-J., Stevens, B., Sullivan, M.D., Tutelman, P.R., Ushida, T., Vader, K., 2020. The revised International Association for the Study of Pain definition of pain: concepts, challenges, and compromises. *Pain* 161, 1976–1982.
<https://doi.org/10.1097/j.pain.0000000000001939>

Ren, D., Li, J.-N., Qiu, X.-T., Wan, F.-P., Wu, Z.-Y., Fan, B.-Y., Zhang, M.-M., Chen, T., Li, H., Bai, Y., Li, Y.-Q., 2022. Anterior Cingulate Cortex Mediates Hyperalgesia and Anxiety Induced by Chronic Pancreatitis in Rats. *Neurosci. Bull.* 38, 342–358.
<https://doi.org/10.1007/s12264-021-00800-x>

Ren, W.-H., Guo, J.-D., Cao, H., Wang, H., Wang, P.-F., Sha, H., Ji, R.-R., Zhao, Z.-Q., Zhang, Y.-Q., 2006. Is endogenous d-serine in the rostral anterior cingulate cortex necessary for pain-related negative affect? *Journal of Neurochemistry* 96, 1636–1647.
<https://doi.org/10.1111/j.1471-4159.2006.03677.x>

Rigney, A.E., Koski, J.E., Beer, J.S., 2018. The functional role of ventral anterior cingulate cortex in social evaluation: disentangling valence from subjectively rewarding opportunities. *Soc Cogn Affect Neurosci* 13, 14–21. <https://doi.org/10.1093/scan/nsx132>

Riva-Posse, P., Choi, K.S., Holtzheimer, P.E., Crowell, A.L., Garlow, S.J., Rajendra, J.K., McIntyre, C.C., Gross, R.E., Mayberg, H.S., 2018. A connectomic approach for subcallosal cingulate deep brain stimulation surgery: prospective targeting in treatment-resistant depression. *Mol Psychiatry* 23, 843–849. <https://doi.org/10.1038/mp.2017.59>

Roiser, J.P., Levy, J., Fromm, S.J., Nugent, A.C., Talagala, S.L., Hasler, G., Henn, F.A., Sahakian, B.J., Drevets, W.C., 2009. The effects of tryptophan depletion on neural responses to emotional words in remitted depression. *Biol Psychiatry* 66, 441–450.
<https://doi.org/10.1016/j.biopsych.2009.05.002>

Rolls, E.T., 2019. The cingulate cortex and limbic systems for emotion, action, and memory. *Brain Struct Funct* 224, 3001–3018. <https://doi.org/10.1007/s00429-019-01945-2>

Root, D.H., Zhang, S., Barker, D.J., Miranda-Barrientos, J., Liu, B., Wang, H.-L., Morales, M., 2018. Selective Brain Distribution and Distinctive Synaptic Architecture of Dual Glutamatergic-GABAergic Neurons. *Cell Rep* 23, 3465–3479.
<https://doi.org/10.1016/j.celrep.2018.05.063>

Rushworth, M.F.S., Noonan, M.P., Boorman, E.D., Walton, M.E., Behrens, T.E., 2011. Frontal cortex and reward-guided learning and decision-making. *Neuron* 70, 1054–1069. <https://doi.org/10.1016/j.neuron.2011.05.014>

S

Sakhi, K., Belle, M.D.C., Gossan, N., Delagrangé, P., Piggins, H.D., 2014a. Daily variation in the electrophysiological activity of mouse medial habenula neurones. *J Physiol* 592, 587–603. <https://doi.org/10.1113/jphysiol.2013.263319>

Sakhi, K., Wegner, S., Belle, M.D.C., Howarth, M., Delagrangé, P., Brown, T.M., Piggins, H.D., 2014b. Intrinsic and extrinsic cues regulate the daily profile of mouse lateral habenula neuronal activity. *J Physiol* 592, 5025–5045. <https://doi.org/10.1113/jphysiol.2014.280065>

Salaberry, N.L., Mendoza, J., 2015. Insights into the Role of the Habenular Circadian Clock in Addiction. *Front Psychiatry* 6, 179. <https://doi.org/10.3389/fpsy.2015.00179>

Salvat, E., Yalcin, I., Müller, A., Barrot, M., 2018. A comparison of early and late treatments on allodynia and its chronification in experimental neuropathic pain. *Mol Pain* 14, 174480691774968. <https://doi.org/10.1177/1744806917749683>

Sánchez-Lafuente, C.L., Kalynchuk, L.E., Caruncho, H.J., Ausió, J., 2022. The Role of MeCP2 in Regulating Synaptic Plasticity in the Context of Stress and Depression. *Cells* 11, 748. <https://doi.org/10.3390/cells11040748>

Sandkühler, J., 2007. Understanding LTP in Pain Pathways. *Mol Pain* 3, 1744-8069-3–9. <https://doi.org/10.1186/1744-8069-3-9>

Santello, M., Bisco, A., Nevian, N.E., Lacivita, E., Leopoldo, M., Nevian, T., 2017. The brain-penetrant 5-HT 7 receptor agonist LP-211 reduces the sensory and affective components of neuropathic pain. *Neurobiology of Disease* 106, 214–221. <https://doi.org/10.1016/j.nbd.2017.07.005>

Santomauro, D.F., Herrera, A.M.M., Shadid, J., Zheng, P., Ashbaugh, C., Pigott, D.M., Abbafati, C., Adolph, C., Amlag, J.O., Aravkin, A.Y., Bang-Jensen, B.L., Bertolacci, G.J., Bloom, S.S., Castellano, R., Castro, E., Chakrabarti, S., Chattopadhyay, J., Cogen, R.M., Collins, J.K., Dai, X., Dangel, W.J., Dapper, C., Deen, A., Erickson, M., Ewald, S.B., Flaxman, A.D., Frostad, J.J., Fullman, N., Giles, J.R., Giref, A.Z., Guo, G., He, J., Helak, M., Hulland, E.N., Idrisov, B., Lindstrom, A., Linebarger, E., Lotufo, P.A., Lozano, R., Magistro, B., Malta, D.C., Månsson, J.C., Marinho, F., Mokdad, A.H., Monasta, L., Naik, P., Nomura, S., O'Halloran, J.K., Ostroff, S.M., Pasovic, M., Penberthy, L., Jr, R.C.R., Reinke, G., Ribeiro, A.L.P., Sholokhov, A., Sorensen, R.J.D., Varavikova, E., Vo, A.T., Walcott, R., Watson, S., Wiysonge, C.S., Zigler, B., Hay, S.I., Vos, T., Murray, C.J.L., Whiteford, H.A., Ferrari, A.J., 2021. Global prevalence and burden of depressive and anxiety disorders in 204 countries and territories in 2020 due to the COVID-19 pandemic. *The Lancet* 398, 1700–1712. [https://doi.org/10.1016/S0140-6736\(21\)02143-7](https://doi.org/10.1016/S0140-6736(21)02143-7)

- Sartorius, A., Henn, F.A., 2007. Deep brain stimulation of the lateral habenula in treatment resistant major depression. *Medical Hypotheses* 69, 1305–1308.
<https://doi.org/10.1016/j.mehy.2007.03.021>
- Sartorius, A., Kiening, K.L., Kirsch, P., Gall, C.C. von, Haberkorn, U., Unterberg, A.W., Henn, F.A., Meyer-Lindenberg, A., 2010. Remission of Major Depression Under Deep Brain Stimulation of the Lateral Habenula in a Therapy-Refractory Patient. *Biological Psychiatry* 67, e9–e11. <https://doi.org/10.1016/j.biopsych.2009.08.027>
- Scholz, J., Finnerup, N.B., Attal, N., Aziz, Q., Baron, R., Bennett, M.I., Benoliel, R., Cohen, M., Cruccu, G., Davis, K.D., Evers, S., First, M., Giamberardino, M.A., Hansson, P., Kaasa, S., Korwisi, B., Kosek, E., Lavand'homme, P., Nicholas, M., Nurmikko, T., Perrot, S., Raja, S.N., Rice, A.S.C., Rowbotham, M.C., Schug, S., Simpson, D.M., Smith, B.H., Svensson, P., Vlaeyen, J.W.S., Wang, S.-J., Barke, A., Rief, W., Treede, R.-D., Classification Committee of the Neuropathic Pain Special Interest Group (NeuPSIG), 2019. The IASP classification of chronic pain for ICD-11: chronic neuropathic pain. *Pain* 160, 53–59.
<https://doi.org/10.1097/j.pain.0000000000001365>
- Schweinhart, P., Bushnell, M.C., 2010. Pain imaging in health and disease — how far have we come? *J. Clin. Invest.* 120, 3788–3797. <https://doi.org/10.1172/JCI43498>
- Sellmeijer, J., Mathis, V., Hugel, S., Li, X.-H., Song, Q., Chen, Q.-Y., Barthas, F., Lutz, P.-E., Karatas, M., Luthi, A., Veinante, P., Aertsen, A., Barrot, M., Zhuo, M., Yalcin, I., 2018. Hyperactivity of Anterior Cingulate Cortex Areas 24a/24b Drives Chronic Pain-Induced Anxiodepressive-like Consequences. *J. Neurosci.* 38, 3102–3115.
<https://doi.org/10.1523/JNEUROSCI.3195-17.2018>
- Seminowicz, D.A., Laferriere, A.L., Millicamps, M., Yu, J.S.C., Coderre, T.J., Bushnell, M.C., 2009. MRI structural brain changes associated with sensory and emotional function in a rat model of long-term neuropathic pain. *NeuroImage* 47, 1007–1014.
<https://doi.org/10.1016/j.neuroimage.2009.05.068>
- Seno, M.D.J., Assis, D.V., Gouveia, F., Antunes, G.F., Kuroki, M., Oliveira, C.C., Santos, L.C.T., Pagano, R.L., Martinez, R.C.R., 2018. The critical role of amygdala subnuclei in nociceptive and depressive-like behaviors in peripheral neuropathy. *Sci Rep* 8, 13608.
<https://doi.org/10.1038/s41598-018-31962-w>
- Seo, J.-S., Zhong, P., Liu, A., Yan, Z., Greengard, P., 2018. Elevation of p11 in lateral habenula mediates depression-like behavior. *Mol Psychiatry* 23, 1113–1119.
<https://doi.org/10.1038/mp.2017.96>
- Serafini, R.A., Pryce, K.D., Zachariou, V., 2020. The Mesolimbic Dopamine System in Chronic Pain and Associated Affective Comorbidities. *Biol Psychiatry* 87, 64–73.
<https://doi.org/10.1016/j.biopsych.2019.10.018>
- Shabel, S.J., Proulx, C.D., Piriz, J., Malinow, R., 2014. GABA/glutamate co-release controls habenula output and is modified by antidepressant treatment. *Science* 345, 1494–1498.
<https://doi.org/10.1126/science.1250469>

- Shabel, S.J., Proulx, C.D., Trias, A., Murphy, R.T., Malinow, R., 2012. Input to the Lateral Habenula from the Basal Ganglia Is Excitatory, Aversive, and Suppressed by Serotonin. *Neuron* 74, 475–481. <https://doi.org/10.1016/j.neuron.2012.02.037>
- Shackman, A.J., Salomons, T.V., Slagter, H.A., Fox, A.S., Winter, J.J., Davidson, R.J., 2011. The Integration of Negative Affect, Pain, and Cognitive Control in the Cingulate Cortex. *Nat Rev Neurosci* 12, 154–167. <https://doi.org/10.1038/nrn2994>
- Shao, F., Fang, J., Qiu, M., Wang, S., Xi, D., Shao, X., He, X., Fang, J., Du, J., 2021a. Electroacupuncture Ameliorates Chronic Inflammatory Pain-Related Anxiety by Activating PV Interneurons in the Anterior Cingulate Cortex. *Front. Neurosci.* 15, 691931. <https://doi.org/10.3389/fnins.2021.691931>
- Shao, F., Fang, J., Wang, S., Qiu, M., Xi, D., Jin, X., Liu, J., Shao, X., Shen, Z., Liang, Y., Fang, J., Du, J., 2021b. Anxiolytic effect of GABAergic neurons in the anterior cingulate cortex in a rat model of chronic inflammatory pain. *Mol Brain* 14, 139. <https://doi.org/10.1186/s13041-021-00849-9>
- Shao, X., Shen, Z., Sun, J., Fang, F., Fang, Jun-fan, Wu, Y., Fang, Jian-qiao, 2015. Strong Manual Acupuncture Stimulation of “Huantiao” (GB 30) Reduces Pain-Induced Anxiety and p-ERK in the Anterior Cingulate Cortex in a Rat Model of Neuropathic Pain. *Evidence-Based Complementary and Alternative Medicine* 2015, 1–11. <https://doi.org/10.1155/2015/235491>
- Shelton, L., Becerra, L., Borsook, D., 2012. Unmasking the mysteries of the habenula in pain and analgesia. *Progress in Neurobiology* 96, 208–219. <https://doi.org/10.1016/j.pneurobio.2012.01.004>
- Shen, Z., Zhang, H., Wu, Z., He, Q., Liu, J., Xu, Y., Yao, S., He, X., Chen, Y., Liang, Y., Liu, B., Jiang, Y., Fang, Junfan, Du, J., Zhu, X., Wu, M., Wu, Y., Sun, J., Xu, C., Fang, Jianqiao, Shao, X., 2021. Electroacupuncture Alleviates Chronic Pain-Induced Anxiety Disorders by Regulating the rACC-Thalamus Circuitry. *Front. Neurosci.* 14, 615395. <https://doi.org/10.3389/fnins.2020.615395>
- Sheng, J., Liu, S., Wang, Y., Cui, R., Zhang, X., 2017. The Link between Depression and Chronic Pain: Neural Mechanisms in the Brain. *Neural Plasticity* 2017, 1–10. <https://doi.org/10.1155/2017/9724371>
- Shi, Y., Yao, S., Shen, Z., She, L., Xu, Y., Liu, B., Liang, Y., Jiang, Y., Sun, J., Wu, Y., Du, J., Zhu, Y., Wu, Z., Fang, J., Shao, X., 2020. Effect of Electroacupuncture on Pain Perception and Pain-Related Affection: Dissociation or Interaction Based on the Anterior Cingulate Cortex and S1. *Neural Plasticity* 2020, 1–10. <https://doi.org/10.1155/2020/8865096>
- Shin, L.M., Whalen, P.J., Pitman, R.K., Bush, G., Macklin, M.L., Lasko, N.B., Orr, S.P., McInerney, S.C., Rauch, S.L., 2001. An fMRI study of anterior cingulate function in posttraumatic stress disorder. *Biol Psychiatry* 50, 932–942. [https://doi.org/10.1016/s0006-3223\(01\)01215-x](https://doi.org/10.1016/s0006-3223(01)01215-x)

- Silva, J., Shao, A.S., Shen, Y., Davies, D.L., Olsen, R.W., Holschneider, D.P., Shao, X.M., Liang, J., 2020. Modulation of Hippocampal GABAergic Neurotransmission and Gephyrin Levels by Dihydropyridin Improves Anxiety. *Front. Pharmacol.* 11, 1008.
<https://doi.org/10.3389/fphar.2020.01008>
- Silva-Cardoso, G.K., Lazarini-Lopes, W., Hallak, J.E., Crippa, J.A., Zuardi, A.W., Garcia-Cairasco, N., Leite-Panissi, C.R.A., 2021. Cannabidiol effectively reverses mechanical and thermal allodynia, hyperalgesia, and anxious behaviors in a neuropathic pain model: Possible role of CB1 and TRPV1 receptors. *Neuropharmacology* 197, 108712.
<https://doi.org/10.1016/j.neuropharm.2021.108712>
- Singh, A., Patel, D., Li, A., Hu, L., Zhang, Q., Liu, Y., Guo, X., Robinson, E., Martinez, E., Doan, L., Rudy, B., Chen, Z.S., Wang, J., 2020. Mapping Cortical Integration of Sensory and Affective Pain Pathways. *Current Biology* 30, 1703-1715.e5.
<https://doi.org/10.1016/j.cub.2020.02.091>
- Smith, M.L., Asada, N., Malenka, R.C., 2021. Anterior cingulate inputs to nucleus accumbens control the social transfer of pain and analgesia. *Science* 371, 153–159.
<https://doi.org/10.1126/science.abe3040>
- Sorge, R.E., Totsch, S.K., 2017. Sex Differences in Pain: Sex Differences in Pain. *Journal of Neuroscience Research* 95, 1271–1281. <https://doi.org/10.1002/jnr.23841>
- Spijker, J., Claes, S., 2014. [Mood disorders in the DSM-5]. *Tijdschr Psychiatr* 56, 173–176.
- Srinivasan, L., Asaad, W.F., Ginat, D.T., Gale, J.T., Dougherty, D.D., Williams, Z.M., Sejnowski, T.J., Eskandar, E.N., 2013. Action Initiation in the Human Dorsal Anterior Cingulate Cortex. *PLOS ONE* 8, e55247. <https://doi.org/10.1371/journal.pone.0055247>
- Stephenson-Jones, M., Floros, O., Robertson, B., Grillner, S., 2012. Evolutionary conservation of the habenular nuclei and their circuitry controlling the dopamine and 5-hydroxytryptophan (5-HT) systems. *Proc Natl Acad Sci U S A* 109, E164–E173.
<https://doi.org/10.1073/pnas.1119348109>
- Stephenson-Jones, M., Yu, K., Ahrens, S., Tucciarone, J.M., van Huijstee, A.N., Mejia, L.A., Penzo, M.A., Tai, L.-H., Wilbrecht, L., Li, B., 2016. A basal ganglia circuit for evaluating action outcomes. *Nature* 539, 289–293. <https://doi.org/10.1038/nature19845>
- Steru, L., Chermat, R., Thierry, B., Simon, P., 1985. The tail suspension test: A new method for screening antidepressants in mice. *Psychopharmacology* 85, 367–370.
<https://doi.org/10.1007/BF00428203>
- Stevens, F.L., Hurley, R.A., Taber, K.H., 2011. Anterior cingulate cortex: unique role in cognition and emotion. *J Neuropsychiatry Clin Neurosci* 23, 121–125.
<https://doi.org/10.1176/jnp.23.2.jnp121>
- Stopper, C.M., Floresco, S.B., 2014. What’s better for me? Fundamental role for lateral habenula in promoting subjective decision biases. *Nat Neurosci* 17, 33–35.
<https://doi.org/10.1038/nn.3587>
- Su, S., Li, M., Wu, D., Cao, J., Ren, X., Tao, Y.-X., Zang, W., 2021. Gene Transcript Alterations in the Spinal Cord, Anterior Cingulate Cortex, and Amygdala in Mice Following Peripheral Nerve Injury. *Front. Cell Dev. Biol.* 9, 634810. <https://doi.org/10.3389/fcell.2021.634810>

- Sun, N., Yu, L., Gao, Y., Ma, L., Ren, J., Liu, Y., Gao, D.S., Xie, C., Wu, Y., Wang, L., Hong, J., Yan, M., 2021. MeCP2 Epigenetic Silencing of Oprm1 Gene in Primary Sensory Neurons Under Neuropathic Pain Conditions. *Front. Neurosci.* 15, 743207. <https://doi.org/10.3389/fnins.2021.743207>
- Sun, T., Wang, J., Li, X., Li, Y.-J., Feng, D., Shi, W.-L., Zhao, M.-G., Wang, J.-B., Wu, Y.-M., 2016. Gastrodin relieved complete Freund's adjuvant-induced spontaneous pain by inhibiting inflammatory response. *International Immunopharmacology* 41, 66–73. <https://doi.org/10.1016/j.intimp.2016.10.020>
- Sych, Y., Chernysheva, M., Sumanovski, L.T., Helmchen, F., 2019. High-density multi-fiber photometry for studying large-scale brain circuit dynamics. *Nat Methods* 16, 553–560. <https://doi.org/10.1038/s41592-019-0400-4>
- T**
- Tajerian, M., Leu, D., Zou, Y., Sahbaie, P., Li, W., Khan, H., Hsu, V., Kingery, W., Huang, T.T., Becerra, L., Clark, J.D., 2014. Brain Neuroplastic Changes Accompany Anxiety and Memory Deficits in a Model of Complex Regional Pain Syndrome. *Anesthesiology* 121, 852–865. <https://doi.org/10.1097/ALN.0000000000000403>
- Tan, L.L., Pelzer, P., Heintz, C., Tang, W., Gangadharan, V., Flor, H., Sprengel, R., Kuner, T., Kuner, R., 2017. A pathway from midcingulate cortex to posterior insula gates nociceptive hypersensitivity. *Nat Neurosci* 20, 1591–1601. <https://doi.org/10.1038/nn.4645>
- Tang, J., Ko, S., Ding, H.-K., Qiu, C.-S., Calejesan, A.A., Zhuo, M., 2005. Pavlovian Fear Memory Induced by Activation in the Anterior Cingulate Cortex. *Mol Pain* 1, 1744-8069-1–6. <https://doi.org/10.1186/1744-8069-1-6>
- Tao, W., Chen, C., Wang, Y., Zhou, W., Jin, Y., Mao, Y., Wang, H., Wang, L., Xie, W., Zhang, X., Li, Jie, Li, Juan, Li, X., Tang, Z.-Q., Zhou, C., Pan, Z.Z., Zhang, Z., 2020. MeCP2 mediates transgenerational transmission of chronic pain. *Progress in Neurobiology* 189, 101790. <https://doi.org/10.1016/j.pneurobio.2020.101790>
- Thibault, K., Lin, W.K., Rancillac, A., Fan, M., Snollaerts, T., Sordoillet, V., Hamon, M., Smith, G.M., Lenkei, Z., Pezet, S., 2014. BDNF-Dependent Plasticity Induced by Peripheral Inflammation in the Primary Sensory and the Cingulate Cortex Triggers Cold Allodynia and Reveals a Major Role for Endogenous BDNF As a Tuner of the Affective Aspect of Pain. *Journal of Neuroscience* 34, 14739–14751. <https://doi.org/10.1523/JNEUROSCI.0860-14.2014>
- Thompson, J.M., Neugebauer, V., 2019. Cortico-limbic pain mechanisms. *Neuroscience Letters* 702, 15–23. <https://doi.org/10.1016/j.neulet.2018.11.037>
- Toth, I., Neumann, I.D., 2013. Animal models of social avoidance and social fear. *Cell Tissue Res* 354, 107–118. <https://doi.org/10.1007/s00441-013-1636-4>
- Treede, R.-D., Jensen, T.S., Campbell, J.N., Cruccu, G., Dostrovsky, J.O., Griffin, J.W., Hansson, P., Hughes, R., Nurmikko, T., Serra, J., 2008. Neuropathic pain: Redefinition and a grading system for clinical and research purposes. *Neurology* 70, 1630–1635. <https://doi.org/10.1212/01.wnl.0000282763.29778.59>

- Treede, R.-D., Rief, W., Barke, A., Aziz, Q., Bennett, M.I., Benoliel, R., Cohen, M., Evers, S., Finnerup, N.B., First, M.B., Giamberardino, M.A., Kaasa, S., Korwisi, B., Kosek, E., Lavand'homme, P., Nicholas, M., Perrot, S., Scholz, J., Schug, S., Smith, B.H., Svensson, P., Vlaeyen, J.W.S., Wang, S.-J., 2019. Chronic pain as a symptom or a disease: the IASP Classification of Chronic Pain for the International Classification of Diseases (ICD-11). *Pain* 160, 19–27. <https://doi.org/10.1097/j.pain.0000000000001384>
- Treede, R.-D., Rief, W., Barke, A., Aziz, Q., Bennett, M.I., Benoliel, R., Cohen, M., Evers, S., Finnerup, N.B., First, M.B., Giamberardino, M.A., Kaasa, S., Kosek, E., Lavand'homme, P., Nicholas, M., Perrot, S., Scholz, J., Schug, S., Smith, B.H., Svensson, P., Vlaeyen, J.W.S., Wang, S.-J., 2015. A classification of chronic pain for ICD-11. *Pain* 156, 1003–1007. <https://doi.org/10.1097/j.pain.0000000000000160>
- Trusel, M., Nuno-Perez, A., Lecca, S., Harada, H., Lalive, A.L., Congiu, M., Takemoto, K., Takahashi, T., Ferraguti, F., Mameli, M., 2019. Punishment-Predictive Cues Guide Avoidance through Potentiation of Hypothalamus-to-Habenula Synapses. *Neuron* 102, 120-127.e4. <https://doi.org/10.1016/j.neuron.2019.01.025>

U

- Ullsperger, M., von Cramon, D.Y., 2003. Error monitoring using external feedback: specific roles of the habenular complex, the reward system, and the cingulate motor area revealed by functional magnetic resonance imaging. *J Neurosci* 23, 4308–4314. <https://doi.org/10.1523/JNEUROSCI.23-10-04308.2003>
- Urban, R., Scherrer, G., Goulding, E.H., Tecott, L.H., Basbaum, A.I., 2011. Behavioral indices of ongoing pain are largely unchanged in male mice with tissue or nerve injury-induced mechanical hypersensitivity. *PAIN* 152, 990. <https://doi.org/10.1016/j.pain.2010.12.003>

V

- Vacca, V., Marinelli, S., Pieroni, L., Urbani, A., Luvisetto, S., Pavone, F., 2014. Higher pain perception and lack of recovery from neuropathic pain in females: A behavioural, immunohistochemical, and proteomic investigation on sex-related differences in mice. *Pain* 155, 388–402. <https://doi.org/10.1016/j.pain.2013.10.027>
- Valentinova, K., Mameli, M., 2016. mGluR-LTD at Excitatory and Inhibitory Synapses in the Lateral Habenula Tunes Neuronal Output. *Cell Reports* 16, 2298–2307. <https://doi.org/10.1016/j.celrep.2016.07.064>
- Van der Linden, A., Van Camp, N., Ramos-Cabrera, P., Hoehn, M., 2007. Current status of functional MRI on small animals: application to physiology, pathophysiology, and cognition. *NMR in Biomedicine* 20, 522–545. <https://doi.org/10.1002/nbm.1131>
- van Hecke, O., Austin, S.K., Khan, R.A., Smith, B.H., Torrance, N., 2014. Neuropathic pain in the general population: A systematic review of epidemiological studies. *Pain* 155, 654–662. <https://doi.org/10.1016/j.pain.2013.11.013>

- van Heukelum, S., Mars, R.B., Guthrie, M., Buitelaar, J.K., Beckmann, C.F., Tiesinga, P.H.E., Vogt, B.A., Glennon, J.C., Havenith, M.N., 2020. Where is Cingulate Cortex? A Cross-Species View. *Trends in Neurosciences* 43, 285–299. <https://doi.org/10.1016/j.tins.2020.03.007>
- Vogt, B.A., 2005. Pain and emotion interactions in subregions of the cingulate gyrus. *Nat Rev Neurosci* 6, 533–544. <https://doi.org/10.1038/nrn1704>
- Vogt, B.A., Derbyshire, S., Jones, A.K.P., 1996. Pain Processing in Four Regions of Human Cingulate Cortex Localized with Co-registered PET and MR Imaging. *European Journal of Neuroscience* 8, 1461–1473. <https://doi.org/10.1111/j.1460-9568.1996.tb01608.x>
- Vogt, B.A., Paxinos, G., 2014. Cytoarchitecture of mouse and rat cingulate cortex with human homologies. *Brain Struct Funct* 219, 185–192. <https://doi.org/10.1007/s00429-012-0493-3>
- Von Korff, M., Crane, P., Lane, M., Miglioretti, D.L., Simon, G., Saunders, K., Stang, P., Brandenburg, N., Kessler, R., 2005. Chronic spinal pain and physical–mental comorbidity in the United States: results from the national comorbidity survey replication. *Pain* 113, 331–339. <https://doi.org/10.1016/j.pain.2004.11.010>

W

- Wager, T.D., Atlas, L.Y., Lindquist, M.A., Roy, M., Woo, C.-W., Kross, E., 2013. An fMRI-Based Neurologic Signature of Physical Pain. *N Engl J Med* 368, 1388–1397. <https://doi.org/10.1056/NEJMoa1204471>
- Wagner, F., Bernard, R., Derst, C., French, L., Veh, R.W., 2016. Microarray analysis of transcripts with elevated expressions in the rat medial or lateral habenula suggest fast GABAergic excitation in the medial habenula and habenular involvement in the regulation of feeding and energy balance. *Brain Struct Funct* 221, 4663–4689. <https://doi.org/10.1007/s00429-016-1195-z>
- Wagner, F., Stroh, T., Veh, R.W., 2014. Correlating habenular subnuclei in rat and mouse by using topographic, morphological, and cytochemical criteria. *J Comp Neurol* 522, 2650–2662. <https://doi.org/10.1002/cne.23554>
- Wallace, M.L., Huang, K.W., Hochbaum, D., Hyun, M., Radeljic, G., Sabatini, B.L., 2020. Anatomical and single-cell transcriptional profiling of the murine habenular complex. *Elife* 9, e51271. <https://doi.org/10.7554/eLife.51271>
- Wang, H., Ren, W.-H., Zhang, Y.-Q., Zhao, Z.-Q., 2005. GABAergic disinhibition facilitates polysynaptic excitatory transmission in rat anterior cingulate cortex. *Biochemical and Biophysical Research Communications* 338, 1634–1639. <https://doi.org/10.1016/j.bbrc.2005.10.132>
- Wang, X., Yue, J., Hu, L., Tian, Z., Yang, L., Lu, L., Zhao, M., Liu, S., 2019. Effects of CPEB1 in the anterior cingulate cortex on visceral pain in mice. *Brain Research* 1712, 55–62. <https://doi.org/10.1016/j.brainres.2019.02.001>

- Wang, X., Zhang, L., Zhan, Y., Li, D., Zhang, Y., Wang, G., Zhang, M., 2017. Contribution of BDNF/TrkB signalling in the rACC to the development of pain-related aversion via activation of ERK in rats with spared nerve injury. *Brain Research* 1671, 111–120. <https://doi.org/10.1016/j.brainres.2017.07.010>
- Wang, Y., Li, C.-M., Han, R., Wang, Z.-Z., Gao, Y.-L., Zhu, X.-Y., Yu, X., Du, G.-Y., Wang, H.-B., Tian, J.-W., Fu, F.-H., 2020. PCC0208009, an indirect IDO1 inhibitor, alleviates neuropathic pain and co-morbidities by regulating synaptic plasticity of ACC and amygdala. *Biochemical Pharmacology* 177, 113926. <https://doi.org/10.1016/j.bcp.2020.113926>
- Wang, Y., Liu, C., Guo, Q.-L., Yan, J.-Q., Zhu, X.-Y., Huang, C.-S., Zou, W.-Y., 2011. Intrathecal 5-azacytidine inhibits global DNA methylation and methyl- CpG-binding protein 2 expression and alleviates neuropathic pain in rats following chronic constriction injury. *Brain Research* 1418, 64–69. <https://doi.org/10.1016/j.brainres.2011.08.040>
- Watanabe, H., Fitting, S., Hussain, M.Z., Kononenko, O., Iatsyshyna, A., Yoshitake, T., Kehr, J., Alkass, K., Druid, H., Wadensten, H., Andren, P.E., Nylander, I., Wedell, D.H., Krishtal, O., Hauser, K.F., Nyberg, F., Karpyak, V.M., Yakovleva, T., Bakalkin, G., 2015. Asymmetry of the Endogenous Opioid System in the Human Anterior Cingulate: a Putative Molecular Basis for Lateralization of Emotions and Pain. *Cerebral Cortex* 25, 97–108. <https://doi.org/10.1093/cercor/bht204>
- Watanabe, S., Al Omran, A., Shao, A.S., Liang, J., 2022a. Social Isolation Model: A Noninvasive Rodent Model of Stress and Anxiety. *JoVE* 64567. <https://doi.org/10.3791/64567>
- Watanabe, S., Al Omran, A.J., Shao, A.S., Zhang, Z., Xue, C., Zhang, J., Watanabe, J., Liang, J., 2022b. Social isolation induces succinate dehydrogenase dysfunction in anxious mice. *Neurochemistry International* 161, 105434. <https://doi.org/10.1016/j.neuint.2022.105434>
- Watanabe, S., Omran, A.A., Shao, A.S., Xue, C., Zhang, Z., Zhang, J., Davies, D.L., Shao, X.M., Watanabe, J., Liang, J., 2022c. Dihydropyridine improves social isolation-induced cognitive impairments and astrocytic changes in mice. *Sci Rep* 12, 5899. <https://doi.org/10.1038/s41598-022-09814-5>
- Weiss, T., Veh, R.W., 2011. Morphological and electrophysiological characteristics of neurons within identified subnuclei of the lateral habenula in rat brain slices. *Neuroscience* 172, 74–93. <https://doi.org/10.1016/j.neuroscience.2010.10.047>
- Weissman, M.M., Bland, R.C., Canino, G.J., Faravelli, C., Greenwald, S., Hwu, H.-G., Joyce, P.R., Karam, E.G., Lee, C.-K., Lellouch, J., Lépine, J.-P., Newman, S.C., Rubio-Stipec, M., Wells, J.E., Wickramaratne, P.J., Wittchen, H.-U., Yeh, E.-K., 1996. Cross-National Epidemiology of Major Depression and Bipolar Disorder. *JAMA* 276, 293–299. <https://doi.org/10.1001/jama.1996.03540040037030>
- Weissman, M.M., Bland, R.C., Canino, G.J., Greenwald, S., Hwu, H.G., Lee, C.K., Newman, S.C., Oakley-Browne, M.A., Rubio-Stipec, M., Wickramaratne, P.J., 1994. The cross national epidemiology of obsessive compulsive disorder. The Cross National Collaborative Group. *J Clin Psychiatry* 55 Suppl, 5–10.

- Wen, J., Xu, Y., Yu, Z., Zhou, Y., Wang, W., Yang, J., Wang, Y., Bai, Q., Li, Z., 2022. The cAMP Response Element- Binding Protein/Brain-Derived Neurotrophic Factor Pathway in Anterior Cingulate Cortex Regulates Neuropathic Pain and Anxiodepression Like Behaviors in Rats. *Front. Mol. Neurosci.* 15, 831151. <https://doi.org/10.3389/fnmol.2022.831151>
- Whiteford, H.A., Degenhardt, L., Rehm, J., Baxter, A.J., Ferrari, A.J., Erskine, H.E., Charlson, F.J., Norman, R.E., Flaxman, A.D., Johns, N., Burstein, R., Murray, C.J., Vos, T., 2013. Global burden of disease attributable to mental and substance use disorders: findings from the Global Burden of Disease Study 2010. *The Lancet* 382, 1575–1586. [https://doi.org/10.1016/S0140-6736\(13\)61611-6](https://doi.org/10.1016/S0140-6736(13)61611-6)
- Williams, L.S., 2003. Prevalence and impact of depression and pain in neurology outpatients. *Journal of Neurology, Neurosurgery & Psychiatry* 74, 1587–1589. <https://doi.org/10.1136/jnnp.74.11.1587>
- Wirtshafter, D., Asin, K.E., Pitzer, M.R., 1994. Dopamine agonists and stress produce different patterns of Fos-like immunoreactivity in the lateral habenula. *Brain Res* 633, 21–26. [https://doi.org/10.1016/0006-8993\(94\)91517-2](https://doi.org/10.1016/0006-8993(94)91517-2)
- Woolfe, G., Macdonald, A.D., 1944. The Evaluation of the Analgesic Action of Pethidine Hydrochloride (demerol). *J Pharmacol Exp Ther* 80, 300–307.
- World Health Organization. Regional Office for South-East Asia, 2009. Regional report on status of road safety: the South-East Asia Region, A call for policy direction. WHO Regional Office for South-East Asia, New Delhi.

X

- Xiao, C., Liu, D., Du, J., Guo, Y., Deng, Y., Hei, Z., Li, X., 2021. Early molecular alterations in anterior cingulate cortex and hippocampus in a rodent model of neuropathic pain. *Brain Research Bulletin* 166, 82–91. <https://doi.org/10.1016/j.brainresbull.2020.11.020>

Y

- Yalcin, I., Barrot, M., 2014. The anxiodepressive comorbidity in chronic pain. *Current Opinion in Anaesthesiology* 27, 520–527. <https://doi.org/10.1097/ACO.0000000000000116>
- Yalcin, I., Bohren, Y., Waltisperger, E., Sage-Ciocca, D., Yin, J.C., Freund-Mercier, M.-J., Barrot, M., 2011. A Time-Dependent History of Mood Disorders in a Murine Model of Neuropathic Pain. *Biological Psychiatry* 70, 946–953. <https://doi.org/10.1016/j.biopsych.2011.07.017>
- Yalcin, I., Megat, S., Barthas, F., Waltisperger, E., Kremer, M., Salvat, E., Barrot, M., 2014. The Sciatic Nerve Cuffing Model of Neuropathic Pain in Mice. *JoVE* 51608. <https://doi.org/10.3791/51608>
- Yang, Y., Cui, Y., Sang, K., Dong, Y., Ni, Z., Ma, S., Hu, H., 2018. Ketamine blocks bursting in the lateral habenula to rapidly relieve depression. *Nature* 554, 317–322. <https://doi.org/10.1038/nature25509>

- Yanguas, J., Pinazo-Henandis, S., Tarazona-Santabalbina, F.J., 2018. The complexity of loneliness. *Acta Bio Medica Atenei Parmensis* 89, 302–314.
<https://doi.org/10.23750/abm.v89i2.7404>
- Yasuda, S., Yoshida, M., Yamagata, H., Iwanaga, Y., Suenaga, H., Ishikawa, K., Nakano, M., Okuyama, S., Furukawa, Y., Furukawa, S., Ishikawa, T., 2014. Imipramine Ameliorates Pain-related Negative Emotion via Induction of Brain-derived Neurotrophic Factor. *Cell Mol Neurobiol* 34, 1199–1208. <https://doi.org/10.1007/s10571-014-0097-y>
- Yi, M., Zhang, H., Lao, L., Xing, G.-G., Wan, Y., 2011. Anterior cingulate cortex is crucial for contra- but not ipsi-lateral electro-acupuncture in the formalin-induced inflammatory pain model of rats. *Mol Pain* 7, 61. <https://doi.org/10.1186/1744-8069-7-61>
- Yoon, C., Wook, Y.Y., Sik, N.H., Ho, K.S., Mo, C.J., 1994. Behavioral signs of ongoing pain and cold allodynia in a rat model of neuropathic pain. *Pain* 59, 369–376.
[https://doi.org/10.1016/0304-3959\(94\)90023-X](https://doi.org/10.1016/0304-3959(94)90023-X)

Z

- Zahm, D.S., Root, D.H., 2017. Review of the cytology and connections of the lateral habenula, an avatar of adaptive behaving. *Pharmacology Biochemistry and Behavior* 162, 3–21.
<https://doi.org/10.1016/j.pbb.2017.06.004>
- Zeltser, R., Beilin, B.-Z., Zaslansky, R., Seltzer, Z., 2000. Comparison of autotomy behavior induced in rats by various clinically-used neurectomy methods. *Pain* 89, 19–24.
[https://doi.org/10.1016/S0304-3959\(00\)00342-0](https://doi.org/10.1016/S0304-3959(00)00342-0)
- Zeng, J., Li, S., Zhang, C., Huang, G., Yu, C., 2018. The Mechanism of Hyperalgesia and Anxiety Induced by Remifentanyl: Phosphorylation of GluR1 Receptors in the Anterior Cingulate Cortex. *J Mol Neurosci* 65, 93–101. <https://doi.org/10.1007/s12031-018-1072-8>
- Zhang, H., Liu, S., Qin, Q., Xu, Z., Qu, Y., Wang, Yadi, Wang, J., Du, Z., Yuan, S., Hong, S., Chang, Z., He, W., Yan, X., Lang, Y., Tang, R., Wang, Yan, Zhu, L., Jiang, X., 2023. Genetic and Pharmacological Inhibition of Astrocytic Mym1 Alleviates Depressive-Like Disorders by Promoting ATP Production. *Advanced Science* 10, 2204463.
<https://doi.org/10.1002/advs.202204463>
- Zhang, L., Wang, G., Ma, J., Liu, C., Liu, X., Zhan, Y., Zhang, M., 2016. Brain-derived neurotrophic factor (BDNF) in the rostral anterior cingulate cortex (rACC) contributes to neuropathic spontaneous pain-related aversion via NR2B receptors. *Brain Research Bulletin* 127, 56–65. <https://doi.org/10.1016/j.brainresbull.2016.08.016>
- Zhang, M.-M., Liu, S.-B., Chen, T., Koga, K., Zhang, T., Li, Y.-Q., Zhuo, M., 2014. Effects of NB001 and gabapentin on irritable bowel syndrome-induced behavioral anxiety and spontaneous pain. *Mol Brain* 7, 47. <https://doi.org/10.1186/1756-6606-7-47>
- Zhang, Q., Manders, T., Tong, A.P., Yang, R., Garg, A., Martinez, E., Zhou, H., Dale, J., Goyal, A., Urien, L., Yang, G., Chen, Z., Wang, J., 2017. Chronic pain induces generalized enhancement of aversion. *eLife* 6, e25302. <https://doi.org/10.7554/eLife.25302>

- Zhang, W.-W., Chen, T., Li, S.-Y., Wang, X.-Y., Liu, W.-B., Wang, Yu-Quan, Mi, W.-L., Mao-Ying, Q.-L., Wang, Yan-Qing, Chu, Y.-X., 2023. Tachykinin receptor 3 in the lateral habenula alleviates pain and anxiety comorbidity in mice. *Front. Immunol.* 14, 1049739. <https://doi.org/10.3389/fimmu.2023.1049739>
- Zhang, X., Liu, P., He, X., Jiang, Z., Wang, Q., Gu, N., Lu, Y., 2021. The PKC γ neurons in anterior cingulate cortex contribute to the development of neuropathic allodynia and pain-related emotion. *Mol Pain* 17, 174480692110619. <https://doi.org/10.1177/17448069211061973>
- Zhang, Y., Ji, F., Wang, G., He, D., Yang, L., Zhang, M., 2018. BDNF Activates mTOR to Upregulate NR2B Expression in the Rostral Anterior Cingulate Cortex Required for Inflammatory Pain-Related Aversion in Rats. *Neurochem Res* 43, 681–691. <https://doi.org/10.1007/s11064-018-2470-6>
- Zhang, Y., Meng, X., Li, A., Xin, J., Berman, B.M., Lao, L., Tan, M., Ren, K., Zhang, R.-X., 2011. Acupuncture Alleviates the Affective Dimension of Pain in a Rat Model of Inflammatory Hyperalgesia. *Neurochem Res* 36, 2104–2110. <https://doi.org/10.1007/s11064-011-0534-y>
- Zhao, H., Xue, Q., Li, C., Wang, Q., Han, S., Zhou, Y., Yang, T., Xie, Y., Fu, H., Lu, C., Meng, F., Zhang, M., Zhang, Y., Wu, X., Wu, S., Zhuo, M., Xu, H., 2020. Upregulation of Beta4 subunit of BKCa channels in the anterior cingulate cortex contributes to mechanical allodynia associated anxiety-like behaviors. *Mol Brain* 13, 22. <https://doi.org/10.1186/s13041-020-0555-z>
- Zheng, Z., Guo, C., Li, M., Yang, L., Liu, P., Zhang, X., Liu, Y., Guo, X., Cao, S., Dong, Y., Zhang, C., Chen, M., Xu, J., Hu, H., Cui, Y., 2022. Hypothalamus-habenula potentiation encodes chronic stress experience and drives depression onset. *Neuron* 110, 1400-1415.e6. <https://doi.org/10.1016/j.neuron.2022.01.011>
- Zhong, S., Zhang, S., Fan, X., Wu, Q., Yan, L., Dong, J., Zhang, H., Li, L., Sun, L., Pan, N., Xu, X., Tang, F., Zhang, J., Qiao, J., Wang, X., 2018. A single-cell RNA-seq survey of the developmental landscape of the human prefrontal cortex. *Nature* 555, 524–528. <https://doi.org/10.1038/nature25980>
- Zhong, X.-L., Wei, R., Zhou, P., Luo, Y.-W., Wang, X.-Q., Duan, J., Bi, F.-F., Zhang, J.-Y., Li, C.-Q., Dai, R.-P., Li, F., 2012. Activation of Anterior Cingulate Cortex Extracellular Signal-Regulated Kinase-1 and -2 (ERK1/2) Regulates Acetic Acid-Induced, Pain-Related Anxiety in Adult Female Mice. *Acta Histochem. Cytochem.* 45, 219–225. <https://doi.org/10.1267/ahc.12002>
- Zhou, H., Zhang, Q., Martinez, E., Dale, J., Hu, S., Zhang, E., Liu, K., Huang, D., Yang, G., Chen, Z., Wang, J., 2018. Ketamine reduces aversion in rodent pain models by suppressing hyperactivity of the anterior cingulate cortex. *Nat Commun* 9, 3751. <https://doi.org/10.1038/s41467-018-06295-x>

- Zhou, W., Jin, Y., Meng, Q., Zhu, X., Bai, T., Tian, Y., Mao, Y., Wang, L., Xie, W., Zhong, H., Zhang, N., Luo, M.-H., Tao, W., Wang, H., Li, Jie, Li, Juan, Qiu, B.-S., Zhou, J.-N., Li, X., Xu, H., Wang, K., Zhang, X., Liu, Y., Richter-Levin, G., Xu, L., Zhang, Z., 2019. A neural circuit for comorbid depressive symptoms in chronic pain. *Nat Neurosci* 22, 1649–1658. <https://doi.org/10.1038/s41593-019-0468-2>
- Zhou, Y.-S., Meng, F.-C., Cui, Y., Xiong, Y.-L., Li, X.-Y., Meng, F.-B., Niu, Z.-X., Zheng, J.-X., Quan, Y.-Q., Wu, S.-X., Han, Y., Xu, H., 2022. Regular Aerobic Exercise Attenuates Pain and Anxiety in Mice by Restoring Serotonin-Modulated Synaptic Plasticity in the Anterior Cingulate Cortex. *Medicine & Science in Sports & Exercise* 54, 566–581. <https://doi.org/10.1249/MSS.0000000000002841>
- Zhu, D.-Y., Cao, T.-T., Fan, H.-W., Zhang, M.-Z., Duan, H.-K., Li, J., Zhang, X.-J., Li, Y.-Q., Wang, P., Chen, T., 2022. The increased in vivo firing of pyramidal cells but not interneurons in the anterior cingulate cortex after neuropathic pain. *Mol Brain* 15, 12. <https://doi.org/10.1186/s13041-022-00897-9>
- Zhu, X., Tang, H.-D., Dong, W.-Y., Kang, F., Liu, A., Mao, Y., Xie, W., Zhang, X., Cao, P., Zhou, W., Wang, H., Farzinpour, Z., Tao, W., Song, X., Zhang, Y., Xue, T., Jin, Y., Li, J., Zhang, Z., 2021. Distinct thalamocortical circuits underlie allodynia induced by tissue injury and by depression-like states. *Nat Neurosci* 24, 542–553. <https://doi.org/10.1038/s41593-021-00811-x>
- Zhu, X., Xu, Yingling, Shen, Z., Zhang, H., Xiao, S., Zhu, Y., Wu, M., Chen, Y., Wu, Z., Xu, Yunyun, He, X., Liu, B., Liu, J., Du, J., Sun, J., Fang, J., Shao, X., 2022. Rostral Anterior Cingulate Cortex–Ventrolateral Periaqueductal Gray Circuit Underlies Electroacupuncture to Alleviate Hyperalgesia but Not Anxiety-Like Behaviors in Mice With Spared Nerve Injury. *Front. Neurosci.* 15, 757628. <https://doi.org/10.3389/fnins.2021.757628>
- Zhuang, Z.-F., Wu, H.-Y., Song, Y.-Y., Li, L., Cui, X., Yang, J., Xu, X.-Q., Cui, W.-Q., 2022. N-Methyl D-aspartate receptor subtype 2B/Ca²⁺/calmodulin-dependent protein kinase II signaling in the lateral habenula regulates orofacial allodynia and anxiety-like behaviors in a mouse model of trigeminal neuralgia. *Front. Cell. Neurosci.* 16, 981190. <https://doi.org/10.3389/fncel.2022.981190>
- Zhuo, M., 2016. Neural Mechanisms Underlying Anxiety–Chronic Pain Interactions. *Trends in Neurosciences* 39, 136–145. <https://doi.org/10.1016/j.tins.2016.01.006>

Appendix

Longitudinal genomic study

In addition to my PhD project, I participated in a transversal genomic study in our team.

My work consisted in generating three different batches of neuropathic animals, composed of 12 sham and 12 cuff. Each batch corresponded to a specific time point of the cuff model: TP1 with only the mechanical hypersensitivity, TP2 with both the mechanical hypersensitivity and the anxiodepressive-like behaviours, and TP3 with only the depressive-like behaviours but with no mechanical hypersensitivity anymore. I performed the behaviour of all three batches (von Frey, splash test and novelty suppressed feeding test -NSF-).

Then, we dissected and collected 7 different brain regions in both sham and cuff animals for each batch at their respective time points: the anterior cingulate cortex, the insular cortex, the nucleus accumbens, the habenula, the basolateral amygdala, the ventral tegmental area and the dorsal raphe nucleus. I then proceeded to RNA and DNA extractions for all the samples.

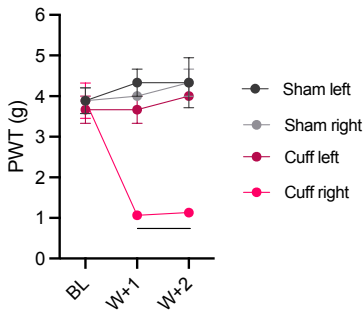
The RNA samples were sent for RNA sequencing and the data is currently being analysed by a bioinformatician.

This work will allow for a transcriptional comprehension of the longitudinal changes induced by the cuff model in brain regions associated with pain, anxiety and depression.

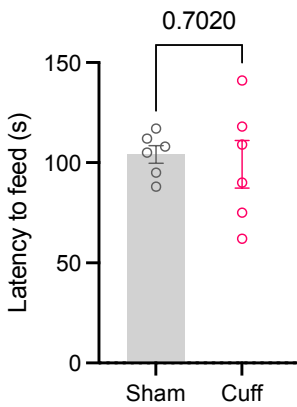
You can find the behaviour of the animals selected for RNA sequencing on the following page for each time point. * $<.05$, ** $<.01$. n= 6-8 animals/group

TP1

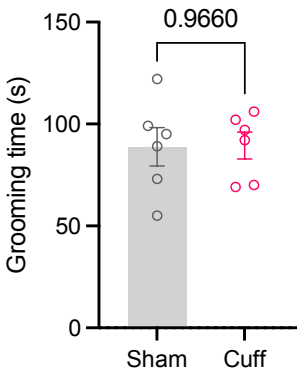
von Frey



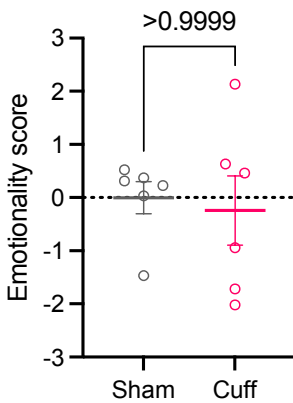
NSF



Splash

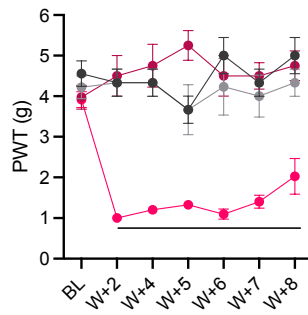


Emotionality

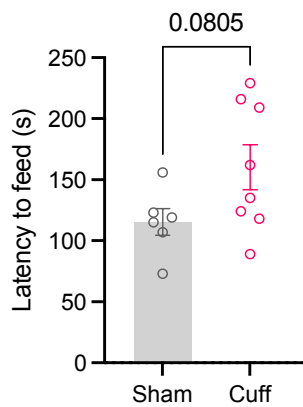


TP2

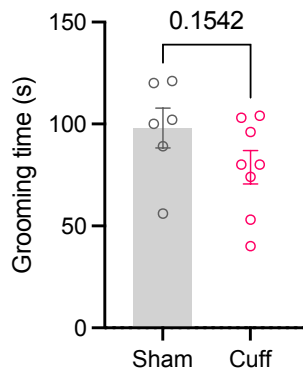
von Frey



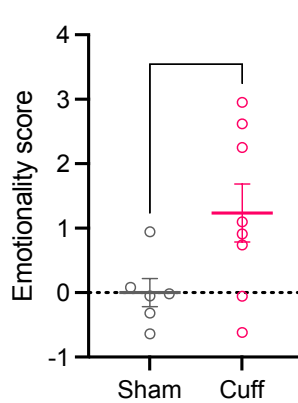
NSF



Splash

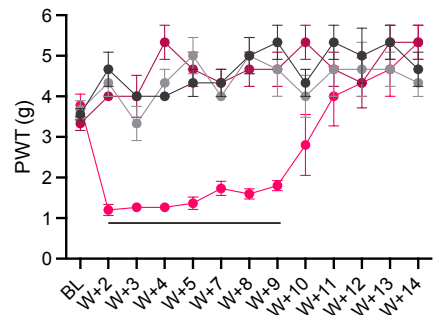


Emotionality

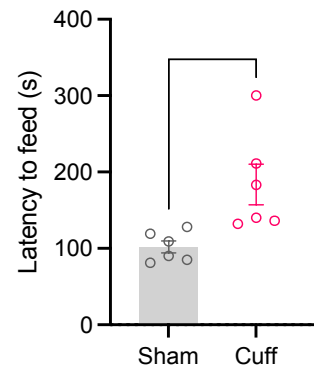


TP3

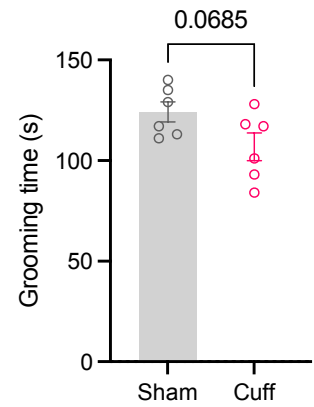
von Frey



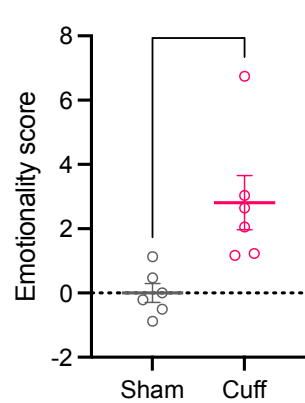
NSF

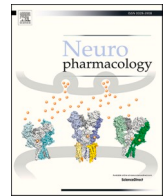


Splash



Emotionality





Antiallodynic action of phosphodiesterase inhibitors in a mouse model of peripheral nerve injury

Salim Megat^a, Sylvain Hugel^a, Sarah H. Journée^a, Yohann Bohren^{a,b}, Adrien Lacaud^a, Vincent Lelièvre^a, Stéphane Doridot^c, Pascal Villa^d, Jean-Jacques Bourguignon^e, Eric Salvat^{a,b}, Remy Schlichter^a, Marie-José Freund-Mercier^a, Ipek Yalcin^{a,*},¹, Michel Barrot^{a,**},¹

^a Centre National de la Recherche Scientifique, Université de Strasbourg, Institut des Neurosciences Cellulaires et Intégratives, Strasbourg, France

^b Hôpitaux Universitaires de Strasbourg, Centre d'Évaluation et de Traitement de la Douleur, Strasbourg, France

^c Centre National de la Recherche Scientifique, Université de Strasbourg, Chronobiotron, Strasbourg, France

^d Université de Strasbourg, Centre National de la Recherche Scientifique, Plateforme de Chimie Biologique Intégrative de Strasbourg, UAR3286, Illkirch, France

^e Université de Strasbourg, Centre National de la Recherche Scientifique, Laboratoire d'Innovation Thérapeutique, Illkirch, France

ARTICLE INFO

Keywords:

antidepressant
Phosphodiesterase inhibitors
Allodynia
TNF α
Pain
Rolipram

ABSTRACT

Neuropathic pain arises as a consequence of a lesion or disease affecting the somatosensory nervous system. It is accompanied by neuronal and non-neuronal alterations, including alterations in intracellular second messenger pathways. Cellular levels of 3',5'-cyclic adenosine monophosphate (cAMP) and 3',5'-cyclic guanosine monophosphate (cGMP) are regulated by phosphodiesterase (PDE) enzymes. Here, we studied the impact of PDE inhibitors (PDEi) in a mouse model of peripheral nerve injury induced by placing a cuff around the main branch of the sciatic nerve. Mechanical hypersensitivity, evaluated using von Frey filaments, was relieved by sustained treatment with the non-selective PDEi theophylline and ibudilast (AV-411), with PDE4i rolipram, etazolol and YM-976, and with PDE5i sildenafil, zaprinast and MY-5445, but not by treatments with PDE1i vinpocetine, PDE2i EHNA or PDE3i milrinone. Using pharmacological and knock-out approaches, we show a preferential implication of delta opioid receptors in the action of the PDE4i rolipram and of both mu and delta opioid receptors in the action of the PDE5i sildenafil. Calcium imaging highlighted a preferential action of rolipram on dorsal root ganglia non-neuronal cells, through PDE4B and PDE4D inhibition. Rolipram had anti-neuroimmune action, as shown by its impact on levels of the pro-inflammatory cytokine tumor necrosis factor- α (TNF α) in the dorsal root ganglia of mice with peripheral nerve injury, as well as in human peripheral blood mononuclear cells (PBMCs) stimulated with lipopolysaccharides. This study suggests that PDEs, especially PDE4 and 5, may be targets of interest in the treatment of neuropathic pain.

1. Introduction

3',5'-cyclic adenosine monophosphate (cAMP) and 3',5'-cyclic guanosine monophosphate (cGMP) are important second messengers implicated in many biological processes (Friebe et al., 2020; Gancedo, 2013; Houslay, 2010). Their cellular levels are regulated by phosphodiesterase (PDE) enzymes belonging to an eleven-family group (PDE1-PDE11) that can be further divided into multiple isoforms, encoded by different genes and/or resulting from alternative splicing (Ahmad et al., 2015; Azevedo et al., 2014; Francis et al., 2001; Soderling

and Beavo, 2000). The PDE families differ in their ability to hydrolyze cAMP and/or cGMP, in their tissue and subcellular distribution, as well as in their sensitivity to pharmacological inhibitors (Ahmad et al., 2015; Azevedo et al., 2014; Francis et al., 2011). Either clinically or in pre-clinical models, these PDE inhibitors (PDEi) have been shown to be effective in a variety of pathological conditions, including major depressive disorder, sexual dysfunction, chronic obstructive pulmonary dysfunction, psoriasis and chronic pain (Ahmad et al., 2015; Azevedo et al., 2014; Bollenbach et al., 2019; Keravis and Lugnier, 2012; Mayer et al., 2005; Page and Spina, 2011; Renau, 2004; Wittmann and

* Corresponding author. INCI CNRS, 8 allée du Général Rouvillois, 67000 Strasbourg, France.

** Corresponding author. INCI CNRS, 8 allée du Général Rouvillois, 67000 Strasbourg, France.

E-mail addresses: yalcin@inci-cnrs.unistra.fr (I. Yalcin), mbarrot@inci-cnrs.unistra.fr (M. Barrot).

¹ The last two authors contributed equally to this work.

Helliwell, 2013).

Neuropathic pain is a chronic pain arising as a consequence of a lesion or a disease affecting the somatosensory nervous system (Scholz et al., 2019; Treede et al., 2019). Interestingly, antidepressant drugs acting on monoamine uptake are amongst first line treatments for neuropathic pain (Attal et al., 2010; Attal, 2019; Barrot et al., 2009; Wright and Rizzolo, 2017). Their primary targets are the noradrenergic and serotonergic transporters, with also some potential direct action on voltage-gated sodium channels (Barber et al., 1991; Micó et al., 2006; Kremer et al., 2016). The pain-relieving action through noradrenergic transmission has been shown to be mediated by the secondary recruitment of β_2 adrenoceptors at peripheral level and/or α_2 adrenoceptors centrally (Choucair-Jaafar et al., 2009; Barrot et al., 2010; Bohren et al., 2013; Kremer et al., 2018; Yalcin et al., 2009a, 2009b; Zhang et al., 2009), by the recruitment of the opioid system (Micó et al., 2006; Kremer et al., 2016, 2018; Marchand et al., 2003; Üçel et al., 2015; Wattiez et al., 2011), and by the reduction of peripheral cytokine tumor necrosis factor (TNF)- α in the dorsal root ganglia (Bohren et al., 2013; Kremer et al., 2018). Since: 1) PDE4 inhibitors have been preclinically investigated for their antidepressant effects (Bobon et al., 1988); 2) PDE4 has been shown to be the main PDE to mediate the hydrolysis of cAMP formed by the activation of β_2 adrenoceptors (Ye et al., 1997); 3) increasing cAMP levels suppresses the activation of glial cells and the production of proinflammatory cytokines such as TNF α , and PDEi can enhance the anti-TNF α activity of a β_2 adrenoceptor agonist (Christiansen et al., 2011), we sought to investigate whether a long-term treatment with PDEi could alleviate mechanical hypersensitivity following peripheral nerve injury.

In this study, our pharmacological screening showed that only PDE4i and PDE5i significantly relieved mechanical hypersensitivity in a dose-dependent manner. Using pharmacological and knock-out approaches, we further showed a differential implication of opioid receptors in the antiallodynic effect of the PDE4i rolipram and the PDE5i sildenafil. Calcium imaging highlighted a preferential action of rolipram on dorsal root ganglia non-neuronal cells, through PDE4B and PDE4D inhibition. In addition, long-term treatment with rolipram decreased levels of the pro-inflammatory cytokine TNF α in the dorsal root ganglia.

2. Material and methods

2.1. Animals

Experiments were performed in adult male mice, housed three to five per cage under a 12 h light/dark cycle with *ad libitum* access to water and food, and weighing 25–30 g at surgery time. C57BL/6J mice (Chronobiotron UMS3415, Strasbourg, France), as well as wild-type (WT) and MOR $^{-/-}$, DOR $^{-/-}$, KOR $^{-/-}$ littermate mice were used. The generation of mice lacking the μ (MOR), δ (DOR) or κ (KOR) opioid receptor has been previously described (Filliol et al., 2000; Simonin et al., 1998). These mice were backcrossed on a C57BL/6J background for at least 10 generations, and heterozygote mice (MOR $^{+/-}$, DOR $^{+/-}$, KOR $^{+/-}$) were bred in our facilities and genotyped upon weaning. The animal facilities are legally registered for animal experimentation under Animal House Agreement C67-482-1. Experiments were approved by the regional ethical committee (CREMEAS).

2.2. Model and test

Peripheral nerve injury was induced by inserting a cuff around the main branch of the right sciatic nerve (Benbouzid et al., 2008b; Yalcin et al., 2014). Surgeries were done under ketamine (17 mg/mL)/xylazine (2.5 mg/mL) anesthesia (intraperitoneal, 4 mL/kg) (Centravet, Taden, France). The common branch of the right sciatic nerve was exposed and a 2 mm section of split PE-20 polyethylene tubing (Harvard Apparatus, Les Ulis, France) was placed around it (Cuff group). The shaved skin was closed using suture. Sham-operated mice underwent the same

procedure, without implantation of the cuff (Sham group). Mechanical allodynia being a symptom of neuropathic pain, we measured mechanical thresholds of hindpaw withdrawal using von Frey hairs and the results were expressed in grams (Barrot, 2012; Bohren et al., 2010; Yalcin et al., 2014). Mice were placed in clear Plexiglas® boxes (7 cm \times 9 cm \times 7 cm) on an elevated mesh screen and calibrated von Frey filaments (Bioseb, Chaville, France) were applied to the plantar surface of each hindpaw in a series of ascending forces until they bent. Gram value of the lower filament that induced at least 3 paw responses out of 5 trials was considered as the paw withdrawal threshold for this animal.

2.3. Drug treatments

Ibutilast (AV-411) and MY-5445 were purchased from Tocris Biosciences (Bristol, United Kingdom). Rolipram, theophylline, naltrindole and naloxonazine were purchased from Sigma-Aldrich (St Quentin Fallavier, France). Erythro-9-(2-hydroxy-3-nonyl)adenine (EHNA), etazolate, milrinone, sildenafil, vinpocetine, YM-976 and zaprinast were purchased from Biotrend Chemikalien GmbH (Köln, Germany). For studies in mice, drugs were suspended in 1% methylcellulose in 0.9% NaCl. PDEi and vehicle solutions were injected intraperitoneally, twice per day (morning and evening) in a volume of 5 mL/kg body weight. Chronic treatments began after at least a two-week delay post-surgery and lasted at least 12 days, except for the non-selective PDEi ibutilast that was given for 7 days. In order to measure the effect of chronic treatments, behavioral tests were done in mornings before the first daily injection and at least twice per week during treatments, except for ibutilast for which the test was done at day 7 only. Experimental designs are detailed in their corresponding figures (Figs. 1–3). For the study in human peripheral blood mononuclear cells (PBMCs), rolipram was re-suspended in dimethyl sulfoxide (DMSO) and tested at different concentrations (final DMSO concentration was adjusted to 1% maximum for each testing well).

2.4. Immunoblot

After 21 days of rolipram or control treatment, dorsal root ganglia corresponding to lumbar levels L4, L5 and L6 were dissected. Total protein was extracted in 150 μ L of lysis buffer (20 mM Tris pH 7.5; 150 mM NaCl; 10% glycerol (v/v); 1% NP40 (v/v); Protease Inhibitor EDTA-free (Roche)) and quantified with DC protein assay kits (Bio-Rad). Fifteen μ g of proteins were resolved on 12% polyacrylamide-SDS electrophoresis gel under reducing conditions, and transferred to PVDF membranes (Immobilion, Millipore, #IPVH00010). Blots were incubated 1 h in blocking agent (ECL Blocking Agent, Advance Western Blotting Detection System Kit) and overnight with anti-TNF α (1:500, RD systems, #AF-410-NA) and anti- β -tubulin (1:10000, Abcam, #Ab108342) antibodies. Blots were then incubated with anti-goat and anti-rabbit HRP-conjugated secondary antibodies (1:5000, Chemicon, #AF106P and #AP187P) at room temperature, and revealed by chemiluminescence (Advance Detection System Kit, Amersham, #RPN2135) using Hyperfilm substrates (Hyperfilm, Amersham Biosciences, #RPN1674K). Protein expression was quantified using the densitometry tool of Adobe Photoshop software CS5.

2.5. Dorsal root ganglia culture

Dorsal root ganglia cell cultures were prepared from adult mice. Immediately after dissection, lumbar dorsal root ganglia were collected in a phosphate-buffered saline solution, enzymatically dissociated for 20 min at 37 °C with trypsin-EDTA (0.5 g/L, Seromed) and 2 mg/mL of collagenase IA/dispase (Invitrogen). Following enzymatic dissociation, culture medium consisting of MEM α (minimum essential medium α , Gibco, France) with 50 IU/mL penicillin-streptomycin (Gibco) and 10% v/v heat inactivated horse serum (Gibco) was added. Cells were then further dissociated by trituration with polished Pasteur pipettes of

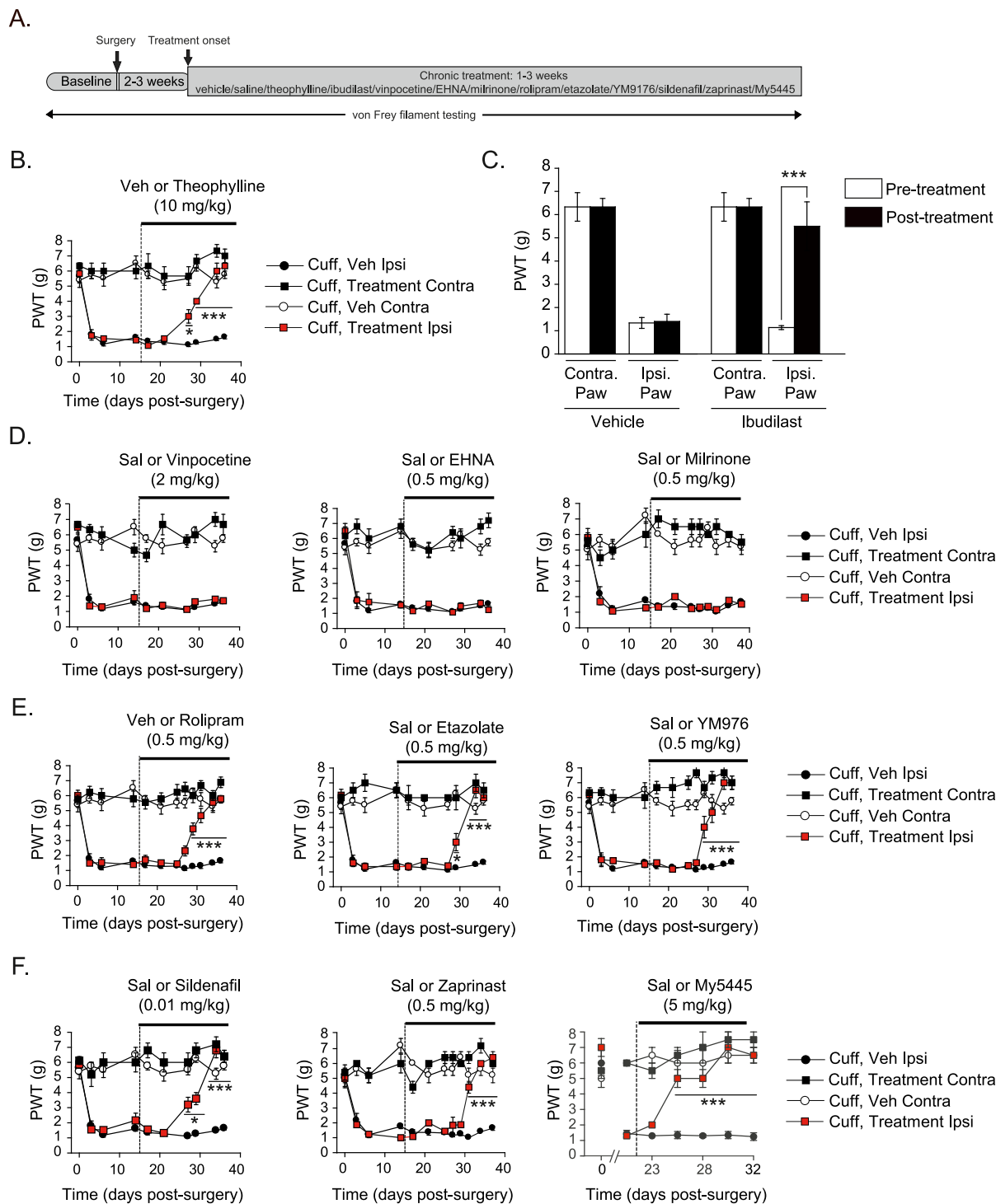
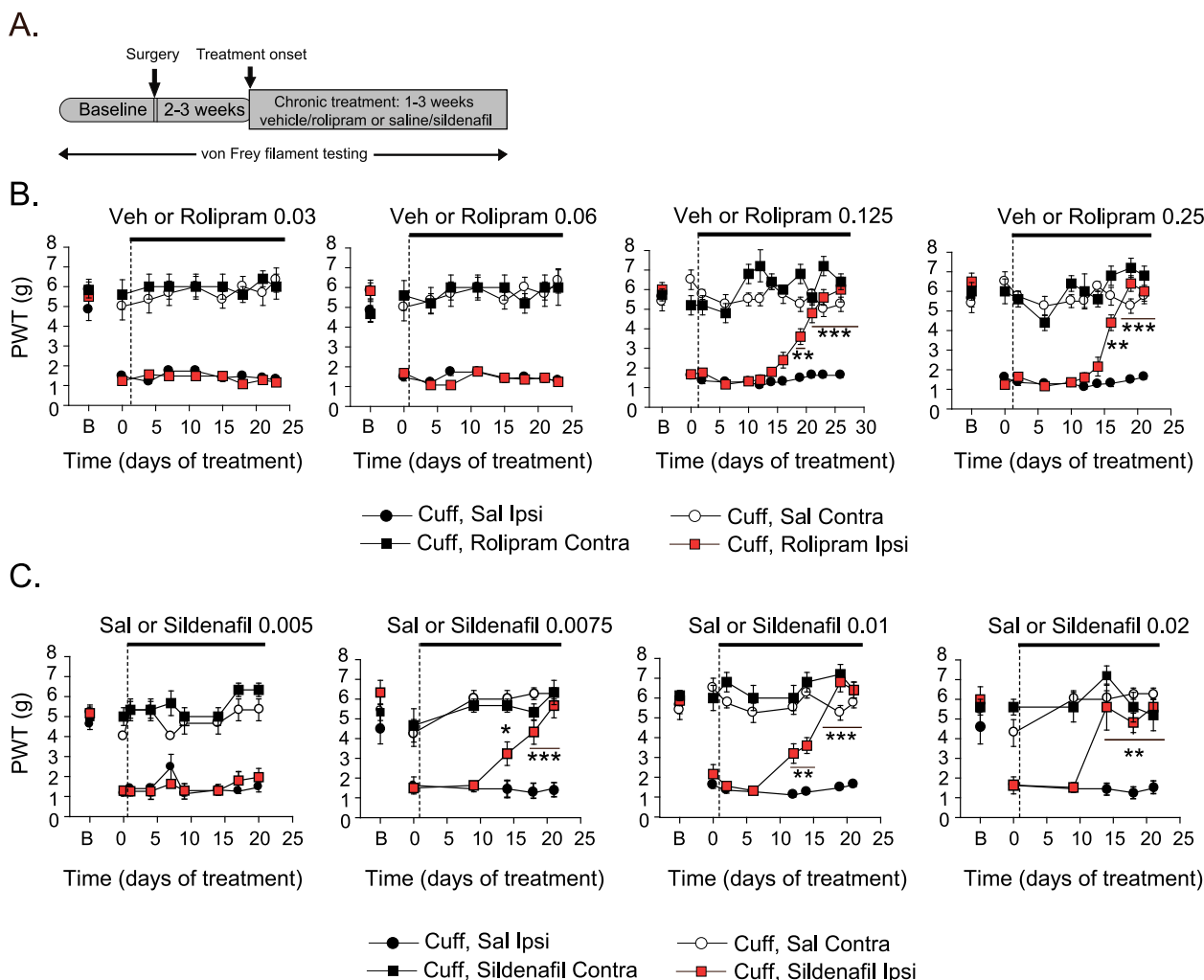


Fig. 1. Non-selective PDEi and selective PDE4i and PDE5i relieve mechanical hypersensitivity. (A) Time course of the experiments. Peripheral nerve injury was induced by inserting a cuff around the main branch of the sciatic nerve. Treatments started after at least 2 weeks postsurgery. Mechanical sensitivity was tested using von Frey filaments. (B,C) Chronic treatment with the non-selective PDEi theophylline ($n = 5-7$ /group; post-hoc Duncan: $*p < 0.05$ and $***p < 0.001$ vs. Cuff Veh Ipsi) or ibudilast ($n = 5-6$ /group; post-hoc: $***p < 0.001$) relieved mechanical hypersensitivity. (D) Prolonged treatments with vinpocetine (PDEi1), EHNA (PDEi2) or milrinone (PDEi3) ($n = 5-6$ /group) did not reverse mechanical hypersensitivity. (E) The PDE4i rolipram suppressed mechanical allodynia after chronic treatment ($n = 5-6$ /group; post-hoc: $***p < 0.001$ vs. Cuff Veh Ipsi), and this effect was also observed with 2 other PDE4i: etazolate ($n = 4-5$ /group; post-hoc: $*p < 0.05$ and $***p < 0.001$ vs. Cuff Veh Ipsi) and YM-976 ($n = 5-6$ /group; post-hoc: $***p < 0.001$ vs. Cuff Veh Ipsi). (F) Treatment with the selective PDE5i sildenafil ($n = 5$ /group; post-hoc: $*p < 0.05$ and $***p < 0.001$ vs. Cuff Veh Ipsi), zaprinast ($n = 5$ /group; post-hoc: $***p < 0.001$ vs. Cuff Veh Ipsi) and MY-5445 ($n = 5-7$ /group; post-hoc: $***p < 0.001$ vs. Cuff Veh Ipsi) also relieved mechanical hypersensitivity. Data are presented as mean \pm SEM. Contra, contralateral; Ipsi, ipsilateral; PWT, paw withdrawal thresholds; Sal, saline; Veh, vehicle.



decreasing tip-diameter. Dorsal root ganglia cells were then plated on 15 mm glass coverslips coated with poly-D-lysine (0.02 mg/mL), and cultures were placed in a controlled atmosphere (95% O₂, 5% CO₂). Calcium imaging experiments were performed 24–36 h after seeding.

2.6. Calcium imaging

2.6. Calcium imaging

Calcium imaging was performed on dorsal root ganglia cell cultures from Sham and Cuff mice. Cells were incubated in a solution containing 2 μ M Fura-2 acetoxyethyl ester (F1201, Molecular Probes, USA) and 0.01% pluronic acid (Molecular Probes) for 1 h at room temperature. During calcium measurements, cells were continuously perfused with an extracellular solution (130 mM NaCl; 5 mM KCl; 1 mM CaCl₂; 1 mM MgCl₂; 10 mM glucose; 10 mM HEPES pH 7.3). Fluorescence measurements were performed on an inverted microscope (Axiovert 35, Zeiss) with a 40X oil-immersion objective (Fluo 40, NA 1.30, Nikon) using a real-time imaging system with a cooled CCD camera (CoolSnap HQ, Photometrics) and an imaging analysis software (Imaging Workbench software 4.0, Axon Instruments). Fluorescence was alternatively excited at 340 nm and 380 nm with a Lambda-10 filter wheel (Sutter Instruments) and the emitted light was collected above 520 nm. Images

were acquired every 2 s and intracellular calcium concentration was expressed using the fluorescence ratio F340/F380 after background subtraction. Responses to UTP (50 μ M), KCl (50 mM) and rolipram (1, 10 and 100 μ M) were tested. Neurons and non-neuronal cells were identified using successive application of UTP, a P2Y receptor agonist, and high KCl which triggers calcium responses selectively in neurons. Cells that clearly showed calcium responses to UTP but not to KCl were considered as non-neuronal cells, while cells that responded to KCl with or without responses to UTP were considered as neurons.

2.7. siRNA experiments

In order to determine the PDE4 subtype involved in the neuronal and non-neuronal effects of rolipram, we performed siRNA-mediated knockdown of *Pde4b* and *Pde4d* in dorsal root ganglia cell cultures. Knockdown of *Pde4b* and *Pde4d* mRNA were performed using ACCELL siRNA (#E-049576-00 and #E-043744-00, respectively) designed and validated by ThermoFisher/Dharmacon (Lafayette, CO, USA). A non-targeting siRNA (#D-001910-10-05) was used as a negative control. Stock solutions for the targeted and scrambled siRNA (#D-001910-10-05) were prepared at 100 μ M in 1x siRNA Buffer (diluted from

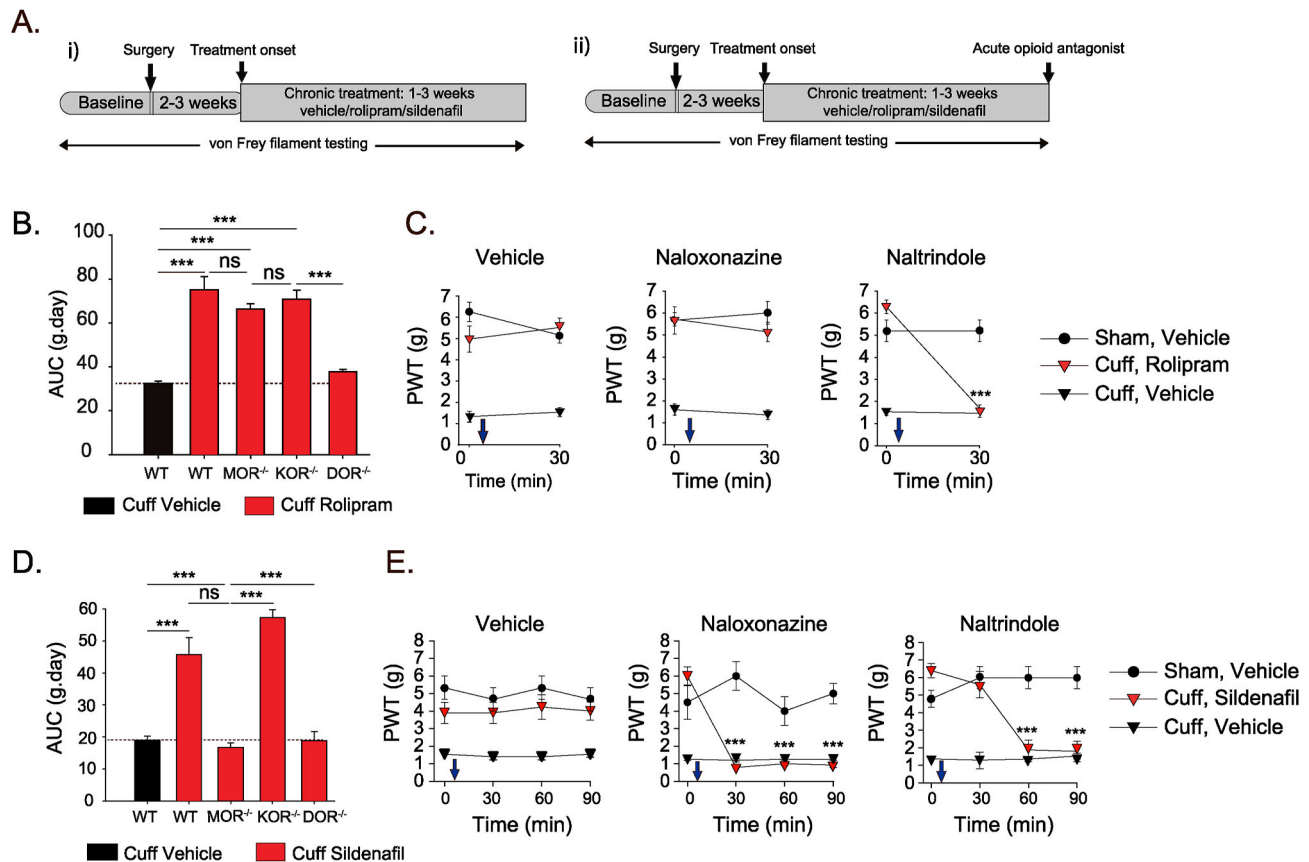


Fig. 3. Opioid receptors are necessary for PDE4i and PDE5i antiallodynic action. (A) Time course of experiments. Peripheral nerve injury was induced by cuffing the sciatic nerve and treatments started at least 2 weeks postsurgery. Mechanical sensitivity was tested using von Frey filaments. Opioid receptor implication was assessed using WT, MOR^{-/-}, KOR^{-/-} and DOR^{-/-} mice, and, in a separate set of experiments, by testing the MOR antagonist naloxonazine (30 mg/kg, s.c) and the DOR antagonist naltrindole (5 mg/kg, s.c) compared to vehicle injection (methylcellulose 1%, s.c) in mice that had fully recovered from mechanical hypersensitivity with chronic rolipram or sildenafil treatment. All data are presented for the right paw, ipsilateral to the surgery. (B) Data are expressed as area under the curve (AUC, g·day) over the period of treatment. Rolipram had an antiallodynic action in WT, MOR^{-/-} and KOR^{-/-} mice, but was ineffective in DOR^{-/-} mice (n = 5–6/group; post-hoc Duncan: ***p < 0.001; ns, non-significant). (C) Acute injection of naloxonazine failed to block chronic rolipram-induced alleviation of mechanical hypersensitivity (n = 5), while naltrindole suppressed rolipram effect (n = 5–6; post-hoc Duncan: ***p < 0.001 vs. Sham Vehicle and vs. Cuff Rolipram at time 0). (D) Long-term sildenafil treatment had an antiallodynic action in WT and KOR^{-/-} mice, while no effect was present in MOR^{-/-} and DOR^{-/-} mice (n = 6–7; post-hoc: ***p < 0.001). (E) Acute injection of either naloxonazine (n = 5–7; post-hoc: ***p < 0.001) or naltrindole (n = 5; post-hoc: ***p < 0.001) induced a relapse of allodynia in sildenafil treated mice. Data are presented as mean ± SEM.

Dharmacon 5x siRNA Buffer, #B-002000-UB-100). Dorsal root ganglia cells were plated and allowed to attach to culture dishes for 30 min in standard culture medium. Then, medium was replaced by 1 mL of serum-free medium (Thermo scientific, #B-005000-500) containing 1 μM siRNA or the scrambled negative control. The cultures were tested 24–36 h after transfection.

2.8. Real time quantitative PCR (RT-qPCR)

Quantification of gene expression was done by RT-qPCR. Total mRNA was extracted using RNAeasy kit (Qiagen) and the cDNA was generated using *iScript cDNA synthesis kit* (Biorad). RT-qPCR was performed on a Thermocycler Biorad MylQ, using Biorad IQ Syber Green Supermix assay, with initialization step at 95 °C for 3 min followed by amplification for 40 cycles of 20 s 95 °C denaturation, 20 s 95 °C annealing and 20 s 60 °C extension. Experiments were performed with triplicate sample deposits on the amplification plate. Relative abundance of each RNA target gene transcript was normalized to the endogenous control gene *Gapdh* RNA. Data were analyzed according to the standard curve method. Primers were designed from *Mus Musculus* using gene data bank and Primer Blast as follows: *Pde4b*: forward 5'-AAATTCTGAACCTTGCTTTGATGT-3' and reverse 3'-GAAAGATGTCGCAGTGTCTCT-5'; *Pde4d*: forward 5'-AGAGCCTGTCTTGTAAAGCATTTC-3' and reverse 5'-GGTGGCGCTCTCAGTAGTTT-3'; and

Gapdh: forward 5'-GGCCTTCCGTGTTCTAC-3' and reverse 3' TGTCATCATACTTGGCAGGTT-5'.

2.9. Anti-TNFα activity in human peripheral blood mononuclear cells (PBMCs)

PBMCs were prepared from the peripheral blood of healthy donors (Etablissement Français du Sang) as described by Kümmerle et al. (2012) PBMCs were isolated using Histopaque gradient (Sigma-Aldrich), washed in Hanks' balanced salt solution (Sigma-Aldrich) and were then cultured in RPMI-1640 medium (Sigma-Aldrich) supplemented with 10% (v/v) fetal bovine serum (PAA Laboratories), 100 U/mL penicillin and 100 μg/mL streptomycin (PAA Laboratories). PBMCs were seeded in 24-well plates (5 × 10⁵ cells/well) and stimulated with 5 μg/mL lipopolysaccharide (LPS) (Sigma-Aldrich, L2630), in a total volume of 1 mL per well. Cells without LPS stimulation were considered as bio-inactive control (basal level of cytokine). Incubation with rolipram was performed at 37 °C (5% CO₂) for 24 h and TNFα was measured on culture supernatant by ELISA as previously described (Kümmerle et al., 2012). Cell viability was also controlled using the WST-1 (Ozyme) assay described previously (Houël et al., 2015). Briefly, after the supernatant was transferred for cytokine determination, WST-1-containing medium was added to cells and cell viability was measured using the Victor³

reader (PerkinElmer) after 2-h incubation at 37 °C. Each measurement was performed in triplicate with three independent experiments, and results expressed as means of the three independent experiments.

2.10. Statistical analysis

Data are expressed as mean \pm SEM. Statistical analyses were performed using multifactorial analysis of variance (ANOVA). Surgical procedures (Sham or Cuff) and treatments (saline vs. drug injections) were taken as between-group factors. When needed, the time of test (either time course or pre-injection vs. post-injection data) was taken as within-subject factor. Duncan test was used for *post-hoc* multiple comparisons. For calcium imaging experiments, the fraction of cells responding or not to rolipram in sham and nerve injury conditions were compared by a contingency table with a Fischer's exact test. For quantitative PCR and immunoblotting experiments, statistical analyses were done using Kruskal-Wallis non-parametric test and a comparison between groups was performed with Mann-Whitney *U* test. Significance level was set at $p < 0.05$.

3. Results

3.1. PDEi relieves mechanical hypersensitivity

For the experimental design, see Fig. 1A. We first tested the non-selective PDEi theophylline which, given intraperitoneally twice a day, relieved mechanical hypersensitivity over time ($F_{27,216} = 3.98$, $p < 0.001$) (Fig. 1B). Similarly, seven days of twice daily treatment with another non-selective PDEi, ibudilast (AV-411), also suppressed mechanical hypersensitivity ($F_{4,80} = 8.14$, $p < 0.001$) (Fig. 1C). To assess the respective role of different PDE subtypes, we then tested more selective compounds. Neither the PDE1i vinpocetine ($F_{27,264} = 0.96$, $p = 0.52$) nor the PDE2i EHNA ($F_{27,242} = 0.50$, $p = 0.95$) or the PDE3i milrinone ($F_{33,242} = 1.42$, $p = 0.1$) suppressed mechanical hypersensitivity of the paw with sciatic nerve cuffing (Fig. 1D). However, chronic treatment with PDE4i, such as rolipram ($F_{33,330} = 4.47$, $p < 0.001$), etazolate ($F_{27,180} = 9.90$, $p < 0.001$) and YM-976 ($F_{30,264} = 6.99$, $p < 0.001$) relieved hypersensitivity (Fig. 1E). Besides, we also observed that treatments with PDE5i, including sildenafil ($F_{27,198} = 6.51$, $p < 0.001$), zaprinast ($F_{33,197} = 3.91$, $p < 0.001$) and MY-5445 ($F_{18,54} = 12.19$, $p < 0.001$), reversed mechanical hypersensitivity (Fig. 1F).

3.2. PDE4i and PDE5i reverse mechanical hypersensitivity in a dose-dependent manner

To identify the threshold doses leading to allodynia relief, we then assessed the dose-response effect of the PDE4i rolipram and PDE5i sildenafil (see Fig. 2A for experimental design). After around two weeks of treatment, rolipram exerted an antiallodynic action at doses 0.25 mg/kg ($F_{27,242} = 3.77$, $p < 0.001$) and 0.125 mg/kg ($F_{33,208} = 2.83$, $p < 0.001$), but not at lower doses (0.06 mg/kg: $F_{24,144} = 0.32$, $p = 0.99$; 0.03 mg/kg: $F_{24,144} = 0.42$, $p = 0.99$) (Fig. 2B). Chronic sildenafil was effective against mechanical hypersensitivity at doses 0.02 mg/kg ($F_{15,100} = 4.03$, $p < 0.01$), 0.01 mg/kg ($F_{21,198} = 6.51$, $p < 0.001$) and down to 0.0075 mg/kg ($F_{15,110} = 3.77$, $p < 0.01$), but not at 0.005 mg/kg ($F_{24,110} = 0.53$, $p = 0.72$) (Fig. 2C).

3.3. The opioid system is necessary for PDE4i and PDE5i antiallodynic action

Since the presence of opioid receptors has been shown to be necessary to the antiallodynic action of antidepressant drugs (Benbouzid et al., 2008a; Kremer et al., 2016, 2018) and of agonists of β_2 adrenoceptors (Choucair-Jaafar et al., 2014; Yalcin et al., 2010), we tested whether opioid receptors also contributed to PDE4i and PDE5i antiallodynic action. For this, we used mice deficient for MOR, DOR and

KOR, and opioid receptor antagonists (Fig. 3A).

The antiallodynic action (area under the curve over 9 days) of repeated treatment with rolipram (0.5 mg/kg, s.c. twice a day) ($F_{3,23} = 19.13$, $p < 0.01$) was similar between WT, MOR^{-/-} and KOR^{-/-} mice, while rolipram lost its action in DOR^{-/-} mice (Fig. 3B). Likewise, pharmacological antagonism of DOR by naltrindole 5 mg/kg acutely reversed the therapeutic effect of chronic rolipram ($F_{2,14} = 97.9$, $p < 0.01$), while there was no relapse following the acute administration of a MOR antagonist, naloxonazine 30 mg/kg ($F_{2,14} = 2.16$, $p = 0.7$) (Fig. 3C). While only DOR appeared critical to rolipram antiallodynic action, the situation differed for sildenafil. Indeed, sildenafil (0.01 mg/kg, s.c. twice a day) (area under the curve over 6 days; $F_{3,16} = 27.26$, $p < 0.001$) failed to impact mechanical hypersensitivity in MOR^{-/-} mice as well as in DOR^{-/-} mice, whereas allodynia relief was observed in WT and KOR^{-/-} (Fig. 3D). In agreement, relief of mechanical hypersensitivity by chronic sildenafil was acutely reversed by an injection of either naloxonazine ($F_{6,39} = 21.71$, $p < 0.001$) or naltrindole ($F_{6,39} = 16.74$, $p < 0.001$) (Fig. 3E).

3.4. Neuronal PDE4B and non-neuronal PDE4D/4B are implicated in rolipram action

We then further explored the mechanism of the PDE4i rolipram, with the hypothesis that it may share mechanistic features with antidepressant treatment of neuropathic pain (Bohren et al., 2013; Kremer et al., 2018). Using calcium imaging on lumbar dorsal root ganglia, we observed an increased proportion of neurons (19% vs. 7.2%; $p = 0.017$) and of non-neuronal cells (32% vs. 5.2%; $p = 0.0389$) responding to rolipram at very high dose (100 μ M) in the dorsal root ganglia of mice with peripheral nerve injury (Fig. 4A and B). A dose-response study, however, supports the idea that non-neuronal cells were preferential targets. Indeed, the neuronal response disappeared at lower doses (1.4% at 10 μ M; 4.7% at 1 μ M; $p < 0.01$ vs. 100 μ M in both cases); whereas the proportion of responding non-neuronal cells remained similar at 1 μ M (32% at 10 μ M; 25% at 1 μ M; $p > 0.05$ vs. 100 μ M in both cases) (Fig. 4C). To test whether responses to rolipram depended on extracellular calcium, we used a calcium-free medium. This led to a dramatic decrease in the proportion of responding cells (rolipram 100 μ M: neurons: 2.6% vs. 16.5%, $p = 0.0055$; non-neuronal cells: 5.4% vs. 21.9%, $p = 0.0051$) (Fig. 4D).

PDE4 is a family of proteins encoded by 4 different genes. Antidepressant's action in neuropathic pain depends on β_2 -adrenoceptors (Bohren et al., 2013; Kremer et al., 2018; Yalcin et al., 2009a, 2009b), and cAMP regulation downstream of β_2 -adrenoceptors has been preferentially associated with *Pde4b* and *Pde4d*. We thus used siRNA to selectively knockdown these genes in dorsal root ganglia cell cultures from mice with peripheral nerve injury. The selectivity of siRNA approach was controlled by RT-qPCR (*Pde4b*: $F_{3,16} = 40.09$, $p < 0.0001$. *Pde4d*: $F_{3,15} = 99.54$, $p < 0.0001$) (Fig. 4E). The neuronal response present at a very high concentration of rolipram (100 μ M) was prevented by *Pde4b* (5.8% vs. 14.2%; $p = 0.036$) but not *Pde4d* siRNA (Fig. 4F); while both *Pde4b* ($p = 0.0136$) and *Pde4d* ($p = 0.048$) contributed to the response of non-neuronal cells at low rolipram concentration (1 μ M) (Fig. 4F).

3.5. The PDE4i rolipram decreases TNF α expression in mouse dorsal root ganglia and human peripheral blood mononuclear cells (PBMCs)

The antiallodynic action of chronic antidepressant treatment relies on an inhibition of neuropathy-induced neuroimmune mechanisms, including the inhibition of dorsal root ganglia TNF α production (Bohren et al., 2013; Kremer et al., 2018). This indirect anti-TNF α action depends upon β_2 adrenoceptors (Bohren et al., 2013). We thus tested whether chronic rolipram action would impact this cytokine levels. Our results confirmed that peripheral nerve injury increased levels of membrane-bound TNF α (mTNF α) in dorsal root ganglia and chronic

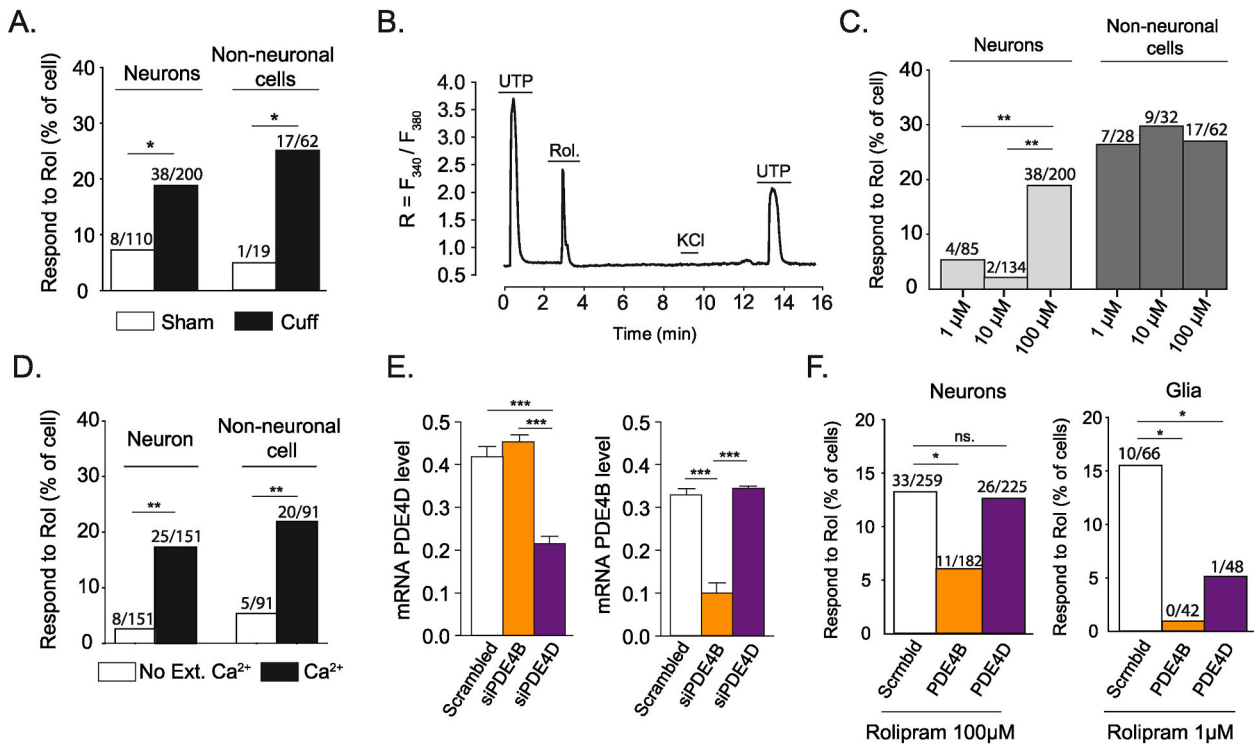


Fig. 4. PDE4B and PDE4D are main targets of rolipram in dorsal root ganglia. For all calcium imaging data, the numbers of responding cells and of analyzed cells are indicated over bars; the number of animals is detailed below. (A) Rolipram at 100 μM increased intracellular calcium concentration in dorsal root ganglia neurons and non-neuronal cells from mice with peripheral nerve injury ($n = 10\text{--}12$ mice/group; Fisher's exact test: $*p < 0.05$). (B) Representative trace showing a non-neuronal cell responding to an application of UTP while no change in intracellular calcium was observed after application of 50 mM KCl. (C) Rolipram induced a calcium response at 100 μM , but not at 10 or 1 μM in neurons ($n = 3$ mice/group; Fisher's exact test: $**p < 0.01$), while a similar proportion of non-neuronal cells responded at the 3 doses. (D) Rolipram-induced calcium response was dependent on extracellular calcium. ($n = 4$ mice/group; Fisher's exact test, $**p < 0.01$). (E) RT-qPCR analysis confirmed siRNA selectivity for *Pde4b* and *Pde4d* (post-hoc: $****p < 0.0001$). (F) *In vitro* treatment with siRNA targeting *Pde4b* and *Pde4d* abolished calcium responses in non-neuronal cells (Fisher's exact test, $*p < 0.05$), while only *Pde4b* influenced neuronal response at a high dose of rolipram (Fisher's exact test, $*p < 0.05$). Rol, rolipram; Scrambl, scrambled control; UTP, uridine-5'-triphosphate.

rolipram (0.5 mg/kg, s.c. twice a day) suppressed this overexpression ($H_{2,18} = 9.36$, $p = 0.0039$) (Fig. 5A and B). We then tested rolipram action on TNF α production in human PBMCs stimulated with LPS. Rolipram blocked TNF α release from PBMCs in a dose-dependent manner with an IC_{50} of 133 nM (Fig. 5C).

4. Discussion

The present study demonstrates that a long-term treatment with non-

selective PDEis, as well as PDE4i and PDE5i, alleviates mechanical hypersensitivity in a dose-dependent manner in a model of peripheral nerve injury. This action requires the endogenous opioid system. For PDE4i, we show that rolipram preferentially recruits dorsal root ganglia non-neuronal cells, acting through both PDE4B and PDE4D, and reverses TNF α overexpression.

Among all the PDEis tested in this study, only PDE4i and PDE5i reversed mechanical hypersensitivity in the model of peripheral nerve injury induced by sciatic nerve cuffing in mice. The selective PDE4i

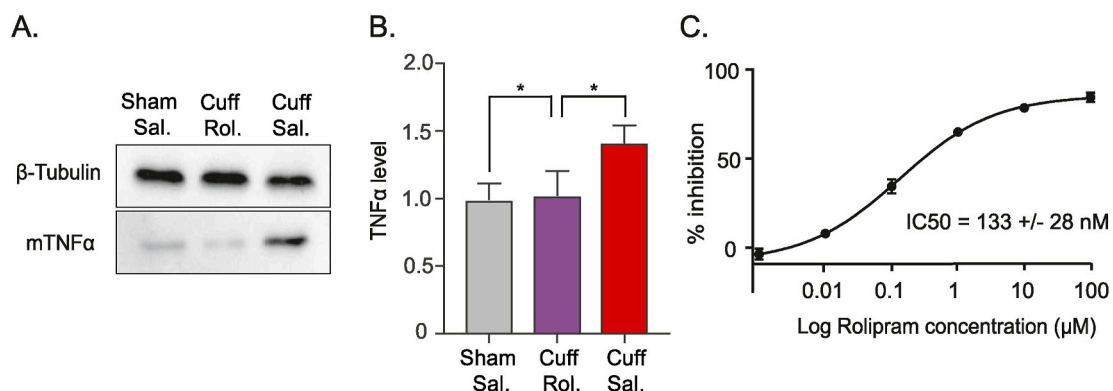


Fig. 5. Rolipram decreases TNF α production in mouse dorsal root ganglia and in human peripheral blood mononuclear cells (PBMCs). (A,B) Membrane-bound TNF α (mTNF α) expression increased in the lumbar dorsal root ganglia of mice with peripheral nerve injury, which was reversed by chronic rolipram (0.5 mg/kg, s.c. twice a day) treatment ($n = 6$ /group; post-hoc: $*p < 0.05$). Rol, rolipram; Sal, saline. (C) In human PBMC, rolipram inhibited TNF α secretion induced by LPS in a dose-dependent manner ($\text{IC}_{50} = 133$ nM).

rolipram has been shown to also be acutely effective in a model of chemotherapy-induced peripheral neuropathy (Kim et al., 2017). However, the dose necessary to obtain such acute and transient action was high (3 mg/kg), which would question the therapeutic potential. In the present study, we showed that a ten-time lower dose was able to completely suppress mechanical hypersensitivity after a twice daily treatment. It was a lasting effect as the mice were tested after an overnight delay following the previous injection. These findings suggest that a long-term treatment may be necessary to achieve disease-modifying properties. However, the present study addressed only mechanical hypersensitivity, and was conducted on male animals only. It would be of interest in future studies to also assess other nociceptive and pain-related parameters, such as thermal hypersensitivity and ongoing pain (Barthas et al., 2015; King et al., 2009), and control female response to the treatments. Sildenafil, a PDE5i, has also been shown to attenuate mechanical hypersensitivity in a model of peripheral nerve injury (Huang et al., 2010), as well as in a model of painful diabetic neuropathy (Wang et al., 2011) and of alcohol-induced neuropathy (Kaur et al., 2017). Similarly, another PDE5i, zaprinast, attenuated both mechanical and cold hypersensitivity in a model of chronic constriction injury (Rojewska et al., 2019). In agreement with those findings, we showed here that sildenafil, zaprinast, as well as MY-5445, all being selective PDE5i, suppressed mechanical hypersensitivity in mice with sciatic nerve cuffing. Interestingly, we also showed that a sustained treatment with sildenafil produced its effect at doses as low as 7.5 µg/kg, which is twenty to a hundred times lower than the doses reported in previous studies to have an acute (Vale et al., 2007) or chronic (Wang et al., 2011) action.

Experimental evidence suggests that the activation of the nitric oxide-cGMP (NO-cGMP) pathway can have both pro- and anti-nociceptive actions (Schmidtke, 2015). PDE5 is the enzyme responsible for cGMP hydrolysis and previous findings reported that spinal injection of a low dose of 8-bromo cGMP, a non-hydrolysable cGMP analog, alleviated inflammatory pain while at higher doses it aggravated hyperalgesia (Tegeader et al., 2002). High doses of NO donors activate protein kinase G, which has been proposed to underlie the pro-nociceptive effect, while the antinociceptive effect seems to be independent from this activation (Cury et al., 2011). We show here that the antiallodynic action of the PDE5i sildenafil requires both MORs and DORs. Similarly, tadalafil, another PDE5i, has been shown to display an antinociceptive action relying on both NO/cGMP pathway and opioid receptors (Mehanna et al., 2018). This is also in line with previous data showing that NO favored opioid release (Armstead, 1998). The co-requirement of MORs and DORs might reflect a sequential or parallel recruitment of separate pathways, but it could also suggest the implication of cells co-expressing both opioid receptors (Erbs et al., 2015) that have even been proposed to potentially form heterodimers (Derouiche and Massotte, 2019; Zhang et al., 2020).

DORs are necessary to the antiallodynic action of chronic treatments with antidepressant drugs (Benbouzid et al., 2008a; Ceredig et al., 2018; Choucair Jaafar et al., 2014; Kremer et al., 2016, 2018) and with β_2 adrenoceptor agonists (Ceredig et al., 2020; Choucair Jaafar et al., 2014; Kremer et al., 2020). In agreement with these findings, we found here that the action of a chronic treatment with the PDE4i rolipram on mechanical hypersensitivity also required DORs. Previous reports evidenced a prominent role of the peripheral nervous system (Bohren et al., 2013; Kremer et al., 2018), and more particularly of peripheral DORs present in dorsal root ganglia neurons expressing Nav1.8 sodium channels (Ceredig et al., 2018, 2020), in the antiallodynic effect of chronic treatments with antidepressant drugs or β_2 adrenoceptor agonists. Although the mechanistic link between β_2 adrenoceptor, PDE4i and DORs is not completely understood, data suggest that treatment with a β_2 adrenoceptor can activate the cAMP/PKA pathway and favor the release of opioid peptides from immune cells (Binder et al., 2004).

Using calcium imaging, it has been shown that the efficacy of β_2 adrenoceptor coupling to its transduction pathway was enhanced in

lumbar dorsal root ganglia under neuropathic conditions (Bohren et al., 2013). Here, we show that PDE4i dose-dependent action on intracellular free calcium concentration is also amplified in dorsal root ganglia non-neuronal cells from mice with peripheral nerve injury. Together, these findings suggest that nerve injury can sensitize the cAMP/PKA pathway (Mironov et al., 2009). Interestingly, *in vitro* low concentrations of rolipram (that are likely more relevant to the *in vivo* treatments) only activated the dorsal root ganglia non-neuronal cells, whereas higher concentrations also recruited neurons. Previous findings support a pro-nociceptive role of cAMP in neurons (Huang et al., 2012; Song et al., 2006). Indeed, increasing cAMP in neurons was shown to contribute to sensory neuron hyperexcitability and to behavioral hyperalgesia in a peripheral nerve injury model. Conversely, elevation of cAMP levels in glial cells was shown to decrease the release of pro-inflammatory cytokines such as TNF- α (Zhu et al., 2001). Interestingly, rolipram was also shown to decrease the production of TNF- α in homogenates of spinal cord, dorsal root ganglia and in activated human mononuclear cells (Guo et al., 2016; Kim et al., 2017; Pearse et al., 2004; Semmler et al., 1993). After peripheral nerve injury, a production of TNF- α has been observed in satellite glial cells of the dorsal root ganglia, which was reversed by stimulation of β_2 adrenoceptors (Bohren et al., 2013). A potential mechanism for such action could rely on the stimulation of the cAMP/PKA pathway which can inhibit I κ B α degradation, thus preventing the nuclear translocation of the nuclear factor κ B (NF κ B) and the transcription of pro-inflammatory cytokines such as TNF α (Farmer and Pugin, 2000). Here we observed that a long-term treatment with rolipram indeed decreased TNF- α levels in the dorsal root ganglia of mice with peripheral nerve injury, as well as in lipopolysaccharide-activated human PBMCs.

Rolipram provides a non-selective inhibition of the different PDE4 subtypes, which differ in their cellular and subcellular distribution (Ahmad et al., 2015; Azevedo et al., 2014; Francis et al., 2011; Johansson et al., 2012; Pérez-Torres et al., 2000; Soderling and Beavo, 2000). The PDE4B subtype has been identified in activated microglia under peripheral nerve injury condition and in bone cancer pain (Guo et al., 2016; Ji et al., 2016; Whitaker et al., 2008), and a selective knock-down of PDE4B attenuated mechanical allodynia (Ji et al., 2016). Here we showed that PDE4B seems necessary for rolipram-induced calcium release in neurons at high dose, while PDE4D and PDE4B are both important in non-neuronal cells. PDE4D is known to be associated with the β_2 adrenoceptor signaling pathway (Bruss et al., 2008), suggesting that in glial cells PDE4D could be the main enzyme responsible for the hydrolysis of cAMP upon activation of β_2 adrenoceptor.

In this study, we showed that a sustained treatment with PDE inhibitors, particularly PDE4i and PDE5i, alleviated mechanical hypersensitivity in a dose-dependent manner. These actions require components of the endogenous opioid system. Based on present findings and previous data, we propose that antidepressant drugs, β_2 adrenoceptor agonists and PDE4i could all be sharing a common mechanism contributing to the relief of mechanical hypersensitivity. This mechanism would involve cAMP signaling in non-neuronal cells of the dorsal root ganglia, inhibiting the production of TNF α . While emetic properties have limited the clinical potential of PDE4i (Li et al., 2018), the pre-clinical action of sustained treatment at low doses is interesting. Some compounds with PDE4i properties are clinically used against asthma (Ntontsi et al., 2019; Phillips, 2020), and the development of PDE4 inhibitors with improved subtype specificity (Kagayama et al., 2009), dual inhibition properties (Blöcher et al., 2018; Chlón-Rzepa et al., 2018) and/or with peripheral action may be of interest in the context of peripheral neuropathic pain.

Author contribution

MB and IY designed the study. IY performed surgeries; SM, YB and ES conducted and analyzed behavioral experiments; SH and SM performed and analyzed the imaging studies; SM and AL and VL performed

molecular analyses; PV and JJB designed, conducted and analyzed the PBMC study; SD did genotyping and animal care; SM, SJ, MB and IY wrote and revised the paper. All authors contributed to the writing of the manuscript.

Declaration of competing interest

No conflict of interest to declare.

Acknowledgement

We thank Adeline Knittel-Obrecht for her excellent technical work, and the staff from the Chronobiotron UAR3415 for animal care. This research was supported by the Centre National de la Recherche Scientifique and the Université de Strasbourg (contracts UPR3212, UMR7200, UMS3415, UMS3286), by the Neurex network (Program Interreg IV Upper Rhine), and by the Agence Nationale de la Recherche (Euridol ANR-17-EURE-0022), by the Région Grand-Est (Fonds Régional de Coopération pour la Recherche, CLueDol project) and by the CeNAF (Centre National des Associations de Fibromyalgiques). Authors declare no conflict of interest.

References

- Ahmad, F., Murata, T., Shimizu, K., Degerman, E., Maurice, D., Manganiello, V., 2015. Cyclic nucleotide phosphodiesterases: important signaling modulators and therapeutic targets. *Oral Dis.* 21 (1), e25–e50. <https://doi.org/10.1111/odi.12275>.
- Armstead, W.M., 1998. Nitric oxide contributes to opioid release from glia during hypoxia. *Brain Res.* 813 (2), 398–401. [https://doi.org/10.1016/s0006-8993\(98\)01022-1](https://doi.org/10.1016/s0006-8993(98)01022-1).
- Attal, N., 2019. Pharmacological treatments of neuropathic pain: the latest recommendations. *Rev. Neurol.* 175 (1–2), 46–50. <https://doi.org/10.1016/j.neurol.2018.08.005>.
- Attal, N., Cruccu, G., Baron, R.A., Haanpää, M., Hansson, P., Jensen, T.S., Nurmiikko, T., 2010. EFNS guidelines on the pharmacological treatment of neuropathic pain: 2010 revision. *Eur. J. Neurol.* 17 (9) <https://doi.org/10.1111/j.1468-1331.2010.02999.x>, 1113–e88.
- Azevedo, M.F., Fauz, F.R., Bimpaki, E., Horvath, A., Levy, I., de Alexandre, R.B., Ahmad, F., Manganiello, V., Stratakis, C.A., 2014. Clinical and molecular genetics of the phosphodiesterases (PDEs). *Endocr. Rev.* 35 (2), 195–233. <https://doi.org/10.1210/er.2013-1053>.
- Barber, M.J., Starmer, C.F., Grant, A.O., 1991. Blockade of cardiac sodium channels by amitriptyline and diphenhydantoin. Evidence for two use-dependent binding sites. *Circ. Res.* 69 (3), 677–696. <https://doi.org/10.1161/01.RES.69.3.677>.
- Barrot, M., 2012. Tests and models of nociception and pain in rodents. *Neuroscience* 211, 39–50. <https://doi.org/10.1016/j.neuroscience.2011.12.041>.
- Barrot, M., Yalcin, I., Choucair-Jaafar, N., Benbouzid, M., Freund-Mercier, M.J., 2009. From antidepressant drugs to beta-mimetics: preclinical insights on potential new treatments for neuropathic pain. *Recent Pat. CNS Drug Discov.* 4 (3), 182–189. <https://doi.org/10.2174/157488909789104794>.
- Barrot, M., Yalcin, I., Tessier, L.H., Freund-Mercier, M.J., 2010. Antidepressant treatment of neuropathic pain: looking for the mechanism. *Future Neurol.* 5 (2), 247–257. <https://doi.org/10.2217/fnl.09.82>.
- Barthas, F., Sellmeijer, J., Hugel, S., Waltisperger, E., Barrot, M., Yalcin, I., 2015. The anterior cingulate cortex is a critical hub for pain-induced depression. *Biol. Psychiatr.* 77, 236–245.
- Benbouzid, M., Gavériaux-Ruff, C., Yalcin, I., Waltisperger, E., Tessier, L.H., Muller, A., Kieffer, B.L., Freund-Mercier, M.J., Barrot, M., 2008a. Delta-opioid receptors are critical for tricyclic antidepressant treatment of neuropathic allodynia. *Biol. Psychiatr.* 63 (6), 633–636. <https://doi.org/10.1016/j.biopsych.2007.06.016>.
- Benbouzid, M., Pallage, V., Rajalu, M., Waltisperger, E., Doridot, S., Poisbeau, P., Freund-Mercier, M.J., Barrot, M., 2008b. Sciatic nerve cuffing in mice: a model of sustained neuropathic pain. *Eur. J. Pain* 12 (5), 591–599. <https://doi.org/10.1016/j.ejpain.2007.10.002>.
- Binder, W., Mousa, S.A., Sitte, N., Kaiser, M., Stein, C., Schäfer, M., 2004. Sympathetic activation triggers endogenous opioid release and analgesia within peripheral inflamed tissue. *Eur. J. Neurosci.* 20 (1), 92–100. <https://doi.org/10.1111/j.1460-9568.2004.03459.x>.
- Blöcher, R., Wagner, K.M., Gopireddy, R.R., Harris, T.R., Wu, H., Barnych, B., Hwang, S. H., Xiang, Y.K., Proschak, E., Morisseau, C., Hammock, B.D., 2018. Orally available soluble epoxide hydrolase/phosphodiesterase 4 dual inhibitor treats inflammatory pain. *J. Med. Chem.* 61 (8), 3541–3550. <https://doi.org/10.1021/acs.jmedchem.7b01804>.
- Bobon, D., Breulet, M., Gerard-Vandenhove, M.A., Guiot-Goffioul, F., Plomteux, G., Sastre-y-Hernandez, M., Schratz, M., Troisfontaines, B., Von Frenckell, R., Wachtel, H., 1988. Is Phosphodiesterase inhibition a new mechanism of antidepressant action? *Eur. Arch. Psychiatry Neurol. Sci.* 238 (1), 2–6. <https://doi.org/10.1007/bf00381071>.
- Bohren, Y., Karavelic, D., Tessier, L.H., Yalcin, I., Gavériaux-Ruff, C., Kieffer, B.L., Freund-Mercier, M.J., Barrot, M., 2010. Mu-opioid receptors are not necessary for nortriptyline treatment of neuropathic allodynia. *Eur. J. Pain* 14 (7), 700–704. <https://doi.org/10.1016/j.ejpain.2009.11.014>.
- Bohren, Y., Tessier, L.H., Megat, S., Petitjean, H., Hugel, S., Daniel, D., Kremer, M., Fournel, S., Hein, L., Schlichter, R., Freund-Mercier, M.J., 2013. Antidepressants suppress neuropathic pain by a peripheral β 2-adrenoceptor mediated anti-TNF α mechanism. *Neurobiol. Dis.* 60, 39–50. <https://doi.org/10.1016/j.nbd.2013.08.012>.
- Bollenbach, M., Lugnier, C., Kremer, M., Salvat, E., Megat, S., Bihel, F., Bourguignon, J. J., Barrot, M., Schmitt, M., 2019. Design and synthesis of 3-aminophthalazine derivatives and structural analogues as PDE5 inhibitors: anti-allodynic effect against neuropathic pain in a mouse model. *Eur. J. Med. Chem.* 177, 269–290. <https://doi.org/10.1016/j.ejmech.2019.05.026>.
- Bruss, M.D., Richter, W., Horner, K., Jin, S.L.C., Conti, M., 2008. Critical role of PDE4D in beta2-adrenoceptor-dependent cAMP signaling in mouse embryonic fibroblasts. *J. Biol. Chem.* 283 (33), 22430–22442. <https://doi.org/10.1074/jbc.m803306200>.
- Ceredig, R.A., Pierre, F., Doridot, S., Alduntzin, U., Salvat, E., Yalcin, I., Gavériaux-Ruff, C., Barrot, M., Massotte, D., 2018. Peripheral delta opioid receptors mediate duloxetine antiallodynic effect in a mouse model of neuropathic pain. *Eur. J. Neurosci.* 48 (5), 2231–2246. <https://doi.org/10.1111/ejn.14093>.
- Ceredig, R.A., Pierre, F., Doridot, S., Alduntzin, U., Hener, P., Salvat, E., Yalcin, I., Gavériaux-Ruff, C., Barrot, M., Massotte, D., 2020. Peripheral delta opioid receptors mediate formoterol anti-allodynic effect in a mouse model of neuropathic pain. *Front. Mol. Neurosci.* 12, 324. <https://doi.org/10.3389/fnmol.2019.00324>.
- Choiñ-Rzepa, G., Ślusarczyk, M., Jankowska, A., Gawalska, A., Bucki, A., Kotaczkowski, M., Świerczek, A., Pocięcha, K., Wyska, E., Zygmunt, M., Kazek, G., Sałat, K., Pawłowski, M., 2018. Novel amide derivatives of 1, 3-dimethyl-2, 6-dioxopurin-7-yl-alkylcarboxylic acids as multifunctional TRPA1 antagonists and PDE4/7 inhibitors: a new approach for the treatment of pain. *Eur. J. Med. Chem.* 158, 517–533. <https://doi.org/10.1016/j.ejmech.2018.09.021>.
- Choucair-Jaafar, N., Salvat, E., Freund-Mercier, M.J., Barrot, M., 2014. The antiallodynic action of nortriptyline and terbutaline is mediated by β 2adrenoceptors and δ opioid receptors in the ob/ob model of diabetic polyneuropathy. *Brain Res.* 1546, 18–26. <https://doi.org/10.1016/j.brainres.2013.12.016>.
- Choucair-Jaafar, N., Yalcin, I., Rodeau, J.L., Waltisperger, E., Freund-Mercier, M.J., Barrot, M., 2009. β 2-Adrenoceptor agonists alleviate neuropathic allodynia in mice after chronic treatment. *Br. J. Pharmacol.* 158 (7), 1683–1694. <https://doi.org/10.1111/j.1476-5381.2009.00510.x>.
- Christiansen, S.H., Selige, J., Dunkern, T., Rassov, A., Leist, M., 2011. Combined anti-inflammatory effects of β 2-adrenergic agonists and PDE4 inhibitors on astrocytes by upregulation of intracellular cAMP. *Neurochem. Int.* 59 (6), 837–846. <https://doi.org/10.1016/j.neuint.2011.08.012>.
- Cury, Y., Picolo, G., Gutierrez, V.P., Ferreira, S.H., 2011. Pain and analgesia: the dual effect of nitric oxide in the nociceptive system. *Nitric Oxide - Biol Chem* 25 (3), 243–254. <https://doi.org/10.1016/j.niox.2011.06.004>.
- Derouiche, L., Massotte, D., 2019. G protein-coupled receptor heteromers are key players in substance use disorder. *Neurosci. Biobehav. Rev.* 106, 73–90. <https://doi.org/10.1016/j.neubiorev.2018.09.026>.
- Erbs, E., Faget, L., Scherrer, G., Matifas, A., Filliol, D., Vonesch, J.L., Koch, M., Kessler, P., Hentsch, D., Birling, M.C., Koutsourakis, M., Vasseur, L., Veinante, P., Kieffer, B.L., Massotte, D., 2015. A mu-delta opioid receptor brain atlas reveals neuronal co-occurrence in subcortical networks. *Brain Struct. Funct.* 220 (2), 677–702. <https://doi.org/10.1007/s00429-014-0717-9>.
- Farmer, P., Pugin, J., 2000. beta-adrenergic agonists exert their “anti-inflammatory” effects in monocytic cells through the I κ B/NF- κ B pathway. *Am. J. Physiol. Lung Cell Mol. Physiol.* 279 (4), L675–L682. <https://doi.org/10.1152/ajplung.2000.279.4.l675>.
- Filliol, D., Ghozland, S., Chluba, J., Martin, M., Matthes, H.W., Simonin, F., Befort, K., Gavériaux-Ruff, C., Dierich, A., LeMeur, M., Valverde, O., Maldonado, R., Kieffer, B. L., 2000. Mice deficient for δ - and μ -opioid receptors exhibit opposing alterations of emotional responses. *Nat. Genet.* 25 (2), 195–200. <https://doi.org/10.1038/76061>.
- Francis, S.H., Blount, M.A., Corbin, J.D., 2011. Mammalian cyclic nucleotide phosphodiesterases: molecular mechanisms and physiological functions. *Physiol. Rev.* 91 (2), 651–690. <https://doi.org/10.1152/physrev.00030.2010>.
- Francis, S.H., Turko, I.V., Corbin, J.D., 2001. Cyclic nucleotide phosphodiesterases: relating structure and function. *Prog. Nucleic Acid Res. Mol. Biol.* 1–52. [https://doi.org/10.1016/s0079-6603\(00\)65001-8](https://doi.org/10.1016/s0079-6603(00)65001-8).
- Friebe, A., Sandner, P., Schmidtke, A., 2020. cGMP: a unique 2nd messenger molecule—recent developments in cGMP research and development. *N-S Arch Pharmacol* 393 (2), 287–302. <https://doi.org/10.1007/s00210-019-01779-z>.
- Gancedo, J.M., 2013. Biological roles of cAMP: variations on a theme in the different kingdoms of life. *Biol. Rev.* 88 (3), 645–668. <https://doi.org/10.1111/brv.12020>.
- Guo, C.H., Bai, L., Wu, H.H., Yang, J., Cai, G.H., Wang, X., Wu, S.X., Ma, W., 2016. The analgesic effect of rolipram is associated with the inhibition of the activation of the spinal astrocytic JNK/CCL2 pathway in bone cancer pain. *Int. J. Mol. Med.* 38 (5), 1433–1442. <https://doi.org/10.3892/ijmm.2016.2763>.
- Houël, E., Fleury, M., Odonne, G., Nardella, F., Bourdy, G., Vonthron-Sénécheau, C., Villa, P., Obrecht, A., Eparvier, V., Deharo, E., Stien, D., 2015. Antiplasmodial and anti-inflammatory effects of an antimalarial remedy from the Wayana Amerindians, French Guiana: takamalaimé (Psidium acutangulum Mart. Ex DC., Myrtaceae). *J. Ethnopharmacol.* 166, 279–285. <https://doi.org/10.1016/j.jep.2015.03.015>.
- Houslay, M.D., 2010. Underpinning compartmentalised cAMP signalling through targeted cAMP breakdown. *Trends Biochem. Sci.* 35 (2), 91–100. <https://doi.org/10.1016/j.tibs.2009.09.007>.


- Yalcin, I., Tessier, L.H., Petit-Demoulière, N., Waltisperger, E., Hein, L., Freund-Mercier, M.J., Barrot, M., 2010. Chronic treatment with agonists of β 2-adrenergic receptors in neuropathic pain. *Exp. Neurol.* 221 (1), 115–121. <https://doi.org/10.1016/j.expneurol.2009.10.008>.
- Yalcin, I., Megat, S., Barthas, F., Waltisperger, E., Kremer, M., Salvat, E., Barrot, M., 2014. The sciatic nerve cuffing model of neuropathic pain in mice. *JoVE* 89. <https://doi.org/10.3791/51608>.
- Ye, Y., Conti, M., Houslay, M.D., Farooqui, S.M., Chen, M., O'Donnell, J.M., 1997. Noradrenergic activity differentially regulates the expression of rolipram-sensitive, high-Affinity cyclic AMP phosphodiesterase (PDE4) in rat brain. *J. Neurochem.* 69 (6), 2397–2404. <https://doi.org/10.1046/j.1471-4159.1997.69062397.x>.
- Zhang, H.T., Whisler, L.R., Huang, Y., Xiang, Y., O'donnell, J.M., 2009. Postsynaptic α -2 adrenergic receptors are critical for the antidepressant-like effects of desipramine on behavior. *Neuropsychopharmacology* 34 (4), 1067–1077. <https://doi.org/10.1038/npp.2008.184>.
- Zhang, L., Zhang, J.T., Hang, L., Liu, T., 2020. Mu opioid receptor heterodimers emerge as novel therapeutic targets: recent progress and future perspective. *Front. Pharmacol.* 11, 1078. <https://doi.org/10.3389/fphar.2020.01078>.
- Zhu, J., Mix, E., Winblad, B., 2001. The antidepressant and antiinflammatory effects of rolipram in the central nervous system. *CNS Drug Rev.* 7 (4), 387–398. <https://doi.org/10.1111/j.1527-3458.2001.tb00206.x>.

The basolateral amygdala-anterior cingulate pathway contributes to depression-like behaviors and comorbidity with chronic pain behaviors in male mice

Received: 24 July 2022

Accepted: 3 April 2023

Published online: 17 April 2023

 Check for updates

Léa J. Becker^{1,9}, Clémentine Fillinger¹, Robin Waegaert¹, Sarah H. Journée¹, Pierre Hener¹, Beyza Ayazgok^{1,2,10}, Muris Humo^{1,10}, Meltem Karatas^{1,3,10}, Maxime Thouaye¹, Mithil Gaikwad^{1,4}, Laetitia Degiorgis³, Marie des Neiges Santin³, Mary Mondino³, Michel Barrot¹, El Chérif Ibrahim⁵, Gustavo Turecki⁶, Raoul Belzeaux^{5,7}, Pierre Veinante¹, Laura A. Harsan³, Sylvain Hugel¹, Pierre-Eric Lutz^{1,8,11} & Ipek Yalcin^{1,4,11} ✉

While depression and chronic pain are frequently comorbid, underlying neuronal circuits and their psychopathological relevance remain poorly defined. Here we show in mice that hyperactivity of the neuronal pathway linking the basolateral amygdala to the anterior cingulate cortex is essential for chronic pain-induced depression. Moreover, activation of this pathway in naive male mice, in the absence of on-going pain, is sufficient to trigger depressive-like behaviors, as well as transcriptomic alterations that recapitulate core molecular features of depression in the human brain. These alterations notably impact gene modules related to myelination and the oligodendrocyte lineage. Among these, we show that *Sema4a*, which was significantly upregulated in both male mice and humans in the context of altered mood, is necessary for the emergence of emotional dysfunction. Overall, these results place the amygdalo-cingulate pathway at the core of pain and depression comorbidity, and unravel the role of *Sema4a* and impaired myelination in mood control.

Major depressive disorder (MDD) and chronic pain are long-lasting detrimental conditions that significantly contribute to the worldwide burden of disease^{1,2}. These two pathologies are highly comorbid, which results in increased disability and poorer prognosis compared to either condition alone^{3,4}. Despite their high prevalence and co-occurrence,

available treatments remain ineffective, urging for a better understanding of their pathophysiological convergence.

The frontal cortex, particularly the anterior cingulate cortex (ACC), is at the center of emotional and pain processing⁵. A large body of evidence documents major alterations in ACC neuronal activity in

¹Centre National de la Recherche Scientifique, Université de Strasbourg, Institut des Neurosciences Cellulaires et Intégratives, Strasbourg, France.

²Department of Biochemistry, Faculty of Pharmacy, University of Hacettepe, Ankara, Turkey. ³Laboratory of Engineering, Informatics and Imaging (ICube), Integrative multimodal imaging in healthcare (IMIS), CNRS, UMR 7357, University of Strasbourg, Strasbourg, France. ⁴Department of Psychiatry and Neuroscience, Université Laval, Québec, QC G1V 0A6, Canada. ⁵Aix-Marseille Univ, CNRS, INT, Inst Neurosci Timone, Marseille, France. ⁶Department of Psychiatry, McGill University and Douglas Mental Health University Institute, Montreal, QC, Canada. ⁷Department of Psychiatry, CHU de Montpellier, Montpellier, France. ⁸Douglas Mental Health University Institute, Montreal, QC, Canada. ⁹Present address: Department of Anesthesiology, Center for Clinical Pharmacology Washington University in St. Louis, St. Louis, MO, USA. ¹⁰These authors contributed equally: Beyza Ayazgok, Muris Humo, Meltem Karatas. ¹¹These authors jointly supervised this work: Pierre-Eric Lutz, Ipek Yalcin. ✉e-mail: yalcin@inci-cnrs.unistra.fr

patients with either chronic pain or MDD, as well as in rodent models of each condition^{6–9}. Among other findings, our group previously showed that a lesion¹⁰ or the optogenetic inhibition¹¹ of the ACC alleviates anxiodepressive-like consequences of neuropathic pain in mice, while activation of this structure is sufficient to trigger emotional dysfunction in naive animals. These results highlight a critical role of the ACC in the comorbidity between pain and MDD. However, the mechanisms priming ACC dysfunction remain poorly understood.

MDD originates from alterations affecting both the subcortical processing of external and internal stimuli, and their integration into perceived emotions by higher-level cortical structures¹². It is, therefore, critical to understand how subcortical inputs to the ACC contribute to the emergence of emotional dysfunction. Among these, the anterior part of the basolateral nucleus of the amygdala (BLA) shows dense, direct and reciprocal connections with areas 24a/b of the ACC^{13,14}, which have been poorly studied in animal models of pain and mood disorders. The BLA plays a critical role in emotional processes, since its neurons encode stimulus with a positive valence, such as rewards^{15,16}, as well as those with a negative valence, including fear¹⁶ or pain states¹⁷. In humans, neuroimaging studies have consistently found that depressed patients^{7,18} and individuals suffering from chronic pain^{6,19} exhibit pathological ACC and BLA hyperactivity.

In this context, we hypothesized that the neuronal pathway linking the BLA and the ACC might represent a core substrate underlying the comorbidity between pain and MDD. First, using retrograde tracing and neuronal activity markers, as well as rodent brain functional magnetic resonance imaging (MRI), we demonstrate that this pathway is hyperactive when chronic pain triggers depressive-like behaviors. Then, by optogenetically manipulating this circuit, we show that its hyperactivity is both necessary for neuropathic pain-induced depressive-like (NPID) behaviors, and sufficient to trigger similar deficits in naive animals, in the absence of chronic pain-like behavior. We next characterize transcriptomic changes occurring in the ACC when BLA–ACC hyperactivity triggers mood dysfunction, and find that they strikingly resemble the molecular blueprint of depression in humans. These results, which notably include alterations affecting oligodendrocytes and myelination, are coherent with our mouse imaging data showing altered tissue anisotropy along the BLA–ACC pathway, and establish the translational relevance of our BLA–ACC optogenetic model of MDD. Finally, we leverage gene-network approaches to prioritize *Semaphorin 4a* (*Sema4a*) as a gene significantly upregulated in both mice and humans in the context of altered mood. Using a gene knockdown approach, we demonstrate that, following optogenetic BLA–ACC stimulation, upregulation of *Sema4a* is necessary for the emergence of depressive-like behaviors. Overall, these results uncover the BLA–ACC pathway as a core substrate of pain and MDD comorbidity.

Results

Chronic neuropathic pain induces hyperactivity in the BLA–ACC pathway

To confirm the anatomical connection between the BLA and ACC, we first injected the retrograde tracer cholera toxin subunit B (CTB) into the areas 24a/b of the ACC (Fig. 1a). Consistent with previous reports, strongly labeled cell bodies were found in the BLA (Fig. 1b)^{13,20,21}. Next, considering that we¹¹, and others^{5,8,22}, have found that the ACC is hyperactive when chronic pain triggers depressive-like behaviors, we wondered whether the BLA is similarly affected. To address this question, we quantified the immediate early gene c-Fos in our well-characterized NPID model^{23,24}. In this model, right-sided peripheral nerve injury leads to immediate and long-lasting mechanical hypersensitivity, with delayed anxiodepressive-like behaviors (significant at 7 weeks post-operation, PO; Fig. 1c–f). In our previous study, increased c-Fos immunoreactivity was found in the ACC at 8 weeks PO²⁵. Here, a similar c-Fos increase was found in the BLA (Supplementary Fig. 1a, b).

This indicates concurrent neuronal hyperactivity of the two structures when anxiodepressive-like behaviors are present. Next, we studied whether these c-Fos positive cells in the BLA directly innervate the ACC (Fig. 1g). The retrograde tracer fluorogold (FG) was injected into the ACC of neuropathic animals, and we quantified its co-localization with c-Fos in the BLA at 8 weeks PO (Fig. 1c). Similar numbers of BLA neurons projecting to the ACC (FG+) were found in both sham and NPID groups, indicating that neuropathic pain does not modify the number of neurons in this pathway (Fig. 1h, i). Compared to shams, an increase in the total number of c-Fos+ cells was observed in the ipsilateral, but not in the contralateral, BLA of NPID mice (Fig. 1j, k), confirming results from our previous cohort (Supplementary Fig. 1a, b). Importantly, this neuronal hyperactivity in the NPID group notably concerned neurons that project to the ACC, as shown by an increase in cells positive for both FG and c-Fos (Fig. 1m, n) in the BLA ipsilateral to nerve injury. Again, no change was observed in the contralateral BLA (Fig. 1l). While similar lateralization has already been reported in the central amygdala during chronic pain^{26,27}, especially at a later timepoint²⁸, our results extend these findings to the BLA in the context of NPID. Also, a recent systematic review of 70 human imaging studies further supports our observation, as pain concomitant with depression was found to strongly associate with enhanced connectivity of the right amygdala, particularly with the prefrontal cortex²⁹. Finally, as a complementary strategy to assess the connectivity of the ACC and the BLA, we took advantage of imaging data recently generated in our NPID model using resting-state functional Magnetic Resonance Imaging (rs-fMRI). Consistent with above histological analyses, we observed that functional connectivity between the two structures was enhanced at 8, but not 2, weeks PO in NPID animals compared to sham controls (Fig. 1o and Supplementary Fig. 1c, d for behavioral characterization). Altogether, these results indicate that chronic pain induces hyperactivity of BLA neurons projecting to the ACC.

Optogenetic inhibition of the BLA–ACC pathway prevents NPID

We next hypothesized that this hyperactivity may be responsible for emotional dysfunction. To address this, we inhibited the pathway using an AAV5-CamKIIa-ArchT3.0-EYFP vector injected bilaterally in the BLA (Fig. 2a, b). To characterize the effects of green light illumination on BLA neurons, we performed ex vivo electrophysiological recordings 6 weeks after viral injection (Fig. 2c). Patch-clamp recordings at the level of the BLA showed that light stimulation resulted in neuronal inhibition, proportional to light intensity, as indicated by outward currents recorded in voltage-clamp mode (Fig. 2d, e).

To assess behavioral effects of inhibiting the BLA–ACC pathway during NPID, the same viral vector was injected bilaterally in the BLA, followed by implantation of an optic fiber in the ACC, to specifically inhibit axon terminals coming from the BLA (Fig. 2f; for BLA viral injection localization, see Supplementary Fig. 2a). Acute inhibition did not impact mechanical thresholds, measured using von Frey filaments, in sham (Supplementary Fig. 2b, c) or nerve-injured animals at either 3 or 6 weeks PO (Fig. 2g, h). The BLA–ACC pathway is, therefore, not essential for mechanical hypersensitivity, consistent with what several groups reported when manipulating the whole ACC^{10,30–32}. Likewise, the BLA–ACC pathway does not drive ongoing pain-like behavior, since we did not observe any significant conditioned place preference (CPP) during optogenetic inhibition (Fig. 2i). Inhibiting the whole ACC was however sufficient to induce CPP in our previous work¹¹. Therefore, modulation of pain states by the ACC likely relies on other afferent structures than the BLA³³.

We next assessed the effect of inhibiting the BLA–ACC pathway on anxiodepressive-like behaviors. Optogenetic inhibition was applied just before (for light/dark, LD, and forced swim tests, FST) or during (splash test, ST) behavioral testing. As expected, NPID animals displayed significantly higher anxiety-like behaviors in the LD at 7 weeks PO (Fig. 2j), as well as higher depressive-like behaviors at 8 weeks PO

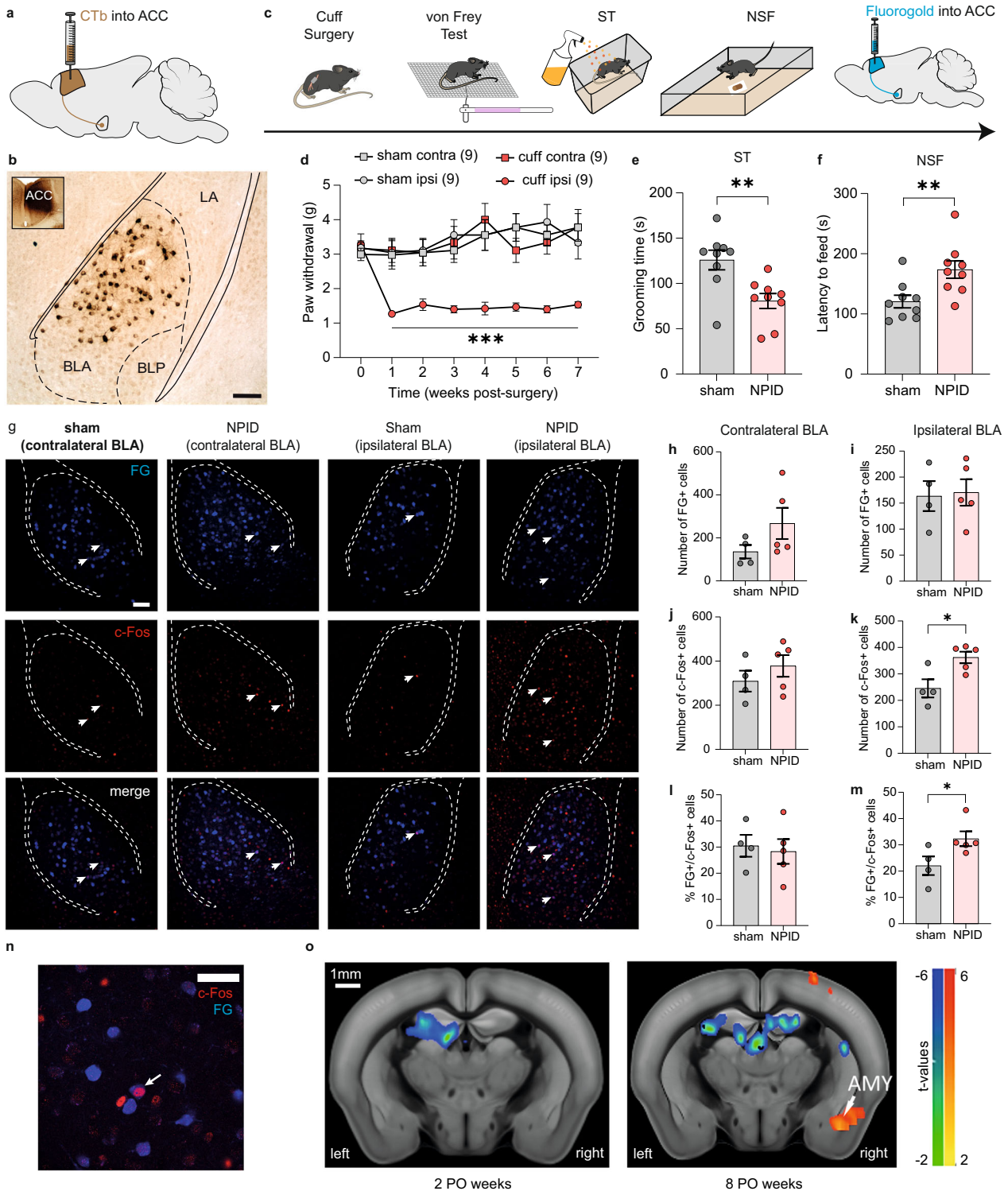


(Fig. 2k, l) in both the ST and FST^{11,24}. Inhibiting the BLA–ACC pathway had no impact in the LD test, suggesting that other pathways may control anxiety-like consequences of chronic pain. In contrast, BLA–ACC inhibition completely reversed pain-induced decreased grooming in the ST (Fig. 2k), and significantly decreased immobility in the FST (Fig. 2l), revealing potent antidepressant-like effects. No effect of optogenetic inhibition was observed in sham animals, indicating that these antidepressant-like effects selectively manifest in the context of chronic pain. As a more general measure of emotionality³⁴, we also calculated z-scores for each animal across all three tests (LD, ST, FST). Results indicated that NPID mice showed global emotional deficit

compared to sham controls, as indicated by lower z-scores, an effect that was prevented by inhibition of the BLA–ACC pathway (Supplementary Fig. 2d). Overall, these results demonstrate that hyperactivity of BLA neurons targeting the ACC is necessary for the selective expression of chronic pain-induced depressive-like behaviors.

Repeated activation of the BLA–ACC pathway triggers depressive-like behaviors in naive mice

We next determined whether BLA–ACC hyperactivity is sufficient to induce depressive-like behaviors in naive mice, in the absence of neuropathic pain. An AAV5-CamKIIa-ChR2-EYFP vector was injected

Fig. 1 | Neuropathic pain-induced depression (NPID) triggers hyperactivity in BLA neurons projecting to the ACC and increases functional connectivity between the ACC and BLA.

a Retrograde tracing strategy, with the injection of the cholera toxin B subunit (CTB) into the anterior cingulate cortex (ACC).

b Representative image of retrogradely labeled cell bodies in the anterior part of the basolateral nucleus of the amygdala (BLA). Scale bar = 100 μ m. c Experimental design for quantifying the activity of BLA neurons projecting to the ACC, during NPID. d–f Peripheral nerve injury induced an ipsilateral mechanical hypersensitivity (d; $F_{(21,224)} = 2.710$; $P < 0.0001$; post hoc 1–7 weeks $P < 0.05$), decreased grooming in the splash test (ST) (e; sham: 125.90 ± 10.80 ; NPID: 80.67 ± 8.22 ; $P = 0.0042$) and increased latency to feed in novelty-suppressed feeding (NSF) (f; sham: 120.7 ± 10.49 ; NPID: 173.7 ± 14.38 ; $P = 0.0089$) ($n = 9$ mice/group). g Representative images showing positive cells for fluorogold (FG+, upper panel), c-Fos (c-Fos+, middle), or co-labeled (bottom), in the contralateral (sham: right column; NPID: middle right) or ipsilateral BLA (sham: middle left; NPID: left). Scale bar = 100 μ m. h–m Quantification of FG+, c-Fos+ cells and their co-localization revealed that, at 8 weeks postoperative (PO), the number of FG+ cells was not altered (h);

contralateral BLA: sham: 135.8 ± 31.52 ; NPID: 267.2 ± 72.58 ; $P = 0.21$; i; ipsilateral BLA: sham: 163.5 ± 28.85 ; NPID: 170.6 ± 25.43 ; $P = 0.3651$), as well as c-Fos+ (j; sham: 309.3 ± 47.60 ; NPID: 378.2 ± 49.10 ; $P = 0.14$) and % of FG+/c-Fos+ (l; sham: 30.50 ± 4.20 ; NPID: 28.33 ± 4.72 ; $P = 0.45$) cells in the contralateral BLA. In contrast, the number of c-Fos+ (k; sham: 245.5 ± 34.37 ; NPID: 362.4 ± 21.62 ; $P = 0.0238$) and % of FG+/c-Fos+ cells (m sham 22.06 ± 3.55 ; NPID: 32.32 ± 2.81 ; $P = 0.0159$) were increased in the ipsilateral BLA (sham: $n = 4$ mice; NPID: $n = 5$ mice). n Close-up image showing the co-localization of c-Fos+ and FG+ cells. Scale bar = 20 μ m. o Inter-group statistical comparisons showed increased functional connectivity between ACC and amygdala (AMY) at 8 (right image) but not 2 (left) PO weeks. FWER corrected at cluster level for $P < 0.05$. Data are mean \pm SEM. * $P < 0.05$; ** $P < 0.01$, *** $P < 0.001$. Two-way ANOVA repeated measures (Time \times Surgery; VF); two-sided unpaired t test (ST and NSF); one-sided Mann–Whitney test (FG, c-Fos quantification). Contra contralateral, ipsi ipsilateral, BLP posterior part of the BLA, LA lateral amygdala. Sagittal mouse brain cartoons (a, c) were created with Biorender.com. Source data are provided as a Source Data file.

bilaterally in the BLA, and patch-clamp recordings confirmed that blue light stimulation (wavelength: 475 nm, pulse duration: 10 ms; frequency: 10 Hz) evoked inward currents in eYFP-expressing BLA neurons, as well as evoked excitatory postsynaptic currents in pyramidal ACC neurons (Fig. 3a–h). In the BLA, optogenetic stimulation of cell bodies induced inward currents, with a plateau reached at 40% of maximal light intensity, while pulsed 10 Hz stimulation produced strong and stable currents (Fig. 3b–d). In the ACC, stimulating BLA axon terminals induced strong inward currents, with a plateau at 80% of maximal light (Fig. 3g, h), indicating activation of ACC neurons.

Having established this stimulation protocol, we explored its behavioral impact in naive mice. An optic fiber was implanted in the ACC, and blue light pulse stimulation applied for 20 min (with parameters validated ex vivo; see Supplementary Fig. 3a for BLA viral injection localization). We first found that a single stimulation session was not sufficient to trigger any alteration in spontaneous locomotor activity, real-time place avoidance or anxiodepressive-like assays (Supplementary Fig. 3b–e). Thus, we next tested the effects of repeated stimulations over 3 consecutive days each week, during 3 weeks (Fig. 4a, b). Behavioral tests were performed at 3 timepoints (i.e. at the end of week 1, 2, or 3), following each block of three activating sessions. A subset of mice was also used to document the impact of our optogenetic stimulation on neuronal activity in vivo. To do so, a 10th session of optogenetic stimulation was applied (5 days after the 9th stimulation), followed by quantification of c-Fos immunoreactivity (90 mn post-stimulation). Results showed robust increase in c-Fos+ cells throughout the ACC (Supplementary Fig. 3f), as expected. At the behavioral level, no effect of stimulations was found on locomotor activity (Supplementary Fig. 3g) or anxiety-like behaviors (Fig. 4b, LD/NSF) at any of the 3 timepoints. This is consistent with above NPID results indicating that optogenetic inhibition of the pathway did not rescue pain-induced anxiety-like behaviors. In contrast, depressive-like behaviors progressively emerged: (i) After the first 3 stimulations, no changes were observed in ST, Nest test, or FST; (ii) After 6 stimulations, immobility in the FST significantly increased, with a tendency for decreased nest building, without significant effects in the ST; (iii) After 9 stimulations, emotional deficits further strengthened, with increased immobility in the FST accompanied by a significantly poorer nest score, along with decreased grooming in the ST (Fig. 4b). Similar to previous NPID experiments, we also computed emotionality z-score at each timepoint (Fig. 4c). Although no effect of repeated BLA–ACC activation was observed after three stimulations, emotionality z-score showed a tendency for a decrease after 6 stimulations ($P = 0.094$), which became significant after 9 stimulations, confirming the progressive emergence of emotional dysfunction. Of note, none of these behavioral effects remained detectable 1 week after the last stimulation (Supplementary Fig. 3h, i), indicating a reversible phenotype.

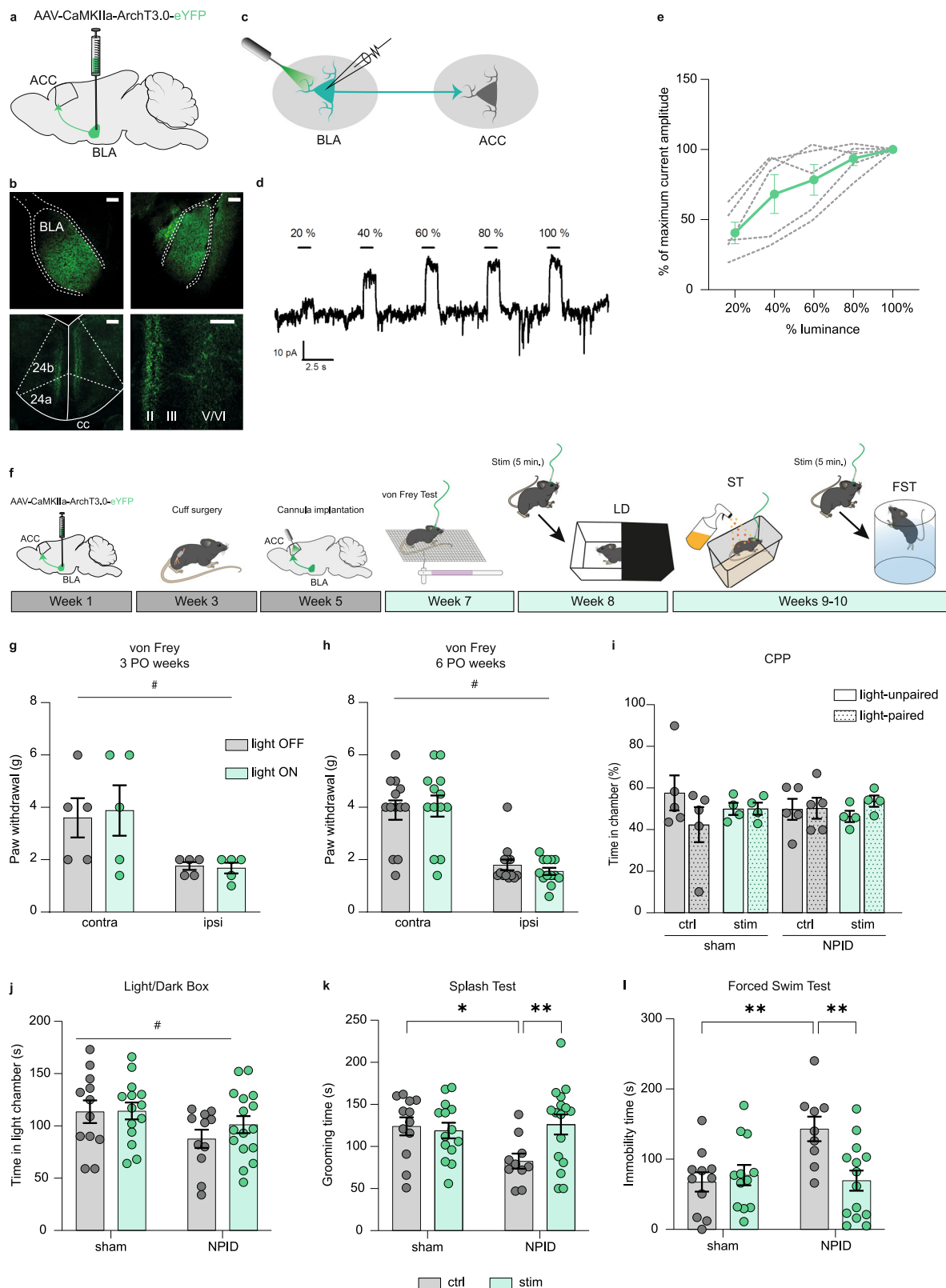
Overall, it is possible to speculate that this kinetic bears an analogy with our results in the NPID model, in which emotional deficits also progressively emerged, and required tonic hyperactivity of the BLA–ACC pathway. Compared to the human disorder, this short-lasting phenotype might be considered to model proximal causes of depression (such as environmental stressors or recent life events), which trigger acute variations in thymic states, rather than underlying endophenotypes (constitutive biological traits thought to act as distal risk factor).

To determine which neuronal cell types are recruited in the ACC by the repeated optogenetic activation paradigm, we next quantified *c-fos* expression and its co-localization with markers of excitatory (glutamatergic, *Slc17a7*) and inhibitory (GABAergic, *Gad2*) neurons, this time 48 h after the 9th stimulation, matching behavioral deficits (in the absence of any new stimulation). Repeated optogenetic activation induced a strong increase in *c-fos* expression, predominantly in glutamatergic but also in GABAergic cells (Fig. 4d, e and Supplementary Fig. 4a, b, e) of the ACC (24a/24b), while global numbers of *Gad2*+ or *Slc17a7*+ cells remained unaltered (Supplementary Fig. 4c, d). Altogether, these results show that repeated activation of the BLA–ACC pathway is sufficient to activate major neuronal cell types in the ACC, and to trigger the progressive emergence of a depressive-like phenotype.

Repeated activation of the BLA–ACC pathway produces transcriptional alterations similar to those observed in human depression

The need for repeated activations to produce behavioral effects suggests transcriptomic alterations. To understand the underlying molecular mechanisms, we used RNA Sequencing to identify gene expression changes occurring in the ACC (Supplementary Data File 1) after 9 stimulations (Fig. 5a), when behavioral deficits are maximal. We generated 2 animal cohorts ($n = 12$ controls and $n = 10$ stimulated mice in total) and, before harvesting ACC tissue, confirmed the development of depressive-like behaviors (Fig. 5b). Analysis of gene expression changes was conducted as described previously³⁵ (“Methods”). Using Principal Component Analysis, robust differences were observed across groups at the genome-wide level (Supplementary Fig. 5a). At nominal P value ($P < 0.05$), 2611 genes were significantly dysregulated in stimulated mice compared to controls, with 54 genes remaining significant after Benjamini–Hochberg correction for multiple testing (Fig. 5c). Over-Representation Analysis³⁶ (ORA) uncovered alterations in Gene Ontology (GO) terms related to myelination, dendritic transport, neurogenesis and cytoskeleton (Supplementary Data File 1 and Supplementary Fig. 5b).

To test the relevance of these data to human depression, we compared them to our recent postmortem study³⁷. In the latter, similar



RNA-Seq was used to compare ACC tissue from individuals who died during a major depressive episode ($n = 26$; Supplementary Table 1) and healthy individuals without any psychiatric history ($n = 24$). Because only males were used in our mouse paradigm, we reprocessed human data to restrict differential expression analysis to men (for a similar analysis in both sexes pooled, see Supplementary Fig. 6). We then used 3 strategies to compare men and mice, focusing on 13,572

orthologues (see “Methods” for detail). First, 398 genes were identified as differentially expressed (DEG, nominal P value < 0.05) in both species (common DEGs; Supplementary Fig. 5c). These represented 29.6% of all DEGs in mice (34.9% when considering both sex; Supplementary Fig. 6a, b), indicating robust overlap between species (Supplementary Fig. 5d). ORA performed on common DEGs revealed enrichments in GO terms related to neurogenesis, cytoskeleton or myelin sheath

Fig. 2 | Optogenetic inhibition of the BLA–ACC pathway blocks NPID.

a Graphical representation of virus delivery to the mouse BLA for voltage-clamp recordings. **b** Representative images of eYFP+ cell bodies in the BLA (upper panels) and eYFP+ axon terminals in the ACC (lower panels). Scale bars = 100 μ m. **c** Graphical representation of patch-clamp recording in the BLA. **d** Representative trace of outward currents. **e** Amplitude of currents induced by optogenetic stimulations of BLA neurons ($n = 5$ cells/2 mice, green trace = mean; gray traces = individual responses). **f** Graphical representation of the experimental design for in vivo optogenetic inhibition of the BLA–ACC pathway. **g, h** At 3 or 6 weeks PO, mechanical hypersensitivity was not affected by the inhibition of BLA–ACC pathway (ipsi vs contra; 3 PO weeks, cuff: $n = 5$ mice, $F_{(1,4)} = 7.752$; $P = 0.0496$; 6 PO weeks, cuff: $n = 13$ mice $F_{(1,12)} = 55.80$; $P < 0.0001$; light-off vs light-on; 3 PO weeks $F_{(1,4)} = 0.669$; $P = 0.4592$; 6 PO weeks $F_{(1,12)} = 2.971$; $P = 0.1104$). **i** Optogenetic inhibition of the BLA–ACC pathway did not induce a place preference at 6 weeks PO (sham-ctrl: $n = 5$ mice; sham-stim: $n = 4$ mice; NPID-ctrl: $n = 5$; NPID-stim: $n = 4$ mice; $F_{(3,13)} = 0.153$; $P = 0.9998$). **j** At 7 weeks PO, BLA–ACC inhibition had no effect on the

decrease in time spent in the lit chamber observed in nerve-injured animals (sham-ctrl: $n = 12$ mice; sham-stim: $n = 14$ mice; NPID-ctrl: $n = 11$; NPID-stim: $n = 16$ mice; sham vs NPID: $F_{(1,49)} = 4.703$; $P = 0.035$; ctrl vs stim: $F_{(1,49)} = 0.634$; $P = 0.43$). **k** At 8 weeks PO, BLA–ACC pathway inhibition reversed the decreased grooming observed in nerve-injured non-stimulated animals ($F_{(1,48)} = 4.991$; $P = 0.03$; post hoc: sham-ctrl ($n = 12$ mice) > NPID-ctrl ($n = 10$ mice); $P < 0.05$; NPID-ctrl ($n = 10$ mice) < NPID-stim ($n = 16$ mice); $P < 0.05$ sham-ctrl ($n = 12$ mice) = sham-stim ($n = 14$ mice)). **l** At 8 weeks PO, BLA–ACC inhibition blocked the increased immobility observed in nerve-injured non-stimulated animals ($F_{(1,42)} = 7.539$; $P = 0.008$, post hoc: sham-ctrl ($n = 11$ mice) > NPID-ctrl ($n = 9$ mice), $P < 0.05$; NPID-ctrl ($n = 9$ mice) > NPID-stim ($n = 14$ mice), $P < 0.01$; sham-ctrl ($n = 11$ mice) = sham-stim ($n = 12$ mice)). Data are mean \pm SEM. #, main effect; * $P < 0.05$; ** $P < 0.01$. Two-way ANOVA repeated measures (von Frey); two-way ANOVA (Surgery \times Stimulation; LD, ST and FST). ACC anterior cingulate cortex, PO postoperative, 24a/24b areas 24a/b of the ACC, II, III, V/VI ACC layers, cc corpus callosum. Sagittal mouse brain cartoons (**a, f**) were created with Biorender.com. Source data are provided as a Source Data file.

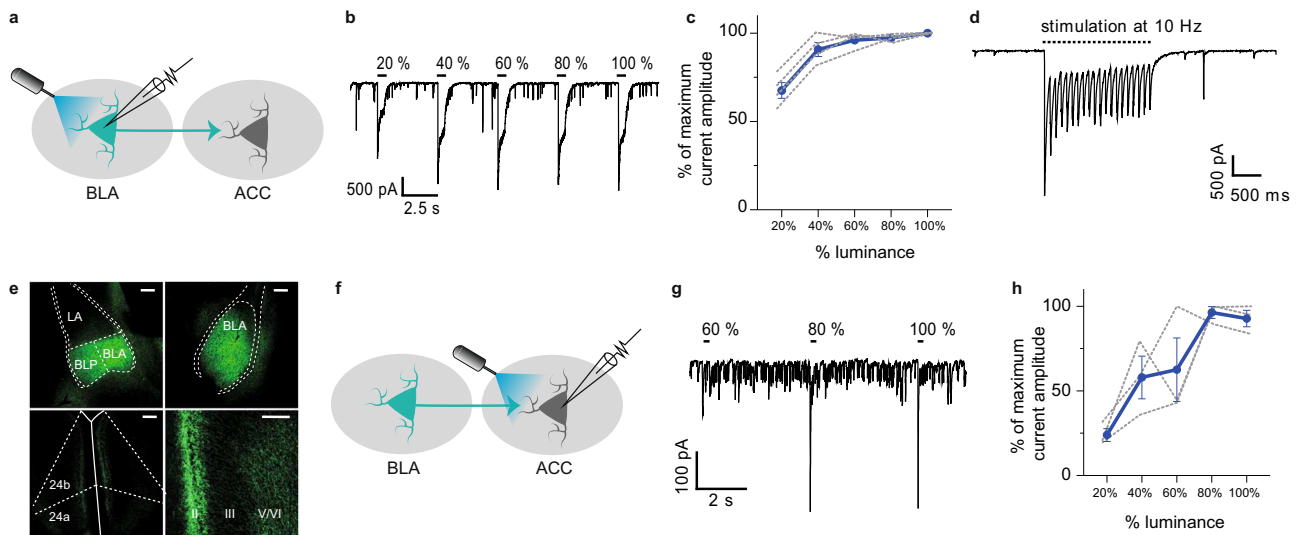


Fig. 3 | ChR2 expression in BLA neurons drives robust light-induced activation of BLA and ACC neurons. **a** Graphical representation of ex vivo voltage-clamp recordings in the BLA. **b** Representative trace of the outward currents induced by optogenetic stimulation with increased luminance in a BLA neuron. **c** Amplitude of currents evoked by optogenetic stimulation of BLA neurons as a function of light stimulation intensity ($n = 4$ cells/3 mice, blue trace = mean; gray traces = individual responses). **d** Representative trace of response of BLA neurons to 10 Hz optogenetic activation showing that after an initial decrease in the amplitude of light-induced currents, a plateau is reached. **e** Representative images of eYFP+ cell bodies in the BLA (upper panels) and eYFP+ axon terminals in the ACC (lower panels). Scale bars = 100 μ m. **f** Graphical representation of the configuration for

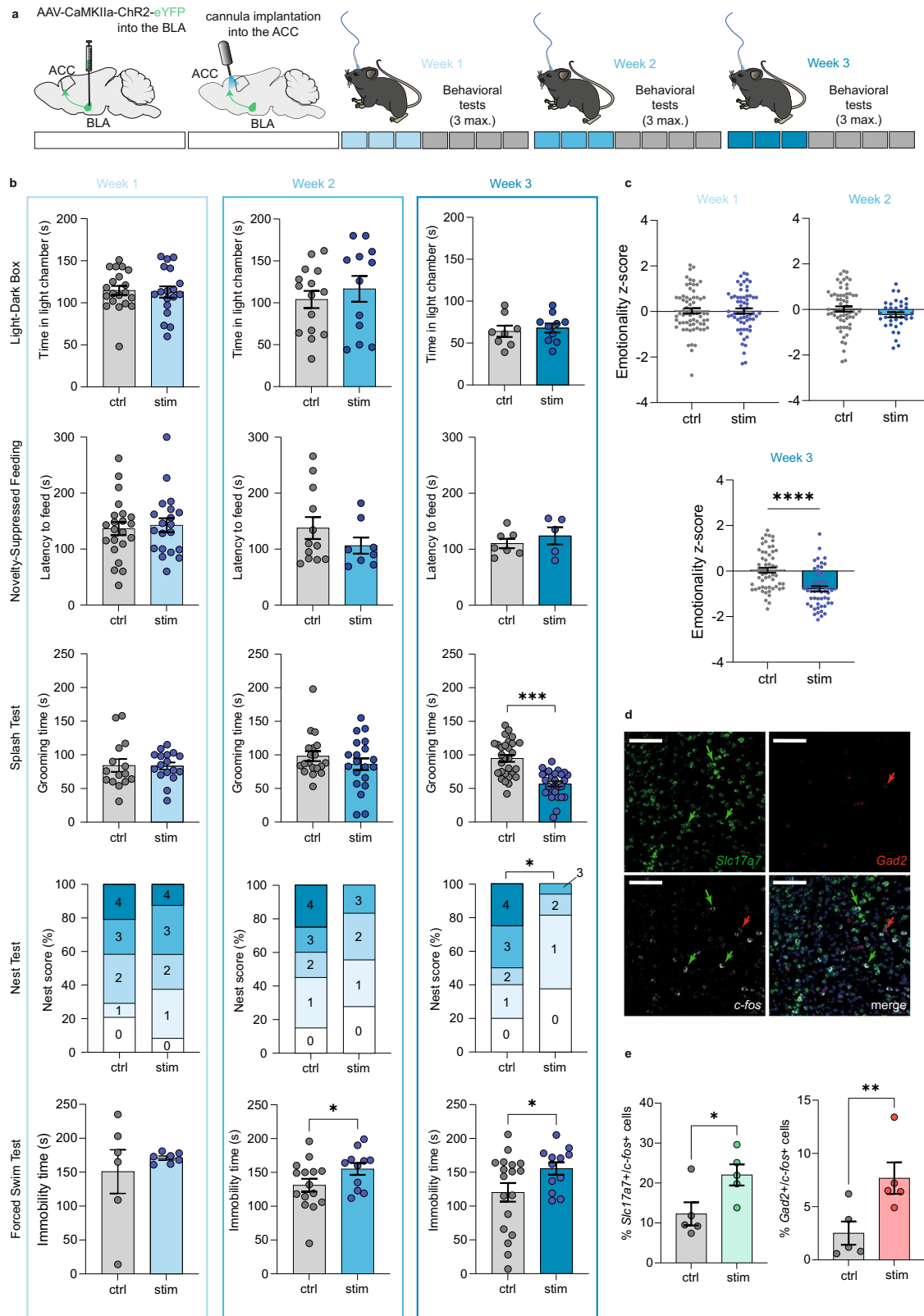
ex vivo voltage-clamp recordings in the ACC. **g** Representative trace of the inward currents induced by optogenetic activation of BLA terminals within the ACC with increased luminance. **h** Amplitude of currents evoked by optogenetic stimulations of BLA terminals recorded in ACC pyramidal neurons as a function of light stimulation intensities ($n = 3$ cells/3 mice, blue trace = mean; gray traces = individual responses). Data are represented as mean \pm SEM. 24a, 24b: areas 24a and 24b of the ACC, II, III, V/VI cortical layers of the ACC, BLA anterior part of the basolateral nucleus of the amygdala, BLP posterior part of the basolateral nucleus of the amygdala, cc corpus callosum, LA lateral amygdala. Source data are provided as a Source Data file.

(Supplementary Fig. 5e). Second, for a more systematic threshold-free comparison, we used RRHO2, (Rank-Rank Hypergeometric Overlap³⁸). This analysis uncovered large patterns of transcriptional dysregulation in similar directions as a function of MDD in men, and of optogenetic activation in mice. Indeed, strong overlaps were observed between species for both upregulated and downregulated genes (Fig. 5d), notably affecting pathways related to oligodendrocyte cell fate and myelination (Supplementary Data Files 2 and 3). Third, because results repeatedly pointed toward myelin, we used Gene Set Enrichment Analysis (GSEA, Fig. 5e–g) to interrogate a well-characterized list of 76 genes primarily expressed by oligodendrocytes, encompassing their major biological functions³⁹. Among these, 48 (63%; Fig. 5e) were downregulated in stimulated mice, and 57 in men with MDD (75%; Fig. 5f). This pattern of myelin downregulation is strikingly similar across species (Fig. 5g). Altogether, these 3 approaches (common DEG, RRHO2 and GSEA) converged to

reveal significant dysregulation of the myelination gene program (see Supplementary Figs. 5e–g and 6c–e).

Gene ontology pathways affected in mice and men point towards altered oligodendrocyte function

To better capture the modular disorganization of gene expression in MDD, we then used weighted gene co-expression network analysis, WGCNA⁴⁰, similar to our recent work⁴¹. Gene networks, constructed independently in each species, were composed of 25 and 29 gene modules in mice and humans, respectively. Using Fischer's exact t test, we found that the gene composition of 14 mice modules (56%) was significantly enriched in human modules, indicating their conservation (Benjamini–Hochberg, $P < 0.05$; Fig. 6a, Supplementary Data File 4, see Supplementary Fig. 6f, and Supplementary Data File 5 when including both sex). To identify which modules are most significantly impacted, we computed correlations between each module's eigengene



(a measure that summarizes co-expression) and optogenetic activation or MDD. In humans, 12 module eigengenes significantly correlated with MDD; in mice, 6 modules associated with optogenetic stimulations (Fig. 6b and Supplementary Fig. 6g). Importantly, among these, 8/12 and 5/6 modules were also conserved across species. Therefore, human MDD and repeated optogenetic activation of the BLA-ACC pathway impact conserved modules in the ACC.

We then conducted ORA of conserved but disorganized modules. Enriched GO terms were related to synaptic activity, mitochondria or RNA processing (Supplementary Table 2), consistent with previous studies of MDD⁴²⁻⁴⁴. Importantly, the 2 most strongly conserved modules (Men/Yellow and Mouse/Brown) again implicated myelin, with enrichments related to oligodendrocytes and myelination (Fig. 6c). To assess where myelin genes are located

Fig. 4 | Repeated activation of the BLA–ACC pathway triggers depressive-like behaviors in naive mice. **a, b** Repeated optogenetic activation of the BLA–ACC pathway did not induce anxiety-like behaviors in the LD (3 stim: ctrl: $n = 20$ mice; 114.8 ± 5.34 ; stim: $n = 18$ mice; 112.9 ± 6.75 ; $P = 0.82$; 6 stim: ctrl: $n = 15$ mice; 104.0 ± 10.31 ; stim: $n = 12$ mice; 116.7 ± 15.37 ; $P = 0.49$; 9 stim: ctrl: $n = 8$ mice; 64.0 ± 6.73 ; stim: $n = 10$ mice; 68.0 ± 5.34 ; $P = 0.64$) nor NSF (3 stim: ctrl: $n = 22$ mice; 136.5 ± 11.65 ; stim: $n = 20$ mice; 142.6 ± 12.44 ; $P = 0.72$; 6 stim: ctrl: $n = 12$ mice; 137.8 ± 19.52 ; stim: $n = 8$ mice; 106.4 ± 14.51 ; $P = 0.26$; 9 stim: ctrl: $n = 7$ mice; 110.3 ± 8.36 ; stim: $n = 5$ mice; 123.8 ± 15.24 ; $P = 0.42$) tests. Three stimulations did not change grooming in the splash test (ST, ctrl: $n = 15$ mice; 84.20 ± 9.37 ; stim: $n = 17$ mice; 83.41 ± 5.33 ; $P = 0.94$), nest building (ctrl: $n = 24$ mice; stim: $n = 24$ mice; Chi-square=0.012; $P = 0.91$) nor immobility in the FST (ctrl: $n = 6$ mice; 150.8 ± 32.29 ; stim: $n = 7$ mice; 171.0 ± 2.89 ; $P = 0.26$). Six stimulations did not alter grooming (ctrl: $n = 19$ mice; 98.16 ± 7.37 ; stim: $n = 20$ mice; 86.10 ± 8.7 ; $P = 0.51$) nor nesting (ctrl: $n = 20$ mice; stim: $n = 18$ mice; Chi-square=2.81; $P = 0.094$), but increased immobility in the FST (ctrl: $n = 15$ mice; 131.1 ± 9.47 ; stim: $n = 11$ mice; 155.1 ± 8.71 ; $P = 0.042$). The latter increase was still present after 9 stimulations (ctrl: $n = 18$ mice; 120.3 ± 13.69 ; stim: $n = 12$ mice; 155.5 ± 9.15 ; $P = 0.033$), along

with decreased grooming (ctrl: $n = 29$ mice; 94.79 ± 5.02 ; stim: $n = 26$ mice; 56.81 ± 3.96 ; $P < 0.0001$) and nest quality (ctrl: $n = 20$ mice; stim: $n = 16$ mice; Chi-square=7.35; $P = 0.0067$). **c** Emotionality z-scores across tests and timepoints: three stimulations had no effect (ctrl: $n = 67$ mice; 0.033 ± 0.11 ; stim: $n = 64$ mice; 0.023 ± 0.11 ; $P = 0.97$), while a tendency for a decrease emerged after 6 stimulations (ctrl: $n = 40$ mice; -0.004 ± 0.082 ; stim: $n = 35$ mice; -0.232 ± 0.109 ; $P = 0.095$) and became significant after 9 (ctrl: $n = 59$ mice; 0.042 ± 0.11 ; stim: $n = 52$ mice; -0.78 ± 0.12 ; $P < 0.0001$). **d** Representative RNAscope images of *Slc17a7* (upper-left panel), *Gad2* (upper-right), *c-fos* (lower-left) mRNAs and their co-localization (lower-right) in the ACC. Scales = 100 μ m. **e** Proportions of *Slc17a7*+/*c-fos*+ (green) and *Gad2*+/*c-fos*+ (red) cells increased in stimulated animals (ctrl: $n = 5$ mice; stimulated: $n = 5$ mice; *Gad2*+/*c-fos*+ : ctrl: 2.52 ± 1.09 ; stim: 7.68 ± 1.48 , $P = 0.008$; *Slc17a7*+/*c-fos*+ : ctrl: 12.28 ± 2.89 ; stim: 22.04 ± 2.64 , $P = 0.028$). Data are mean \pm SEM. * $P < 0.05$; ** $P < 0.01$; *** $P < 0.001$; **** $P < 0.0001$. Two-sided unpaired *t* test (LD, NSF, ST, z-score); chi-square test for trend (Nest); one-sided Mann–Whitney test (mRNA quantification). 24a/b: areas 24a/b of the ACC, II, III, V/VI ACC layers. Sagittal mouse brain cartoons (a) were created with Biorender.com. Source data are provided as a Source Data file.

within these modules, we analyzed their module membership (MM), a measure of module centrality. Myelin-related genes displayed higher absolute values (i.e., higher centrality) compared to means among their host modules, in both species (Fig. 6d). Among the 235 genes belonging to the intersection between the 2 Men/Yellow and Mouse/Brown modules, 36 were myelin-related (Fig. 6e, red dots), and a strong correlation between mouse and human MM was found, indicating that the same set of genes is centrally located among the two modules. Finally, we also observed among these 2 modules a strong correlation in the directionality of gene expression changes across species, with a majority of downregulated genes (Fig. 6f). Altogether, this suggests that myelination transcriptional deficiency, a feature of MDD pathophysiology in the ACC, is recapitulated in our optogenetic paradigm.

We next validated RNA-sequencing results using microfluidic qPCR and a new mouse cohort generated with the same optogenetic protocol ($n = 8$ control and 7 stimulated mice). Behavioral effects of stimulations were first confirmed (Fig. 6g), followed by dissection of the ACC tissue and analysis of the expression of most abundant myelin sheath proteins (*Plp1*, *Mal*, *Mog*, *Mag*, *Mbp*), enzymes involved in the synthesis of myelin lipids (*Aspa*, *Ugt8*), as well as positive (*Ernn*) and negative (*Sema4a*, *Lingo1*) regulators of myelination (Fig. 6h, i). Results significantly correlated with RNA-sequencing data, with similar downregulation of myelin proteins, or synthesis enzymes, as well as upregulation of 2 well-known negative regulators of myelination, *Sema4a* and *Lingo1*.

Finally, as complementary approaches to document how these myelin gene expression changes translate at cellular and network levels, we used immunohistochemistry (Fig. 7a) and brain imaging (Fig. 7e). We first assessed the number of ACC cells expressing *Olig2*, a transcription factor essential for proliferation and differentiation in the oligodendrocyte lineage, as well as PDGFRA, a marker of oligodendrocyte progenitor cells (OPC; Fig. 7b). Our results showed that the number of *Olig2*+ (Fig. 7b, c), but not PDGFRA+ (Fig. 7b, d) cells decreased after nine stimulations, when depressive-like consequences are maximal (Supplementary Fig. 7a). This suggests that loss of mature oligodendrocytes underlies the decreased expression of myelin genes observed in bulk tissue. Of note, this decrease in *Olig2*+ cells was not observed one week after the 9th stimulation, when behavioral deficits are no longer present (Supplementary Fig. 7b, c), indicating a rapid recovery matching the behavioral kinetic. Finally, in a different cohort (Supplementary Fig. 7d for behavioral validation), we also performed MRI with DTI acquisition sequences, to analyze microstructural changes induced by optogenetic activation. Interestingly, stimulated animals displayed lower fractional anisotropy (FA) compared to controls in the ACC, amygdala and along the pathway connecting the two

regions (Fig. 7f). This effect significantly correlated with increased depressive-like behavior (Supplementary Fig. 7e). Since myelination is an important determinant of the structural connectivity assessed by DTI^{45,46}, these results reinforce the notion that repeated activation of the BLA–ACC pathway disrupts the transcriptional program and the survival of mature oligodendrocytes within the ACC, leading to altered connectivity between the two structures.

Prompted by these consistent transcriptomic, histological and imaging findings, we then asked whether myelin dysregulation might also occur during chronic pain. To address this possibility, we took advantage of recent work by Dai and collaborators in a chronic neuropathic pain model (spared nerve injury), which provided transcriptomic analysis in both the PFC and ACC⁴⁷. For consistency, these data were reprocessed in our differential expression analysis pipeline, and compared to those obtained after optogenetic stimulations (using RRHO2). Results uncovered strong similarity across the 2 datasets, including the downregulation of myelin- and oligodendrocyte-related genes and GO terms (Supplementary Fig. 8). Therefore, it is possible that impaired transcriptional activity of the myelination program may also contribute to mood dysregulation during chronic neuropathic pain.

Sema4a is necessary for the emergence of optogenetically induced depressive-like states

While the relationship between myelination and the expression of depressive-like behaviors has already been documented^{48–52}, little is known about underlying molecular substrates. A few rodent studies have investigated the effect of depleting myelin sheath protein⁵³ or positive regulator of myelination⁵⁴ on depressive-like behaviors. In contrast, upstream factors that prime myelin deficits and lead to behavioral dysregulation are unknown. Hence, we decided to focus on *Sema4a*, which was upregulated in the ACC of animals showing depressive-like behaviors (Fig. 6i). *Sema4a* has indeed known cytotoxic effects on oligodendrocytes^{55,56} and has been associated with white matter defects^{57,58}.

To block the over-expression of *Sema4a* in our model, we first established a knockdown (KD) approach. Three different shRNAs (#108, 576, 791; Fig. 8a) targeting exon 15 of *Sema4a* were designed, packed into AAV plasmids with mCherry reporter, and transfected in HEK cells overexpressing the targeted *Sema4a* exon, in fusion with eGFP. Among these, we prioritized shRNA-791 because it yielded the most profound KD, as shown by a near complete loss of eGFP signal at 2 days post-transfection (Fig. 8b). To characterize its in vivo efficiency, shRNA-791, was then packaged into an AAV vector and injected in the ACC of adult mice, followed 6 weeks later by qPCR quantification of *Sema4a* (Fig. 8c, d). Compared with a control vector expressing the

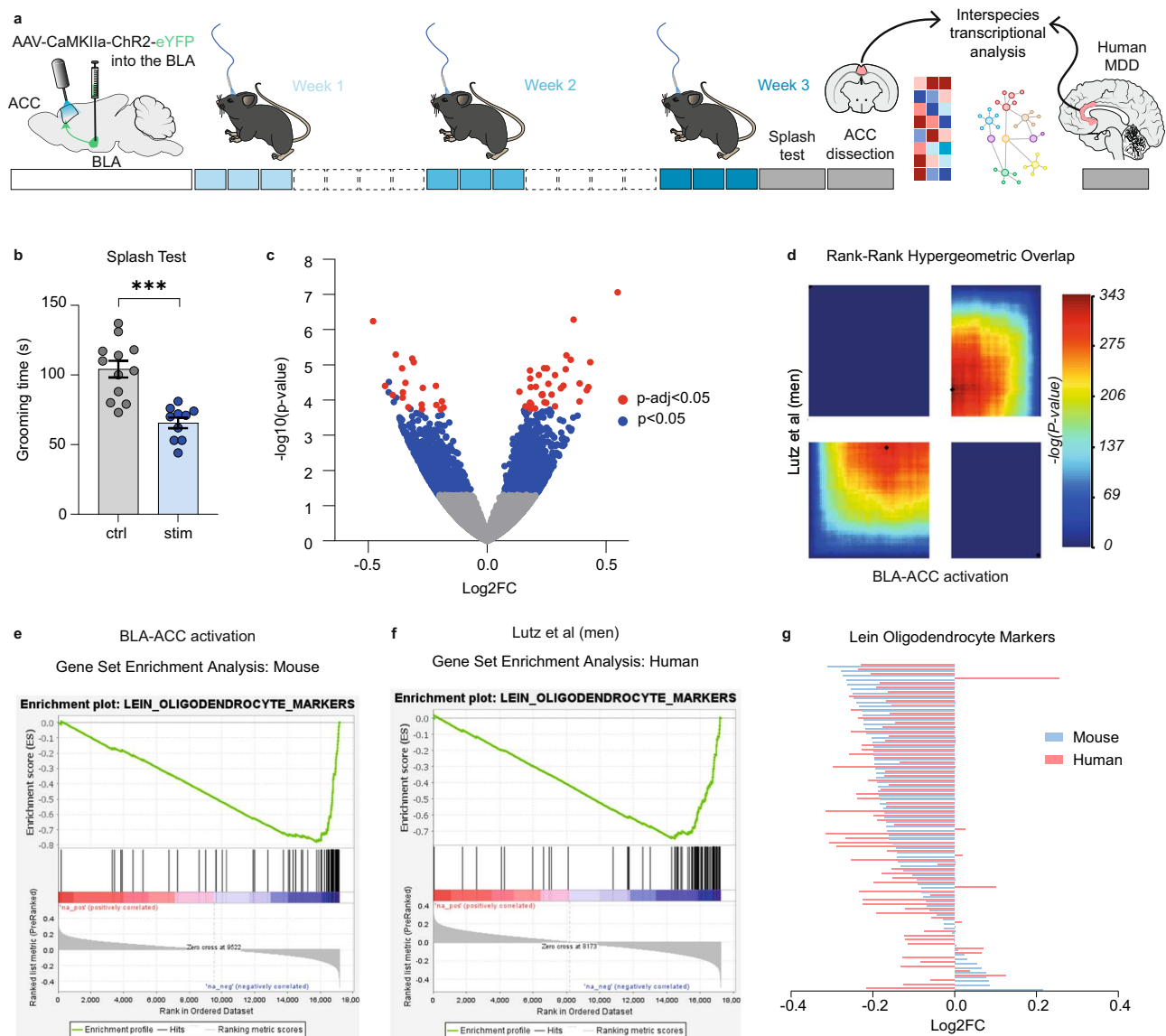


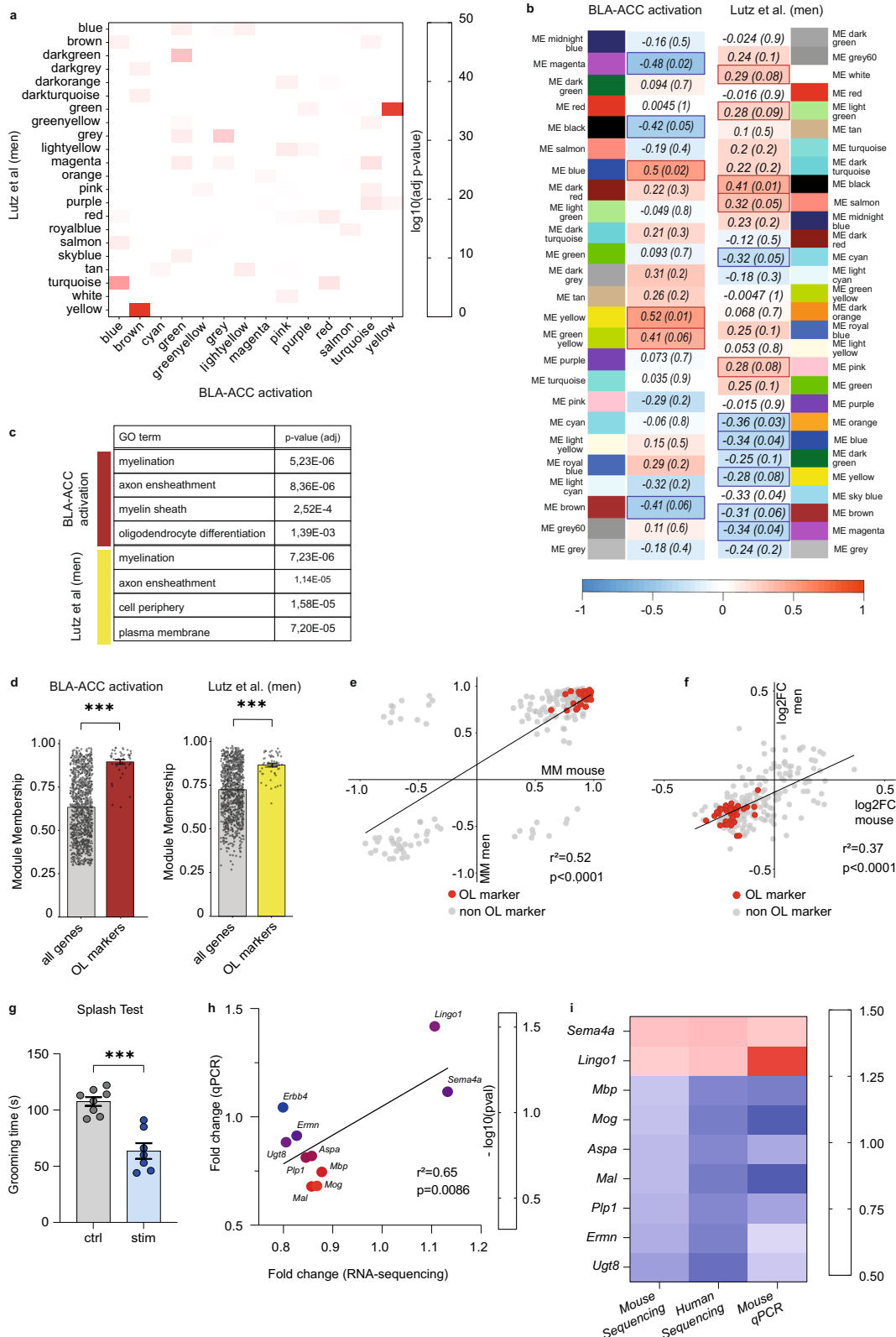
Fig. 5 | Repeated activation of the BLA-ACC pathway induces transcriptional alterations similar to those observed in human-depressed patients. **a** Graphical representation of experimental design, including virus delivery into the BLA, cannula implantation into the ACC, 9 sessions of optogenetic activation, ACC extraction in mice, and transcriptomic analysis in mice and humans. **b** Nine sessions of optogenetic activation of the BLA-ACC pathway decreased grooming behaviors in stimulated animals used for RNA Sequencing (ctrl: $n = 12$ mice; 104.2 ± 6.0 ; stim: $n = 10$ mice; 65.60 ± 3.80 ; $P < 0.0001$). **c** Volcano plot showing the 2611 (blue dot, 6.9% of all genes) genes differentially expressed (nominal P values < 0.05 ; Wald test) between stimulated ($n = 10$) and control animals ($n = 12$). Red circles depict the 54 genes that showed a significant dysregulation after multiple testing correction ($P_{adj} < 0.05$, Benjamini and Hochberg correction). **d** Rank-Rank Hypergeometric

Overlap (RRHO) identified shared transcriptomic changes in the ACC across mice and men as a function of optogenetic stimulation (mouse) or a diagnosis of major depressive disorder (MDD). Levels of significance for the rank overlap between men and mice are color-coded, with a maximal one-sided Fisher's Exact Test (FET) $P < 1.0E-343$ for upregulated genes (lower-left panel), and a maximal FET $P < 1.0E-315$ for downregulated genes (upper-right panel). **e-g** Gene set enrichment analysis (GSEA) revealed an enrichment for genes specifically expressed by oligodendrocytes and showing evidence of downregulation as a function of optogenetic stimulation (**e**) or MDD diagnosis (**f**). The direction of the changes correlated across mice and humans (**g**; $r^2 = 0.15$, $P = 0.0005$). Behavioral data are mean \pm SEM, *** $P < 0.001$, two-sided unpaired t test. Brain cartoons (**a**) were created with Biorender.com. Source data are provided as a Source Data file.

mCherry and a scrambled shRNA, the AAV-shRNA-791 achieved a 62% reduction of *Sema4a* expression, demonstrating its efficacy.

Finally, we hypothesized that knocking down *Sema4a* prior to optogenetic stimulations may prevent the emergence of depressive-like behaviors. Cohorts of mice (Fig. 8e) went through bilateral injections of the Chr2-expressing virus in the BLA (see Supplementary Fig. 9 for injection placement), bilateral injections of the AAV-shRNA-791 vector (or the Scrambled control) in the ACC (Fig. 8f), followed, 2 weeks later, by optogenetic cannula implantation in the ACC. Behavioral testing was performed after 9 stimulations over 3 weeks, corresponding to the 6-week timepoint at which we documented

shRNA-791 in vivo efficiency (Fig. 8d). In the splash test, knocking down *Sema4a* did not affect the decreased grooming observed in stimulated animals (Fig. 8g). However, in the FST (Fig. 8h), we detected a significant interaction between optogenetic stimulations and *Sema4a* KD, with a potent increase in depressive-like behaviors of stimulated mice, which did not occur when *Sema4a* was knocked-down. Analysis of emotional reactivity across ST and FST tests further strengthened these results, as global emotional dysfunction induced by BLA-ACC activation was reversed by *Sema4a* KD (Fig. 8i). Of note, *Sema4a* KD had no effect in unstimulated mice across any tests, indicating that it is not sufficient to trigger emotional dysfunction in naive animals.



Altogether, these results indicate that silencing *Sema4a* in the ACC prevents the emergence of emotional deficits driven by activation of the BLA-ACC pathway.

Discussion

Given the complexity of the emotional consequences of chronic pain, disentangling the circuitries involved in its different components is

crucial for uncovering new therapeutic leads and strategies. The ACC is considered to play a pivotal role in these processes^{10,32,59}. However, while its connectome has been robustly established using neuroanatomical^{13,14} and imaging approaches, how it integrates in polysynaptic neuronal circuits that may differentially regulate mood and nociception is poorly understood⁶⁰. To address this gap, here we focused on the BLA-ACC pathway, based on their reciprocal

Fig. 6 | Gene-network analysis points toward alterations of myelination and oligodendrocyte in mice and men. **a** Heatmap representing the level of significance of overlaps between mice and men gene modules (two-sided Fisher Exact Test). The highest overlap ($P = 8.36E-49$) was obtained for the man/yellow and mouse/brown modules. **b** WGCNA gene modules in the mouse and men ACC. The tables depict associations between each module's eigengene and optogenetic stimulation in mice (left panel), or MDD diagnosis in men (right), and show both r correlation coefficients and P values (in brackets). **c** Gene Ontology analysis for man/yellow and mouse/brown modules, with most significant findings for myelin-related terms in both species (two-sided Fisher Exact Test). **d** The absolute value of the module membership (MM) of oligodendrocytes (OL) markers (OL genes) was significantly higher than the MM of all genes in each module, for both mouse/brown ($n = 1088$ genes total, $n = 43$ OL genes; left panel; P value $< 2.2E-16$) or man/yellow ($n = 1049$ genes total, $n = 52$ OL genes, right panel; P value $< 2.2E-16$) modules (two-sided paired t test). **e** Significant Pearson correlation between mouse/brown and man/yellow MM rankings ($r^2 = 0.52$, $P = 0.0001$). Red dots indicate myelin- and

oligodendrocyte-related genes/genes also present in the Lein-Oligodendrocytes-Markers database. **f** Pearson linear regression of fold changes measured by RNA sequencing for men and mouse, showing a significant positive correlation in the direction of the change in expression of the genes in mouse/brown and man/yellow modules ($r^2 = 0.37$, $P < 0.0001$). Red dots indicate myelin and oligodendrocyte-related genes. **g** Repeated activation of the BLA-ACC decreased grooming time in stimulated animals in the splash test (ctrl $n = 8$ mice; 107.6 ± 3.65 ; stim $n = 7$ mice; 63.57 ± 6.96 ; $P < 0.0001$). **h** Linear regression of fold changes measured by RNA sequencing and qPCR, showing a significant positive correlation between the two methods ($r^2 = 0.42$, $P = 0.0025$). **i** Downregulation of the myelin-related genes (*Mbp*, $P = 0.044$; *Mog*, $P = 0.026$; *Aspa*, $P = 0.078$; *Mal*, $P = 0.038$; *Plp1*, $P = 0.080$; *Ermn*, $P = 0.180$; *Ugt8*, $P = 0.133$) and upregulation of inhibitors of the myelination process (*Lingo1*, $P = 0.114$; *Sema4a*, $P = 0.154$) were consistent across mice and men in RNA-Sequencing data, and validated in mice by qPCR, after nine stimulations. Data are mean \pm SEM, *** $P < 0.0001$, two-tailed (Splash Test) and one-tailed (qPCR) unpaired t test. Source data are provided as a Source Data file.

anatomical connections and well-known functions. By leveraging 2 optogenetic strategies for neuronal activation or inhibition in the mouse, we manipulated ACC inputs coming from the BLA. Our translational results uncover a critical role of this discrete pathway in mood, both in the context of chronic pain or in the absence of neuropathy.

First, we found that inhibiting the BLA-ACC pathway blocks the expression of depressive-like consequences of chronic pain, without affecting anxiety-like behaviors, aversiveness, or mechanical hypersensitivity. Because acute inhibition is sufficient to produce this effect, depressive-like features seem to be mediated by ongoing hyperactivity of the pathway. In contrast, our previous work had shown that inhibition of CaMKII α cells in the ACC, regardless of their connectivity features, attenuated both anxiety and depressive-like consequences of chronic pain¹¹. This suggests that distinct ACC inputs differentially contribute to various aspects of the pain experience, consistent with data from other groups^{33,61}. Accordingly, Gao et al showed that, in the sciatic nerve chronic constriction injury model, inhibiting projections from the ACC to the mesolimbic pathway (nucleus accumbens and ventral tegmental area) induced CPP, without affecting evoked pain³³. In parallel, Hirschberg et al. found that ACC inputs coming from the locus coeruleus (LC) are involved in anxiety-like and aversive consequences of pain⁶¹. Combined with ours, these results suggest functional segregation, with a LC-ACC-mesolimbic circuit preferentially involved in pain-induced aversion, while BLA and LC inputs targeting the ACC may predominantly mediate depressive- and anxiety-like consequences of chronic pain, respectively.

Second, we show that, in the absence of neuropathy, in naïve mice, repeated but not acute BLA-ACC activation is sufficient to trigger depressive-like effects. This is in line with our previous study showing that chronic but not acute activation of the whole ACC induces emotional deficits^{10,25}. The lack of detectable impact of this optogenetic manipulation on anxiety-like responses also strengthens the aforementioned notion that ACC inputs coming from the BLA selectively modulate mood states. Interestingly, activation of BLA terminals in other subparts of the PFC (i.e., areas 25/32, located more rostrally), different from those recruited in the present work (ACC areas 24a/24b), induced anxiety-like behavior⁶²⁻⁶⁵. These results therefore suggest differential control of emotional responses by multiple pathways that originate in the BLA but target separate cortical regions. Finally, because it is likely that the depressive-like phenotype induced by chronic BLA-ACC activation requires molecular and circuit plasticity, we next conducted open-ended transcriptomic analysis, along with direct comparison with the human MDD signature.

Based on convergent bioinformatic analyses (common DEG, RRHO2, GSEA, WGCNA), we found that transcriptomic changes occurring in our optogenetic paradigm recapitulated a series of adaptations previously associated with human MDD, notably affecting the mitochondria^{44,66}, chromatin remodeling factors⁶⁷, synaptic

function, translational regulation⁴² or myelination^{37,68}. These results document the translational relevance of our paradigm. They also indicate that selective manipulation of a restricted neuronal pathway may represent a valuable strategy to model MDD, at both behavioral and molecular levels. Because recent studies suggest that the various mouse models available for this disorder may capture distinct aspects of its molecular pathophysiology⁴⁴, we argue that our optogenetic model provides a complementary approach. While it is based on an artificially induced neuronal hyperactivation, it opens the possibility of modeling some of the effects of internal insults or states, such as chronic pain. Finally, this paradigm, and its potential extension to other neuronal circuits, also enables deciphering what is sufficient for the emergence of mood dysfunction.

Most widespread alterations affected oligodendrocytes and the myelination process, which were consistently identified across human and mouse data. Global downregulation of myelin sheath proteins (*Plp1*, *Mal*, *Mog*, *Mbp*) and enzymes involved in the synthesis of myelin lipids (*Aspa*, *Ugt8*), as well as upregulation of myelination inhibitors (*Lingo1*, *Sema4a*) were observed in the ACC of animals displaying depressive-like behaviors. These findings further translated at the cellular level, since a decrease in the number of mature oligodendrocytes was detected after repeated BLA-ACC activation. Of note, one week after the cessation of optogenetic stimulations, when behavioral deficits were no longer present, the loss of Olig2+ cells was reversed. Similarly rapid kinetics were previously characterized in the context of motor learning, with an increase in oligodendrocyte proliferation 4–11 days after mice exercised on a complex wheel⁶⁹. By analogy, quick changes in oligodendroglia might also underlie the emotional fluctuation seen in our optogenetic model, a hypothesis that will need to be further investigated. These results are also congruent with previous studies reporting deficits in myelination^{37,70}, white matter tract organization⁷¹⁻⁷³ or oligodendrocytes integrity^{50,74}, in the ACC of MDD patients (in cross-sectional comparisons of symptomatic patients and euthymic controls). The crucial role of myelination in MDD pathophysiology is further supported by preclinical studies^{52,75,76}. Depletion of the myelin sheath component CNP⁵³, or of the positive regulator of myelination ErbB4⁵⁴, as well as cellular depletion of oligodendrocyte progenitors⁷⁷, have all been shown to induce emotional dysfunction in rodents. Conversely, the pharmacological compound Clemastine, which enhances oligodendrocyte differentiation and myelination, exerts antidepressant-like effects in socially defeated⁷⁶ or isolated⁷⁴ mice. Molecular mechanisms mediating such effects, however, remain poorly characterized. Here, using gene-network theory, we prioritized *Sema4a* as one of the most prominently upregulated genes in a myelin-enriched gene module strongly affected by BLA-ACC activation. Previous reports had shown that increased *Sema4a* function contributes to the broad loss of mature oligodendrocytes and demyelination observed in neurological

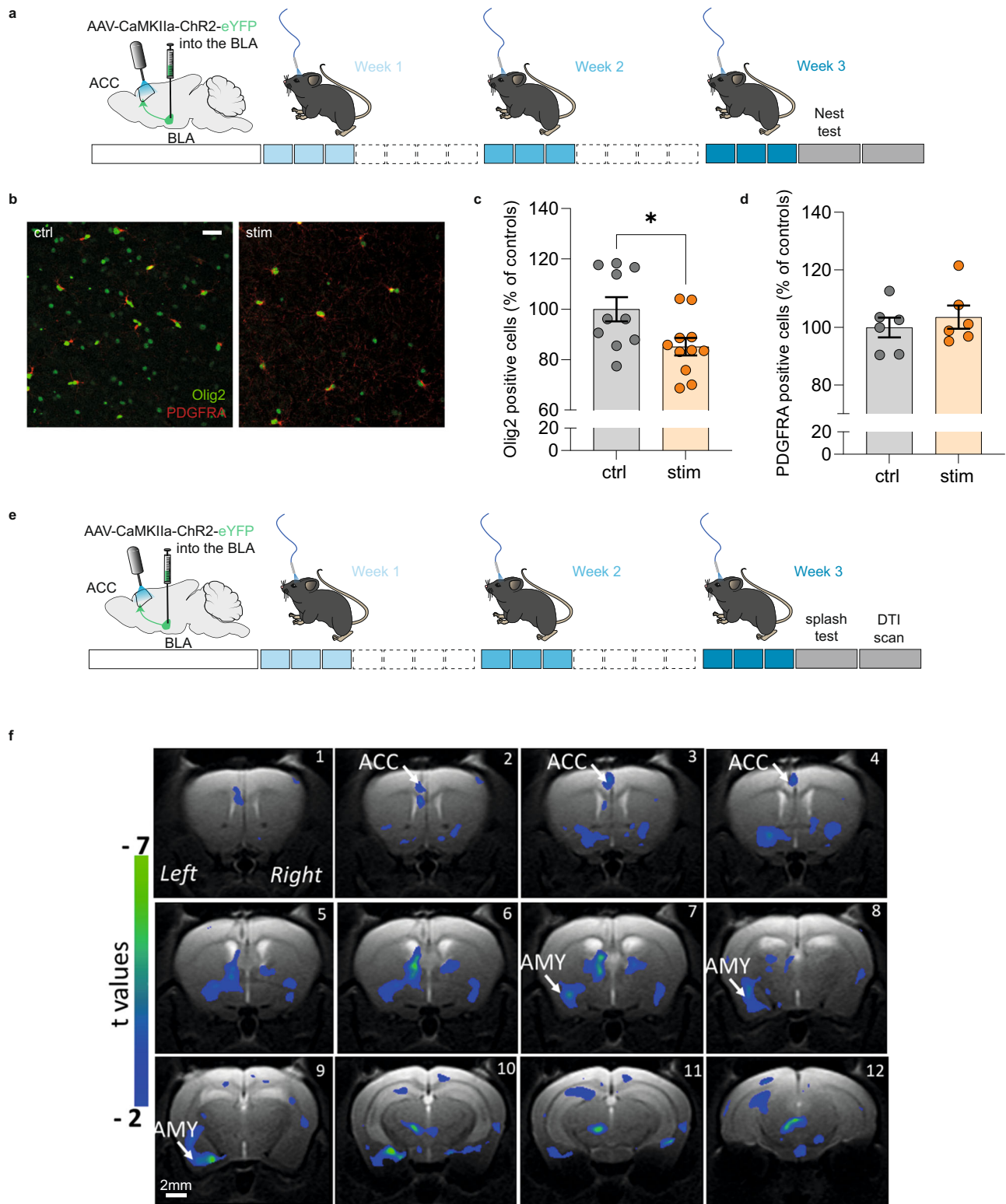
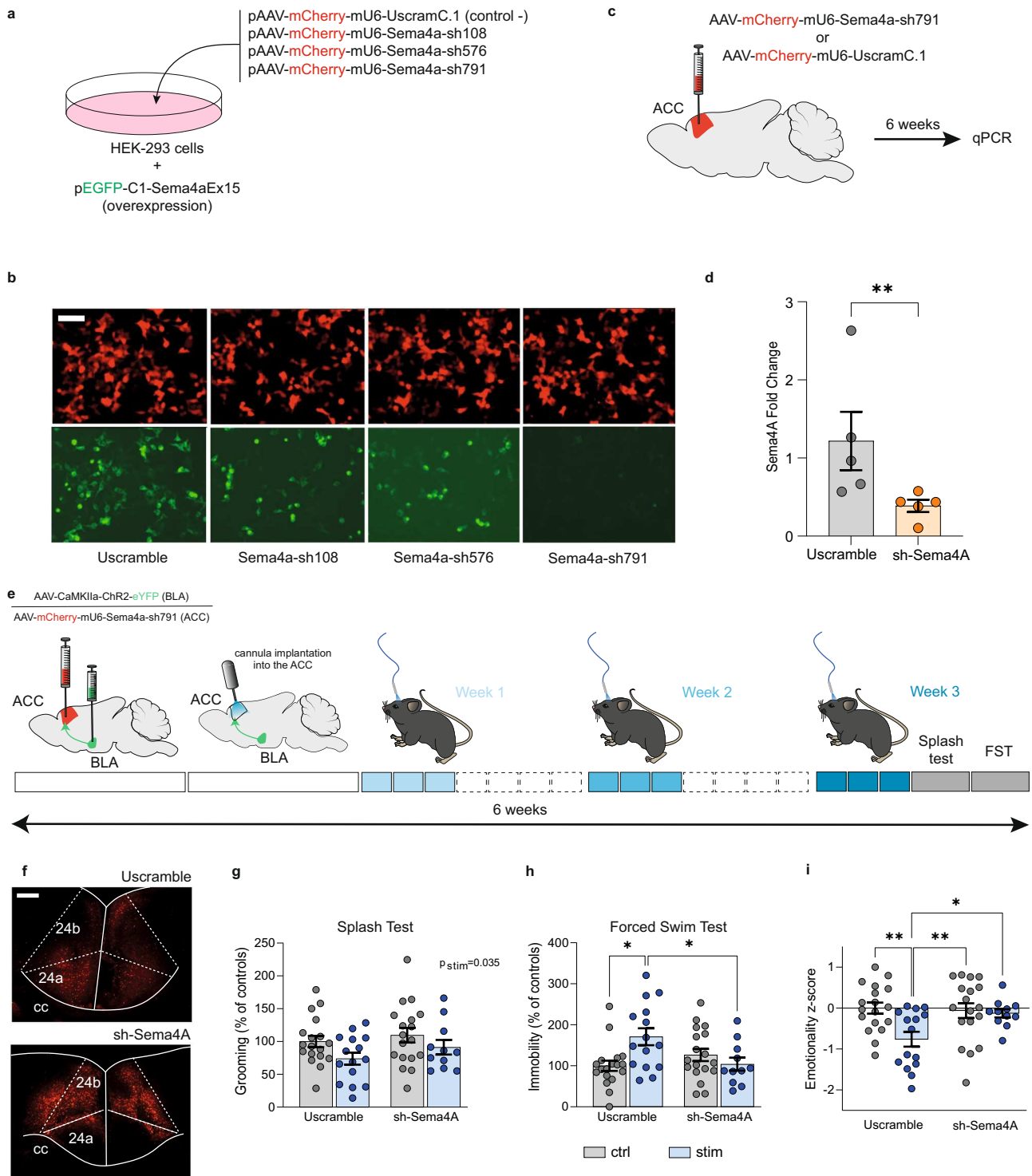


Fig. 7 | Repeated activation of the BLA-ACC pathway impairs myelination.

a Graphical representation of the experimental design, including virus delivery into the BLA, cannula implantation into the ACC and the nine sessions of optogenetic activation. **b** Representative fluorescence images showing cells that are Olig2+ (green) or PDGFRA+ (red) in non-stimulated (left panel) and stimulated mice (right panel). Scale bar = 50 μ m. **c, d** Quantification of Olig2 and PDGFRA-positive cells showed that nine optogenetic stimulations of the BLA-ACC pathway decreased the number of Olig2+ cells without affecting the number of PDGFRA+ cells (**c**: ctrl: $n = 6$ mice; 99.97 ± 3.45 ; stim: $n = 6$ mice; 103.6 ± 4.00 ; $P = 0.41$) in the ACC (**d**: ctrl: $n = 10$

mice; 100.00 ± 4.83 ; stim: $n = 11$ mice; 85.11 ± 3.48 ; $P = 0.01$). **e** Graphical representation of the experimental design for the DTI experiment, including virus delivery into the BLA, cannula implantation into the ACC and the nine sessions of optogenetic activation. **f** Representative coronal MRI images showing in blue the areas with a significant decrease of FA along the left BLA-ACC pathway in stimulated animals compared to the control group (ctrl: $n = 7$; stim: $n = 6$; GLM $P < 0.001$ uncorrected). Data are mean \pm SEM. * $P < 0.05$; ** $P < 0.01$. one-sided Mann-Whitney test (Olig2 and PDGFRA quantification). Sagittal mouse brain cartoons (**a, e**) were created with Biorender.com. Source data are provided as a Source Data file.



and autoimmune disorders, such as multiple sclerosis^{55-58,78}. Our results extend these findings in the context of mood regulation, and involve a milder and possibly more localized dysregulation of *Sema4a* within the ACC. Its knockdown in this region was sufficient to prevent the development of depressive-like behaviors induced by repeated activation of incoming BLA fibers. Therefore, we document those changes in *Sema4a* expression may play a pivotal role in mood regulation, and represent a putative therapeutic target. Among others, avenues for future work will include characterizing the mechanisms by which *Sema4a* modulates oligodendrocytes, identifying in which ACC cell types such processes are recruited by BLA afferents, and

describing putative sex differences in these aspects of pain and emotional processing.

Accordingly, a limitation of the present study is that we focused on males only. Since sexual differences have been described in relation to chronic pain and associated emotional dysregulation⁷⁹⁻⁸¹, future studies will be necessary to investigate sex as a biological variable in behavioral and transcriptomic consequences of various models (including NPID), as well as in interactions among structures such as the BLA and the ACC (with no concrete evidence available to date).

In conclusion, our results demonstrate that the BLA-ACC pathway critically mediates the interplay between chronic pain and depression.

Fig. 8 | Semaphorin-4A is essential for the depressive-like behaviors induced by the activation of the BLA-ACC pathway. **a** Graphical representation of the experimental design for shRNA validation in vitro. HEK-293 cells were transfected with plasmids expressing the mouse *Sema4a* exon 15 (green), and 1 out of 3 shRNAs tested for knockdown efficiency (red; with 1 scrambled shRNA as control). **b** Representative fluorescence images showing that the pAAV-mCherry-mU6-Sema4A-sh791 plasmid was the most efficient. Scale bar = 50 μm . **c** Graphical representation of the bilateral virus injection in the ACC for in vivo validation of the selected sh791, inserted into an AAV vector. **d** qPCR analysis showing a down-regulation of *Sema4a* expression level in the ACC of mice injected with Sema4A-sh791 (Uscramble: $n = 5$ mice; 1.22 ± 0.37 ; sh-Sema4A: $n = 5$ mice; 0.39 ± 0.07 ; $P = 0.0079$). **e** Graphical representation of the experimental design, including bilateral virus delivery in the BLA (AAV5-CaMKIIa-ChR2(H134R)-EYFP) and the ACC (rAAV-mCherry-scrambleUsh or rAAV-mCherry-Sema4A-sh791), cannula implantation, optogenetic stimulation and behavioral testing. **f** Representative images of mCherry+ cells in the ACC after the injection of Uscramble (upper panel) or

sh-Sema4A (lower panel). Scale bars = 100 μm . **g–i** Effect of *Sema4a* knockdown on optogenetically induced emotional deficits (Uscramble-Ctrl: $n = 18$ mice; Uscramble-Stim: $n = 15$ mice; sh-Sema4A-Ctrl: $n = 18$ mice; sh-Sema4A-Stim: $n = 11$ mice). Grooming time in the ST was decreased by repeated activation of the BLA-ACC pathway (**g**: $F_{(1,58)} = 4.623$; $P = 0.036$) but was not affected by knocking down *Sema4a* in the ACC (**g**: $F_{(1,58)} = 1.694$; $P = 0.20$). Knocking down *Sema4a* in the ACC counteracted the increased immobility time observed in stimulated animals in the FST (**h**: $F_{(1,58)} = 8.032$; $P = 0.006$; post hoc: Uscramble-Ctrl < Uscramble-Stim; $P < 0.05$; sh-Sema4A-Stim < Uscramble-Stim; $P = 0.05$). Knocking down *Sema4a* in the ACC normalized the emotionality z-score (i: $F_{(1,58)} = 4.39$; $P = 0.041$; post hoc: Uscramble-Ctrl > Uscramble-Stim; $p < 0.01$; Uscramble-Stim < sh-Sema4A-Ctrl; $P < 0.01$ Uscramble-Stim < sh-Sema4A-Stim; $P < 0.05$; sh-Sema4A-Ctrl = sh-Sema4A-Stim; $p > 0.05$). Data are mean \pm SEM. * $P < 0.05$; ** $P < 0.01$; one-tailed Mann-Whitney test (*Sema4a* quantification), two-way ANOVA (Stimulation \times KnockDown; ST, FST and z-score). Sagittal mouse brain cartoons (**c**, **e**) were created with Biorender.com. Source data are provided as a Source Data file.

By combining animal and human studies, we define the behavioral relevance of this pathway, and uncover the essential role of impaired myelination and *Sema4a* signaling in depression.

Methods

Animals

Experiments were conducted using male adult C57BL/6J (RRID: IMSR JAX: 000664) mice (Charles River, France), 8 weeks old at the beginning of experimental procedures, group-housed with a maximum of five animals per cage and kept under a reversed 12 h light/dark cycle (room temperature $24 \pm 1^\circ\text{C}$, humidity around 50%). After the optic fiber implantation, animals were single housed to avoid possible damage to the implant. We conducted all the behavioral tests during the dark phase, under red light. Our animal facility (Chronobiotron) is registered for animal experimentation (Agreement A67-2018-38), and protocols were approved by the local ethical committee of the University of Strasbourg (CREMEAS, APAFIS183-2016121317103584).

Surgical procedures

Surgical procedures were performed under zoletil/xylazine anesthesia (zoletil 50 mg/ml, xylazine 2.5 mg/ml; i.p., 4 ml/kg, Centravet). For stereotaxic surgery, a local anesthetic was delivered subcutaneously at the incision site (bupivacaine, 2 mg/kg).

Neuropathic pain induction: cuff surgery

For the BLA-ACC inhibition study, we used a well-characterized chronic pain-induced depression model^{11,23}. Before surgery, mice were assigned to experimental groups so that these groups did not initially differ in mechanical nociceptive threshold or body weight. Chronic neuropathic pain was induced by placing a 2 mm polyethylene tubing (Cuff, Harvard Apparatus, Les Ulis, France) around the right common branch of the sciatic nerve²⁴. The Sham group underwent the same procedure without cuff implantation.

Virus injection

After general anesthesia, mice were placed in a stereotaxic frame (Kopf Instruments). In total, 0.5 μl of AAV5-CaMKIIa-ChR2(H134R)-EYFP or AAV5-CaMKIIa-eArchT3.0-EYFP (UNC Vector core) were injected bilaterally into the BLA using a 5- μl Hamilton syringe (0.05 $\mu\text{l}/\text{min}$, coordinates for the BLA, anteroposterior (AP): -1.4 mm from bregma, lateral (L): ± 3.2 mm, dorsoventral (DV): 4 mm from the brain surface). The same method was used to bilaterally inject the rAAV-mCherry-scrambleUsh or the rAAV-mCherry-Sema4A-sh791 into the ACC (coordinates: AP: +0.7 mm, L: ± 0.2 mm, DV: -2 mm, from the bregma). After injection, the 32-gauge needle remained in place for 10 min before being removed and then the skin was sutured. Following surgery, animals were left undisturbed for at least two weeks before cannula implantation. To check viral injection localization at the end of

the experiment, animals were anesthetized with Euthasol (182 mg/kg) and perfused with 30 mL of 0.1 M phosphate buffer (PB, pH 7.4) followed by 100 mL of 4% paraformaldehyde solution (PFA) in 0.1 M PB. Brains were extracted and postfixed overnight and kept at 4°C in 0.1 M PB saline (PBS) until cutting. Coronal sections (40 μm) were obtained using a vibratome (VT 1000 S, Leica, Deerfield, IL) and were serially collected in PBS. Sections were serially mounted with Vectashield medium (Vector laboratories) and localization of the fluorescence was checked using an epifluorescence microscope (Nikon 80i, FITC filter). Only animals well-injected bilaterally in the BLA were kept for further analyses.

Tracer injections

Analysis of afferent neurons from the BLA to the ACC was performed by injecting the retrograde tracer hydroxystilbamidine methanesulfonate (FluoroGold[®], Molecular Probes, 0.5 μl) bilaterally in the ACC, using a microsyringe pump controller (UMC4, World precision instruments) and a 5- μl Hamilton syringe (100 nl/min, coordinates for the ACC, AP: +0.7 mm from bregma, L: ± 0.2 mm, DV: -2 mm from the bregma). 7 days after the tracer injection, mice were anesthetized with Euthasol (182 mg/kg) and perfused with 30 ml of 0.1 M phosphate buffer (PB, pH 7.4) followed by 150 ml of 4% paraformaldehyde solution (PFA) in 0.1 M PB. Brains were removed, postfixed overnight in PFA at 4°C , and then kept at 4°C in 0.1 M PB saline (PBS, pH 7.4) until cutting. Coronal sections (40 μm) were obtained with a Vibratome (VT 1000 S, Leica, Deerfield, IL) and serially collected in PBS.

Optic fiber cannula implantation

At least two weeks after virus injection, both control and stimulated animals underwent a unilateral optic fiber cannula implantation into the ACC. The optic fiber cannula was 1.7-mm long and 220 μm in diameter. The cannula was inserted 1.5-mm deep in the brain at the following coordinates: AP: +0.7 mm L: ± 0.2 mm (MFC 220/250-0.66 1.7 mm RM3 FLT, Doric Lenses)¹⁰. For behavioral experiments, cannulas were implanted in the left hemisphere in half of each experimental group, whereas the other half received the implant in the right hemisphere. For DTI protocol, all mice were implanted in the left hemisphere. Animals were then left undisturbed for 3 to 7 days before undergoing optogenetic stimulation and behavioral testing.

Optogenetic stimulation procedures

BLA-ACC pathway inhibition. The BLA-ACC pathway was inhibited using a green light-emitting laser with a peak wavelength of 520 nm (Miniature Fiber Coupled Laser Diode Module, Doric Lenses). From the light source, the light passes through the fiber optic patch cable (MFP 240/250/900-0.63 0.75 m FC CM3, Doric Lenses) to the implant cannula. Green light was delivered in a continuous manner during 5 min prior (Forced Swim Test and Dark/light test) or during behavioral

testing (Splash test, Novelty-Suppressed Feeding Test and von Frey test). The onset and end of stimulation were manually controlled. Light intensity was measured before implantation at the fiber tip using a photodetector (UNO, Gentec, Quebec, Canada) and was set at 16 mW. All control animals underwent the same procedure but the light remained switched off.

BLA-ACC pathway activation. Activation of the BLA-ACC pathway was achieved using a blue light-emitting diode (LED) with a peak wavelength of 463 nm (LEDFRJ-B FC, Doric Lenses). From the light source, the light passes through the fiber optic patch cable (MFP 240/250/900-0.63 0.75 m FC CM3, Doric Lenses) to the implant cannula. Blue light was delivered by pulses generated through a universal serial bus connected transistor-transistor logic pulse generator (OPTG 4, Doric Lenses) connected to a LED driver (LEDRV 2CH v.2, Doric Lenses). Transistor-transistor logic pulses were generated by an open-source software developed by Doric Lenses (USBTTL V1.9). For acute activation of the BLA-ACC pathway, the stimulation was delivered during behavioral testing. For repeated activation of the pathway, stimulated animals received repetitive stimulation sequences of 3 s consisting of 2 s at 10 Hz with 10 ms pulses and 1 s without stimulation. The whole sequence was repeated for 20 min each day for 3 consecutive days for 3 weeks. Each stimulation session was performed in the animals' home cage. Light intensity was measured as described above and set between 3 mW and 5 mW. All control animals underwent the same procedure, but the light remained switched off.

Behavioral assessment

Behavioral testing was performed during the dark phase, under red light. While each mouse went through different tests, they were never submitted to more than 3 tests per week. The forced swimming test (FST) was always performed as a final test. Body weights were measured weekly. Experimenters were always blind to the pain conditions and optogenetic stimulation, except during the von Frey and Splash test concerning the inhibition paradigm condition and during the RTA, NSF and Splash test concerning the acute activation paradigm. A summary of the tests performed by each animal cohort for repeated activation paradigm is provided in Supplementary Data File 6.

Nociception-related behavior. The mechanical threshold of hind paw withdrawal was evaluated using von Frey hairs (Bioseb, Chaville, France)²³. Mice were placed in clear Plexiglas® boxes (7 × 9 × 7 cm) on an elevated mesh screen²⁴. Filaments were applied to the plantar surface of each hind paw in a series of ascending forces (0.4–8 g). Each filament was tested five times per paw, being applied until it just bent, and the threshold was defined as 3 or more withdrawals observed out of the five trials. All animals were tested before the cuff surgery to determine the basal threshold every week after cuff surgery to ensure the development of mechanical allodynia and during optogenetic stimulation to assess the effect of the inhibition of the BLA-ACC on mechanical hypersensitivity.

Locomotor activity. Spontaneous locomotor activity was monitored for each experimental group. Mice were individually placed in activity cages (32 × 20 cm floor area, 15 cm high) with seven photocell beams. The number of beam breaks was recorded over 30 min using Polyplace software (Imetronic, Pessac, France).

Real-time place avoidance (RTA) and conditioned place preference (CPP). The apparatus consists of two connected Plexiglas chambers (size 20 × 20 × 30 cm) distinguished by the wall patterns. On the first day (pre-test), animals are free to explore the apparatus for 5 min (CPP) or 10 min (RTA), and the time spent in each chamber is measured to control for the lack of spontaneous preference for one compartment. Animals spending more than 75% or less than 25% of the total time in

one chamber were excluded from the study. For RTA, the second day (test), animals are plugged to the light source placed between the two chambers and let free to explore for 10 min. Light is turned on when the mouse enters its head and forepaws in the stimulation-paired chamber and turned off when it quits the compartment. The total time spent in the stimulation-paired chamber is measured. For CPP, on the second and third days (conditioning), animals are maintained for 5 min in one chamber, where optogenetic stimulation occurs, and 4 h later placed for 5 min in the other chamber, without optogenetic stimulation. On the 4th day (test), the time spent in each chamber is recorded for 5 min.

Dark-light box test. The apparatus consists of connected light and dark boxes (18 × 18 × 14.5 cm each). The lit compartment was brightly illuminated (1000 lux). This test evaluates the conflict between the exploratory behavior of the rodent and the aversion created by bright light. Mice were placed in the dark compartment in the beginning of the test, and the time spent in the lit compartment was recorded during 5 min¹⁰. For inhibition experiment, the test was performed immediately after the light stimulation.

Novelty-suppressed feeding test. The apparatus consisted of a 40 × 40 × 30 cm plastic box with the floor covered with 2 cm of sawdust. Twenty-four hours prior to the test, food was removed from the home cage. At the time of testing, a single pellet of food was placed on a paper in the center of the box. The animal was then placed in the corner of the box and the latency to eat the pellet was recorded within a 5-min period. This test induces a conflict between the drive to eat the pellet and the fear of venturing in the center of the box⁸². For inhibition experiments, optogenetic stimulation was conducted during the test.

Splash test. This test, based on grooming behavior, was performed as previously described^{24,82}. Grooming duration was measured for 5 min after spraying a 20% sucrose solution on the dorsal coat of the mouse. Grooming is an important aspect of rodent behavior and decreased grooming in this test is considered related to the loss of interest in performing self-oriented minor tasks⁸³. For inhibition experiments, optogenetic stimulation was conducted during the test.

Nest test. This test, based on a rodent innate behavior, was performed in cages identical to the home cages of animals. Each mouse was placed in a new cage with cotton square in the center. Water and food were provided ad libitum. After 5 h, mice were placed back in their original cages and pictures of the constructed nest were taken. A score was given blindly to each nest as follows: 0 corresponds to an untouched cotton square, 1 to a cotton square partially shredded, 2 if the cotton is totally shredded but not organized, 3 if cotton is totally shredded and organized in the center of the cage, 4 if the cotton is totally shredded and shows a well-organized shape in the corner of the cage, like a nest^{84,85}.

Forced swim test. FST⁸⁶ was conducted by gently lowering the mouse into a glass cylinder (height 17.5 cm, diameter 12.5 cm) containing 11.5 cm of water (23–25 °C). The test duration was 6 min. The mouse was considered immobile when it floated in the water, in an upright position, and made only small movements to keep its head above water. Since little immobility was observed during the first 2 min, the duration of immobility was quantified over the last 4 min of the 6 min test. Concerning inhibition experiments, the test was performed just after the stimulation.

Ex vivo electrophysiological recordings

We performed whole-cell patch-clamp recordings of BLA neurons or ACC pyramidal neurons. In the BLA, we recorded from eYFP-expressing neurons of mice bilaterally injected with an AAV driving the

expression of either the archaerhodopsin ArchT3.0 or the channelrhodopsin 2 under control of the CaMKIIa promoter (with AAV5-CamKIIa-ArchT3.0-EYFP and AAV5-CamKIIa-ChR2(H134R)-EYFP, respectively). In the ACC, we recorded from pyramidal neurons surrounded by eYFP-positive fibers. For these experiments, mice were anesthetized with urethane (1.9 g/kg) and killed by decapitation, their brain was removed and immediately immersed in cold (0–4 °C) sucrose-based ACSF containing the following (in mM): 2 kynurenic acid, 248 sucrose, 11 glucose, 26 NaHCO₃, 2 KCl, 1.25 KH₂PO₄, 2 CaCl₂, and 1.3 MgSO₄ (bubbled with 95% O₂ and 5% CO₂). Transverse slices (300- μ m thick) were cut with a vibratome (VT1000S, Leica). Slices were maintained at room temperature in a chamber filled with ACSF containing the following (in mM): 126 NaCl, 26 NaHCO₃, 2.5 KCl, 1.25 NaH₂PO₄, 2 CaCl₂, 2 MgCl₂, and 10 glucose (bubbled with 95% O₂ and 5% CO₂; pH 7.3; 310 mOsm measured). Slices were transferred to a recording chamber and continuously superfused with ACSF saturated with 95% O₂ and 5% CO₂. BLA neurons expressing eYFP were recorded in the whole-cell patch-clamp configuration. Recording electrodes (3.5–4.5 M Ω) were pulled from borosilicate glass capillaries (1.2 mm inner diameter, 1.69 mm outer diameter, Warner Instruments, Harvard Apparatus) using a P1000 electrode puller (Sutter Instruments). Recording electrodes were filled with, in mM: 140 KCl, 2 MgCl₂, 10 HEPES, 2 MgATP; pH 7.3. The pH of intrapipette solutions was adjusted to 7.3 with KOH, and osmolarity to 310 mOsm with sucrose. BLA or ACC were illuminated with the same system used for the *in vivo* experiments (see above) triggered with WinWCP 4.3.5, the optic fiber being localized in the recording chamber at 3 mm from the recorded neuron. The holding potential was fixed at –60 mV. Recordings were acquired with WinWCP 4.3.5 (courtesy of Dr. J. Dempster, University of Strathclyde, Glasgow, UK). All recordings were performed at 34 °C.

MRI data acquisition

Animals were scanned 48 h after the 9th stimulation. Mouse brain resting-state functional MRI scans were performed with a 7 T Bruker BioSpec 70/30 USR animal scanner, a mouse head adapted room temperature surface coil combined with a volume transmission coil for the acquisition of the MRI signal and ParaVision software version 6.0.1 (Bruker, Ettlingen, Germany). Imaging was performed at baseline, 2 weeks, and 8 weeks after peripheral nerve injury in the cuff model (Cuff $n=7$ and Sham $n=7$). For rs-fMRI the animals were briefly anesthetized with isoflurane for initial animal handling. The anesthesia was further switched to medetomidine sedation (MD, Domitor, Pfizer, Karlsruhe, Germany), initially induced by a subcutaneous (sc) bolus injection (0.15 mg MD per kg body weight (kg bw) in 100 μ l 0.9% NaCl-solution). 10 min later, the animals received a continuous sc infusion of MD through an MRI-compatible catheter (0.3 mg/kg bw/h) inserted at the mouse shoulder level. During the whole acquisition a 2-mm thick agar gel (2% in NaCl) was applied on the mouse head to reduce any susceptibility artifacts arising at the coil/tissue interface. Respiration and body temperature were monitored throughout the imaging session. Acquisition parameters for rs-fMRI were: single shot GE-EPI sequence, 31 axial slices of 0.5 mm thickness, FOV = 2.12 \times 1.8 cm, matrix=147 \times 59, TE/TR = 15 ms/2000ms, 500 image volumes, 0.14 \times 0.23 \times 0.5 mm³ resolution. Acquisition time was 16 min. Morphological T2-weighted brain images (resolution of 0.08 \times 0.08 \times 0.4 mm³) were acquired with a RARE sequence using the following parameters: TE/TR = 40 ms/4591 ms; 48 slices, 0.4-mm slice thickness, interlaced sampling, RARE factor of 8, 4 averages; an acquisition matrix of 256 \times 256 and FOV of 2.12 \times 2 cm². Brain Diffusion Tensor MRI (DT-MRI) acquisition in the BLA-ACC optogenetically stimulated animals was performed with the 7 T animal scanner, but using a combination of a transmit–receive volume coil (86 mm) and a mouse brain adapted loop surface coil allowing the passage of the optogenetic cannulas (MRI, Bruker, Germany). Stimulated animals ($n=6$) and their controls ($n=7$) were brain imaged under isoflurane anesthesia (1.5% for maintenance) using a 4-shot DTI-EPI

sequence (TE/TR = 24 ms/3000 ms), 8 averages; with diffusion gradients applied along 45 nonlinear directions, gradient duration [δ] = 5.6 ms and gradient separation [Δ] = 11.3 ms and a b-factor of 1000 s/mm². Images with a b-factor = 0 s/mm² were also acquired. In total, 30 axial slices with 0.5 mm thickness were acquired, covering the whole brain with a FOV of 1.9 \times 1.6 cm² and an acquisition matrix of 190 \times 160 resulting in an image resolution of 0.1 \times 0.1 \times 0.5 mm³. The total acquisition time was 1 h and 20 min.

MRI data processing

Rs-fMRI images were spatially normalized into a template using Advanced Normalization Tools (ANTs) software⁸⁷ using SyN algorithm and smoothed (FWHM = 0.28 \times 0.46 \times 1 mm³) with SPM8. Seed-based functional connectivity analysis was performed with a MATLAB tool developed in-house. Regions of interest (ROI) were extracted from Allen Mouse Brain Atlas³⁹ which were later normalized into the template space. Resting-state time series were de-trended, band-pass filtered (0.01–0.1 Hz) and regressed for the cerebrospinal fluid signal from the ventricles. Principal component analysis (PCA) of the BOLD time courses across voxels within a given ROI was performed, and first principal component accounting for the largest variability was selected as the representative time course for further analysis. Spearman correlations between the PCA time course of single ROIs and each voxel of the brain was computed at the group and individual levels and r values were converted to z using Fisher's r -to- z transformation. Individual connectivity maps for baseline rs-fMRI acquisitions were subtracted from 2 and 8 PO weeks counterparts for each subject. Baseline subtracted connectivity maps were subsequently used for two sample t test with SPM8 to perform group comparison. Family-wise error rate (FWER) correction was applied at the cluster level ($P < 0.05$) for each statistical image. Preprocessing of diffusion-weighted images included denoising⁸⁸, removal of Gibbs ringing artifacts⁸⁹, motion correction⁹⁰, and bias field inhomogeneity correction⁹¹. Diffusion tensor was estimated⁷¹ using weighted least-squares (WLS) approach and the following tensor-derived parameters were computed: fractional anisotropy (FA), axial diffusivity (AD), mean diffusivity (MD) and radial diffusivity (RD). All these processing steps were done using MRtrix3 (<https://www.mrtrix.org>); except the motion correction step, done using Advanced Normalisation Tools (ANTs, <http://stnava.github.io/ANTs/>). Based on $b=0$ s/mm² images (i.e., the volume without diffusion weighting), these images were then spatially registered in a common space using the SyN registration method of ANTs to build a study-specific template, which was then registered onto the Allen Brain Atlas template. Each mouse tensor-derived maps was warped in this common space. These registered images were finally smoothed by a 0.5 mm full-width half maximum (FWHM) Gaussian kernel. Inter-group differences for all the DTI-derived parameters were assessed using the SPM12 General Linear Model (GLM). The results were analyzed according to a level of statistical significance, $P < 0.001$ without correction. Further, correlational analyses were performed between the DTI metrics (voxel level) and the results from splash tests (statistical significance was $P < 0.001$, uncorrected).

Immunohistochemistry

c-Fos immunoperoxidase. On the 5th day after the last stimulation, animals were stimulated once with the same procedure as described before (for BLA-ACC activation). 90 min later, animals were anesthetized with Euthasol (182 mg/kg) and perfused with 30 ml of 0.1 M PB (pH 7.4) followed by 100 ml of 4% PFA in 0.1 M PB. Brains were removed, postfixed overnight and kept at 4 °C in 0.1 M PBS (pH 7.4) until cutting. Coronal sections (40 μ m) were obtained using a vibratome (VT 1000 S, Leica, Deerfield, IL) and were serially collected in PBS. Sections were incubated 15 min in a 1% H₂O₂/50% ethanol solution and washed in PBS (3 \times 10 min). Sections were then pre-incubated in PBS containing Triton X-100 (0.3%) and donkey serum (5%) for 45 min.

Sections were then incubated overnight at room temperature in PBS containing Triton X-100 (0.3%), donkey serum (1%) and rabbit anti-c-Fos (1:10,000, Santa Cruz Biotechnology, EI008). Sections were then washed in PBS (3×10min), incubated with biotinylated donkey anti-rabbit secondary antibody (1:300) in PBS containing Triton X-100 (0.3%), donkey serum (1%) for 2 h and washed in PBS (3 × 10 min). Sections were incubated with PBS containing the avidin-biotin-peroxidase complex (ABC kit; 0.2% A and 0.2% B; Vector laboratories) for 90 min. After being washed in Tris-HCl buffer, sections were incubated in 3,3'-diaminobenzidine tetrahydrochloride (DAB) and H₂O₂ in Tris-HCl for approximately 4 min and washed again. Sections were serially mounted on gelatin-coated slides, air dried, dehydrated in graded alcohols, cleared in Roti-Histol (Carl Roth, Karlsruhe, Germany) and coverslipped with Eukitt. c-Fos immunohistochemistry then allowed controlling for both the implant location and the activation of the ACC by the optogenetic procedure. Animals having c-Fos induction outside of the ACC, for instance, in the motor cortex, were excluded from analysis.

c-Fos immunofluorescence. One week after the Fluorogold injection in the ACC, animals were anesthetized with Euthasol (182 mg/kg) and perfused with 30 ml of 0.1 M PB (pH 7.4) followed by 100 ml of 4% PFA in 0.1 M PB. Brains were removed, postfixed overnight, and kept at 4 °C in 0.1 M PBS (pH 7.4) until cutting. Coronal sections (40 μm) were obtained using a vibratome (VT 1000 S) and were serially collected in PBS. Sections were washed in PBS (3 × 10min) and pre-incubated in PBS containing Triton X-100 (0.3%) and donkey serum (5%) for 45 min. Sections were then incubated overnight at room temperature in PBS containing Triton X-100 (0.3%), donkey serum (1%) and rabbit anti-c-Fos (1:1000, Synaptic System, 226-003). Sections were then washed in PBS (3×10min), incubated with Alexa fluor 594 donkey anti-rabbit secondary antibody (1:400) in PBS containing Triton X-100 (0.3%), donkey serum (1%) for 2 h and washed in PBS (3 × 10 min). Sections were finally serially mounted with vectashield medium (Vector laboratories).

Olig2 immunofluorescence. Twenty-four hours after the last behavioral test, animals were anesthetized with Euthasol (182 mg/kg) and perfused with 30 ml of 0.1 M PB (pH 7.4) followed by 100 ml of 4% PFA in 0.1 M PB. Brains were removed, postfixed overnight and kept at 4 °C in 0.1 M PBS (pH 7.4) until cutting. Coronal sections (40 μm) were obtained using a vibratome (VT 1000 S) and were serially collected in PBS. Sections were washed in PBS (3 × 10 min) and pre-incubated in PBS containing Triton X-100 (0.3%) and donkey serum (5%) for 1 h. Sections were then incubated overnight at +4 °C in PBS containing Triton X-100 (0.3%) and rabbit anti-Olig2 (1:200, Merck-Millipore, AB9610). Sections were then washed in PBS (3×10min), incubated with Cy3 donkey anti-rabbit secondary antibody (1:400, Jackson ImmunoResearch, 711-165-152) in PBS containing Triton X-100 (0.3%) for 2 h and washed in PBS (3×10min). Sections were finally serially mounted with Fluoromount-G (Electron Microscopy Sciences, EM-17984-25).

Olig2 and PDGFRa co-staining. Twenty-four hours after the last behavioral test, animals were anesthetized with Euthasol (182 mg/kg) and perfused with 30 ml of 0.1 M PB (pH 7.4) followed by 100 ml of 4% PFA in 0.1 M PB. Brains were removed, postfixed overnight and kept at 4 °C in 0.1 M PBS (pH 7.4) until cutting. Coronal sections (40 μm) were obtained using a vibratome (VT 1000 S) and were serially collected in PBS. Sections were mounted on a Superfrost slide (Eprelia reference J1800AMNZ) and dried for 30 min at room temperature. Slides were dipped 2 times in H₂O and incubated for 15 min at 98 °C in RNAscope target retrieval buffer (ACDBio ref. 322001). Slides were quickly rinsed in H₂O, washed in PBS (2×10 min) and pre-incubated in PBS containing Triton X-100 (0.3%) and donkey serum (5%) for 1 h and 30 min. Sections were then incubated overnight at +4 °C in PBS containing Triton

X-100 (0.3%), goat anti-PDGFRa (1:200, RandD systems, AF1062) and rabbit anti-Olig2 (1:200, Merck-Millipore, AB9610). Sections were then washed in PBS (3 × 10 min), incubated with Cy3 donkey anti-goat secondary antibody (1:400, Jackson ImmunoResearch, 705-165-147) and Alexa Fluor 647 donkey anti-rabbit (1:400, Invitrogen, A31573) in PBS containing Triton X-100 (0.3%) for 2 h and washed in PBS (3 × 10 min). Sections were finally serially mounted with Fluoromount-G (Electron Microscopy Sciences, EM-17984-25).

Fluorogold and c-Fos quantification

Single-layer images were acquired using a laser-scanning microscope (confocal Leica SP5 Leica Microsystems CMS GmbH) equipped with a ×20 objective. Excitation wavelengths were sequentially diode 405 nm, argon laser 488 nm, and diode 561 nm. Emission bandwidths are 550-665 nm for Fluorogold fluorescence and 710-760 nm for Alexa594 signal. Segmentation and classification of c-Fos+ cells were performed from three sections for each animal using a deep learning model. The model was trained from scratch for 400 epochs on 10 paired image patches (image dimensions: (160,160), patch size: (160,160)) with a batch size of 2 and a mae loss function, using the StarDist 2D ZeroCostDL4Micnotebook (v1.11)⁹². Key python packages used include tensorflow (v0.1.12), Keras (v2.3.1), csbdeep (v0.6.2), numpy (v1.19.5), cuda (v11.0.221). The training was accelerated using a Tesla K80 GPU and the dataset was augmented by a factor of 4. Segmentation and classification of Fluorogold signal was done using Stardist 2D_ versatile_fluo^{93,94} pre-trained model. Fluorogold masks and c-Fos masks were then overlaid to count the double-positive cells using Fiji⁹⁵.

PDGFRa and Olig2 quantification

Three field of view by three single-layer mosaics were acquired using a laser-scanning microscope (confocal Leica Stellaris 8 Leica Microsystems CMS GmbH) equipped with ×10 objective. Excitation wavelengths were sequentially white light laser 554 nm and 653 nm. Emission bandwidths are 559–632 nm for Cy3 signal and 663–839 nm for Alexa Fluor 647 signal. Positive cells were counted in the whole ACC using Fiji⁹⁵.

RNAscope

Forty-eight hours after the last stimulation, brain samples were immersed in isopentane and immediately placed at –80 °C. Frozen samples were embedded in OCT compound and 14-μm thick sections were performed on cryostat, mounted on slides and put back in –80 °C freezer. Sections were fixed, dehydrated and pre-treated using the “RNAscope Sample Preparation and Pre-treatment Guide for Fresh Frozen Tissue using RNAscope Fluorescent Multiplex Assay” protocol (Advanced Cell Diagnostics). Hybridation of *Slc17a7* (ACD, 416631), *Gad2* (ACD, 415071-C2) and *c-fos* (ACD, 316921) probes and development of the different signals with Opal 520, 590, and 690 fluorophores were performed in accordance with the “RNAscope Multiplex Fluorescent Reagent Kit v2 Assay” instructions (Advanced Cell Diagnostics). Single-layer images were acquired using a laser-scanning nanoscope (S60; Hamamatsu Photonics) at ×40 magnification. Quantifications were performed from two sections for each animal on QuPath 0.3.0 software⁹⁶. First, the region of interest was delimited using the polygon annotation tool. Then nuclei were detected within regions of interest using the cell detection module on the Dapi staining. To determine the *c-fos*, *Gad2*, and *Slc17a7* positive cells on our regions of interest, object classifiers were trained in Qupath using Random trees classifiers. We selected all the features by output class (Nucleus mean, Nucleus sum, Nucleus standard deviation, Nucleus maximum, Nucleus minimum, Nucleus range, Cell mean, Cell standard deviation, Cell maximum, Cell minimum, Cytoplasm mean, Cytoplasm standard deviation, Cytoplasm maximum, Cytoplasm minimum), and annotated manually a minimum of 20 points for positive cells and negative cells.

Classifiers were then applied sequentially on the whole region of interest to determine the *c-fos*, *Gad2*, and *Slc17a7* positive cells.

RNA extraction

Two different batches of animals were generated for RNA sequencing, with a third one for Fluidigm validation of RNA-sequencing results. Forty-eight hours after the last stimulation, bilateral ACC was freshly dissected from animals killed by cervical dislocation and tissues were stored at -80°C . Total RNA was extracted from ACC tissue with the Qiagen RNeasy Mini Kit (Hilden Germany). Around 20 mg of ACC tissue was disrupted and homogenized with a Kinematica Polytron 1600E in 1.2 ml QIAzol Lysis reagent, for 30 s, and then left at room temperature for 5 min. Next, 240 μl of chloroform was added and mixed before centrifugation for 15 min at $17,000 \times g$ at 4°C . The aqueous phase (600 μl) was transferred to a new collection tube and mixed with 600 μl of 70% ethanol. The mix was transferred into a RNeasy spin column in a 2-ml collection tube, and centrifuged at $12,000 \times g$ for 15 s. Next, 350 μl of RW1 buffer was added and centrifuged at $12,000 \times g$, for 15 s, before adding 10 μl of DNase and 70 μl of RDD buffer. The mix was left at room temperature for 15 min and 350 μl of RW1 buffer was added and centrifuged at $12,000 \times g$ for 15 s. The column was then transferred to a new 2 ml collection tube and washed with 500 μl of RPE buffer, before being centrifuged at $12,000 \times g$. Finally, the column was dry centrifuged at $12,000 \times g$ for 5 min, and transferred to a new 1.5 ml collection tube to which 18 μl of RNase-free water was added. Finally, the RNA was eluted by centrifugation for 1 min at $12,000 \times g$. Samples were kept at -80°C until use.

Mouse RNA sequencing

RNA sequencing was performed by the Genomeast platform at IGBMC. Full length cDNAs were generated from 5 ng of total RNA using the Clontech SMARTSeq v4 Ultra Low Input RNA kit for Sequencing (PN 091817, Takara Bio Europe, Saint-Germain-en-Laye, France) according to the manufacturer's instructions, with 10 cycles of PCR for cDNA amplification by Seq-Amp polymerase. Six hundred pg of pre-amplified cDNA were then used as input for Tn5 transposon tagmentation by the Nextera XT DNA Library Preparation Kit (PN 15031942, Illumina, San Diego, CA), followed by 12 PCR cycles of library amplification. Following purification with Agencourt AMPure XP beads (BeckmanCoulter, Villepinte, France), the size and concentration of libraries were assessed by capillary electrophoresis. Libraries were then sequenced using an Illumina HiSeq 4000 system using single-end 50 bp reads. Reads were trimmed using cutadapt v1.10, mapped onto the mm10 assembly of the *Mus musculus* genome, using STAR version 2.5.3a⁹⁷. Gene expression quantification was performed from uniquely aligned reads using htseq-count⁹⁸ version 0.6.1p1, with annotations from Ensembl version 95. Read counts were then normalized across samples with the median-of-ratios method proposed by Anders and Huber⁹⁹, to make these counts comparable between samples. Principal Component Analysis was computed on regularized logarithm-transformed data calculated with the method proposed by Love and collaborators¹⁰⁰. Differential expression analysis was performed using R and the Bioconductor package DESeq2 version 1.22.1¹⁰⁰, using RIN values and batches as covariates. Because we generated two batches of mice, the lfcShrink function was used instead of betaPrior in order to calculate *P* values from the log₂ Fold changes unshrunk and to perform the shrinkage afterward. RIN and sample batches can be found in Supplementary Table 1.

Human RNA-sequencing data

Human gene expression data, obtained from our previous publication³⁷ (archived on GEO Datasets under the reference series: "GSE151827" samples: GSM5026548-97), were generated initially using postmortem ACC tissue from the Douglas-Bell Canada Brain Bank. This cohort was composed of 26 subjects who died by suicide during a major

depressive episode, and 24 psychiatrically healthy controls. Groups were matched for age, postmortem interval and brain pH, and included both man (19 in control group and 19 in MDD group) and woman (5 in control group, 7 in MDD group) subjects. All control subjects corresponded to healthy individuals with no psychiatric history. Depressed individuals had a history of early-life adversity (ELA), but did not suffer from comorbid psychosis or bipolar disorder (exclusion criteria). Demographics for the cohort can be found in Supplementary Table 1. While differential expression analysis for the whole cohort (both males and females) was reported previously³⁷, during the present work we also reprocessed raw gene counts from male individuals only, and conducted a new differential expression analysis to compare men with MDD and healthy control men, taking into account RIN, and age, as in ref. 37. Matching of self-reported gender and biological sex was validated by inspecting relative expression levels of well-known sex-specific genes (e.g., *XIST*, *KDM5D*, *ZFY*, *UTY*, *EIF1AY*).

Rank-rank hypergeometric overlap (RRHO) analysis

In order to compare mouse and human RNA-Sequencing data, we used the RRHO2 procedure, as described previously¹⁰¹, using the R package available at <https://github.com/Caleb-Huo/RRHO2>. Mice-human orthologous genes were first obtained using the R package BioMart, leaving a total of 13572 genes. Genes in each dataset were ranked based on the following metric: $-\log_{10}(P \text{ value}) \times \text{sign}(\log_2 \text{ Fold Change})$. Then, the RRHO2 function was applied to the two gene lists at default parameters (with step size equal to the square root of the list length). The significance of hypergeometric overlaps between human and mouse gene expression changes are reported as log₁₀ *P* values, corrected using the Benjamini–Yekutieli procedure.

Gene set enrichment analysis (GSEA)

Mouse and human genes were ranked independently based on the fold changes obtained from their respective differential expression analysis. GSEA was performed as previously described¹⁰² using the GSEA-Preranked tool and the Lein Oligodendrocyte markers gene set.

Weighted gene co-expression network analysis (WGCNA)

WGCNA⁴⁰ was used to construct gene networks in mice and humans using RNA-seq expression data and then identify conserved gene modules between the two species. The RNA-sequencing expression data were normalized for batch and RIN in mice; and for age and RIN in humans (as well as sex included when analyzing the whole cohort). First, a soft-threshold power was defined (mouse: 4, human: 8) to reach a degree of independence superior to 0.8 and thus ensure the scale-free topology of the network. To construct the network and detect modules, the blockwiseModules function of the WGCNA algorithm was used, with the minimum size of modules set at 30 genes. Then, the eigengene of each module was correlated with our traits of interest (optogenetic stimulation of the BLA-ACC pathway in mice, or MDD in humans) and gene significance (GS), defined as the correlation between each individual gene and trait, was calculated. Inside each module a measure of the correlation between the module eigengene and the gene expression profile, or module membership (MM), was also assessed. Conservation of WGCNA modules across mice and humans was assessed by Fisher's exact test. Modules were considered as significantly overlapping, and therefore conserved, when *Padj* < 0.05. Among the modules displaying a significant overlap between human and mice, only those with a significant (*Padj* < 0.1) association between the module eigengene and trait, in both species, were kept for further analysis.

Gene ontology

Enrichments for functional terms in differentially expressed genes (DEGs) in humans and mice were performed using WEBGSTALL for biological process, cellular component, and molecular function³⁶. Analysis was restricted to DEG with nominal *P* values < 0.05. The same

procedure was applied to the list of genes obtained by RRHO, dysregulated in similar directions in mice and humans, and corresponding to the best one-sided Fisher exact *t* test *P* value.

Fluidigm

cDNA was generated by subjecting 50 ng of RNA from each sample to reverse transcriptase reaction (Reverse Transcription Master Mix Kit Fluidigm P/N-100-6297). Then, 1.25 μ L of each cDNA solution was used to generate a preamp mix containing a pool of the 26 primers pairs and the PreAmp Master Mix Kit (Fluidigm P/N-100-5744). Preamp mixes were run for 14 cycles and the remaining primers were digested with Exonuclease I (New England Biolabs, P/N MO293L, LOT 0191410). Preamp samples were analyzed for the expression of 22 genes of interest (for primer sequences, see Supplementary Table 3) using the BioMark qPCR platform (Fluidigm, San Francisco, CA, USA). Data were normalized to *Gadph*, *B2m*, *Actb* and *Gusb* (from the same animal) and fold changes were calculated using the $2^{-\Delta\Delta C_t}$ method⁹⁴.

Plasmid construction

For the expression of shRNAs, long oligonucleotide linkers were designed containing the *Hind*III and *Bgl*II restriction sites at the 5' and 3' extremities, respectively. Each linker contained the loop TTCAA GAGA separating a forward and a reverse copy of the following shRNA sequences: GGAAGAGCCAGACAGGTTTCT for mouse *Sema4a* exon 15, GCCACAACGCTATATCATGG for eGFP and GCGCTTAGCTGTAGG ATTC for a universal scramble. Linkers were cloned by restriction/ligation downstream the mouse U6 promoter into the pAAV-CMV-mCherry-mU6 construct derived from pAAV-MCS (Agilent). For the construction of the plasmid for the sh efficiency testing in cells, the *Sema4a* exon 15 was amplified from C57Bl/6 embryonic stem cell genomic DNA and cloned at the C-terminal end of eGFP into pEGFP-C1 by SLIC using the following primers:

GTACAAGTCCGGACTCAGATCTCGAGCTATTAAGAAGTCCTGA CAGTCCC and GATCAGTTATCTAGATCCGGTGGATCCTTAAGCCACT TCGGCGCC.

AAV production

Recombinant adenoassociated virus AAV serotype 5 (AAV5) were generated by a triple transfection of HEK293T-derived cell line using polyethylenimine (PEI) transfection reagent and the three following plasmids: pAAV-CMV-mCherry-mU6-shRNA, pXR5 (deposited by Dr Samulski, UNC Vector Core) encoding the AAV serotype 5 capsid and pHelper (Agilent) encoding the adenovirus helper functions. 48 h after transfection, AAV5 vectors were harvested from cell lysate treated with Benzonase (Merck) at 120 U/ml. They were further purified by gradient ultracentrifugation with Iodixanol (OptiprepTM density gradient medium) followed by dialysis and concentration against Dulbecco's PBS using centrifugal filters (Amicon Ultra-15 Centrifugal Filter Devices 100 K, Millipore). Viral titers were quantified by Real-Time PCR using the LightCycler480 SYBR Green I Master (Roche) and primers targeting mCherry sequence. Titers are expressed as genome copy per milliliter (GC/ml).

Validation of *Sema4a* shRNAs in cell culture

The efficiency of the different shRNA sequences in inhibiting the expression of *Sema4a* was evaluated in a cell culture test. For this purpose, 5×10^5 HEK293T cells were seeded in each well of a six-well plate and transfected (6 h after seeding) with 1 mg of each of the pAAV-mCherry-U6-sh-*Sema4a* plasmids, combined with 1 mg of the peGFP-*Sema4a*-ex15 plasmid. The peGFP plasmid used in this test was constructed by cloning, into the peGFP-C1 backbone, the *Sema4a* exon 15 sequence downstream the eGFP gene. The inhibition of the *Sema4a* mRNA by a specific shRNA induces a decrease in the GFP expression and, therefore, a decrease of the green fluorescence intensity. The fluorescence intensity of the wells transfected with peGFP-*Sema4a*-

ex15 and pAAV-U6-sh-*Sema4a* was measured 48 h after transfection and compared with the fluorescence intensity of cells transfected with the same concentration of peGFP-*Sema4a*-ex15 and pAAV-U6-shScramble (negative control) or pAAV-U6-shGFP (positive control).

Statistics and reproducibility

Statistical analyses were performed in GraphPad Prism v9.0 software. Data are expressed as mean \pm SEM, with statistical significance set as **P* < 0.05, ***P* < 0.01, ****P* < 0.001. Student's *t* test (paired and unpaired), One-way analysis of variance (ANOVA), one-way repeated measures ANOVA, and two-way ANOVA followed by Newman–Keuls post hoc test were used when appropriate. If data failed the Shapiro–Wilk normality test, Mann–Whitney non-parametric (one- or two-tailed) analysis was used when comparing two independent groups, and the Chi-Square test for trend was used to compare the distribution of nest scores between groups. Experiments for brain morphological analysis (immunohistochemistry, RNAscope) were repeated independently with similar results in at least three animals using a minimum of three sections per side and per animal. Electrophysiological recordings were performed in at least two mice.

Emotionality z-scores

Emotionality z-scores were computed as previously described by³⁴. First, individual z-score values were calculated for each mouse in each test using Eq. (1):

$$z = \frac{X - \mu}{\sigma} \quad (1)$$

where *X* represents the individual data for the observed parameter while μ and σ represent the mean and standard deviation of the control group. The directionality of scores was adjusted so that decreased score values reflect increased dimensionality (anxiety- or depressive-like behaviors). For instance, increased immobility time in the FST was converted into negative standard deviation changes compared to group means indicating increased behavioral deficits. Finally, z values obtained for each test were averaged to obtain a single emotionality score using Eq. (2):

$$\text{Emotionality } z - \text{score} = \frac{Z_{\text{test1}} + Z_{\text{test2}} + \dots + Z_{\text{testn}}}{\text{Number of tests}} \quad (2)$$

Reporting summary

Further information on research design is available in the Nature Portfolio Reporting Summary linked to this article.

Data availability

Raw and processed human data reported in this study using post-mortem brain tissue from the ACC are publicly available on NCBI's GEO Datasets website, via the Gene Expression Omnibus accession number "GSE151827" (samples: GSM5026548-97). Raw and processed mouse RNA-Sequencing data related to transcriptional signature of neuropathic pain, published by Dai et al. and used in this study for comparison with optogenetic activation of the BLA–ACC pathway (Supplementary Fig. 8) are publicly available via the Gene Expression Omnibus accession number "GSE197233". Finally, raw and processed RNA-sequencing data regarding transcriptional effects, in the ACC, of optogenetic activation of the BLA–ACC pathway, are publicly available via the Gene Expression Omnibus accession number "GSE227159". Source data are provided with this paper.

Code availability

The source code generated during this study is provided in Supplementary information (Supplementary Note 1).

References

1. Bair, M. J., Robinson, R. L., Katon, W. & Kroenke, K. Depression and pain comorbidity: a literature review. *Arch. Intern. Med.* **163**, 2433–2445 (2003).
2. Rayner, L. et al. Depression in patients with chronic pain attending a specialised pain treatment centre: prevalence and impact on health care costs. *Pain* **157**, 1472–1479 (2016).
3. Arnow, B. A. et al. Comorbid depression, chronic pain, and disability in primary care. *Psychosom. Med.* **68**, 262–268 (2006).
4. Gallagher, R. M. & Verma, S. Managing pain and comorbid depression: a public health challenge. *Semin. Clin. Neuropsychiatry* **4**, 203–220 (1999).
5. Thompson, J. M. & Neugebauer, V. Cortico-limbic pain mechanisms. *Neurosci. Lett.* **702**, 15–23 (2019).
6. Apkarian, A. V., Bushnell, M. C., Treede, R.-D. & Zubieta, J.-K. Human brain mechanisms of pain perception and regulation in health and disease. *Eur. J. Pain* **9**, 463–484 (2005).
7. Drevets, W. C., Savitz, J. & Trimble, M. The subgenual anterior cingulate cortex in mood disorders. *CNS Spectr.* **13**, 663–681 (2008).
8. Kummer, K. K., Mitrić, M., Kalpachidou, T. & Kress, M. The medial prefrontal cortex as a central hub for mental comorbidities associated with chronic pain. *Int. J. Mol. Sci.* **21**, 3440 (2020).
9. Xiao, C. et al. Early molecular alterations in anterior cingulate cortex and hippocampus in a rodent model of neuropathic pain. *Brain Res. Bull.* **166**, 82–91 (2021).
10. Barthas, F. et al. The anterior cingulate cortex is a critical hub for pain-induced depression. *Biol. Psychiatry* **77**, 236–245 (2015).
11. Sellmeijer, J. et al. Hyperactivity of anterior cingulate cortex areas 24a/24b drives chronic pain-induced anxiodepressive-like consequences. *J. Neurosci. J. Soc. Neurosci.* **38**, 3102–3115 (2018).
12. LeDoux, J. E. & Brown, R. A higher-order theory of emotional consciousness. *Proc. Natl Acad. Sci. USA* **114**, E2016–E2025 (2017).
13. Fillinger, C., Yalcin, I., Barrot, M. & Veinante, P. Afferents to anterior cingulate areas 24a and 24b and midcingulate areas 24a' and 24b' in the mouse. *Brain Struct. Funct.* **222**, 1509–1532 (2017).
14. Fillinger, C., Yalcin, I., Barrot, M. & Veinante, P. Efferents of anterior cingulate areas 24a and 24b and midcingulate areas 24a' and 24b' in the mouse. *Brain Struct. Funct.* **223**, 1747–1778 (2018).
15. Kesner, R. P., Walser, R. D. & Winzenried, G. Central but not basolateral amygdala mediates memory for positive affective experiences. *Behav. Brain Res.* **33**, 189–195 (1989).
16. Namburi, P. et al. A circuit mechanism for differentiating positive and negative associations. *Nature* **520**, 675–678 (2015).
17. Veinante, P., Yalcin, I. & Barrot, M. The amygdala between sensation and affect: a role in pain. *J. Mol. Psychiatry* **1**, 9 (2013).
18. Drevets, W. C. Neuroimaging abnormalities in the amygdala in mood disorders. *Ann. N. Y. Acad. Sci.* **985**, 420–444 (2003).
19. Simons, L. E. et al. The human amygdala and pain: Evidence from neuroimaging. *Hum. Brain Mapp.* **35**, 527–538 (2012).
20. Åhrlund-Richter, S. et al. A whole-brain atlas of monosynaptic input targeting four different cell types in the medial prefrontal cortex of the mouse. *Nat. Neurosci.* **22**, 657–668 (2019).
21. Hintiryan, H. et al. Connectivity characterization of the mouse basolateral amygdalar complex. *Nat. Commun.* **12**, 2859 (2021).
22. Zhuo, M. Neural mechanisms underlying anxiety-chronic pain interactions. *Trends Neurosci.* **39**, 136–145 (2016).
23. Yalcin, I. et al. A time-dependent history of mood disorders in a murine model of neuropathic pain. *Biol. Psychiatry* **70**, 946–953 (2011).
24. Yalcin, I. et al. The sciatic nerve cuffing model of neuropathic pain in mice. *J. Vis. Exp. JoVE* 51608 <https://doi.org/10.3791/51608> (2014).
25. Barthas, F. et al. Cingulate overexpression of mitogen-activated protein kinase phosphatase-1 as a key factor for depression. *Biol. Psychiatry* **82**, 370–379 (2017).
26. Allen, H. N., Bobnar, H. J. & Kolber, B. J. Left and right hemispheric lateralization of the amygdala in pain. *Prog. Neurobiol.* **196**, 101891 (2021).
27. Ji, G. & Neugebauer, V. Hemispheric lateralization of pain processing by amygdala neurons. *J. Neurophysiol.* **102**, 2253–2264 (2009).
28. Gonçalves, L. & Dickenson, A. H. Asymmetric time-dependent activation of right central amygdala neurones in rats with peripheral neuropathy and pregabalin modulation. *Eur. J. Neurosci.* **36**, 3204–3213 (2012).
29. Zheng, C. J., Van Drunen, S. & Egorova-Brumley, N. Neural correlates of co-occurring pain and depression: an activation-likelihood estimation (ALE) meta-analysis and systematic review. *Transl. Psychiatry* **12**, 1–16 (2022).
30. Johansen, J. P., Fields, H. L. & Manning, B. H. The affective component of pain in rodents: direct evidence for a contribution of the anterior cingulate cortex. *Proc. Natl Acad. Sci. USA* **98**, 8077–8082 (2001).
31. LaGraize, S. C., Labuda, C. J., Rutledge, M. A., Jackson, R. L. & Fuchs, P. N. Differential effect of anterior cingulate cortex lesion on mechanical hypersensitivity and escape/avoidance behavior in an animal model of neuropathic pain. *Exp. Neurol.* **188**, 139–148 (2004).
32. Qu, C. et al. Lesion of the rostral anterior cingulate cortex eliminates the aversiveness of spontaneous neuropathic pain following partial or complete axotomy. *Pain* **152**, 1641–1648 (2011).
33. Gao, S.-H. et al. The projections from the anterior cingulate cortex to the nucleus accumbens and ventral tegmental area contribute to neuropathic pain-evoked aversion in rats. *Neurobiol. Dis.* **140**, 104862 (2020).
34. Guilloux, J.-P., Seney, M., Edgar, N. & Sibille, E. Integrated behavioral z-scoring increases the sensitivity and reliability of behavioral phenotyping in mice: relevance to emotionality and sex. *J. Neurosci. Methods* **197**, 21–31 (2011).
35. Kremer, M. et al. A dual noradrenergic mechanism for the relief of neuropathic allodynia by the antidepressant drugs duloxetine and amitriptyline. *J. Neurosci. J. Soc. Neurosci.* **38**, 9934–9954 (2018).
36. Liao, Y., Wang, J., Jaehnig, E. J., Shi, Z. & Zhang, B. WebGestalt 2019: gene set analysis toolkit with revamped UIs and APIs. *Nucleic Acids Res.* **47**, W199–W205 (2019).
37. Lutz, P.-E. et al. Association of a history of child abuse with impaired myelination in the anterior cingulate cortex: convergent epigenetic, transcriptional, and morphological evidence. *Am. J. Psychiatry* **174**, 1185–1194 (2017).
38. Cahill, K. M., Huo, Z., Tseng, G. C., Logan, R. W. & Seney, M. L. Improved identification of concordant and discordant gene expression signatures using an updated rank-rank hypergeometric overlap approach. *Sci. Rep.* **8**, 9588 (2018).
39. Lein, E. S. et al. Genome-wide atlas of gene expression in the adult mouse brain. *Nature* **445**, 168–176 (2007).
40. Langfelder, P. & Horvath, S. WGCNA: an R package for weighted correlation network analysis. *BMC Bioinforma.* **9**, 559 (2008).
41. Zhou, Y., Lutz, P.-E., Wang, Y. C., Ragoussis, J. & Turecki, G. Global long non-coding RNA expression in the rostral anterior cingulate cortex of depressed suicides. *Transl. Psychiatry* **8**, 224 (2018).
42. Bansal, Y. & Kuhad, A. Mitochondrial Dysfunction in Depression. *Curr. Neuropharmacol.* **14**, 610–618 (2016).
43. Howard, D. M. et al. Genome-wide meta-analysis of depression identifies 102 independent variants and highlights the importance of the prefrontal brain regions. *Nat. Neurosci.* **22**, 343–352 (2019).

44. Scarpa, J. R. et al. Shared transcriptional signatures in major depressive disorder and mouse chronic stress models. *Biol. Psychiatry* **88**, 159–168 (2020).
45. Hübner, N. S. et al. The connectomics of brain demyelination: functional and structural patterns in the cuprizone mouse model. *NeuroImage* **146**, 1–18 (2017).
46. Cerina, M. et al. Myelination- and immune-mediated MR-based brain network correlates. *J. Neuroinflammation* **17**, 186 (2020).
47. Dai, W. et al. Sex-specific transcriptomic signatures in brain regions critical for neuropathic pain-induced depression. *Front. Mol. Neurosci.* **15**, 886916 (2022).
48. Boda, E. Myelin and oligodendrocyte lineage cell dysfunctions: New players in the etiology and treatment of depression and stress-related disorders. *Eur. J. Neurosci.* **53**, 281–297 (2021).
49. Hemanth Kumar, B. S. et al. Demyelinating evidences in CMS rat model of depression: a DTI study at 7 T. *Neuroscience* **275**, 12–21 (2014).
50. Hercher, C., Turecki, G. & Mechawar, N. Through the looking glass: examining neuroanatomical evidence for cellular alterations in major depression. *J. Psychiatr. Res.* **43**, 947–961 (2009).
51. Miguel-Hidalgo, J. J., Moulana, M., Deloach, P. H. & Rajkowska, G. Chronic unpredictable stress reduces immunostaining for connexins 43 and 30 and myelin basic protein in the rat prelimbic and orbitofrontal cortices. *Chronic Stress* **2**, 2470547018814186 (2018).
52. Takahashi, K. et al. Disturbance of prefrontal cortical myelination in olfactory bulbectomized mice is associated with depressive-like behavior. *Neurochem. Int.* **148**, 105112 (2021).
53. Hagemeyer, N. et al. A myelin gene causative of a catatonia-depression syndrome upon aging. *EMBO Mol. Med.* **4**, 528–539 (2012).
54. Roy, K. et al. Loss of erbB signaling in oligodendrocytes alters myelin and dopaminergic function, a potential mechanism for neuropsychiatric disorders. *Proc. Natl Acad. Sci. USA* **104**, 8131–8136 (2007).
55. Chiou, B., Neely, E., Kallianpur, A. & Connor, J. R. Semaphorin4A causes loss of mature oligodendrocytes and demyelination in vivo. *J. Neuroinflammation* **16**, 28 (2019).
56. Leitner, D. F., Todorich, B., Zhang, X. & Connor, J. R. Semaphorin4A is cytotoxic to oligodendrocytes and is elevated in microglia and multiple sclerosis. *ASN NEURO* **7**, 1759091415587502 (2015).
57. Chiou, B., Lucassen, E., Sather, M., Kallianpur, A. & Connor, J. Semaphorin4A and H-ferritin utilize Tim-1 on human oligodendrocytes: a novel neuro-immune axis. *Glia* **66**, 1317–1330 (2018).
58. Eiza, N., Garty, M., Staun-Ram, E., Miller, A. & Vadasz, Z. The possible involvement of sema3A and sema4A in the pathogenesis of multiple sclerosis. *Clin. Immunol.* **238**, 109017 (2022).
59. Bliss, T. V. P., Collingridge, G. L., Kaang, B.-K. & Zhuo, M. Synaptic plasticity in the anterior cingulate cortex in acute and chronic pain. *Nat. Rev. Neurosci.* **17**, 485–496 (2016).
60. Becker, L. J., Journée, S. H., Lutz, P.-E. & Yalcin, I. Comorbidity of chronic pain and anxiety disorders: deciphering underlying brain circuits. *Neurosci. Biobehav. Rev.* **115**, 131–133 (2020).
61. Hirschberg, S., Li, Y., Randall, A., Kremer, E. J. & Pickering, A. E. Functional dichotomy in spinal- vs prefrontal-projecting locus coeruleus modules splits descending noradrenergic analgesia from ascending aversion and anxiety in rats. *eLife* **6**, e29808 (2017).
62. Padilla-Coreano, N. et al. Direct ventral hippocampal-prefrontal input is required for anxiety-related neural activity and behavior. *Neuron* **89**, 857–866 (2016).
63. Lowery-Gionta, E. G. et al. Chronic stress dysregulates amygdalar output to the prefrontal cortex. *Neuropharmacology* **139**, 68–75 (2018).
64. Felix-Ortiz, A. C., Burgos-Robles, A., Bhagat, N. D., Leppla, C. A. & Tye, K. M. Bidirectional modulation of anxiety-related and social behaviors by amygdala projections to the medial prefrontal cortex. *Neuroscience* **321**, 197–209 (2016).
65. Marcus, D. J. et al. Endocannabinoid signaling collapse mediates stress-induced amygdalo-cortical strengthening. *Neuron* **105**, 1062–1076.e6 (2020).
66. Gong, Y., Chai, Y., Ding, J.-H., Sun, X.-L. & Hu, G. Chronic mild stress damages mitochondrial ultrastructure and function in mouse brain. *Neurosci. Lett.* **488**, 76–80 (2011).
67. Gross, J. A. et al. Gene-body 5-hydroxymethylation is associated with gene expression changes in the prefrontal cortex of depressed individuals. *Transl. Psychiatry* **7**, e1119 (2017).
68. Nagy, C. et al. Single-nucleus transcriptomics of the prefrontal cortex in major depressive disorder implicates oligodendrocyte precursor cells and excitatory neurons. *Nat. Neurosci.* **23**, 771–781 (2020).
69. McKenzie, I. A. et al. Motor skill learning requires active central myelination. *Science* **346**, 318–322 (2014).
70. Tham, M. W., Woon, P. S., Sum, M. Y., Lee, T.-S. & Sim, K. White matter abnormalities in major depression: evidence from post-mortem, neuroimaging and genetic studies. *J. Affect. Disord.* **132**, 26–36 (2011).
71. Bae, J. N. et al. Dorsolateral prefrontal cortex and anterior cingulate cortex white matter alterations in late-life depression. *Biol. Psychiatry* **60**, 1356–1363 (2006).
72. Bhatia, K. D., Henderson, L. A., Hsu, E. & Yim, M. Reduced integrity of the uncinat fasciculus and cingulum in depression: a stem-by-stem analysis. *J. Affect. Disord.* **235**, 220–228 (2018).
73. Hyett, M. P., Perry, A., Breakspear, M., Wen, W. & Parker, G. B. White matter alterations in the internal capsule and psychomotor impairment in melancholic depression. *PLoS ONE* **13**, e0195672 (2018).
74. Zhou, B., Zhu, Z., Ransom, B. R. & Tong, X. Oligodendrocyte lineage cells and depression. *Mol. Psychiatry* **26**, 103–117 (2021).
75. Cathomas, F. et al. Oligodendrocyte gene expression is reduced by and influences effects of chronic social stress in mice. *Genes Brain Behav.* **18**, e12475 (2019).
76. Liu, J. et al. Impaired adult myelination in the prefrontal cortex of socially isolated mice. *Nat. Neurosci.* **15**, 1621–1623 (2012).
77. Birey, F. et al. Genetic and stress-induced loss of NG2 glia triggers emergence of depressive-like behaviors through reduced secretion of FGF2. *Neuron* **88**, 941–956 (2015).
78. He, B. et al. Interactions among nerve regeneration, angiogenesis, and the immune response immediately after sciatic nerve crush injury in Sprague-Dawley rats. *Front. Cell. Neurosci.* **15**, 717209 (2021).
79. Unruh, A. M. Gender variations in clinical pain experience. *Pain* **65**, 123–167 (1996).
80. Jefferson, T., Kim, H. R. & Martina, M. Impaired muscarinic modulation of the rat prelimbic cortex in neuropathic pain is sexually dimorphic and associated with cold allodynia. *Front. Cell. Neurosci.* **17**, 984287 (2023).
81. Michailidis, V., Lidhar, N. K., Cho, C. & Martin, L. J. Characterizing sex differences in depressive-like behavior and glial brain cell changes following peripheral nerve injury in mice. *Front. Behav. Neurosci.* **15**, 758251 (2021).
82. Santarelli, L. et al. Requirement of hippocampal neurogenesis for the behavioral effects of antidepressants. *Science* **301**, 805–809 (2003).

83. Yalcin, I., Coubard, S., Bodard, S., Chalon, S. & Belzung, C. Effects of 5,7-dihydroxytryptamine lesion of the dorsal raphe nucleus on the antidepressant-like action of tramadol in the unpredictable chronic mild stress in mice. *Psychopharmacol. (Berl.)* **200**, 497–507 (2008).
84. Deacon, R. M. J. Assessing nest building in mice. *Nat. Protoc.* **1**, 1117–1119 (2006).
85. Otabi, H., Goto, T., Okayama, T., Kohari, D. & Toyoda, A. The acute social defeat stress and nest-building test paradigm: A potential new method to screen drugs for depressive-like symptoms. *Behav. Process.* **135**, 71–75 (2017).
86. Can, A. et al. The mouse forced swim test. *J. Vis. Exp. JoVE* e3638 <https://doi.org/10.3791/3638> (2012).
87. Avants, B. B. et al. A reproducible evaluation of ANTs similarity metric performance in brain image registration. *NeuroImage* **54**, 2033–2044 (2011).
88. Veraart, J., Fieremans, E. & Novikov, D. S. Diffusion MRI noise mapping using random matrix theory. *Magn. Reson. Med.* **76**, 1582–1593 (2016).
89. Kellner, E., Dhital, B., Kiselev, V. G. & Reisert, M. Gibbs-ringing artifact removal based on local subvoxel-shifts. *Magn. Reson. Med.* **76**, 1574–1581 (2016).
90. Avants, B. B., Tustison, N. & Johnson, H. Advanced normalization tools (ANTs). *Insight J* **2**, 1–35 (2009).
91. Tustison, N. J. et al. N4ITK: improved N3 bias correction. *IEEE Trans. Med. Imaging* **29**, 1310–1320 (2010).
92. Chamier, L. von et al. Democratising deep learning for microscopy with ZeroCostDL4Mic. *Nat Commun.* **12**, 2276 (2020).
93. Schmidt, U., Weigert, M., Broaddus, C. & Myers, G. Cell detection with star-convex polygons. in *Medical Image Computing and Computer Assisted Intervention—MICCAI 2018: 21st International Conference, Granada, Spain, September 16–20, 2018, Proceedings, Part II* Vol. 11071, 265–273 (Springer International Publishing, 2018).
94. Weigert, M., Schmidt, U., Haase, R., Sugawara, K. & Myers, G. Star-convex polyhedra for 3D object detection and segmentation in microscopy. in *2020 IEEE Winter Conference on Applications of Computer Vision (WACV)* 3655–3662 (IEEE, 2020).
95. Schindelin, J. et al. Fiji: an open-source platform for biological-image analysis. *Nat. Methods* **9**, 676–682 (2012).
96. Bankhead, P. et al. QuPath: open source software for digital pathology image analysis. *Sci. Rep.* **7**, 16878 (2017).
97. Dobin, A. et al. STAR: ultrafast universal RNA-seq aligner. *Bioinformatics* **29**, 15–21 (2013).
98. Anders, S., Pyl, P. T. & Huber, W. HTSeq—a Python framework to work with high-throughput sequencing data. *Bioinformatics* **31**, 166–169 (2015).
99. Anders, S. & Huber, W. Differential expression analysis for sequence count data. *Genome Biol.* **11**, R106 (2010).
100. Love, M. I., Huber, W. & Anders, S. Moderated estimation of fold change and dispersion for RNA-seq data with DESeq2. *Genome Biol.* **15**, 550 (2014).
101. Lutz, P.-E. et al. Non-CG methylation and multiple histone profiles associate child abuse with immune and small GTPase dysregulation. *Nat. Commun.* **12**, 1132 (2021).
102. Subramanian, A. et al. Gene set enrichment analysis: a knowledge-based approach for interpreting genome-wide expression profiles. *Proc. Natl Acad. Sci. USA* **102**, 15545–15550 (2005).
- (FdF N° Engt:00081244; I.Y., P.E.L., R.B., and E.C.I.), a NARSAD Young Investigator Grant from the Brain & Behavior Research Foundation (24736; I.Y.), the French National Research Agency (ANR) through the Programme d’Investissement d’Avenir EURIDOL graduate school of pain ANR-17-EURE-0022 (L.J.B.), ANR-18-CE37-0004 (I.Y.), ANR-18-CE19-0006-03 (I.Y.) and ANR-19-CE37-0010 (P.E.L.), Hacettepe University Scientific Research Projects Coordination Unit (HUBAB), International Cooperation Project TBI-2018-17569 (B.A.), the Scientific and Technological Research Council of Turkey (TUBITAK) through international post-doctoral research fellowship program (B.A.), IdEx Young Investigator award of University Strasbourg (I.Y.), IdEx postdoctoral fellow of University of Strasbourg (M.T.) and EU Erasmus Mundus Neurotime program (M.K., I.Y., and L.H.). This work received support from the European Union’s Horizon 2020 research and innovation program under the Marie Skłodowska-Curie grant agreement N°955684 (M.G., P.E.L., and I.Y.). The authors would also like to acknowledge the CAIUS High-Performance Computing Center of the University of Strasbourg for providing scientific support and access to computing resources. Part of the computing resources was funded by the Equipex Equip@Meso project (Program Investissements d’Avenir) and the CPER Alsacalcul/Big Data. We would like to thank the UMS3415 Chronobiotron for animal care, the In Vitro UAR 3156 imaging platform, Pascale Koebel and Paola Rossolillo from IGBMC for virus preparations, Jennifer Kaufling, Khaled Abdallah, Noémie Willem and Quentin Leboulleux for technical support, Violaine Alunni from IGBMC for the Fluidigm experiment and Daniel Almeida for English editing. Behavioral and microscopy platforms were supported by the Région Grand-Est (Fonds Régional de la Coopération pour la Recherche, CLueDol project). Sequencing was performed by the GenomEast platform, a member of the ‘France Génomique’ consortium (ANR-10-INBS-0009). We would like to acknowledge that images were adapted from “Mouse brain (sagittal cut)”, “Mouse brain (coronal cut)”, and “Brain (sagittal cut)” by BioRender.com (2023). Retrieved from <https://app.biorender.com/biorender-templates>.

Author contributions

Behavioral experiments: L.J.B., R.W., C.F., S.H.J., M.H., M.T., and I.Y.; molecular experiments: L.J.B., P.E.L., and I.Y.; electrophysiological recordings: S.H.; human data acquisition: G.T. and P.E.L.; imaging: L.J.B., M.K., L.D., M.M., M.N.S., and L.A.H.; immunohistochemistry: R.W., B.A., and M.B.; neuroanatomy: R.W., C.F., and P.V.; experimental design: P.E.L. and I.Y.; data analyses: L.J.B., R.W., P.H., M.G., B.A., P.E.L., and I.Y.; fundings: I.Y., P.E.L., E.C.I., and R.B.; manuscript preparation: L.J.B., R.W., S.H., L.A.H., P.E.L., and I.Y.

Competing interests

The authors declare no competing interests.

Additional information

Supplementary information The online version contains supplementary material available at <https://doi.org/10.1038/s41467-023-37878-y>.

Correspondence and requests for materials should be addressed to Ipek Yalcin.

Peer review information *Nature Communications* thanks the anonymous reviewers for their contribution to the peer review of this work. Peer reviewer reports are available.

Reprints and permissions information is available at <http://www.nature.com/reprints>

Publisher’s note Springer Nature remains neutral with regard to jurisdictional claims in published maps and institutional affiliations.

Acknowledgements

This work was supported by the Centre National de la Recherche Scientifique (contract UPR3212), the University of Strasbourg, the Fondation pour la Recherche Médicale (FRM, FDT202012010622; FDT201805005527) (L.J.B. and M.H.), the Fondation de France

Open Access This article is licensed under a Creative Commons Attribution 4.0 International License, which permits use, sharing, adaptation, distribution and reproduction in any medium or format, as long as you give appropriate credit to the original author(s) and the source, provide a link to the Creative Commons license, and indicate if changes were made. The images or other third party material in this article are included in the article's Creative Commons license, unless indicated otherwise in a credit line to the material. If material is not included in the article's Creative Commons license and your intended use is not permitted by statutory regulation or exceeds the permitted use, you will need to obtain permission directly from the copyright holder. To view a copy of this license, visit <http://creativecommons.org/licenses/by/4.0/>.

© The Author(s) 2023



ARTICLE OPEN



Node of Ranvier remodeling in chronic psychosocial stress and anxiety

Maija-Kreetta Koskinen^{1,2,3,6}, Mikaela Laine^{1,2,3,6} , Ali Abdollahzadeh⁴ , Adrien Gigliotta^{1,2,3}, Giulia Mazzini^{1,2,3}, Sarah Journée^{1,2} , Varpu Alenius^{1,2,3}, Kalevi Trontti^{1,2,3}, Jussi Tohka⁴, Petri Hyytiä⁵ , Alejandra Sierra⁴ and Iiris Hovatta^{1,2,3} ✉

© The Author(s) 2023

Differential expression of myelin-related genes and changes in myelin thickness have been demonstrated in mice after chronic psychosocial stress, a risk factor for anxiety disorders. To determine whether and how stress affects structural remodeling of nodes of Ranvier, another form of myelin plasticity, we developed a 3D reconstruction analysis of node morphology in C57BL/6NCrI and DBA/2NCrI mice. We identified strain-dependent effects of chronic social defeat stress on node morphology in the medial prefrontal cortex (mPFC) gray matter, including shortening of paranodes in C57BL/6NCrI stress-resilient and shortening of node gaps in DBA/2NCrI stress-susceptible mice compared to controls. Neuronal activity has been associated with changes in myelin thickness. To investigate whether neuronal activation is a mechanism influencing also node of Ranvier morphology, we used DREADDs to repeatedly activate the ventral hippocampus-to-mPFC pathway. We found reduced anxiety-like behavior and shortened paranodes specifically in stimulated, but not in the nearby non-stimulated axons. Altogether, our data demonstrate (1) nodal remodeling of the mPFC gray matter axons after chronic stress and (2) axon-specific regulation of paranodes in response to repeated neuronal activity in an anxiety-associated pathway. Nodal remodeling may thus contribute to aberrant circuit function associated with anxiety disorders.

Neuropsychopharmacology; <https://doi.org/10.1038/s41386-023-01568-6>

INTRODUCTION

Anxiety disorders are the most common psychiatric disorders, affecting up to 14% of the population [1], with a large socioeconomic burden [2]. Anxiety disorders are complex diseases with both genetic and environmental risk factors [3, 4], however, little is known about the mechanisms underlying these gene-environment interactions. Chronic psychosocial stress increases the risk to develop anxiety disorders [5, 6]. Understanding the mechanisms mediating vulnerability to stress, and resilience to it, is crucial for the development of much-needed treatment and prevention strategies.

By employing the chronic social defeat stress (CSDS) model, a well-validated animal model of psychosocial stress and anxiety-like behavior in male mice [7, 8], we recently demonstrated using four inbred mouse strains that behavioral responses to stress are strongly influenced by genetic background [9]. CSDS, consisting of confrontations between intruder and resident mice, leads to social avoidance in a subset of mice (stress-susceptible), while others retain social approach (stress-resilient) like non-stressed mice. For example, most (~95%) DBA/2NCrI (D2) mice show social avoidance after CSDS, and are thus classified as stress-susceptible, while the majority (~70%) of C57BL/6NCrI (B6) mice are stress-resilient [9].

Our prior unbiased gene expression profiling study, aimed to identify biological pathways mediating stress-induced anxiety and

resilience to it, discovered statistical over-representation of myelin-related genes among differentially expressed genes in mice after CSDS [9]. Both the genetic background, as well as resilience and susceptibility to stress modulated this effect. Changes in gene expression were accompanied by strain- and susceptibility/resilience-dependent differences in myelin sheath thickness in the medial prefrontal cortex (mPFC), ventral hippocampus (vHPC), and bed nucleus of stria terminalis (BNST), regions involved in the regulation of anxiety [10]. Altogether, these findings, also supported by others [11–15], highlight the involvement of myelin plasticity in stress response and suggest an important role for myelination in mediating susceptibility and resilience to stress.

Myelin plasticity, or adaptive myelination, encompasses various alterations in myelin structure, density, and function in response to specific experiences and consequent changes in neuronal activity [16, 17]. In addition to changes in myelin thickness and de novo myelination of previously non-myelinated axons or axonal segments, myelin plasticity involves modulation of nodes of Ranvier [18], small unmyelinated segments between myelin sheaths which enable saltatory conduction [19]. They consist of unmyelinated node gaps containing a high density of voltage-gated sodium ion channels that are flanked by paranodes, where myelin sheaths attach to axons. Juxtaparanodes are located adjacent to paranodes, and contain a high density of potassium

¹SleepWell Research Program, Faculty of Medicine, University of Helsinki, Helsinki, Finland. ²Department of Psychology and Logopedics, Faculty of Medicine, University of Helsinki, Helsinki, Finland. ³Neuroscience Center, Helsinki Institute of Life Science HiLIFE, University of Helsinki, Helsinki, Finland. ⁴A.I. Virtanen Institute for Molecular Sciences, University of Eastern Finland, Kuopio, Finland. ⁵Department of Pharmacology, Faculty of Medicine, University of Helsinki, Helsinki, Finland. ⁶These authors contributed equally: Maija-Kreetta Koskinen, Mikaela Laine. ✉email: iiris.hovatta@helsinki.fi

Received: 26 September 2022 Revised: 7 February 2023 Accepted: 3 March 2023

Published online: 22 March 2023

channels [19–21]. Similar to changes in myelin thickness and sheath length node of Ranvier remodeling can also have profound changes on axonal conduction [22–25], and thus critically impact connectivity of neuronal networks [26]. Whether node of Ranvier morphology in the cortical gray matter is affected in chronic psychosocial stress, and whether activity-dependent nodal changes occur in anxiety-associated circuits remain unclear.

Here, we first investigated whether modulation of node of Ranvier structure occurs in response to CSDS, and whether these changes are influenced by genetic background or resilience or susceptibility to stress-induced social avoidance, a symptom of anxiety. We identify strain-dependent effects of chronic stress on nodal structures using a novel 3D segmentation method, allowing refined structural node analysis. In a second set of experiments, we test neuronal activation as a possible mechanism underlying morphological changes of nodes of Ranvier, and demonstrate that repeated chemogenetic activation of the vHPC-to-mPFC pathway reduces anxiety-like behavior and induces axon-specific shortening of paranode length, suggesting that activity and axon-specific nodal remodeling may contribute to shaping of neuronal connectivity in anxiety circuits.

MATERIALS AND METHODS

Detailed materials and methods can be found in the Supplementary information.

Animals

C57BL6/NCrI (B6) and DBA/2NcrI (D2) male mice (5 weeks old upon arrival, Charles River Laboratories) were purchased for all experiments. All animal procedures were approved by the Regional State Administration Agency for Southern Finland (ESAVI/2766/04.10.07/2014 and ESAVI/9056/2020) and conducted in accordance with directive 2010/63/EU of the European Parliament and of the Council.

Experiment 1: CSDS

CSDS was performed as previously described [9, 27]. Seven-week-old male mice underwent a 10-day CSDS paradigm, consisting of a 5–10 min daily physical confrontation and constant sensory interaction. One day after the end of CSDS mice were tested for social avoidance (SA). A social interaction (SI) ratio was calculated for each mouse. Susceptible mice were defined as having SI ratios below a boundary defined as the strain-specific control mean score minus one standard deviation [9].

RNA-sequencing and differential gene expression analysis

We re-analyzed RNA sequencing data from brain samples of B6 and D2 mice after CSDS, published by us previously [9] (GEO accession GSE109315). Briefly, mice were sacrificed 6–8 days after the last CSDS session and RNA was extracted. Sequencing libraries were prepared with ScriptSeq v2 RNA-seq library preparation kit (Epicentre) and sequencing was performed on NextSeq500 (single-end 96 bp; Illumina). Differential expression analysis on voom normalized [28] gene expression values was performed using limma eBayes [29, 30], comparing resilient and susceptible mice to their same-strain controls. Here, we conducted gene set enrichment analysis (GSEA Desktop v4.1.0 [31, 32]) using the differential expression results published in [9].

Experiment 2: DREADD—stereotaxic surgery

Stereotaxic surgeries were performed under isoflurane anesthesia. AAV_{retro}-Cre was injected into the mPFC (AP: +2.22 mm, ML: ±0.35 mm, DV: –2.1 mm) for retrograde transport to vHPC neurons projecting to the mPFC. For the vHPC viral construct (AP: –3.4 mm, ML: ±2.9 mm, DV: –4.5 mm), mice were randomly assigned to receive either the control virus (AAV8-Dio-mCherry) or the DREADD virus (AAV8-Dio-hM3D(Gq)-mCherry).

Experiment 2: DREADD—behavioral testing and CNO injections

Mice were tested in the elevated zero maze (EZM) test 20–30 min after receiving a clozapine-N-oxide (CNO, 1 mg/kg) injection (i.p.). The total time spent in open and closed areas was recorded over 5 min and analyzed

using Ethovision XT10 software. CNO injections were continued once per day for a total of 15 days.

On day 13, prior to receiving CNO, the open field test (OFT) was performed. Each mouse was allowed to explore an arena for 5 min. The time the mice spent in the center vs. periphery was computed. On day 14, the EZM was repeated with slight modifications (EZM2). To test for effects of chronic vHPC-mPFC activation on social avoidance behavior, we performed the SA test on day 15. Each mouse went through two trials of the SA test similarly as after CSDS. To explore whether the chronic activation had affected the acute response to CNO, we performed an additional test of anxiety-like behavior following a priming injection (day 16). Each mouse received an injection of CNO and after 20–30 min they were tested in an elevated plus maze (EPM).

Nodes of Ranvier immunohistochemistry

Mice were transcardially perfused, post-fixed and brains cut into 35–40 µm sections. The used antibodies were: rabbit anti-Nav1.6 (1:250, #ASC-009, Alomone labs), mouse anti-CASPR (1:5000, #75-001, Neuromab), goat anti-rabbit Alexa Fluor 568 (1:400, #A-11011, Thermo Fisher Scientific), goat anti-mouse Alexa Fluor 488 (1:400, #A28175, Thermo Fisher Scientific), and goat anti-mouse Alexa 647 (1:400, #ab150115, Abcam).

Imaging

Imaging was performed with ZEISS LSM 880 Confocal Laser Scanning microscope with AiryScan (Zeiss). To image individual nodes within a field of view, a region around a node was cropped, and a z-stack of the cropped region was acquired. Z-stacks were acquired at a resolution of 0.04 × 0.04 × 0.10 µm.

3D segmentation and morphometry of paranodes and juxtapanodes

We developed an automated pipeline to segment and analyze the morphology of paranodes and juxtapanodes, as well as to measure the length of nodes of Ranvier in the acquired 3D microscopy images (Fig. S4).

Statistical analysis

We assessed group differences in node and paranode morphology using a mixed model design, in which individual mice and paranode dependency (two paranodes originate from the same node) were treated as random factors and group (control, resilient, and susceptible) and staining batch as fixed factors. Unpaired (two-tailed) Student's *t* test or a Mann–Whitney *U* test were used to assess behavioral test differences. Two-way repeated ANOVA was used to analyze repeated testing in the EZM task. Mixed model was performed using R (4.2.2) and other statistical analyses using Prism 8.

RESULTS

Node of Ranvier-related genes are differentially expressed in response to chronic psychosocial stress

In our previous study, we discovered changes in the expression of myelin-related genes in response to CSDS [9]. These changes were accompanied by differences in myelin thickness, which occurred in a brain region- and strain-dependent manner, altogether demonstrating myelin plasticity as an integral part of the stress response [9]. These findings prompted us to further investigate whether chronic stress impacts other myelin features, such as nodes of Ranvier. To investigate differential expression of genes involved in the structure and function of nodes of Ranvier (Fig. 1a and Table S1), we re-analyzed our previously published RNA-sequencing dataset from the mPFC (including the prelimbic, infralimbic, and anterior cingulate cortex regions) of B6 and D2 mice, performed 1 week after cessation of a 10-day CSDS [9]. We examined 40 genes associated with the Gene Ontology term node of Ranvier. Twelve genes (30%) were differentially expressed in B6 susceptible mice compared to controls, with 11 of them (28%) being expressed at a lower level in the susceptible compared to control mice (Fig. 1b). These genes encoded for voltage-dependent ion channels (e.g., *Kcnq2*; *Kv7.2* and *Scn1a*; *Nav1.1*) and structural components of the nodes (e.g., *Gjc*; *Connexin-47*;

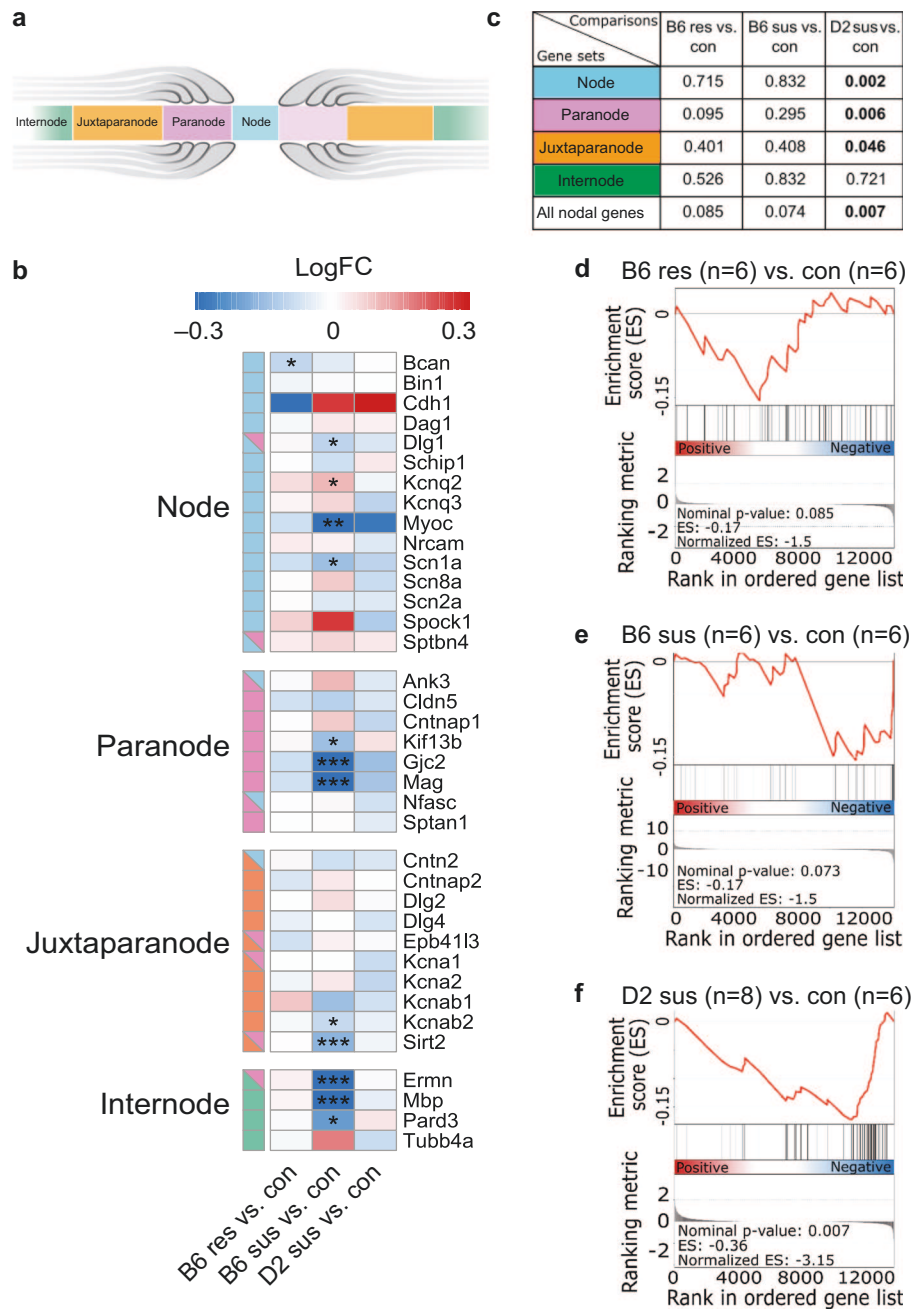


Fig. 1 Differential expression of nodes of Ranvier genes after chronic social defeat stress. **a** Schematic representation of the node of Ranvier subregions. **b** Heatmap showing the expression fold change (logFC) and significance of differential expression for genes associated with nodes of Ranvier subcomponents (node, light blue; paranode, pink; juxtaparanode, orange; internode, green) in B6 and D2 defeated mice in the mPFC. **c** Gene Set Enrichment Analysis (GSEA) of genes associated with the individual structural subcomponents of the nodes of Ranvier (node, paranode, juxtaparanode, internode) and combined analysis of all nodal genes ($N = 40$ genes, see Supplementary Table 1). **d–f** GSEA enrichment score figures of all nodal genes. The top portion of the plot shows the enrichment score, which reflects the degree of overrepresentation of the gene set at the top or bottom of a ranked gene list. The middle portion of the plot shows the position of the genes in the ranked list. The bottom portion of the plot shows the value of the ranking metric as the analysis walks down the list of ranked genes. B6: C57BL/6Ncrl; D2: DBA/2Ncrl; Con control, Res resilient, Sus susceptible. * $p < 0.05$, ** $p < 0.01$, *** $p < 0.001$.

Mag; Myelin associated glycoprotein). In addition, to examine whether genes encoding for structural subcomponents of the nodes of Ranvier (Fig. 1a) were over-represented among the up- or downregulated genes, we conducted Gene Set Enrichment Analysis (GSEA) [31] on differential gene expression lists of B6 resilient, B6 susceptible, and D2 susceptible mice compared to controls (Fig. 1c, d). As D2 resilient mice are found very infrequently, they were not available in the cohort used for this

experiment. We found that paranodal, juxtaparanodal, and nodal genes were significantly overrepresented among the downregulated genes in the D2 susceptible mice compared to same-strain controls. In B6 susceptible mice, we observed a statistical trend for overrepresentation of node of Ranvier genes among the downregulated genes. GSEA performed with all 40 genes associated with nodes of Ranvier produced similar results (Fig. 1c, d). Taken together, these results suggest that chronic psychosocial

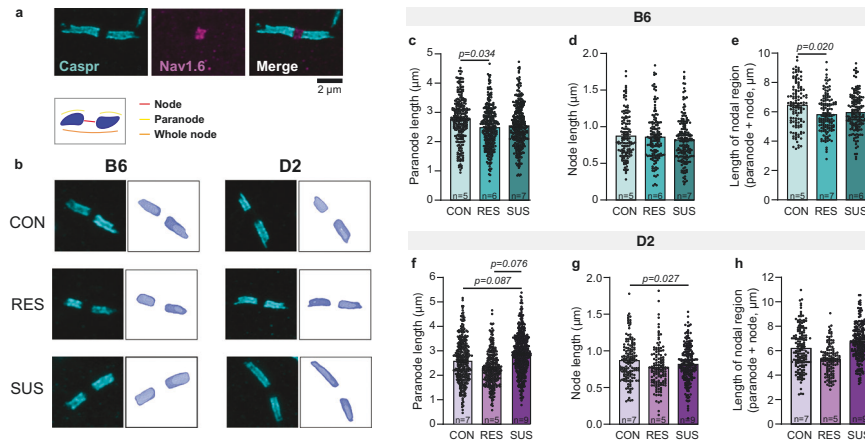


Fig. 2 Strain-dependent changes in nodal morphology after chronic social defeat stress. **a, b** Examples of 3D reconstructed paranodes in the anterior cingulate cortex layer V/VI in B6 and D2 mice after chronic social defeat stress. Quantification of paranode length (**c, f**), node width (**d, g**), total nodal region length (**e, h**). **c** Paranode length B6: Con = 266 paranodes from 5 mice, Res = 311 paranodes from 6 mice, Sus = 286 paranodes from 7 mice. Statistical differences were identified by linear mixed-effect modeling with pairwise comparisons: Con vs. Res, $t(13.5) = -2.356$, $p = 0.034$; Con vs. Sus, $t(13.8) = -1.488$, $p = 0.159$; Res vs. Sus, $t(9.4) = 1.148$, $p = 0.279$. **d** Node length B6: Con = 132 nodes from 5 mice, Res = 152 nodes from 6 mice, Sus = 168 nodes from 7 mice. Con vs. Res, $t(9.4) = -0.141$, $p = 0.891$; Con vs. Sus, $t(9.5) = -0.972$, $p = 0.355$. **e** Nodal region length B6: Con = 124 nodes from 5 mice, Res = 136 nodes from 6 mice, Sus = 152 nodes from 7 mice. Con vs. Res, $t(13.6) = -2.630$, $p = 0.020$; Con vs. Sus, $t(13.7) = -1.628$, $p = 0.126$. **f** Paranode length D2: Con = 334 paranodes from 7 mice, Res = 274 paranodes from 5 mice, Sus = 476 paranodes from 9 mice. Con vs. Res, $t(16.6) = 0.040$, $p = 0.968$; Con vs. Sus, $t(16.8) = 1.889$, $p = 0.076$; Res vs. Sus, $t(10.5) = 1.885$, $p = 0.087$. **g** Node length D2: Con = 151 nodes from 7 mice, Res = 131 nodes from 5 mice, Sus = 215 nodes from 9 mice. Con vs. Res, $t(17.5) = -0.487$, $p = 0.632$; Con vs. Sus, $t(18.1) = -2.402$, $p = 0.027$. **h** Nodal region length D2: Con = 154 nodes from 7 mice, Res = 124 nodes from 5 mice, Sus = 219 nodes from 9 mice. Con vs. Res, $t(15.7) = 0.043$, $p = 0.966$; Con vs. Sus, $t(15.6) = 1.035$, $p = 0.317$. B6: C57BL/6NCrI; D2: DBA/2NCrI; Con control, Res resilient, Sus Susceptible.

stress alters the expression levels of genes involved in node of Ranvier structure and function in the mPFC of B6 and D2 susceptible mice.

Strain-dependent alterations of mPFC nodal morphology after chronic psychosocial stress

To investigate whether the observed gene expression differences are associated with changes in node of Ranvier morphology, we developed a novel 3D reconstruction analysis of nodal subdomains. Particularly in gray matter nodes of Ranvier can present highly variable orientations, and as a result, two-dimensional maximum projection analysis of morphology can induce significant distortions of measured parameters. By measuring nodes as they exist in three-dimensional space, we can obtain accurate morphological measures. We analyzed nodal subdomains after CSDS in the anterior cingulate cortex subregion of the mPFC, a critical hub for the regulation of anxiety [33]. This brain region contains several short- and long-range connections [34] as well as excitatory and inhibitory neurons, both of which are known to be myelinated [35]. To investigate whether genetic background or susceptibility or resilience to stress influence nodal modifications in response to stress, we conducted the morphological analysis both in B6 and D2 mice, classified either as stress-resilient or -susceptible based on social avoidance behavior following CSDS [9, 27] (Fig. S1).

We found that B6 resilient mice had shorter paranodes (by 10.3%), identified by contactin-associated protein (CASPR) immunoreactivity (Fig. 2a, b) compared to same strain controls (Fig. 2c). In D2 mice we found a statistical trend toward increased paranode length in susceptible mice compared both to same strain resilient (by 27.0%) and control mice (by 11.1%) (Fig. 2f). Moreover, node width, defined as the distance between two flanking paranodes (Fig. 2a, b), was shorter (by 5.2%) in D2 susceptible mice compared to same strain control mice (Fig. 2g), but not in B6 mice (Fig. 2d). In accordance with shorter paranodes, total nodal region length was shorter in resilient B6 mice (by 8.4%) compared to same strain controls (Fig. 2e, h). These changes in paranode length are similar in magnitude with previous findings in multiple sclerosis, in which

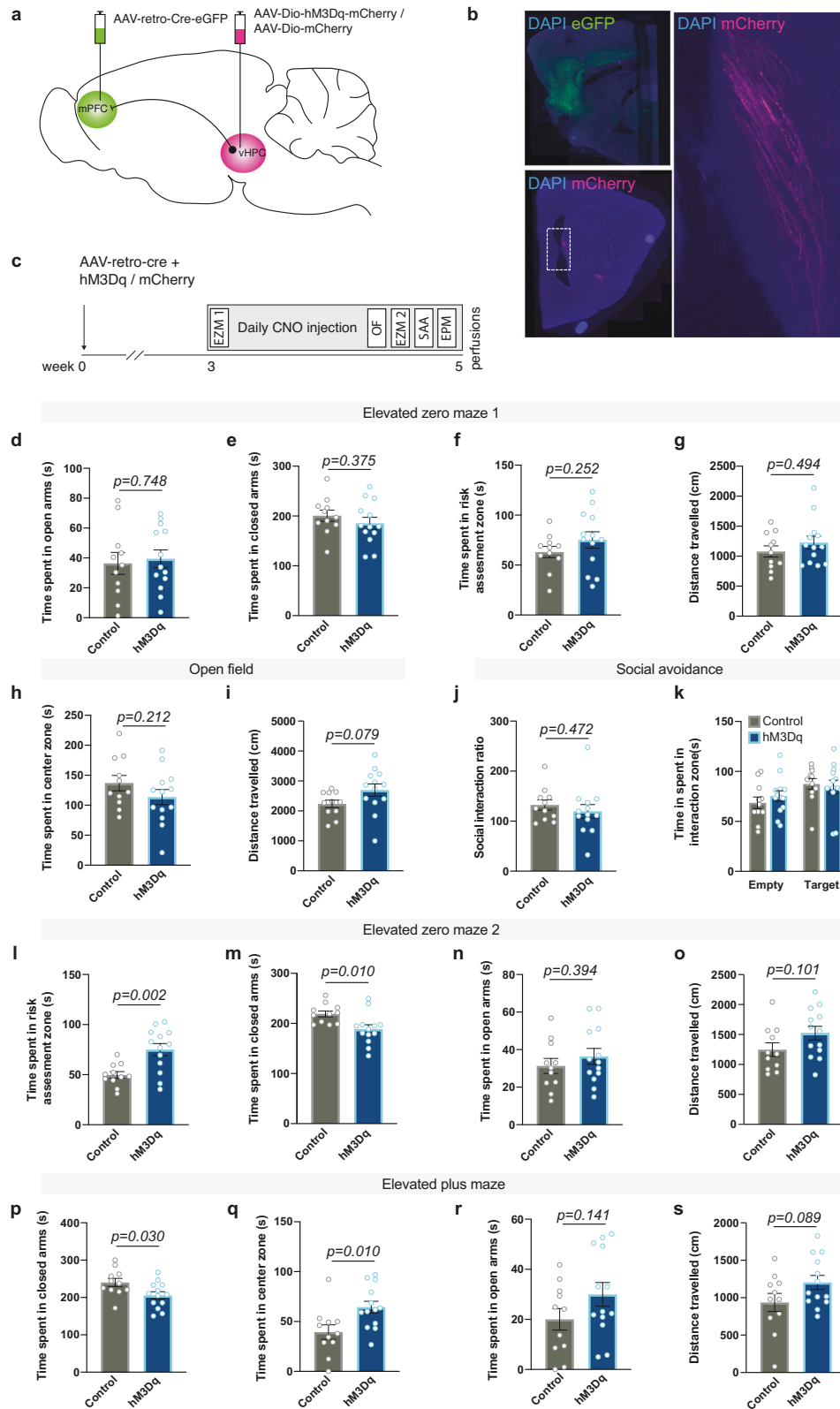
paranodal changes associate with predicted changes in conduction velocity [36].

Strain-dependent alterations of nodal morphology in forceps minor

In addition to cortical gray matter, we analyzed nodal morphology in response to CSDS in the forceps minor (Fig. S2a), a white matter tract adjacent to the mPFC. Paranode length was longer in B6 stress-resilient (by 7.0%) compared to same strain controls, and there was a statistical trend toward longer paranodes (by 4.4%) in stress-susceptible mice (Fig. S2b). Paranode length in D2 mice or node width in either B6 or D2 mice did not change in response to CSDS (Fig. S2c–e). Altogether, our analysis demonstrates that chronic stress alters node of Ranvier morphology both in the mPFC gray matter and in the forceps minor white matter. These effects were strongly influenced by genetic background and brain region, and they depended on the individual stress response.

Repeated activation of the vHPC-mPFC pathway reduces anxiety-like behavior and paranode length in axon-specific manner

Mechanisms underlying experience-dependent changes in node of Ranvier structure are largely unknown. We hypothesized that neuronal activity may be one such mechanism because it influences oligodendrocyte precursor cell proliferation, oligodendrogenesis, and myelin thickness [37, 38]. Furthermore, transcranial magnetic stimulation affects node of Ranvier width in the stimulated area [23]. However, whether activity-dependent nodal remodeling occurs in circuits involved in the regulation of anxiety-like behavior, and whether such effects are specific to activated axons, are not known. To study the effects of neuronal activation on nodal morphology, we chemogenetically activated neurons projecting from the vHPC to the mPFC, a pathway previously shown to increase anxiety-like behavior upon acute stimulation [39, 40]. To achieve projection-specific expression of excitatory hM3Dq-receptors, we bilaterally injected a retrograde Cre-carrying virus (AAV_{retro}-Cre-eGFP) into the mPFC, while a Cre-dependent hM3Dq (AAV8-Dio-hM3Dq-mCherry) or an mCherry (AAV8-Dio-mCherry) control



vector was injected into the vHPC (Fig. 3a) of male C57BL/6NCr1 mice. Immunohistochemical analysis confirmed the accuracy of the labeling by showing robust eGFP labeling in the mPFC and mCherry expression in the vHPC CA3/1 regions, as well as eGFP/mCherry-double positive axons along the pathway (Fig. 3b).

Behavioral tests confirmed that the activation of this specific pathway was effective in modulating anxiety-like behavior (Fig. 3c), although the effects differed from those previously published for acute stimulation [39, 40]. We first assessed the effects of an acute chemogenetic activation of Gq signaling on anxiety-like behavior

Fig. 3 DREADD-mediated activation of vHPC-to-mPFC projection neurons reduces anxiety-like behavior. **a** Projection-specific expression of hM3Dq/mCherry was achieved by injecting a retrograde Cre-carrying virus (retro-Cre-eGFP) into the mPFC and a Cre-dependent hM3Dq (Dio-hM3Dq-mCherry) or a control virus (Dio-mCherry) into the vHPC CA3 subregion. **b** Representative examples showing eGFP expression in the mPFC and mCherry-expressing axons in the hippocampal fimbria. **c** Experimental timeline. Open zone (**d**), closed zone (**e**) risk assessment (RA) zone (**f**) time and the number of stretch-attend postures in the RA zone (**g**) in the acute elevated zero maze test (EZM1) (two-sided Student's *t* tests). Time spent in the center of the open field (OF) test (**h**) and distance traveled (**i**) during the OF test (two-sided Student's *t* tests). **j** Quantification of social interaction ratio in the social approach (SA) task (two-sided Student's *t* test). **k** Time spent in the interaction zone during empty and target sessions of the SA test (two-way repeated ANOVA: group \times session $F(1,22) = 0.703$, $p = 0.402$; session $F(1,22) = 6.111$, $p = 0.022$; group $F(1,22) = 0.100$, $p = 0.755$). Time spent in the open zone (**l**), closed zone (**m**) (two-sided Student's *t* tests), risk assessment zone (**n**) (two-sided Welch's *t*-test) and the number of stretch-attend postures in the RA zone (**o**) in the EZM2 test after repeated activation of vHPC-to-mPFC pathway. Time spent in the closed arms (**p**), center zone (**q**), open arms (**r**) and the number of stretch-attend postures (**s**) in the elevated plus maze (EPM) test (two-sided Student's *t* tests). Control $n = 11$; hM3Dq $n = 13$; Error bars represent \pm SEM.

by testing the mice in the elevated zero maze (EZM) 20–30 min after a single clozapine-*N*-oxide (CNO) injection, which activates the hM3Dq receptors. In the EZM, the hM3Dq and control groups spent equal amount of time in the open areas, closed areas, and in the risk assessment zone, and we did not observe differences in stretch-attend postures or general activity (Figs. 3d–g and S3a), suggesting ineffectiveness of the acute manipulation to alter anxiety-like behavior in this assay. After the acute test, we continued daily CNO injections to assess the effects of a repeated manipulation of vHPC-to-mPFC activity on anxiety-like behavior. After 12 days of CNO injections, we carried out the open field (OF) test. Anxiety-like behavior or general activity did not differ between the groups, as demonstrated by similar time spent in the center zone and the distance traveled (Fig. 3h, i). On the following day, and after another CNO injection, we tested the mice in the EZM task. In contrast to the acute CNO effects, after the repeated manipulation hM3Dq mice spent more time in the risk-assessment zone, compared to controls (Fig. 3n). This was accompanied with reduced closed area time (Fig. 3m), with no differences in the time spent in the open areas (Fig. 3l) or general activity (Fig. S3b). The behavior of the control mice did not differ between the acute and chronic EZM tests (Fig. S3c–f), supporting the feasibility of repeated testing in the EZM.

On the following day (after 14 days of CNO injections), we tested the effects of the repeated activation of the vHPC-to-mPFC projection on social behavior in the social approach (SA) task. hM3Dq and control mice spent equal amounts of time interacting with a social target (Fig. 3j, k), suggesting no effects on social avoidance behavior.

Lastly, we tested the priming effects of an acute hM3Dq activation on anxiety-like behavior. After receiving daily CNO injections for 15 days, the mice received a single CNO injection 30 min prior to testing in the elevated plus maze (EPM), to avoid a habituation effect from repeated testing in the EZM. An acute activation in primed animals resulted in reduced exploration of the closed arms in hM3Dq mice, which was accompanied with increased center zone time and increased number of stretch-attend postures compared to controls, with no change in open arm time or in locomotor activity (Figs. 3p–s and S3e). Taken together, our behavioral data demonstrate that prolonged manipulation of vHPC-to-mPFC activity decreases anxiety-like behavior, reflected particularly as increased risk assessment in the EZM test, together with reduced closed arm exploration and increased engagement in stretch-attend postures in the EPM test.

Finally, we assessed whether DREADD-mediated activation, changing anxiety-like behavior, altered nodal morphology along labeled vHPC-to-mPFC axons. For this, we imaged paranodes (identified with CASPR) on mCherry-expressing (mCherry+) axons within the hippocampal fimbria, where robust labeling of mPFC-projecting vHPC axons was observed in both hM3Dq and control mice (Fig. 4a, b). To tease out manipulation-specific effects, we also studied paranodes on non-labeled axons (mCherry–) within the same brain region. In mice with vHPC-to-mPFC projection neurons expressing hM3Dq, paranodes were significantly shorter

(13.9%) than in controls (Fig. 4c). Importantly, the effect was specific for paranodes on mCherry-labeled axons, as no difference in paranode length was present between the groups in non-labeled axons. Furthermore, paranode length did not differ between labeled and non-labeled axons in control mice. In concordance with reduced paranode length, the total nodal region was shorter in hM3Dq-expressing neurons compared to control neurons (Fig. 4e). The DREADD-mediated activation did not affect node width (Fig. 4d). These results demonstrate that manipulation of neuronal activity specifically affected paranode length, and, importantly, the modification occurred in the activated, but not in the non-activated, axons, supporting our hypothesis on activity-dependent remodeling of nodes.

DISCUSSION

In this study, we first investigated morphology of nodes of Ranvier after chronic psychosocial stress. These studies were based on our initial finding of differential expression of node of Ranvier-related genes within the mPFC of mice exposed to CSDS. The observed gene expression differences were accompanied by altered node of Ranvier morphology. Secondly, to identify mechanisms which could drive nodal remodeling, we assessed whether altered neuronal activity in an anxiety-associated pathway produces nodal changes. In such a pathway, we showed shortened paranodes along DREADD-stimulated axons. Our data demonstrate that DREADD-mediated chronic activation can alter node of Ranvier morphology along active axons, and that such changes can be accompanied by changes in anxiety-like behavior.

We found shorter paranodes in B6 stress-resilient mice compared to controls in the mPFC gray matter after CSDS. In D2 stress-susceptible mice node gap was shorter compared to controls. These findings suggest that nodal remodeling may influence resilience and susceptibility to stress. For example, in B6 the ability to adjust the paranode length, according to the need of the pathway, may promote resilience, a process which may fail in susceptible mice.

Myelination both in the white and gray matter contribute to experience-dependent shaping of neural circuits [18, 41]. Therefore, we also assessed nodal remodeling after chronic stress in the white matter within the forceps minor, the anterior part of the corpus callosum. We found longer paranodes in stress-resilient B6 mice compared to same strain controls, as also previously observed after chronic restraint stress [42]. Different effects of chronic stress on nodal remodeling in the gray and white matter demonstrate that nodal changes are highly brain region-dependent, possibly echoing differences in their activity in response to stress.

What drives the remodeling of the nodes of Ranvier after chronic stress? We hypothesized that behavioral response to chronic stress could be affected by activity-dependent nodal remodeling that takes place selectively in stress-associated circuits. As pathway-specific nodal remodeling in anxiety circuits has to date not been established, we set out to test this

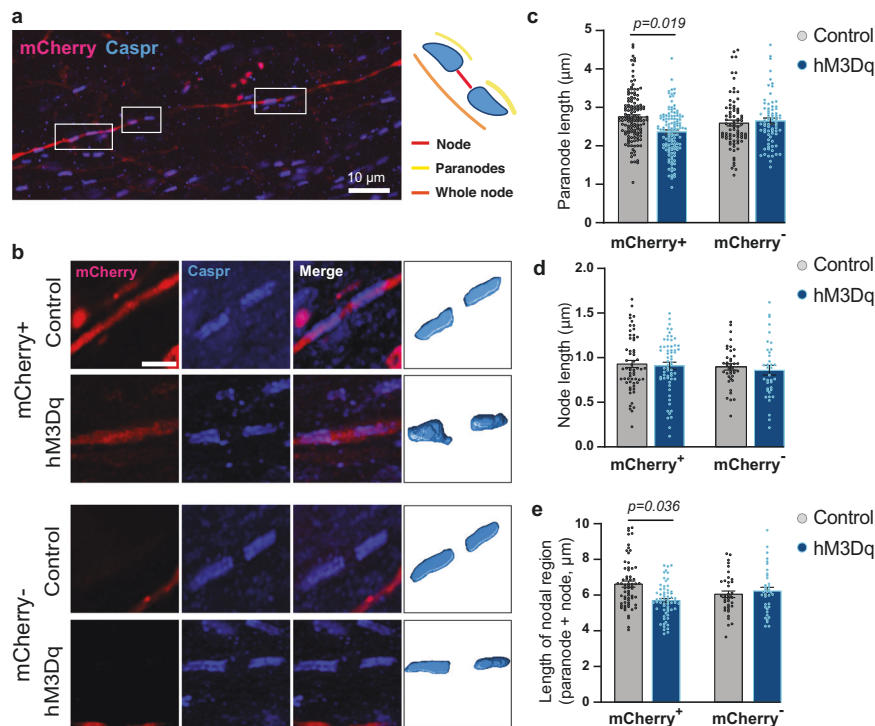


Fig. 4 Repeated activation of vHPC-to-mPFC projection neurons reduces paranodal length. **a** A sagittal section containing the vHPC immunolabeled with CASPR antibody in mice expressing an mCherry-labeled hM3Dq or a control virus in vHPC-to-mPFC projection neurons. Outlines demonstrating paranodes along an mCherry-labeled axon. **b** 3D reconstruction of paranodes on labeled and non-labeled axons. **c** Quantification of paranode length (**c** Linear mixed model: Group_virus $t(16.8) = -0.187$, $p = 0.854$; Axon_type $t(210) = 0.954$, $p = 0.341$; Group_virus \times Axon_type $t(205) = -2.463$, $p = 0.015$; pairwise comparisons: hM3Dq-mCherry⁺ vs. Control-mCherry⁺ $t(11) = -2.732$, $p = 0.019$; hM3Dq-mCherry⁻ vs. Control-mCherry⁻ $t(9.7) = -0.047$, $p = 0.963$). **d** Quantification of node length (**d** Group_virus $t(18.6) = -0.060$, $p = 0.953$; Axon_type $t(193) = 0.507$, $p = 0.613$; Group_virus \times Axon_type $t(191) = 0.158$, $p = 0.874$). **e** Quantification of total nodal region length (**e** Group_virus $t(17.8) = 0.244$, $p = 0.810$; Axon_type $t(193) = 1.622$, $p = 0.106$; Group_virus \times Axon_type $t(191) = -2.569$, $p = 0.011$; pairwise comparisons: hM3Dq-mCherry⁺ vs. Control-mCherry⁺ $t(9.8) = -2.425$, $p = 0.036$; hM3Dq-mCherry⁻ vs. Control-mCherry⁻ $t(9.2) = 0.308$, $p = 0.765$). **c** hM3Dq: 73 mCherry⁻ and 123 mCherry⁺ paranodes from 6 animals; Control: 80 mCherry⁻ and 134 mCherry⁺ paranodes from 6 animals. **d** hM3Dq: 37 mCherry⁻ and 62 mCherry⁺ nodes from 6 animals; Control: 39 mCherry⁻ and 61 mCherry⁺ nodes from 6 animals. **e** hM3Dq: 37 mCherry⁻ and 62 mCherry⁺ total nodal regions from 6 animals; Control: 37 mCherry⁻ and 64 mCherry⁺ total nodal regions from 6 animals. **b** Size bar 2 μm . Error bars represent \pm SEM.

hypothesis by using a chemogenetic approach in the vHPC-to-mPFC pathway, previously shown to regulate anxiety-like behavior [39, 40]. We found that prolonged DREADD-mediated activation of vHPC-to-mPFC projection neurons resulted in increased risk-assessment and reduced closed arm exploration, suggesting decreased anxiety-like behavior. An acute inhibition of the pathway has previously been shown to decrease anxiety-like behavior [39, 40], while an acute activation elicited an anxiogenic effect [40]. Altogether, these data demonstrate that vHPC-to-mPFC pathway is critical for the regulation of anxiety-like behavior, yet it underscores a divergent impact of an acute and chronic activation of the pathway on anxiety. We next asked whether nodal changes occur in an activity-dependent and pathway-specific manner in the vHPC-to-mPFC pathway.

Whether activity-related nodal alterations result from generalized activity changes within a brain region, or whether nodal modulation occurs at the level of individual axons, has remained unanswered until recently [43]. Here, we studied whether axon-specific nodal remodeling occurs along axons that mediate anxiety-like behavior. To study this, we used chemogenetics as this method allowed us to repeatedly stimulate specific neurons regulating anxiety-like behavior, while visualizing the manipulated axons for morphological analysis of nodes. Notably, paranodes were specifically modified on activated axons, but not on non-activated axons within the same brain region, suggesting that neuronal activity directly elicits paranodal plasticity along the stimulated axons, as described previously for the formation of

myelin sheaths [37, 38], and recently in the motor cortex following learning [43]. Altogether, these findings suggest that node remodeling may play an important role in modulating neuronal communication in anxiety circuits.

Axon-specific modulation of nodes of Ranvier likely adds to fine-tuning of axonal conduction, enabling circuit-specific adaptation to changing processing needs. However, it could also underlie some of the persistent maladaptations associated with stress-related psychiatric disorders. We found that the main nodal effect of CSDS was shortening of paranodes in the mPFC gray matter and lengthening of paranodes in the forceps minor white matter in B6 stress-resilient mice. Similar to the effects observed in the mPFC in B6 stress-resilient mice, DREADD-mediated stimulation led to shorter paranodes in the vHPC-to-mPFC pathway, an effect that was accompanied with reduced anxiety-like behavior. Conversely, in the D2 strain, paranodes appeared longer in the mPFC gray matter in stress-susceptible mice, although these changes did not reach statistical significance. We have previously shown that chronic stress can associate both with thicker or thinner myelin sheaths, depending on whether the mice are stress-susceptible or -resilient and on the genetic background [9]. Similar to dynamic modulation of myelin sheaths [41], bidirectional and brain region-specific modulation of paranodes likely contributes to the capacity to adapt according to the needs of specific circuits and networks [22].

Overall, our data demonstrate genetically controlled remodeling of nodes of Ranvier after chronic stress. Much of the work on

myelin plasticity and stress has been conducted using only one mouse strain, typically a B6 substrain. Our findings highlight the need to study more than one genetic background, as appreciating genetically dependent outcomes could improve translational validity of preclinical models. We propose that nodes of Ranvier remodeling associated with CSDS result from stress-induced changes in neuronal activity patterns in distinct gray and white matter regions. Together with other forms of myelin plasticity, i.e., alterations in oligodendrocyte precursor and mature oligodendrocyte function, and changes to myelin distribution and thickness, nodal changes may either promote susceptibility or resilience to stress. We cannot, based on our data, characterize the observed modifications as pathological or adaptive. As anxiety disorders are increasingly considered to involve circuit-level dysfunction, rather than a disruption of a single neurotransmitter system or a single brain region [44], nodal remodeling may contribute to aberrant circuit function in these conditions. Future studies should be aimed not only to understand how nodes of Ranvier remodeling influences conduction velocity along single axons, but to understand its role in circuit- and network level communication. Understanding the mechanisms driving node of Ranvier changes may help pave the way for novel treatment practices for anxiety disorders.

REFERENCES

- Kessler RC. The global burden of anxiety and mood disorders: putting the European Study of the Epidemiology of Mental Disorders (ESEMeD) findings into perspective. *J Clin Psychiatry*. 2007;68:10–19.
- Yang X, Fang Y, Chen H, Zhang T, Yin X, Man J, et al. Global, regional and national burden of anxiety disorders from 1990 to 2019: results from the Global Burden of Disease Study 2019. *Epidemiol Psychiatr Sci*. 2021;30:e36.
- Hettema JM, Neale MC, Kendler KS. A review and meta-analysis of the genetic epidemiology of anxiety disorders. *Am J Psychiatry*. 2001;158:1568–78.
- Sharma S, Powers A, Bradley B, Ressler KJ. Gene × environment determinants of stress- and anxiety-related disorders. *Annu Rev Psychol*. 2016;67:239–61.
- Heim C, Nemeroff CB. The impact of early adverse experiences on brain systems involved in the pathophysiology of anxiety and affective disorders. *Biological Psychiatry*. 1999;46:1509–22.
- Faravelli C. Childhood stressful events, HPA axis and anxiety disorders. *World J Psychiatry*. 2012;2:13.
- Krishnan V, Han M-H, Graham DL, Berton O, Renthal W, Russo SJ, et al. Molecular adaptations underlying susceptibility and resistance to social defeat in brain reward regions. *Cell*. 2007;131:391–404.
- Hollis F, Kabbaj M. Social defeat as an animal model for depression. *ILAR J*. 2014;55:221–32.
- Laine MA, Trontti K, Misiewicz Z, Sokolowska E, Kulcskaya N, Heikkinen A, et al. Genetic control of myelin plasticity after chronic psychosocial stress. *Eneuro*. 2018;5:ENEURO.0166-18.2018.
- Calhoun GG, Tye KM. Resolving the neural circuits of anxiety. *Nat Neurosci*. 2015;18:1394–404.
- Zhang H, Yan G, Xu H, Fang Z, Zhang J, Zhang J, et al. The recovery trajectory of adolescent social defeat stress-induced behavioral, 1H-MRS metabolites and myelin changes in Balb/c mice. *Sci Rep*. 2016;6:27906.
- Lehmann ML, Weigel TK, Elkahloune AG, Herkenham M. Chronic social defeat reduces myelination in the mouse medial prefrontal cortex. *Sci Rep*. 2017;7:46548.
- Liu J, Dietz K, Hodes GE, Russo SJ, Casaccia P. Widespread transcriptional alterations in oligodendrocytes in the adult mouse brain following chronic stress: stress alters oligodendrocyte transcription. *Devel Neurobio*. 2018;78:152–62.
- Bonnefil V, Dietz K, Amatruda M, Wentling M, Aubry AV, Dupree JL, et al. Region-specific myelin differences define behavioral consequences of chronic social defeat stress in mice. *ELife*. 2019;8:e40855.
- Cathomas F, Azzinnari D, Bergamini G, Sigrist H, Buerge M, Hoop V, et al. Oligodendrocyte gene expression is reduced by and influences effects of chronic social stress in mice. *Genes Brain Behav*. 2019;18:e12475.
- Mount CW, Monje M. Wrapped to adapt: experience-dependent myelination. *Neuron*. 2017;95:743–56.
- Monje M. Myelin plasticity and nervous system function. *Annu Rev Neurosci*. 2018;41:61–76.
- de Faria O, Pivonkova H, Varga B, Timmler S, Evans KA, Kárádóttir RT. Periods of synchronized myelin changes shape brain function and plasticity. *Nat Neurosci*. 2021;24:1508–21.
- Lubetzki C, Sol-Foulon N, Desmazières A. Nodes of Ranvier during development and repair in the CNS. *Nat Rev Neurol*. 2020;16:426–39.
- Poliak S, Peles E. The local differentiation of myelinated axons at nodes of Ranvier. *Nat Rev Neurosci*. 2003;4:968–80.
- Nelson AD, Jenkins PM. Axonal membranes and their domains: assembly and function of the axon initial segment and node of Ranvier. *Front Cell Neurosci*. 2017;11:136.
- Arancibia-Cárcamo IL, Ford MC, Cossell L, Ishida K, Tohyama K, Attwell D. Node of Ranvier length as a potential regulator of myelinated axon conduction speed. *ELife*. 2017;6:e23329.
- Cullen CL, Pepper RE, Clutterbuck MT, Pitman KA, Oorschot V, Auderset L, et al. Periaxonal and nodal plasticities modulate action potential conduction in the adult mouse brain. *Cell Rep*. 2021;34:108641.
- Dutta DJ, Woo DH, Lee PR, Pajevic S, Bukalo O, Huffman WC, et al. Regulation of myelin structure and conduction velocity by perinodal astrocytes. *Proc Natl Acad Sci USA*. 2018;115:11832–7.
- Ford MC, Alexandrova O, Cossell L, Stange-Marten A, Sinclair J, Kopp-Scheinpflug C, et al. Tuning of Ranvier node and internode properties in myelinated axons to adjust action potential timing. *Nat Commun*. 2015;6:8073.
- Noori R, Park D, Griffiths JD, Bells S, Frankland PW, Mabbott D, et al. Activity-dependent myelination: a glial mechanism of oscillatory self-organization in large-scale brain networks. *Proc Natl Acad Sci USA*. 2020;117:13227–37.
- Golden SA III, Berton O, Russo SJ. A standardized protocol for repeated social defeat stress in mice. *Nat Protoc*. 2011;6:1183.
- Law CW, Chen Y, Shi W, Smyth GK. voom: precision weights unlock linear model analysis tools for RNA-seq read counts. *Genome Biol*. 2014;15:R29.
- Ritchie ME, Phipson B, Wu D, Hu Y, Law CW, Shi W, et al. limma powers differential expression analyses for RNA-sequencing and microarray studies. *Nucleic Acids Res*. 2015;43:e47.
- Phipson B, Lee S, Majewski IJ, Alexander WS, Smyth GK. Robust hyperparameter estimation protects against hypervariable genes and improves power to detect differential expression. *Ann Appl Stat*. 2016;10:946–63.
- Subramanian A, Tamayo P, Mootha VK, Mukherjee S, Ebert BL, Gillette MA, et al. Gene set enrichment analysis: a knowledge-based approach for interpreting genome-wide expression profiles. *Proc Natl Acad Sci USA*. 2005;102:15545–50.
- Mootha VK, Lindgren CM, Eriksson K-F, Subramanian A, Sihag S, Lehar J, et al. PGC-1 α -responsive genes involved in oxidative phosphorylation are coordinately downregulated in human diabetes. *Nat Genet*. 2003;34:267–73.
- Bishop S, Duncan J, Brett M, Lawrence AD. Prefrontal cortical function and anxiety: controlling attention to threat-related stimuli. *Nat Neurosci*. 2004;7:184–8.
- Riga D, Matos MR, Glas A, Smit AB, Spijker S, Van den Oever MC. Optogenetic dissection of medial prefrontal cortex circuitry. *Front Syst Neurosci*. 2014;8:00230.
- Stedehouder J, Couey JJ, Brizee D, Hosseini B, Slotman JA, Dirven CMF, et al. Fast-spiking parvalbumin interneurons are frequently myelinated in the cerebral cortex of mice and humans. *Cereb Cortex*. 2017;27:5001–13.
- Gallego-Delgado P, James R, Browne E, Meng J, Umashankar S, Tan L, et al. Neuroinflammation in the normal-appearing white matter (NAWM) of the multiple sclerosis brain causes abnormalities at the nodes of Ranvier. *PLoS Biol*. 2020;18:e3001008.
- Gibson EM, Purger D, Mount CW, Goldstein AK, Lin GL, Wood LS, et al. Neuronal activity promotes oligodendrogenesis and adaptive myelination in the mammalian brain. *Science*. 2014;344:1252304.
- Mitew S, Gobius I, Fenlon LR, McDougall SJ, Hawkes D, Xing YL, et al. Pharmacogenetic stimulation of neuronal activity increases myelination in an axon-specific manner. *Nat Commun*. 2018;9:306.
- Padilla-Coreano N, Bolkan SS, Pierce GM, Blackman DR, Hardin WD, Garcia-Garcia AL, et al. Direct ventral hippocampal-prefrontal input is required for anxiety-related neural activity and behavior. *Neuron*. 2016;89:857–66.
- Parfitt GM, Nguyen R, Bang JY, Aqrabawi AJ, Tran MM, Seo DK, et al. Bidirectional control of anxiety-related behaviors in mice: role of inputs arising from the ventral hippocampus to the lateral septum and medial prefrontal cortex. *Neuropsychopharmacology*. 2017;42:1715–28.
- Bonetto G, Belin D, Kárádóttir RT. Myelin: a gatekeeper of activity-dependent circuit plasticity? *Science*. 2021;374:eaba6905.
- Miyata S, Taniguchi M, Koyama Y, Shimizu S, Tanaka T, Yasuno F, et al. Association between chronic stress-induced structural abnormalities in Ranvier nodes and reduced oligodendrocyte activity in major depression. *Sci Rep*. 2016;6:23084.
- Bacmeister CM, Huang R, Osso LA, Thornton MA, Conant L, Chavez AR, et al. Motor learning drives dynamic patterns of intermittent myelination on learning-activated axons. *Nat Neurosci*. 2022;25:1300–13.
- Hare BD, Duman RS. Prefrontal cortex circuits in depression and anxiety: contribution of discrete neuronal populations and target regions. *Mol Psychiatry*. 2020;25:2742–58.

ACKNOWLEDGEMENTS

We thank Kai Kaila and Hovatta lab members for helpful discussions and comments on the manuscript. Imaging was performed at the Biomedicum Imaging Unit and Genome Biology Unit and behavioral analyses at the Mouse Behavioural Phenotyping Facility, all supported by the Helsinki Institute of Life Science (HiLIFE) and Biocenter Finland.

AUTHOR CONTRIBUTIONS

M-KK, ML and IH designed the experiments, interpreted results, and wrote the manuscript. M-KK performed immunohistochemical studies, microscopy imaging and data analysis with the assistance of SJ and VA. ML performed the CSDS experiment, DREADD manipulation, behavioral testing, immunohistochemical and data analysis with the help of GM and PH. AA performed 3D reconstructions under the supervision of AS and JT who established the method. AG and KT performed gene expression and GSEA data analyses. All of the authors commented on the manuscript.

FUNDING

This work was funded by the Academy of Finland (316282; to IH; 323385; to AS), European Research Council Starting Grant (GenAnx; to IH), Sigrid Jusélius Foundation (to IH), and Finnish Cultural Foundation (to M-KK). Open Access funding provided by University of Helsinki including Helsinki University Central Hospital.

COMPETING INTERESTS

The authors declare no competing interests.

ADDITIONAL INFORMATION

Supplementary information The online version contains supplementary material available at <https://doi.org/10.1038/s41386-023-01568-6>.

Correspondence and requests for materials should be addressed to Iiris Hovatta.

Reprints and permission information is available at <http://www.nature.com/reprints>

Publisher's note Springer Nature remains neutral with regard to jurisdictional claims in published maps and institutional affiliations.



Open Access This article is licensed under a Creative Commons Attribution 4.0 International License, which permits use, sharing, adaptation, distribution and reproduction in any medium or format, as long as you give appropriate credit to the original author(s) and the source, provide a link to the Creative Commons license, and indicate if changes were made. The images or other third party material in this article are included in the article's Creative Commons license, unless indicated otherwise in a credit line to the material. If material is not included in the article's Creative Commons license and your intended use is not permitted by statutory regulation or exceeds the permitted use, you will need to obtain permission directly from the copyright holder. To view a copy of this license, visit <http://creativecommons.org/licenses/by/4.0/>.

© The Author(s) 2023

Résumé

La douleur chronique est l'une des principales causes d'invalidité à l'échelle mondiale et est largement associée aux troubles émotionnels. En effet, près de 50% des patients souffrant de douleur chronique développent des troubles de l'humeur ou anxieux au cours de leur vie. De nombreuses études chez l'Homme ou dans des modèles animaux ont suggéré un rôle important pour le cortex cingulaire antérieur (CCA) et l'habénula latérale (HbL) dans le développement et le maintien de la comorbidité entre douleur chronique et troubles émotionnels.

L'objectif de cette thèse était d'apporter une caractérisation comportementale, fonctionnelle et moléculaire de la voie CCA-HbL dans les conséquences émotionnelles de la douleur chronique chez des souris mâles. Nous avons premièrement mis en évidence, via des enregistrements calciques de « fiber photometry » des neurones du CCA projetant vers l'HbL, que ces derniers répondaient particulièrement à des stimuli aversifs. Dans un second temps, en manipulant par l'optogénétique cette voie, nous avons montré que l'activation chronique, mais pas aiguë, de la voie CCA-HbL induisait des comportements de type anxio-dépressif chez des animaux naïfs. D'autre part, l'inhibition de cette voie chez des souris douloureuses chroniques a permis de réduire les comportements de type anxio-dépressif, mais pas chez des souris stressées chroniquement. Enfin, notre analyse transcriptomique des neurones du CCA projetant vers l'HbL a révélé des dérégulations associées à des processus épigénétiques et de traitement des ARN chez les souris douloureuses chroniques.

Pour conclure, ces résultats ont souligné l'importance de la voie CCA-HbL dans la comorbidité entre douleur chronique et troubles émotionnels.

Mots-clés : Cortex cingulaire antérieur, Habénula latérale, Douleur chronique, Anxiété, Dépression

Résumé en anglais

Chronic pain is one of the leading causes of disability worldwide and is widely associated with emotional disorders. Indeed, around 50% of chronic pain patients develop mood or anxiety disorders during their lifespan. Compelling evidence from human studies and animal models suggest an important role of the anterior cingulate cortex (ACC) and the lateral habenula (LHb) in the development and maintenance of the chronic pain and emotional disorders comorbidity.

The objective of this thesis was to provide a behavioural, functional and molecular characterization of the ACC-LHb pathway in chronic pain-induced emotional consequences in male mice. We first highlighted with *in vivo* fiber photometry calcium recording of LHb projecting ACC neurons that they are specifically responding to aversive stimuli. Secondly, by optogenetically manipulating this pathway, our results show that chronic, but not acute, activation of the ACC-LHb pathway induces anxiodepressive-like behaviours in naive animals. On the other hand, inhibiting this pathway alleviates chronic pain induced anxiodepressive-like behaviours, but not in chronically stressed animals. Finally, transcriptomic analysis of LHb projecting ACC neurons revealed dysregulation associated with epigenetic adaptations and RNA processing in chronic pain mice.

Altogether, these results highlight the importance of the ACC-LHb pathway in the chronic pain and emotional disorders dyad.

Keywords: Anterior cingulate cortex, Lateral habenula, Chronic pain, Anxiety, Depression